THE PHYSICAL REVIEW

VOLUME 86 Second Series NUMBER

MAY 1, 1952

Published by the

AMERICAN PHYSICAL SOCIETY

at the

American Institute of Physics

Lancaster, Pa. and New York, N. Y.

THE PHYSICAL REVIEW

A journal of experimental and theoretical physics established by E. L. Nichols in 1893

Published by the American Institute of Physics for the

AMERICAN PHYSICAL SOCIETY

Officers

President

J. H. VAN VLECK
Harvard University
Cambridge, Massachusetts

Vice-President

ENRICO FERMI
Institute for Nuclear Studies
University of Chicago
Chicago 37, Illinois

Secretary

K. K. DARROW
Bell Telephone Laboratories
Office:
Columbia University
New York 27, New York

Treasurer

G. B. PEGRAM
Columbia University
New York 27, New York

Local Secretary for the Pacific Coast

J. KAPLAN
University of California at Los Angeles
Los Angeles, California

Managing Editor

S. A. GOUDSMIT
Brookhaven National Laboratory
Upton, Long Island
New York

BOARD OF EDITORS

Editor

S. A. GOUDSMIT

Assistant Editor

H. FESHBACH

Associate Editors

HARVEY BROOKS	M. GOLDHABER	W. F. ALLIS
R. F. CHRISTY	R. HOFSTADTER	F. G. BEDEWELL
C. L. CRITCHFIELD	A. W. LAWSON	W. B. FRETTER
M. DEUTSCH	A. PAIS	CHUNING HERRING
T. H. JOHNSON	R. SERBER	H. W. LEVERENZ
BRUNO ROSSI	C. H. TOWNES	ARNOLD NORDSIECK

Manuscripts for publication should be submitted to S. A. Goudsmit, Brookhaven National Laboratory, Upton, Long Island, New York. The authors' institutions are requested to pay a publication charge of $6 per page which, if honored, entitles them to 100 free reprints. Instructions will be sent with galley proofs.

Proof and all correspondence concerning papers in the process of publication should be addressed to the Publication Manager, American Institute of Physics, 57 East 55 Street, New York 22, New York.

Subscription Price

United States and Canada.....$15.00
Elsewhere.....$17.00

Back Numbers[1]

Yearly back number rate when complete year is available:
Prior to 1949: $20.00
Thereafter: $27.00
Single copies: $2.00 each, prior to July, 1929;
$1.00 each, July, 1929–December, 1941;
$2.00 each, January, 1942–December, 1946;
$1.00 each, January, 1947–December, 1948;
$1.25 each, thereafter.
General index, 1893–1930: $8.00.

Subscriptions, renewals, and orders for back numbers should be addressed to the American Institute of Physics, 57 East 55 Street, New York 22, New York.

Changes of address in the case of members of the American Physical Society should be addressed to the Treasurer; in the case of other subscribers to the American Institute of Physics.

[1] For Series I reprint of Physics Department, Cornell University, Ithaca, New York.

This Physical Review is published semi-monthly at Prince and Lemon Streets, Lancaster, Pennsylvania.

Entered as second-class matter March 9, 1917, at the Post Office at Lancaster, Pennsylvania, under the Act of March 3, 1879.

Acceptance for mailing at special rate of postage provided for in paragraph (d-2), section 34.40, P. L. & R. of 1948, authorized January 20, 1949.

THE
PHYSICAL REVIEW

A journal of experimental and theoretical physics established by E. L. Nichols in 1893

SECOND SERIES, VOL. 86, NO. 3 MAY 1, 1952

Monte Carlo Study of Shower Production

ROBERT R. WILSON
Cornell University, Ithaca, New York
(Received December 26, 1951)

Electron- and photon-initiated showers in lead have been calculated in a simple Monte Carlo manner for energies from 20 to 500 Mev. The results, exhibited in a series of transition curves, show considerable differences from the results of conventional cascade theory in that the number of electrons at the maximum are fewer and the shower is more penetrating.

The effects of multiple Coulomb scattering of the electrons have been included and depend markedly on the measurement considered. Thus, ionization currents are only slightly changed (the transition curves are foreshortened by about one-half radiation length) while the number of electrons counted behind lead plates in a cloud chamber can be reduced by as much as 50 percent by effects of multiple scattering. This result is nearly independent of the incident energy.

The final curves obtained are compared with the ionization measurement of Blocker, Kenney, and Panofsky and the cloud-chamber measurements of A. M. Shapiro. The agreement is satisfactory.

A simple quasi-analytic cascade theory is developed in which known low energy solutions are used to obtain successively higher energy solutions.

I. INTRODUCTION

THE cascade theory of shower production in light elements such as air has been worked out rather completely for very high energy initiating electrons or photons.[1] For energies of less than one Bev in lead, however, the cascade theory cannot be expected to apply very accurately: ionization losses are important, the cross sections for radiation and pair production change rapidly with energy, and not many generations occur. None of the calculations include effects of multiple scattering except for lateral spreading. The shower problem is inherently a stochastic one and lends itself naturally to a straightforward treatment by the Monte Carlo method. The calculations described here are all for lead and were done in two steps: first neglecting multiple scattering so that the results could be compared to conventional theory, and then including multiple scattering for the final results.

[1] H. J. Bhabha and W. Heitler, Proc. Roy. Soc. (London) **159**, 432 (1937); J. F. Carlson and J. R. Oppenheimer, Phys. Rev. **51**, 220 (1937); B. Rossi and K. Greisen, Revs. Modern Phys. **13**, 24 (1941); H. S. Snyder, Phys. Rev. **76**, 1563 (1949); I. B. Bernstein, Phys. Rev. **80**, 995 (1950).

II. THE MONTE CARLO MACHINE

The procedure used was a simple graphical and mechanical one. The distance into the lead was broken into intervals of one-fifth of a radiation length (about one mm). The electrons or photons were followed through successive intervals and their fate in passing through a given interval was decided by spinning a wheel of chance; the fate being read from one of a family of curves drawn on a cylinder, the unwrapped surface of which is shown in Fig. 1. The energy ordinate is parallel to the axis of the cylinder. For electrons, curves were drawn in such a way that the ratio of the distance between two adjacent curves to the peripheral distance of the cylinder was equal to the probability of radiation of a quantum, the energy of which was marked on each curve. For photons, dotted lines were drawn in a similar way to give the probability of electron pair production, the energies of the resulting electrons being read from the curves. Compton scattering was also included as is indicated. Accurate values of the probabilities, determined by the calculations of Bethe and Heitler[2] ad-

[2] H. A. Bethe and W. Heitler, Proc. Roy. Soc. (London) **146**, 84 (1934).

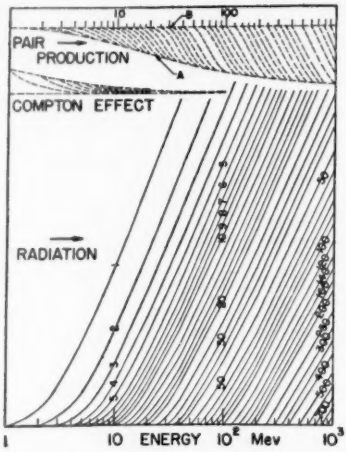

FIG. 1. The unwrapped surface of the cylinder of the wheel of chance.

justed to fit experiments,[3] were used in determining the curves.

A word about the wheel of chance: The cylinder, 4 in. outside diameter by 12 in. long, is driven by a high speed motor geared down by a ratio of about 20 to 1. The motor armature is heavier than the cylinder and determines where the cylinder stops. The motor was observed to stop at random and, in so far as the cylinder is concerned, its randomness is multiplied by the gear ratio. It appeared adequate for the operator simply to turn the motor on and then, after many revolutions of the cylinder, turn it off. As an improvement a simple switch was constructed which the operator turned on but which a Geiger counter, activated by cosmic-ray particles, turned off after a few seconds. It was also possible to set the position of the cylinder using a graduated dial and a table of random numbers. This was, of course, the most satisfactory procedure for obtaining true randomness but the operators found it considerably more tedious than using the motor. Many obvious tests of randomness have been made which indicate that the machine is more than adequately random for the accuracy aimed at in this treatment.

III. CALCULATIONS NEGLECTING MULTIPLE SCATTERING

Figure 2 exhibits a typical photon shower calculation for an initiating photon of 100 Mev. The energy of the electrons or photons of the cascade is plotted as ordinate, and distance into the Pb is the abscissa, each division corresponding to one interval (0.2 radiation length). The horizontal dotted lines are photons; the black sloping lines are electrons. The procedure of calculation is to follow the initial photon through successive intervals, spinning the cylinder at each interval until the stationary index falls between the dotted curves A and B, at the energy of the photon. The nearest curve to the index at that point indicates the energy of one of the electrons formed in pair production. The energy of the other electron is obtained by subtraction from the initial photon energy since energy is conserved. A further subtraction of one Mev for the rest mass of the electrons was made. The photon track disappears and one of the pair electrons is now followed. At each interval, the wheel is spun and the energy radiated by the electron is indicated on the black radiation curve nearest the index line at the electron energy. The newly created photon energy is plotted on the graph at that point. The energy of the radiating electron has now been reduced by the emitted photon energy plus a constant ionization loss of 1.5 Mev per interval. In this way the electron is followed until it has lost all its energy and so stops. The operator then goes back and follows the other electron and photons in turn until the whole shower is dead. The graph is thus a record of the history of that particular shower. The procedure is then successively repeated, until the statistics are adequate. Variations in form and complexity of each shower from that shown in Fig. 2 are indeed striking.

In practice photons are indicated but are not followed once their energy falls below 10 Mev because their mean free path by them is too long. The mean free path is nearly constant between 10 Mev and 1 Mev, and there is little difficulty in calculating the propagation of such radiation. The number of electrons n_2 at a

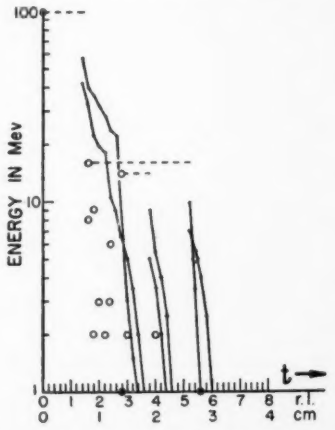

FIG. 2. A typical shower resulting from a 100-Mev photon. The dotted lines indicate photon paths and the solid lines indicate electron paths, the ordinate in each case giving the energy. The open circles are photons that were not followed. Distance in the Pb is measured in radiation lengths.

[3] DeWire, Beach, and Ashkind, Phys. Rev. **83**, 505 (1951); J. L. Lawson, Phys. Rev. **75**, 433 (1949); R. L. Walker, Phys. Rev. **76**, 1440 (1949).

distance t due to this radiation is given by

$$n_2(t) = \int_0^t [w(t')/\beta] e^{-(t-t')\sigma_m} dt', \qquad (1)$$

where $w(t')dt'$ is the average energy per shower starting as gamma-rays below 10 Mev in the interval dt' at t'. It is obtained from the shower charts by adding up the energy of all the indicated photons of energy less than 10 Mev which occur in intervals of distance that were chosen to be one radiation length and then dividing by the number of charts to get the average. The assumption is made that this energy propagates in the forward direction as $e^{-(t-t')\sigma_m}$ where σ_m is the average cross section per radiation length of the photon radiation below 10 Mev and above 1 Mev. The value of 0.24 was chosen for σ_m in lead. In obtaining (1), the assumption is also made that after the energy is absorbed the resulting electrons give up all of their energy into ionization in a region small compared to the mean free path of the radiation. The track length contributed in that region by these electrons is $w(t')/\beta$, where β is the ionization per radiation length or the critical energy; β is assumed to be 7.5 Mev for lead.

It is customary to present shower calculations in the form of curves giving the average number of electrons as a function of distance into the lead. This is done in Fig. 3 for incident photons. The number of electrons n, which is the ordinate, is the sum of n_2, the electrons as t due to low energy photons, and n_1, the electrons at t due to photons of energy greater than 10 Mev. The number n_1 is obtained directly from the shower charts by adding up all the electrons seen at a given distance and then dividing by the number of charts used. In general one or two hundred shower histories were made for each curve; thus the statistical accuracy of each point is roughly 10 percent. Actually the curves have been normalized by a few percent as follows: the initial slope of the curves for gamma-rays must be equal to $2\sigma_\pi + \sigma_C$, where the cross sections are for pair production and Compton scattering, respectively; the curves must all finally fall off as $e^{-\sigma_m t}$, and the integral, $\int_0^\infty \beta n dt$, must be equal to the initial energy. The purpose of the Monte Carlo method is thus to determine the shape of the curves in the intermediate region.

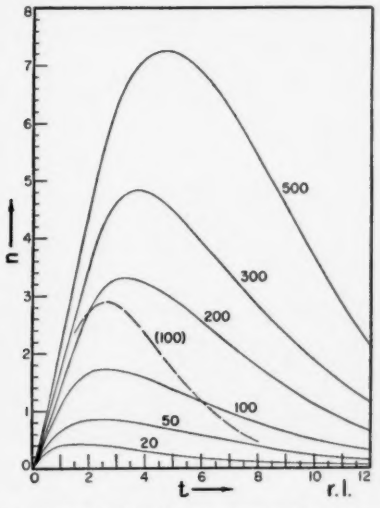

FIG. 3. Photon initiated shower curves in lead without consideration of multiple scattering. The solid curves give the Monte Carlo results and the dashed curve is calculated by conventional cascade theory. The energy in Mev is indicated on the curves. Depth units are in radiation units.

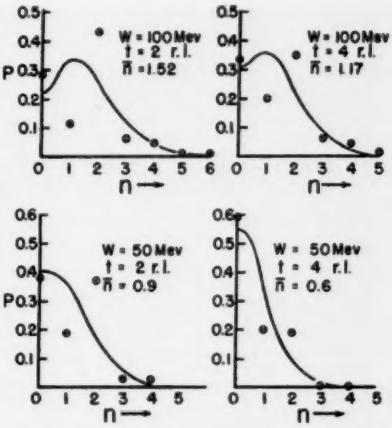

FIG. 4. Fluctuations in the number of electrons seen at a given distance. The circles are given by the Monte Carlo method and the curve is a Poisson distribution for the average number indicated. Only electrons resulting from photons above 10 Mev are shown here.

The labor becomes excessive for initial energies above 300 Mev, and for these energies the photons and electrons were followed down to 50 Mev where solutions already obtained by the Monte Carlo method were fed in numerically. For purposes of comparison, the results of the theory as given in Rossi and Greisen[1] including ionization loss are shown as a dotted curve for 100-Mev initiating photons.[4] There is no agreement in shape or absolute values for reasons already given in the introduction. The comparison is equally poor with the numerical calculations of Arley.[5]

In Fig. 4 are plotted distributions of the empirical expectancy of observing various numbers of electrons at given depths in the lead (electrons below 10 Mev are

[4] I am indebted to Dr. L. Brown for calculating this curve and the one shown in Fig. 10.

[5] Niels Arley, *On the Theory of Stochastic Processes and their Application to the Theory of Cosmic Radiation* (G. E. C. Gad, Copenhagen, 1943).

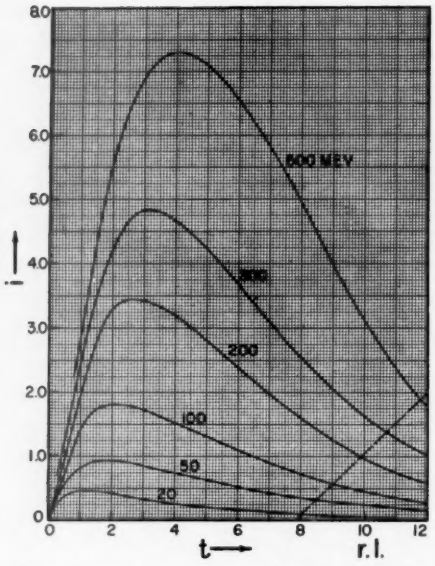

FIG. 5. Transition curves that would obtain in ionization measurements with incident photons whose energy in Mev is marked on each curve. Multiple scattering effects are included. The quantity i is defined in the text and would be proportional to the current measured in a thin ionization chamber. Beyond the oblique dashed line the curves are exponentials decaying with an absorption coefficient of 0.24. Depth units are in radiation lengths.

neglected here). Poisson distributions adjusted to the mean numbers are also drawn. It is seen that the empirical points have quite different values from those predicted by the Poisson distribution. The differences are largely inherent in the mechanism of pair production and in the fairly long range of electrons. Thus, if one member of a pair of electrons is observed, it is likely that the other electron will also be observed. Single electrons are infrequently seen by themselves and double electrons occur nearly twice as frequently as predicted by the Poisson curve. It is interesting that the expectancy of zero electrons agrees with the Poisson prediction well within the statistical accuracy.

For the experimentalist a sheaf of the history graphs is about as good a representation as any. He can leaf through the set and get a feeling for the fluctuations that are likely to occur. For a given set of experimental conditions, such as an arrangement that measures the ionization between the second and fourth radiation lengths, the graphs can be consulted directly to get an approximate answer. If one attempts a calculation, a cursory examination of the graphs gives valuable clues as to what is significant and as to what can be neglected.

IV. CALCULATIONS INCLUDING MULTIPLE SCATTERING

In principle one could include multiple scattering at the same time that the shower is being calculated by spinning an auxiliary wheel to find the multiple scattering angle of an electron as it passed through each interval of length. This would be far too laborious. Instead the effects of multiple scattering on the range of individual electrons has been worked out theoretically in a separate paper,[6] in which the results were checked with the Monte Carlo method. A two-group theory was assumed, in which the electron paths were considered as straight until the energy had been degraded to a critical value E_r after which the motion was considered to be completely random. It was found that the random energy E_r was nearly independent of the initial energy of the electron and is given in Mev by the approximate formula[7]

$$E_r \approx 20/\beta^{\frac{1}{2}}. \tag{2}$$

Once the electron reaches this energy further displacement is negligible because the residual range is spent in a tight random motion. This means that one of the

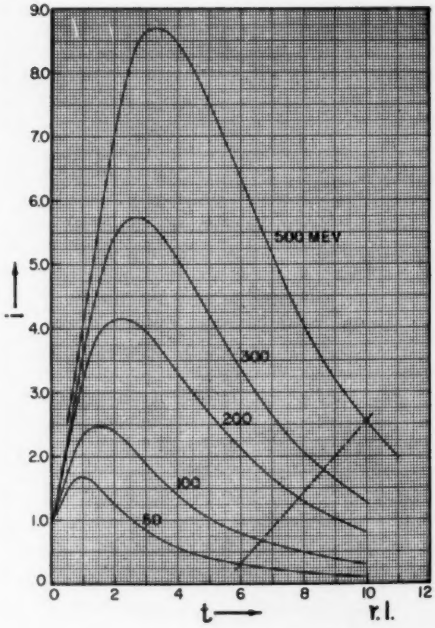

FIG. 6. Same as Fig. 5 but for incident electrons.

[6] R. R. Wilson, Phys. Rev. 84, 100 (1951).
[7] The formula appears different than in reference 6 because different units are used. More exact values are given by Eq. (14) of the same paper.

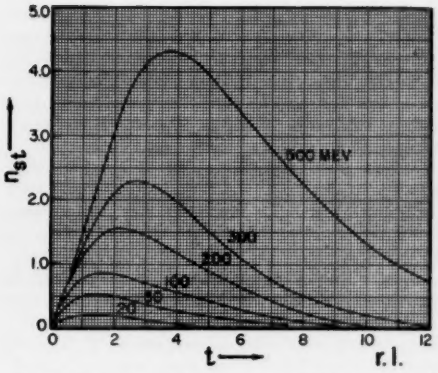

FIG. 7. The number of electrons that would be counted in the core of a shower and with paths in the direction of the shower is plotted against t, in radiation lengths, for incident photons. The energy is marked on the curves in Mev.

effects of multiple scattering is to shorten the paths of all electrons in a shower by an amount r, the range of an electron with energy E_r. This range was shown[6] to be given in radiation lengths by

$$r/\ln 2 = \ln(1+E_r/\beta \ln 2), \tag{3}$$

where β is the critical energy in the same units as E_r.

In presenting the effects of multiple scattering on curves such as those in Fig. 3 showing n against t, it is necessary to delineate the problem a little more closely in terms of measurement. One might try to measure such a curve with a thin ionization chamber inserted in the material, or the experimenter might endeavor to count the number of electrons at a given depth using a Geiger counter, or using a cloud chamber in which many plates were inserted. Quite different results would be obtained in lead in each case.

In the case of an ionization measurement, electrons moving with random motion contribute considerably to the ionization, especially those electrons moving nearly parallel to the plane of the chamber. Let us call the measured quantity i, defined as the ionization charge collected per incident electron or photon divided by the charge that would be collected were one straight electron path to cross the chamber normally. Thus if multiple scattering were negligible, i would equal n. As an approximation, we obtain curves of i as a function of t from the curves of Fig. 3 by simply shortening all the abscissas of the curves by an amount r to correspond to the decrease in electron range. Clearly this procedure breaks down for small values of t, in which case the abscissas are shortened by an amount,

$$\Delta t = r(1-e^{-t}). \tag{4}$$

This expression was chosen arbitrarily. It expresses the fact that most of the electrons in a shower have their energy near the critical energy and hence have a range of roughly one radiation length. In a more accurate theory it would be necessary to make a better determination of Δt. The fore-shortened curve should now be renormalized because the integral $\int_0^\infty i\beta dt$ must still be equal to the initial energy—this renormalization takes care of the oblique electron traversals of the ion chamber. Curves of i as a function of t for various energies of initiating electrons and photons are shown in Figs. 5 and 6.

Now for the second case in which the electrons are counted, let us discuss the example of the cloud chamber: the case of the Geiger counter will follow from this discussion. There are two possibilities in counting electrons in the cloud chamber: all the electrons appearing in the chamber between two plates can be counted, n_e; or just those electron tracks in the core and with a forward direction, say within 30°, can be counted, n_{st}. In the latter case the shower is just cut off at the energy E_r, for nearly all electrons below this energy will be either off the shower axis or if on the axis will be oriented in the wrong direction. This is a good procedure in counting because it discriminates against background electrons produced throughout the chamber. Curves of n_{st} against distance obtained by cutting showers off at E_r (8 Mev for lead) are shown in Figs. 7 and 8.

Finally we treat the case where all electron paths between successive plates are counted. Now we must add to n_{st}, just calculated for straight paths, the electrons which are moving randomly. This can be done most easily by taking the difference Δn between i given in Figs. 5 or 6 and n_{st} given in Figs. 7 or 8. The difference is the track length due to randomly moving electrons. Only the component of track length along the initial direction of the electron or photon is of interest now, and this is $\cos\theta$ times the track length, where θ is the direction of the electron with respect to the initial direction. The average of $\cos\theta$ over a hemisphere is $\frac{1}{2}$, hence we add one-half Δn to n_{st} to obtain

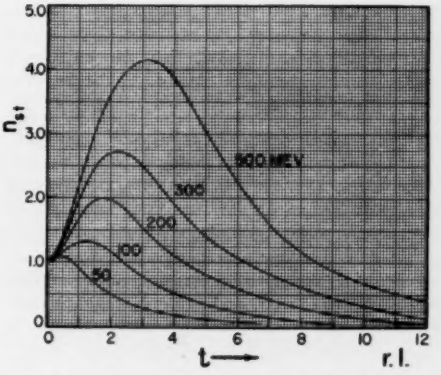

FIG. 8. Same as Fig. 7 but for incident electrons.

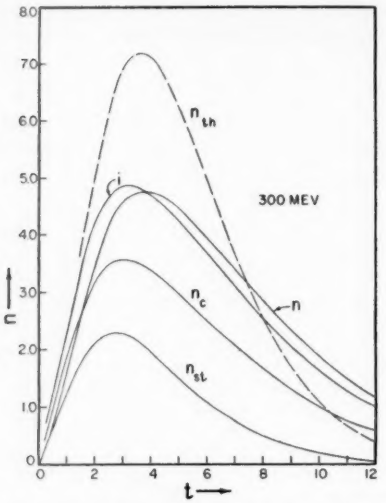

FIG. 9. The effects of multiple scattering on the transition curve of a 300-Mev incident photon. The ordinate plotted corresponds to the quantity labeled on the curve and these quantities are defined in the text for various conditions of measurement . . . the dashed curve is the result of conventional theory. (See reference 4.)

our result n_c. Curves are not given for this quantity because it can be so easily obtained from the curves of i and n_{st}.

In general one will count those electrons having an angle with respect to the initial direction less than say θ_1. In that case a fraction $\langle\cos\theta\rangle_{Av}=(1-\cos^2\theta_1)/4$ of Δn should be added to n_{st}. One must not forget the crudeness of this approximation.

Comparisons between the four above quantities n, i, n_c, and n_{st} for 300-Mev initiating electrons and photons are given in Fig. 9. The effects of multiple scattering were also calculated at 300 Mev by Mrs. Elizabeth Baranger[8] by inserting the multiple scattering in detail into the Monte Carlo calculations and her work will be published separately. Her results are statistically indistinguishable from those obtained by the simplified treatment given here.

V. EXTENSION OF CALCULATIONS TO OTHER MATERIALS

The above calculations apply to lead. For neighboring elements the results will be similar but the ordinates of the curves must be multiplied by the ratio of critical energy of the new substance to that of lead. For light elements conventional theory should apply for incident particles of high energy: at low energy or for elements of intermediate Z, the method of Bernstein[1] or the simple theory outlined in the appendix should be used.

Multiple scattering effects become relatively smaller at low Z for two reasons: (*a*) The cascade tends to cut off at an energy β which varies roughly as $1/Z$, and (*b*) E_r, the energy below which random motion sets in, varies as $1/\beta$ and hence as $Z^{\frac{1}{2}}$. Thus the relative number of electrons in a shower with energy below E_r decreases rapidly with Z.

Conventional theory can be easily corrected, if curves of i *vs* t are desired, by simply fore-shortening values of t by the amount given by Eqs. (2) and (3), as was done in this paper for the Monte Carlo results in lead, together with a renormalization of the curve. To obtain curves of n_{st} and n_c *vs* t, we must find the total track length below E_r. The computations of Richards and Nordheim[9] show that the integral track length for low energy electrons is nearly independent of Z. Their results can be expressed, at low energy and very roughly (about 10 percent), by the empirical formula

$$F(E)=W(1-e^{-2E/\beta})/\beta, \tag{5}$$

where $F(E)$ is the integral track length of electrons *up to* energy E and W is the initial particle energy. Hence we compute n_{st} by subtracting $F(E_r)$ from i as obtained above: n_c is obtained by subtracting $F(E_r)/2$. This procedure cannot be expected to work near the beginning of the shower when the calculations of track length do not apply. On the other hand it may be fairly

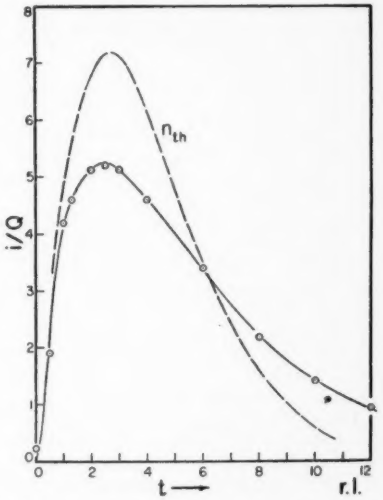

FIG. 10. A comparison of theory and experiment. The circles are the measurements in lead of ionization resulting from incident 330-Mev bremsstrahlung radiation. The solid curve which fits the points is the Monte Carlo theory and the dashed curve is the result of conventional shower theory (see reference 4). The areas of the curves are all adjusted to the same value.

[8] E. Baranger, Master's thesis, Cornell University (1951).

[9] J. Richards and L. Nordheim, Phys. Rev. **74**, 1106 (1948).

reliable near the shower maximum. Incidently, this calculation shows that the effects of multiple scattering are essentially independent of initial energy.

VI. COMPARISON WITH EXPERIMENT

Ionization curves have been measured for lead by Blocker *et al.*[10] for incident bremsstrahlung from 330-Mev electrons. Assuming the photon spectrum given by theory,[2] Monte Carlo values taken from Fig. 5 were added numerically to give the theoretical ionization curves of Fig. 10. The experimental points are also shown and the excellent agreement must be considered as partly fortuitous. The curve marked n_{th} is that given by conventional theory.[4]

Shapiro[11] has used a cloud chamber in which were placed a number of lead plates. With 200-Mev electrons incident, obtained from the Cornell synchrotron, he counted the number of electron paths in the core of the shower between the plates. His average numbers as well as the fluctuations from the averages are in very good agreement with the Monte Carlo results. An extensive comparison will be published by Shapiro.

There is an experimental check on the variation of multiple scattering effects with Z. Blocker *et al.*[10] measured the ionization current essentially at shower maximum with and without material behind the ion chamber. The difference is presumably due to multiple scattering effects. The increase in ionization resulting from back scatter was 0.41 of the total ionization in lead, 0.20 in copper, 0.09 in aluminum, and 0.04 in carbon. Our theory requires the backscattering to be proportional to the number of electrons below E_r. Using values of E_r given by Eq. (2) and the corresponding integral track lengths for lead and air given by Richards and Nordheim,[9] and assuming that half the source of randomly moving electrons is removed upon taking away the material behind the chamber, we calculate 0.38 for the backscattering in lead and 0.03 for carbon. Using Eq. (3) to interpolate track length for Cu and Al we get 0.20 and 0.07 for the backscattering respectively, instead of 0.20 and 0.08 as measured. The effects of reflections will tend to destroy this rather fortuitous agreement.

It is a pleasure to acknowledge the cooperation of Miss Leonilda Altman and Miss Ruth Seiwatz who did all of the tedious running of the machine and who carried out miscellaneous numerical calculations. Without their help the work would not have been done. I am also indebted to Mrs. Elizabeth Baranger for her work at 300 Mev on the inclusion of effects of multiple scattering.

APPENDIX. A SIMPLE SHOWER THEORY

The Monte Carlo method as used here has suggested the following simple analytic method of computing cascade phenomena. It is presented because it can be useful in extending the present results to higher energy. It is applicable to all substances, retains the use of actual cross sections for photon absorption, and should give considerably more accurate results than does the Monte Carlo method.

The theory will be described first for incident photons and then extended later on to incident electrons. The central idea is to feed in known low energy shower curves and to get out high energy curves, which can be used in turn to get ever higher energy curves. Basic for the calculation is the theory of the propagation of individual electrons, and this has been developed separately in reference 6. There it was shown that the average range R of an electron of energy E_0 is, in shower units,[12]

$$R=\ln(E_0+1), \tag{6}$$

and that the mean square straggling of the range is

$$y=(1-R/E_0)^2R. \tag{7}$$

It was also shown that the average range of the electrons of a pair produced by a photon of energy W is

$$R=(1-1/W)\ln(W+1)-1, \tag{8}$$

and that the spacial distribution of a pair of electrons produced at $t=0$, i.e., the number of electrons reaching a distance t or more, is given approximately by[13]

$$n=2\exp(-t/R_\tau). \tag{9}$$

A two-group theory is used for the shower calculation, in which the first group of electrons will be the pair made directly on the initial absorption of the incident gamma-ray. The second group will then correspond to all of the electrons resulting from the photons radiated by the initial pair electrons. We will call the electron groups primary and secondary, respectively.

The primary electron distribution $n_1(t)$ can be obtained readily from (9), i.e.,

$$\begin{aligned} n_1(t)&=2\sigma\int_0^t e^{-\sigma x}e^{-(t-x)/R_\tau}dx \\ &=2\sigma(e^{-t/R_\tau}-e^{-\sigma t})/(\sigma-1/R_\tau), \end{aligned} \tag{10}$$

where σ is the absorption cross section of the initial photon.

The secondary electrons will be calculated by first obtaining the average spectrum and source strength of the secondary photons, i.e., those emitted by the primary pair electrons. These photons will be of much

[10] Blocker, Kenney, and Panofsky, Phys. Rev. **79**, 419 (1950).
[11] A. M. Shapiro, Phys. Rev. **82**, 307 (1951).

[12] Shower units of length and energy are used in this appendix as in reference 6. Shower lengths are radiation lengths times ln2, and energies are here measured in units equal to ln2 times the critical energy, i.e., $E=E_{Mev}/\beta\ln 2$.

[13] The exponential expression applies for energies of the order of magnitude of the critical energy. For much higher energies, the integral Gaussian form (21) should be used, substituting the pair range, R_τ, for R. Actually at such high energies the primary electrons will be completely masked by the secondaries and the approximation (9) will introduce little if any error.

lower energy in general than the initial photon, and a shower curve can then be calculated for this spectrum either by feeding in known shower curves such as the Monte Carlo results given in this paper or by going down to such a low energy compared to the critical energy that the shower curves will be given directly by (10), i.e., at low enough energy that the secondary group is negligible compared to the primary group. The spacial distribution, on the average, of the source strength of the secondary photons must also be computed, and then the distribution of secondary electrons will be obtained numerically through the knowledge of how such photons propagate, namely, by knowing the averaged secondary photon shower curve.

Now for the actual calculation of the secondary electrons: it is assumed that an electron in going dt emits a spectrum of photons given by

$$w(k)dkdt=dkdt/k. \tag{11}$$

which is cut off at $k=E_0$. We wish to find the average spectrum of photons from an electron of energy E_0 going a distance corresponding to its average range. The integral number of photons of energy k emitted by an electron will be obtained by integrating over that part of the range where the energy of the electron is greater than k. Assuming that the energy of the electron is related to the residual range as given by (6), then the interval of integration must be from zero to $R-t_k$, where $t_k=\ln(k+1)$ corresponds to the residual range of an electron of energy k and in this range no photons of energy k can be emitted. Accordingly, the average distribution of photons from an electron will be given by

$$w'(k)dk=(dk/k)\ln[(E_0+1)/(k+1)]. \tag{12}$$

We notice that this distribution cuts out the high energy photons. In fact a fair approximation is to assume a dk/k distribution which cuts off at $k_1=E_0-R$, the cutoff being chosen here to give the correct amount of total energy radiated compared to ionization loss which is, of course, just R in these units. This may be more accurate than using (12), for it automatically takes into account the effects of large fluctuations—an important consideration in the derivation of (6).

The spectrum of photons (12) must now be averaged over the energies of the pair electrons. Assuming that the energy of the pair is split between electron and positron such that it is equally probable for the electron to receive any fraction of the photon energy W between 0 and 1, then the average photon spectrum from the pair is

$$\begin{aligned} w''(k)dk&=\int_k^W (2dk/k)\ln[(E+1)/(k+1)]dE/W \\ &=2(dk/kW)\{(W+1)\ln[(W+1)/(k+1)] \\ &\qquad -(W-k)\}. \end{aligned} \tag{13}$$

Here the photons are degraded even farther in comparison to the initial photon energy W, and again we can approximate (but less accurately) with a simple $2dk/k$ spectrum with cutoff at $k_1=W-2R_\tau$.

To calculate $n_2(t)$, the distribution of electrons due to secondary photons, we must now know the distribution in space of the sources of secondary photons represented by (13). The total energy radiated in photons from an electron as it goes dt is given by[14]

$$-dE/dt=E,$$

and solving (6) for the average energy of an electron E as a function of the residual range r gives $E=e^r-1$; hence

$$-dE/dt=e^r-1. \tag{14}$$

An electron which starts at $t=0$ will have a photon source S_1 which is proportional to $-dE/dt$ and which varies as the energy of the electron varies. It will be given by

$$S_1(t)=e^{R-t}-1. \tag{15}$$

Assume now that the members of the initial pair of electrons both have just the average pair range given by (8). Then the source distribution from the pair produced by the initial photon will be given by

$$S_2(t)=2\sigma\int_{t-R_\tau}^{t}(e^{R_\tau-t+t'}-1)e^{-\sigma t'}dt',$$

where the lower limit is zero for $t<R_\tau$. After integration we get, for $t<R_\tau$,

$$S_2(t)=2\sigma(e^{-R_\tau-\sigma t}-e^{R_\tau-t})/(1-\sigma)-2(e^{-\sigma t}-1) \tag{16}$$

and for $t>R_\tau$,

$$\begin{aligned} S_2(t)&=2\sigma(e^{-R_\tau-\sigma t}-e^{-(t-R_\tau)\sigma})/(1-\sigma) \\ &\qquad -2(e^{-\sigma t}-e^{-(t-R_\tau)\sigma}). \end{aligned} \tag{17}$$

At this point we must calculate $n'(t)$, the shower curve due to a unit source at $t=0$ for the spectrum of photons given by (13) or by the approximate $2dk/k$ spectrum with cutoff at $k=W-2R_\tau$. Then, knowing the distribution of the sources as given above, we get at once the secondary electron distribution $n_2(t)$ by numerical integration, namely,

$$n_2(t)=\int_0^t S_2(t')\cdot n'(t-t')dt'. \tag{18}$$

The normalization of $n_2(t)$ can be checked by noticing that all the energy in the shower must be given up to ionization energy; thus

$$\int_0^\infty n_1 dt=2R_\tau, \tag{19}$$

[14] The ln2 term does not appear because of the effects of fluctuations, see reference 6.

and hence

$$\int_0^\infty n_2 dt = W - 2R_\tau. \tag{20}$$

The sum of n_1 and n_2 gives the resulting shower curve, and then one proceeds to progressively higher energies by feeding this solution back into the method.

For the case of incident electrons the procedure is exactly the same, except that the primary distribution $n_1(t)$ is due to the incident electron itself and, as shown in reference 6, is given by the integral Gaussian form,

$$n_1(t) = \tfrac{1}{2}\{1 - \mathrm{erf}[(x-R)/(2y)^{\frac{1}{2}}]\}, \tag{21}$$

R and y being given by (6) and (7). The photon spectrum is given by (12) or by its simple approximation dk/k with cutoff at $k = E_0 - R$. The spacial source distribution is given by (15).

Multiple scattering effects are included in much the same manner as in the Monte Carlo work. We calculate the number of electrons below the random energy, given in shower units of energy, approximately by

$$E_r = (10/\beta)^{\frac{1}{2}}, \tag{22}$$

or more accurately by Eq. (14) of reference 6. (Notice that β is in Mev in these formulas.) The fraction of the primary electrons, n_1, below E_r is just r/R for an incident electron or r/R_τ for an incident photon, where $r = \ln(E_r+1)$. The fraction of the secondary electrons n_2 below E_r is just $r/\bar{R}$, where $\bar{R}$ is the pair range given by (7) averaged over the spectrum (12) or (13).

PHYSICAL REVIEW VOLUME 86, NUMBER 3 MAY 1, 1952

Comparative Models in Nuclear Scattering*

D. C. PEASLEE
Columbia University, New York, New York

(Received January 9, 1952)

The "optical" and "compound" methods for treating nucleon-nucleus encounters are compared on the basis of a very simple model. It is concluded that the optical procedure is valid for incident energies $E > \sim 80$ Mev, the compound for $E < \sim 30$ Mev. The statistical model of the excited nucleus can be applied only when the excitation energies of individual nucleons may all be considered to be within the lower limit. For π-mesons incident on nuclei similar considerations show that the optical method must be used under all circumstances.

1. INTRODUCTION

ELASTIC scattering and absorption of nucleons have been treated by two different methods, which may be designated as the optical[1] and compound[2] procedures. The present note compares these approaches and attempts to define their respective regions of validity, with a view toward determining which approach is suitable for π-meson scattering and absorption by nuclei; it appears that the optical model is preferred under all circumstances.

In the compound procedure the logarithmic derivative f at the nuclear surface is represented by a suitable phenomenological form that reflects the complex situation inside the compound nucleus; namely,

$$f = -K_0 \tan\{\pi/D(E - E_0 + i\Gamma_a/2)\}$$

where $K_0 \approx 10^{13}$ cm^{-1} is a wave number appropriate to the interior of the nucleus and corresponds to a potential well about 30 Mev deep. The energy of the system is E, a resonance energy is E_0, the average spacing of successive resonance levels is D, and Γ_a is the half-width for absorption. This approach yields the Breit-Wigner form for isolated levels at low energy and has been extended[3] to incident nucleon energies as high as 25 Mev, where the resonances are completely smeared out.

The optical method has been used for incident nucleon energies on the order of 90 Mev or more and consists in integrating the phase difference over all paths through the nucleus. The wave number external to the nucleus is k, internally is $k' = k + k_1 + iK/2$, where $|k' - k| \ll k$. The beam may be analyzed into partial waves of angular momentum l, for which the appropriate W.K.B. path length extends radially from R to r_l, the classical turning point radius. A characteristic feature of this treatment is the complete neglect of reflection at the nuclear surface, which implies an infinitely diffuse boundary.

A superficial difference between the models is the question of "sharp" *vs* "diffuse" boundaries: to argue that it is unimportant, consider the error introduced by assuming a sharp boundary when a diffuse boundary is correct. The parameter measuring the sharpness of the boundary is $1/(k\Delta R)$, where the uncertainty in nuclear radius ΔR happens roughly to equal $1/K_0$ in magnitude. In the simplest case of no external potential the phase shift is given by

$$k \cot(kR + \delta) = k \cot K'R + (K' - k) \cot K'R, \tag{1}$$

* This work is supported by the research program of the AEC.

[1] Fernbach, Serber, and Taylor, Phys. Rev. **75**, 1352 (1949).

[2] See, for example, Feshbach, Peaslee, and Weisskopf, Phys. Rev. **71**, 145 (1947).

[3] H. Feshbach and V. F. Weisskopf, Phys. Rev. **76**, 1550 (1949).

TABLE I. Ratio N_1/N_2 for various incident energies E_0.

E_0(Mev)	≈0	10	25	50	75	100
Γ(Mev)	0.3×10^{-6}	1.5	4	8	12	16
v/c	0.2	0.3	0.3	0.4	0.4	0.4
$\lambda(10^{-13}$ cm)	1.4	1.4	2	3	4	5
$\bar{\lambda}(10^{-13}$ cm)	1.4	1.4	1.4	2.1	2.8	3.5
f	1	0.85	0.71	0.3	0.1	0.03
N_2/N_1	10^6	26	6	1	0.2	0.07

where $K'=(k^2+K_0^2)^{\frac{1}{2}}$ is the wave number of the interior region. The first term on the right-hand side of (1) would be given by a perfectly diffuse boundary, leading to a phase shift $\delta=(K'-k)R$; the second becomes dominant as the hard sphere condition is approached. The relative importance of reflection at the boundary is thus measured by $(K'-k)/k$; and under the diffuse boundary condition, $K_0/k\ll1$, this becomes $(K'-k)/k\approx\frac{1}{2}(K_0/k)^2\ll1$, so that no appreciable error is made by insertion of the sharp boundary in this case. With long-range potentials $V(r)$ in the internal and external regions, the relation (1) may be approximately preserved by replacing k with $k_{\text{eff}}=[k^2-2MV(R)/\hbar^2]^{\frac{1}{2}}$. Then the sharp boundary holds for $k_{\text{eff}}\ll K_0$ and $k_{\text{eff}}\gg K_0$, being respectively necessary and inconsequential. In any situation, only a minor fraction of the partial waves will satisfy $k_{\text{eff}}\approx K_0$, so that a relatively small total error is expected by assuming sharp boundaries throughout. There is some experimental sanction for a sharp boundary with 90-Mev neutrons,[4] as well as at 25 Mev and 14 Mev.[3]

2. COMPARISON OF METHODS

The underlying physical models constitute the essential difference between the methods: in the optical case the entire incident energy is focused in a single nucleon, and one computes its elastic or inelastic scattering (absorption) in passing through the nucleus. On the other hand, the resonances always implied if not resolved in the compound model involve the sharing and exchange of the incident energy among many nucleons; elastic scattering is achieved only if the energy is relocalized in a single nucleon before being degraded. The models are generically related, since absorption of a nucleon in the optical model is a necessary first step in the establishment of an excited compound state. It is not a sufficient step, however, for the nucleus may lose energy by inelastic emission in an early stage of the sharing and exchange process. Thus if a large number of such systems are being formed by bombardment at a constant rate, the relative numbers in the optical (1) and compound (2) states are given by the formula familiar from a simple radioactive decay chain:

$$N_2/N_1=(\tau_2/\tau_1)f \tag{2}$$

where τ_1, τ_2 are the respective mean lives and f is the fraction of state 1 that upon decay ultimately leads to state 2.

The fraction f is roughly the probability that the incident energy will become uniformly distributed over the nucleus before any of it escapes by nucleon emission (γ- and α-emission are negligible in comparison). The ultimate simplification is one in which all collisions in the nucleus are averaged to produce at each encounter two nucleons of half the original energy. Then the numbers of participating nucleons at any time is $n(t)=e^{0.7t/\tau}$, where $\tau=\lambda/v$ is the mean interval between collisions. The nucleons that escape between successive collisions lie in a surface layer of depth λ, and the fraction of these with the proper direction of motion to escape is about $\frac{1}{2}\int_0^1(1-\mu)d\mu=\frac{1}{4}$. If $P(t)$ is the probability that no nucleons have escaped by time t, and $n(t)$ is assumed uniformly distributed over the volume of the nucleus,

$$dP=-\tfrac{1}{4}\left\{\frac{4\pi R^2\lambda}{(4/3)\pi R^3}\right\}n(t)\left[\frac{vdt}{\lambda}\right]P$$

$$P(t)/P(0)=P(t)=\exp\left\{-(3/4)v/R\int_0^t n(t)dt\right\}$$

$$\approx\exp\{-(\lambda/R)[n(t)-1]\}. \tag{3}$$

Then $f=P(t_0)$, where t_0 is the earliest time at which the excited nucleons cannot escape. Assuming the average binding of a nucleon in the Fermi well to be about 15 Mev, and including the incident nucleon, one has $n(t_0)\approx E_0/15+1$ where E_0 is the incident kinetic energy, and

$$f\approx\exp\{-\bar{\lambda}E_0/15R\}. \tag{4}$$

The mean free path $\bar{\lambda}$ in (4) is an average over the slowing-down process, while $\tau_1=\lambda/v$ with $\lambda>\bar{\lambda}$ the mean free path of the incident nucleon and v its velocity inside the nucleus. The mean life $\tau_2=\hbar/\Gamma$, where for high excitation energies E_0 the compound model[5] gives the order of magnitude $\Gamma\approx\frac{2}{3}E_0A^{\frac{1}{3}}$. In computing "representative" values of N_2/N_1, an average was taken between the values of Γ and of f for $A^{\frac{1}{3}}=3$ and $A^{\frac{1}{3}}=6$. The indicated assumptions of λ, $\bar{\lambda}$ lead to the estimates given in Table I. The values of N_2/N_1 cannot be taken too literally but suggest that in the region around 30–80 Mev neither model is adequate alone and a mixture must be used with both states at least 20 percent abundant. Measurements in this region would be especially complicated to analyze.

3. APPLICATIONS

An obvious corollary of the foregoing conclusion is that the evaporation model for nuclear reactions[6] cannot be relied upon for excitation energies much above 30 Mev for the individual nucleons. This feature is allowed for in describing the production of stars in nuclear emulsions and the diffusion of the nucleonic

[4] S. Pasternack and H. S. Snyder, Phys. Rev. **80**, 921 (1950).

[5] V. F. Weisskopf and D. H. Ewing, Phys. Rev. **57**, 472 (1940).

component in cosmic rays. As a first approximation the production of secondary nucleons in high energy nuclear events can be described entirely by methods appropriate to the optical model;[6] the statistical model can be applied as a correction to the nucleons remaining inside the nucleus with excitations of 30 Mev or less.

The present analysis is in harmony with the interpretation of the high energy tail in γ-n excitation curves[7] as largely due to a direct photoelectric effect, especially in light elements. It strongly suggests, however, that this interpretation is not to be applied to the large resonances found in the 17-Mev region among medium and heavy elements, as is already clear from the large peak cross sections.

In case the incident particle to be elastically scattered or absorbed is a π-meson, an important modification is made by the possibility of catastrophic absorption in which the incident particle is destroyed. If this occurs, the nucleus will be excited by more than 140 Mev, and the arguments above indicate that fast nucleon emission will preclude the formation of a compound state. On the other hand, if a compound state is to be formed with the meson as one particle, catastrophic absorption must be avoided for a relatively long time and is the dominant factor determining f. Thus,

$$N_2/N_1 \approx (\tau_2/\tau_1)\dot{p}^n \approx n\dot{p}^n, \tag{5}$$

where $n \approx \tau_2/\tau_1$ is the number of collisions made by the meson during the establishment of a compound state, and $\dot{p}$ is the average probability per collision of escaping catastrophic absorption. It appears,[8] at least at moderate energies, that $\dot{p} \ll 1$; then maximizing (5) shows that $(N_2/N_1)_{\max} \ll 1$, and that this maximum is achieved for $n \ll 2$, which is certainly too few collisions to establish a compound state. Thus one concludes that only the optical model is applicable to calculation of π-mesons on nuclei for all energies. The argument concerning sharp *vs* diffuse boundaries, however, still holds in favor of including nuclear boundary effects in meson calculations.

The author wishes to thank Professor R. Serber for stimulating comments, and Dr. J. M. Miller for an interesting discussion.

[6] M. L. Goldberger, Phys. Rev. **74**, 1269 (1948).
[7] R. Sagane, Phys. Rev. **84**, 587 (1951).
[8] Brueckner, Serber, and Watson, Phys. Rev. **84**, 258 (1951).

PHYSICAL REVIEW VOLUME 86, NUMBER 3 MAY 1, 1952

Extinction Effects in Neutron Transmission of Polycrystalline Media*

R. J. Weiss
Watertown Arsenal, Watertown, Massachusetts
(Received November 29, 1951)

The effects of primary and secondary extinction are considered for neutron transmission work in the energy region where diffraction is important. It is shown that in typical studies the grain size is the most important parameter affecting extinction, with the mosaic block size and the angular spread of the mosaic blocks of secondary importance. Experiments were performed to corroborate the theory, and criteria are set up to avoid extinction effects. It is shown how to determine the mosaic block size and the angular spread of the mosaic blocks in substances with large grain size by using fine resolution near the last crystalline cutoff, where the breadth of the Bragg peak becomes large compared to the angular misalignment of the mosaic blocks.

IT is convenient in neutron transmission studies of polycrystalline media to have the apparent cross section per nucleus of the sample, as given by the usual expression $\bar{\sigma} = (\ln I_0/I)/Nx$ (where N is the number of nuclei per cc and x is the thickness of the sample), proportional to the coherent cross section of the nuclei. Previous theoretical treatments[1,2] have assumed this to be the case under the experimental conditions that the microcrystals are randomly oriented and are small enough to give negligible primary extinction. Microcrystals are small coherent domains (commonly called mosaic blocks) and are usually misaligned over a range of several seconds in perfect crystals to several minutes in the macroscopic grains of imperfect crystals like metals. (In large single crystals the gross lineage may cause further misalignment to the extent of several degrees,[2] but we shall confine our attention here to small grains $<10^{-1}$ cm.) It is the purpose of this note to show that the conditions postulated in references 1 and 2 are not sufficient and to point out under what conditions the proportionality between the apparent and coherent nuclear cross sections are assured. We shall also show how it is possible to secure information about the mosaic block size even if primary extinction is negligible.

To begin, we consider the cross section for scattering into Bragg peaks of a perfect microcrystal small enough to make use of the Born approximation,

$$\sigma = \frac{\sigma_{\text{coh}}}{4\pi} \prod_{ijk} \frac{\sin^2(N_i s d\mathbf{q}\cdot\mathbf{i})}{\sin^2(s d\mathbf{q}\cdot\mathbf{i})}, \tag{1}$$

* Research carried out at Brookhaven National Laboratory under contract with AEC.
[1] Halpern, Hamermesh, and Johnson, Phys. Rev. **59**, 981 (1941).
[2] Fermi, Sturm, and Sachs, Phys. Rev. **71**, 589 (1947).
[3] Weiss, Hastings, and Corliss, Phys. Rev. **83**, 863 (1951).

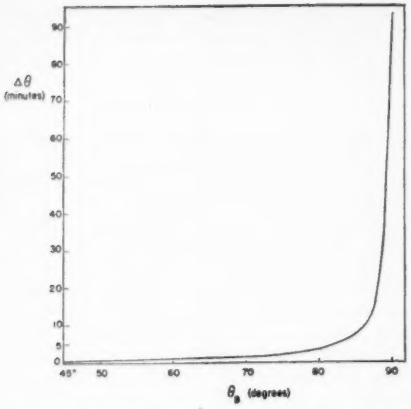

FIG. 1. Half-width in minutes of the 111 Bragg peak in aluminum as a function of Bragg angle for a microcrystal size $t_0=2\times10^{-4}$ cm.

where $\mathbf{q}$ is the unit scattering vector; $\mathbf{i}$, $\mathbf{j}$, $\mathbf{k}$, are unit vectors along the crystallographic axes, N_i is the number of nuclei in the microcrystal in the $\mathbf{i}$ direction, $s=4\pi\sin\theta_B/\lambda$, d=grating space of the diffracting plane, and θ_B is the Bragg angle. When the Bragg conditions are fulfilled, $\mathbf{q}\cdot\mathbf{j}=\mathbf{q}\cdot\mathbf{k}=0$, $\mathbf{q}\cdot\mathbf{i}=1$, $sd=2\pi$, and $\sigma=\sigma_{\rm coh}N_i^2N_j^2N_k^2=\sigma_{\rm coh}N^6$. The angle, θ, at which $\sigma=\frac{1}{2}\sigma_{\rm coh}N^6$ is given by

$$\sin\theta_B-\sin\theta\cong\lambda/2.6l_0, \tag{2}$$

where $l_0=Nd$=size of the microcrystal. When the Bragg angle is not too near the cut-off wavelength, i.e., $\lambda<2d$; $\theta_B<\pi/2$, then (2) becomes

$$\Delta\theta=0.8\lambda/l_0\cos\theta_B. \tag{3}$$

This is the full width at half-maximum of the diffraction peak. When $\theta_B\to\pi/2$

$$\Delta\theta\to(3\lambda/l_0)^{\frac{1}{2}}. \tag{4}$$

This is the full width of the diffraction peak at the cutoff.

For $l_0=2\times10^{-4}$ cm, $\lambda=1$A, and $\theta_B\ll\pi/2$, we find $\Delta\theta\cong15$ seconds, and the assumption in typical differential cross-section studies that microcrystals scatter independently for all but the most perfect crystals appears reasonable. However, for typical transmission studies when $\theta_B\to\pi/2$, and for $l_0=5\times10^{-5}$ cm and $\lambda=4$A, we find $\Delta\theta\cong1.5$ degrees. Since the angle between microcrystals is much less than this, it follows that microcrystals in a grain will either scatter coherently or at least will all satisfy the Bragg conditions simultaneously. Figure 1 is a plot of the half-width as a function of the Bragg angle for the (111) peak in aluminum for a microcrystal size $l_0=2\times10^{-4}$ cm, and it indicates the very rapid rise in half-width as $\theta_B\to\pi/2$. The sharpness of the cutoff, however, is negligibly affected by this large uncertainty in θ_B. To see this we differentiate the Bragg equation and obtain the resolution for the (111) cutoff in aluminum,

$$\frac{\Delta\lambda}{\lambda}=\frac{\Delta\theta}{\tan\theta_B}=\frac{(3\lambda/l_0)^{\frac{1}{2}}}{\tan(\frac{1}{2}\pi-\frac{1}{2}\Delta\theta)}\cong7.8\times10^{-4}, \tag{5}$$

which is much better than the resolution generally obtainable with present instruments.

The effect of this diffraction broadening will be to introduce primary extinction if the grains scatter coherently, or secondary extinction if they do not. When extinction is present, multiple scattering within the crystal redirects a portion of the scattered beam back into the main beam and the exponential decrease in intensity is not observed. It has been pointed out[4] that if the "mosaic block" picture is correct, primary extinction will not be present since the distorted regions between mosaic blocks introduce arbitrary phase differences which destroy the coherence between mosaic blocks. Secondary extinction does become important and, in fact, the experimental evidence below supports this. However, to prove this point a general treatment of both primary and secondary extinction applicable to neutron transmission studies follows. We first consider primary extinction.

PRIMARY EXTINCTION

The integrated reflecting power of a perfect crystal plate of thickness t, i.e., the reflecting power integrated over the angular range of reflections of the crystal is, neglecting temperature effects,[5,6]

$$R^p=\frac{\lambda^3NF[|\gamma_H|/|\gamma_0|]^{\frac{1}{2}}}{g\sin2\theta_B}\tanh A, \tag{6}$$

where

$$F=(\sigma_{\rm coh}/4\pi)^{\frac{1}{2}}\sum_{hkl}\exp[2\pi i(hx/a+ky/b+lz/c)],$$

γ_H and γ_0 are the direction cosines of the diffracted and incident beams with the normal to the surface of the crystal, g is the number of atoms per unit cell, and A, the extinction factor, is given by

$$A=N\lambda Ft/g[|\gamma_H|/|\gamma_0|]^{\frac{1}{2}}. \tag{7}$$

If we introduce the solid angle factor, $(\cos\theta_B)/2$, for randomly oriented crystals in a powder sample and substitute $\sin\theta_B=\lambda/2d$, we have

$$R^p=(d\lambda F/2g)[|\gamma_H|/|\gamma_0|]^{\frac{1}{2}}\tanh A=N\bar{\sigma}t/\gamma_0\ll1, \tag{8}$$

$$\bar{\sigma}=(d\lambda F/2gt)[|\gamma_H|/|\gamma_0|]^{\frac{1}{2}}\tanh A. \tag{9}$$

We now distinguish two cases:

Case 1: $A<0.24$, $\tanh A\approx A$, and $\bar{\sigma}$, the apparent cross section per nucleus is given by

$$\bar{\sigma}=\lambda^2NF^2d/2g^2. \tag{10}$$

[4] S. Pasternack, private communication.
[5] W. H. Zachariasen, *Theory of X-Ray Diffraction in Crystals* (John Wiley & Sons, Inc., New York, 1945).
[6] G. E. Bacon and R. D. Lowde, Acta Cryst. **1**, 303 (1948).

If we introduce the Debye-Waller factor, e^{-2W}, the multiplicity, j, and sum over all planes $\lambda \leq 2d$, we have for typical transmission work

$$\bar{\sigma} = \sum_{\lambda \leq 2d} \frac{\lambda^2 N F^2 j d}{2g^2} e^{-2W} \tag{11}$$

in agreement with former authors.[1,2] The condition, then, to insure negligible primary extinction is,

$$t < 0.24 g \langle [\,|\gamma_0 \gamma_H|\,]^{\frac{1}{2}} \rangle_{Av} / N\lambda F \approx 0.16 g / N\lambda F. \tag{12}$$

Case 2: $10^3 > A > 2$, $\tanh A \to 1$, and

$$\bar{\sigma} = (\lambda d F / \pi g l). \tag{13}$$

$\bar{\sigma}$ is now proportional to $(\sigma_{coh})^{\frac{1}{2}}$ and inversely proportional to l, making this an inconvenient condition.

In actual grains, if the microcrystals scatter coherently as $\theta_B \to \pi/2$, t becomes an effective thickness (called t^{eff}), which may be large compared to the microcrystal size and less than or equal to the grain size. We shall assume that the microcrystals follow a Gaussian distribution given by

$$W(\epsilon) = \frac{1}{\eta(2\pi)^{\frac{1}{2}}} \exp(-\epsilon^2/2\eta^2), \tag{14}$$

where ϵ is the angle the neutron makes with the mean angle of the blocks and $2(2 \ln 2)^{\frac{1}{2}}$ is the half-width. If t^{eff} is proportional to the number of microcrystals in the range $\Delta\epsilon$, then for $\Delta\epsilon \ll \eta$,

$$t^{eff} \cong T\Delta\epsilon / 2\eta = T\lambda / (2\eta l_0 \cos\theta_B), \tag{15}$$

where T = grain size. Introducing the solid angle factor into (15) and substituting this into (13), we have

$$\bar{\sigma} = (4\eta l_0 d F / \pi g T). \tag{16}$$

$\bar{\sigma}$ is then independent of λ.

If $\Delta\epsilon > \eta$ the entire grain scatters coherently and

$$\bar{\sigma} = (d\lambda F / \pi g \bar{T}), \tag{17}$$

where $\bar{T}$ is an average grain size. Even though the extinction in the grains is complete under these conditions, the angular range over which they reflect is still proportional to λ.

While the sharpness of the cutoff is theoretically limited by (5), it may in practice be limited by the geometry of the detector and sample. The reason for this is that at the cut-off wavelength, the multiply scattered beams are spread out over a small angular range in the forward and backward direction (each scattering deviates the neutron by 180°). The second scattering, even though not in the same grain, may cause the neutron to enter the detector. The use of the exponential law assumes that all scattered neutrons are lost. This effect can be minimized by making the geometry from scatterer to detector less than $(3\lambda/l_0)^{\frac{1}{2}}$ near the cutoff.

It should be noted that Eq. (11) assumes completely random orientation of grains. Preferred orientation is generally present in cold-worked metals and may even be present in annealed metals and compressed powders. To insure the validity of (11) it is suggested that loosely packed powders be used.

SECONDARY EXTINCTION

The integrated reflecting power of a layer of mosaic blocks is given by Zachariasen,[4] Eq. (4.18). We have used Eq. (3.158) for the reflecting power, P_H/P_0, of each mosaic block. This gives for the reflectivity per unit thickness of imperfect crystal

$$\sigma = \frac{A^2}{t_0 \eta \sqrt{2}[1/2\eta^2 + A^2 q^2/\pi]^{\frac{1}{2}}} \times \exp\left(-\left\{\frac{Aq}{(\pi)^{\frac{1}{2}}}\left[1 - \frac{A^2 Z}{\pi}\right]^{\frac{1}{2}}(\theta - \theta_B) + \frac{Ah}{\pi}\left[1 - \frac{A^2 Z}{\pi}\right]^{\frac{1}{2}}\right\}^2\right), \tag{18}$$

where

$$q = \pi\, l_0\, \gamma_0 \sin 2\theta_B / A\lambda, \quad Z = q^2 \Big/ \left(\frac{1}{2\eta^2} + \frac{q^2 A^2}{\pi}\right),$$

$$h = (1 - \gamma_0/\gamma_H)/2F[\gamma_0/\gamma_H]^{\frac{1}{2}},$$

and where the half-width of the diffracted beam from a mosaic block is $(\pi \ln 2)^{\frac{1}{2}}/qA$. The integrated reflecting power for nonabsorbing crystals (i.e., $\sigma \gg \mu$, where μ = absorption per unit thickness) is

$$\mathcal{R}_\theta = \int_{-\infty}^{+\infty} \frac{\sigma T}{1 + \sigma T} d\theta. \tag{19}$$

This integral has been evaluated numerically and yields

$$\mathcal{R}_\theta = \frac{\pi^{\frac{1}{2}} f(s)}{Aq[1 - \pi^{-1} A^2 Z]^{\frac{1}{2}}} = \frac{N\bar{\sigma}T}{\gamma_0} \ll 1, \tag{20}$$

where $f(s)$ is plotted in Fig. 2 and where $s = (\sigma T)_{\theta = \theta_B}$.

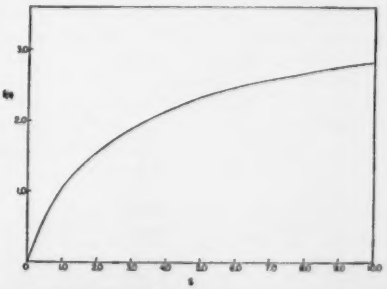

FIG. 2. Extinction factor $f(s)$ for the integrated reflecting power of an imperfect crystal as a function of s, $[s = (\sigma T)_{\theta = \theta_B}]$.

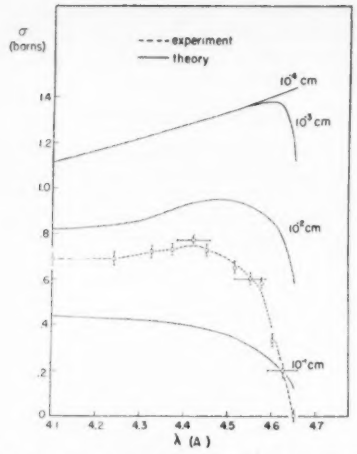

FIG. 3. Total cross section in barns of 111 peak in $\sim 2\times 10^{-2}$ cm polycrystalline aluminum as a function of neutron wavelength, with capture and inelastic scattering subtracted. Included are theoretical curves for varying gram sizes using 1.5 barn for σ_{COH}.

The general expression for the cross section is, including all factors,

$$\bar{\sigma} = \sum_{\lambda \leq 2d} \frac{\gamma_0 \pi^{\frac{1}{2}} f(s) j e^{-2w} \cos\theta_B}{2NAqT[1-\pi^{-1}A^2Z]^{\frac{1}{2}}}. \tag{21}$$

For $\sigma T \ll 1$, $f(s) = \pi^{\frac{1}{2}}(\sigma T)_{\theta=\theta_B}$ and the cross section reduces to (11). The condition for negligible secondary extinction (less than 5 percent) is $T \leq 0.05/\sigma_{\theta=\theta_B}$, where σ is given by (18).

When $\theta_B \to \pi/2$ for the last peak and for large σT, $f(s) \to \sim 3$ and $A^2q^2/\pi \ll 1/2\eta^2$. We then have

$$\bar{\sigma} \cong \frac{3dje^{-2w}}{2\pi^{\frac{1}{2}} t_0 NT}. \tag{22}$$

In this case $\bar{\sigma}$ is independent of λ. Likewise, for σT large but $\theta_B < \pi/2$, $A^2q^2/\pi \gg 1/2\eta^2$ and

$$\bar{\sigma} \cong \frac{3\sqrt{2}\eta \cos\theta_B j e^{-2w}}{\pi NT}. \tag{23}$$

In this case $\bar{\sigma}$ decreases with λ.

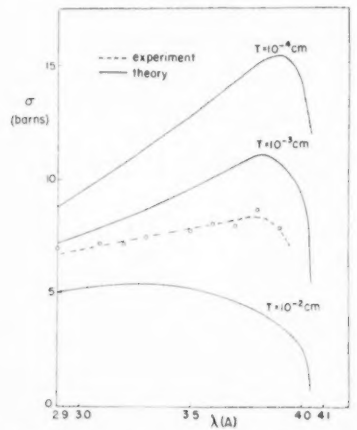

FIG. 4. Total cross section of 110 peak in Armco iron of grain size $\sim 7\times 10^{-3}$ cm as a function of neutron wavelength, with capture, incoherent, and inelastic scattering subtracted. Included are theoretical curves for varying grain sizes using 11.4 barn for σ_{COH}.

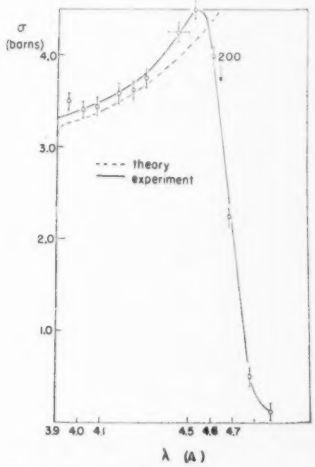

FIG. 5. Total cross section of 200 peak in very finely powdered NaF with capture, incoherent, inelastic and a small 111 scattering contribution subtracted. Included is a theoretical curve assuming no extinction, and using 1.5 barn for σ_{COH} of Na and 3.8 barn for σ_{COH} of F.

By observing the cross section for large σT far (23) and very close (22) to the cutoff we can experimentally determine η and t_0. The comments of the last two paragraphs under Primary Extinction are also applicable in the case of secondary extinction.

COMPARISON WITH EXPERIMENT

Figure 3 is a curve for polycrystalline 2S aluminum taken with a spectrometer at Brookhaven consisting of a lead crystal for selecting monochromatic neutrons, plus a beryllium filter to eliminate higher orders. This method gives good resolution and high intensity from 3.6A to 5.7A. Included in Fig. 3 are the theoretical curves for varying grain sizes (assuming $\eta = 10^{-3}$), and they indicate the approach to extinction. It is quite

evident that primary extinction is not taking place, since application of Eq. (17) in the range 4.3 to 4.65A, where $\Delta\epsilon > \eta$, yields a cross section $\bar{\sigma} = 0.06$ barn. The grain size of the aluminum is $\sim 2\times10^{-2}$ cm. By increasing η to 2×10^{-3} cm better agreement is obtained.

Figure 4 is a similar curve for Armco iron of $\sim 7\times10^{-2}$ cm grain size, taken by Hughes *et al.* at the Argonne National Laboratory.[7] The presence of extinction is quite apparent. Figure 5 is a curve (taken with the lead crystal) of very finely powdered NaF, together with a theoretical curve calculated from (11). We find good agreement with the theory for negligible extinction.

The determination of the mosaic block size from Eq. (22) requires better resolution than was obtained by the spectrometer used above. A resolution, $\Delta\lambda/\lambda$, of approximately 0.005 is required, whereas we have a resolution of 0.02. Such resolution is feasible and is planned for a future project.

We wish to express our thanks to D. J. Hughes, S. Pasternack, A. W. McReynolds, L. D. Jaffé, J. C. Slater, D. Kleinman, L. Corliss, and J. Hastings for many interesting discussions and suggestions.

[7] Hughes, Wallace, and Holtzman, Phys. Rev. **73**, 1277 (1948).

PHYSICAL REVIEW VOLUME 86, NUMBER 3 MAY 1, 1952

Evidence for *K*-Shell Ionization Accompanying the Alpha-Decay of Po^{210}

W. C. BARBER* AND R. H. HELM
Department of Physics, Stanford University, Stanford, California
(Received October 8, 1951)

The radiations of Po^{210} have been studied using NaI scintillation counters. In agreement with Grace, Allen, West, and Halban, it is concluded that the soft electromagnetic component probably entirely consists of x-rays of lead. The region from 25 kev to 2.5 Mev has been examined and, with the exception of the known γ-ray of 800 kev, no nuclear γ-rays were observed. The ratio of the number of K x-rays to the number of 800-kev γ-rays was measured as 0.134 ± 0.025 to 1. The K shell internal conversion coefficient of the 800-kev transition has been reported as about 0.05, and hence the K x-ray intensity is too great to be explained by internal conversion alone. The residual x-rays are attributed to the process whereby the emission of the alpha-particle causes ionization of the atom. Comparison of the relative intensity of K x-rays and alpha-particles shows qualitative agreement with the probability of this ionization process as calculated by Migdal.

I. INTRODUCTION

ZAJAC, Broda, and Feather[1] have reported γ-rays of energy 84 ± 4 kev in the decay of 138-day Po^{210}. In investigating Po^{210} radiations with NaI scintillation counters we have observed radiation in this energy region, but our measurements yield a mean energy of 76 kev. In attempting to understand the origin of this radiation we have measured its intensity relative to the intensity of the 800-kev γ-ray, and we have looked for coincidences between the 800- and the 76-kev radiations. The results of our investigations are consistent with the interpretation of the softer radiation as x-rays of lead, whereas its interpretation as a nuclear γ-ray would lead to an unlikely decay scheme. The energy resolution of our counters is not sufficient to resolve the K_α and K_β x-rays of lead, and hence we would not be able to distinguish a 76-kev nuclear γ-ray from the lead K x-ray spectrum. However, during the time our measurements were being made, Grace, Allen, West, and Halban[2] reported the result of an investigation of the Po^{210} spectrum where the soft radiations were detected in proportional counters. In their work lines interpretable as the K_α and K_β were observed, and with the help of critical absorption measurements they were determined to be x-rays of lead. Grace *et al.*[2] measured the number of K x-rays relative to alpha-particles and also the number of conversion electrons relative to alpha-particles. Noting that these were experimentally equal they explained the x-rays as the result of the internal conversion of the 800-kev γ-ray.

Our results for the most part are in agreement with the work of Grace *et al.*,[2] but on the question of the relative intensity of K x-rays and conversion electrons we find evidence for more quanta than can be accounted for by internal conversion alone. Since this is the most important contribution of the present paper, we should like to note, as will be shown in the concluding section, that when the data of Grace *et al.*[2] are corrected for the Auger effect and the K/L internal conversion ratio they are not in disagreement with our conclusion.

II. EXPERIMENTAL METHODS

The polonium was supplied by the Eldorado Mining and Refining Company, who report radioactive impurities (of unspecified form) of about 6×10^{-6} mg of Ra-equivalent per millicurie of Po. The sources were prepared for use and further purified by precipitation

* Now at Microwave Laboratory, Stanford University, Stanford, California.
[1] Zajac, Broda, and Feather, Proc. Phys. Soc. (London) **60**, 501 (1948).
[2] Grace, Allen, West, and Halban, Proc. Phys. Soc. (London) **64**, 493 (1951).

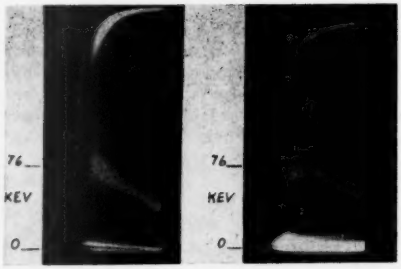

FIG. 1. Photographs of the pulse distributions produced in the same scintillation counter by lead x-rays (left) and Po^{210} (right). Each photograph shows large pulses which overload the amplifier, a band of pulses about 4/10 of full height which are the result of the K x-rays, and small pulses caused by noise and L x-rays.

on nickel foils in 0.1N HCl. Later, some of the polonium was purified a second time in the manner described by Lee and Libby.[3] No spurious lines were observed in the spectra of the sources either before or after purification.

The sources used for alpha-counting were prepared on 0.005-inch foils, thick enough to stop alphas completely, so that only one side was effective for alpha-counting. The activity was found to be somewhat concentrated on the edges of the foil so the edges were trimmed away, leaving a nearly uniform source.

Various sources were used, each with a strength of about one millicurie. The sources were studied using scintillation counters consisting of NaI (Tl) crystals mounted on RCA 5819 photomultiplier tubes. The output of the phototubes was amplified by Model 501 pulse amplifiers and then fed to a differential discriminator, a synchroscope, or in some cases, a coincidence circuit. The power supplies for the electronic equipment were all electronically regulated. Constant voltage transformers were used to stabilize the system against line voltage fluctuations. The final stability was sufficiently good that differential discriminator measurements could be made over periods of one week or more without any significant errors due to instability. The NaI crystals (obtained from the Harshaw Chemical Company) were clear single crystals of about one square cm area and of thicknesses which varied from about 0.2 to 1 cm. The sources were always mounted within one cm of the crystals and no collimation was used.

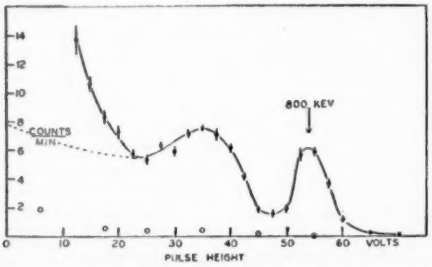

FIG. 2. Differential discriminator curve showing the distribution of pulses resulting from the 800-kev Po γ-ray. The solid curve gives the distribution of pulses due to the source after the background (shown as circles) has been subtracted. Not all of the small pulses are due to the direct effect of the 800-kev γ-ray. The calculated distribution due to this γ-ray only is shown as a dashed curve. The curve was taken with an amplifier gain of 1250 and a 1.5 volt differential discriminator channel width.

When alpha-particles were to be detected, the crystals were cleaved in a dry-box and mounted on a multiplier tube in a box containing silica gel as drying agent. So treated, the crystals could be used for several weeks without appreciable deterioration. When only γ-rays were to be detected, the crystals were further protected by a thin film of mineral oil. Conversion electrons were screened from the crystal by layers of Cellophane or mica. In all cases a film of oil was used to provide good optical contact between the multiplier face and the bottom of the crystal.

Gamma-ray energies were measured by studying the pulse-height distributions either by means of a differential discriminator or by photographing synchroscope presentations of the pulse heights. The details of these measurements followed closely the methods described by Hofstadter and McIntyre.[4]

The relative intensities of the various radiations were determined by measuring the areas under the differential discriminator curves and using calculated values for the efficiency of the NaI crystals for the radiations in question.

III. ENERGY MEASUREMENTS

The pulse distribution produced by the γ-rays of Po^{210} showed clearly the presence of the 800-kev component as well as a component in the energy range reported by Zajac *et al.*[1] No other lines of comparable intensity could be detected in the spectrum which was examined in the range from 25 kev to 2.5 Mev. By comparison with the pulse-height distribution produced in the crystal by incidence of monochromatic x-rays from a calibrated Bragg spectrometer, the mean energy of the softer component was determined as 76±4 kev.

Because 76 kev is approximately the mean energy of the K x-radiation of lead, the daughter element of the polonium decay, we made a direct comparison with the fluorescent x-radiation of lead. Figure 1 shows on the right a photograph of the low energy part of the Po^{210} pulse distribution (exposure time 45 minutes). For comparison Fig. 1 (left) shows a photograph of the pulse distribution of fluorescent lead x-rays, detected in the same crystal under the same conditions. The lead x-rays were produced by exposing a slab of lead placed over the crystals to a strong γ-ray source. The crystal was shielded from the direct γ-rays by several inches of lead. The exposure time was 5 minutes.

The broad line near the center of the polonium

[3] D. D. Lee and W. F. Libby, Phys. Rev. **55**, 252 (1939).

[4] R. Hofstadter and J. A. McIntyre, Phys. Rev. **80**, 631 (1950).

picture is the same height as the K-line in the lead x-ray picture. The band of pulses near the base line of the polonium picture is attributed to L and M x-rays of lead, x-rays of Ni produced by alpha-bombardment of the source backing, and photomultiplier tube noise.

The similarity of the Po radiation and the lead K x-rays has also been checked by taking differential discriminator curves of the two pulse distributions shown in Fig. 1. The resulting curves are similar to Fig. 3. When the two curves are normalized to the same area, subtraction of one from the other yields a curve which is everywhere zero within statistical error.

These experiments do not prove that the soft Po radiations are lead x-rays. However, the results are in agreement with the recent work of Grace *et al.*[2] in which the K_α and K_β lines were resolved by using proportional counters, and were shown by critical absorption measurements to correspond with the x-rays of lead and not of neighboring elements. Neither our experiments nor those of Grace *et al.*[2] rule out the possible

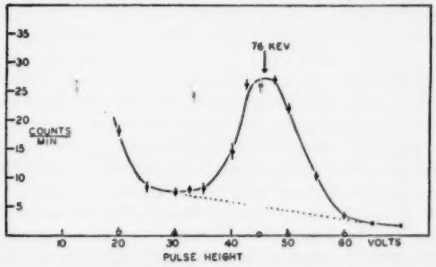

FIG. 3. Differential discriminator curve showing the distribution of pulses resulting from lead x-rays from the Po^{210} source. The curve was taken with an amplifier gain of 10,000 and a 1.5-volt discriminator channel width. The background (shown as circles near the baseline) has been subtracted.

existence of a weak nuclear γ-ray in addition to the lead x-rays. However, the combined experimental results would limit the intensity of a nuclear γ-ray in the 80–90 kev region to less than 10 percent of the K x-ray intensity.

IV. COINCIDENCE EXPERIMENTS

An attempt was made to observe coincidences between the 800-kev and 76-kev radiations by triggering the synchroscope on coincidences between pulses in two crystals, and photographing the pulse-height distributions from either crystal in the usual way. The proper operation of this system and the resolving time of the coincidence circuit (12 μsec) were checked by measuring γ–γ coincidences from a Co^{60} source.

The 76-kev line was observed to be in coincidence with softer radiation, presumably L x-rays, which were also observed in the pulse-height photographs, but was not in immediate coincidence with the 800-kev γ-ray. Because of the low counting rate the presumed K–L coincidences were not measured quantitatively. In the case of the 76- and 800-kev quanta the estimated upper limit for the number of coincidences is fewer than 0.05 of the number to be expected if each 76-kev quantum were accompanied by an 800-kev quantum. Thus these radiations could be in cascade only if the lifetime of the intermediate state is considerably greater than the 12×10^{-6} sec resolving time of the coincidence circuit.

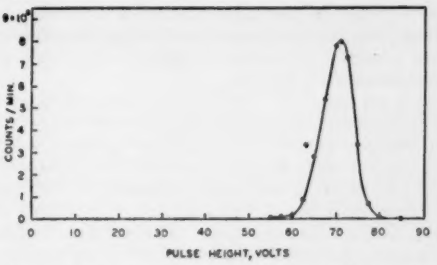

FIG. 4. Differential discriminator curve resulting from Po^{210} α-particles. The discriminator channel width was 1.5 volts and the amplifier gain was about 350.

V. INTENSITY RATIOS

Figures 2, 3, and 4 show differential discriminator curves which were used in determining intensities of the radiations. A thick crystal was used to determine the relative intensity of the 76- and 800-kev radiations. Figure 2, taken with an amplifier gain of 1250, shows the curve for the 800-kev radiation. Figure 3 was taken with all conditions the same except that the amplifier gain was increased to 10,000 to show the effect of the

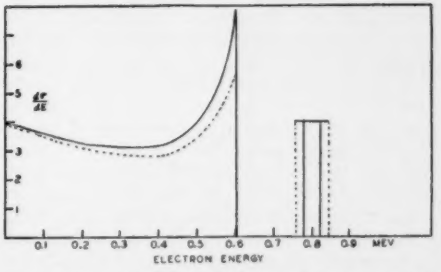

FIG. 5. Energy distribution of electrons produced by an 800-kev γ-ray in a NaI crystal. The solid curve below 0.6 Mev shows the distribution of Compton electrons resulting from the primary interaction only (ordinate scale in arbitrary units). The photoelectric effect gives monoenergetic electrons and is important only for the K-electrons of iodine. The relative number of photoelectrons is given by the area of the solid rectangle at 0.8 Mev. Secondary processes produce electrons which also lose energy in the crystal. The most important secondary process is the capture of Compton scattered photons with the result that the full energy of the γ-ray is spent in ionization of the crystal. The dashed curve shows how this secondary process increases the number of events where the full energy of the γ-ray is expended in ionization at the expense of a loss in number of events where only part of the γ-ray energy is involved.

76-kev radiation. The background when no source was present has been subtracted from both of these curves (the amount of background is shown by the circles at the bottom of the figures).

The low energy part of the 800-kev distribution curve is partly due to the 76-kev line and partly the result of radiation scattered from the brass container which encloses the multiplier and crystal. In order to estimate the part due to the direct effect of the 800-kev radiation, we have made use of the theoretical curves shown in Fig. 5. The solid curve below 600 kev shows the distribution of Compton electrons due to the primary interaction only. The ordinate gives the number of electrons per unit energy interval (arbitrary units) as calculated from the Klein-Nishina formula. In order to show the importance of the photoelectric effect the cross section for the photoelectric absorption in NaI of an 800-kev photon was calculated from the data given by Heitler.[5] In Fig. 5 the relative importance of the photoelectric cross section is indicated by the area of the solid rectangle (should be a delta-function) which is centered at 800 kev.

When γ-rays interact with a NaI crystal multiple processes occur. The most important multiple process is the capture of the scattered photons which result from a primary Compton effect. The result of this process is that pulses corresponding with the full energy of the γ-ray are observed instead of pulses corresponding with the energy of a Compton electron. The magnitude of this effect can be estimated by calculating the expected absorption of Compton scattered photons in the crystal. An experimental check on this calculation is provided by comparison of the number of the observed full energy pulses with the number to be expected due to direct photoelectric absorption. For the crystal used in obtaining the data of Fig. 2, the calculations indicate that the total number of full energy pulses is somewhat more than twice the number due to direct photoelectric absorption. The dotted lines in Fig. 5 show the calculated effect of this multiple process. The area subtracted from the Compton distribution has been added to the rectangle at the full energy. An ideal scintillation counter should reproduce the energy loss curve of Fig. 5. Inhomogeneities in the crystal and the photo surface, together with statistical fluctuations in the counting process, give a spread to the pulses resulting in a distribution like the experimental curve, Fig. 2. We have used the theoretical curve, Fig. 5, to estimate what fraction of the small pulses in Fig. 2 are due to the direct effect of the 800-kev γ-ray. The dotted line in Fig. 2 shows the result.

TABLE I. Intensity ratios of the 76- and 800-kev radiations and the alpha-particles.

	N_{76}/N_{800}	N_{76}/N_{α}	N_{800}/N_{α}
Present expts.	0.134 ± 0.025	$2.00\pm0.38\times10^{-6}$	$1.5\pm0.4\times10^{-5}$
Grace *et al.*	0.083 ± 0.03	$1.5\pm0.5\times10^{-6}$	$1.8\pm0.14\times10^{-5}$

Since the 76-kev quantum always interacts near the surface of the crystal, whereas the 800-kev penetrates throughout the volume and is only partly absorbed, the counting efficiencies for the two radiations are not the same. The calculation of the efficiencies involves an integration over the volume of the crystal and the area of the source. These calculations have been carried out by numerical integrations which should give an accuracy of better than ten percent for the ratio of the two efficiencies. The absorption coefficient in NaI was taken from x-ray tables as 12.6 cm^{-1} for the 76-kev quanta and 0.244 cm^{-1} (computed from the sum of the theoretical Compton and photoelectric effects) for 800 kev.

In the experiment corresponding to Figs. 2 and 3, the crystal was 1.19 cm by 1.17 cm on the top face and 0.953 cm thick; the source was approximately 0.5 cm square and was centered 0.10 cm above the top face of the crystal. The calculated efficiencies in this case were $\epsilon_{76}=0.41$, and $\epsilon_{800}=0.060$.

Two slight additional corrections must be made to the above calculations: (1) In the 800-kev case the escape from surface layers of the crystal of photoelectrons or energetic Compton electrons has the effect of distorting the electron distribution in Fig. 5 by increasing the relative number of low energy electrons. The importance of this effect was estimated from the average range of the electrons to be about 5 percent. (2) K x-rays of iodine escape from the crystal because the 76-kev quantum is absorbed predominantly by photoelectric effect in the surface layers of the crystal. The escape line was observed in photographs but not measured quantitatively in the present experiments. The process has been studied quantitatively by West, Meyerhof, and Hofstadter,[6] and their unpublished data show that the escape peak is 7 percent of the main peak when 76-kev x-rays are incident. Since our integration of the 76-kev differential discriminator curve did not include the region of the escape peak, we should add 7 percent to the measured area.

Two independent determinations were made of the ratio of the intensities of the 76- and 800-kev radiations. Different sources and crystals were used each time. The experiment corresponding to Figs. 2 and 3 is believed to be the more reliable because the source was repurified one extra time, the geometry was measured more carefully, and greater effort was expended in calculating the efficiency factors. Combining the efficiency factors with the ratio of areas (area 76 kev/area 800-kev = 0.90) obtained from Figs. 2 and 3 and making the corrections discussed above we get $N_{76}/N_{800}=0.134$ for the relative rate of emission of the 76- and 800-kev quanta.

An early experiment using a different source and slightly different geometry gave $N_{76}/N_{800}=0.14$. This agrees with the later result within the experimental

[5] W. Heitler, *Quantum Theory of Radiation* (Oxford University Press, London, 1944), Chapter III.

[6] West, Meyerhof, and Hofstadter, Phys. Rev. **81**, 141 (1951).

error, but because of the presumed greater reliability of the later experiment we use it as a final result.

The chief sources of error in the determination of this ratio are: (1) uncertainties in the measurement of the crystal and its position relative to the source, (2) approximations in the numerical integration used to calculate counting efficiency, (3) statistical errors in the determination of the differential discriminator curves, and (4) uncertainties in the corrections made necessary by the multiple processes which have been discussed. We estimate that the error could be as high as 10 percent for each of the last three effects and 5 percent for the first; while these are not all random-type errors, we simply have combined them statistically to give the approximate probable error as 18 percent. The final result is then $N_{76}/N_{800}=0.134\pm0.025$.

The number of 76-kev quanta relative to alpha-particles was measured in a similar manner. The source was plated on both sides of a 0.005-inch nickel foil, so that the alpha-particles were only detected from one side while the x-rays were detected from both sides (except for a 6 percent correction for absorption). In order to reduce the alpha-counting rate to a suitable level, a steel shutter 0.0025 cm thick containing a pinhole 0.033 cm in diameter was mounted between the source and crystal. The differential discriminator curve for the alpha-particles, taken with an amplifier gain of about 350, is shown in Fig. 4. (The width of this curve is partially due to straggling and partially due to the fact that the source has finite size and particles from different parts of the source traverse different air paths before striking the crystal.) With the steel shutters blocking the alphas (the absorption of 76-kev quanta in the shutter is negligible) a curve very similar to Fig. 3 was obtained for the 76-kev quanta.

The relative efficiencies of the detector for the alpha-particles and the 76-kev quanta were calculated by numerical integration. In the case of the 76 kev, the calculation is of the same type as described before. In the case of the alpha-particles it is only necessary to average the solid angle, defined by the pinhole, over the area of the source; the geometry was such that all particles passing through the pinhole struck the crystal and were assumed to be counted.

In sweeping the pinhole across the crystal the alpha-counting rate was found to fall off smoothly and symmetrically on either side of a broad central maximum, showing that the crystal could not have had any serious non-uniformities in its surface. The differential discriminator curve was taken at the position of the maximum, corresponding to the assumed condition that the pinhole was centered over the crystal. The source was also checked and found to have the same activity on each side. The calculated efficiency factors are $\epsilon_{76}=0.100$ and $\epsilon_\alpha=1.81\times10^{-4}$. The ratio of the areas under the differential discriminator curves was (area of 76 kev)/(area of α)$=1.93\times10^{-3}$. Making a 6-percent correction for absorption of the x-rays from the back side of the nickel foil, a 7-percent correction for escape of iodine K x-rays in counting 76-kev quanta, and allowing for the fact that only one side of the foil was effective for α-counting, we get

$$N_{76}/N_\alpha=(2.00\pm0.38)\times10^{-6}.$$

The error in this result was estimated on the basis of the same considerations as those described in the determination of N_{76}/N_{800}.

No direct comparison of the 800-kev γ-ray intensity relative to that of alpha-particles was made, but the combination of the last quoted result of the comparison of the 76- and 800-kev intensities gives

$$N_{800}/N_\alpha=(1.5\pm0.4)\times10^{-5}.$$

A comparison of these results with the results for the same ratios as measured by Grace *et al.*[2] is shown in Table I.

Assuming that the 76-kev line is entirely K x-radiation, a correction of 11 percent for the Auger effect as observed in heavy elements[7] gives the results shown in Table II.

VI. CONCLUSIONS

The only radiation in the Po^{210} spectrum which is definitely a nuclear γ-ray is the 800-kev line. If other nuclear γ-rays are present in the range from 25 kev to 2.5 Mev their intensity is less than ten percent of that of the 800 kev γ-ray.

TABLE II. Intensity ratios after correction for the Auger effect.

	N_K/N_{800}	N_K/N_α
Present expts.	0.15 ± 0.028	$2.2\pm0.42\times10^{-6}$
Grace *et al.*	0.093 ± 0.033	$1.7\pm0.56\times10^{-6}$

Our results combined with those of Grace *et al.*[2] indicate that the 76-kev radiation is at least 90 percent and probably entirely due to K-shell ionization, but the observed intensity is too great to be explained by internal conversion of the 800-kev transition, as is shown by the following argument.

The number of K-shell ionizations due to internal conversion divided by the number of γ-rays is equal to the internal conversion coefficient, α_K. The total conversion coefficient of the 800-kev γ-ray has been measured (by counting the number of electrons relative to γ-rays) as 0.067 ± 0.017 by Grace *et al.*[2] and as less than 0.05 by Alburger and Friedlander,[8] who also measured the K/L ratio as 3.7. The value of the K/L ratio is highly accurate, and therefore α_K is not over 3.7/4.7 times the total conversion coefficient. According to Grace *et al.*[2] α_K is then 0.053 ± 0.013 and less than 0.04 according to Alburger and Friedlander.[8] Both of these numbers are considerably less than our result, 0.15 ± 0.028 for the total number of K-shell ionizations relative to γ-rays, and are also probably less than the result, 0.093 ± 0.033, for the same quantity as determined from the measurements of Grace *et al.*[2]

[7] L. S. Germain, Phys. Rev. **80**, 937 (1950).
[8] D. E. Alburger and G. Friedlander, Phys. Rev. **81**, 141 (1951).

The above calculations indicate that only about one-third or one-half the K-shell ionization can be attributed to internal conversion. The remaining ionization is probably the direct result of the emission of the alpha-particle.

Assuming that the excess K-shell ionization is due to the direct action of the alpha-particle as it leaves the atom, the probability of this process is given by the quantity N_K/N_α multiplied by the fraction of K-shell ionizations not due to internal conversion. Using our values for N_K/N_{300} and N_K/N_α together with the value $\alpha_K=0.053\pm0.013$, we arrive at

$$(2.2\pm0.4)\{1-(0.053\pm0.013)/(0.15\pm0.028)\}\times10^{-6}$$
$$=(1.4\pm0.35)\times10^{-6}$$

for the probability of K-shell ionization by the alpha-particle.

Migdal[9] has made theoretical calculations of the probability of ionization of the daughter atom by a particle which leaves the nucleus. Migdal's theory predicts that the alpha-particle almost always ionizes the atom, but that the ionization probability of a given electron shell decreases rapidly as shells nearer and nearer the nucleus are considered.

The process of direct ionization by the alpha-particle has been suggested as the origin of the L x-rays which are observed in Po^{210} radiations.[10,11]

[9] A. Migdal, J. Phys. (U.S.S.R.) **4**, 449 (1941).
[10] I. Curie and F. Joliot, J. phys. et radium **2**, 20 (1931).
[11] W. Rubinson and W. Bernstein, Phys. Rev. **82**, 334 (1951).

The approximations made in Migdal's calculations include the use of perturbation theory to describe the effect of the alpha-particle, the assumption that the alpha-particle moves with uniform velocity as it leaves the nucleus, and the use of nonrelativistic hydrogen-like wave functions to describe the atom. These approximations are best in the case of K-shell ionization, but even here the error may be appreciable. Migdal's result for the probability of ionization of the K-shell is $2.2(137\ v_\alpha/Z^2c)^2$, where v_α is the velocity of the alpha-particle and Z is the atomic number of the daughter atom. Evaluation of this expression gives 2.6×10^{-6} in the case of Po^{210}.

Migdal's theory thus agrees in order of magnitude with the experimental results, $(1.4\pm0.35)\times10^{-6}$, but the predicted ionization probability is too high to be reconciled with either our results or those of Grace *et al.*[2] Since Migdal's theory neglects the effects of screening of the nucleus from the K electrons, one might argue that the Z in Migdal's theory should be replaced by a smaller "effective" Z. This change would make the predicted ionization probability even higher and thus would increase the discrepancy with experiment. The authors believe that approximations in Migdal's theory may result in an overestimate of the K-shell ionization process.

The authors would like to express their appreciation to Professors R. Hofstadter and W. E. Meyerhof for their valuable suggestions and criticisms concerning this work.

PHYSICAL REVIEW VOLUME 86, NUMBER 3 MAY 1, 1952

The Sign of the Quadrupole Interaction Energy in Diatomic Molecules*†

R. A. Logan, R. E. Coté, and P. Kusch
Columbia University, New York, New York

(Received January 9, 1952)

The molecular beam magnetic resonance method has been used to determine the sign (and the magnitude in those cases where it has not been previously measured) of the quadrupole interaction energy of the alkali nuclei in the homonuclear molecules, that of Na^{23} and Li^7 in the alkali halides, and that of Cl^{35} and Cl^{37} in KCl. An obstacle is inserted into the path of the beam so that its edge coincides with the position of the undeflected beam. Molecules of either positive or negative total magnetic moment are then removed from the beam which arrives at the detector. Certain maxima in the nuclear resonance spectrum at high magnetic fields ($eqQ\ll g_I\mu_0H$) arising from the transitions $\Delta m_I=\pm1$ are suppressed depending on the states removed by the obstacle. It is thus possible to identify the resonance maxima in terms of the transitions which produce them. From this evidence the sign of the quadrupole interaction energy can be deduced. The quadrupole interaction energy, eqQ, is positive for Li^7 and negative for Na^{23} in the homonuclear and the halide molecules. These results suggest that the sign of q at a given nucleus is the same in a rather considerable range of diatomic molecules. The interaction constant, eqQ, is positive for Cs^{133} in Cs_2, and negative for K^{39} in K_2, Rb^{85}, Rb^{87} in Rb_2, and Cl^{35}, Cl^{37} in KCl. The signs of the interaction for K^{39}, Rb^{85}, Rb^{87}, and Cs^{133} in the alkali fluorides, and for Cl^{35}, Cl^{37} in TlCl as determined by the molecular beam electrical resonance method are the same as those for the same nucleus in the molecules here considered.

INTRODUCTION

IT is the purpose of the present paper to discuss in detail a method which permits the determination of the sign of the quadrupole interaction energy in diatomic molecules and to present the results of new measurements on the sign and the magnitude of the quadrupole interaction energies of several nuclei in a considerable range of diatomic molecules. A preliminary description of the method has previously been given.[1]

Unfortunately it is not possible, in general, to deduce

* This research was supported in part by the ONR.
† Submitted by R. A. Logan in partial fulfillment of the requirements for the degree of Doctor of Philosophy, in the Faculty of Pure Science, Columbia University.

[1] P. Kusch, Phys. Rev. **76**, 138 (1949).

the sign and magnitude of the electric quadrupole moment of a nucleus from a knowledge of the quadrupole interaction energy of the nucleus in a particular molecule. The only completely unambiguous exception is in the determination of the quadrupole moment of the deuteron from the experimental value of the quadrupole interaction of the deuteron in HD and D_2. In this case the molecular wave functions are sufficiently well known to permit an exact calculation[2] of q.[3] In the case of the molecule Li_2, Foley[4] has made a calculation of q from the Bartlett-Furry wave functions. These wave functions[5] lead to a dissociation energy and an internuclear distance for Li_2 which agree with the experimentally observed quantities but the extent of their validity in the calculation of q is uncertain. In other cases where the quadrupole interaction has been measured, good wave functions are not available for the determination of q, but in some instances apparently satisfactory approximations have been devised.[6]

The present results themselves do not, therefore, permit a direct determination of either the sign or the magnitude of the nuclear quadrupole moment. They do, however, indicate certain systematic behavior of the quadrupole interaction energy and may thus aid in establishing the validity of the various models and approximations proposed for the determination of the nuclear electric quadrupole moment from observed interaction energies.

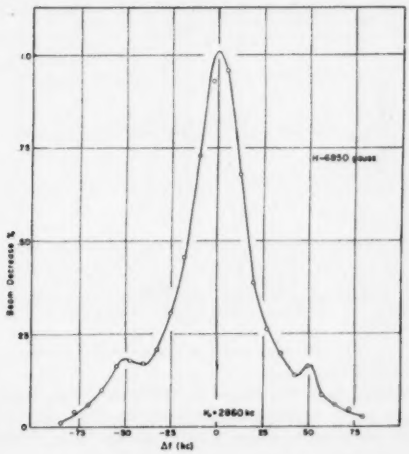

FIG. 1. Nuclear resonance spectrum of Cl^{35} in KCl.

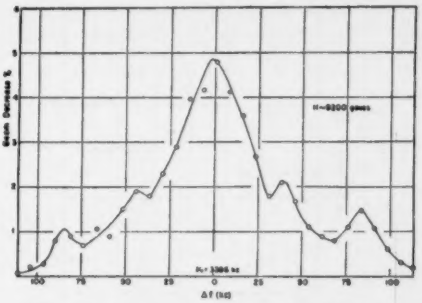

FIG. 2. Nuclear resonance spectrum of Rb^{85} in Rb_2.

THEORY

In the present experiments the high field spectrum arising from a nuclear reorientation in a diatomic molecule is observed. This spectrum has been discussed in detail by Feld and Lamb[7] and by Nierenberg and Ramsey[8] for a diatomic molecule which contains one nucleus possessing both a magnetic dipole moment and an electric quadrupole moment and another nucleus of spin zero. The conclusions are, however, valid for an arbitrary diatomic molecule including the homonuclear molecule[9] when J is large and when the electric quadrupole interaction is large compared to the magnetic interaction between nuclei and that between each nucleus and the field caused by the molecular rotation. All of these criteria are substantially satisfied by the molecules here considered.

The spectrum consists of a series of $2I$ maxima. When I is an odd half-integer, the central peak in the spectrum corresponds to the nuclear resonance frequency, $\nu_0=g_I\mu_0H/h$, and is not, at sufficiently high magnetic fields ($g_I\mu_0H\gg eqQ$), affected by the quadrupole interaction. The width and shape of the central maximum is determined by the interaction of the nuclear moment with the magnetic field due to the molecular rotation and by the resolution effects of the apparatus. The other maxima appear as satellites of the central peak and their position is determined by the magnitude of the quadrupole interaction as given by Feld and Lamb.

A typical high field resonance spectrum when $I=3/2$ is that of Cl^{35} in KCl, shown in Fig. 1. For the magnetic

[2] A. Nordsieck, Phys. Rev. **58**, 310 (1940).

[3] The q employed here was suggested by J. Bardeen and C. H. Townes, Phys. Rev. **73**, 97 (1948), and represents directly the gradient of the electric field at the nucleus in the inward direction along the internuclear axis. This definition of q ascribes a physical significance to the previously defined q' of A. Nordsieck, Phys. Rev. **58**, 310 (1940). The q used by B. T. Feld and W. E. Lamb, Jr., Phys. Rev. **67**, 15 (1945), is expressed in terms of coordinates relative to an axis fixed in space, whereas Nordsieck's q' is expressed relative to a coordinate system fixed in and moving with, the molecule. These definitions are related by

$$q_{\text{Bardeen-Townes}}=2eq'=-[(2J+3)/2J]2eq_{\text{Feld-Lamb}}$$

where e=proton charge, J=rotational quantum number.

[4] A calculation by H. M. Foley quoted in reference 1.

[5] J. H. Bartlett, Jr., and W. H. Furry, Phys. Rev. **38**, 1615 (1931).

[6] C. H. Townes and B. P. Dailey, J. Chem. Phys. **17**, 782 (1949).

[7] B. T. Feld and W. E. Lamb, Jr., Phys. Rev. **67**, 15 (1945).

[8] W. A. Nierenberg and N. F. Ramsey, Phys. Rev. **72**, 1075 (1947).

[9] H. M. Foley, Phys. Rev. **71**, 747 (1947).

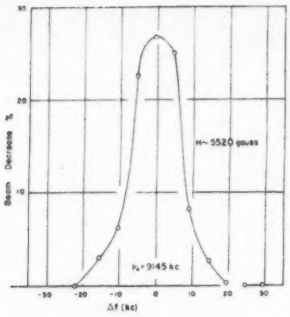

FIG. 3. Nuclear resonance spectrum of Li^7 in Li_2.

fields employed the interaction energy of the nuclear magnetic moment is large compared to the quadrupole interaction energy and genuinely high field conditions prevail. The frequency separation between the two maxima is $eqQ/4h$ and from Fig. 1 and other data it is found that $eqQ/h=0.420$ Mc. When $I=5/2$, as in the case of Rb^{85}, whose spectrum in Rb_2 is shown in Fig. 2, two auxiliary maxima appear on each side of the central maximum. In this case $eqQ/h=1.10$ Mc. In both cases the rapidly varying intensity of other components of the spectrum in the neighborhood of the satellite have the effect of shifting the maximum to the center so that the stated value of eqQ/h represents a lower limit of the quantity. This effect is especially pronounced in the case of Rb^{85} in Rb_2 where the low abundance (<0.5 percent) of molecules in a beam of rubidium evaporated from an oven makes necessary the use of low resolution (which arises due to a large amplitude of rf field) to obtain observable intensities in the spectral envelope. Typical spectra when $I=3/2$ are also shown in Figs. 7 and 8.

A case of special interest is the resonance of Li^7 in Li_2 shown in Fig. 3. In this case the quadrupole interaction is not sufficiently great to resolve the satellites from the central maximum in view of the limited resolving power of the apparatus (natural width of an isolated line in Li_2~3.6 kc) and in view of the effect of the $\mathbf{I}\cdot\mathbf{J}$ interaction in broadening the envelope. The observed envelope, nevertheless, differs in shape from that observed for Li^6 in LiI shown in Fig. 4, where quadrupole effects are known to be negligible.[10] As will be shown later, there is considerable evidence to indicate that there is, in fact, an unresolved quadrupole structure in this envelope and that a reasonable estimate of the quadrupole interaction energy may be obtained on the basis of the assumption that the satellite maxima determine the half-width of the observed pattern.

A detailed quantitative description of the shapes of the resonance curves requires the inclusion of several effects not considered by Feld and Lamb. Among these are the cosine interaction between nuclear spin and molecular rotation, the variation of q with both rotational and vibrational quantum number, the effect of a J, which is small for a not inappreciable fraction of molecules in the beam, and the resolution properties of the apparatus. However, for the purpose of a determination of the sign of the quadrupole interaction energy, these effects do not modify the conclusions which may be deduced from observed data by the use of the simple Feld-Lamb theory.

The spectrum, at high magnetic fields, which occurs as a consequence of a nuclear reorientation in a diatomic molecule, cannot directly yield information about the sign of the quadrupole interaction energy. The observed pattern is entirely symmetrical about the central frequency, ν_0, and it is not possible to identify the satellite maxima in terms of the transitions $\Delta m_I=\pm 1$ which produce them. It will be shown, however, that the

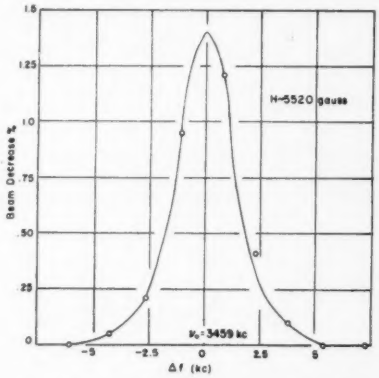

FIG. 4. Nuclear resonance spectrum of Li^6 in LiI.

removal from the beam of molecules with states of positive or negative m_I gives rise to an asymmetry in the resonance spectrum which permits a determination of the sign of eqQ.

The portion of the expression for the energy levels of a diatomic molecule at high magnetic fields ($eqQ \ll g_I\mu_0 H$) which depends on m_I is:

$$W=m_I g_I \mu_0 H - \frac{eqQ[3m_J^2-J(J+1)][3m_I^2-I(I+1)]}{4(2J+3)(2J-1)I(2I-1)} - cm_I m_J.$$

The first term is the interaction energy of the nuclear magnetic moment with the applied magnetic field, H, the second term the interaction energy of the nuclear electric quadrupole moment, Q, with the gradient, q, of the electric field at the nucleus and the third term the interaction energy of the nuclear magnetic moment

[10] P. Kusch, Phys. Rev. **75**, 887 (1949); N. A. Schuster and G. E. Pake, Phys. Rev. **81**, 157 (1951).

with the magnetic field produced by the molecular rotation. Feld and Lamb have shown that the transitions $\Delta m_I = \pm 1$ lead to maxima in the envelope in the region near $m_J = 0$. In this region the quantity $[3m_J^2 - J(J+1)]$ is negative, and except for constant terms and the small term $cm_I m_J$,

$$W = m_I g_I \mu_0 H + \text{constant}(eqQm_I^2).$$

The ordering of the energy levels is determined by the first term of the expression. The various possibilities when $I = 3/2$ are shown in Fig. 5. When g_I is negative, it is evident that the high frequency satellite maximum will correspond to the transition $(-3/2 \leftrightarrow -1/2)$ if eqQ is positive and to the transition $(1/2 \leftrightarrow 3/2)$ if eqQ is negative. The situation is reversed if g_I is positive. The sign of the interaction can thus be determined by an identification of the satellite maxima in terms of the m_I values of the terminal states if the sign of g_I is known.

Since the trajectory of a molecular beam through the sequence of magnets and slits in the molecular beam

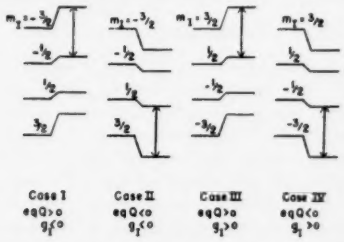

FIG. 5. Detail of nuclear energy level diagram ($I = 3/2$) showing the shift in energy due to the quadrupole interaction energy for the four cases depending on the relative signs of eqQ and g_I. In each case the arrow indicates the transition which gives rise to the high frequency satellite in the nuclear resonance spectrum.

apparatus is determined by the magnetic moment of the molecule, it is possible, by the introduction of suitable obstacles in the trajectories of the molecules, to exclude from observation molecules in which m_I is either positive or negative and hence to affect the intensity distribution in the resonance spectrum.

METHOD

A schematic diagram of the apparatus used in these measurements is shown in Fig. 6. The apparatus, except for the presence of the obstacle between the B and C magnets, is a typical molecular beam apparatus used for the observation of molecular spectra arising from a nuclear reorientation. Refocusing occurs at the detector when the molecule is in the same state in both the A and B magnets; if a transition occurs in the C magnet there will, in general, be a change in magnetic moment and refocusing will not occur.

The beam is a narrow ribbon in the xz plane and is propagated in the positive x-direction from the oven to the detector. The field in the A, B, and C magnets may

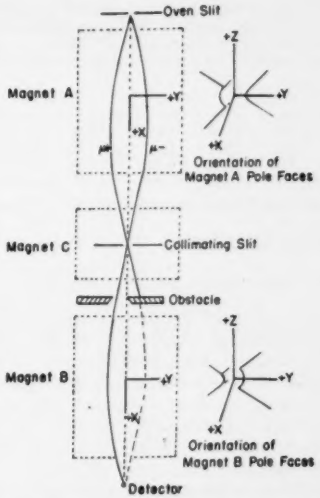

FIG. 6. Schematic diagram of the apparatus showing the arrangement of the magnet pole faces.

be either along the positive or negative y-direction, but is in the same direction in all three magnets. The ratio $(\partial H/\partial y)/H$ in the A and B fields is determined by the shape of the magnet pole faces and is a fixed and generally unalterable property of the apparatus, so that the direction of $\partial H/\partial y$ is reversed when the direction of H is reversed. Hence a particle with a positive component of magnetic moment along H is deflected while passing through the A-field in the positive y-direction, independent of the field direction. The net deflection of the beam at the collimating slit is equal to zero and beyond the collimating slit all molecules of positive moment will have a positive y-coordinate.

An obstacle with a sharp edge, parallel to the other elements which define the beam (source slit, collimating slit and detector) may be interposed between the B and C magnets. If the obstacle is in the region of $+$ y-coordinate and if its edge coincides with the position of the undeflected beam, all particles with a positive component of resultant moment in the A field are removed from the beam which arrives at the detector. In the event that transitions occur in the C region, the spectrum which is observed will not contain lines resulting from transitions for which the initial state is characterized by positive moment.

In the present case we are concerned with diatomic molecules in which there is no net electronic angular momentum, and the magnetic fields employed in the experiments are large ($\approx 10{,}000$ gauss) so that the angular momentum vectors are completely decoupled. The resultant magnetic moment is contributed by the two nuclear moments μ_{I1} and μ_{I2}, and the rotational

TABLE I. Table of allowed values of the total magnetic moment of Li^7I^{127}, in nuclear magnetons, in the direction of the applied field, for the possible m_I of the Li^7 and I^{127} nuclei.

$m_I(I^{127})$ / $m_I(Li^7)$	5/2	3/2	1/2	−1/2	−3/2	−5/2
3/2	6.065	4.942	3.818	2.694	1.570	0.447
1/2	3.894	2.771	1.641	0.523	−0.601	−1.724
−1/2	1.724	0.601	−0.523	−1.641	−2.771	−3.894
−3/2	−0.447	−1.570	−2.694	−3.818	−4.942	−6.065

moment μ_J. The effective moment of the molecule is then:

$$\mu = -(m_{I1}g_{I1} + m_{I2}g_{I2} + m_J g_J)\mu_0.$$

In all cases considered in these experiments, the nuclear g values are negative so that each nucleus contributes a positive moment for a positive value of m_I. The contribution of μ_J to the moment may be ignored since g_J is sufficiently small in comparison with g_I so that $|m_J g_J| \ll |m_I g_I|$. For any m_{I1} and m_{I2}, the moment distribution is affected symmetrically by μ_J since positive and negative values of m_J are equally probable. The effect is to broaden the deflection spectrum at any point in a manner analogous to, though not identical with, that produced by the velocity distribution.

The degree to which molecules in which a given nucleus has a positive (or negative) component of moment in the direction of the field can be separated from the beam depends on the relative values of the two nuclear moments in the molecule. The removal from the beam of nearly all molecules in which μ_{I1} contributes a positive moment requires that $|\mu_{I2}| \ll |\mu_{I1}|$ so that the sign of the magnetic moment of the molecule is determined predominantly by the orientation of μ_{I1}. When this condition holds, the interposition of the obstacle as described above will leave the observable intensity of a line arising from transitions between two states of negative m_{I1}, unaltered, between two states of positive m_{I1} zero, and between two states with m_{I1} of opposite sign, one-half of the original intensity. It is evident in this case that the selective removal of molecules with positive (or negative) m_{I2} cannot be achieved.

As an example, consider the case of Li^7I^{127}. The spin and magnetic moment of the nuclei are, respectively, 3/2, 3.256 nm for Li^7 and 5/2, 2.809 nm for I^{127}. Table I exhibits the possible values of the component of the magnetic moment of Li^7I^{127} in the direction of the applied field. It is evident that if all molecules whose component of magnetic moment in the field direction is positive, are removed from the beam which arrives at the detector, then the central maximum $(1/2 \leftrightarrow -1/2)$ in the nuclear resonance spectrum of Li^7 in Li^7I^{127} will be reduced in intensity by 1/2, while the satellite maximum $(3/2 \leftrightarrow 1/2)$ will be reduced in intensity of 1/6 of its original value and that due to the transitions $(-1/2 \leftrightarrow -3/2)$ will have 5/6 of its original intensity. By this means the satellite maxima are identified in terms of the transitions which produce them, and from this evidence the sign of the quadrupole interaction can be deduced.

As long as $eqQ \gg cJ$, where J is the most probable value of J, it is not necessary that the satellite maxima be resolved from the central peak in order to allow the determination of the sign of the quadrupole interaction energy. The large density of levels near $m_J/J = 0$ gives rise to the satellite maxima, and these maxima contribute directly to the intensity distribution in the unresolved resonance envelope. The removal of molecules containing m_I of a particular sign will suppress the satellites unsymmetrically, and will produce a shift in the center of the observed resonance spectrum. A detailed example of this effect in the Li^7 resonance in Li_2 is given in a later section. When $cJ \gtrsim eqQ$, the maxima in the envelope of the satellite lines become very poorly defined, and when the whole spectrum is unresolved, a detectable shift in the center of the pattern may not occur when molecules containing m_I of a particular sign are removed from the beam.

APPARATUS

The molecular beam apparatus was originally built in 1947. The design is symmetrical about the collimating slit which is located at the center of the homogeneous C-field. The inhomogeneous A and B fields have equal lengths (50.8 cm) and equal ratio of field gradient to field $(\partial H/\partial y)/H = 8$ cm^{-1}. The pole pieces on the deflecting magnets are made of Permendur which has a saturation value considerably in excess of 20,000 gauss. The over-all length of the apparatus from the oven slit to the tungsten detector wire is 175.8 cm. For a gradient of 1.6×10^6 gauss/cm and at an oven temperature of 900°K, a fairly typical temperature in the

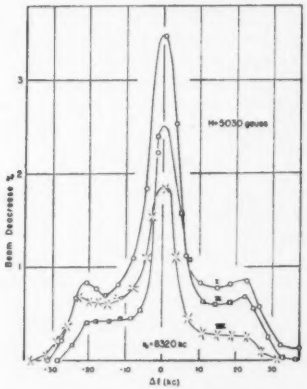

FIG. 7. Nuclear resonance spectrum of Li^7 in LiI; curve I is obtained with full beam, curve II with molecules of positive total moment removed from the beam, and curve III with molecules of negative total moment removed from the beam.

production of beams of the alkali halides,

$$S_\alpha = 5.77 \times 10^{-3} g \text{ cm}$$

where S_α is the deflection of a molecule at the detector which has undergone a transition resulting in a moment change $g_I \mu_0$ and where α is the most probable velocity in the oven. For Cl^{35} ($g_I = 0.55$ nm), $S_\alpha = 3.2 \times 10^{-3}$ cm. The actual change in intensity at the detector which is observed when a transition occurs is determined by the widths of the various defining elements. If the oven slit, collimating slit, and detector each have a width of 2.5×10^{-3} cm the maximum drop in intensity at the detector which may be observed when Cl^{35} undergoes a transition is about 38 percent. Actually, in the cases under consideration, the probability of transition, averaged over the velocity distribution of the molecules, cannot exceed 0.7; a particular nuclear species may have less than 100 percent isotopic abundance, and population in a great number of states (J, m_J) may broaden the spectrum so that the actual observed intensity change may be very much less than the calculated maximum.

The obstacle consists of two parallel quartz edges which are mounted parallel to the z-direction. This structure is movable in the y-direction and can be used to cut the beam on the side of either positive or negative y-coordinate. The obstacle is located between the B and C magnets as shown in Fig. 6. Evidently the optimum position at which to mount the obstacle is at a point in the B magnet where the maximum dispersion occurs in the deflection spectrum of the various molecular moments. However, the introduction of a movable slit at some point along the length of the B magnet leads to considerable mechanical complications. At the position of the actual obstacle, just before the entrance

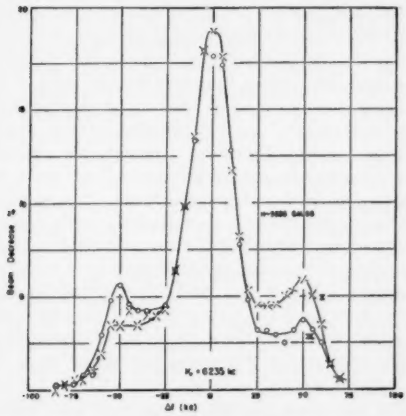

FIG. 8. Nuclear resonance spectrum of Na^{23} in Na_2; curve I is obtained with molecules of negative total moment removed from the beam and curve II with molecules of positive total moment removed from the beam.

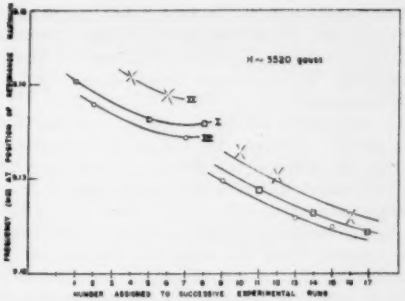

FIG. 9. Successive determinations of the center of the resonance spectrum of Li^7 in Li_2; curve I is obtained with full beam, curve II with molecules of positive total moment removed from the beam, and curve III with molecules of negative total moment removed from the beam.

to the B field, a molecule is subject to deflections by the A field only. When $(\partial H/\partial y)_A = 1.44 \times 10^5$ gauss/cm, a molecule containing an atom of Li^7, and with velocity α, propagated from an oven at a temperature of 900°K, is deflected 5.3×10^{-3} cm when $m_I = 3/2$ and 1.8×10^{-3} cm when $m_I = 1/2$ due to the Li atom only.

The insertion of the obstacle into the beam path makes the beam intensity at the detector more sensitive to mechanical distortion of the apparatus since there are then four elements which define the beam instead of the usual three, and in addition, the umbra or region of constant maximum beam intensity at the detector is reduced in width by the presence of the obstacle. Observation of the resonance spectrum is also made more difficult by the reduction of beam intensity which arises when the obstacle is inserted. Changes in beam intensity of the order of 0.01 percent may be observed under good conditions; it is, nevertheless, difficult to obtain the envelope of a spectrum with sufficient accuracy to make an exact quantitative analysis of the intensity distribution.

RESULTS

The nuclear resonance spectrum of Li^7 in LiI is shown in curve I of Fig. 7 while curve II shows the same resonance when the obstacle removes molecules of positive total moment from the beam, with the consequent suppression of the low frequency satellite. It is thus evident that the low frequency satellite corresponds to the transitions $(1/2 \leftrightarrow 3/2)$ indicating that eqQ is positive. Curve III exhibits the converse effect where molecules of negative total moment have been removed from the beam which arrives at the detector, with the consequent reduction of the intensity of the high frequency satellite.

The observed nuclear resonance spectrum of Na^{23} in the homonuclear molecule Na_2 in which molecules of negative total moment are removed by the obstacle is shown in curve I of Fig. 8. The partial removal of the

low frequency satellite shows that eqQ is negative. The converse effect is exhibited in curve II where molecules of positive total moment have been removed from the beam with the consequent suppression of the high frequency satellite.

In the nuclear resonance spectrum of Li^7 in the homonuclear molecule Li_2 the satellite maxima are unresolved. However, the sign of the quadrupole interaction energy is determined unambiguously by observing the position of the center of the resonance when molecules of either positive or negative total moment are removed from the beam by the obstacle. The suppression of the high frequency satellite in this manner shifts the center of the observed resonance in the direction of lower frequency and vice versa. In Fig. 9, a plot is made of successive determinations of the position of the center of the resonance curve for various positions of the obstacle in each of two separate runs. A slow downwards drift in field is evident from the curves by the slow decrease in ν_0. Curve I indicates the successive positions of the center of the resonance obtained with full beam; when molecules of total positive moment are removed, the center of the resonance is shifted to higher frequency as shown in curve II indicating that the transitions $(3/2\leftrightarrow 1/2)$ give rise to an unresolved low frequency satellite. The converse effect is exhibited in curve III where molecules of total negative moment are removed from the beam and the center of the resonance is shifted to lower frequency, indicating that the high frequency satellite has been suppressed. This identification of the satellite maxima in terms of m_I indicates that eqQ is positive.

The observed shift of the resonance center of about 1.5 kc on inserting the obstacle can be seen to be quite reasonable by the construction of an approximate resonance spectrum from the three component line envelopes. When $I=3/2$, the frequency of the satellite maximum $(3/2\leftrightarrow 1/2)$ for $eqQ\ll g_I\mu_0 H$ is

$$\nu=(g_I\mu_0 H/h)+[eqQ(3z^2-1)/8h]+(czJ/h)$$

where $z=m_J/J$ and $0\leqslant|z|\leqslant 1$. Neglecting the last term, the component lines extend over a frequency range defined by $z=0$ at the maximum to $z=\pm 1$ at the other limit, and $z=\pm 1/\sqrt{3}$ at the central frequency ν_0. Since the number of transitions in any frequency interval is proportional to the Δz required to cover the interval, the ratio of the satellite area on the side of ν_0 containing the maximum to the area on the other side of ν_0 is $1/(\sqrt{3}-1)=1.37$. Hence we may represent the satellite by a right triangle having its right-angled vertex at $\nu_1=\nu_0-eqQ/8h$ and with the base of the triangle extending from ν_1 to $\nu_2=\nu_0+eqQ/4h$. The area distribution is adjusted by the addition of a very small triangle adjacent to the right-angled vertex. The central structure $(1/2\leftrightarrow -1/2)$ is represented by an isosceles triangle having an area equal to 4/3 that of the satellite, since the total probability of the central line is greater than that for the satellites by this factor. Applying resolution corrections for the natural resonance width of 3.6 kc, and assuming a central half-width of 8 kc and $eqQ/4h=16$ kc, a resonance curve of half-width equal to that of the observed resonance curve was obtained. A similar construction was made in which the component maxima were reduced in intensity corresponding to the removal by the obstacle of molecules of total positive moment. The center of the resonance thus obtained was displaced about 1 kc from ν_0, which agrees fairly well with the observed shift of about 1.5 kc. The result obtained here for the sign of eqQ for Li^7 in Li_2, and the value of q calculated using available molecular wave functions yield a positive value for Q.

Since the positive Q for Li^7 is in contradiction with the predictions of simple nuclear models, an attempt has been made to obtain an independent determination of the sign of $Q(Li^7)$ by a study of LiH. A more dependable value of q may be calculated for LiH than for Li_2, since better wave functions are available. Since on heating, LiH dissociates before sufficient vaporization occurs to produce a molecular beam, various schemes for synthesizing Li and H in a molecular beam oven were tried without success. The detailed experimental investigation[11] of the thermal dissociation properties of LiH, however, indicates that it is not feasible to produce a beam of LiH in a molecular beam apparatus. At the high oven temperatures necessary to vaporize the lithium it is impossible to introduce sufficient hydrogen into the oven to produce a reasonable amount of LiH and still maintain the necessary vacuum in the apparatus.

The magnitude of the quadrupole interaction is determined by the separation $eqQ/4h$ of the satellite maxima when $I=3/2$. In the case of Li^7 in LiI the separation of the observed satellite maxima shown in Fig. 8 yields the result $eqQ/h=172$ kc. In the case of the resonance of Li^7 in Li_2 the two satellite maxima which determine the magnitude of the interaction were unresolved. If the assumption is made that the unresolved satellite maxima determine the half-width of the envelope then $eqQ/h=+60$ kc is found. This assumption is apparently quite reasonable in view of the agreement achieved above in explaining the displacement of the resonance caused by the insertion of the obstacle, where it was assumed that $eqQ/h=64$ kc. A similar situation arises in the case of the Cs^{133} resonance in Cs_2 where $I=7/2$ and the 6 satellite maxima were unresolved. It was assumed that the half-width of the resonance spectrum was determined by the satellites $(3/2\leftrightarrow 5/2)$ and $(-3/2\leftrightarrow -5/2)$ which gives the value $eqQ/h=+0.23$ Mc. The estimate is, of course, quite crude and a large $\mathbf{I}\cdot\mathbf{J}$ interaction might make the estimate of doubtful validity.

The magnitude and sign of the quadrupole interactions that have been determined by the methods

[11] Private communication from Johnson, Hill, and Perlow.

described above and by the electrical resonance method are listed in Table II.

DISCUSSION

The invariance of the sign of the quadrupole interactions of each of the two nuclei, Li^7 and Na^{23}, in the homonuclear molecules and all the halides; of K^{39}, Rb^{85}, Rb^{87} and Cs^{133} in the homonuclear molecules and the fluorides and of Cl^{35} and Cl^{37} in KCl and TlCl suggests that the sign of q, the gradient of the electric field at the nucleus, is the same in a large range of diatomic molecules.

The sign of q is known[9] to be positive in the hydrogen molecule. Recent work[12] has shown that the quadrupole moment, Q, of both chlorine isotopes is negative, and this result applied to the present data indicates that q at the Cl nucleus in KCl and TlCl is positive. Finally, Foley[4] has shown that q is positive at the Li nucleus in Li_2. This result is, of course, less certain than the other two results because of a possible inadequacy in the wave functions used in the calculation.

A positive value of q at one nucleus in a diatomic molecule occurs when the gradient contributed by one nucleus exceeds in magnitude that contributed by the net electronic configuration. The net electric field at the nucleus is, of course, equal to zero. A positive value of q corresponds to a minimum of the electrostatic potential at the nucleus in question. It is an attractive possibility that q at each nucleus in every diatomic molecule is positive. No general theorems have been proved to substantiate this conjecture; however, in the three cases where a test has been made, q is positive and it follows that q is positive in all diatomic molecules in which the signs of the quadrupole interactions of Li and Cl have been determined. It is certain that if the sign of q is reversed in a molecule containing another nucleus, it is reversed in all molecules, here considered, containing that nucleus.

Townes, Foley, and Low[13] have proposed a model which predicts the signs of the quadrupole moments of the nuclei. The sign of the moment of Li^7 is explicitly predicted to be negative and that of K^{39} positive. From the curve presented by these authors, the sign of $Q(Na^{23})$ is positive, though the sign is read from a dotted and presumably doubtful portion of the curve. The model makes no predictions as to the sign of the quadrupole moment of Rb^{85}, Rb^{87}, and Cs^{133}.

[12] V. Jaccarino and J. G. King, Phys. Rev. **83**, 471 (1951).
[13] Townes, Foley, and Low, Phys. Rev. **76**, 1415 (1949).

TABLE II. Magnitude and sign of the quadrupole interaction constant eqQ/h.

Molecule	eqQ/h (Mc)	Reference to sign of eqQ	Reference to magnitude of eqQ
Li^7 resonance			
Li_2	+0.060		
LiF	+0.408		[a]
LiCl	+0.192		[a]
LiI	+0.172		[a]
LiBr	+0.184		[a]
Na^{23} resonance			
Na_2	−0.423		[b]
NaF	−8.12		
NaCl	−5.40		[c]
NaI	−3.88		[c]
NaBr	−4.68		[c]
K^{39} resonance			
K_2	−0.158		[b]
KF	−7.938	[d]	[d]
Rb^{85} resonance			
Rb_2	−1.10		
RbF	−70.31	[e]	[e]
Rb^{87} resonance			[e]
Rb_2	−0.580		
RbF	−34.00	[e]	[e]
Cs^{133} resonance			
Cs_2	+0.23		
CsF	+1.240	[f]	[f]
Cl^{35} resonance			
KCl	−0.420		
TlCl	−15.795	[g]	[g]
Cl^{37} resonance			
KCL	−0.336		
TlCl	−12.446	[g]	[g]

[a] P. Kusch, reference 10.
[b] Kusch, Millman, and Rabi, Phys. Rev. **55**, 1176 (1939).
[c] See reference 8.
[d] L. Grabner and V. Hughes, Phys. Rev. **79**, 819 (1950).
[e] V. Hughes and L. Grabner, Phys. Rev. **79**, 314 (1950).
[f] J. W. Trischka, Phys. Rev. **74**, 718 (1948).
[g] Carlson, Lee, and Fabricand, Phys. Rev. **85**, 784 (1952).

From the data presented in the present paper, the predictions of Townes, Foley, and Low lead to a negative value of q in Li_2 and at the Li nucleus in the lithium halides. This result is opposite to that calculated by Foley.[4] Similarly a negative value of q is predicted at the sodium and potassium nuclei in diatomic molecules. The value of q at the Cl nucleus in the chlorine bearing molecules is positive. While no direct evidence exists to indicate that q cannot, in fact, show this variation, it is nevertheless true that an estimate of the sign of q from a model of nuclear structure and from the sign of the interaction energy eqQ cannot be accepted without reservation.

Electrodynamic Displacement of Atomic Energy Levels. II. Lamb Shift

ROBERT KARPLUS, ABRAHAM KLEIN, AND JULIAN SCHWINGER
Harvard University, Cambridge, Massachusetts

(Received December 26, 1951)

The vacuum fluctuations of the photon and pair fields modify the interaction of an electron with an electromagnetic field. The effects on the energy levels are conveniently described in terms of the mass operator and the vacuum polarization potential. An operator calculus for handling the mass operator is used to separate the contribution of low energy quanta, for which the external electromagnetic field may not be treated as weak. The remainder is given as a power series in the field. The additional displacement of order $Z\alpha$ with respect to the published values for the Lamb shift is calculated by specializing the external field to the Coulomb field of the nucleus and by taking the matrix element of the operators in an S-state of a hydrogen-like atom. It is found that the nS-level is raised by

$$\frac{Z^4\alpha^4}{n^3}\mathrm{Ry}\left(1+\frac{11}{128}-\frac{1}{2}\ln 2+\frac{5}{192}\right).$$

The theoretical value for the Lamb shift of an atom with infinitely heavy nucleus becomes 1058.42 Mc/sec. Effects of finite nuclear mass and size change this value to 1057.8 Mc/sec and 1058.9 Mc/sec for hydrogen and deuterium, respectively.

I. INTRODUCTION

IN a previous paper,[1] we considered the problem of the effects of the vacuum fluctuations of the photon and pair fields on the motion of an electron in a prescribed electromagnetic field. In particular, we developed the approximate mass operator, which describes the consequences of a single virtual photon emission and absorption, in a power series in the field up to quadratic terms. This procedure presupposes the smallness of the potential energy of the electron compared to its kinetic energy. It proved adequate for the computation of corrections, up to relative order $Z\alpha^2$, to the hyperfine structure splitting of the ground state of a hydrogenic atom. Since to this order the effects in question are confined to the neighborhood of an electron Compton wavelength of the nucleus, the basic assumption of the expansion in the field is a valid one. As is well known, this is not the case when one turns to the consideration of the Lamb shift[2]—the electrodynamic displacement of the $2S_{\frac{1}{2}}$ and $2P_{\frac{1}{2}}$ energy levels. The very first treatment of this problem[3] showed that one could account for the order of magnitude of the shift by a nonrelativistic treatment of the motion of the electron and by the use of the dipole approximation for the virtual quanta. Thus, the phenomenon depends in an essential way on the behavior of the electron at distances from the nucleus which are of the order of the Bohr radius, rather than of the electron Compton wavelength. This circumstance dooms to failure any attempt to treat the Lamb shift in its entirety by a straightfoward expansion of self-energy effects in powers of the external field. Subsequent consideration of relativistic refinements[4] to the Bethe calculation showed that the breakdown of the expansion was in fact a mild one. By introducing a low energy cutoff to the relativistic calculation, one could tie it to the nonrelativistic result in a manner which, to the order considered—$Z\alpha\log\alpha$ and $Z\alpha$ corrections to the fine structure formula—was independent of the precise value of the cutoff.

The purpose of this paper is to obtain corrections of relative order $Z\alpha$ to the present formula for the energy shift. The basic problem which must be solved is the separation of nonrelativistic effects, for which the structure of the atom is decisive, from relativistic effects, for which the detailed energy scheme is largely irrelevant. Any attempt to extend the cut-off techniques employed in previous calculations would be cumbersome, since to the order of accuracy which we now contemplate, previous calculations are not cut-off-independent. One can argue, however, that corrections to the nonrelativistic aspects of the level shift arise only from fine-structure corrections to the energy levels of the atom and are therefore of relative order $(Z\alpha)^2$. On the other hand, relativistic effects, which to first order in the field are confined to the origin, will be modified to relative order $Z\alpha$ as soon as one takes adequate account of the behavior of the electron as a nonlocalized entity in an inhomogeneous-field. This is tantamount to the statement that such effects are velocity-dependent. We may therefore expect them to be appreciable only when the velocity of the electron is appreciable, i.e., when the electron is in the vicinity of the nucleus. It is just under such circumstances that the weak field treatment is appropriate. That the foregoing argument is correct will emerge as a consequence of this paper.

We have performed the calculations by working at all stages with operators whose matrix elements are free of infrared divergences. Our ability to do this rests on

[1] R. Karplus and A. Klein, Phys. Rev. **85**, 972 (1952), referred to as I. Our notation follows this paper.
[2] W. E. Lamb and R. C. Retherford, Phys. Rev. **81**, 222 (1951).
[3] H. A. Bethe, Phys. Rev. **72**, 339 (1947).
[4] N. M. Kroll and W. E. Lamb, Phys. Rev. **75**, 380 (1949); J. B. French and V. F. Weisskopf, Phys. Rev. **75**, 1280 (1949); R. P. Feynman, Phys. Rev. **74**, 1430 (1948), and corrections in Phys. Rev. **76**, 269 (1949), footnote 13; J. Schwinger, Phys. Rev. **76**, 790 (1949).

a new technique of handling the mass operator. In Sec. II this method is used to derive the complete first-order level shift formula without the necessity of introducing an artificial cutoff of any kind. The more complete calculation occupies Secs. III–V. It is found that as long as we separate and treat by the method of Sec. II any part of the mass operator which contains the known nonrelativistic result, the remainder of the mass operator, when expanded as for a weak field, yields a perfectly finite matrix element. A critical examination of the structure of the power series expansion serves to clarify the reasons for this fact. The final result which includes a small contribution from vacuum polarization effects (Sec. VI), is stated and discussed in Sec. VII.

II. NEW DERIVATION OF FIRST-ORDER LAMB SHIFT

We propose to explain a method of treating the mass operator which has the following features: It works with the operator proper rather than with a particular representation; the mass renormalization can be carried out to all orders in the external field; the operator can be separated into two parts, one of which contains all the contributions characteristic of a slowly moving particle, whereas the other can be expanded safely in powers of the external field. In this section we shall concentrate on the explanation of the method of extracting nonrelativistic effects. We begin by discussing the structure of the mass operator.

By means of the integral representations, Eqs. (I, 2.3) and (2.5), the mass operator can be written in the form[5]

$$\begin{aligned}\mathbf{M}&=m_0-ie^2\int(2\pi)^{-4}d^4q\int_0^\infty ds\int_0^\infty dt\\&\quad\times\exp[-im^2s]\gamma_\lambda\tfrac{1}{2}\{m-\gamma(\Pi-q),\\&\qquad\times\exp[-is((\Pi-q)^2-e\tfrac{1}{2}\sigma F)-itq^2]\}\gamma_\lambda\\&=m_0-ie^2\int(2\pi)^{-4}d^4q\int_0^\infty sds\int_0^1 u^{-2}du\\&\quad\times\exp[-ism^2u]\gamma_\lambda\tfrac{1}{2}\{m-\gamma(\Pi-q),e^{-i\phi}\}\gamma_\lambda,\end{aligned}\tag{2.1}$$

where

$$\begin{aligned}\phi&=-su^{-1}(\gamma(q-u\Pi))^2+w\mathfrak{K}\\&=su^{-1}(q-u\Pi)^2-sue\tfrac{1}{2}\sigma F+w\mathfrak{K};\end{aligned}\tag{2.2}$$

$\mathfrak{K}$ is the second-order Dirac operator,

$$\mathfrak{K}=-(\gamma\Pi)^2+m^2,\quad \mathfrak{K}\psi=0,\tag{2.3}$$

and the parameters u and w, defined by

$$t=wu^{-1},\quad w=s(1-u),\tag{2.4}$$

have the same significance as in I. In the event that the external field vanishes,

$$[\Pi_\mu,\Pi_\nu]=0,\tag{2.5}$$

there is no obstacle to commuting the Dirac matrices in Eq. (2.1) with the exponential operator and to making the displacement

$$q_\mu\rightarrow(q+\Pi u)_\mu.\tag{2.6}$$

Carrying out the integration over the virtual photon momentum, we find that the mass operator in the absence of a field becomes

$$\begin{aligned}\mathbf{M}_0(\gamma\Pi)=m_0+e^2(4\pi)^{-2}\int_0^\infty s^{-1}ds\int_0^1 du\\\times\exp[-im^2s+iw(\gamma\Pi)^2][4m+2\gamma\Pi(1-u)],\end{aligned}\tag{2.7}$$

of which the Dirac wave function is an eigenfunction with eigenvalue equal to the total mass of the electron.[6] It follows that the mass operator in the presence of an external field must be expressible in the form

$$\mathbf{M}=\mathbf{M}_0(\gamma\Pi)+\bar{\mathbf{M}},\tag{2.8}$$

where $\bar{\mathbf{M}}$ contains the observable effects of the external field.

With the result of the form of Eq. (2.8) in mind, we carry out the preliminary rearrangement

$$\begin{aligned}&\gamma_\lambda\tfrac{1}{2}\{m-\gamma(\Pi-q),e^{-i\phi}\}\gamma_\lambda\\&\quad=-\{2m+\gamma\Pi(1-u),e^{-i\phi}\}-(1-u)[\Pi_\lambda,[\gamma_\lambda,e^{-i\phi}]]\\&\qquad-\tfrac{1}{4}\{m+\gamma\Pi(1-u),[\gamma_\lambda,[\gamma_\lambda,e^{-i\phi}]]\}\\&\qquad+\tfrac{1}{2}\gamma_\lambda\{\gamma(q-u\Pi),e^{-i\phi}\}\gamma_\lambda.\end{aligned}\tag{2.9}$$

The form of Eq. (2.9) is significant in several respects. First of all, it can be seen from Eq. (2.4) that values of the parameter u close to zero corresponds to large values of the photon "proper time" t or small values of the photon momentum. Any infrared divergences that may eventually appear in the mass operator will therefore correspond to divergences at the lower limit, $u=0$, of this parameter. Thus, relative powers of u (and at this stage also of the photon momentum q) serve to catalog the relative low or high energy nature of the contribution of the various terms of Eq. (2.9) to the level shift. We shall find that, at least through terms which are quadratic in the Coulomb field, all infrared difficulties are hidden in the first two terms of Eq. (2.9). (We can set $\gamma\Pi=-m$ if it stands at either wing of a term.)

Of more immediate interest is the fact that the first term of Eq. (2.9) would be the integrand of $M_0(\gamma\Pi)$ if

[5] The absorption of the factor $\exp[iq(x'-x'')]$ from the Fourier representation of the photon Green's function results from the gauge transformation $A_\mu(x)\rightarrow A_\mu(x)+(1/e)\partial_\mu(qx)$, $\Pi_\mu\rightarrow\Pi_\mu-q_\mu$, when one takes account of the resultant change in phase of the Dirac wave functions. Alternatively one may think of the displacement operation

$$\exp[iq(x'-x'')](x'|\,\Pi_\mu\,|x'')=(x'|\,e^{iqx}\Pi_\mu e^{-iqx}\,|x'')=(x'|\,\Pi_\mu-q_\mu\,|x'').$$

[6] J. Schwinger, Phys. Rev. **82**, 664 (1951).

$\exp(-i\phi)$ were replaced by

$$\exp[-i\phi(0)]=\exp[-isu^{-1}q^2-iw\mathfrak{C}] \quad (2.10)$$

and the q integration carried out. The expansion of the physically significant difference

$$[\exp(-i\phi)-\exp(-i\phi(0))]$$

in powers of the field, would then be part of the weak field treatment employed in I. Now, a glance at Eq. (2.2) makes it clear that the practical necessity for having to carry out some form of expansion of $\exp(-i\phi)$ derives from our inability to perform the q integration for the expression as it stands. On the other hand, as already indicated, $\exp(-i\phi(0))$ presents no such obstacle. A procedure alternative to direct expansion which naturally suggests itself is, therefore, to "expand" $\exp(-i\phi)$ about $\exp(-i\phi(0))$. By means to be explained below, we shall then find it possible to derive an operator whose matrix element reproduces the previous known result for the Lamb shift formula complete with Bethe logarithm term. The significance of such an expansion will be more easily understood in retrospect. We proceed from the identity

$$\exp[-i\phi]=\exp[-i\phi(0)]+\int_0^1 d\lambda(\partial/\partial\lambda)\exp[-i\phi(\lambda)], \quad (2.11)$$

where

$$\begin{aligned}\phi(\lambda)&=-su^{-1}[\gamma(q-\lambda u\Pi)]^2+w\mathfrak{C}\\&=su^{-1}(q-\lambda u\Pi)^2-\lambda^2 sue\tfrac{1}{2}\sigma F+w\mathfrak{C}\end{aligned} \quad (2.12)$$

is seen to reduce to ϕ and $\phi(0)$ at the limits $\lambda=1$ and $\lambda=0$, respectively.

The required techniques may be illustrated by a consideration of[7]

$$\begin{aligned}&\int d^4q\int_0^1 d\lambda(\partial/\partial\lambda)\exp[-i\phi(\lambda)]\\&=\int d^4q\int_0^1 d\lambda\int_0^1 dv\exp[-iv\phi(\lambda)]\\&\quad\times[2is(q\Pi-\lambda u\Pi^2)+2i\lambda sue\tfrac{1}{2}\sigma F]\\&\quad\times\exp[-i(1-v)\phi(\lambda)].\end{aligned} \quad (2.13)$$

The spin term in Eq. (2.13) is already explicitly first order in the field. To exhibit the remaining terms in like guise, we perform an integration by parts according to

$$\begin{aligned}&\int d^4q(\partial/\partial q_\mu)\int_0^1 dv\exp[-iv\phi(\lambda)]\Pi_\mu\\&\quad\times\exp[-i(1-v)\phi(\lambda)]=0\\&=\int d^4q\int_0^1 dv\int_0^1 dy\{\exp[-ivy\phi(\lambda)]\\&\quad\times(-2isu^{-1}v)(q-\lambda u\Pi)_\mu\exp[-iv(1-y)\phi(\lambda)]\\&\quad\times\Pi_\mu\exp[-i(1-v)\phi(\lambda)]+\exp[-iv\phi(\lambda)]\Pi_\mu\\&\quad\times\exp[-i(1-v)y\phi(\lambda)](-2isu^{-1}(1-v))\\&\quad\times(q-\lambda u\Pi)_\mu\exp[-i(1-v)(1-y)\phi(\lambda)]\},\end{aligned} \quad (2.14)$$

from which it follows that

$$\begin{aligned}&\int d^4q\int_0^1 dv\exp[-iv\phi(\lambda)]q\Pi\exp[-i(1-v)\phi(\lambda)]\\&=2\lambda u\int d^4q\int_0^1 dv\int_0^v dz\exp[-i(v-z)\phi(\lambda)]\Pi_\mu\\&\quad\times\exp[-iz\phi(\lambda)]\Pi_\mu\exp[-i(1-v)\phi(\lambda)],\end{aligned} \quad (2.15)$$

after appropriate changes of parameter in the two terms of Eq. (2.14). We can now write

$$\begin{aligned}&\int d^4q\int_0^1 d\lambda(\partial/\partial\lambda)\exp[-i\phi(\lambda)]\\&=\int d^4q\int_0^1 d\lambda 2\lambda(\partial/\partial\lambda^2)\exp[-i\phi(\lambda)]\\&=\int d^4q(\partial/\partial\lambda^2)\exp[-i\phi(\lambda)]|_{\lambda=0}\\&\quad-\int d^4q\int_0^1 d(\lambda^2)(\lambda^2-1)(\partial/\partial\lambda^2)^2\\&\quad\times\exp[-i\phi(\lambda)],\end{aligned} \quad (2.16)$$

with

$$\begin{aligned}&\int d^4q(\partial/\partial\lambda^2)\exp[-i\phi(\lambda)]|_{\lambda=0}\\&=\int d^4q isu\exp(-isu^{-1}q^2)\\&\quad\times\Big\{2\int_0^1 dv\int_0^v dz\exp[-i\mathfrak{C}w(v-z)]\Pi_\mu\\&\quad\times\exp[-i\mathfrak{C}wz]\Pi_\mu\exp[-i\mathfrak{C}w(1-v)]\\&\quad-\int_0^1 dv\exp[-i\mathfrak{C}wv](\Pi^2-e\tfrac{1}{2}\sigma F)\\&\quad\times\exp[-i\mathfrak{C}w(1-v)]\Big\},\end{aligned} \quad (2.17)$$

[7] We employ the formula

$$\begin{aligned}&(\partial/\partial\lambda)\exp[-i\phi(\lambda)]\\&=\lim_{\Delta\lambda\to 0}\frac{\exp[-i\phi(\lambda)-i\Delta\lambda\phi'(\lambda)]-\exp[-i\phi(\lambda)]}{\Delta\lambda}\\&=\int_0^1 dv\exp[-iv\phi(\lambda)](-i\phi'(\lambda))\exp[-i(1-v)\phi(\lambda)]\end{aligned}$$

after expanding the first exponential operator and taking the limit.

and

$$\int d^4q(\partial/\partial\lambda^2)^2\exp[-i\phi(\lambda)]$$

$$=\int d^4q\,isu(\partial/\partial\lambda^2)\Big\{2\int_0^1 dv\int_0^v dz$$

$$\times\exp[-i(v-z)\phi(\lambda)]\Pi_\mu\exp[-iz\phi(\lambda)]\Pi_\mu$$

$$\times\exp[-i(1-v)\phi(\lambda)]-\int_0^1 dv\exp[-iv\phi(\lambda)]$$

$$\times(\Pi^2-e\tfrac{1}{2}\sigma F)\exp[-i(1-v)\phi(\lambda)]\Big\}. \quad (2.18)$$

We shall pay no further heed to terms of the form of Eq. (2.18) since it can be shown that they do not contribute to the Lamb shift in first order. On the other hand Eq. (2.17) can be simplified for use in connection with the first term of Eq. (2.9), for the exponential operators which flank the expression may be replaced by unity in virtue of the Dirac equation. The resulting expression, which is now partially a matrix element, can be written[8]

$$\Big\langle\int d^4q(\partial/\partial\Lambda^2)\exp[-i\phi(\lambda)]|_{\lambda=0}\Big\rangle$$

$$=\pi^2u^3s^{-1}\Big\langle e\tfrac{1}{2}\sigma F+2\int_0^1 dv(1-v)\Pi_\lambda$$

$$\times[\exp(-i\mathfrak{C}wv)-1]\Pi_\lambda\Big\rangle, \quad (2.19)$$

after performing the q integration.

We accord similar treatment to the remaining terms of Eq. (2.9); since these terms vanish in the absence of an external field, it should be, and indeed is, possible to extract all first-order contributions without having to compute any λ derivatives. Thus by means of the formula

$$[\gamma_\mu, e^{-i\phi}]$$

$$=-\int_0^1 dv(\partial/\partial v)[\exp(-iv\phi)\gamma_\mu\exp(-i(1-v)\phi)]$$

$$=\int_0^1 dv\exp(-iv\phi)[\gamma_\mu,-i\phi]\exp(-i(1-v)\phi], \quad (2.20)$$

one sees that the second and third terms of Eq. (2.9) are explicitly first order. One of these is

$$\Big\langle(1-u)\int d^4q[\pi_\lambda,[e^{-i\phi},\gamma_\lambda]]\Big\rangle$$

$$=\Big\langle(1-u)\int d^4q\int_0^1 dv[\Pi_\lambda,\exp(-iv\phi)$$

$$\times 2se(\gamma F)_\lambda\exp(-i(1-v)\phi)]\Big\rangle$$

$$=\Big\langle-2i\pi^2u^2(1-u)s^{-1}\int_0^1 dv\{\Pi_\lambda\exp[-i\mathfrak{C}wv]$$

$$\times e(\gamma F)_\lambda-e(\gamma F)_\lambda\exp[-i\mathfrak{C}wv]\Pi_\lambda\}$$

$$+(1-u)\int_0^1 d\lambda\int d^4q(\partial/\partial\lambda)[\Pi_\lambda,\exp(-iv\phi(\lambda))$$

$$\times 2se(\gamma F)_\lambda\exp(-i(1-v)\phi(\lambda))]\Big\rangle. \quad (2.21)$$

To derive Eq. (2.21) we have employed Eq. (I, 4.2d), an equation of the form of Eq. (2.11), and have carried out the integration over the virtual photon momentum and used the Dirac equation in the first term.

A sequence of similar steps for the third term of Eq. (2.9) yields in turn

$$\Big\langle-\tfrac{1}{4}\int d^4q\{m+\gamma\Pi(1-u),[\gamma_\lambda,[\gamma_\lambda,e^{-i\phi}]]\}\Big\rangle$$

$$=\Big\langle-\tfrac{1}{2}u\int d^4q\int_0^1 dv[\gamma_\lambda,\exp(-iv\phi)is$$

$$\times[\gamma_\lambda,e\tfrac{1}{2}\sigma F]\exp(-i(1-v)\phi)]\Big\rangle$$

$$=\Big\langle 4\pi^2mu^3s^{-1}e\tfrac{1}{2}\sigma F-\tfrac{1}{2}\pi^2u^3s^{-1}\int_0^1 dv$$

$$\times\{[\gamma_\lambda,\exp(-i\mathfrak{C}wv)][\gamma_\lambda,e\tfrac{1}{2}\sigma F]$$

$$\times\exp(-i\mathfrak{C}w(1-v))+\exp(-i\mathfrak{C}wv)$$

$$\times[\gamma_\lambda,e\tfrac{1}{2}\sigma F][\gamma_\lambda,\exp(-i\mathfrak{C}w(1-v))]\}$$

$$-\tfrac{1}{2}u\int_0^1 d\lambda\int_0^1 dv\int d^4q(\partial/\partial\lambda)$$

$$\times[\gamma_\lambda,\exp(-iv\phi(\lambda))is[\gamma_\lambda,e\tfrac{1}{2}\sigma F]$$

$$\times\exp(-i(1-v)\phi(\lambda))]\Big\rangle. \quad (2.22)$$

The second term of Eq. (2.22), which belongs to the part of the operator evaluated at $\lambda=0$, is explicitly second order in the field. It has been written in primitive

[8] The brackets $\langle\ \rangle$ will henceforth indicate that a matrix element has been taken in a state satisfying the Dirac equation; the brackets $\langle\ \rangle_0$ will refer to the nS-level matrix element in a hydrogen atom.

form in order to indicate its origin in the noncommutivity of the Dirac matrices.

There remains the evaluation of the last term of Eq. (2.9). Employing an equation of the form

$$\int d^4q\gamma q \exp(-i\phi)$$

$$= \int d^4q \int_0^1 dv \gamma_\lambda \exp(-iv\phi) u\Pi_\lambda \exp(-i(1-v)\phi), \quad (2.23)$$

the proof of which is analogous to that of Eq. (2.15), we can write[9]

$$\int d^4q \{\gamma(q-u\Pi), e^{-i\phi}\}$$

$$= \int d^4q \Big[\int_0^1 dv \{\gamma_\lambda, \exp(-iv\phi)\} u\Pi_\lambda \times \exp(-i(1-v)\phi)\} - \{\gamma\Pi u, e^{-i\phi}\} \Big]$$

$$= \int d^4q \int_0^1 dv \{[\gamma_\lambda, \exp(-iv\phi)]u\Pi_\lambda \times \exp(-i(1-v)\phi) - \exp(-i(1-v)\phi) u\Pi_\lambda \times [\gamma_\lambda, \exp(-iv\phi)] + [\exp(-iv\phi), \gamma\Pi u] \times \exp(-i(1-v)\phi) - \exp(-i(1-v)\phi) \times [\exp(-iv\phi), \gamma\Pi u]\}. \quad (2.24)$$

The first two terms of Eq. (2.24) differ in no essential way from the operator evaluated in Eq. (2.21) and are readily found to have the value

$$\Big\langle 2i\pi^2 u^3 s^{-1} \int_0^1 dv (1-v) \{e(\gamma F)_\lambda \exp(-i\mathfrak{K}wv)\Pi_\lambda - \Pi_\lambda \exp(-i\mathfrak{K}wv) e(\gamma F)_\lambda\} + \int_0^1 d\lambda \int d^4q \int_0^1 dv \int_0^v dz (\partial/\partial\lambda) \times \{\exp[-i(v-z)\phi(\lambda)] 2isue(\gamma F)_\lambda \exp[-iz\phi(\lambda)] \times \Pi_\lambda \exp[-i(1-v)\phi(\lambda)] - \exp[-i(1-v)\phi(\lambda)]\Pi_\lambda \times \exp[-iz\phi(\lambda)] 2isue(\gamma F)_\lambda \times \exp[-i(v-z)\phi(\lambda)]\} \Big\rangle. \quad (2.25)$$

Finally, for the remaining terms of Eq. (2.24), we carry out a rearrangement with successive results

$$\Big\langle \int d^4q \int_0^1 dv \{(1-v)\exp(-iv\phi)(2isu)[q\Pi, \gamma\Pi] \times \exp(-i(1-v)\phi) - v\exp(-iv\phi)(2isu) \times [q\Pi, \gamma\Pi]\exp(-i(1-v)\phi)\} \Big\rangle$$

$$= \Big\langle \int d^4q \int_0^1 dv \int_0^v dz 2isu^2(1-2v) \times \{\exp(-i(v-z)\phi)\Pi_\lambda \exp(-iz\phi)[\Pi_\lambda, \gamma\Pi] \times \exp(-i(1-v)\phi) - \exp(-i(1-v)\phi) \times [\Pi_\lambda, \gamma\Pi]\exp(-iz\phi)\Pi_\lambda \times \exp(-i(v-z)\phi)\} \Big\rangle$$

$$= \Big\langle 2i\pi^2 u^4 s^{-1} \int_0^1 dv v(1-v)\{\Pi_\lambda \exp(-i\mathfrak{K}wv) e(\gamma F)_\lambda - e(\gamma F)_\lambda \exp(-i\mathfrak{K}wv)\Pi_\lambda\} + \int_0^1 d\lambda \int d^4q (\partial/\partial\lambda) \int_0^1 dv \int_0^v dz \times (2isu^2)(1-2v)\{\ \} \Big\rangle, \quad (2.26)$$

where { } stands for the same bracket of the preceding version with ϕ replaced by $\phi(\lambda)$. In arriving at Eq. (2.26) we have employed equations similar to Eq. (2.20), (2.15), transformed parameters as convenient, and performed the q integration.

We now collect the results of Eqs. (2.9), (2.16), (2.17), (2.21), (2.22), (2.25), and (2.26). If we ignore all terms for which the (tacit) claim has been made that they are at least quadratic in the field, we find for the mass operator, Eq. (2.1), the approximate expression

$$\langle \mathbf{M} \rangle = m_0 + (\alpha m/2\pi) \int_0^\infty s^{-1} ds \int_0^1 du(1+u) \times \exp[-ism^2 u] - (i\alpha m/4\pi) \int_0^\infty ds \int_0^1 du \times 2u(1-u)\exp[-ism^2 u]\langle e\tfrac{1}{2}\sigma F\rangle + (i\alpha m/2\pi) \int_0^\infty ds \int_0^1 du 2u(1+u) \times \exp[-ism^2 u] \int_0^1 dv(1-v) \times \langle \Pi_\lambda [\exp(-i\mathfrak{K}wv) - 1]\Pi_\lambda \rangle + (\alpha/2\pi) \int_0^\infty ds \int_0^1 du \exp[-ism^2 u] \times \int_0^1 dv[(1-u)+u(1-v)-u^2 v(1-v)] \times \langle e(\gamma F)_\lambda \exp(-i\mathfrak{K}wv)\Pi_\lambda - \Pi_\lambda \exp(-i\mathfrak{K}wv) e(\gamma F)_\lambda \rangle. \quad (2.27)$$

[9] Note that

$$\tfrac{1}{2}\gamma_\lambda\{\gamma(q-\Pi u), e^{-i\phi}\}\gamma_\lambda = \{\gamma(q-\Pi u), e^{-i\phi}\} + \tfrac{1}{2}\gamma_\lambda\gamma(q-\Pi u)[e^{-i\phi}, \gamma_\lambda] + \tfrac{1}{2}[\gamma_\lambda, e^{-i\phi}]\gamma(q-\Pi u)\gamma_\lambda.$$

The last two terms can be shown to be at least of second order, since the leading term in their λ-expansion vanishes on integration over q.

Within the express limitations of the calculation of this section—first-order explicit field dependence and consideration of a matrix element in a state satisfying the Dirac equation in the prescribed field—the penultimate term of Eq. (2.27) can be recast into the form of the last term. We first integrate by parts with respect to the proper time parameter s according to

$$\int_0^\infty i(m^2u)^{-1}(\partial/\partial s)(\exp[-ism^2u])[\exp(-i\mathfrak{C}uv)-1]ds$$
$$=-v(1-u)(m^2u)^{-1}\int_0^\infty ds$$
$$\times\exp[-ism^2u]\mathfrak{C}\exp[-i\mathfrak{C}uv], \quad (2.28)$$

since the integrated terms vanish. Next, we note the validity of the following rearrangement

$$\langle\Pi_\lambda\mathfrak{C}\exp[-i\mathfrak{C}uv]\Pi_\lambda\rangle$$
$$=\langle\Pi_\lambda(m-\gamma\Pi)(m+\gamma\Pi)\exp[-i\mathfrak{C}uv]\Pi_\lambda\rangle$$
$$=\langle 2m\Pi_\lambda(m+\gamma\Pi)\exp[-i\mathfrak{C}uv]\Pi_\lambda$$
$$-[\Pi_\lambda,\gamma\Pi]\exp[-i\mathfrak{C}uv](m+\gamma\Pi)\Pi_\lambda\rangle$$
$$=\langle -ime(\gamma F)_\lambda\exp[-i\mathfrak{C}uv]\Pi_\lambda$$
$$+im\Pi_\lambda\exp[-i\mathfrak{C}uv]e(\gamma F)_\lambda$$
$$-e^2(\gamma F)_\lambda\exp[-i\mathfrak{C}uv](\gamma F)_\lambda\rangle. \quad (2.29)$$

Ignoring the explicit second-order term in Eq. (2.29), we find, after performing the elementary integrations in the spin term, that the resulting mass operator can be written simply as

$$\langle\mathbf{M}\rangle=m-(\alpha/2\pi)(e/2m)\langle\tfrac{1}{2}\sigma F\rangle$$
$$+(\alpha/2\pi)\int_0^\infty ds\int_0^1 du\exp[-ism^2u]$$
$$\times\int_0^1 dv[1-2v(1-v)-uv+u^2v(1-v)]$$
$$\times\langle e(\gamma F)_\lambda\exp[-i\mathfrak{C}uv]\Pi_\lambda$$
$$-\Pi_\lambda\exp[-i\mathfrak{C}uv]e(\gamma F)_\lambda\rangle; \quad (2.30)$$

m now represents the renormalized mass, the second term is the expected increment in the magnetic moment, and the last term, as we shall proceed to show, contains the correct charge interaction term.

To demonstrate this assertion, we can proceed in several ways. As a preliminary, we note that in the absence of the operator $\exp(-i\mathfrak{C}uv)$ the field dependent structure is

$$e(\gamma F)_\lambda\Pi_\lambda-\Pi_\lambda e(\gamma F)_\lambda=ie\gamma_\lambda J_\lambda, \quad (2.31)$$

where J_λ is the current associated with the external field. In this case the remaining integrations are trivial, but the resulting operator is the unsatisfactory one

$$(\alpha/3\pi m^2)e\gamma J\left[\int_0^1\frac{du}{u}-\frac{5}{8}\right], \quad (2.32)$$

which exhibits a logarithmic divergence, of infrared origin, at the lower limit $u=0$. Equation (2.32) is exactly the result which would have been achieved to lowest order by a straightforward expansion in powers of the field, as in reference 1. On the other hand, all our effort has in fact been directed toward obtaining the exponential operator, which permits us, where it is necessary, to take adequate account of the atomic structure. In the present connection it suffices to consider the term with the factor $(1-2v(1-v))$ which alone diverges in the infrared. We perform an integration by parts

$$\int_0^1 du\exp[-is(m^2u+\mathfrak{C}v(1-u))]$$
$$=\int_0^1 du\exp[-is\mathfrak{C}v(1-u)](-ism^2)^{-1}$$
$$\times(\partial/\partial u)\exp[-ism^2u]$$
$$=(-ism^2)^{-1}[\exp(-ism^2)-\exp(-is\mathfrak{C}v)]$$
$$+\int_0^1 du\mathfrak{C}vm^{-2}\exp[-is(m^2u+\mathfrak{C}v(1-u))]. \quad (2.33)$$

The second term in Eq. (2.33) contributes only in second order by virtue of the structure

$$\langle(\gamma F)_\lambda\exp[-i\mathfrak{C}uv]\mathfrak{C}\Pi_\lambda\rangle$$
$$=\langle(\gamma F)_\lambda\exp[-i\mathfrak{C}uv][\mathfrak{C},\Pi_\lambda]\rangle. \quad (2.34)$$

The operator of interest thus assumes the form

$$(i\alpha/2\pi m^2)\int_0^1 dv(1-2v(1-v))\int_0^\infty s^{-1}ds$$
$$\times\langle e(\gamma F)_\lambda[\exp(-ism^2)-\exp(-is\mathfrak{C}v)]\Pi_\lambda$$
$$-\Pi_\lambda[\exp(-ism^2)-\exp(-is\mathfrak{C}v)]e(\gamma F)_\lambda\rangle$$
$$=-(i\alpha/2\pi m^2)\int_0^1 dv(1-2v(1-v))\langle e(\gamma F)_\lambda$$
$$\times\ln(m^2/\mathfrak{C}v)\Pi_\lambda-\Pi_\lambda\ln(m^2/\mathfrak{C}v)e(\gamma F)_\lambda\rangle$$
$$=(\alpha/3\pi m^2)\langle e\gamma J\rangle\left[\ln\frac{m}{2k_0(n_0,l)}+\frac{13}{12}\right], \quad (2.35)$$

if we make the replacement

$$\langle e(\gamma F)_\lambda\ln(m^2/\mathfrak{C})\Pi_\lambda-\Pi_\lambda\ln(m^2/\mathfrak{C})e(\gamma F)_\lambda\rangle$$
$$\rightarrow\langle ie\gamma J\rangle\ln[m/2k_0(n_0,l)], \quad (2.36)$$

where $k_0(n_0, l)$ is the excitation energy as a function of principal and angular momentum quantum numbers, defined and computed by Bethe *et al.*[10] The justification for this replacement is considered in the appendix. It should be noted that the matrix element of γJ is to be computed in the state $(n_0, 0)$.

The first-order part of the matrix element can now be written in terms of an effective operator,

$$\int \bar{\psi}_0(x')\bar{M}_1(x', x'')\psi_0(x'')d\mathbf{r}'d\mathbf{r}''dt''$$
$$= -(\alpha/2\pi)(e/2m)\langle \tfrac{1}{2}\sigma F\rangle_0 + (\alpha/3\pi m^2)\langle e\gamma J\rangle_0 \times[\ln(m/2k_0(n_0, l)) + (11/24)]. \quad (2.37)$$

In an S-state Eq. (2.37) yields the known result for the energy shift of that state if one includes the contribution $(-1/5)$ from vacuum polarization in the charge interaction term. To complete the computation, we need only observe that the operator in Eq. (2.37) is diagonal in coordinate space. The integration over the coordinates which are doubly primed is then trivial, and the time dependence of the stationary state

$$\psi_0(x) = \psi_0(\mathbf{r})e^{-iE_0t} \quad (2.38)$$

disappears. Further

$$e\gamma J(x) = 4\pi Z\alpha\gamma_0\delta(\mathbf{r}), \quad (2.39)$$

and

$$e\tfrac{1}{2}\sigma F = e\boldsymbol{\alpha}\cdot\mathbf{E}(\mathbf{r}) \rightarrow (e/2m)\boldsymbol{\nabla}\cdot\mathbf{E}(\mathbf{r}) = -(2\pi/m)Z\alpha\delta(\mathbf{r}), \quad (2.40)$$

for a spherically symmetric state after reduction to large and small components. The resulting energy shift including the vacuum polarization term is[10]

$$\Delta E(n_0, 0) = (4/3)(Z\alpha^2/m^2)|\varphi_0(0)|^2 \times[\ln\{m/2k_0(n_0, 0)\} + \tfrac{5}{6} - \tfrac{1}{5}]$$
$$= (8Z^4/n_0^3)(\alpha^3/3\pi)\mathrm{Ry}[\ln\{m/2k_0(n_0, 0)\} + \tfrac{5}{6} - \tfrac{1}{5}]. \quad (2.41)$$

For a state with $l \neq 0$, where only the spin-orbit coupling arising from the spin terms and the logarithm contribute, one finds in an analogous way[10]

$$\Delta E(n_0, l) = \frac{8Z^4}{n_0^3}\cdot\frac{\alpha^3}{3\pi}\mathrm{Ry}\left[\ln\frac{\mathrm{Ry}}{k_0(n_0, l)} + \frac{3}{8}\frac{C_{lj}}{2l+1}\right], \quad (2.42)$$

where

$$C_{lj} = 1/(l+1) \quad \text{for} \quad j = l+\tfrac{1}{2}, \quad (2.43a)$$
$$C_{lj} = -1/l \quad \text{for} \quad j = l-\tfrac{1}{2}. \quad (2.43b)$$

The significance of the treatment of this section may perhaps best be understood on the basis of the remark that instead of expanding the field dependent exponential operator about its value for a free particle,

$$i\int_0^\infty ds\int_0^1 \exp[-is\mathfrak{m}^2u] = \frac{1}{\mathfrak{m}^2}\int_0^1\frac{du}{u} \quad (2.44)$$

[see Eq. (2.27) and (2.32)], we have "expanded" about the field dependent combination

$$i\int_0^\infty ds\int_0^1 du\exp[-is(\mathfrak{m}^2u + \mathfrak{K}(1-u)v] = \int_0^1 du\frac{1}{\mathfrak{m}^2u + \mathfrak{K}(1-u)v}. \quad (2.45)$$

[See Eq. (2.33)]. We have thus retained the natural lower limit to the frequency of the virtual quanta, a limit which is determined by the structure of the atom. Our procedure is flexible in that at any stage at which we have convinced ourselves that all nonrelativistic effects have been extracted, it is possible to resort to a straightforward power series expansion of the exact remainder operator which is available after each step in the calculation. The method of making a more complete calculation from this latter point of view is treated in the next section.

III. DECOMPOSITION OF THE MASS OPERATOR

It is possible to formulate the power series expansion and the operation of mass renormalization very compactly in terms of the λ-procedure just described. Such an expression is particularly suitable for isolating relativistic effects, whose contribution to the level shift does not depend on the details of the atomic structure. These terms are conveniently evaluated by means of the power series. The structure dependent corrections that arise from low energy virtual quanta, on the other hand, cannot be treated by a weak field expansion. They will therefore be obtained by the methods of the preceding chapter. It should be pointed out that this separation is by no means unique. The particular procedure that is adopted here was suggested by convenience and by its close relationship to the calculation carried out in reference 1.

We therefore consider the operator

$$\mathfrak{S}(\lambda^2, n) = -ie^2\int(2\pi)^{-4}d^4q\int_0^\infty sds u^{-2} \times\exp[-is\mathfrak{m}^2u]\tfrac{1}{2}\gamma_\mu\{m - \gamma\Pi(1-u) + \lambda\gamma(q - \lambda\Pi u), \exp[-i\phi(\lambda)]\}\gamma_\mu. \quad (3.1)$$

The value of the integral of this operator over u is clearly equal to the electrodynamic addition to the mass of the electron when $\lambda = 1$. In order to separate the change in rest mass from the field dependent effects, we divide the operator into two parts,

$$\mathfrak{S}(\lambda^2, u) = \mathfrak{S}_A(\lambda^2, n) + \mathfrak{S}_B(\lambda^2, u), \quad (3.2)$$

[10] Bethe, Brown, and Stehn, Phys. Rev. **77**, 370 (1950).

that arise naturally when the Dirac matrices γ_μ are eliminated from Eq. (3.1)

$$\mathfrak{F}_A(\lambda^2,u)=ie^2\int(2\pi)^{-4}d^4q\int_0^\infty sdsu^{-2}\exp[-ism^2u]$$
$$\times\{2m+\gamma\Pi(1-u),\exp(-i\phi(\lambda))\};\quad(3.3a)$$

$$\mathfrak{F}_B(\lambda^2,u)=-ie^2\int(2\pi)^{-4}d^4q\int_0^\infty sdsu^{-2}\exp[-ism^2u]$$
$$\times(\tfrac{1}{2}\gamma_\mu\{\lambda\gamma(q-\lambda\Pi u),\exp(-i\phi(\lambda))\}\gamma_\mu$$
$$+\tfrac{1}{4}\{m+\gamma\Pi(1-u),[\gamma_\mu,[\exp[-i\phi(\lambda)],\gamma_\mu]]\}$$
$$+(1-u)[\Pi_\mu,[\exp[-i\phi(\lambda)],\gamma_\mu]]).\quad(3.3b)$$

The first of these has a particularly simple value at $\lambda=0$. The integration over the momentum of the virtual photon can be carried out with the result

$$\int_0^1 du\mathfrak{F}_A(0,u)=\mathbf{M}_0(\gamma\Pi),$$

the mass renormalization discussed in connection with Eq. (2.7). The physically significant contributions to the mass operator are therefore contained in

$$\bar{\mathbf{M}}=\int_0^1 du[\mathfrak{F}(1,u)-\mathfrak{F}_A(0,u)]$$
$$=\int_0^1 du\left[\mathfrak{F}_B(1,u)+\int_0^1 d\lambda^2(\partial/\partial\lambda^2)\mathfrak{F}_A(\lambda^2,u)\right].\quad(3.5)$$

The manipulations carried out in Sec. II have indicated that the first-order effects of the soft virtual quanta are completely included in [see Eqs. (2.19) and (2.21)]

$$\bar{\mathbf{M}}_0=\int_0^1 du[\mathfrak{F}_B(0,u)+\mathfrak{F}_A'(0,u)]\quad(3.6)$$
$$(\mathfrak{F}'=(\partial/\partial\lambda^2)\mathfrak{F}).$$

It follows that the rearrangement

$$\bar{\mathbf{M}}=\bar{\mathbf{M}}_0+\bar{\mathbf{M}}',\quad(3.7)$$

$$\bar{\mathbf{M}}'=\int_0^1 du\int_0^1 d\lambda^2[\mathfrak{F}_B'(\lambda^2,u)+(1-\lambda^2)\mathfrak{F}_A''(\lambda^2,u)],\quad(3.8)$$

displays a contribution for which a power series treatment is certainly inadequate plus a contribution which we may hope to treat by an expansion. Both parts must be evaluated to the desired order of accuracy; the first part will be evaluated by the methods of Sec. II, while the remainder will be obtained as a power series. The adequacy of such treatment remains to be justified. It will follow from the expansion of the operator $\mathfrak{F}(\lambda^2,u)$.

The gauge transformation[5]

$$\Pi_\mu\to\Pi_\mu+(\lambda/\Lambda)q_\mu\quad(3.9)$$

with

$$\Lambda=1-u+\lambda^2u\quad(3.10)$$

of the coordinate matrix element of $\mathfrak{F}(\lambda^2,u)$ expresses this matrix element as the product of the proper time representations of an effective photon Green's function with an effective electron Green's function,

$$(x'|\mathfrak{F}(\lambda^2,u)|x'')$$
$$=-ie^2\int_0^\infty sds\exp[-im^2s](\Lambda/\lambda)^4u^{-2}$$
$$\times(-i)(4\pi t')^{-2}\exp[i(\Delta x)^2/4t']$$
$$\times(x'|\tfrac{1}{2}\gamma_\mu\{m-\Lambda\gamma\Pi,\exp[is'(\gamma\Pi)^2]\}\gamma_\mu|x'').\quad(3.11)$$

The quantities that play the roles of the proper time variables in the two functions are

$$t'=\Lambda w/\lambda^2u,\quad s'=\Lambda s.\quad(3.12)$$

Although this expression has no physical significance for values of λ different from unity, it is very suggestive, for the entire dependence on the electromagnetic field is now contained in operators whose weak field expansions are contained in reference 1. In fact, the matrix element in Eq. (3.10) is obtained directly from Eq. (I, 3.29) by dropping those terms that depend on the proper time w, by replacing s by s' everywhere in the large bracket, and by multiplying all terms that arose from momentum operators by the factor Λ. This adaptation results in the expression

$$(x'|\mathfrak{F}(\lambda^2,u)|x'')$$
$$=-i\alpha(4\pi)^{-2}\int_0^\infty(ds/s)\exp[-im^2s]\Phi(x',x'')$$
$$\times w^{-2}\exp[i(\Delta x)^2/4w](\{4m+\gamma\Delta x/s]$$
$$\times[1+A(s')+C(s')]+2\Lambda\gamma_\mu[A_{+\mu}(s')+C_{+\mu}(s')]$$
$$-\{\Lambda\gamma B_+(s')+(\gamma\Delta x/2s)B(s'),\tfrac{1}{2}\sigma F\}$$
$$+[\Lambda\gamma B_-(s'),\tfrac{1}{2}\sigma F]-\{\Lambda\gamma D_+{}^1(s')$$
$$+(\gamma\Delta x/2s)D^1(s'),\tfrac{1}{2}\sigma F^2\}+[\Lambda\gamma D_-{}^1(s'),\tfrac{1}{2}\sigma F^2]$$
$$-\{\Lambda\gamma D_+{}^2(s')+(\gamma\Delta x(2s)D^2(s'),\tfrac{1}{2}\sigma F^1\}$$
$$+[\Lambda\gamma D_-{}^2(s'),\tfrac{1}{2}\sigma F^1]+i\{\Lambda\gamma G_+(s')$$
$$+(\gamma\Delta x/2s)G(s'),\mathrm{tr}(F^1\sigma F^2)\}$$
$$-i[\Lambda\gamma G_-(s'),\mathrm{tr}(F^1\sigma F^2)]-4mG(s')\gamma_5\tfrac{1}{2}F^1F^{2*}$$
$$+2\Lambda\gamma G_-(s')\gamma_5\tfrac{1}{2}F^1F^{2*}).\quad(3.13)$$

The light-faced $\mathfrak{F}$ represents the power series to second-order terms of the operator $\mathfrak{F}$. The power series for

$\mathfrak{F}_A(\lambda^2, u)$ is obtained in very much the same way. The displacement Eq. (3.9) in Eq. (3.3a) makes the q integration easy and leaves

$$(x'|\,\mathfrak{F}_A(\lambda^2,u)\,|x'')$$
$$=ie^2\int_0^\infty sds\,\exp[-ism^2](\Lambda/\lambda)^4(-i)(4\pi t')^{-2}$$
$$\times\exp[i(\Delta x)^2/4t'](x'|\,\{2m+\gamma\Pi(1-u)$$
$$+(\lambda^2u\gamma\Delta x/2s'),\exp[is'(\gamma\Pi)^2]\}\,|x''). \quad (3.14)$$

The series expansion for this quantity can be transcribed from Eqs. (I, 3.14) and (I, 3.19):

$$(x'|\,\mathfrak{F}_A(\lambda^2,u)\,|x'')$$
$$=-i\alpha(4\pi)^{-3}\int_0^\infty (ds/s)\exp[-im^2s]\Phi(x',x'')$$
$$\times w^{-2}\exp[i(\Delta x)^2/4w]([4m+\gamma\Delta x/s]$$
$$\times[1+A(s')+C(s')]+2(1-u)\gamma_\mu[A_{+\mu}(s')$$
$$+C_{+\mu}(s')]+[(1-u)\gamma B_-(s'),\tfrac{1}{2}\sigma F]$$
$$+\{(1-u)\gamma B_+(s')+(\gamma\Delta x/2s)B(s'),\tfrac{1}{2}\sigma F\}$$
$$+[(1-u)\gamma D_-{}^1(s'),\tfrac{1}{2}\sigma F^2]+\{(1-u)\gamma D_+{}^1(s')$$
$$+(\gamma\Delta x/2s)D^1(s'),\tfrac{1}{2}\sigma F^2\}$$
$$+[(1-u)\gamma D_-{}^2(s'),\tfrac{1}{2}\sigma F^1]+\{(1-u)\gamma D_+{}^2(s')$$
$$+(\gamma\Delta x/2s)D^2(s'),\tfrac{1}{2}\sigma F^1\}-i[(1-u)\gamma G_-(s'),$$
$$\times\mathrm{tr}(F^1\sigma F^2)]-i\{(1-u)\gamma G_+(s')$$
$$+(\gamma\Delta x/2s)G(s'),\mathrm{tr}(F^1\sigma F^2)\}+4m[B(s')\tfrac{1}{2}\sigma F$$
$$+D^1(s')\tfrac{1}{2}\sigma F^2+D^2(s')\tfrac{1}{2}\sigma F^1+G(s')(\gamma_5\tfrac{1}{2}F^1F^{2*}$$
$$-i\,\mathrm{tr}(F^1\sigma F^2))]-2(1-u)$$
$$\times\gamma G_-(s')\gamma_5\tfrac{1}{2}F^1F^{2*}). \quad (3.15)$$

The power series for a matrix element of $\mathfrak{F}_B(\lambda^2, u)$ is obtained most simply by subtracting Eq. (3.15) from Eq. (3.13).

One may note that these power series explicitly display the functions $\mathfrak{F}(\lambda^2, u)$ and $\mathfrak{F}_A(\lambda^2, u)$ as functions of λ^2, for they depend on that variable only through Λ, Eq. (3.10).

IV. THE EVALUATION OF M′

We shall now evaluate the matrix element of the power series for the operators $\mathfrak{F}$, $\mathfrak{F}_A$, and $\mathfrak{F}_B$ in an S-state of a hydrogen-like atom. The procedure parallels precisely that of reference 1, Secs. IV and V. The only difference is that now the external field consists only of the electric field of the nucleus. The rearrangement of Eq. (I, 4.1) applied to $\mathfrak{F}$ and $\mathfrak{F}_A$ yields the term linear in the field,

$$(x'|\,\mathfrak{F}_1(\lambda^2,u)\,|x'')$$
$$=(\alpha/2\pi)\int_0^\infty (ds/s)\exp[-im^2su]\int(2\pi)^{-4}d^4p e^{ip\Delta x}$$
$$\times\exp[-iw(p^2+m^2)]ie\int d^4k\{(2m^2w(2-w/s)$$
$$+iw/s)(e(s')-1)\gamma J/k^2+\tfrac{1}{2}\Lambda(s'+w-v^2(s'-w))$$
$$\times e(s')\gamma J-mw((2-w/s)(e(s')-1)$$
$$-\Lambda e(s'))\tfrac{1}{2}\sigma F\} \quad (4.1)$$

and

$$(x'|\,\mathfrak{F}_{A1}(\lambda^2,u)\,|x'')$$
$$=(\alpha/2\pi)\int_0^\infty (ds/s)\exp[-im^2su]\int(2\pi)^{-4}d^4p e^{ip\Delta x}$$
$$\times\exp[-iw(p^2+m^2)]ie\int d^4k\{(2m^2w(2-w/s)$$
$$+iw/s)(e(s')-1)\gamma J/k^2+\tfrac{1}{2}(1-u)v^2(s'-w)$$
$$\times e(s')\gamma J+m((2s'-w)e(s')$$
$$-w(2-w/s)(e(s')-1))\tfrac{1}{2}\sigma F\}, \quad (4.2)$$

whence

$$(x'|\,\mathfrak{F}_{B1}(\lambda^2,u)\,|x'')$$
$$=(\alpha/2\pi)\int_0^\infty (ds/s)\exp[-im^2su]\int(2\pi)^{-4}d^4p e^{ip\Delta x}$$
$$\times\exp[-iw(p^2+m^2)]ie\int d^4k\{\tfrac{1}{2}(\Lambda(s'+w)$$
$$-\lambda^2uv^2(s'-w))e(s')\gamma J$$
$$-2m\Lambda(s-w)e(s')\tfrac{1}{2}\sigma F\}. \quad (4.3)$$

In addition, the $\mathfrak{F}$'s consist of the explicitly second-order terms C, D, and G, Eqs. (3.13) and (3.15), the analogs of Eq. (I, 4.5), and $\mathfrak{F}$ and $\mathfrak{F}_A$ contain the term

$$(x'|\,\mathfrak{F}_0(u)\,|x'')$$
$$=-i\alpha(4\pi)^{-3}\int_0^\infty (ds/s)w^{-2}\exp[i(\Delta x)^2/4w]$$
$$\times\Phi(x',x'')(4m+\gamma\Delta x/s), \quad (4.4)$$

which is independent of λ.

The Coulomb wave functions that enter the matrix elements may be approximated by the Pauli wave functions, and need to be represented accurately only near the position of the nucleus of the atom [see Eqs. (I, 4.12), (4.20), and (5.1)]. The operators that appear in $\mathfrak{F}$ then vanish or suffer the following transformation in the light of Eqs. (I, 5.2), and (5.4) and with the

understanding of the comment in Eq. (I, 5.5):

$$\bar{\psi}_0(\mathbf{r}')e\gamma J\psi_0(\mathbf{r}'')\rightarrow 2Z\alpha|\,\varphi_0(0)|^2(1-2Z\alpha r'm); \quad (4.5a)$$

$$\bar{\psi}_0(\mathbf{r}')\tfrac{1}{2}e\sigma F\psi_0(\mathbf{r}'')\rightarrow 2Z\alpha|\,\varphi_0(0)|^2(1-2Z\alpha r'm)(-\tfrac{1}{2}); \quad (4.5b)$$

$$\bar{\psi}_0(\mathbf{r}')e^2(\gamma F^1\Delta x)(\Delta x J^2)\psi_0(\mathbf{r}'')\rightarrow (2Z\alpha)^2|\,\varphi_0(0)|^2 2imw^2\Delta v; \quad (4.5c)$$

$$\bar{\psi}_0(\mathbf{r}')\tfrac{1}{2}e^2[\gamma F^1\Delta x,\ \tfrac{1}{2}\sigma F^2]\psi_0(\mathbf{r}'')\rightarrow -(2Z\alpha)^2|\,\varphi_0(0)|^2 iwm/k_2^2; \quad (4.5d)$$

$$\bar{\psi}_0(\mathbf{r}')e^2(A^1\Delta x)(\gamma J^2)\psi_0(\mathbf{r}'')\rightarrow (2Z\alpha)^2|\,\varphi_0(0)|^2 2wm/k_2^2; \quad (4.5e)$$

$$\bar{\psi}_0(\mathbf{r}')e^2(\Delta x J^1)(\Delta x J^2)\psi_0(\mathbf{r}'')\rightarrow (2Z\alpha)^2|\,\varphi_0(0)|^2(4m^2w^2-2iw); \quad (4.5f)$$

$$\psi_0(\mathbf{r}')e^2(\gamma\Delta x)(\Delta x J^1)(\Delta x J^2)\psi_0(\mathbf{r}'')\rightarrow (2Z\alpha)^2|\,\varphi_0(0)|^2(-8w^3m^3+12iw^2m); \quad (4.5g)$$

$$\bar{\psi}_0(\mathbf{r}')e^2\{1;\gamma\Delta x\}J^1J^2\psi_0(\mathbf{r}'')\rightarrow (2Z\alpha)^2|\,\varphi_0(0)|^2\{-1;2wm\}; \quad (4.5h)$$

$$\bar{\psi}_0(\mathbf{r}')e^2\{1;\gamma\Delta x\}[k_2\Delta x(1+v_2)-k_1\Delta x(1-v_1)]\times J^1J^2\psi_0(\mathbf{r}'')\rightarrow (2Z\alpha)^2|\,\varphi_0(0)|^2k^2w\Delta v(2-\Delta v)\{1;-2wm\}; \quad (4.5i)$$

$$\bar{\psi}_0(\mathbf{r}')e^2\{1;\gamma\Delta x\}(iJ^2F^1\Delta x(1-v_1) - iJ^1F^2\Delta x(1+v_2))\psi_0(\mathbf{r}'')\rightarrow (2Z\alpha)^2|\,\varphi_0(0)|^2w\Delta v(2-\Delta v)\{1;-2wm\}; \quad (4.5j)$$

$$\bar{\psi}_0(\mathbf{r}')e^2\{1;\gamma\Delta x\}\tfrac{1}{2}F^1F^2\psi_0(\mathbf{r}'')\rightarrow (2Z\alpha)^2|\,\varphi_0(0)|^2\{-1;2wm\}/k_1^2; \quad (4.5k)$$

$$\bar{\psi}_0(\mathbf{r}')e^2[v_1(\gamma F^1\Delta x)(\Delta x J^2) + v_2(\gamma F^2\Delta x)(\Delta x J^1)]\psi_0(\mathbf{r}'')\rightarrow (2Z\alpha)^2|\,\varphi_0(0)|^2 2iw^2m(\Delta v)^2; \quad (4.5l)$$

$$\bar{\psi}_0(\mathbf{r}')e^2(\gamma J^1)(\Delta x J^2)\psi_0(\mathbf{r}'')\rightarrow \bar{\psi}_0(\mathbf{r}')e^2(\gamma J^2)(\Delta x J^1)\psi_0(\mathbf{r}'')\rightarrow (2Z\alpha)^2|\,\varphi_0(0)|^2 2mw; \quad (4.5m)$$

$$\bar{\psi}_0(\mathbf{r}')([\gamma D_-^1(s'),\ \tfrac{1}{2}\sigma F^2]+[\gamma D_-^2(s'),\ \tfrac{1}{2}\sigma F^1])\psi_0(\mathbf{r}'')\rightarrow -(2Z\alpha)^2|\,\varphi_0(0)|^2 i^2[e_1(s')+e_2(s')]2mws'. \quad (4.5n)$$

Here Eqs. (4.5a), (b) contain operators that occur in $\mathfrak{F}_1$, Eqs. (4.5c)-(e) pertain to the transcript of Eq. (I, 4.5), Eqs. (4.5f)–(k) are relevant to the second-order term $C(s')$, Eqs. (4.5l, m) reduce the second-order term $C_{+\mu}(s')$, and Eq. (4.5n) is self-explanatory. It is interesting to note that the set of terms considered here in connection with the level shift and the set of terms that contributed to the hyperfine structure are mutually exclusive. This fact follows from the orthogonality of the two vector potentials.

When these substitutions are made, the S-state matrix element of the operator $\mathfrak{F}(\lambda^2, u)$ becomes

$$\begin{aligned}\langle\mathfrak{F}(\lambda^2,u)\rangle_0 &= \langle\mathfrak{F}_0(u)\rangle_0+2Z\alpha^2|\,\varphi_0(0)|^2\int_0^\infty(ds/s)\\ &\times\exp[-im^2su]\Big\{i\int_{-1}^1\tfrac{1}{2}dv\int(2\pi)^{-3}d\mathbf{k}d\mathbf{r}'\\ &\times\exp[-iw\tfrac{1}{4}k^2(1-v^2)](1-2Z\alpha r'm)\\ &\times[(2m^2w(2-w/s)+iw/s)(e(s')-1)/k^2\\ &+\tfrac{1}{2}\Lambda(s'+w-v^2(s'-w))e(s')\\ &+\tfrac{1}{2}w((2-w/s)(e(s')-1)-\Lambda e(s'))]\\ &+2Z\alpha\int_{-1}^1\tfrac{1}{2}dv_1\int_{-1}^{v_1}\tfrac{1}{2}dv_2i^2\int(2\pi)^{-3}d\mathbf{k}_1\\ &\times\exp[-iw\tfrac{1}{4}k_1^2(\Delta v)^2][2mw(2m^2w(2-w/s)\\ &-i(2-3w/s))(E(s')-1)/k_1^4\\ &+\tfrac{1}{2}m(2-w/s)s'(w\Delta v(2-\Delta v)-s'\Delta v(3-\Delta v))\\ &\times E(s')/k_1^2+\Lambda mw(w(\Delta v)^2\\ &+s'\Delta v(1-\Delta v))E(s')/k_1^2]\\ &+2Z\alpha\int_{-1}^1\tfrac{1}{2}dv_1\int_{-1}^1\tfrac{1}{2}dv_2i^2\int(2\pi)^{-3}d\mathbf{k}_2\\ &\times\exp[-iw\tfrac{1}{4}k_2^2(\Delta v)^2][4imw(1-w/s)\\ &\times(e_2(s')-1)/k_2^4-mw^2((w/s)(\Delta v)^2\\ &-(2-w/s)v_1\Delta v)(e_2(s')-1)/k_2^2]\Big\}. \quad (4.6)\end{aligned}$$

The remaining coordinate and momentum integrals are of the form Eqs. (I, 4.23) and (I, 5.8) with the addition of

$$\int(2\pi)^{-3}d\mathbf{r}'d\mathbf{k}e^{i\mathbf{k}\cdot\mathbf{r}}(\exp[-is\tfrac{1}{4}k^2\eta_j]-1)(r'/k^2) = -\tfrac{1}{2}(is\eta_j)^{\frac{1}{2}}\pi^{-\frac{1}{2}} \quad (4.7a)$$

and

$$\int(2\pi)^{-3}d\mathbf{k}(\exp[-isk^2\tfrac{1}{4}\eta_j]-1)/k^4=-\tfrac{1}{2}(i\eta_j s/\pi)^{\frac{1}{2}}. \quad (4.7b)$$

The quantities η_j have the following significance:

$$\eta_1=2(1-v)[1-u(1-\tfrac{1}{2}\lambda^2(1+v))]; \qquad \bar{\eta}_1=(1-v^2)(1-u); \quad (4.8a)$$

$$\eta_2=2\Delta v[1-u(1-\tfrac{1}{2}\lambda^2(2-\Delta v))]; \qquad \bar{\eta}_2=(\Delta v)^2(1-u); \quad (4.8b)$$

$$\eta_3=1-v_2^2+(\Delta v)^2-u[(1-v_2^2)(1-\lambda^2)+(\Delta v)^2]; \qquad \bar{\eta}_3=(\Delta v)^2(1-u). \quad (4.8c)$$

The proper time integration finally leaves the integral

$$\langle\bar{\mathfrak{F}}(\lambda^2,u)\rangle_0$$
$$=\langle\bar{\mathfrak{F}}_0(u)\rangle_0+(2Z\alpha^2|\,\varphi_0(0)\,|^2/m^2)$$
$$\times\Big\{\int_{-1}^{1}\tfrac{1}{2}dv\big[-\tfrac{1}{4}\Lambda(1-v^2)u^{-2}(2(1-u^2)-u(1-u))$$
$$+\Lambda u^{-1}(1-u+\tfrac{1}{2}\lambda^2u(1-v^2))-\tfrac{1}{2}u^{-1}(1-u)\Lambda$$
$$+2Z\alpha(u^{-5/2}(\eta_1^{\frac{1}{2}}-\bar\eta_1^{\frac{1}{2}})(\tfrac{1}{2}(1-u^2)-\tfrac{1}{6}u(1-u))$$
$$-u^{-\frac{1}{2}}\Lambda\eta_1^{\frac{1}{2}}(1-u+\tfrac{1}{2}u\lambda^2(1-v^2))$$
$$+\tfrac{1}{2}u^{-\frac{1}{2}}(\Lambda\eta_1^{\frac{1}{2}}(1-u)-(\eta_1^{\frac{1}{2}}-\bar\eta_1^{\frac{1}{2}})(1-u^2)))\big]$$
$$+2Z\alpha\int_{-1}^{1}\tfrac{1}{2}dv_1\int_{-1}^{v_1}\tfrac{1}{2}dv_2\big[-3(1-u)u^{-5/2}$$
$$\times(\eta_2^{\frac{1}{2}}-\bar\eta_2^{\frac{1}{2}})(\tfrac{1}{2}(1-u^2)-\tfrac{1}{6}u(1-3u))$$
$$+\tfrac{1}{2}\Lambda u^{-\frac{1}{2}}\eta_2^{-\frac{1}{2}}(\tfrac{1}{2}(1-u^2)\Delta v(2-\Delta v)-\tfrac{1}{2}(1+u)$$
$$\times\Lambda\Delta v(3-\Delta v)+(1-u)^2(\Delta v^2)$$
$$+(1-u)\Lambda\Delta v(1-\Delta v))\big]$$
$$+2Z\alpha\int_{-1}^{1}\tfrac{1}{2}dv_1\int_{-1}^{1}\tfrac{1}{2}dv_2\big[u^{-\frac{1}{2}}(\eta_2^{\frac{1}{2}}-\bar\eta_2^{\frac{1}{2}})(1-u)$$
$$-\tfrac{1}{2}u^{-\frac{1}{2}}(\eta_2^{-\frac{1}{2}}-\bar\eta_2^{-\frac{1}{2}})(1-u)^2((1-u)(\Delta v)^2$$
$$-(1+u)v_1\Delta v)\big]\Big\}. \quad (4.9)$$

Similar derivations give the expressions for $\bar{\mathfrak{F}}_A(\lambda^2,u)$ and $\bar{\mathfrak{F}}_B(\lambda^2,u)$:

$$\langle\bar{\mathfrak{F}}_A(\lambda^2,u)\rangle_0$$
$$=\langle\bar{\mathfrak{F}}_0(u)\rangle_0+(2Z\alpha^2|\,\varphi_0(0)\,|^2/m^2)$$
$$\times\Big\{\int_{-1}^{1}\tfrac{1}{2}dv\big[-\tfrac{1}{4}\Lambda(1-v^2)u^{-2}(2(1-u^2)$$
$$-u(1-u))-\tfrac{1}{2}\lambda^2v^2(1-u)-\tfrac{1}{2}u^{-1}\Lambda(1+u)$$
$$+2Z\alpha(u^{-5/2}(\eta_1^{\frac{1}{2}}-\bar\eta_1^{\frac{1}{2}})(\tfrac{1}{2}(1-u^2)-\tfrac{1}{6}u(1-u))$$
$$+\tfrac{1}{2}u^{-\frac{1}{2}}\lambda^2\eta_1^{\frac{1}{2}}v^2(1-u)+\tfrac{1}{2}u^{-\frac{1}{2}}\{\Lambda\eta_1^{\frac{1}{2}}(1+u)$$
$$-(\eta_1^{\frac{1}{2}}-\bar\eta_1^{\frac{1}{2}})(1-u^2)\})\big]$$
$$+2Z\alpha\int_{-1}^{1}\tfrac{1}{2}dv_1\int_{-1}^{v_1}\tfrac{1}{2}dv_2\big[-3u^{-5/2}(1-u)$$
$$\times(\eta_2^{\frac{1}{2}}-\bar\eta_2^{\frac{1}{2}})(\tfrac{1}{2}(1-u^2)-\tfrac{1}{6}u(1-3u))$$
$$+\tfrac{1}{2}u^{-\frac{1}{2}}\eta_2^{-\frac{1}{2}}(1-u)(\tfrac{1}{2}(1+u)\Lambda\Delta v(2-\Delta v)$$
$$-\tfrac{1}{2}\Lambda^2\Delta v(3-\Delta v)+(1-u)^2(\Delta v)^2$$
$$+\Lambda(1-u)\Delta v(1-\Delta v))\big]$$
$$+2Z\alpha\int_{-1}^{1}\tfrac{1}{2}dv_1\int_{-1}^{1}\tfrac{1}{2}dv_2\big[u^{-\frac{1}{2}}(\eta_2^{\frac{1}{2}}-\bar\eta_2^{\frac{1}{2}})(1-u)$$
$$-\tfrac{1}{2}u^{-\frac{1}{2}}(\eta_2^{-\frac{1}{2}}-\bar\eta_2^{-\frac{1}{2}})(1-u)^2$$
$$\times((1-u)(\Delta v)^2-(1+u)v_1\Delta v)\big]\Big\} \quad (4.10)$$

and

$$\langle\bar{\mathfrak{F}}_B(\lambda^2,u)\rangle_0$$
$$=(2Z\alpha^2|\,\varphi_0(0)\,|^2/m^2)\Big\{\int_{-1}^{1}\tfrac{1}{2}dv\big[\tfrac{1}{2}u^{-1}(\Lambda(\Lambda+1-u)$$
$$-\lambda^4u^2v^2)+\Lambda-2Z\alpha(\tfrac{1}{2}u^{-\frac{1}{2}}\eta_1^{\frac{1}{2}}(\Lambda(\Lambda+1-u)$$
$$-\lambda^4u^2v^2)+u^{-\frac{1}{2}}\eta_1^{\frac{1}{2}}\Lambda)\big]$$
$$+2Z\alpha\int_{-1}^{1}\tfrac{1}{2}dv_1\int_{-1}^{v_1}\tfrac{1}{2}dv_2\big[\tfrac{1}{2}u^{-\frac{1}{2}}\eta_2^{-\frac{1}{2}}\lambda^2(1-u)$$
$$\times((1-u)(\Delta v)^2+\Lambda(\Delta v)(1-\Delta v))\big]\Big\}. \quad (4.11)$$

Inspection shows that these functions are singular at $u=0$. The first-order terms in $\bar{\mathfrak{F}}_A$ behave as u^{-2} and the second-order terms as $u^{-5/2}$, while the contributions to $\bar{\mathfrak{F}}_B$ have singularities that are one power weaker than these. The dependence of Λ and of the η_j on λ^2, however, implies that differentiation with respect to this variable will reduce the severity of the divergence by one power. It follows that the second derivative of $\bar{\mathfrak{F}}_A$ and the first derivative of $\bar{\mathfrak{F}}_B$ will yield finite integrals over the variable u. The matrix element of the operator defined in Eq. (3.8) can therefore be approximated by a power series; the relevant quantities can be obtained very easily from Eqs. (4.10) and (4.11) and the integrations can be carried out. The result is

$$\langle\bar M'\rangle_0=(2Z\alpha^2|\,\varphi_0(0)\,|^2/m^2)\{(17/12)$$
$$+\pi Z\alpha[-2+(38/105)+(11/64)-\ln2]\}. \quad (4.12)$$

The results of the next section will show that it is instructive to carry out the integration over λ^2 in Eq. (3.8) before performing the other operations. We can then write

$$\langle\bar M'\rangle_0=\int_0^1 du\langle(\bar{\mathfrak{F}}(1,u)-\bar{\mathfrak{F}}_A(0,u))$$
$$-\bar{\mathfrak{F}}_B(0,u)-\bar{\mathfrak{F}}_A'(0,u)\rangle_0, \quad (4.11)$$

where the right-hand side, of course, is still expanded as a power series in the external field; this is indicated by the lightfaced $\mathfrak{F}$. Although the integrals of the individual terms are now infinite—it makes no sense, strictly, to discuss them separately—they will be stated:

$$\int_0^1 du\langle\bar{\mathfrak{F}}(1,u)-\bar{\mathfrak{F}}_A(0,u)\rangle$$
$$=(2Z\alpha^2|\,\varphi_0(0)\,|^2/m^2)\{\tfrac{3}{8}(-\ln u)_{u=0}-\tfrac{1}{6}$$
$$-Z\alpha[(76/36)(u^{-\frac{1}{2}})_{u=0}$$
$$-\pi(2+(11/64)-\ln2)]\}, \quad (4.14)$$

$$\int_0^1 du\langle\mathfrak{F}_B(0,u)\rangle_0$$
$$=(2Z\alpha^2|\varphi_0(0)|^2/m^2)\{(-\ln u)_{u=0}-1$$
$$-Z\alpha[4(u^{-\frac{1}{2}})_{u=0}-4\pi]\}, \quad (4.15)$$

and

$$\int_0^1 du\langle\mathfrak{F}_A'(0,u)\rangle_0$$
$$=(2Z\alpha^2|\varphi_0(0)|^2/m^2)\{-\tfrac{1}{2}(-\ln u)_{u=0}-7/12$$
$$+Z\alpha[(64/35)(u^{-\frac{1}{2}})_{u=0}-(38/105)\pi]\}. \quad (4.16)$$

V. THE EVALUATION OF $\bar{M}_0$

In order to complete the evaluation of the matrix element of the mass operator in an S-state, we must calculate the contribution of Eq. (3.6). The two parts will be discussed in order.

After the commutators are evaluated (Eq. (2.20)) and the momentum integration is carried out, the operator $\mathfrak{F}_B(0,u)$,

$$\langle\mathfrak{F}_B(0,u)\rangle$$
$$=-(\alpha/4\pi)\Big\langle\int_0^\infty ds\exp[-ism^2u]\Big|4imu(1-u)e\tfrac{1}{2}\sigma F$$
$$+e\int_0^1 dv(2-u)(\Pi_\mu\exp[iw\mathfrak{C}v](\gamma F)_\mu$$
$$-(\gamma F)_\mu\exp[-iw\mathfrak{C}v]\Pi_\mu)-e^2\int_0^1 dv4s(1-u)^2$$
$$\times mu(1-v)(\gamma F)_\mu\exp[-iw\mathfrak{C}v](\gamma F)_\mu\Big|\Big\rangle \quad (5.1)$$

can be further decomposed so as to separate first-order from second-order terms. Then, in an S-state and for an explicit second-order term, the field in the exponentials can be neglected and the usual approximation to the wave function can be made. A momentum representation of the exponential facilitates the time integration in the matrix element [see Eq. (I, 4.6)]. The Dirac matrices are eliminated by the observation that only γ_0 and $-\gamma_s^2$ have diagonal elements, and that these are unity. The last term in Eq. (5.1), for instance, becomes

$$e^2\langle(\gamma F)_\mu\exp[-iw\mathfrak{C}v](\gamma F)_\mu\rangle_0\rightarrow$$
$$|\varphi_0(0)|^2e^2\int(2\pi)^{-3}d\mathbf{p}\exp[-iwp^2v]$$
$$\times\Big(\int d\mathbf{r}'F_{\mu\nu}(\mathbf{r}')e^{i\mathbf{p}\cdot\mathbf{r}'}\Big)\Big(\int d\mathbf{r}''F_{\mu\nu}(\mathbf{r}'')e^{-i\mathbf{p}\cdot\mathbf{r}''}\Big)$$
$$=16(Z\alpha)^2|\varphi_0(0)|^2\int(d\mathbf{p}/4\pi p^2)\exp[-iw^2pv]$$
$$=8(Z\alpha)^2|\varphi_0(0)|^2(\pi/iwv)^{\frac{1}{2}}, \quad (5.2)$$

with the help of Eq. (I, 2.18). The first term in Eq. (5.1) is very simple (Eq. (2.40)),

$$\langle mc\tfrac{1}{2}\sigma F(\mathbf{r})\rangle_0=-2\pi Z\alpha|\varphi_0(0)|^2. \quad (5.3)$$

One part of the remaining term in Eq. (5.1) is rearranged according to Eq. (2.33):

$$e\int_0^1 du\exp[-ism^2u]\langle\Pi_\mu\exp[-iw\mathfrak{C}v](\gamma F)_\mu\rangle$$
$$=(ie/m^2s)\langle\Pi_\mu\exp[-iw\mathfrak{C}v-ism^2u](\gamma F)_\mu\rangle|_{u=0}^1$$
$$+(ev/m^2)\int_0^1 du\exp[-im^2su]$$
$$\times\langle\Pi_\mu\mathfrak{C}\exp[-iw\mathfrak{C}v](\gamma F)_\mu\rangle$$
$$=(ie/m^2s)\langle\Pi_\mu(\exp[-im^2s]-\exp[-is\mathfrak{C}v])(\gamma F)_\mu\rangle$$
$$-(ie^2v/m^2)\int_0^1 du\exp[-ism^2u]$$
$$\times\langle(\gamma F)_\mu(m-\gamma\Pi)\exp[-iw\mathfrak{C}v](\gamma F)_\mu\rangle. \quad (5.4)$$

When this expression is symmetrized, the matrix element of the first order terms are evaluated by Eq. (2.35), while the second-order term is treated with the help of the remarks preceding Eq. (5.2). The final contribution is more conveniently integrated by parts with respect to s,

$$e\int_0^\infty ds(-2u+u^2)\exp[-ism^2u]$$
$$\times\langle\Pi_\mu\exp[-iw\mathfrak{C}v](\gamma F)_\mu\rangle$$
$$=(i(2-u)/m^2)\Big[\langle e\Pi_\mu(\gamma F)_\mu\rangle$$
$$-(1-u)v\int_0^\infty ds\exp[-ism^2u]$$
$$\times\langle(\gamma F)_\mu(m-\gamma\Pi)\exp[-iw\mathfrak{C}v](\gamma F)_\mu\rangle\Big]. \quad (5.5)$$

The entire matrix element of $\mathfrak{F}_B(0,u)$, therefore, is equal to [see Eq. (2.35)]

$$\langle\mathfrak{F}_B(0,u)\rangle_0$$
$$=(2Z\alpha^2|\varphi_0(0)|^2/m^2)\int_0^1 dv\Big\{\ln(m/2k_0(n_0,0)v)$$
$$-2+u+(1-u)+Z\alpha\pi^{-\frac{1}{2}}\int_0^\infty ds\exp[-ism^2u]$$
$$\times[-32(ism^2)^{\frac{1}{2}}(1-u)^{\frac{1}{2}}u(1-v)v^{-\frac{1}{2}}$$
$$+16(ism^2)^{-\frac{1}{2}}v^{\frac{1}{2}}(1-u)^{-\frac{1}{2}}$$
$$+16(ism^2)^{-\frac{1}{2}}v^{\frac{1}{2}}(2-u)(1-u)^{\frac{1}{2}}]\Big\} \quad (5.6)$$

whence

$$\int_0^1 du\langle\mathfrak{F}_B(0,u)\rangle_0=(2Z\alpha^2|\varphi_0(0)|^2/m^2)\times\{\ln(m/2k_0(n_0,0))+4\pi Z\alpha\}. \quad (5.7)$$

The operator $\mathfrak{F}_A'(0,u)$ [see Eq. (2.19)],

$$\langle\mathfrak{F}_A'(0,u)\rangle=(\alpha/4\pi)\int_0^\infty ids2m(2+u)\exp[-ism^2u]\times\left\langle\tfrac{1}{2}c\sigma F+2\int_0^1 dv(1-v)\Pi_\mu\times(\exp[-iu\mathfrak{K}v]-1)\Pi_\mu\right\rangle \quad (5.8)$$

is evaluated in the same way. It contributes

$$\int_0^1 du\langle\mathfrak{F}_A'(0,u)\rangle_0=(2Z\alpha^2|\varphi_0(0)|^2/m^2)\{-\tfrac{1}{3}\ln(m/2k_0(n_0,0))-(31/36)-(38/105)\pi Z\alpha\}. \quad (5.9)$$

When these contributions are added to the result of the power series expansion, Eq. (4.12), one obtains the entire shift in an S-level due to the mass operator,[11]

$$\langle\bar{M}\rangle_0=(2Z\alpha^2|\varphi_0(0)|^2/m^2)\{\tfrac{2}{3}\ln(m/2n_0(n_0,0))+(5/9)+2\pi Z\alpha[1+(11/128)-\tfrac{1}{2}\ln 2]\}. \quad (5.10)$$

If we now compare this result with Eq. (4.14), we see that the rigorous evaluation of the effects of the soft quanta can be described by

$$(\tfrac{2}{3}(-\ln u)-(76/35)Z\alpha u^{-\frac{1}{2}})_{u=0}\rightarrow\tfrac{2}{3}\ln(m/2k_0(n_0,0))+13/18. \quad (5.11)$$

The successively more severe infrared divergences in the power series are a result of expanding the logarithm on the right-hand side about the "free particle" null value of the energy k_0. The comparison further shows that there are no corrections of order $Z\alpha$ to the logarithm itself. Since relativistic corrections to the structure of the hydrogen atom are of relative order $(Z\alpha)^2$, this result is not surprising.

VI. VACUUM POLARIZATION

The contribution from the polarization potential induced by the Coulomb field in the pair vacuum remains to be calculated. The perturbation energy is

$$\langle M^P\rangle_0=e\int d\mathbf{r}\bar{\psi}_0(\mathbf{r})V^P(\mathbf{r})\psi_0(\mathbf{r})=\int(2\pi)^{-3}d\mathbf{r}d\mathbf{k}\bar{\psi}_0(\mathbf{r})eV^P(\mathbf{k})e^{i\mathbf{k}\cdot\mathbf{r}}\psi_0(\mathbf{r}) \quad (6.1)$$

where, by Eq. (I, 2.19),

$$eV^P(\mathbf{k})=-Z\alpha^2\int_0^\infty ids\int_0^1 dvv^2(1-\tfrac{1}{3}v^2)\times\exp[-ism^2-is\tfrac{1}{4}k^2(1-v^2)]. \quad (6.2)$$

The usual approximation to the wave function, Eq. (I, 2.22), and the integrals Eq. (I, 4.23) lead immediately to the numerical result

$$\langle M^P\rangle_0=2Z\alpha^2|\varphi_0(0)|^2[-(2/15)+(5/96)\pi Z\alpha]. \quad (6.3)$$

VII. SUMMARY OF RESULTS

The insertion of the value of the hydrogenic wave function at the origin,

$$|\varphi_0(0)|^2=\pi^{-1}(Z\alpha m/n_0)^3$$

(n_0 = principal quantum number), into Eqs. (5.10) and (6.3) leads to the following more familiar form for these results:

$$\langle\bar{M}\rangle_0=\frac{8Z^4}{n_0^3}\frac{\alpha^3}{3\pi}\{\ln(m/2k_0(n_0/0))+\tfrac{5}{6}+3\pi Z\alpha[1+(11/128)-\tfrac{1}{2}\ln 2]\}\mathrm{Ry}_\infty$$

and

$$\langle M^P\rangle_0=\frac{8Z^4}{n_0^3}\frac{\alpha^3}{3\pi}\left\{-\frac{1}{5}+\frac{5}{64}\pi Z\alpha\right\}Ry_\infty.$$

The total effect of the higher order correction calculated in this paper is to raise the $2s$-level an additional amount of[12]

$$\frac{\alpha^3}{3\pi}\left[3\pi\alpha\left(1+\frac{11}{128}-\frac{1}{2}\ln 2+\frac{5}{192}\right)\right]\mathrm{Ry}_\infty=7.14\ \mathrm{Mc/sec}.$$

A complete estimate to relative order α of the $2S_{\frac{1}{2}}-2P_{\frac{1}{2}}$ displacement must also take into account the fourth-order electrodynamic corrections, but of these only the contribution of the magnetic moment is known. It decreases the splitting by 0.94 Mc/sec. Use of the new value of α then leads to the improved theoretical value of

$$\Delta E_\infty=1058.42\ \mathrm{Mc/sec}$$

for the Lamb shift in an atom with infinitely heavy nucleus. This compares favorably with the published experimental value for hydrogen, 1062 ± 5 Mc/sec. The

[11] The same result has been obtained by M. Baranger, Phys. Rev. **84**, 866 (1951) and Ph.D. thesis, Cornell (1951). We are indebted to H. A. Bethe for informing us of this calculation and to Dr. Baranger for supplying us with a copy of his thesis.

[12] A small numerical error made previously [Phys. Rev. **84**, 597 (1951)] has been corrected.

corrections of relative order $\alpha^2 \log\alpha$ that are obtained from a still more accurate treatment of the Coulomb field are probably much less than 1 Mc/sec.

Since much more precise experiments are being carried out to measure the level shift in hydrogen and deuterium, it is worthwhile to calculate the effects of the structure and of the finite mass of these nuclei. In the nonrelativistic approximation,[3] use of the Rydberg constant appropriate to the atom, rather than the one for infinite mass, provides for the reduced mass correction. The result is to reduce the level shift by 0.6 Mc/sec in hydrogen and by 0.3 Mc/sec in deuterium. The most pronounced effect of nuclear structure arises from the motion of the proton inside the deuteron. The resulting change in the Coulomb interaction energy depends on the mean square of the neutron-proton distance in the deuteron,

$$\delta E \cong \tfrac{1}{6}\pi\alpha |\varphi_0(0)|^2 \langle R^2\rangle_{Av}.$$

It can be calculated with sufficient accuracy from the asymptotic form of the deuteron wave function in terms of $d=4.314\times10^{-13}$ cm, the size of the deuteron, and $\rho=1.71\times10^{-13}$ cm, the effective triplet range:

$$\langle R^2\rangle_{Av}=\tfrac{1}{2}d^2(1-\rho/d)^{-1}.$$

The $2S$ level is therefore reached by 0.75 Mc/sec while the $2P$ levels are unaffected. These nuclear interactions change the quoted theoretical value for the level shift to

$$\Delta E_{\mathrm{H}}=1057.8 \text{ Mc/sec and } \Delta E_{\mathrm{D}}=1058.9 \text{ Mc/sec}$$

in hydrogen and deuterium, respectively.

We are indebted to Norman M. Kroll for numerous enlightening conversations.

APPENDIX

In this section we shall justify the replacement made in Eq. (2.36) of the text. We must thus establish the identity, except for terms of order $(Z\alpha)^2$,

$$-\frac{i\alpha}{3\pi m^2}\int \bar\psi_0(x')\left(x'\left|e(\gamma F)_\lambda \ln\frac{m^2}{m^2-(\gamma\Pi)^2}\Pi_\lambda - \Pi_\lambda \ln\frac{m^2}{m^2-(\gamma\Pi)^2}e(\gamma F)_\lambda\right|x''\right)\psi_0(x')d\mathbf{r}'d\mathbf{r}''dt''$$
$$=\frac{2\alpha}{3\pi m^2}\sum_n{}'|\mathbf{p}_{n0}|^2(E_n-E_0)\ln\frac{m}{2|E_n-E_0|}. \quad \text{(A.1)}$$

In the former expression we have a relativistic matrix element, in the latter, the sum over nonrelativistic Schroedinger states computed by Bethe *et al.*[10] We first note that

$$\left\langle e(\gamma F)_\lambda \ln\frac{m^2}{m^2-(\gamma\Pi)^2}\Pi_\lambda - \Pi_\lambda \ln\frac{m^2}{m^2-(\gamma\Pi)^2}e(\gamma F)_\lambda\right\rangle$$
$$=2i\left\langle \Pi_\lambda(\gamma\Pi+m)\ln\frac{m^2}{m^2-(\gamma\Pi)^2}\Pi_\lambda\right\rangle_0$$
$$=2i\left\langle \Pi_\lambda\gamma_0(H^{r1}-E_0{}^r)\ln\frac{m}{2(H^{r2}-E_0{}^r)}\Pi_\lambda\right\rangle_0, \quad \text{(A.2)}$$

after one takes advantage of the stationary character of the state $\psi_0(x)$. The superscript r denotes relativistic, whereas the additional superscript 1 or 2 distinguishes the first-order from the second-order Hamiltonian; the operator Π_λ is represented by

$$\Pi_\lambda=(\mathbf{p}, E_0{}^r-V), \quad \text{(A.3)}$$

where V is the Coulomb potential. It is apparent from the structure of Eq. (A.2) that only the space part of Π_λ need be given further consideration, since the contribution of the fourth component vanishes except for the term involving two factors of the potential energy. The integration over the space-time coordinates which are doubly primed now reduces the matrix element under discussion to the time independent expression

$$\int\psi_0{}^*(\mathbf{r}')\mathbf{p}(H^{r1}-E_0{}^r)\ln\frac{m}{2(H^{r2}-E_0{}^r)}\mathbf{p}\psi_0(\mathbf{r}')d\mathbf{r}'$$
$$=\left\langle \mathbf{p}(H^{r1}-E_0{}^r)\ln\frac{m}{2(H^{r2}-E_0{}^r)}\mathbf{p}\right\rangle_0$$
$$=(\sum_{n+}+\sum_{n-}{}')|\mathbf{p}_{n0}|^2(E_n{}^r-E_0{}^r)\ln\frac{m}{2|E_n{}^r-E_0{}^r|}. \quad \text{(A.4)}$$

The sum over positive energy states may immediately be identified, except for fine structure corrections, with the nonrelativistic sum in Eq. (A.1). In the sum over negative energy states, one is at first confronted with the large energy differences $E_n{}^r-E_0{}^r\sim-2m$. On the other hand, it is easy to prove that $|\mathbf{P}_{0n-}|^2\sim\alpha^4|\mathbf{P}_{0n+}|^2$ so that the sum over negative energy states is indeed negligible for our purposes.

Energy Levels of C^{11} and C^{12} from Photographic Plate Observation of Neutron Spectra*

VIRGIL R. JOHNSON†
University of Wisconsin, Madison, Wisconsin
(Received October 22, 1951)

The energies of neutrons from $B^{10}(d,n)C^{11}$ and $B^{11}(d,n)C^{12}$ reactions have been measured by use of photographic emulsions and enriched B^{10} targets. Neutron groups corresponding to levels in C^{11} at 1.85, 4.23, 4.77, 6.40, 6.77, 7.39, 8.08, 8.39, 8.62, and possibly 8.97 and 9.13 Mev, have been observed. Most of these levels in C^{11} show good correspondence to those previously reported for the mirror nucleus B^{11}. This correspondence supports the assumed equality of n–n and p–p forces. Neutrons from normal boron targets were observed, corresponding to levels in C^{12} at 4.4-, 9.6-, 10.8-, 11.1-, 11.74-, 12.76-, 15.09-, and 16.07-Mev excitation. There were also some indication of additional levels at 13.21-, 13.36-, 14.16-, and 15.52-Mev excitation.

INTRODUCTION

THE hypothesis that the neutron-neutron and proton-proton nuclear forces are equal has been used with considerable success in comparisons of the binding energies of the ground states of pairs of light mirror nuclei.[1] These comparisons show that almost the entire observed energy difference between the ground states can be explained by assuming that the binding energy from nuclear forces is the same in both nuclei and that they differ only in the relatively small Coulomb energies. On the basis of this hypothesis it is also expected that the excited states of mirror nuclei are similar in their excitation energies, and also in their characteristic parameters such as angular momentum and parity. Although differences in excitation energy of some of the mirror levels so far observed are larger than at first expected (particularly in the case of C^{13} and N^{13}),[2] some success has been attained in comparing corresponding excited states of mirror nuclei.[3]

The excited states of the mirror pair, B^{11} and C^{11}, are advantageous to study because of the large range of excitation energy available in these nuclei when produced by (d,p) and (d,n) reactions with B^{10}. In addition, within this excitation range both bound and virtual states occur. It may be expected that the differences in excitation energy of corresponding levels will increase on the average for virtual levels, because of a differential reduction of the Coulomb energy as the wave function spreads out.

Experimental information on B^{11} is quite extensive as to the location of levels below 10 Mev.[4] The energy level spectrum of C^{11} is not so well known. Excited states of C^{11} have been reported at 2.0 Mev by Gibson and at 4.5 and 6.7 Mev by Swann and Hudspeth.[6] The $B^{10}(d,n)C^{11}$ reaction was used in both of these experiments. Excited states at 9.7 and 10.1 Mev have been indicated by resonances in the alpha-particle yield from the $B^{10}(p,\alpha)Be^{7}$ reaction.[7] Since the above experiments did not cover the region between 7.0 and 9.5 Mev, it was desirable to extend the observations in C^{11} to include this energy region and if possible to increase the energy resolution.

EXPERIMENTAL PROCEDURE

The energy levels of C^{11} were observed by measuring the energies of neutrons produced by deuteron bombardment of B^{10} according to the reaction:

$$B^{10}+D\rightarrow C^{11}+n+6.473 \text{ Mev}.^{8} \qquad (1)$$

Monoenergetic deuterons were produced by the Wisconsin electrostatic generator and analyzed by a 90° cylindrical electrostatic analyzer. Thin targets of 96 percent enriched[9] B^{10} were produced by evaporation of elemental B^{10} from a tungsten boat onto tantalum backings. Two separate evaporations of B^{10} were carried out; the thickness of each target, which was determined by weighing before and after evaporation, was about 100 kev for 3.5-Mev deuterons. Energies of the emitted neutrons were obtained by measuring the ranges of recoil hydrogen nuclei produced by the neutrons in 200-micron thick Eastman NTA emulsions mounted 10 centimeters from the target at 0° and 80°

* Work supported by the AEC and the Wisconsin Alumni Research Foundation.
† Now at Midwest Research Institute, Kansas City, Missouri.
[1] Fowler, Delsasso, and Lauritsen, Phys. Rev. **49**, 561 (1935); E. Feenberg and E. Wigner, Phys. Rev. **51**, 95 (1937); H. A. Bethe, Phys. Rev. **54**, 436 (1938); White, Delsasso, Fox, and Creutz, Phys. Rev. **56**, 512 (1939); H. Brown and D. R. Inglis, Phys. Rev. **55**, 1182 (1939); M. Phillips and E. Feenberg, Phys. Rev. **59**, 400 (1941); D. R. Elliot and L. D. P. King, Phys. Rev. **60**, 489 (1941); E. Feenberg and G. Goertzel, Phys. Rev. **70**, 597 (1946).
[2] D. M. Van Patter, Phys. Rev. **76**, 1264 (1949).
[3] R. G. Thomas, Phys. Rev. **80**, 136 (1950); R. K. Adair, Phys. Rev. **81**, 310 (1951); E. Feenberg, Phys. Rev. **81**, 644 (1951); J. B. Ehrman, Phys. Rev. **81**, 412 (1951); D. R. Inglis, Phys. Rev. **82**, 181 (1951); S. Bashkin and H. T. Richards, Phys. Rev. **84**, 1124 (1951).
[4] Van Patter, Buechner, and Sperduto, Phys. Rev. **82**, 248 (1951).
[6] W. M. Gibson, Proc. Phys. Soc. (London) **A62**, 586 (1949).
[6] C. P. Swann and E. L. Hudspeth, Phys. Rev. **76**, 168 (1949).
[7] Brown, Chao, Fowler, and Lauritsen, Phys. Rev. **78**, 88 (1950).
[8] The value of 6.473±0.011 Mev is based on a Q of 9.235±0.011 Mev for the $B^{10}(d,p)B^{11}$ reaction obtained by Strait, Van Patter, Buechner, and Sperduto [Phys. Rev. **81**, 747 (1951)] and a Q of 2.762±0.003 Mev for the $B^{11}(p,n)C^{11}$ reaction as given by Richards, Smith, and Browne [Phys. Rev. **80**, 524 (1950)].
[9] Enriched B^{10} was obtained from the AEC Oak Ridge Laboratory.

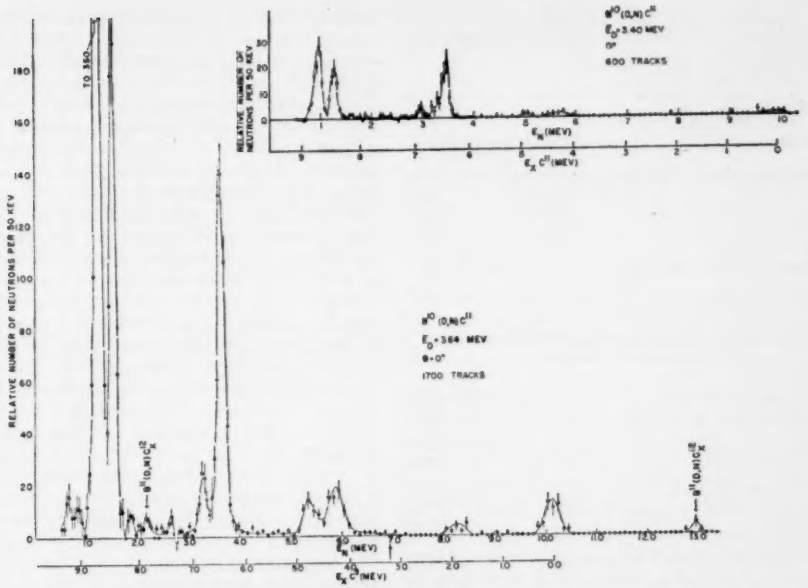

FIG. 1. Neutron spectrum at 0° from deuterons on 96 percent enriched B^{10} target. Upper curve: 3.40-Mev deuterons; lower curve: 3.64-Mev deuterons.

with respect to the incident beam. Conversion from range to energy was accomplished by means of an experimentally determined range-energy curve for the Eastman NTA emulsion. This range-energy curve was the same as that published by Richards *et al.*[10] (The neutron scale shown on the various figures in the present work was based on an earlier range-energy curve which, above 10 Mev, differs appreciably from that of reference 10. The Q values shown in the tables, however, are computed on the most recent data of reference 10.) The method of measurement and the criteria for acceptance of tracks have been described earlier.[11]

In order to eliminate from the resulting neutron spectrum the neutron group arising from the $B^{11}(d,n)C^{12}$ reaction, it was necessary to make an exposure to the neutrons from deuteron bombardment of a normal boron target. A background exposure was also made with the deuteron beam striking a bare tantalum target.

EXPERIMENTAL RESULTS ON C^{11}

One of the B^{10} targets was bombarded with deuterons of mean energy 3.40 Mev. The upper part of Fig. 1 shows the data taken at 0°. Background has been subtracted and a correction has been made for the variation with energy of the $n-p$ cross section[12] and for variation in the probability of the tracks leaving the emulsion.[13] The lower abscissa, labeled "$E_X C^{11}$", gives the excitation energy in C^{11} giving rise to emitted neutrons of the corresponding energy.

Higher energy deuterons, 3.64-Mev mean energy, and the other B^{10} target were used for the second exposure. The 0° data, corrected for background, $n-p$ cross-section variation, and geometry, is given in the lower part of Fig. 1. Because of the much lower intensity of the higher energy neutron groups, most of the measuring time was spent on tracks from neutrons of energies greater than 1.85 Mev; this accounts for the discontinuity in statistical uncertainty at this energy. Before assigning the observed groups to levels in C^{11}, it was necessary to eliminate the possibility that some of the groups might be due to neutrons from deuterons on B^{11} or on the commonly occurring contaminants, oxygen, carbon, and deuterium.

Some neutron groups were assigned to the $B^{11}(d,n)C^{12}$ reaction by comparing the neutron spectrum from the B^{10} targets with that from the normal boron target. The 0° data from the normal boron target is shown in Fig. 2; the mean bombarding deuteron energy was 3.40 Mev.

[10] Richards, Johnson, Ajzenberg, and Laubenstein, Phys. Rev. **83**, 994 (1951).
[11] Johnson, Laubenstein, and Richards, Phys. Rev. **77**, 413 (1950).
[12] R. K. Adair, Revs. Modern Phys. **22**, 249 (1950).
[13] H. T. Richards, Phys. Rev. **59**, 796 (1941).

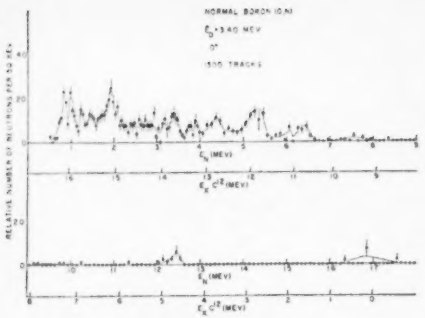

FIG. 2. Neutron spectrum at 0° from 3.40-Mev deuterons on normal boron target.

The peaks which show up in both the enriched B^{10} target data (Fig. 1) and the normal boron target data, are the ones in Fig. 2 which occur at neutron energies of 1.00, 1.25, 1.92, 3.45, and 12.5 Mev. The corresponding groups in the 3.64-Mev data of Fig. 1 are, of course, several hundred kv higher because of the higher E_D. Comparison of the relative intensities from the normal and enriched B^{10} targets shows that of these the 1.92- and 12.5-Mev groups (Fig. 2) result from the $B^{11}(d,n)C^{12}$ reaction, while the other three are from the $B^{10}(d,n)C^{11}$ reaction.

The data at 80° (Fig. 3) is of considerable help in confirming levels and in establishing the absence of contamination neutrons from deuterons on carbon, oxygen, and deuterium in the targets. No neutron groups corresponding to the $d-d$ neutron energies appear in any of the data except the 80° normal boron target data (Fig. 3) at neutron energy of 3.7 Mev. In this case it can be ruled out, since it does not appear at 6.7 Mev in the 0° data for the same target. Secondly, the neutron group at 1.87 Mev in the lower graph of Fig. 1 is at almost the correct energy for $O^{16}(d,n)F^{17}$ neutrons; however, at 80° no group corresponding to neutrons from deuterons on O^{16} appears for the same target, whereas a group does appear which would correspond to a $B^{10}(d,n)C^{11}$ group coming in at 0° at the oxygen neutron energy. Furthermore, there is no evidence on both the 0° and 80° data for neutrons corresponding to F^{17} being left in its 536-kev excited state.[14] Therefore, oxygen is not believed to be a significant contaminant. Large numbers of neutrons from carbon contamination may also be ruled out. In the 3.64-Mev data of Fig. 1 a group of neutrons occurs at 3.28 Mev, which is the energy for the C^{12} neutrons. But at 80° the energy of the neutrons from C^{12} would have shifted with respect to the neutrons from $B^{10}(d,n)C^{11}$ reaction so as to come in on the low energy side of the relatively intense peaks corresponding to formation of a level in C^{11} at 6.40 Mev. The occurrence of neutron groups in both sets of 80° B^{10} target data corresponding to the peak at 3.30-Mev neutron energy at 0° (Fig. 1), is quite good evidence that these groups result from the B^{10} reaction in which C^{11} is left in an excited state at 6.77 Mev.

The presence of some carbon contamination cannot

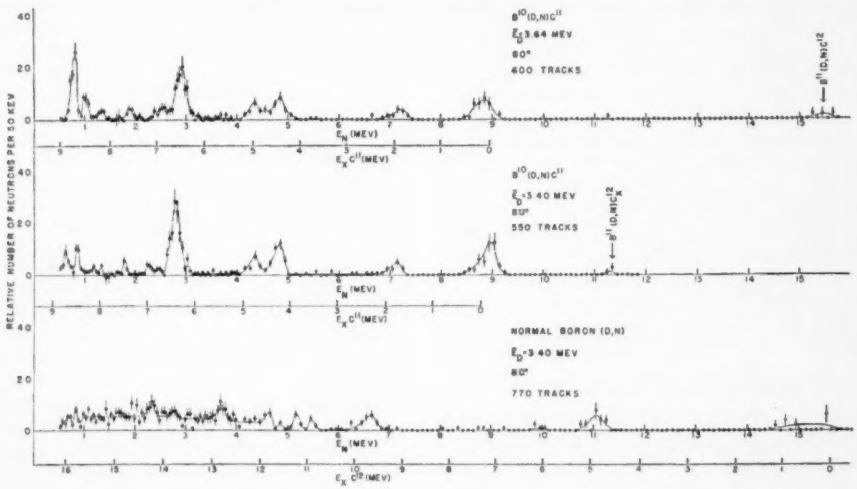

FIG. 3. Neutron spectra at 80° from 3.64-Mev and 3.40-Mev deuterons on 96 percent-enriched B^{10} and 3.40-Mev deuterons on normal boron.

[14] F. Ajzenberg, Phys. Rev. **83**, 693 (1951).

be excluded, however, even though the 6.77-Mev level of C^{11} seems well established. In fact, the weak group in the lower graph of Fig. 1 at 0.85-Mev neutron energy may be due to the $C^{12}(d,n)N^{13*}$ reaction, in which the 2.4-Mev level of N^{13} is formed.[15] Since this group is observed in only one set of data and is poorly resolved there, the level of C^{11} corresponding to it will be listed as uncertain. The low intensity group adjacent to it at 0.65-Mev neutron energy will also be listed as uncertain because it, too, is observed on but one set of data (Fig. 1). It could also possibly result from the $B^{11}(d,n)C^{12}$ reaction. If so, it corresponds to formation of C^{12} in an excited state at 16.7 Mev, a level which has been previously reported.[16]

In summary, all of the neutron groups observed in the B^{10} target data shown in Figs. 1, 2 and 3 are believed to correspond to levels in C^{11} except those marked otherwise. However, the assignment of the two lowest energy groups in the lower graph of Fig. 1 is uncertain.

As mentioned above, the background has been subtracted in all the curves. For comparison purposes the background data is shown in Fig. 4. The amount of background shown results from scanning an area on the 0° plates equivalent (for the total bombardments used) to one-third the area taken for the data of the lower part of Fig. 1 and three-fourths the area for Fig. 2. The background correction did not change the shapes of any of the curves significantly, but it did show up in an increased statistical uncertainty.

The data on C^{11} is summarized in Table I. The uncertainties in Q-values listed are estimated from the fluctuations of different sets of data. Relative intensities are corrected to the center-of-mass system; the ratios of the intensities at 0° to the intensities at 80° lab (ψ in c.m. system) are also from center-of-mass intensities.

COMPARISON OF B^{11} AND C^{11}

A comparison of the levels of B^{11} and C^{11} is shown in Fig. 5. The B^{11} levels shown, with the exception of the dotted level at 7.8 Mev, are those found by Van Patter *et al.*,[4] who used the $B^{10}(d,p)B^{11}$ reaction. A similar, though not so complete, spectrum has also been found by other workers.[17,18] The dotted level at 7.8 Mev in B^{11} was reported in the earlier work[17,18] but is apparently excluded by the recent careful work of Van Patter *et al.*[4] (however, see following discussion). Probable mirror levels are indicated in Fig. 5 by connecting lines. The poorer resolution of the photographic plate technique as compared to the method used by Van Patter *et al.*[4] prevented resolution of levels in C^{11} spaced less than 100 kev apart.

The close similarity of the level structure of B^{11} and C^{11} is very apparent in Fig. 5. There is no ambiguity in identifying the corresponding mirror levels until an excitation energy of about 6.5 Mev is reached. Then the question arises as to whether the close-spaced doublet in B^{11} at 6.76–6.81 Mev shifts to an unresolved doublet at 6.40 Mev in C^{11} or whether there is a differential shift of the members of the doublet so that the 6.77-Mev level in C^{11} corresponds to the upper level of the doublet. Only under the latter circumstance could one get a one-to-one correspondence of the higher mirror levels, if a level of B^{11} around 7.8 Mev is excluded. However, there are intensity objections to such an assignment of corresponding levels. Figure 6 shows the relative yields of the various (dp) and (dn) groups normalized to one for the ground-state transitions. The close similarity in intensity of mirror groups corresponding to <6-Mev excitation is marked. Since the higher member of the B^{11} doublet is very weak, it seems unlikely that it corresponds to the 6.77-Mev level in C^{11}. The best correspondence of intensities is obtained if one postulates that the mirror to 7.39 level of C^{11} has

TABLE I. $B^{10}(d,n)C^{11}$ yield data and the levels of C^{11}.

Excitation energy of C^{11} level (Mev)	Weighted mean Q-value (Mev)	Relative intensity in c.m. system at 0° for data of Fig. 2	Ratio of intensity at 0° to intensity at $\phi°$ in c.m. system	$\phi°$ c.m. system
0	(6.473±0.011)[a]	1.1	1.1	84.3°
1.85	4.62±0.06	0.3	0.8	84.8
4.23	2.24±0.06	1.4	1.6	85.8
4.77	1.70±0.06	1.0	1.9	87.1
6.40	0.07±0.04	5.9	3.5	87.4
6.77	−0.30±0.04	1.0	2.1	88.5
7.39	−0.92±0.04	0.2	0.8	89.2
8.08	−1.61±0.02	0.2	1.3	91.1
8.39	−1.92±0.02	5.0	12.2	92.0
8.62	−2.15±0.02	9.2	8.3	94.2
8.97[b]	−2.50±0.02[b]	0.3[b]		
9.13[b]	−2.66±0.02[b]	0.3[b]		

[a] Calculated from $B^{10}(d,p)B^{11}$ and $B^{11}(p,n)C^{11}$ reaction energies, Q_{dp} = 9.235±0.011 Mev (Strait *et al.*, Phys. Rev. **81**, 747 (1951)) and Q_{pn} = −2.762±0.003 Mev (Richards *et al.*, Phys. Rev. **80**, 524 (1950)).
[b] Assignment to C^{11} uncertain.

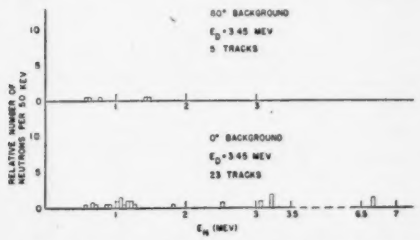

FIG. 4. Neutron background from 3.45-Mev deuteron beam on tantalum target backing.

[15] G. Goldhaber and R. M. Williamson, Phys. Rev. **82**, 495 (1951).
[16] Herb, Kerst, and McKibben, Phys. Rev. **51**, 691 (1937); Curran, Lee, and Petrzilka, Proc. Roy. Soc. (London) **A169**, 269 (1938).
[17] H. W. Fullbright and R. R. Bush, Phys. Rev. **74**, 1323 (1948).
[18] W. O. Bateson, Phys. Rev. **78**, 337 (1950); Phys. Rev. **80**, 982 (1950).

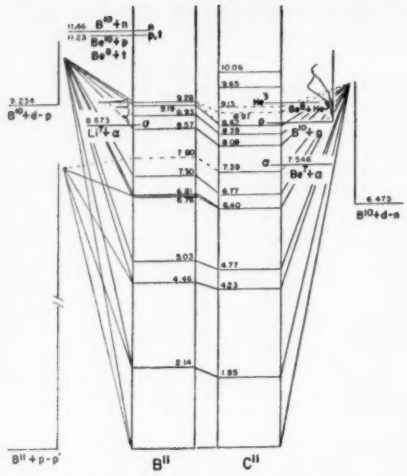

FIG. 5. Comparison of levels of B^{11} and C^{11} (ground state of C^{11} normalized to B^{11} ground state).

escaped observation in B^{11} because of its very low intensity. This hypothesis is reasonable, since the mirror proton group at Van Patter's bombarding voltage might be expected to fall in a momentum interval near the intense group of contamination protons from the $O^{16}(d,p)O^{17*}$ reaction. In fact, in Fig. 2 of reference 4 there is perhaps indication at $H\rho = 211$ kilograuss-cm of a weak group on the enriched B^{10} data which is not present on the normal boron data.[19]

Another significant feature of Fig. 6 deserves comment. One notes that experimentally, for both the (d,p) and (d,n) yields, the most intense groups correspond to low energy outgoing neutrons or protons. This result is exactly opposite to that predicted on a compound nucleus picture where one expects the intensity distribution of completely resolved groups to be weighted by the momentum of the outgoing nucleon. The marked forward bunching (by a factor of ten) in the c.m. system of some groups of the outgoing neutrons (see Table I) is also not expected on the compound nucleus picture. However, such angular distributions and intensity distributions are readily understood if the reaction proceeds chiefly by a stripping process (e.g., see Butler[20]). Also, according to Butler, the very strong forward bunching occurs only for $l=0$ deuterons. Therefore, the experimental ratio of intensities (last column, Table I) probably indicates that the 6.4-, 8.39-, and 8.62-Mev levels of C^{11} are even parity and $3/2 \leq J \leq 9/2$.

[19] Recently, Dr. A. B. Lillie of the Rice Institute has found evidence for a B^{11} level at about 8 Mev from an experiment on the $N^{14}(n,\alpha)$ reaction using 14-Mev monoenergetic neutrons. The author is grateful for permission to publish this note.

[20] S. T. Butler, Phys. Rev. **80**, 1095 (1950).

In conclusion, the correspondence of levels of the mirror nuclei B^{11} and C^{11} seems to be reasonably well established, and hence the close equality of neutron-neutron and proton-proton forces is evidenced.

LEVELS OF C^{12}

The data from the normal boron target was taken primarily for the purpose of checking assignments of neutron groups from the enriched B^{10} target. As a result, the normal boron data lack sufficient statistics to resolve clearly some of the weaker neutron groups corresponding to excited states of C^{12}. (For many of the levels, the poor statistics are partially compensated by the occurence of the corresponding neutron groups at both 0° and 80°.) There are strong $B^{10}(d,n)C^{11}$ groups (normal boron is 20 percent B^{10}) which obscure some regions of the $B^{11}(d,n)C^{12}$ spectrum. Therefore, it is emphasized that the present spectrum on C^{12} is certainly not complete. Nevertheless, several new levels in C^{12} are certainly established by the present data which is the first to explore the excitation interval 10–16 Mev and to overlap the proton capture levels observed in the $B^{11}(p,\gamma)C^{12}$ reaction.

The three intense $B^{10}(d,n)C^{11}$ neutron groups (upper part of Fig. 1) appear at the same energies (~1.0, 1.2, and 3.3 Mev) in the normal boron data (Fig. 2) and hence these groups are identified with the C^{11} level system. All the remaining groups apparently result from excited states of C^{12}.

Table II lists our best estimates of the Q-values of these groups. The indicated uncertainty is somewhat subjective, but is believed to be conservative. The present data is in agreement with previous neutron spectra concerning the existence of C^{12} levels at 4.4 and 9.6 Mev.[21] No group was resolved corresponding to

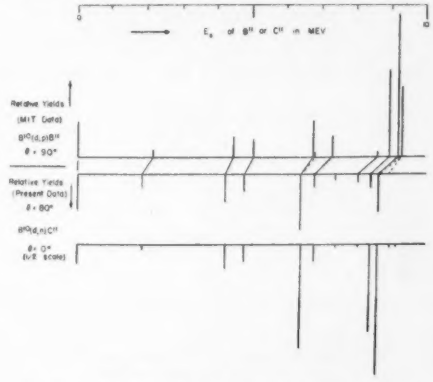

FIG. 6. Relative intensities of neutron and proton groups from $B^{10}(d,p)B^{11}$ and $B^{10}(d,n)C^{11}$.

[21] Hornyak, Lauritsen, Morrison, and Fowler, Revs. Modern Phys. **22**, 325 (1950); R. Malm and W. W. Buechner, Phys. Rev. **81**, 519 (1951).

the previously reported 7-Mev level, although a few recoil tracks were observed in this region. The 10.8-Mev level here observed has also been inferred from a neutron threshold in the $Be^9(\alpha,n)C^{12}$ reaction and possibly from the B^{12} beta-decay and $C^{12}(p,p')C^{12}$ reaction (see reference 21).

In addition to producing neutron groups of discrete energies, one must consider the possibility that deuterons on B^{11} can produce a continuum of neutron energies by the three- and four-particle break-up of the compound nucleus. For example, the following modes of disintegration are energetically possible: Be^8+He^4+n or $3\ He^4+n$, or, more likely, by the "cascade" disintegration of C^{13} first into $Be^{9*}+He^4$ or Be^8+He^5 and then into Be^8+He^4+n. The presence of a continuum corresponding to C^{13} excitation energies between 11.5 and 16.3 Mev cannot be ruled out on the basis of the data obtained. However, the occurrence of some unresolved or very broad states of C^{13} would account adequately for the "background" in this energy range.

The author is indebted to Dr. H. T. Richards for invaluable help throughout the course of the work. The author is also grateful to Miss Fay Ajzenberg for development of the plates and for help in exposing the plates and to Dr. G. Goldhaber for assistance in exposing the plates.

TABLE II. Q-values for the $B^{11}(d,n)C^{13}$ reaction and the corresponding energy levels of C^{13}.

Q value (Mev)	Excitation energy C^{13} Mev
(13.740 ± 0.014)[a]	0
(9.30 ± 0.02)[a]	4.44
4.1 ± 0.1	9.6
2.9 ± 0.1	10.8
2.6 ± 0.1	11.1
2.00 ± 0.08	11.74
0.98 ± 0.08	12.76
0.53 ± 0.05	13.21
0.38 ± 0.05 one level (?)	13.36 one level at 13.3 (?)
-0.42 ± 0.05 (?)	14.16 (?)
-1.35 ± 0.03	15.09
-1.78 ± 0.03 (?)	15.52 (?)
-2.33 ± 0.03	16.07

[a] These Q-values are computed from disintegration data (as described in reference 10) not from the present neutron data.

A New "Double Resonance" Method for Investigating Atomic Energy Levels. Application to Hg $^3P_1$*

JEAN BROSSEL† AND FRANCIS BITTER
Research Laboratory of Electronics, Massachusetts Institute of Technology, Cambridge, Massachusetts
(Received December 17, 1951)

Excitation of atoms in a vapor by polarized light produces unequal population of the magnetic sublevels of the excited state. The emitted optical resonance radiation is therefore partly polarized. The application of radiofrequency or microwave fields at a magnetic resonance frequency will induce transitions between sublevels of the excited state. The degree of polarization of the emitted optical resonance radiation is altered when the magnetic resonance condition is fulfilled. As suggested by Brossel and Kastler, this effect may be used to reveal the structure of the energy level. A detailed theory applicable to, and experiments on the $^3P_1$ state of all the isotopes of mercury are reported. The results obtained indicate that double resonance phenomena constitute a valuable new tool for investigating the structure of atomic energy levels. The mean life of the $^3P_1$ state is shown by observations on the resonance line widths to be 1.55×10^{-7} sec for all the isotopes. The g-factor of the $^3P_1$ state for isotopes with zero spin, measured in terms of the proton g-factor, is 1.4838 ± 0.0004.

INTRODUCTION

THE only means available at present for investigating the internal structure of nuclei involves accurate determinations of nuclear moments and hyperfine structures.[1] These determinations have previously been made by magnetic resonance experiments on the ground state of atoms or molecules in a beam or on diamagnetic liquids. In such experiments magnetic dipole transitions are induced by an oscillating magnetic field. If, in the sample being investigated, there is an initial inequality in the population of the magnetic sublevels of any given state, the net effect of the transitions induced by the oscillating magnetic field is to change this inequality and therefore to modify any property depending on it. In an atomic or molecular beam experiment the number of particles having a given trajectory through the apparatus is altered. In a nuclear resonance experiment, the degree of magnetization of the core of a coil, and therefore its impedance, is altered. A further possibility, having the great advantage of extending observations to the excited states of atoms, is to detect magnetic resonance in an energy level by observing changes in the optical radiation involving transitions from or to that level.[2]

The present paper gives an analysis and a detailed description of effects first observed in 1950,[3] based on suggestions put forward by Brossel and Kastler.[4] Excitation of a level by optical resonance radiation with polarized light provides the initial inequality of population in the Zeeman pattern of the excited state. The degree of polarization of the light spontaneously reemitted depends on this initial inequality and changes when it is altered by magnetic resonance absorption. This is the physical basis of the observations reported below.

Changes in frequency of the optical resonance radiation caused by magnetic resonance among the sublevels of either the upper or lower of the energy levels involved in the radiation process have also been predicted.[2] Such changes have been observed by Autler and Townes[5] in a somewhat analogous case in molecular spectra but are much too small to be significant for the atomic spectra discussed in the following.

GENERAL DISCUSSION OF EFFECTS IN MERCURY VAPOR

Mercury was the element studied experimentally. Naturally occurring mercury was used for the investigation of isotopes with even mass number and zero nuclear spin. Samples enriched in Hg^{199} and Hg^{201} were supplied by the Atomic Energy Commission for the investigation of these isotopes. Isotopic abundances of the samples used are shown in Table I.

The level studied was the $^3P_1$ excited state reached by excitation with the intercombination line $^1S_0-^3P_1$, having a wavelength 2537A. A diagram of the transitions involved and of the hyperfine structure of the line is shown in Fig. 1. The ground state is a diamagnetic $^1S_0$ state. The optical transition probabilities have been computed using the formulas of Hill[6] and Inglis[7] and are shown in Fig. 2 for the weak field case of no decoupling of the nuclear and electronic angular momenta. In this diagram the vertical arrows correspond

* This work has been supported in part by the Signal Corps, the Air Materiel Command, and ONR.
† Joint fellow of Spectroscopy Laboratory and Laboratory for Nuclear Science and Engineering.
[1] A. Bohr, Phys. Rev. **73**, 1109 (1948); F. Bitter, Phys. Rev. **76**, 150 (1949); A. Bohr and F. Weisskopf, Phys. Rev. **77**, 94 (1950).
[2] F. Bitter, Phys. Rev. **76**, 833 (1949); M. L. Pryce, Phys. Rev. **77**, 136 (1950).
[3] Brossel, Sagalyn, and Bitter, Phys. Rev. **79**, 196, 225 (1950). Attention is also called to the pioneering work of E. Fermi and F. Rasetti [Nature **115**, 764 (1925); and Z. Physik **33**, 246 (1925)], who first observed the depolarization of the resonance radiation of mercury by radiofrequency magnetic fields.
[4] J. Brossel and A. Kastler, Compt. rend. **229**, 1213 (1949).
[5] S. H. Autler and C. H. Townes, Phys. Rev. **78**, 340 (1950).
[6] E. H. Hill, Proc. Nat. Acad. Sci. **15**, 779 (1929).
[7] D. Inglis, Z. Phys. **84**, 466 (1933).

to transitions with $\Delta m_F=0$, or plane polarized π-radiation in absorption or emission with the electric vector parallel to the applied field, and diagonal arrows correspond to transitions with $\Delta m_F=\pm 1$ or circularly polarized σ-radiation.

For isotopes with even mass number [shown in Fig. 2(a)] π-excitation leads to the middle upper state only, and in the absence of perturbations, the reemitted radiation contains this π-component only. The experiment then consists of the application of a radio-frequency field which transfers atoms to the states with $m=\pm 1$ when the magnetic resonance condition $\omega=\gamma H_z$ is fulfilled. Here ω is the frequency of the oscillating field, H_z is the constant magnetic field, and γ is the gyromagnetic ratio of the state in question, namely, the $^3P_1$ state. When the resonance condition is fulfilled, the intensity of the π-component diminishes, and that of the σ-component increases. These changes were observed and used to detect resonance.

Collisions involving excited atoms will modify the aforementioned simple description, since atoms can then be reoriented not only by the absorption of rf energy, but also as a result of inelastic collisions. According to previous work,[8] the vapor pressure of mercury at -15°C is low enough so that the effect of such collisions is negligible, but this is not true at 0°C, the temperature used in the experiments to be described. At this temperature a considerable fraction of the atoms excited to the level with $m=0$ are transferred by collisions to the levels with $m=\pm 1$, and the reemitted light is partly depolarized even in the absence of an oscillating field. This depolarization of resonance radiation as a result of inelastic collisions will reduce the magnitude of the signal to be expected when an oscillating field is applied, and will shorten the mean life of an atom in any given excited level. No experimental investigation of these effects was undertaken. It is simply assumed that magnetic relaxation phenomena may affect the two quantities just mentioned, but may otherwise be neglected.

The effects to be expected have been analyzed in considerable detail.[9] A summary of results will be given here. The problem concerns the reorientation of a magnetic dipole with fixed total angular momentum. This situation was analyzed in a very general way by Majorana[10] and by Rabi,[11] who derived the expressions for the required transition probabilities. An angular momentum F in one of its substates m_F is in a rotating field H_1 at right angles to a constant field H_z. Under these conditions the probability of transitions to another state m_F' is considered. For simplicity we shall write the magnetic quantum numbers without the subscript F. Modifications caused by use of linearly oscillating rather than rotating fields have been considered by Bloch and Siegert.[12] These modifications are negligible

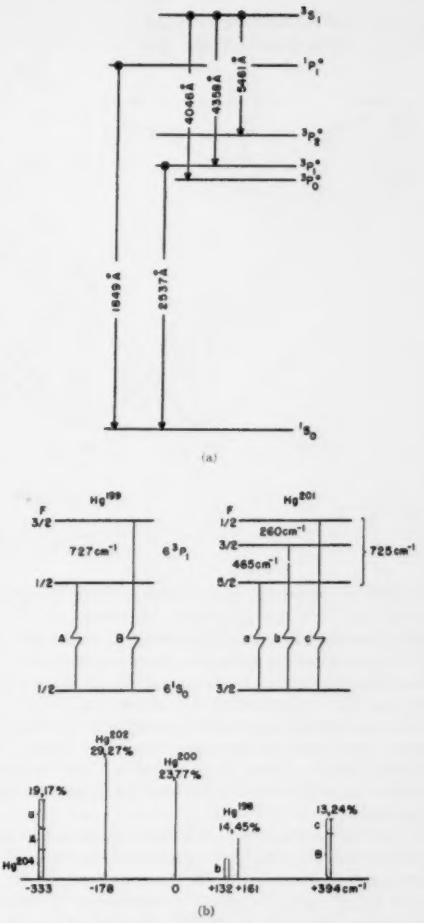

FIG. 1. (a) The low-lying energy levels of mercury; (b) the hyperfine structure of the resonance line.

TABLE I. Isotopic abundances of the samples of mercury used.

	Percent of isotopes with even mass number	Percent 199	Percent 201
Natural Hg	69.80	17.0	13.2
Enriched Hg^{199}	32.27	62.5	5.23
Enriched Hg^{201}	37.3	4.76	57.9

[8] V. von Keussler, Ann. Physik **82**, 793 (1927).
[9] F. Bitter and J. Brossel, Technical Report No. 176, Research Laboratory of Electronics, M.I.T. (hereafter called simply Technical Report No. 176).
[10] E. Majorana, Nuovo cimento **9**, 43 (1932).
[11] I. I. Rabi, Phys. Rev. **51**, 652 (1932).
[12] F. Bloch and A. Siegert, Phys. Rev. **57**, 522 (1940).

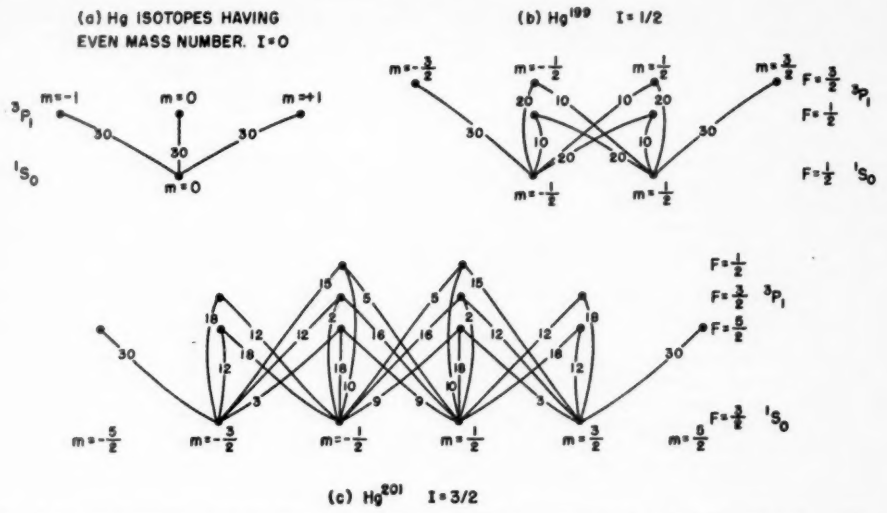

FIG. 2. Transition probabilities for the components of the resonance line of mercury (a) for isotopes and even mass number, (b) for Hg^{199} with $I=1/2$, and (c) for Hg^{201} with $I=3/2$.

for most purposes. We shall return to their discussion further on. For rotating fields Majorana and Rabi derive an expression for the probability that a system of total angular momentum F, known to be in a state m at time $t=0$, shall be in a state m' at some later time t. We designate this transition probability by $P(F, m, m', t)$. It is rigorously derived from the Schroedinger time dependent equation and is not arrived at by perturbation theory. It is therefore valid for large amplitudes of the rotating field and for large values of the time.

Let ω be the frequency, in radians per second, of the rotating field H_1. The gyromagnetic ratio is $\gamma=ge/2Mc$. The Larmor frequency ω_0 in the constant field H_z is given by $\omega_0=\gamma H_z$. The Landé g-factors for the various isotopes of mercury in the $^3P_1$ state in question are given in Table II. The values listed have only a limited validity, since g_J is computed on the assumption of L-S coupling which is surely not rigorously valid for the $^3P_1$ state of mercury. If it were, transitions to the ground state, which is a singlet state, would be forbidden, whereas in fact, the life of the metastable triplet state is of the order of 10^{-7} sec.

We now define an angle, α, by the relation

$$\sin^2\frac{\alpha}{2}=\frac{(\omega/\gamma H_1)^2}{1+[1+(H_z/H_1)]^2}\cdot\frac{(\gamma H_1)^2}{(\gamma H_1)^2+(\omega-\omega_0)^2}\cdot\sin^2\tfrac{1}{2}[(\gamma H_1)^2+(\omega-\omega_0)^2]^{\frac{1}{2}}t. \quad (1)$$

This is a periodic function of the time. The amplitude of this periodic function is shown in Fig. 3. From an inspection of this illustration it is clear that for $H_z/H_1 \gtrsim 10$ the function plotted has a maximum near $\omega=\omega_0$, and Eq. (1) may be written, to a good approximation,

$$\sin^2\frac{\alpha}{2}=\frac{(\gamma H_1)^2}{(\gamma H_1)^2+(\omega-\omega_0)^2}\times\sin^2\tfrac{1}{2}[(\gamma H_1)^2+(\omega-\omega_0)^2]^{\frac{1}{2}}t. \quad (2)$$

In terms of this angle α the required transition probabilities given by the Majorana formula are

$$P(F, m, m', t)=(\cos\tfrac{1}{2}\alpha)^{4F}(F+m)!(F+m')!(F-m)!(F-m')!\times\left[\sum_{n=0}^{2F}\frac{(-1)^n(\tan\tfrac{1}{2}\alpha)^{2n-m+m'}}{n!(n-m+m')!(F+m-n)!(F-m'-n)!}\right]^2. \quad (3)$$

The simplest case is for $F=1/2$. The aforementioned formula then reduces to

$$P(\tfrac{1}{2}, \tfrac{1}{2}, -\tfrac{1}{2}, t)=\sin^2\left(\frac{\alpha}{2}\right)=\frac{(\gamma H_1)^2}{(\gamma H_1)^2+(\omega-\omega_0)^2}\times\sin^2\tfrac{1}{2}[(\gamma H_1)^2+(\omega-\omega_0)^2]^{\frac{1}{2}}t.$$

Transitions induced by the oscillating field will take place with appreciable probability in a radiating vapor if the above transition probability has an appreciable value within the lifetime of the excited state. For example, for lifetimes of the order of 10^{-7} sec we must

have γH_1, of the order of 10^7 sec^{-1}, or since $\gamma \sim 10^7$, we must have rotating fields of the order of a gauss.

Effects caused by transitions induced by the rotating magnetic field must now be combined with effects caused by transitions involving optical resonance radiation. We shall describe here procedures to be followed in making the calculations and leave the discussion of specific formulas to later parts of this paper where they will be compared with experimental results.

Let n be the number of optical quanta absorbed per second involving transitions from some one particular magnetic sublevel of the ground state, designated by m_g, to one particular magnetic sublevel of the excited state, designated by the two quantum numbers F and m. The number of atoms excited in an interval of time dt at the time $t=0$ is then ndt. If T_e is the mean life of atoms in the excited state, the number of atoms remaining in the excited state after a time t has elapsed is $ndte^{-t/T_e}$. If the excited atoms were in a rotating magnetic field during the entire time interval t, the number in a sublevel m' of the excited state at the time t is $nP(F, m, m', t)e^{-t/T_e}dt$.

We wish to compute the total number of excited atoms in a vapor in the sublevel m'. We have just derived the number which had been in the excited state for a time between t and $t+dt$. Evidently, the total number may be arrived at by integrating

$$N_{m'} = \int_0^\infty nP(F, m, m', t)e^{-t/T_e}dt. \tag{4}$$

In this expression the excitation rate is obtained from the steady state condition $n=N_m/T_e$, where $N_m \sim A_{m,m_g}N_{m_g}I_0$. The coefficient A_{m,m_g} is the transition probability between an excited sublevel m and a ground state sublevel m_g shown in Fig. 2. N_{m_g} is the number of atoms in the ground state sublevel in question, and I_0 is the intensity of the light used to produce the excitation. The only one of these quantities requiring further discussion is N_{m_g}. For practically realizable intensities of illumination the fraction of the atoms in a vapor which are in an excited state at any instant is very small and may be neglected in comparison with the number in the ground state. Normally thermal relaxation processes insure that the various magnetic sublevels of the ground state are equally populated. The use of polarized resonance radiation may upset this thermal equilibrium, particularly when circularly polarized radiation is used. Such effects are not important in the experiments discussed here, and we shall therefore neglect them in this discussion. For isotopes with even mass number N_{m_g} is simply the total number of such atoms present. For Hg^{199} with a spin of $\frac{1}{2}$ there are two ground-state sublevels, and $N_{m_g}=N_{199}/2$. For Hg^{201} with a spin of $\frac{3}{2}$ there are four sublevels, and $N_{m_g}=N_{201}/4$.

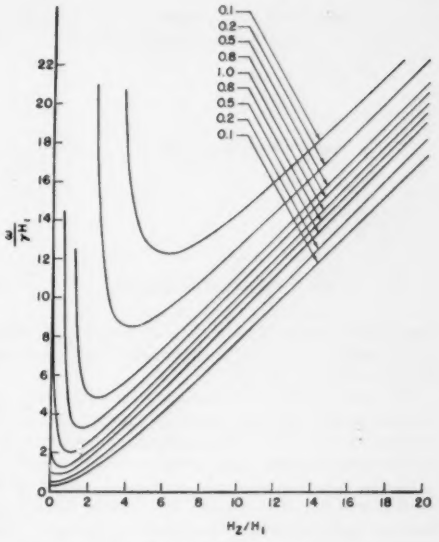

FIG. 3. A contour plot of
$(\omega/\gamma H_1)^2/1+[1+(H_z/H_1)]^2\cdot(\gamma H_1)^2/[(\gamma H_1)^2+(\omega-\omega_0)^2]$.

The intensity of the light radiated by atoms which have been excited from m_g to m, transferred from m to m', and which finally decay from m' to m_g' is proportional to

$$N_{m'}A_{m',m_g'}.$$

$N_{m'}$ is given by Eq. (4), and the transition probability A is that shown in Fig. 2. The dependence of the state of polarization of the resonance radiation on the magnitude and frequency of the rotating magnetic field may then be obtained by summing over the various levels involved. In general, in a vapor containing a mixture of isotopes, several optical frequencies will be absorbed and some assumption must be made regarding the structure of the resonance line used [see Fig. 1(b)].

TABLE II. The Landé g-factors for the $^3P_1$ state of the isotopes of mercury computed from the relation

$$g_F = g_J\frac{F(F+1)+J(J+1)-I(I+1)}{2F(F+1)} - g_I\frac{F(F+1)+I(I+1)-J(J+1)}{2F(F+1)}$$

$$g_J = 1+\frac{2J(J+1)+S(S+1)-L(L+1)}{2J(J+1)}.$$

Isotopes with even mass number	F / I	g_F / $3/2$
Hg^{199}	3/2	$1-1.81\times10^{-4}$
	1/2	$2+1.81\times10^{-4}$
Hg^{201}	5/2	$\frac{5}{3}+1.19\times10^{-4}$
	3/2	$\frac{2}{3}+1.46\times10^{-4}$
	1/2	$-1+3.31\times10^{-4}$

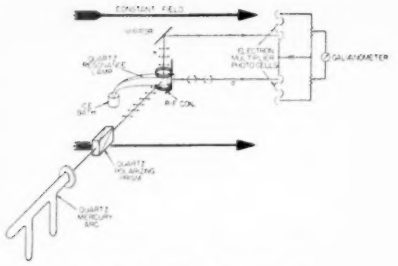

FIG. 4. Diagram of the apparatus.

The simplest assumption is that of "broad line" excitation, and this was used in the detailed calculations of Technical Report No. 176.

The aforementioned transitions refer exclusively to changes in the magnetic quantum number of a rigid rotator with a given total angular momentum F. Observations involving such transitions may be used to determine the gyromagnetic ratio of an atom in a particular state. High frequency magnetic fields may also be used to induce transitions resulting in the reorientation of the nucleus in the field of the electrons. Observations on such transitions give information on the hyperfine structure of a level and may be used to compute nuclear moments. Such transitions, however, are not reported in this paper.

EXPERIMENTAL ARRANGEMENTS

The apparatus used is illustrated in Fig. 4. Light from a low pressure mercury lamp made by Hanovia, operated at 150 ma and cooled with an air blast, is collimated by a quartz lens and polarized by a Glazebrook prism cemented with glycerine. This light is allowed to fall on one of the five mutually perpendicular faces of a fused quartz resonance lamp. The liquid mercury in the tail of the lamp was kept at a temperature of 0°C. The light incident on the lamp was polarized with its electric vector parallel to the constant field H_z. In other words, only the π-component was used for excitation in these experiments. A magnetic field of a few hundred gauss is produced by Helmholtz coils. The σ-component of the resonance radiation may be observed in the direction of this constant field, and both σ- and π-components may be observed at right angles to this field. Around the lamp are a few turns of water-cooled copper tubing forming part of a tuned radiofrequency circuit inductively coupled to a generator capable of supplying up to 100 watts. At maximum rf power the resonance lamp lights up if it is not very well evacuated or if traces of mercury have deposited on the windows of the lamp. The axis of the rf coils is at right angles to the constant field.

In the first experiments attempted, changes were observed in the intensity of the σ-component of the resonance radiation in the direction of the constant field. The intensity of the light emitted by the mercury arc lamp was found to be constant to only about 3 percent, so that small changes in intensity were difficult to measure against this fluctuating background. The sensitivity of the apparatus was greatly improved by the introduction of an optical bridge.[13] Two photomultiplier tubes are used. One of these receives the σ-component in the direction of the field, and the other receives the π-component or the π- and σ-components emitted at right angles to the field. The resistors shown in the illustration are so adjusted that under normal operation no current flows in the galvanometer. This was found to eliminate fluctuations in the galvanometer deflection resulting from fluctuations in the brightness of the light source. When magnetic resonance increases the intensity of the σ-component at the expense of the π-component, the balance of the bridge is upset, and the resulting galvanometer deflection measures directly the quantity desired. The response is linear. Galvanometers with sensitivities up to 10^{-11} amp/mm and periods from 10 to 40 seconds were used. The fluctuation in zero of the galvanometer was about that to be expected due to the IP28 phototubes, but some of this noise may have been caused by spontaneous fluctuations of the polarization of the resonance radiation. Without the optical bridge the random movements of the galvanometer were about 30 times as large.

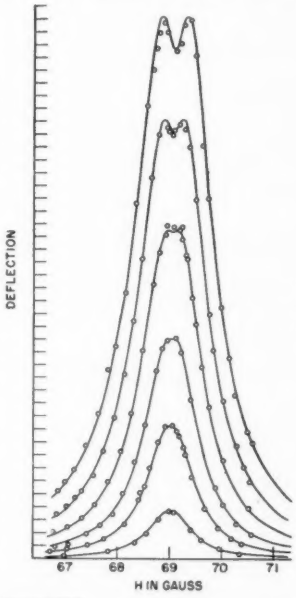

FIG. 5. Resonances observed in isotopes having even mass number and zero nuclear spin.

[13] O. Oldenberg and H. P. Broida, J. Opt. Soc. Am. **40**, 381 (1950).

No measurements were made of the absolute magnitude of the oscillating field. Relative measurements were made by means of a crest voltmeter in an auxiliary inductively coupled circuit and are considered reliable to about 1 percent.

Magnet currents were measured with a Leeds and Northrup Type K_2 potentiometer, with the auxiliary shunt kept at 0°C. Two magnets were used. The first, having a uniformity of only about one part in 10^3 over the volume of the resonance lamp, was used for the determination of line shape and of the mean life of the $^3P_1$ state. The second was uniform to better than one part in 10^4 over the region occupied by the lamp and was used in the determination of the gyromagnetic ratio. This magnet was calibrated by means of proton resonances at 1.6, 0.812, 0.530, and 0.350 Mc/sec. The local earth's field was evaluated by making resonance measurements with the magnet current flowing in both senses through the magnet.

OBSERVATIONS ON ISOTOPES WITH EVEN MASS NUMBER

With the aforementioned apparatus operated at frequencies from 50 to 150 Mc/sec, resonance curves such as are plotted in Fig. 5 are obtained. They show, at one given frequency, galvanometer deflections as a function of the applied constant field for various rf amplitudes. Increasing the rf amplitude produces a stronger and wider line and also produces characteristic changes in the line shape. All of these features, as we shall see, are accounted for by Eq. 4. In Technical Report No. 176 it is shown that for the case in question involving integrals containing $P(1, 0, 1, t)$, the galvanometer deflection should be proportional to a quantity which we call B:

$$B=\frac{I_0}{2}\frac{(\gamma H_1)^2}{(\gamma H_1)^2+(\omega-\omega_0)^2}\left[\frac{(\gamma H_1)^2}{(1/T_e)^2+4(\gamma H_1)^2+(\omega-\omega_0)^2}+\frac{(\omega-\omega_0)^2}{(1/T_e)^2+(\gamma H_1)^2+(\omega-\omega_0)^2}\right]. \quad (5)$$

This represents a bell-shaped curve for values of $\gamma H_1 \ll 1/T_e$, but for $\gamma H_1 \gg 1/T_e$ the curve has two maxima. The separation between these maxima is $\sqrt{2}H_1$, and the ratio of the intensity at maximum to that at resonance is, in the limit for large rf power, 4/3.

A detailed check of Eq. (5) was undertaken. One finds for the intensity at resonance

$$B_r=k\frac{(\gamma H_1)^2}{4(\gamma H_1)^2+(1/T_e)^2}, \quad (6)$$

where k is an arbitrary constant. In order to check this equation the quantity H_1^2/B_r was plotted as a function of H_1^2 in arbitrary units. The result is shown in Fig. 6(a). It is clear that this aspect of the theory is well borne out by the experiments. In the absence of an absolute determination of H_1, however, it is not possible to deduce T_e from this relation. Another procedure was adopted to determine this quantity. From Eq. (6) it is possible to compute the width of the resonance line $\Delta\omega$ when the amplitude is half its value at resonance, as a function of H_1. For our purposes the complete expression is not important. The first two terms in a power series expansion are

$$\Delta\omega^2=(4/T_e^2)[1+5.8(\gamma H_1 T_e)^2]. \quad (7)$$

The form of this expression is also experimentally verified for the range of rf amplitudes used, as is shown in Fig. 6(b) where the experimental data are plotted in arbitrary units. It is possible, however, to plot this data using the correct units. The half-width of the resonance curve in frequency units may be obtained from the observed half-width in gauss and the known

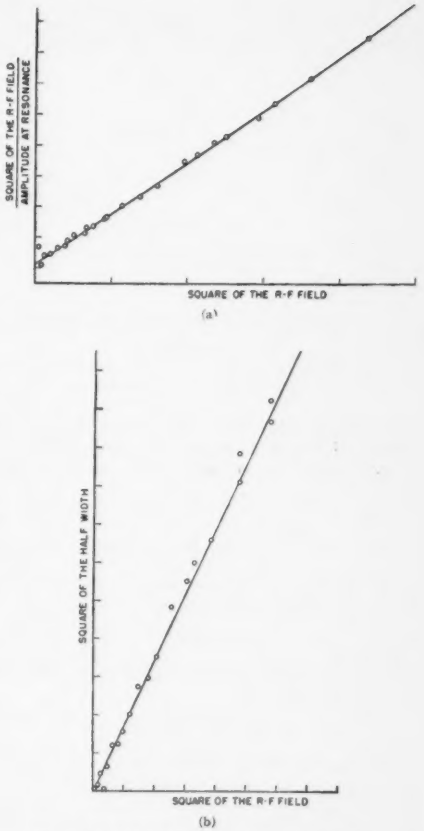

FIG. 6. (a) A plot of Eq. (6); (b) a plot of Eq. (7).

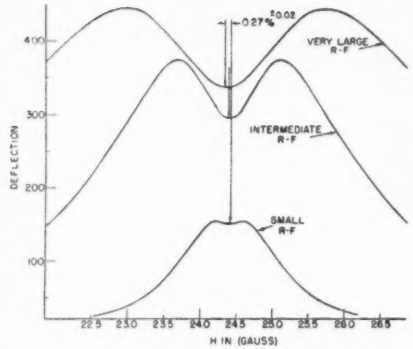

FIG. 7. Experimental verification of the expected shift of the resonant frequency with rf amplitude.

gyromagnetic ratio. The value of $(\gamma H_1 T_e)^2$ for any arbitrary setting of the rf amplitude may be obtained as follows. Calling the ordinate of Fig. 6(a) y, we may write

$$y=\frac{H_1^2}{B_r}=[4(\gamma H_1 T_e)^2+1]/k\gamma^2 T_e^2, \tag{8}$$

and for the value of y when $H_1=0$,

$$y_0=1/k\gamma^2 T_e^2. \tag{9}$$

Combining (8) and (9), we have the measurable dimensionless quantity

$$(y-y_0)/y_0=4(\gamma H_1 T_e)^2, \tag{10}$$

which may be used in plotting Eq. (7). By means of this procedure the value of the numerical coefficient 5.8 was verified, and the mean life of the excited state was obtained by extrapolation to zero amplitude of the rf field. This was done at frequencies of 50, 100, 120, and 144 Mc/sec. The same value was obtained from all these measurements with a total spread of 1 percent. The value obtained in this way for the mean life of the $^3P_1$ state of the even isotopes of Hg is 1.55×10^{-7} sec.[14] The true value may be somewhat longer because the broadening of the line as a result of collisions and field inhomogeneities was not explicitly taken into account. The above value is about 30 percent longer than the previously accepted value, obtained, not too consistently, by conventional optical methods. As we shall report further on, the same value was found for Hg^{199} and Hg^{201} within the experimental error.

The line shape itself, as given by Eq. (5), was then checked in the following way. T_e was given the above value. H_1 was obtained from experimental determinations of $\gamma H_1 T_e$ as aforementioned. The arbitrary constant determining the magnitude of the galvanometer deflection was chosen so that the greatest deflection at resonance coincided with the observed value. The parameters I_0, T_e, and H_1 being determined, a complete plot of Eq. (5) was made. This is shown in the solid curves of Fig. 5. In these curves the parameter $\gamma H_1 T_e$ assumes values up to 0.7. The experimental points corresponding to these curves are also plotted. The agreement seems to be entirely satisfactory and leaves little doubt as to the adequacy of the above theoretical discussion. Observations made at different frequencies proved that the resonant frequency is a linear function of the magnetic field to within one part in 5000.

At 50 Mc a slight shift in the resonance frequency with rf amplitude was observed at large rf amplitudes, as predicted by Bloch and Siegert,[12] when a linearly oscillating rather than a rotating field is used. As shown in Fig. 7, at high rf fields the resonant field for a given frequency is smaller than at low rf fields. The shift is predicted to be proportional to $(H_1/H_s)^2$. This dependence was roughly verified, but the magnitude of the observed shifts was 30 percent greater than the predicted shift. This discrepancy is not considered significant because the equivalent rotating field H_1 was arrived at only indirectly and because the oscillating field was certainly not completely linear, but somewhat elliptical.

The Landé g-factor for the $^3P_1$ state of the isotopes with zero spin was determined by measuring both the frequency and the field required to establish the resonance condition illustrated in Fig. 5. Frequency determinations were made with a Signal Corps BC 221 frequency meter and are considered reliable to one part in 10,000. The field was measured in terms of a proton resonance, so the computation takes the form

$$g=g_{\text{proton}}\times\frac{m}{M}\times\frac{\omega_{\text{Hg}}}{\omega_{\text{proton}}}. \tag{11}$$

Using 5.58501 for the gyromagnetic ratio of the proton[15] and 1836.12 for the ratio of the mass of the proton to

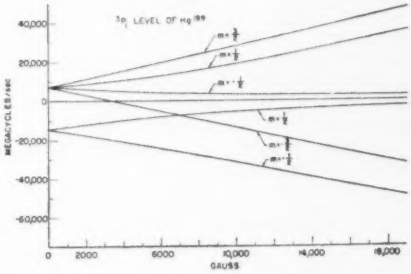

FIG. 8. Zeeman effect of the hyperfine structure of the $^3P_1$ level of Hg^{199}.

[14] J. Brossel, Phys. Rev. **83**, 210 (1951).

[15] Sommer, Thomas, and Hipple, Phys. Rev. **82**, 697 (1951).

that of the electron,[15] we find for the desired g-factor

$$g=1.4838+0.0004. \quad (12)$$

EXPERIMENTS ON Hg^{199} AND Hg^{201}

The 199 isotope with a nuclear spin of 1/2 has two hyperfine structure levels in the $^3P_1$ state with $F=1/2$ and $F=3/2$, as shown in Fig. 8. The use of π-excitation does not lead to any inequality of population of levels with $m=\pm 1/2$ [see Fig. 2(b)]. For this reason excitation to $F=1/2$ and magnetic resonance in this level produces no changes in polarization of the resonance radiation. Magnetic resonance in this level can therefore not be observed. However, magnetic resonance in the level with $F=3/2$ was observed and studied in some detail.

At 144 Mc the decoupling of I and J is sufficient to make the three frequencies $(-3/2\rightarrow -1/2)$, $(-1/2\rightarrow 1/2)$, and $(1/2\rightarrow 3/2)$ slightly different. The Zeeman effect of this case was computed following Inglis[7] and is shown in Fig. 8. The line corresponding to the transition $(-1/2\rightarrow 1/2)$ is not observable with π-excitation because the levels in question are equally populated. The other two transitions are displaced with respect to each other by an amount, in frequency units, equal to (Zeeman separation)^2/hfs separation, or $(150\times 10^6)^2/2\times 10^{10}$. This separation is only a small fraction of the line width, and therefore the two components were not resolved in the fields used.

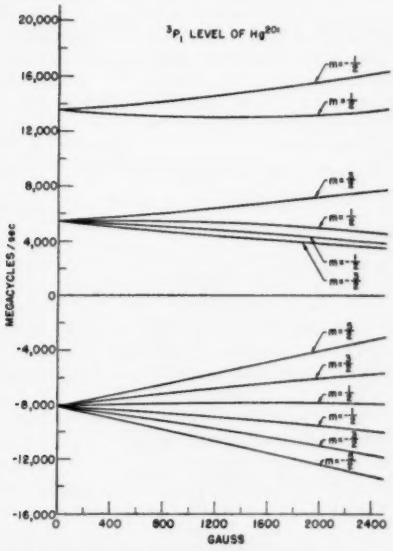

FIG. 9. The Zeeman effect of the hyperfine structure of the $^3P_1$ level of Hg^{201}.

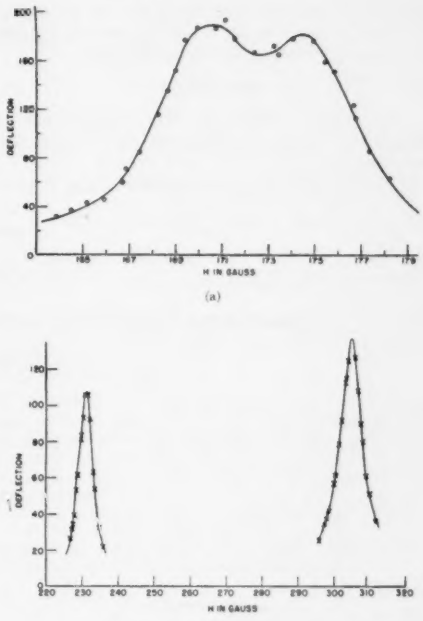

FIG. 10. Resonances observed at 144 Mc in the $^3P_1$ state of Hg^{20} (a) for the level $F=5/2$ and (b) for the level $F=3/2$.

Estimates of the mean life of the excited state of this isotope were made by computing $\gamma H_1 T_e$ for both the even and 199 isotopes [see Eq. (10)]. The ratio of the two values obtained for a fixed value of H_1 should give the ratio of the γ's if the mean life is the same for both isotopes. This was found to be the case at 50, 100, and 144 Mc to within 2 percent.

For the isotope Hg^{201} with a spin of 3/2, resonances were observed in the levels $F=5/2$ and $F=3/2$. Because of the small g-values, high rf field intensities are needed. These resonances are much less marked than those previously described, being only about 5 times the noise level. At frequencies above 50 Mc the decoupling of I and J is considerable, as may be seen from the inequality in spacing of the Zeeman levels in Fig. 9. At 50 Mc very broad resonances were observed for both the $F=3/2$ and $F=5/2$ levels. At 144 Mc the $F=5/2$ resonance shown in Fig. 10(a) was observed. This resonance consists of four unresolved components corresponding to the transitions $(5/2\rightarrow 3/2)$, $(3/2\rightarrow 1/2)$, $(-1/2\rightarrow -3/2)$, and $(-3/2\rightarrow -5/2)$. The resonances in the $F=3/2$ level consist of two well-resolved lines corresponding to the transitions $(3/2\rightarrow 1/2)$ and $(-1/2\rightarrow -3/2)$. The width of these lines agrees to

within 2 percent with that found for the isotopes of even mass number, again indicating that all isotopes have the same mean life in the excited state.

SUMMARY

1. An effective method has been demonstrated for extending rf absorption measurements to the excited states of atoms.

2. The g-factor and the level widths for the $^3P_1$ state of mercury have been studied. These levels could be examined in sufficient detail to establish their center to within 2 percent of the level widths.

3. The method can be extended to measurements of the hyperfine structure.

4. Other promising fields of observation include the Stark effect, the quenching and depolarization of resonance radiation, and in general, problems related to magnetic relaxation phenomena in vapors.

PHYSICAL REVIEW VOLUME 86, NUMBER 3 MAY 1, 1952

Effect of the Atomic Core on the Magnetic Hyperfine Structure*

R. STERNHEIMER
Brookhaven National Laboratory, Upton, New York
(Received December 20, 1951)

Equations have been obtained for the magnetic field at the nucleus due to the current induced in the electron core by an external valence electron. The magnetic field is written as $-4\mu_0[\mathbf{j}/(j(j+1))]\langle r^{-3}\rangle_p(1+R_m)$, where $\langle r^{-3}\rangle_p$ is the average over the valence electron function, assumed in a p state, R_m is the correction due to the core, μ_0 = Bohr magneton, j = angular momentum. R_m is of importance in obtaining the nuclear quadrupole moment Q from the value of the magnetic moment μ_I and the ratio b/a of the splittings due to Q and μ_I. The electric field gradient at the nucleus, $-\frac{1}{2}e\langle r^{-3}\rangle_p(1+R)$, which determines b, contains a similar term R for the distortion of the core by the valence electron. It is shown that R_m approximately cancels the exchange terms of R, so that the correction factor for Q is that predicted by the Thomas-Fermi model.

I. INTRODUCTION

IN the calculation of the effect of the quadrupole moment induced in the electron shells on the nuclear quadrupole coupling,[1] it was pointed out that the electron core may exert a similar effect on the coupling of the nuclear magnetic moment with the electrons. The closed shells are distorted by the electrostatic interaction with the valence electron. The exchange part of this interaction leads to additional terms in the core density for the electrons with spin parallel to the valence electron spin, which are not present for the electrons with antiparallel spin. Moreover, the density induced by the exchange depends on the magnetic quantum number of the core substate. Both terms in the core density give rise to a magnetic field at the nucleus, and hence to an interaction with the nuclear magnetic moment.

The purpose of this paper is to calculate the magnetic effect and to show that it approximately cancels the exchange terms in the quadrupole coupling correction. Therefore, the correction to nuclear quadrupole moments is essentially that predicted by the Thomas-Fermi model. Values of the correction are given for the nuclei whose Q has been determined.

II. THE MAGNETIC EFFECT

The magnetic splitting is determined by the component along $\mathbf{j}$ (angular momentum of atom) of the magnetic field at the nucleus $\mathbf{H}(0)$:

$$\mathbf{H}(0)\cdot\mathbf{j}=-2\mu_0\left\langle\sum_i\left(\frac{\mathbf{l}_i\cdot\mathbf{j}}{r_i^3}+\frac{3(\mathbf{s}_i\cdot\mathbf{r}_i)(\mathbf{r}_i\cdot\mathbf{j})}{r_i^5}-\frac{\mathbf{s}_i\cdot\mathbf{j}}{r_i^3}\right)\right\rangle, \quad (1)$$

where $\mathbf{l}_i$ and $\mathbf{s}_i$ are the orbital angular momentum and the spin of the ith electron, whose radius vector is $\mathbf{r}_i$; μ_0 = Bohr magneton. The excitation of s states will be considered first. To be specific, we consider the perturbation of $1s$ by the $3p$ electron in Al. The unperturbed wave function of the three electrons for the $^2P_{3/2}$ state with magnetic quantum number $m_j=3/2$ is

$$\Psi=3^{-\frac{1}{2}}[\psi(1,2,3)+\psi(2,3,1)+\psi(3,1,2)], \quad (2)$$

where

$$\psi(1,2,3)=\psi_{1s}(1)\psi_{1s}(2)\psi_{3p,1}(3)\times[2^{-\frac{1}{2}}\{a(1)b(2)-b(1)a(2)\}a(3)]. \quad (2a)$$

Here ψ_{1s} is the $1s$ function, $\psi_{3p,m}$ is the $3p$ function with magnetic quantum number m, $a(i)$ and $b(i)$ are spin functions for the z component of the spin of i, $s_{iz}=1/2$, and $-1/2$, respectively.

To obtain the perturbation of ψ due to exchange, we write the Schrödinger equation

$$\left[-\sum_i\left(\nabla_i^2+\frac{2Z}{r_i}\right)+\sum_{i>j}\frac{2}{r_{ij}}\right]\psi=E\psi, \quad (3)$$

where ∇_i is the gradient for the coordinates of i (in Bohr units a_H), $r_{ij}=|\mathbf{r}_i-\mathbf{r}_j|$, E is the energy (in Ry units).

* Work done under the auspices of the AEC.
[1] R. Sternheimer, Phys. Rev. **80**, 102 (1950); **84**, 244 (1951). The latter paper will be referred to as I.

Let $V_0(r_i)$ denote the potential due to the nucleus plus the spherical part of the Coulomb potential due to the electrons other than i. We write

$$\psi=\psi_0+\psi_1, \tag{4}$$

where ψ_0 is the wave function obtained from V_0 and ψ_1 is the perturbation due to exchange. ψ_0 satisfies

$$\sum_i[-\nabla_i^2+V_0(r_i)]\psi_0=E_0\psi_0, \tag{5}$$

where E_0 would be the energy if the potential were exactly V_0. If E_1 is the energy due to exchange, so that

$$E=E_0+E_1, \tag{6}$$

we obtain from (3)–(6):

$$\sum_i(-\nabla_i^2+V_0(r_i))\psi_1-E_0\psi_1=-\sum_{i>j}\frac{2}{r_{ij}}\psi_0+E_1\psi_0. \tag{7}$$

Equation 7 holds to first order in the perturbation; the small term $E_1\psi_1$ was omitted. In the right-hand side of (7) we must be careful to include only the exchange with the valence electron, since the perturbation due to the Coulomb potential of the valence electron produces no net magnetic field at the nucleus. ψ_1 consists of excited s and d waves. We consider the term $(-2/r_{13})\psi_0$, so that we are interested in the perturbation

$$\psi_1=\sum_{mm'}a_{mm'}\psi_{3p,m}(1)\psi_{d,m'}(3)+a'\psi_{3p,1}(1)\psi_s'(3), \tag{8}$$

where $\psi_{d,m}$ is the d wave with component m, ψ_s' is the s wave, $a_{mm'}$ and a' are coefficients.

In order to obtain the equations for ψ_s' and $\psi_{d,m}$ we consider the wave $\psi_{3p,1}(1)[a_{10}\psi_{d,0}(3)+a'\psi_s'(3)]$. We define radial functions u_0', v', $u_{1,d}$ and $u_{1,s}$ as follows:

$$\begin{aligned} r\psi_{1s}&=u_0'\Theta_0^0, \quad r\psi_{3p,1}=v'\Theta_1^1,\\ a_{10}r\psi_{d,0}&=u_{1,d}\Theta_2^0, \quad a'r\psi_s'=u_{1,s}\Theta_0^0, \end{aligned} \tag{9}$$

where

$$\Theta_l^m=[(2l+1)/2]^{\frac{1}{2}}P_l^m\exp[im\varphi]F(m), \tag{9a}$$

with P_l^m = Legendre polynomial of order l; $F(m)=(-1)^m$ for $m>0$ and 1 for $m\leq 0$. The normalization is

$$\int_0^\infty u_0'^2dr=\int_0^\infty v'^2dr=\int_0^\pi|\Theta_l^m|^2\sin\theta d\theta=1.$$

Equation (7) gives

$$\begin{aligned}(-\nabla_3^2+V_0-E_{1s})\{u_{1,d}\Theta_2^0+u_{1,s}\Theta_0^0\}(3)\{v'\Theta_1^1\}(1)\\ =[-(2/r_{13})+E_1]\{u_0'\Theta_0^0\}(1)\{v'\Theta_1^1\}(3),\end{aligned} \tag{10}$$

where E_{1s} is the unperturbed $1s$ energy and (1), (3) indicate that the coordinates are $\mathbf{r}_1$ and $\mathbf{r}_3$, respectively. Upon multiplying (10) by $\{v'\Theta_1^{1*}\}(1)$ and integrating over $\mathbf{r}_1$, we obtain with the aid of the expansion of $1/r_{13}$ in spherical harmonics

$$\begin{aligned}(-\nabla_3^2+V_0-E_{1s})(u_{1,d}\Theta_2^0+u_{1,s}\Theta_0^0)\\ =\tfrac{2}{3}fv'(\Theta_2^0/\sqrt{5}-\Theta_0^0),\end{aligned} \tag{11}$$

where

$$f(r)=\frac{1}{r^2}\int_0^r u_0'v'r'dr'+r\int_r^\infty u_0'v'r'^{-2}dr'. \tag{11a}$$

The effect of the s wave on $\mathbf{H}(0)$ is discussed below. The d wave $u_{1,d}$ may be written as $(2/3\sqrt{5})u_1'$, where u_1' satisfies

$$-d^2u_1'/dr^2+6u_1'/r^2+V_0u_1'-E_{1s}u_1'=fv'. \tag{11b}$$

The $\psi_{d,m}$ will be defined by

$$\psi_{d,m}=(u_1'/r)\Theta_2^m,$$

so that $a_{10}=2/(3\sqrt{5})$. By a similar calculation, using the perturbed waves $\psi_{d,1}$ and $\psi_{d,2}$, it can be shown that $a_{mm'}$ is given by

$$a_{mm'}=-2\int_0^\pi\Theta_0^0P_1^m\Theta_1^{m*}d\Omega_1\int_0^\pi\Theta_1^1P_1^{-m}\Theta_2^{m'*}d\Omega_3, \tag{12}$$

with $d\Omega_i=\sin\theta_i d\theta_i$. Evaluation of (12) gives for the perturbation

$$\begin{aligned}\psi_1=\frac{2}{3\sqrt{5}}\psi_{3p,1}(1)\psi_{d,0}(3)-\frac{2}{\sqrt{15}}\psi_{3p,0}(1)\psi_{d,1}(3)\\ +\frac{2\sqrt{2}}{\sqrt{15}}\psi_{3p,-1}(1)\psi_{d,2}(3).\end{aligned} \tag{13}$$

The function u_1' is completely determined by (11b) and the condition of regularity at $r=0$ and large r. As shown below, $\mathbf{H}(0)$ involves only the value of $\int_0^\infty(u_0'u_1'/r^2)dr$. This integral, which will be denoted by L, can be obtained from the earlier work.[1(a)] The following equation is solved in I (Eq. (7)):

$$-d^2\bar{u}_1'/dr^2+6\bar{u}_1'/r^2+V_0\bar{u}_1'-E_{1s}\bar{u}_1'=u_0'/r^3. \tag{14}$$

We show that L equals the integral

$$\bar{L}=\int_0^\infty u_0'v'\left(\frac{1}{r^2}\int_0^r\bar{u}_1'v'r'dr'+r\int_r^\infty\bar{u}_1'v'r'^{-2}dr'\right)dr, \tag{14a}$$

which is evaluated in I [see Eqs. (44), (47)]. By partial integration and from the definition of f, we have

$$\bar{L}=\int_0^\infty\bar{u}_1'fv'dr. \tag{14b}$$

[1(a)] We note that the integrations performed in I to obtain the perturbation u_1' of the core wave functions due to Q were carried out numerically, using the appropriate atomic potential for each Z. The integrations were started at large r by means of $A\exp[-|E_0|^{\frac{1}{2}}r]$ and were continued inward, using numerical values of the Thomas-Fermi potential V_0 down to the radius r_1 ($\sim 0.03a_H$) where the numerical solution was matched with the power series expansion, e.g., Eq. (10) of I. The calculations were carried out for several values of A and the appropriate values of A and of the constant a_3 in the expansion (10) were obtained from the conditions of continuity of u_1' and du_1'/dr at $r=r_1$.

With

$$M=-d^2/dr^2+6/r^2+V_0-E_{1s},$$

we obtain from (11b)

$$\bar{L}=\int_0^\infty \bar{u}_1' M u_1' dr=\int_0^\infty u_1' M \bar{u}_1' dr. \qquad (14c)$$

The last equality follows by partial integration. From (14), $M\bar{u}_1'$ equals u_0'/r^3, so that $L=\bar{L}$.

We note[2] that (13) is the correct combination of one-electron products to give a function of angular momentum $l=1$, $(m=1)$. This is expected since $1/r_{13}$ commutes with $\mathbf{l}$.

If the unperturbed function is $\psi_{1s}(1)\psi_{2p,0}(3)$, the $a_{mm'}$ are obtained from (12) by replacing $\Theta_1{}^1$ in the second integral by $\Theta_1{}^0$. The resulting perturbation is

$$\psi_1=\frac{2}{\sqrt{15}}\psi_{2p,1}(1)\psi_{d,-1}(3)-\frac{4}{3\sqrt{5}}\psi_{3p,0}(1)\psi_{d,0}(3)+\frac{2}{\sqrt{15}}\psi_{3p,-1}(1)\psi_{d,1}(3). \qquad (15)$$

Upon multiplying (13) by Ψ^* and integrating over $\mathbf{r}_1$ and $\mathbf{r}_2$, we obtain terms of the form $\psi_{1s}{}^*(3)\psi_{d,m}(3)$. Since ψ_{1s} and $\psi_{d,m}$ have different l, the $\mathbf{l}_3\cdot\mathbf{j}$ and $\mathbf{s}_3\cdot\mathbf{j}$ terms of $\mathbf{H}(0)\cdot\mathbf{j}$ do not contribute. In order to calculate $\langle(\mathbf{s}_3\cdot\mathbf{r}_3)(\mathbf{r}_3\cdot\mathbf{j})/r_3{}^5\rangle$, we obtain the effect of the spin functions in (2a). Let $\psi_{1/2}{}^{(s)}(1,2,3)$ be the function in square brackets in (2a). We have

$$\int \psi_{\pm 1/2}{}^{(s)*}(2,3,1)s_{3s}\psi_{\pm 1/2}{}^{(s)}(1,2,3)=\mp 1/4, \qquad (16)$$

$$\int \psi_{1/2}{}^{(s)*}(2,3,1)(s_{3x}+is_{3y})\psi_{-1/2}{}^{(s)}(1,2,3)=-1/2, \qquad (16a)$$

where $\psi_{-1/2}{}^{(s)}$ is obtained from $\psi_{1/2}{}^{(s)}(1,2,3)$ by replacing $a(3)$ by $b(3)$. To obtain the complete effect, we note the presence of a second term in the perturbed function, arising from the exchange of 3 and 2:

$$\psi_1=\frac{2}{3\sqrt{5}}\psi_{2p,1}(2)\psi_{d,0}(3)-\frac{2}{\sqrt{15}}\psi_{2p,0}(2)\psi_{d,1}(3)+\frac{2\sqrt{2}}{\sqrt{15}}\psi_{2p,-1}(2)\psi_{d,2}(3). \qquad (17)$$

We take into account both terms (13) and (17) by using for the spin integrals twice the values of (16), (16a). The terms $i=1, 2, 3$, in (1) are identical, so that the effect of the three electrons is obtained by omitting the factors $3^{-\frac{1}{2}}$ which multiply the $\psi(i, j, k)$ in Eq. (2).

We consider the state ${}^2P_{3/2}, mj=3/2$. The calculation of the magnetic field $\mathbf{H}^{(1)}(0)$ due to $(s_{3z}z_3{}^2j_z)/r_3{}^5$ is given in detail. If $\psi_{m_l}{}^{(l)}$ is the space part of the unperturbed function with magnetic quantum number m_l and $\psi_{m_l,P}{}^{(l)}$ is the perturbation, we have

$$\mathbf{H}^{(1)}(0)\cdot\mathbf{j}=9\mu_0\int \psi_1{}^{(l)*}(2,3,1)(z_3{}^2/r_3{}^5)\psi_{1,P}{}^{(l)}(1,2,3), \qquad (18)$$

where a factor 2 has been included to take into account the presence of two terms in the perturbed density $\Psi^*\Psi$. Evaluation of the integral using (13) gives

$$\mathbf{H}^{(1)}(0)\cdot\mathbf{j}=(4/5)\mu_0 L, \qquad (19)$$

with

$$L=\int_0^\infty (u_0'u_1'/r^3)dr. \qquad (19a)$$

Evaluation of the other terms of $\langle(\mathbf{s}_2\cdot\mathbf{r}_2)(\mathbf{r}_2\cdot\mathbf{j})/r_2{}^5\rangle$ gives for the total field $\mathbf{H}^{(d)}(0)$ due to $s\rightarrow d$:

$$\mathbf{H}^{(d)}(0)\cdot\mathbf{j}=(4/3)\mu_0 L. \qquad (20)$$

The field due to $3p$ is given by

$$\mathbf{H}^{(0)}(0)\cdot\mathbf{j}=-4\mu_0\langle r^{-3}\rangle_{3p}, \qquad (21)$$

independent of j. The total $\mathbf{H}(0)\cdot\mathbf{j}$ can be written

$$\mathbf{H}(0)\cdot\mathbf{j}=-4\mu_0\langle r^{-3}\rangle_{3p}(1+R_m), \qquad (21a)$$

where

$$R_m=-L/(3\langle r^{-3}\rangle_{3p}). \qquad (22)$$

For the ${}^2P_{1/2}$ state, the function

$$\Psi=[-\sqrt{2}\psi_1{}^{(l)}\psi_{-1/2}{}^{(s)}+\psi_0{}^{(l)}\psi_{1/2}{}^{(s)}]/\sqrt{3} \qquad (23)$$

leads to

$$\mathbf{H}^{(d)}(0)\cdot\mathbf{j}=-(8/3)\mu_0 L, \qquad (24)$$

$$R_m=2L/(3\langle r^{-3}\rangle_{3p}). \qquad (25)$$

The excitation of the $2p$ shell of Al in the ${}^2P_{3/2}$, $m_j=3/2$ state will now be considered. The wave function for the 7 electrons consisting of the $2p$ shell and $3p$ is

$$\Psi=(\sqrt{\tfrac{1}{3}}\psi_{2p,1}(1)\psi_{u,-1}-\sqrt{\tfrac{1}{3}}\psi_{2p,0}(1)\psi_{u,0}+\sqrt{\tfrac{1}{3}}\psi_{2p,-1}(1)\psi_{u,1})\psi_{3p,1}(7)\cdot[\sqrt{\tfrac{1}{2}}(a(1)b(u)-b(1)a(u))a(7)], \qquad (26)$$

$\psi_{u,m}$ is the space part of the wave function of electrons $2, \cdots 6$ in the $2p$ shell; it has $l=1$; $a(u)$ and $b(u)$ are spin functions for the 5 electrons, whose total spin is $1/2$. For the term $\psi_{2p,1}(1)\psi_{3p,1}(7)$ the perturbation due to exchange of $2p$ with $3p$ is

$$\psi_1=\sum_{mm'} b_{mm'}\psi_{2p,m}(1)\psi_{p,m'}(7)+\sum_{mm'} c_{mm'}\psi_{3p,m}(1)\psi_{f,m'}(7), \qquad (27)$$

where $\psi_{p,m}$ and $\psi_{f,m}$ are excited p and f functions, $b_{mm'}$

[2] It can be verified that (13) gives the correct term in the quadupole coupling. The perturbed density ρ with $m=0$ is $-(2/3)u_0'u_1'P_2{}^0/r^3$, where the $-$ sign is due to exchange. The interaction energy of ρ with the potential $-QP_2{}^0/r^3$ due to Q is $(4/15)QL$, or $(4/3)(L/\langle r^{-3}\rangle_{3p})$ times the interaction of Q with $3p$ in the $m=1$ state. This agrees with Eq. (47) of I.

and $c_{mm'}$ are coefficients. The wave $(b_{11}\psi_{p,1}(7)+c_{11}\psi_{f,1}(7))\psi_{3p,1}(1)$ will be considered first. We define radial functions w_1 and y_1, by

$$b_{11}\psi_{p,1}=(w_1/r)\Theta_1^1, \quad c_{11}\psi_{f,1}=(y_1/r)\Theta_3^1. \tag{27a}$$

Upon inserting (27a) into (7), one obtains

$$(-\nabla_7^2+V_0-E_{2p})\{w_1\Theta_1^1+y_1\Theta_3^1\}(7)\{v'\Theta_1^1\}(1) =[-(2/r_{17})+E_1]\{u_0'\Theta_1^1\}(1)\{v'\Theta_1^1\}(7), \tag{28}$$

where E_{2p} is the $2p$ energy; the radial functions u_0', v' are defined by

$$\psi_{2p,m}=(u_0'/r)\Theta_1^m, \quad \psi_{3p,m}=(v'/r)\Theta_1^m. \tag{28a}$$

Equation (28) is multiplied by $\{v'\Theta_1^{1*}\}(1)$ and integrated over $\mathbf{r}_1$. With the aid of the expansion of $1/r_{17}$ one finds

$$(-\nabla_7^2+V_0-E_{2p})(w_1\Theta_1^1+y_1\Theta_3^1) =-2(gv'+fv'/25)\Theta_1^1+[12(7/2)^{\frac{1}{2}}/175]fv'\Theta_3^1, \tag{29}$$

where

$$g=\frac{1}{r}\int_0^r u_0'v'dr'+\int_r^\infty u_0'v'r'^{-1}dr', \qquad f=\frac{1}{r^3}\int_0^r u_0'v'r'^2dr'+r^2\int_r^\infty u_0'v'r'^{-3}dr'. \tag{29a}$$

We consider first the p wave. From (29), one obtains

$$w_1=-2w_1'-(2/25)w_1'', \tag{30}$$

where w_1' and w_1'' are determined by

$$M_pw_1'=gv'+\alpha u_0', \tag{31}$$

$$M_pw_1''=fv'+\beta u_0', \tag{31a}$$

where α and β are constants and

$$M_p=-d^2/dr^2+2/r^2+V_0-E_{2p}. \tag{31b}$$

Equations (31) are obtained directly from (29), except for the terms $\alpha u_0'$ and $\beta u_0'$. In order to obtain these terms we note that

$$\int_0^\infty w_1'M_pu_0'dr=\int_0^\infty u_0'M_pw_1'dr=0. \tag{32}$$

Inserting (31) into (32), one finds

$$\int^\infty u_0'(gv'+\alpha u_0')dr=0,$$

so that

$$\alpha=-\int_0^\infty gu_0'v'dr. \tag{33}$$

A similar argument using (31a) gives

$$\beta=-\int_0^\infty fu_0'v'dr. \tag{33a}$$

As for the $s\rightarrow d$ wave, we are interested in the integrals

$$L_1=\int_0^\infty (u_0'w_1'/r^3)dr, \tag{34}$$

$$L_2=\int_0^\infty (u_0'w_1''/r^3)dr. \tag{34a}$$

By a proof similar to that for $s\rightarrow d$, it can be shown that L_1 equals the following integral of I:

$$L_1=\int_0^\infty u_0'v'\vartheta dr, \tag{35}$$

where ϑ (see Eq. (62) of I) is defined by

$$\vartheta=\frac{1}{r}\int_0^r u_{1,p}'v'dr'+\int_r^\infty u_{1,p}'v'r'^{-1}dr', \tag{35a}$$

in terms of the function $u_{1,p}'$ which satisfies (see Eq. (22) of I)

$$M_pu_{1,p}'=u_0'(r^{-3}-\langle r^{-3}\rangle_{2p}). \tag{35b}$$

L_2 is equal to

$$L_2\equiv\int_0^\infty u_0'v'f_e dr, \tag{36}$$

where (see Eq. (61) of I)

$$f_e=\frac{1}{r^3}\int_0^r u_{1,p}'v'r'^2dr'+r^2\int_r^\infty u_{1,p}'v'r'^{-3}dr'. \tag{36a}$$

The perturbed p wave will be written

$$\psi_1=\sum_{mm'}b_{mm'}'\psi_{3p,m}(1)\psi_{p,m'}'(7) +\sum_{mm'}b_{mm'}''\psi_{3p,m}(1)\psi_{p,m'}''(7), \tag{37}$$

where $\psi_{p,m}'$ and $\psi_{p,m}''$ are defined by

$$\psi_{p,m}'=(w_1'/r)\Theta_1^m, \quad \psi_{p,m}''=(w_1''/r)\Theta_1^m. \tag{37a}$$

Thus, for the excitation of $\psi_{2p,1}(1)\psi_{3p,1}(7)$, $b_{11}'=-2$, $b_{11}''=-2/25$, For the general case of the excitation of $\psi_{2p,m_1}\psi_{3p,m_2}$ one obtains

$$b_{mm'}''=-2\int_0^\pi \Theta_1^{m_1}P_2^{m_2-m_1}\Theta_1^{m*}d\Omega_1 \times\int_0^\pi \Theta_1^{m_2}P_2^{m_1-m}\Theta_1^{m'*}d\Omega_7; \tag{38}$$

$b_{mm'}'$ is obtained from (38) by replacing $P_2^{\pm(m-m_1)}$ by P_0. Upon evaluating (38) and inserting the perturbations into (26), one finds

$$\psi_{1,P}^{(1)}=-(2/\sqrt{3})(\psi_{3p,1}\psi_{u,-1}-\psi_{3p,0}\psi_{u,0} +\psi_{3p,-1}\psi_{u,1})\psi_{p,1}'-(2/25\sqrt{3})[\psi_{u,-1}\psi_{p,1}''\psi_{3p,1} -\psi_{u,0}(3\psi_{p,0}''\psi_{2p,1}-2\psi_{p,1}''\psi_{3p,0}) +\psi_{u,1}(6\psi_{p,-1}''\psi_{3p,1} -3\psi_{p,0}''\psi_{3p,0}+\psi_{p,1}''\psi_{3p,-1})]. \tag{39}$$

The coordinates of ψ_{3p} are $\mathbf{r}_1$, those of $\psi_{p,m}'$ and $\psi_{p,m}''$ are $\mathbf{r}_7$.

The perturbation of the state for which $3p$ has $m_2=0$ is also required. The space part of the unperturbed function is then

$$\psi_0^{(1)}=(1/\sqrt{3})[\psi_{2p,1}(1)\psi_{u,-1}-\psi_{2p,0}(1)\psi_{u,0}+\psi_{2p,-1}(1)\psi_{u,1}]\psi_{3p,0}(7). \quad (40)$$

The perturbation is obtained from (38):

$$\psi_{0,P^{(1)}}=-(2/\sqrt{3})(\psi_{3p,1}\psi_{u,-1}-\psi_{3p,0}\psi_{u,0}+\psi_{3p,-1}\psi_{u,1})\psi_{p,0}'+(2/25\sqrt{3})[\psi_{u,-1}(2\psi_{p,0}''\psi_{3p,1}-3\psi_{p,1}''\psi_{3p,0})-\psi_{u,0}(3\psi_{p,1}''\psi_{3p,-1}-4\psi_{p,0}''\psi_{3p,0}+3\psi_{p,-1}''\psi_{3p,1})+\psi_{u,1}(2\psi_{p,0}''\psi_{3p,-1}-3\psi_{p,-1}''\psi_{3p,0})]. \quad (40a)$$

The complete wave function contains in addition to (26) terms which are obtained from (26) by permuting the electron coordinates. If (26) is denoted by $\psi(1, 7)$, the only term with which (39) gives an overlap is $-\psi^*(7, 1)$. If the spin functions are denoted by $\psi_{\pm 1/2}^{(s)}(i, j)$ one finds

$$-\int \psi_{\pm 1/2}^{(s)*}(7, 1)s_{7z}\psi_{\pm 1/2}^{(s)}(1, 7)=\mp\tfrac{1}{4}, \quad (41)$$

$$-\int \psi_{\mp 1/2}^{(s)*}(7, 1)(s_{7x}\mp is_{7y})\psi_{\pm 1/2}^{(s)}=-\tfrac{1}{2}. \quad (41a)$$

In the sum over i in (1), there are 6 equal terms for the exchange of $2p$ with $3p$. Each term has a factor $1/3$ arising from the $1/\sqrt{3}$ in (26). Therefore, the effect of the complete $2p$ shell is obtained by omitting the $1/3$ and replacing s_{7s} by $\mp 1/2$ for $\psi_{\pm 1/2}^{(s)}$ and $(s_{7x}\pm is_{7y})$ by -1. When no spin operators are involved, the spin integral is replaced by -1.

The calculation of the field due to $\mathbf{l}_7\cdot\mathbf{j}/r_7^3$ is given in detail. The functions $\psi_{ml}^{(1)}\sqrt{3}$ and $\psi_{ml,P}^{(1)}\sqrt{3}$ are denoted by $\bar{\psi}_{ml}^{(1)}$ and $\bar{\psi}_{ml,P}^{(1)}$, respectively. We have

$$l_{7z}j_z\bar{\psi}_{1,P^{(1)}}=-3(\psi_{3p,1}\psi_{u,-1}-\psi_{3p,0}\psi_{u,0}+\psi_{3p,-1}\psi_{u,1})\psi_{p,1}'-(3/25)[\psi_{u,-1}\psi_{p,1}''\psi_{3p,1}+2\psi_{u,0}\psi_{p,1}''\psi_{3p,0}-6\psi_{u,1}\psi_{p,-1}''\psi_{3p,1}+\psi_{u,1}\psi_{p,1}''\psi_{3p,-1}].$$

The contribution of this term of $\mathbf{H}(0)\cdot\mathbf{j}$ is

$$\mathbf{H}^{(1)}(0)\cdot\mathbf{j}=4\mu_0\int\bar{\psi}_1^{(1)*}(7, 1)(l_{7z}j_z/r_7^3)\bar{\psi}_{1,P^{(1)}}=-\mu_0[12L_1-(12/5)L_2], \quad (42)$$

where a factor -2 arises from the two terms in the density $\Psi^*\Psi$ and from the spin integral. For $\frac{1}{2}(l_x+il_{7y})\times(j_x-ij_y)$, only the term $\sqrt{2}\psi_0^{(1)}\psi_{1/2}^{(s)}$ of $(j_x-ij_y)\Psi$ contributes. We have

$$(1/\sqrt{2})(l_{7x}+il_{7y})\bar{\psi}_{0,P^{(1)}}=-2(\psi_{3p,1}\psi_{u,-1}-\psi_{3p,0}\psi_{u,0}+\psi_{3p,-1}\psi_{u,1})\psi_{p,1}'+(2/25)[2\psi_{u,-1}\psi_{p,1}''\psi_{3p,1}+\psi_{u,0}(4\psi_{p,1}''\psi_{3p,0}-3\psi_{p,0}''\psi_{3p,1})+\psi_{u,1}(2\psi_{p,1}''\psi_{3p,-1}-3\psi_{p,0}''\psi_{3p,0})].$$

The contribution to $\mathbf{H}(0)\cdot\mathbf{j}$ is

$$\mathbf{H}^{(2)}(0)\cdot\mathbf{j}=4\mu_0\int\bar{\psi}_1^{(1)*}(7, 1)(1/\sqrt{2})(l_{7x}+il_{7y})\bar{\psi}_{0,P^{(1)}}=-\mu_0(8L_1-8L_2/5). \quad (43)$$

Evaluation of the spin terms of (1) gives for the total magnetic field due to the $p\rightarrow p$ wave

$$\mathbf{H}^{(p)}(0)\cdot\mathbf{j}=-\mu_0[16L_1-(104/25)L_2]. \quad (44)$$

For $^2P_{1/2}$, one finds

$$\mathbf{H}^{(p)}(0)\cdot\mathbf{j}=-\mu_0[16L_1-(32/25)L_2]. \quad (45)$$

For the excitation of the $2p$ electrons into f states, (29) gives a wave $[12(7/2)^{\frac{1}{2}}/175]y_1'\Theta_3^1$, where y_1' is determined by

$$M_f y_1'=fv', \quad (46)$$

with

$$M_f=-d^2/dr^2+12/r^2+V_0-E_{2p}. \quad (46a)$$

The integral

$$L_3=\int_0^\infty(u_0'y_1'/r^3)dr \quad (47)$$

which enters in $\mathbf{H}(0)$ is equal to $\bar{L}_3$ of I [see Eqs. (54), (56)] defined by

$$\bar{L}_3\equiv\int_0^\infty u_0'v'f_b dr, \quad (47a)$$

where

$$f_b=\frac{1}{r^3}\int_0^r u_{1,f}'v'r'^2dr'+r^2\int_r^\infty u_{1,f}'v'r'^{-3}dr', \quad (47b)$$

and $u_{1,f}'$ is the function determined by

$$M_f u_{1,f}'=u_0'/r^3. \quad (47c)$$

The $\psi_{f,m}$ of (27) are defined by

$$\psi_{f,m}=(y_1'/r)\Theta_3^m.$$

For the $c_{mm'}$ of the perturbation of $\psi_{2p,m_1}(1)\psi_{3p,m_2}(7)$, one finds

$$c_{mm'}=-2\int_0^\pi\Theta_1^{m_1}\Theta_1^{m*}P_2^{m-m_1}d\Omega_1\times\int_0^\pi\Theta_1^{m_2}\Theta_3^{m'*}P_2^{m_1-m}d\Omega_7. \quad (48)$$

The perturbed waves for $m_2=1$ and $m_2=0$ are

$$\psi_{1,P}{}^{(1)}=\frac{1}{175\sqrt{3}}\Big[\psi_{u,-1}\Big(12\sqrt{\frac{7}{2}}\psi_{3p,0}\psi_{f,1}-6\sqrt{70}\psi_{3p,0}\psi_{f,2}+12\sqrt{\frac{105}{2}}\psi_{3p,-1}\psi_{f,3}\Big)-\psi_{u,0}\Big(6\sqrt{21}\psi_{3p,1}\psi_{f,0}-24\sqrt{\frac{7}{2}}\psi_{3p,0}\psi_{f,1}+6\sqrt{70}\psi_{3p,-1}\psi_{f,2}\Big)+\psi_{u,1}\Big(12\sqrt{\frac{7}{2}}\psi_{3p,1}\psi_{f,-1}-6\sqrt{21}\psi_{3p,0}\psi_{f,0}+12\sqrt{\frac{7}{2}}\psi_{3p,-1}\psi_{f,1}\Big)\Big], \quad (49)$$

$$\psi_{0,P}{}^{(1)}=\frac{1}{175\sqrt{3}}[\psi_{u,-1}(6\sqrt{21}\psi_{3p,1}\psi_{f,0}-6\sqrt{56}\psi_{3p,0}\psi_{f,1}+6\sqrt{70}\psi_{3p,-1}\psi_{f,2})-\psi_{u,0}(12\sqrt{14}\psi_{3p,1}\psi_{f,-1}-12\sqrt{21}\psi_{3p,0}\psi_{f,0}+12\sqrt{14}\psi_{3p,-1}\psi_{f,1})+\psi_{u,1}(6\sqrt{70}\psi_{3p,1}\psi_{f,-2}-6\sqrt{56}\psi_{3p,0}\psi_{f,-1}+6\sqrt{21}\psi_{3p,-1}\psi_{f,0})]. \quad (49a)$$

As for the $s\rightarrow d$ wave, only the $(\mathbf{s}_7\cdot\mathbf{r}_7)(\mathbf{r}_7\cdot\mathbf{j})/r_7{}^5$ term contributes. One finds for $^2P_{3/2}$ and $^2P_{1/2}$

$$\mathbf{H}^{(1)}(0)\cdot\mathbf{j}=(36/25)\mu_0 L_3, \qquad (^2P_{3/2}) \quad (50)$$

$$\mathbf{H}^{(1)}(0)\cdot\mathbf{j}=-(72/25)\mu_0 L_3. \qquad (^2P_{1/2}) \quad (51)$$

The s wave perturbation of $1s$ will now be considered. From Eq. (11) $u_{1,s}$ may be written $-(2/3)u_1'$ where u_1' satisfies

$$-\frac{d^2u_1'}{dr^2}+V_0u_1'-E_{1s}u_1'=fv'-\sum_{n=1}^{3}\Big(\int_0^\infty fv'u_{0,ns}'dr\Big)u_{0,ns}'\equiv I(r), \quad (52)$$

with $u_{0,ns}'$ = radial ns function. Equation (52) is obtained directly from (11), except for the sum on the right. The term $n=1$ of this sum arises in the same manner as $\beta u_0'$ in (31a); $n=2$ and $n=3$ are Lagrangian terms which ensure that u_1' is orthogonal to the $u_{0,ns}'$. This can be seen by regarding the right side (denoted by $I(r)$) as equivalent to a small potential $-I/u_{0,1s}'$ acting on $u_{0,1s}'$. The perturbation is given by

$$u_1'=\sum_{n=2}^{\infty}\frac{\int_0^\infty Iu_{0,ns}'dr}{E_{ns}-E_{1s}}u_{0,ns}'. \quad (52a)$$

The coefficients of $u_{0,2s}'$ and $u_{0,3s}'$ are zero. After a particular solution of (52) is obtained, it is made orthogonal to u_0' by adding a suitable multiple of $u_{0,1s}'$. To obtain the effect on $\mathbf{H}(0)\cdot\mathbf{j}$, we note that for s states, Eq. (1) must be replaced by[3]

$$\mathbf{H}(0)\cdot\mathbf{j}=2\hbar ec\Big\langle\frac{d}{dr_i}\Big(\frac{1}{E_T+mc^2+eA_0}\Big)\times\Big[\frac{\mathbf{s}_i\cdot\mathbf{j}}{r_i{}^2}-\frac{(\mathbf{s}_i\cdot\mathbf{r}_i)(\mathbf{r}_i\cdot\mathbf{j})}{r_i{}^4}\Big]\Big\rangle, \quad (1a)$$

where E_T is the energy of the s state, including the rest energy, A_0 is the Coulomb potential of the nucleus. By means of (16), (16a), one finds for $^2P_{3/2}$

$$\mathbf{H}(0)\cdot\mathbf{j}=\frac{20\hbar ec}{9}\int_0^\infty\frac{d}{dr_i}\Big(\frac{1}{E_T+mc^2+eA_0}\Big)\frac{u_1'u_{0,1s}'}{r_i{}^2}dr_i.$$

Evaluation of the integral in the manner of Fermi[4] and Breit[3] gives

$$\mathbf{H}(0)\cdot\mathbf{j}=-\frac{20\mu_0}{9}\lim_{r_i=0}\Big(\frac{u_1'u_{0,1s}'}{r_i{}^2}\Big). \quad (53)$$

For $^2P_{1/2}$ one obtains

$$\mathbf{H}(0)\cdot\mathbf{j}=\frac{4\mu_0}{9}\lim_{r_i=0}\Big(\frac{u_1'u_{0,1s}'}{r_i{}^2}\Big). \quad (53a)$$

Equation (52) was solved[4(a)] for the case of Cl. For the $u_{0,ns}'$ we used the Hartree-Fock functions[5] for Cl^-. The integration was carried out as follows. Assume that u_0' is known at $r_n-\delta$, r_n, $r_n+\delta$; here r_n is a selected point and δ is the interval of the numerical integration. Let $V_0-E_{1s}\equiv P(r)$; $u_1'(r_n+\delta)$ is obtained from

$$u_1'(r_n+\delta)=\{2+\delta^2[P(r_n)-I(r_n)/u_1'(r_n)]\}u_1'(r_n)-u_1'(r_n-\delta). \quad (54)$$

$P(r_n)$ was obtained from the requirement that it shall reproduce $u_0'(r_n)$:

$$P(r_n)=[u_0'(r_n-\delta)+u_0'(r_n+\delta)-2u_0'(r_n)]/u_0'(r_n)\delta^2. \quad (54a)$$

Near $r=0$, u_1' is proportional to $u_{0,1s}'$. The integration was started with two values of u_1' proportional to $u_{0,1s}'$. After u_1' is calculated,[6] the perturbation $\bar{u}_1'$ is

[3] G. Breit and F. W. Doermann, Phys. Rev. **36**, 1732 (1930).

[4] E. Fermi, Z. Phys. **60**, 320 (1930).

[4(a)] Similar calculations for the case of Ga have been carried out by G. Koster, [Phys. Rev. **85**, 148 (1952)]. I am indebted to Dr. Koster for showing me a copy of his paper in advance of publication.

[5] D. R. Hartree, Proc. Roy. Soc. (London) **156**, 56 (1936).

[6] If δ were very small, u_1' would be regular for large r, since $\int_0^\infty Iu_{0,1s}'dr=0$ ensures that u_1' is well-behaved at infinity. In practice, this is not true, because of the finite δ. $I(r)$ was therefore modified by adding a small term $\xi u_{0,1s}'$. The constant ξ was determined from the condition that u_1' obtained with $I+\xi u_{0,1s}'$ is regular at large r. In all cases ξ was small, indicating that δ was adequate.

TABLE I. Values of $R_{m,ns}(^2P_{3/2})$ for Cl.

State	γ	a_1^2	$R_{m,ns}(^2P_{3/2})$
$1s$	-4.6×10^{-5}	18,600	-0.082
$2s$	6.5×10^{-4}	1460	0.091
$3s$	-5.7×10^{-3}	128	-0.071

obtained from

$$\tilde{u}_1'=u_1'-\left(\int_0^\infty u_1'u_{0,1s}'dr\right)u_{0,1s}'. \tag{54b}$$

If the series expansions of $\tilde{u}_1'$ and $u_{0,1s}'$ start as a_3r and a_1r, respectively, we may write $R_{m,1s}(^2P_{3/2})$ for the $1s\to s$ wave as follows, using (53) and (21):

$$R_{m,1s}=5\gamma a_1^2/(9\langle r^{-3}\rangle_p), \tag{55}$$

with $\gamma=a_3/a_1$. Table I gives values of γ, a_1^2 and $R_{m,ns}(^2P_{3/2})$ for Cl. The sign of γ can be explained as follows. In view of (52a) and the completeness theorem, u_1' is approximated by $I(r)(E_{ns}-E_{1s})^{-1}$, where the bracket is an average energy denominator. From the numerical solutions it was found that u_1' is fairly well represented near $r=0$ by taking $\langle E_{ns}-E_{n's}\rangle=400$ ry, 40 ry, and 18 ry for $n'=1, 2, 3$, respectively. Thus the sign of γ is determined by that of $I(r)$ near $r=0$. The term fv' goes as r^3 and is therefore small compared to the terms proportional to $u_{0,ns}'(\propto r)$. For $1s$, the main term $-(\int_0^\infty fv'u_{0,1s}'dr)u_{0,1s}'<0$, because fv' and $u_{0,1s}'$ are both positive. For $2s$, $fv'<0$; the $u_{0,1s}'$ term predominates and gives $I>0$. For $3s$ the dominant $u_{0,3s}'$ term is negative, but its effect is considerably reduced by the $u_{0,1s}'$ and $u_{0,2s}'$ terms which have opposite sign. It is seen that $R_{m,1s}$ and $R_{m,2s}$ almost cancel, so that a good value of $\sum_{n=1}^{3}R_{m,ns}$ requires very accurate calculations of the $R_{m,ns}$ for each shell.

We can now write the total magnetic correction for an atom consisting of closed s and p shells and a valence electron (or hole) in a p state. The ratios $L/\langle r^{-3}\rangle_p$, $L_1/\langle r^{-3}\rangle_p$, where $\langle r^{-3}\rangle_p$ is the average over the valence wave function, will be denoted by L' and L_1', respectively. For the $s\to s$ wave, $\gamma a_1^2/\langle r^{-3}\rangle_p$ is denoted by K. From (22), (25), (44), (45), (50), (51), (55) we obtain

$$R_m(^2P_{3/2})=\sum_{n_1}\left(\frac{5K}{9}-\frac{L'}{3}\right)+\sum_{n_2}\left(4L_1'-\frac{26}{25}L_2'-\frac{9}{25}L_3'\right), \tag{56}$$

$$R_m(^2P_{1/2})=\sum_{n_1}\left(-\frac{K}{9}+\frac{2L'}{3}\right)+\sum_{n_2}\left(4L_1'-\frac{8}{25}L_2'+\frac{18}{25}L_3'\right), \tag{56a}$$

where the n_1-sum extends over the s shells and the n_2-sum over the p shells. Equation (56) may be compared with the correction to the quadrupole coupling:[1]

$$R=R_d+\sum_{n_1}\frac{4L'}{3}+\sum_{n_2}\left(4L_1'+\frac{4}{25}L_2'+\frac{36}{25}L_3'\right), \tag{57}$$

where R_d is a negative term arising from the direct interaction of the valence electron and the core ($R_d=E_{\Delta Q}/E_Q$ of I). The term $\sum_{n_2}4L_1'(=E'^{(0)}/E_Q$ of I) is the largest in R and hence leads to $R>0$. However, (56) shows that R_m has an equal term independent of j. This was expected, since $\psi_{p,m}'$ behaves like $\psi_{3p,m}$ in the unperturbed Ψ [see Eqs. (39), (40)] and $4L_1'$ is the ratio of $\langle r^{-3}\rangle$ for the density $4\psi_{2p,m}{}^*\psi_{p,m}'$ and the valence density. Table II gives R_m for Cl and R for Cl, Al, and Li. The row (L', L_2', L_3') includes all exchange terms other than those due to $\psi_{p,m}'$ and the $s\to s$ waves (see E'/E_Q of I).

The magnetic hfs splitting a is given by

$$a=2l(l+1)\mu_0\mu_I F(j)\langle r^{-3}\rangle_p(1+R_m)/[Ij(j+1)h], \tag{58}$$

where μ_I=nuclear magnetic moment, I=nuclear spin, and $F(j)$ is a relativistic correction. For Cl^{37}, a has been measured both for the $^2P_{3/2}$ and the $^2P_{1/2}$ state.[7] The values are $a^{37}(3/2)=170.681$ Mc, $a^{37}(1/2)=863.350$ Mc. From (58) we have

$$\frac{5a^{37}(3/2)}{a^{37}(1/2)}=\frac{F(3/2)\,[1+R_m(^2P_{3/2})]}{F(1/2)\,[1+R_m(^2P_{1/2})]}.$$

With[8] $F(3/2)/F(1/2)=0.978$, we obtain

$$[1+R_m(^2P_{3/2})]/[1+R_m(^2P_{1/2})]=1.011$$

From Table II this ratio is $1.358/1.482=0.916$. The disagreement may be due to the uncertainty in the radial functions. Thus for $3s\to s$, fv' is negative up to the node of $3p$ at $0.55a_H$ and positive for $r>0.55a_H$. The values of

$$X_n\equiv\left(\int_0^\infty fv'u_{0,ns}'dr\right)\left(\frac{u_{0,ns}'}{r}\right)_{r\to0}$$

are -0.011, -0.006, 0.025 for $n=1, 2, 3$, respectively. If $u_{0,3s}'$ were, in fact, more internal than the Hartree-Fock function, fv' would have larger values near $r=0$, resulting in larger X_1 and X_2, while X_3 would be nearly unchanged. As a result, $I>0$ giving $R_{m,3s}>0$. We have calculated that if the normalized $u_{0,3s}'$ were bigger by a factor 1.7 for $r<0.70a_H$, $R_{m,3s}$ would be raised to ~0.05, giving $[1+R_m(^2P_{3/2})]/[1+R_m(^2P_{1/2})]=1.02$, in approximate agreement with experiment. Although the required change in $u_{0,3s}'$ is rather large, this calculation shows that inaccuracy of the wave functions may be

[7] V. Jaccarino and J. G. King, private communication.

[8] H. B. G. Casimir, *On the Interaction between Atomic Nuclei and Electrons* (Teyler's Tweede Genootschap, Haarlem, Holland, 1936).

TABLE II. Values of R_m and R.

	$R_m(^2P_{3/2})_{Cl}$	$R_m(^2P_{1/2})_{Cl}$	R_{Cl}	R_{Al}	R_{Li}
$\sum_{n_2} 4L_1'$	0.47	0.47	0.47	0.17	0
(L_1', L_2', L_3')	−0.05	0.00	0.04	0.03	0.06
$\sum_{n=1}^{3} R_{m,ns}$	−0.062	0.012	...	...	...
R_d	...	...	−0.094	−0.006	−0.166
R_m or R	0.358	0.482	0.42	0.19	−0.11
$1/[1+R_d(1+\sum_{n_2} 4L_1')^{-1}]$	...	...	1.068	1.005	1.20

responsible for the disagreement. We note that the difference between the radial $3p$ functions for $^2P_{1/2}$ and $^2P_{3/2}$, which was disregarded, may contribute to the discrepancy.

III. THE QUADRUPOLE CORRECTION

The splitting due to the quadrupole moment is

$$b=-2Ie^2Q\langle r^{-3}\rangle_p(1+R)/(2I+3)h. \tag{59}$$

In the experiments[9] on Cl and Al, μ_I is known independently and Q can be obtained from b/a by means of

$$Q=-(2I+3)(I+1)\mu_0\mu_I b(1+R_m)/[j(j+1)Ie^2a(1+R)]. \tag{59a}$$

In order to obtain the factor $(1+R_m)/(1+R)$ we make use of the experimental fact[7] that $5a(3/2)/a(1/2)\approx 1$ both for Cl and Al. This indicates that the true $s\rightarrow s$ term is small. The other important R_m term, $\sum_{n_2}4L_1'$, appears also in the exchange part of R. The remaining exchange terms (L_1', L_2', L_3') are small compared to $\sum_{n_2}4L_1'$, as shown in Table II. Since they are probably not accurately given by the present calculation, it seems reasonable to omit them and to replace $(1+R_m)/(1+R)$ by

$$\frac{1+R_m}{1+R}\approx\frac{1+\sum_{n_2}4L_1'}{1+R_d+\sum_{n_2}4L_1'}=1\Big/\left\{1+\frac{R_d}{1+\sum_{n_2}4L_1'}\right\}. \tag{60}$$

In the correction (60) for Q, exchange does not change the sign of the effect, but merely decreases its magnitude by a factor $(1+\sum_{n_2}4L_1')$. This is contrary to the result obtained if only the effect of the core on the quadrupole coupling is taken into account. However, when exchange is included, it is not legitimate to disregard the magnetic effect, which approximately cancels the exchange term of R. R_d is negative, so that (60) is such as to increase Q.

Equation (60) is approximated by the Thomas-Fermi value of the quadrupole correction, which, however, does not take into account the $p\rightarrow p$ waves and the $(1+\sum_{n_2}4L_1')^{-1}$ factor. The latter is probably less important than the uncertainty of $\langle r^{-3}\rangle_p$. The $p\rightarrow p$ waves induced by the nuclear moment Q cannot be predicted from the statistical model. As discussed in I, their effect may be either to shield or reinforce the nuclear Q. However, the following argument shows that for medium and heavy atoms the net $np\rightarrow p$ term is small compared to the angular excitations represented by the statistical model. For each p shell, the induced moment is shielding inside the outermost maximum of the wave function, where $u_0'u_{1,p}'>0$, and antishielding outside $(u_0'u_{1,p}'<0$, see Figs. 3 and 4 of I). Thus the antishielding of the nuclear moment by the np shell tends to be cancelled by the shielding by the $(n+1)p$ shell inside its principal maximum. This is brought out by the case of Cl where the shielding due to $3p\rightarrow p$ compensates for the $2p\rightarrow p$ term. The cancellation should become more complete for heavy atoms, with increasing number of shells.

We conclude that the statistical model is probably adequate, except for light atoms. In I, it was shown that the Thomas-Fermi correction R' should be reduced by a factor 1.5 for light atoms, to give closer agreement with the calculations using wave functions. Therefore the best correction factor is $C\equiv 1/(1-R'/1.5)$, where R' is the Thomas-Fermi value given in Tables II and III. For medium and heavy atoms ($Z>17$) where calculations using wave functions have not been carried out, we take $C\equiv 1/(1-R')$. Upon using $R'=0.095$ for Al, 0.073 for Cl, 0.194 for Li, we find $C=1.067$ for Al, 1.052 for Cl, and 1.148 for Li. For Cl and Li, C agrees fairly well with the values of (60) listed in Table II; for Al, C is too large because of $2p\rightarrow p$ antishielding. Upon applying the correction (60) to the values[9-11] of Q for Cl and Al, we obtain $Q(Cl^{35})=-0.0843\times10^{-24}$ cm^2, $Q(Cl^{36})=-0.0183\times10^{-24}$ cm^2, $Q(Cl^{37})=-0.0664\times10^{-24}$ cm^2, $Q(Al^{27})=0.157\times10^{-24}$ cm^2.

In cases where $\langle r^{-3}\rangle_p$ is obtained from the fine-structure splitting, the correction is also given by (60), and hence approximately by the Thomas-Fermi value. In order to derive this result, we note that the fine structure is due to the total spin density of the atom, interacting with the orbital motion. If we multiply $\bar{\psi}_{1,P}^{(1)}$ (Eq. (39)) by $-2\sqrt{3}\psi^*(7,1)$ and integrate over

[9] Davis, Feld, Zabel, and Zacharias, Phys. Rev. **76**, 1076 (1949); H. Lew, Phys. Rev. **76**, 1086 (1949).

[10] V. Jaccarino and J. G. King, Phys. Rev. **83**, 471 (1951).

[11] C. H. Townes and L. C. Aamodt, Phys. Rev. **76**, 691 (1949).

TABLE III. Values of the quadrupole correction.

Nucleus	$Q/(10^{-24}\ \mathrm{cm}^2)$	Method	State	nl	$C(nl)$[a]
$B^{10,11}$	0.06, 0.03	Wf	$2p$	$2p$	1.124
N^{14}	0.02	Wf	$2p^3$	$2p$	1.101
Al^{27}	0.156	Ah	$3p$	$3p$	1.005[b]
$S^{33,35}$	−0.08, 0.06	Wf	$3p^4$	$3p$	1.052[c]
$Cl^{35,36,37}$	−0.07894, −0.0172, −0.06213	Ah	$3p^5$	$3p$	1.068[b]
$Cu^{63,65}$	−0.26, −0.15	Sh	$3d^94s^2$	$3d$	1.229
$Ga^{69,71}$	0.232, 0.146	Ah	$4p$	$4p$	1.046
Ge^{73}	−0.21	Wf	$4p^2$	$4p$	1.044
As^{75}	0.3	Wf	$4p^3$	$4p$	1.043
$Br^{79,81}$	0.26, 0.21	Wf	$4p^5$	$4p$	1.040
Kr^{83}	0.15	Wf	$4p^55s$	$4p$	1.038
$In^{113,115}$	1.144, 1.161	Ah	$5p$	$5p$	1.032
$Sb^{121,123}$	−0.3, −1.2	Sf	$5p^3$	$5p$	1.030
$I^{127,129}$	−0.59, −0.43	Wf	$5p^5$	$5p$	1.029
$Eu^{151,153}$	1.2, 2.5	Sf	$4f^76s6p$	$6p$	1.026
Yb^{173}	3.9	Sf	$6s6p$	$6p$	1.026
$Lu^{175,176}$	5.9, 7	Sf	$5d6s^2$	$5d$	1.107
Ta^{181}	6	Sf	$5d^36s^2$	$5d$	1.103
$Re^{185,187}$	2.8, 2.6	Sf	$5d^56s6p$	$6p$	1.023
Hg^{201}	0.5	Sf	$6s6p$	$6p$	1.019
Bi^{209}	−0.4	Sf	$6p^3$	$6p$	1.019

[a] $C=1/(1-R'/1.5)$ for B and N. The other Thomas-Fermi values were taken as $1/(1-R')$.
[b] This value is obtained from Eq. (60).
[c] This value is obtained by interpolation of (60) for Al and Cl.

$\mathbf{r}_1, \cdots \mathbf{r}_6$, we obtain for the spin density due to $2p\rightarrow p$:

$$\rho_c=4\psi_{p,1}'\psi_{2p,1}^*+(4/25)(\psi_{p,1}''\psi_{2p,1}^*+3\psi_{p,0}''\psi_{2p,0}^*+6\psi_{p,-1}''\psi_{2p,-1}^*). \quad (61)$$

By means of (37a) we obtain

$$\int_0^\pi \rho_c d\Omega_7=4\frac{u_0'w_1'}{r^2}+\frac{8}{5}\frac{u_0'w_1''}{r^2}. \quad (62)$$

The $s\rightarrow d$ and $p\rightarrow f$ waves do not contribute, because the angular integral is zero. For $m=0$, $\bar{\psi}_{0,P^{(1)}}$ also leads to (62). The $np\rightarrow p$ terms are added to the valence density $|\psi_{2p,m}|^2$. Thus, in the approximation where $(1/r)(\partial V_0/\partial r)\sim -Z_i e/r^3$ (Z_i=effective Z), the fine-structure splitting is given by

$$\nu=\tfrac{3}{4}Z_i R\alpha^2 a_H^3\langle r^{-3}\rangle_p[1+\textstyle\sum n_2(4L_1'+(8/5)L_2')], \quad (63)$$

with R=Ry, α=fine structure constant. Upon neglecting the L_2' term, we obtain $(1+\sum n_2 4L_1')/(1+R)$ for the correction factor for Q, in agreement with Eq. (60).

Table III gives C for the nuclei whose Q is known. The values of Q are those given in the paper of Mack[12] which also lists the references. The method of determination is indicated as follows: W=microwave absorption, S=line spectra, A=atomic beam magnetic resonance; h indicates that $\langle r^{-3}\rangle$ was obtained from the hfs splitting and μ_I; f means that the fine structure was used. The next two columns list the atomic state and the orbital which gives the quadrupole coupling. In order to obtain C for Eu, Yb, and Re, we have calculated R' for the $6p$ orbital for $Z=63$ and $Z=71$. The values are as follows:[13] $\langle r^{-3}\rangle=5.6a_H^{-3}$, $\langle V_1\rangle=0.56a_H^{-3}$, $R'=0.025$ for $Z=63$; $\langle r^{-3}\rangle=10.8a_H^{-3}$, $\langle V_1\rangle=1.1a_H^{-3}$, $R'=0.025$ for $Z=71$. We note that for Eu and Re, only $6p$ contributes to the quadrupole coupling, because the configurations $4f^7$ and $5d^6$ are in S states. For D and Li^7 a correction is not called for, because the electric field gradient was determined from a molecular wave function. When molecules are used for microwave measurements, the p orbitals are mixed with excited s states.[14] However, the correction C still applies, since the valence electron contributes to the quadrupole coupling only when it is in the p state, in which case it interacts with the shielded moment.

I would like to thank Professor H. Snyder for much encouragement and several helpful discussions. I am also indebted to Professor J. Slater for valuable discussions.

[12] J. E. Mack, Revs. Modern Phys. **22**, 64 (1950).

[13] Here $\langle r^{-3}\rangle$ is the average over the $6p$ function; $\langle V_1\rangle$ is the average of V_1, defined by Eq. (74), of I (see Table III of I).

[14] C. H. Townes and B. P. Dailey, J. Chem. Phys. **17**, 782 (1949).

Interpretation of Experiments on the Photonuclear Effect in Heavy Elements*

L. EYGES
Radiation Laboratory, Department of Physics, University of California, Berkeley, California†
(Received December 26, 1951)

An analysis of the experiments to date on photonuclear reactions in heavy nuclei leads to the following results. There is a correlation between the energy at which the (γ,n) cross section is a maximum and the $(\gamma,2n)$ threshold. The shape of the total photon absorption cross sections in Sb and Ta can be estimated up to 22 Mev, and there is an indication that the cross section drops off strongly above that energy. Using the estimate of the shape of the total cross section in Ta, one can calculate the neutron yield to be expected in experiments with 330-Mev bremsstrahlung. The calculated value is only about 60 percent of the experimental value. Evidence is presented that the discrepancy is due to neutrons produced by high energy photons, presumably due to mesonic effects. The integrated cross sections for Zn^{64}, Sb, and Ta^{181} can be evaluated and by comparison with the Levinger-Bethe formula lead to values of 0.56, >0.44, and 0.50, respectively, for the fraction of exchange force in the neutron-proton interaction, assuming that all of the photoeffect is due to electric dipole transition.

THERE have been many experiments on the photonuclear effect.[1–39] Some of these have been interpreted as agreeing with Bohr's model of the compound nucleus, whereas others have seemed to disagree. Thus, Hirzel and Wäffler[2] measured the ratio of emitted protons to neutrons from nuclei irradiated by 17.5-Mev γ-rays and found that this ratio was much higher than that predicted by compound nucleus theory. Another apparent discrepancy arose when it was established that the (γ,n) cross section in medium weight elements had a maximum around 20 Mev and dropped off sharply for higher energies. According to compound nucleus theory, this drop-off should be due to the competition to the (γ,n) reaction afforded by the $(\gamma,2n)$. But experimentally, it appeared that the $(\gamma,2n)$ cross section was much too small to furnish appreciable competition. It was this discrepancy, among others, that led Goldhaber and Teller[40] to propose their special model of nuclear dipole vibrations. Finally, various observers have found that the angular distribution of high energy protons from (γ,p) reactions is not spherically symmetrical, in contradiction to the predictions of the compound nucleus.

On the other hand, there were experiments which were in good agreement with compound nucleus theory. Thus, the angular distribution of the low energy neutrons and protons produced in the nuclear photoeffect was measured by various workers and found to be spherically symmetrical.[10,11,30] Also, the energy distribution of the neutrons and protons was in good agreement with the compound nucleus model.[11] Moreover, Byerly and Stephens[16] measured the ratio of neutrons to protons emitted from Cu when irradiated with 24-Mev bremsstrahlung and found excellent agreement with the predictions of Weisskopf and Ewing,[41] which were based on the compound nucleus model.

These apparently contradictory results are, we think, resolved in part by the suggestion of Courant[42] that there may be a direct photoeffect on protons, in which they are ejected from the nucleus without a compound nucleus being formed. The cross section for this process can be quite small and still explain the anomalously large number of protons in Hirzel and Wäffler's experiment. Also, this hypothesis explains naturally the

* This work was performed under the auspices of the AEC.
† Present address: American Embassy, 2 Ave. Gabriel, Paris 8, France.

[1] G. C. Baldwin and G. S. Kaiber, Phys. Rev. **70**, 259 (1946).
[2] O. Hirzel and H. Wäffler, Helv. Phys. Acta. **19**, 373 (1947).
[3] J. L. Lawson and M. L. Perlman, Phys. Rev. **74**, 1190 (1948).
[4] M. L. Perlman and G. Friedlander, Phys. Rev. **74**, 445 (1948); M. L. Perlman, Phys. Rev. **75**, 988 (1949).
[5] H. Wäffler and O. Hirzel, Helv. Phys. Acta. **21**, 200 (1948).
[6] N. W. Curtis *et al.*, Phys. Rev. **77**, 290 (1950).
[7] E. R. Gaerttner and M. L. Yeater, Phys. Rev. **77**, 570, 714 (1950).
[8] G. A. Price and D. W. Kerst, Phys. Rev. **77**, 806 (1950).
[9] H. L. Poss, Phys. Rev. **79**, 539 (1950).
[10] D. W. Kerst and G. A. Price, Phys. Rev. **79**, 725 (1950).
[11] B. C. Diven and G. M. Almy, Phys. Rev. **80**, 407 (1950).
[12] A. K. Mann and J. Halpern, Phys. Rev. **80**, 470 (1950).
[13] Seishi Kikuchi, Phys. Rev. **80**, 492 (1950).
[14] McDaniel, Walker, and Stearns, Phys. Rev. **80**, 807 (1950).
[15] H. E. Johns, *et al.*, Phys. Rev. **80**, 1062 (1950).
[16] P. R. Byerly, Jr., and W. E. Stephens, Phys. Rev. **81**, 473 (1951).
[17] R. N. H. Haslam and H. M. Skarsgard, Phys. Rev. **81**, 479 (1951).
[18] L. Katz and A. S. Penfold, Phys. Rev. **81**, 815 (1951).
[19] L. Katz and A. S. Penfold, Phys. Rev. **83**, 169 (1951).
[20] N. Sugarman and R. Peters, Phys. Rev. **81**, 951 (1951).
[21] Karl Strauch, Phys. Rev. **81**, 973 (1951).
[22] Seishi Kickuchi, Phys. Rev. **81**, 1060 (1951).
[23] Richard D. Miller, Phys. Rev. **82**, 260 (1951).
[24] Haslam, Johns, and Horsely, Phys. Rev. **82**, 270 (1951).
[25] L. Katz *et al.*, Phys. Rev. **82**, 271 (1951).
[26] E. R. Gaerttner and M. L. Yeater, Phys. Rev. **82**, 461 (1951).
[27] Stephens, Halpern, and Sher, Phys. Rev. **82**, 511 (1951).
[28] M. E. Toms and W. E. Stephens, Phys. Rev. **82**, 709 (1951).
[29] A. K. Mann and J. Halpern, Phys. Rev. **82**, 733 (1951).
[30] Terwilliger, Jones, and Jarmie, Phys. Rev. **82**, 820 (1951).
[31] C. Levinthal and A. Silverman, Phys. Rev. **82**, 822 (1951).
[32] P. R. Byerly, Jr., and W. E. Stephens, Phys. Rev. **83**, 54 (1951).
[33] E. R. Gaerttner and M. L. Yeater, Phys. Rev. **83**, 146 (1951).
[34] R. Sagane, Phys. Rev. **83**, 174 (1951).
[35] Marshall, Rosenfeld, and Wright, Phys. Rev. **83**, 305 (1951).
[36] L. Lundby and L. Marshall, Phys. Rev. **83**, 323 (1951).
[37] L. Marshall, Phys. Rev. **83**, 345 (1951).
[38] J. Halpern and A. K. Mann, Phys. Rev. **83**, 370 (1951).
[39] D. H. Wilkinson and J. H. Carver, Phys. Rev. **83**, 466 (1951).
[40] M. Goldhaber and E. Teller, Phys. Rev. **74**, 1046 (1948).
[41] V. Weisskopf and D. H. Ewing, Phys. Rev. **57**, 472 (1940).
[42] E. Courant, Phys. Rev. **82**, 703 (1951).

TABLE I. Summary of data on photonuclear reactions.

Isotope	Threshold	W_{max}	Half-width	$\int \sigma dW$ (Mev-barns)	Reference
		(γ,n) reactions			
C^{12}	18.7	22.4	···	0.047	24
C^{12}	···	···	···	0.086	35
C^{12}	···	···	···	0.107	21
Al^{27}	14	19.6	···	···	···
I^{121}	12.4	19.0	7.5	0.120	18
Fe^{54}	18.3	···	5.7	0.42	25
Ni^{58}	18.5	···	4.6	0.33	25
Cu^{63}	10.9	17.5	6.0	0.70	15
Cu^{63}	10.9	···	···	0.77±0.15	35
Cu^{63}	10.9	17.5	···	0.60	11
Cu^{65}	10.2	19.0	6.0	1.40	15
Cu^{66}	···	19.0		0.89	21[a]
Zn^{64}	19.0	···	···	0.61	21[a]
Zn^{64}	18.5	···	7.1	0.83	25
Zn^{64}	···	···	···	0.77	35
Ag^{109}	···	16.5	···	1.65	11
Sb^{121}	9.3	14.5	5.5	>1.2	15
Sb^{122}	9.3	14.5	5.5	2.0	15
Ta^{181}	8.0	13.5	4.5	>0.39	15
		(γ,p) reactions			
C^{12}		21.5±0.5	1.7	0.063±0.016	38
Mg^{25}		21	···	0.056±0.03	28
Al^{29}		21.2±0.5	5.4	0.12±0.03	38
Ni {67% Ni^{58}, 27% Ni^{60}}		18.7	5.4	0.32±0.08	38
$^{27}Co^{62}$		21.5	5.7	0.14±0.04	38
$^{30}Zn^{68}$		···	···	0.068	21
$^{41}Cb^{93}$		21.3	6.6	0.12±0.03	38
		Higher order reactions			
Reaction					
$S^{32}(\gamma,np+d)$				0.004	18
$Zn^{64}(\gamma,pn)Cu^{63}$				0.26	21[a]
$Zn^{66}(\gamma,pn)Cu^{64}$				0.13	21[a]
$Zn^{64}(\gamma,2n)Zn^{62}$				0.047	21[a]
$Cu^{63}(\gamma,2n)Cu^{61}$				0.035	34[a]

[a] In this reference the measurements of integrated cross sections are relative to that of Cu^{63}. To convert these relative values to the absolute ones given in this table we have taken as the integrated cross-section for Cu^{63} the mean of the three values given above, i.e., 0.69-Mev barn.

angular asymmetry of high energy protons mentioned above. Moreover, it does not destroy the agreement with the compound nucleus theory that Byerly and Stephens found. The directly-ejected protons are important only when the proton binding energy is so high that the number of evaporated protons is small. This is the case in the experiments of Hirzel and Wäffler but is not so for Cu^{63}, the element measured by Byerly and Stephens.

There is also no contradiction between compound nucleus theory and the fact mentioned above, that the $(\gamma,2n)$ cross section in Cu^{63} is much too small to provide competition for the (γ,n) reaction. It appears experimentally that the (γ,np) cross section is much larger than the $(\gamma,2n)$ cross section and, indeed, is sufficiently large to afford competition.

There is some other evidence that has not been presented before for the validity of the statistical model. For heavy nuclei, the emission of a proton is strongly inhibited by the Coulomb barrier. The only important processes appear to be the emission of neutrons. If the statistical theory and the idea of competition is correct, we would expect to find a correlation between the energy at which the (γ,n) cross section is maximum and the threshold of the $(\gamma,2n)$ reaction. Evidence for such a correlation is presented in Sec. III.

The statistical model predicts what happens after the nucleus absorbs a photon. There are also theories which say something about the absorption of the photon in the first place. In particular, we shall consider the work of Levinger and Bethe.[43] Using so-called "sum rules" these authors calculate the integrated cross section for dipole absorption of a photon. They get the formula

$$\int_0^\infty \sigma_{\text{total}}(W)dW = 0.060(NZ/A)(1+0.8x). \quad (1)$$

Here x is the fraction of exchange force in the neutron-proton potential (assumed to be due to central forces only). $\sigma_{\text{total}}(W)$ is the sum of all processes in which a photon is absorbed, i.e., it is the sum of the cross sections for all such processes as (γ,n), (γ,p), $(\gamma,2n)$, etc. If we have an experimental value for this sum, we have a means of deducing the fraction of exchange force in the neutron-proton potential, always remembering the assumption of dipole transition. The integral in Eq. (1) can be evaluated from the available data in some cases. This is discussed in Sec. VI.

The experiments that we have analyzed to obtain the results stated above have been of two major kinds. The first kind is that in which the integrated cross section and sometimes the detailed shape of a particular reaction is measured, detecting the reaction by the method of induced radioactivity. The second kind is that in which the total neutron yield is measured from a target irradiated by bremsstrahlung or some other source of photons. The latter method has the advantage that one gets information about all reactions in which a neutron is emitted, but it has the corresponding disadvantage that one cannot immediately isolate the contribution to the total cross section from particular reactions. This disadvantage can be overcome to some extent by comparing the results of experiments done at different maximum bremsstrahlung energies. Among the experiments which we shall use, are those of McDaniel *et al.*[14] on neutron yields using photons from the $Li(p,\gamma)$ reaction, that of Price and Kerst[8] using bremsstrahlung at 18- and 22-Mev maximum energy and those of Terwilliger *et al.*[20] and of Kerst[10] using bremsstrahlung at about 330-Mev maximum energy. By comparing the difference between the 18- and 22-Mev yields, one gets information about the cross section for neutron emission between these energies; this is mainly information about the $(\gamma,2n)$ cross section for heavy elements. By further comparing the 22-Mev results with the 330-Mev results, we can find something about the contribution of the cross section between 22 and 330 Mev.

In the next section, we present a compilation of the

[43] J. S. Levinger and H. A. Bethe, Phys. Rev. **78**, 115 (1950).

data on individual reactions and in the following section, show that for heavy elements there is a strong correlation between the $(\gamma,2n)$ threshold and the peak of the (γ,n) cross section. In Sec. IV, we try to estimate the magnitude of the $(\gamma,2n)$ cross section in some elements by comparing the 18- and 22-Mev data of Kerst and Price and by using the results of McDaniel mentioned above. We can then use this estimate and the 330-Mev bremsstrahlung data to try to find something about the cross section between 22 and 330 Mev. This work, plus other evidence presented in Sec. V, indicates that the total cross section drops off quite sharply above 22 Mev and begins to rise again at energies of the order of 200 Mev. This rise may be due to mesonic effects. In Sec. VI, we use our deductions from the experimental data to calculate the integrated cross section and hence the fraction of exchange force in the n-p interaction.

II. SUMMARY OF DATA

In Table I we present a summary of the data available on photonuclear reactions. There are some interesting features to note in this table. The first is the rather regular rise of the integrated cross section for (γ,n) reactions. Also, there is a slight indication that for elements heavier than Cu, the (γ,n) half-width decreases slowly with Z. As opposed to the (γ,n) reactions, the integrated cross section for (γ,p) reactions rises with Z up to about $Z=28$ and then begins to drop off. This trend is confirmed by the work of Mann and Halpern,[39] who measure the yields of (γ,p) reactions as a function of Z. These yields are roughly proportional to the integrated cross section. Mann and Halpern also find a maximum yield at around $Z=30$. At this point the yields are of the same order of magnitude as for the (γ,n) reaction. Beyond $Z=30$, however, the proton yield drops off rapidly and at $Z=50$ is about one-hundredth the neutron yield. This is easily understandable as due to the effect of the Coulomb barrier. It suggests that in heavy elements one can confine attention to processes in which a neutron is emitted. The last point to be noted in Table I is that the integrated cross section for the (γ,pn) reaction in a medium weight element can be much larger than that for the $(\gamma,2n)$ reaction. For $_{30}Zn^{64}$, e.g., the integrated (γ,pn) cross section is about 0.4 of the integrated (γ,n) cross section. This suggests that, if the statistical model holds, competition in medium weight elements may be provided by (γ,pn) rather than $(\gamma,2n)$ reactions.

III. CORRELATION BETWEEN ENERGY AT WHICH (γ,n) CROSS SECTION IS MAXIMUM AND THRESHOLD OF THE $(\gamma,2n)$ REACTION

According to the Bohr concept of the compound nucleus, the cross section $\sigma_{\gamma,a}(W)$ for a reaction in which a particle a[44] is emitted when a photon of energy W is incident on a nucleus, is $\sigma_{\gamma,a}(W)=\sigma_{abs}(W)\times P_a(W)$. Here $\sigma_{abs}(W)$ is the cross section for absorption of a photon of energy W, and $P_a(W)$ is the probability that at excitation energy W, the nucleus emits a particle type a. Now, as is well known, the cross section of the (γ,n) reaction, $\sigma_{\gamma,n}(W)$, has a maximum around 19 Mev for medium weight elements and at somewhat smaller values for heavier elements. In all measured cases, the cross section is small or zero near threshold and rises sharply to the maximum. We will say nothing about this initial rise here. A maximum in the (γ,n) absorption cross section could be caused by a maximum in $\sigma_{abs}(W)$, or, if we assume that $\sigma_{abs}(W)$ is more or less flat near W_m, the maximum could be caused by a dropping off of $P_a(W)$. The last assumption seems to us to be much less restrictive.

If we make it, we would expect to find a correlation in heavy elements between the energy W_m at which the (γ,n) cross section is maximum and the $(\gamma,2n)$ threshold. We have restricted this statement to heavy elements because, as we have discussed in the introduction, it is only for these that one can be reasonably certain *a priori*, that essentially only neutrons are emitted. For medium weight elements, we would expect a correlation if the $(\gamma,2n)$ process dominated the (γ,pn). We are reasonably sure that this is the case for Cu^{63}, for which Byerly and Stephens have found that proton emission is small compared with neutron emission. Thus, we include Cu^{63} along with four other heavy elements in Table II, which seems to show that there is a real correlation between W_m and the $(\gamma,2n)$ threshold.

A word about the method of calculating the $(\gamma,2n)$ thresholds given in the third column of Table II may be useful here. That for Ag^{109} is obtained by adding the value given by Sher *et al.*[45] for the photoneutron threshold in Ag^{109} to Harvey's[46] value for the photoneutron threshold in Ag^{108}. Similarly, for Sb^{123} we have used Sher's value for the threshold in Sb^{123} and Harvey's for the threshold in Sb^{121}. For the other elements, we have had to add the measured values of the (γ,n) threshold (from Harvey and/or Sher) in the original nucleus and the value calculated from the semi-empirical mass formula for the final nucleus, or vice versa. The measured values have probable errors of about 0.2 Mev. A comparison of Harvey's data on some neighboring

TABLE II. Comparison of the $(\gamma,2n)$ threshold and energy W_m at which the (γ,n) cross section is maximum.

Element	W_m	$(\gamma,2n)$ threshold
$_{29}Cu^{63}$	19.0	18.1
$_{47}Ag^{109}$	16.5	16.05±0.28
$_{51}Sb^{121}$	14.5	15.6±0.3
$_{51}Sb^{123}$	14.5	15.4
$_{73}Ta^{181}$	14.0[a]	14.1

[a] This value is a later one than that presented in Table I and is taken from a preprint of a paper by R. N. H. Haslam, L. A. Smith, and J. G. V. Taylor.

[44] We shall let the subscript a signify several particles if the excitation energy W is high enough that they can be emitted.

[45] Sher, Halpern, and Mann, Phys. Rev. **84**, 387 (1951).

[46] J. A. Harvey, Phys. Rev. **81**, 353 (1951).

elements with the calculated values for those elements, indicates that the calculated values that enter here should be good to within 0.3 or 0.4 Mev. Therefore, we expect the $(\gamma,2n)$ thresholds given in Table II for Cu, Sb^{123}, and Ta to be accurate to perhaps 0.5 Mev. Probably, this is the magnitude of error in the position in the maximum of the cross section. Thus, our values seem to be sufficiently accurate as not to destroy the correlation, if there is one.

IV. ESTIMATE OF (γ,n) AND $(\gamma,2n)$ CROSS SECTION FOR Sb AND Ta

In this section, we attempt to estimate the (γ,n) and $(\gamma,2n)$ cross sections as a function of photon energy and hence, the total cross section below the $(\gamma,3n)$ threshold, for Sb and Ta. The reason for limiting ourselves to these two elements will appear shortly.

The shape of the (γ,n) cross section for Ta^{181} (the only isotope of Ta) is known from the work of Johns *et al.*,[15] but the absolute magnitude is not. Naturally occurring Sb consists of two isotopes, Sb^{121} (56 percent) and Sb^{123} (44 percent). The (γ,n) cross section for Sb^{123} has been measured by Johns *et al.*[14] The shape of the (γ,n) cross section in Sb^{121}, for those reactions in which the nucleus is left in the 16.4-minute isomeric state, has also been measured. The shape of this cross section curve is, within experimental error, the same as that for Sb^{123}. We will assume here that the shape of the (γ,n) reaction in which Sb is left in the ground state is the same as that measured for the reaction in which Sb is left in the isomeric state.[47] Thus, both isotopes of Sb will be assumed to have the same total cross section shape. It would be very natural, both *a priori* and in view of the assumed similarity in shape between the cross sections in Sb^{121} and Sb^{123}, to assume further that the magnitudes are the same. We shall not do this here, but instead shall estimate independently the magnitude of the cross section in Sb^{121}; we shall find that it does come out to be very close to that for Sb^{123}.

We already know something about the total cross section in Sb and Ta, since we know the shape of the (γ,n) cross section and up to the $(\gamma,2n)$ threshold this is the total cross section. In the last section, we found that the (γ,n) cross section had a maximum, i.e., was flat just at and below the $(\gamma,2n)$ threshold. In view of the correlation we have found between the energy at which the (γ,n) reaction is maximum and the $(\gamma,2n)$ threshold, it seems very reasonable to assume that the total cross section is fairly flat just beyond the maximum. Starting from this, we can estimate the total cross section above the $(\gamma,2n)$ threshold in more detail using the data of Price and Kerst[8] on neutron yields with 18- and 22-Mev bremsstrahlung and the data of McDaniel *et al.*[14] on neutron yields with γ-rays from the $Li^7(p,\gamma)$ reaction.

Price and Kerst have made measurements of the neutron yields from a large number of elements, using 18- and 22-Mev bremsstrahlung. The ratio of these yields is a smoothly varying function of Z for Z greater than about 30. The difference in yields between the 18- and 22-Mev experiments is due to the difference in the bremsstrahlung spectra at these energies, weighted by the cross section [mainly $(\gamma,2n)$]. We know what the difference between the 18- and 22-Mev spectra looks like from the work of Schiff.[48] Thus, we can estimate roughly what the $(\gamma,2n)$ cross section must be between these energies to agree with Kerst and Price's experiment. This first estimate is rather ambiguous, since there is, of course, more than one shape which will give agreement, but it is a starting point, and we shall see later how it can be made more accurate.

Now, using our guess of the shape of the $(\gamma,2n)$ cross section we can estimate the absolute cross sections in a way which is insensitive to errors in the $(\gamma,2n)$ cross section. Price and Kerst have also measured the relative neutron yields of various elements at 18 Mev, among them Cu. Now, the (γ,n) cross sections for Cu^{63} and Cu^{65} are quite well known. The integrated cross section for Cu^{63} has been measured by three different observers[11,14,32] with fairly good agreement among the three measurements. The measurements of the Cu^{63} cross section by Diven and Almy[11] and by Johns *et al.*[15] agree quite well with each other. The cross section curve for Cu^{65} has been measured only by Johns *et al.*, but it agrees very well with the Cu^{63}:Cu^{65} cross-section ratio measurements at 17.5 Mev of Hirzel and Wäffler. Thus, there is reason to have considerable confidence in an average of the different sets of measurements on Cu^{63} and of Johns' measurements of Cu^{65}. Then, using the 18-Mev bremsstrahlung spectrum due to Schiff, we can calculate the absolute neutron yield to be expected from natural copper. Using the relative cross-section shapes as estimated above for the element considered, we can also calculate what the absolute magnitude must be to agree with Kerst's 18-Mev data on the yield relative to Cu.

To successfully carry out the analysis outlined above, we must know the shape of the (γ,n) cross section. This is known for all the isotopes in Table II. But now we see why the only elements we can use are Sb and Ta and not Ag and Cu. This is because Kerst and Price use natural isotopic mixtures of the elements, and Ag^{109} and Cu^{65} represent only 48.1 percent and 29.9 percent of the natural isotopic mixture, respectively. On the other hand Ta^{181}, and Sb^{121} and Sb^{123} together, account

[47] Evidence for the correctness of this assumption is had from the work of R. Montalbetti and L. Katz, Phys. Rev. **83**, 892 (1951). These authors have measured the cross-section curves for $Mo^{99}(\gamma,n)Mo^{91}$ when Mo^{91} is left both in the ground state and in a 15.5-min isomeric state. They find a peak for both reactions at 18.7 Mev and also find that above 15.5 Mev the shape of the cross-section curves are the same. The cross sections begin to differ below 15.5 Mev, but they are small compared to their peak values in that region. Similar results have been found by R. Sagane (private communication).

[48] L. I. Schiff, Phys. Rev. **83**, 252 (1951).

for approximately 100 percent of the isotopic abundances of Ta and Sb.

Our estimate of the absolute magnitude of the (γ,n) cross section is insensitive to the estimated shape of the $(\gamma,2n)$ cross sections, since most of the neutron yield with 18-Mev bremsstrahlung from Sb and Ta comes from the (γ,n) reaction.

We can check and refine the above rough estimates using other experimental data. McDaniel *et al.*[4] have measured the neutron yield relative to Cu from various elements irradiated with the γ-rays from the $Li^7(p,\gamma)$ reaction. These γ-rays comprise a sharp line at 17.6 Mev and another component of about half the intensity with a half-width of about 2 Mev centered at 14.8 Mev. Since we know the cross sections for Cu and have an estimate of the cross sections for other elements, we can calculate the relative yields to be expected in the experiment of McDaniel and if necessary, correct our previous estimates. The relative yields in McDaniel's experiment are particularly sensitive to the absolute value of the $(\gamma,2n)$ cross section at 17.6 Mev. Our results are given in Fig. 1.

The curves in this figure are such as to agree within a few percent with the experimental data we have used to check them, namely the ratio of neutrons yields to that of Cu in the experiments of Kerst and Price, and of McDaniel and the ratio of the 18- and 22-Mev yields in the Kerst and Price experiment. We estimate that they are not in error by more than 15 percent. Although we have drawn in the total cross section up to 22 Mev, the data does not really tell much about the cross sections above 20 Mev. Thus, as far as this data goes, it is quite possible that above 20 Mev the cross-section curve for Sb does not drop off as sharply as indicated, i.e., that there may be a long flat tail which contributes appreciably to the integrated cross sections. For Ta, the situation is quite different. Here the cross section has dropped to less than one-fifth of its maximum value by 20 Mev; hence it seems very unlikely that there is appreciable contribution to the integrated cross section from energies above 22 Mev.

The integrated cross section for the (γ,n) reaction up to 22 Mev in Sb is given by our estimates as 1.82-Mev barns, which is very close to the value of 2.0 Mev-barns found by Katz for Sb^{123}. This is very reasonable, as we have discussed earlier, in the light of the similarity in cross-section shape between Sb^{121} and Sb^{123}.

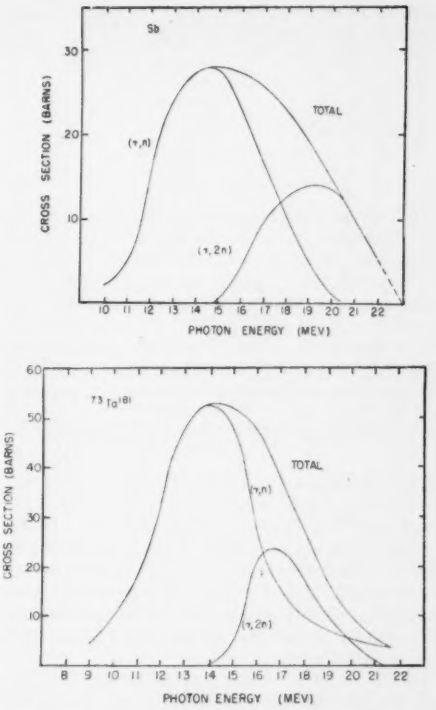

FIG. 1. Estimate of the (γ,n) and $(\gamma,2n)$ cross sections in Sb: (56 percent Sb^{121}+44 percent Sb^{123}) and $_{73}Ta^{181}$. The shape of the (γ,n) cross section is assumed known from the work of Johns *et al.* The shape of the total cross section (and hence of the $(\gamma,2n)$ cross section) is estimated roughly from Price and Kerst's data on the ratio of neutron yields with 18- and 22-Mev bremsstrahlung. The absolute magnitude of the cross sections can then be found by using the known cross sections in Cu and comparing Price and Kerst's yield at 18 Mev for the element concerned with that for Cu. This estimate is insensitive to errors in the shape of the $(\gamma,2n)$ cross section. Finally, the procedure is checked and refined by using the data of McDaniel *et al.* on the yields relative to Cu using γ-rays from the $Li(p,\gamma)$ reaction. This data is particularly sensitive to the absolute value of the $(\gamma,2n)$ cross section at 17.6 Mev.

V. YIELDS WITH 330-MEV BREMSSTRAHLUNG. EVIDENCE FOR AN INCREASE IN THE TOTAL CROSS SECTION AT HIGH ENERGIES

Terwilliger *et al.*[10] and Kerst[9] have measured the absolute yields of neutrons using bremsstrahlung with a 330-Mev maximum energy. We can calculate the yields to be expected in Sb and Ta from the (γ,n) and $(\gamma,2n)$ reactions by photons of energy up to 22 Mev by using the results given in Fig. 1 for the shape and absolute magnitude of the cross-section curves. The formula for the yields with 330-Mev bremsstrahlung is

$$\text{Yield}\left(\frac{\text{neutrons}}{\text{erg}\times\text{mole/cm}^2}\right)$$

$$=1.77\times10^3\int[(\sigma_{\gamma,n}(W)+2\sigma_{\gamma,2n}(W)\cdots)]\frac{dW}{W},$$

for cross sections in barns. Computing from this formula, one gets for the yields up to 22 Mev of Ta^{181} and the natural isotopic mixture of Sb, 526 and 320 neutrons/(erg×mole/cm^2), respectively. The measured

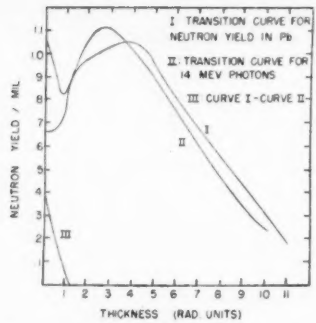
I TRANSITION CURVE FOR NEUTRON YIELD IN Pb
II TRANSITION CURVE FOR 14 MEV PHOTONS
III CURVE I - CURVE II
NEUTRON YIELD / MIL
THICKNESS (RAD. UNITS)

FIG. 2. Decomposition of the transition curve for neutron yield due to 330-Mev bremsstrahlung in Pb. Curve *I* is the original transition curve as measured by Terwilliger *et al.* Curve *II* is the transition curve for a spectrum of photons with peak energy at 14 Mev. Curve *III* is the difference between curves *I* and *II* and is presumably the transition curve due to neutrons produced by mesons. It corresponds to an energy of the order 200 Mev.

yields[19] are 940 and 552 neutrons/(erg×mole/cm²), and are thus higher than the calculated yields by almost a factor two. Thus, there is evidence that a considerable fraction of the neutron yield in experiments with 330-Mev bremsstrahlung comes from photons with energy greater than 22 Mev. *A priori*, there is no way to decide whether the photon absorption cross section drops off fairly quickly beyond the maximum or whether there is an appreciable tail.

For Sb, as we have seen, one cannot say with any certainty whether such a tail exists or not. For Ta the situation is different. Here, our reconstruction of the cross-section curves indicates that the total cross section is small at 22 Mev and that there is no evidence for an appreciable tail. Moreover, for Pb there is other evidence that shows much more strongly that the extra neutrons which are needed above 22 Mev to give agreement with the 330-Mev data come not from a long tail to the photon absorption cross section, but rather from an increase in the neutron yield for photon energies of the order of 200 Mev.

This evidence is as follows: Terwilliger *et al.* have measured the transition curve for the neutron yield in Pb due to 330-Mev photons, i.e., the curve of yield per unit thickness vs thickness in Pb. This curve is reproduced in Fig. 2. Now, we would expect the photon absorption cross section for Pb to be quite similar to that for Ta, except that the maximum should be shifted to a somewhat lower energy, say 14 Mev. But we have a good idea of what a transition curve resulting from a spectrum of photons with maximum energy around 14 Mev should look like. Such a transition curve is essentially determined by the energy in the photon absorption cross section for which the cross section is a maximum. Its main features do not depend on whether the cross section has a tail or not, provided it is not very large. Strauch[21] has measured transition curves for photon spectra with peaks at 16 and 19 Mev (the (γ,n) cross sections in Ag^{109} and Cu^{63}, respectively). These curves, normalized to unity at the origin, do not differ by more than 30 percent at most and usually by much less than that. One can then quite reliably extrapolate them to find the transition curve due to a photon spectrum with 14-Mev maximum energy. This extrapolated curve is shown in Fig. 2, as curve *II*, normalized to Terwilliger's curve at radiative units. We see that for thicknesses greater than a radiation length, this curve has the same shape within the experimental error as the transition curve in Pb measured by Terwilliger *et al.* If we subtract the two, we get the transition curve for neutron yield from those photons which are not contained in the spectrum around 14 Mev. The subtracted curve is given by curve *III* of Fig. 2. We see that it falls off very sharply and thus corresponds to a very high

TABLE III. Evaluation of $\int\sigma_{\text{tot}n}dW$ and x, the fraction of exchange force in the neutron-proton interaction, for $_{30}Zn^{64}$.

Reaction	$\int\sigma dW$ (Mev-barns)	Source
(γ,n)	0.730	Arithmetic mean of the values in references 21, 25, and 36.
(γ,p)	0.14	Estimated from evaporation model.
$(\gamma,2n)$	0.047	Reference 21.
$(\gamma,2p)$	~0	Reference 4.
(γ,pn)	0.260	Reference 21.
$(\gamma,p2n)$	~0.12	From values in reference 21 for $_{30}Zn^{66}$, multiplied by two to take account of the fact that $\int\sigma_{\gamma,pn}dW$ for $_{30}Zn^{64}$ is twice that for $_{30}Zn^{66}$.
$(\gamma,p3n)$	~0.066	
$(\gamma,p4n)$	~0.028	

$\int\sigma_{\text{tot}n}dW = 1.39$; $x = 0.56$.

energy. We estimate this energy to be of the order of 200 Mev. The obvious explanation of the source of this high energy yield of neutrons is from the stars produced by mesons, either real or virtual.

The relative contribution to the neutron yield due to the high energy photons as compared with those around 14 Mev in the Terwilliger *et al.* experiments is given approximately by the relative height of the two transition curves at $t=0$, since in these experiments the thickness of the targets was small compared with a radiation length. From the relative heights at $t=0$, we conclude that for Pb the high energy photon component contributes about 40 percent of the neutron yield and the low energy component about 60 percent. This is in excellent agreement with our results for Ta, where we concluded that the high energy component contributed 44 percent of the neutron yield.

If we make the guess indicated by the dotted line in Fig. 1 for the cross section of Sb above 22 Mev, we find that this cross section gives an absolute yield of 328 neutrons/(erg×mole/cm²). This is 59 percent of the yield found by Terwilliger *et al.* Thus for this estimate

[19] The values of Kerst are 27 percent lower than those of Terwilliger. We have taken as the measured value the arithmetic mean of Terwilliger's and Kerst's values.

of the Sb cross section, 41 percent of the yield comes from high energy photons.

Finally, our hypothesis that the photon absorption cross section for heavy elements drops off quite sharply beyond the maximum is supported by direct experimental evidence. Anderson and Duffield[50] have measured the total absorption cross section of U^{238} and find that at 23 Mev, the cross section is a small fraction of its value at 15 Mev, the energy at which the maximum cross section occurs.

VI. EVALUATION OF $\int\sigma_{\text{total}}dW$. COMPARISON WITH LEVINGER-BETHE FORMULA

In this section, we try to evaluate the total integrated cross section for photon absorption from experimental data. When this is done we can use this value in Eq. (1) to try to find the fraction of exchange force x in the n-p interaction. The total cross section for photon absorption is the sum of the cross sections for all processes in which a photon is absorbed and a particle (or photon) is emitted. There is sufficient data for the elements $_{30}Zn^{64}$ and $_{73}Ta^{181}$ to evaluate the total cross section with reasonable accuracy. Also, one can get a lower limit from the data on Sb. First, we present our data in

TABLE IV. Evaluation of $\int_0^{23}\sigma_{\text{total}}dW$ and x, the fraction of exchange force in the neutron-proton interaction, for Sb.

Reaction	$\int\sigma dW$ (Mev-barns)	Source
(γ,n)	1.82	Secs. II and III
$(\gamma,2n)$	0.59	Secs. II and III
$(\gamma,n>2)$	?	
$\int_0^{23}\sigma_{\text{total}}dW>2.41$; $x>0.44$.		

Tables III, IV, and V, and then we discuss the data briefly.

We consider first, the data for $_{30}Zn^{64}$ given in Table III. There are several reactions listed, the source of which is the work of Strauch.[21] Strauch has measured only values of the integrated cross sections relative to that of Cu^{63}. To obtain absolute values from his data, we have combined his relative measurements with three measurements of the integrated cross sections for the (γ,n) reaction on Cu^{63} by Johns *et al.*, Marshall, and Diven and Almy. These authors give this integrated cross section as 0.70, 0.77±0.15 and 0.60 Mev-barns, respectively. We have used the mean of these three values, 0.69 Mev-barns, to get absolute values from Strauch's relative measurements.

The integrated cross section for the (γ,p) reaction is obtained from the known (γ,n) cross section combined with the calculations of Weisskopf and Ewing on the relative probability of evaporation of a proton or neutron. This should give a fairly reliable estimate, since the proton is bound much less tighly than the neutron. As we have discussed in the introduction, in such a case

[50] R. E. Anderson and R. B. Duffield, Bull. Am. Phys. Soc. **26**, No. 6, 32 (1951).

TABLE V. Evaluation of $\int\sigma_{\text{total}}dW$ and x, the fraction of exchange force in the neutron-proton interaction, for $_{73}Ta^{181}$.

Reaction	$\int\sigma dW$ (Mev-barns)	Source
(γ,n)	2.96	Secs. II and III
$(\gamma,2n)$	0.81	Secs. II and III
$(\gamma,n>2)$	~0	Secs. II and III
$\int\sigma_{\text{total}}dW=3.77$; $x=0.56$.		

the evaporation theory probably predicts the relative numbers of neutrons and protons fairly accurately. Our calculation neglects the protons which are emitted below the threshold for neutron production, but it is very likely that the number of such protons is small. We would expect the integrated $(\gamma,2p)$ cross section to be very small, since the integrated (γ,p) cross section is small. There is also evidence for this from the data of Perlman[4] on the neighboring element Cu^{63}. Perlman finds that the relative yields for the $Cu^{63}(\gamma,n)$ and $Cu^{63}(\gamma,2p)$ reactions from 50-Mev bremsstrahlung are 35 and 0.16, respectively. Assuming that the energy at which the $(\gamma,2p)$ cross section is a maximum is about twice that for the (γ,n) gives the result that the integrated $(\gamma,2p)$ cross section is about 1 percent of the integrated (γ,n) cross section. We would expect a similar result from Zn. Also, we would expect that the cross sections for higher order reactions involving two protons as $(\gamma,2pn)$, $(\gamma,2p2n)$, etc., are small, as well as the (γ,γ) and (γ,α) reaction. Thus, it is likely that the data listed in Table II includes all reactions whose integrated cross sections are appreciable and that the value for $\int\sigma_{\text{total}}dW$ is fairly accurate. Putting this value into the formula (1) gives a value $x=0.56$ for the fraction of the exchange force in the n-p interaction. This is in good agreement with the ratio postulated by Serber to explain the high energy n-p scattering. In Tables IV and V, we present data for the evaluation of $\int\sigma_{\text{total}}dW$ for Sb and $_{73}Ta^{181}$. As we have noted before, the cross section for Sb is not known above 22 Mev. Hence, the integrated cross section given must be considered to be a lower limit. For Ta, on the other hand, we expect the integrated cross to be, to a good approximation, the sum of the (γ,n) and $(\gamma,2n)$ integrated cross sections. Comparing the total integrated cross sections with formula (1), one gets the values of x shown. Considering the errors involved in their calculation, the three values of x deduced here must be considered to be in good agreement with one another. In these calculations we have had to neglect contributions to the electric-dipole photoeffect from photons with energy greater than 330 Mev, but we expect this to be a very small contribution.

Katz and Penfold[18] have made similar calculations to that of this section for S^{32} and conclude that the integrated cross section is much less, about $\frac{1}{4}$ of that expected from the Levinger-Bethe formula. We think the reason for this disagreement is that among other things, they neglect to include the cross sections for

higher order reactions in which two or more neutrons are produced. The evidence for this is as follows. We have taken their estimate for the (γ,n) cross section and their measurements of the (γ,pn) cross section and calculated the yield of neutrons to be expected in Jarmie, Jones, and Terwilliger's experiments. The yield comes out to be too low by a factor five. Thus, there seems to be an appreciable cross section from reactions which Katz and Penfold have not taken into account. Of course, this yield might come from neutrons produced by high energy photons in a similar process to the one we have to postulate above to explain the Terwilliger transition curve. In this case the high energy process would have to account for 80 percent of the neutrons observed with 330-Mev bremsstrahlung. This seems rather high. If we assume arbitrarily, that as for heavy elements the high energy process accounts for about 40 percent of the neutron yield, then the (γ,n) cross section alone is too small by a factor three to secure agreement with Terwilliger's results. Thus, the estimate of the (γ,n) cross section is either much too low or else there are higher order reactions with integrated cross sections comparable to that for the (γ,n) process. At any rate, it seems that it would be premature to claim disagreement with the Levinger-Bethe formula until more measurements are made.

PHYSICAL REVIEW VOLUME 86, NUMBER 3 MAY 1, 1952

Nuclear Phenomena Deducible from μ-Pair Theory with Pseudoscalar Coupling*

L. M. TANNENWALD†
Department of Physics, University of Chicago, Chicago, Illinois
(Received November 21, 1951)

The case of pseudoscalar coupling between nucleons and μ-field is considered within the framework of μ-pair theory. Besides the usual perturbation treatment, the strong coupling approximation for this case is developed. Both methods are applied to the problems of scattering of μ-mesons by nucleons and the nucleon-nucleon interaction. Interpolation between the extremes of weak and strong coupling suggests that this μ-pair theory may be promising with an intermediate coupling strength, a condition also required by the μ-pair theory of the π-meson.

1. INTRODUCTION

BESIDES the Yukawa theory of nuclear forces, some attention has in the past been devoted to the so-called pair theories according to which the interaction between nucleons may be pictured as being transmitted by a pair of particles instead of a single particle (π-meson). The quanta of a pair may be either bosons[1] or fermions.[2] The latter were first taken to be electron-neutrino or electron-positron pairs and later μ-meson pairs.[3]

One recommending feature of pair theories is the saturation characteristics of the nuclear forces.[2,4–6] A second is the possibility of interpreting the π-meson as a pair of μ-mesons bound together due to a small admixture of a virtual nucleon-pair state,[7] and the possible explanation of the V-particles[8] as excited nuclear states resulting from the binding of μ-mesons, say, by a bare nucleon. The fact that the spin of such excited states may be integral or half-integral, depending on whether an odd or even number of fermions has been bound, may be helpful in understanding the long lifetime of the neutral V-particle (10^{-10} sec), in particular its stability against γ-decay into the neutron ground state.

The most serious objection against pair theories may well be the role played by the momentum cutoff which must be introduced to achieve convergence and which dominantly affects the predictions of the theory in the high energy region. Since it turns out that the cutoff also determines the range of the nuclear forces and the density of nucleons in heavy nuclei,[5] its order of magnitude is roughly that of the meson mass (times c). Therefore, if one takes the cut-off prescription seriously to the extent of applying it, for example, to the scattering of μ-mesons by nucleons, then one would expect at kinetic energies much greater than 100 Mev a very small cross section, while a substantially larger value for energies of the order 100 Mev or somewhat less. According to the measurements of Amaldi and Fidecaro[9] the cross section is at most 4.5×10^{-29} cm^2 per nucleon for μ-energies between 200 and 320 Mev, and above 320 Mev it is at most 2.3×10^{-30} cm^2 per nucleon. The cutoff therefore offers an explanation for the presently

* This paper was written as a Ph.D. thesis in the Department of Physics, University of Chicago, Chicago, Illinois.

† Present address: U. S. Naval Ordnance Test Station, Inyokern, China Lake, California.

[1] W. Pauli and N. Hu, Revs. Modern Phys. **17**, 267 (1945), for literature until 1945.

[2] G. Wentzel, Prog. Theoret. Phys. **5**, 584 (1950), for literature until 1950.

[3] R. Marshak, Phys. Rev. **57**, 1101 (1940).

[4] Wigner, Critchfield, and Teller, Phys. Rev. **56**, 530 (1939).

[5] G. Wentzel, Helv. Phys. Acta **15**, 111 (1942).

[6] A. Houriet, Helv. Phys. Acta **16**, 529 (1943).

[7] G. Wentzel, Phys. Rev. **79**, 710 (1950).

[8] G. D. Rochester and C. C. Butler, Nature **160**, 855 (1947); Seriff, Leighton, Hsiao, Cowan, and Anderson, Phys. Rev. **79**, 204 (1950).

[9] E. Amaldi and G. Fidecaro, Phys. Rev. **81**, 339 (1951).

known data, though not a very satisfactory one. Similar is the situation with regard to the μ-pair creation in high energy nucleon-nucleon and photon-nucleon collisions.[7,10] As a result of the cutoff, μ-pairs are much more likely to come out in the bound state, i.e., as a π-meson.

The interaction Hamiltonian of fermion pair theories has the general form

$$\text{const}\int d^3x\Phi^*O\Phi\psi^*O\psi \tag{1.1}$$

where Φ and ψ are the field operators of the nucleons and mesons, respectively. If transitions between neutrons and protons are to be considered, the ψ-field must be of a mixed charged-neutral type. This also appears necessary for any μ-pair theory if it is to give an explanation for the $\pi^{\pm}$ meson within its framework. For the sake of simplicity, however, we shall always associate ψ with charged (+) μ-mesons, so that any pair produced by (1.1) will have total charge zero. Any more complete treatment with respect to the inclusion of neutral mesons is straightforward and is easily carried out in perturbation theory.[11] The symbol O in (1.1) stands for one of the five types of matrix operators well known from β-decay theory: scalar, vector, tensor, pseudovector, and pseudoscalar coupling. All except the last have been extensively investigated with respect to nuclear forces and μ-scattering. In the "static" case (nucleons infinitely heavy and at rest), there exist exact solutions for scalar and vector coupling,[6,12] whereas in the tensor and pseudovector cases only weak or strong coupling approximations are available.[2,3,13] Very little, however, is known about the pseudoscalar coupling ($O=\beta\gamma_5=i\beta\alpha_1\alpha_2\alpha_3$) because (1.1) vanishes in the strictly static limit, and even in the lowest nonstatic approximation the problems are considerably more involved than in the static tensor and pseudovector cases.

This paper is intended to fill the gap in our knowledge at least partially. Weak and strong coupling approximations will be applied to the pseudoscalar problem, with emphasis on the more difficult strong coupling case. The particular problems to be studied are the scattering of μ-mesons by nucleons (Sec. III), and the two nucleon forces (Sec. IV). The more involved problems (saturation properties, isobar states, magnetic moments) have been left aside. Two other reasons may be mentioned that give relevance to a treatment of the pseudoscalar case. The first is based on our presently held belief of the pseudoscalar nature of the π-meson. The explanation of this particular π-meson type as a bound μ-pair is only possible with pseudoscalar or pseudovector coupling types O, or a mixture of the two,[7] and for pure pseudoscalar coupling, there can be only one bound state, namely, the pseudoscalar one. Secondly, if the coupling constant in (1.1) is determined from the π-meson mass (binding energy), the pseudoscalar coupling leads to a much smaller μ-scattering cross section than all other coupling types. This follows from the fact that the matrix elements of $\Phi^*\beta\gamma_5\Phi$ for small nucleon velocities are proportional to the recoil velocity, which is small as the meson-nucleon mass ratio μ/M. Therefore, it turns out that in the μ-scattering problem, a weak coupling approximation is permissible (even though the π-binding energy requires an intermediate coupling strength), and the cross section becomes comparatively small, due to the factor $(\mu/M)^2$. The pseudoscalar coupling is unique in this respect. Furthermore, for very small meson velocities the cross section will practically vanish. This version of the theory is therefore more likely to be compatible with the fact that no strong nuclear μ-scattering has been observed so far.

[10] P. Wolff, Phys. Rev. **81**, 1056 (1951).
[11] N. Kemmer, Phys. Rev. **52**, 906 (1937).
[12] J. W. Weinberg, Phys. Rev. **59**, 776 (1941); J. Jauch, Helv. Phys. Acta **15**, 175 (1942).
[13] J. Blatt, Phys. Rev. **69**, 285 (1946).

2. APPROXIMATIONS

Inserting $O=\beta\gamma_5$ in (1.1), in the limit of large nucleon mass, $\Phi^*O\Phi$ may be replaced by

$$\textstyle\sum_n \delta(\mathbf{x}-\mathbf{x}_n)(\boldsymbol{\sigma}_n\cdot\mathbf{p})/2M,$$

where $\mathbf{p}=-i\nabla$ and n enumerates the various nucleons (Mass$=M$) present. The situation is well known from pseudoscalar Yukawa theory. Indeed, if the nonrelativistic Pauli approximation for the nucleon eigenfunctions is used, the matrix elements of $\int d^3x\Phi^*O\Phi F(\mathbf{x})$ are correctly calculated with this substitution. $F(\mathbf{x})$ is in Yukawa theory the pseudoscalar field operator, and in pair theory it is the bilinear product $\psi^*\beta\gamma_5\psi$. Therefore

$$H_i=\textstyle\sum_n f_n[(\boldsymbol{\sigma}_n\cdot\mathbf{p}_n)/2M]\psi^*(\mathbf{x}_n)\beta\gamma_5\psi(\mathbf{x}_n).$$

(The coupling parameter f_n may be chosen different for neutrons and protons.)

The momentum cutoff which will now be introduced is equivalent to replacing $\psi(\mathbf{x}_n)$ by a spatially averaged operator

$$\bar{\psi}(\mathbf{x}_n)=\int d^3x u(\mathbf{x}_n-\mathbf{x})\psi(\mathbf{x}). \tag{2.1}$$

The source function u is given the property of being different from zero only for $|\mathbf{x}-\mathbf{x}_n|\cong A^{-1}$ and being a real, spherically symmetric function. With this modification

$$H_i=(1/2M)\textstyle\sum_n f_n(\boldsymbol{\sigma}_n\cdot\mathbf{p}_n)\bar{\psi}^*(\mathbf{x}_n)\beta\gamma_5\bar{\psi}(\mathbf{x}_n). \tag{2.2}$$

This is the cut-off procedure customary in pair theories and we shall adopt it here.

The total Hamiltonian is then

$$H=H_\mu+H_i, \tag{2.3}$$

where

$$H_\mu=\int d^3x\psi^*(\mathbf{x})[(\boldsymbol{\alpha}\cdot\mathbf{p})+\mu\beta]\psi(\mathbf{x}). \tag{2.3}$$

The spinor components of the field operators obey the usual anti-commutation relations

$$\psi_\rho^*(\mathbf{x})\psi_\sigma(\mathbf{x}')+\psi_\sigma(\mathbf{x}')\psi_\rho^*(\mathbf{x})=\delta_{\rho\sigma}\delta(\mathbf{x}-\mathbf{x}'), \text{ etc.} \quad (2.4)$$

Next we shall develop the strong coupling approximation. In doing so, we may closely follow a paper of Blatt[13] in which the tensor coupling case is treated along similar lines.

The common aim of all such theories is the isolation of the modes on which the dominant term H_i depends most. This is achieved by splitting the field operator $\psi(\mathbf{x})$ into parts having the $\mathbf{x}$ dependence of the various source functions $u(\mathbf{x}-\mathbf{x}_n)$ and of their derivatives, and another part $\psi'(\mathbf{x})$ orthogonal to every source function and its derivatives.

$$\psi(\mathbf{x})=\textstyle\sum_n N^{-\frac{1}{2}}Q_n u(\mathbf{x}-\mathbf{x}_n) +\sum_n \mathfrak{N}^{-\frac{1}{2}}(\mathfrak{Q}_n\cdot\nabla)u(\mathbf{x}-\mathbf{x}_n)+\psi'(\mathbf{x}) \quad (2.5)$$

with

$$\int d^3x\psi'(\mathbf{x})u(\mathbf{x}-\mathbf{x}_n)=0 \quad (2.6)$$

$$\int d^3x\psi'(\mathbf{x})\nabla u(\mathbf{x}-\mathbf{x}_n)=0. \quad (2.7)$$

Note that due to (2.6, 7) the ψ'-part in $\bar{\psi}(\mathbf{x}_n)$ and in $p_n\bar{\psi}(\mathbf{x}_n)$ vanishes, and therefore H_i (2.2) causes no coupling of the ψ'-field with the bare nucleons.

This kind of separation is characteristic of all strong coupling theories. The term n in (2.5) will describe the mesons bound to the nth nucleon, whereas $\psi'(\mathbf{x})$ describes the free mesons whose interaction with "real" or "physical" nucleons turns out to be weak. The normalization factors N and $\mathfrak{N}$ in (2.5) are conveniently defined by

$$N=\int d^3x\,|u(\mathbf{x})|^2, \quad \mathfrak{N}=\tfrac{1}{3}\int d^3x\,|\nabla u(\mathbf{x})|^2. \quad (2.8, 9)$$

Assuming for the present that the distance between nucleons is larger than A^{-1}, no overlap between the various sources will occur.

$$\int d^3x u(\mathbf{x}-\mathbf{x}_n)u(\mathbf{x}-\mathbf{x}_m)=0 \quad (m\neq n). \quad (2.10)$$

Then it follows from (2.5, 6, 7, 8, 9) that

$$Q_{m\rho}=N^{-\frac{1}{2}}\int d^3x\psi_\rho(\mathbf{x})u(\mathbf{x}-\mathbf{x}_m)$$
$$\mathfrak{Q}_{m\rho}{}^{(j)}=\mathfrak{N}^{-\frac{1}{2}}\int d^3x\psi_\rho(\mathbf{x})(\partial/\partial x_j)u(\mathbf{x}-\mathbf{x}_m). \quad (2.11)$$

The spinor operators $Q_{m\rho}$ and $\mathfrak{Q}_{m\rho}{}^{(j)}$ are the variables of the "physical" nucleons; the nonvanishing anti-commutators containing these are

$$[Q_{m\rho}{}^*, Q_{m'\rho'}]_+=\delta_{\rho\rho'}\delta_{mm'},$$
$$[\mathfrak{Q}_{m\rho}{}^{(j)}, \mathfrak{Q}_{m'\rho'}{}^{(j')}]_+=\delta_{\rho\rho'}\delta_{mm'}\delta_{jj'}, \quad (2.12)$$

as is easily seen from (2.4) and (2.11). Similarly,

$$[Q_{m\rho}, \psi_\sigma^*(\mathbf{x})]_+=N^{-\frac{1}{2}}\delta_{\rho\sigma}u(\mathbf{x}-\mathbf{x}_m),$$
$$[\mathfrak{Q}_{m\rho}{}^{(j)}, \psi_\sigma^*(\mathbf{x})]_+=\mathfrak{N}^{-\frac{1}{2}}\delta_{\rho\sigma}(\partial/\partial x_j)u(\mathbf{x}-\mathbf{x}_m). \quad (2.12')$$

From (2.4, 12, and 12′) it then follows that

$$[\psi_\rho{}'^*(\mathbf{x}), \psi_\sigma'(\mathbf{x}')]_+ =\delta_{\rho\sigma}[\delta(\mathbf{x}-\mathbf{x}')-\textstyle\sum_n N^{-1}u(\mathbf{x}-\mathbf{x}_n)u(\mathbf{x}'-\mathbf{x}_n) -\mathfrak{N}^{-1}\nabla u(\mathbf{x}-\mathbf{x}_n)\nabla' u(\mathbf{x}'-\mathbf{x}_n)]. \quad (2.13)$$

The Hamiltonian (2.2, 3) may now be split into three parts,

$$H=H^0+H'+\Omega,$$
$$H^0=\textstyle\sum_n H^0(n), \quad (2.14)$$

$$H^0(n)=i(f/2M)(N\mathfrak{N})^{-\frac{1}{2}}\boldsymbol{\sigma}_n\cdot\{\mathfrak{Q}_n{}^*\beta\gamma_5 Q_n+Q_n{}^*\beta\gamma_5\mathfrak{Q}_n\} +i(\mathfrak{N}/N)^{\frac{1}{2}}\{Q_n{}^*(\boldsymbol{\alpha}\cdot\mathfrak{Q}_n)-(\mathfrak{Q}_n{}^*\cdot\boldsymbol{\alpha})Q_n\} +\mu\{Q^*\beta Q+\mathfrak{Q}^*\beta\mathfrak{Q}\}. \quad (2.15^0)$$

$$H'=\int d^3x\psi'^*(\mathbf{x})[(\boldsymbol{\alpha}\cdot\mathbf{p})+\mu\beta]\psi'(\mathbf{x}) \quad (2.15')$$

$$\Omega=\textstyle\sum_n \Omega(n)$$

$$\Omega(n)=\mathfrak{N}^{-\frac{1}{2}}\int d^3x[\psi'^*(\mathbf{x})(\boldsymbol{\alpha}\cdot\mathbf{p})(\mathfrak{Q}\cdot\nabla)u(\mathbf{x}-\mathbf{x}_n) +\text{c.c.}]. \quad (2.15^\Omega)$$

Similarly, the expressions for the charge and the angular momentum of the system may be split up (with no cross terms such as Ω appearing), but they will not be needed here.

The term Ω, in H, which is bilinear in the bound and free meson variables, describes the emission or absorption of free mesons by the physical nucleons. Ω must be a weak perturbation if the separation (2.14) is to be useful. This leads to the "strong coupling condition" which, following the argument of Pauli and Hu, turns out to be

$$(f/2M)A^2\gg 1, \quad (2.16)$$

provided that $A>\mu$. In any strong coupling calculation, condition (2.16) will be assumed to hold, that is to say, Ω will be disregarded. In this approximation there is a complete separation of the variables describing the various physical nucleons $Q_{m\rho}$, $\mathfrak{Q}_{m\rho}{}^{(j)}$ and the free meson variables $\psi'(x)$. The Hamiltonians concerning the various nucleons (H^0) and the free meson field (H') may be studied separately.

In the following applications, namely, the μ-scattering and two-nucleon forces, we will be concerned with the H' problem only. H^0 can be considered an additive constant. A general scheme for solving the H' problem rigorously is the following: Introduce a complete set of orthonormal functions (spinors) ϕ_m subject to the

orthogonality restrictions

$$\int d^3x\phi_{m,\rho}^*(\mathbf{x})u(\mathbf{x}-\mathbf{x}_n)=0, \quad (2.17)$$

$$\int d^3x\phi_{m,\rho}^*(\mathbf{x})(\partial/\partial x_i)u(\mathbf{x}-\mathbf{x}_n)=0, \quad (2.18)$$

where $\rho=1, 2, 3, 4$; $i=1, 2, 3$; $m=1, 2, \cdots$; and $n=1, 2, \cdots$. In addition, of course,

$$\int d^3x\phi_m^*\phi_m-1=0. \quad (2.19)$$

These functions, together with

$$N^{-\frac{1}{2}}u(\mathbf{x}-\mathbf{x}_n)C(\sigma) \quad \text{and} \quad \mathfrak{N}^{-\frac{1}{2}}(\partial/\partial x_i)u(\mathbf{x}-\mathbf{x}_n)C(\sigma)$$

(where $C(\sigma)\{\sigma=1, \cdots 4\}$ designate four spinors obeying $C^*(\sigma)C(\sigma')=\delta_{\sigma\sigma'}$, e.g. $C_\rho(\sigma)=\delta_{\rho\sigma}$) form a complete set suitable for the expansion of the complete field ψ [see (2.5)]. For the part ψ', subject to the orthogonality conditions (2.6, 7) and to the commutation rules (2.13), the most general expansion is

$$\psi_\rho'(\mathbf{x})=\sum_m a_m\phi_{m,\rho}(\mathbf{x}), \quad (2.20)$$

where the a's obey the well-known anticommutation relations

$$[a_m^*, a_{m'}]_+=\delta_{mm'}, \quad [a_m, a_{m'}]_+=[a_m^*, a_{m'}^*]_+=0.$$

The ϕ_m's are conveniently constructed as eigenfunctions of the variational problem

$$\delta\int d^3x\phi_m^*(\mathbf{x})[(\boldsymbol{\alpha}\cdot\mathbf{p})+\mu\beta]\phi_m(\mathbf{x})=0, \quad (2.21)$$

with the constraints (2.17, 18, 19). Introducing for these constraints, respectively, Lagrangian multipliers $\lambda_{n\rho}$, $\Lambda_{n\rho}^{(i)}$ and E, one obtains the set of linear equations

$$(\boldsymbol{\alpha}\cdot\mathbf{p}+\mu\beta)\phi=E\phi+\sum_n(\lambda_n+\boldsymbol{\Lambda}_n\cdot\mathbf{p})u(\mathbf{x}-\mathbf{x}_n). \quad (2.22)$$

Then, with (2.20) inserted into (2.15'), H' assumes the diagonal form

$$H'=\sum_m a_m^*a_mE_m. \quad (2.23)$$

Note that the coupling parameter f does not appear in the H' problem. Finally it may be noted that the introduction of an additional neutral meson field (doubling of all ϕ-components, with O involving isotopic spin operators) causes no computational changes in the H' problem. Of course, the number of eigenvalues E, per interval ΔE, is doubled.

3. ONE-NUCLEON PROBLEM

In the one-nucleon case (2.22) reduces to

$$(\boldsymbol{\alpha}\cdot\mathbf{p}+\mu\beta-E)\phi=(\lambda+\boldsymbol{\Lambda}\cdot\mathbf{p})u(\mathbf{x}). \quad (3.1)$$

To study the μ-scattering, we insert for $\phi(\mathbf{x})$ a plane, incoming wave plus an outgoing spherical wave

$$\phi(\mathbf{x})=\phi_0e^{i(\mathbf{p}_0\cdot\mathbf{x})}+\int_C d^3k a(\mathbf{k})e^{i(\mathbf{k}\cdot\mathbf{x})}. \quad (3.2)$$

ϕ_0 obeys the "source free" equation

$$(\boldsymbol{\alpha}\cdot\mathbf{p}_0+\mu\beta-E)\phi_0=0, \quad E=+(p_0^2+\mu^2)^{\frac{1}{2}} \quad (3.3)$$

and C denotes the countour to be taken in the complex $|\mathbf{k}|$ plane which gives rise only to outgoing waves.

Multiplying (3.1) with $(\boldsymbol{\alpha}\cdot\mathbf{p}+\mu\beta+E)$, one finds

$$(p^2-p_0^2)\phi(\mathbf{x})=(\boldsymbol{\alpha}\cdot\mathbf{p}+\mu\beta+E)(\lambda+\boldsymbol{\Lambda}\cdot\mathbf{p})u(\mathbf{x}). \quad (3.4)$$

Let

$$u(\mathbf{x})=\int d^3k g(\mathbf{k})e^{i(\mathbf{k}\cdot\mathbf{x})}. \quad (3.5)$$

Inserting (3.2, 5) into (3.4) yields at once

$$a(\mathbf{k})=g(\mathbf{k})(\boldsymbol{\alpha}\cdot\mathbf{k}+\mu\beta+E)(\lambda+\boldsymbol{\Lambda}\cdot\mathbf{k})/(k^2-p_0^2); \quad (3.6)$$

λ and $\boldsymbol{\Lambda}$ are still to be determined from (2.19, 20)

$$\int d^3x u(\mathbf{x})\phi(\mathbf{x})=\int d^3x u(\mathbf{x})\mathbf{p}\phi(\mathbf{x})=0.$$

Choosing the "3" axis in the p_0 direction one finds

$$\lambda=\frac{g(p_0)}{p_0^2I(p_0)-3J(p_0)}[p_0\alpha_3-(E-\mu\beta)]\phi_0,$$

$$\Lambda_i=\frac{p_0^{-1}g(p_0)}{p_0^2I(p_0)-3J(p_0)}[\alpha_i\alpha_3(E-\mu\beta)-p_0\alpha_i]\phi_0; \quad (i=1, 2), \quad (3.7)$$

$$\Lambda_3=-p_0^{-1}g(p_0)\left[(E-\mu\beta)\left(\frac{1}{J(p_0)}+\frac{1}{p_0^2I(p_0)-3J(p_0)}\right)-\frac{p_0\alpha_3}{p_0^2I(p_0)-3J(p_0)}\right]\phi_0,$$

where

$$I(p_0)=\int_C dk\frac{k^2g^2(k)}{k^2-p_0^2}, \quad J(p_0)=\tfrac{1}{3}\int_C dk\frac{k^4g^2(k)}{k^2-p_0^2}. \quad (3.8)$$

The contour C is of course the same as in (3.2). From (3.6, 7)

$$a(\mathbf{k})=\frac{b(\mathbf{k})}{k^2-p_0^2}\phi_0, \quad (3.9)$$

where

$$b(\mathbf{k})=\frac{g(k)g(p_0)}{p_0^2I(p_0)-3J(p_0)}(\boldsymbol{\alpha}\cdot\mathbf{k}+\mu\beta+E)$$

$$\times\left[(\boldsymbol{\alpha}\cdot\mathbf{p}_0)-(E-\mu\beta)-\frac{(\boldsymbol{\alpha}\cdot\mathbf{k})(\boldsymbol{\alpha}\cdot\mathbf{p}_0)}{p_0^2}(E-\mu\beta)+(\boldsymbol{\alpha}\cdot\mathbf{k})-\frac{p_0^2I(p_0)-3J(p_0)}{J(p_0)}\left(\frac{\mathbf{k}\cdot\mathbf{p}_0}{p_0^2}\right)(E-\mu\beta)\right].$$

Finally one may in the usual way evaluate the k integral in (3.2) for the wave zone ($|\mathbf{k}|\,|\mathbf{x}|\gg 1$)

$$\phi(\mathbf{x})=[e^{i\mathbf{p}_0\cdot\mathbf{x}}+2\pi^2 b(\boldsymbol{\kappa})\exp(i|\boldsymbol{\kappa}|\,|\mathbf{x}|)/|\mathbf{x}|]\phi_0. \quad (3.10)$$

Here, $\boldsymbol{\kappa}$ stands for the momentum of the meson scattered in the x direction $\boldsymbol{\kappa}=|\mathbf{p}_0|\mathbf{x}/|\mathbf{x}|$. Note that if ϕ_0 refers to a positive energy state ($E>0$), then also the scattered wave contains only positive energy states, as is indicated by the factor $(E+\boldsymbol{\alpha}\cdot\boldsymbol{\kappa}+\mu\beta)$ in (3.9). Therefore, the scattering cross section averaged over the initial polarizations, is simply

$$d\sigma/d\Omega=2\pi^4\,\mathrm{Sp}[b^*(\boldsymbol{\kappa})b(\boldsymbol{\kappa})(E+\boldsymbol{\alpha}\cdot\mathbf{p}_0+\mu\beta)/2E]$$
$$=8\pi^4\left|\frac{1}{J(p_0)}\right|^2\frac{(\boldsymbol{\kappa}\cdot\mathbf{p}_0)^2}{p_0^2}(p_0^2+\boldsymbol{\kappa}\cdot\mathbf{p}_0)g^4(p_0). \quad (3.11)$$

We have evaluated the cross section for the simple cut-off law

$$g(k)=(1+k^2/A^2)^{-1} \quad (3.12)$$

which corresponds to the source function

$$u(x)=2\pi^2A^3(e^{-Ax}/Ax) \quad (3.13)$$

as defined by (3.5). In this special case

$$I(p_0)=i\pi^2[2p_0-iA(1-p_0^2/A^2)]g^2(p_0)$$
$$3J(p_0)=i\pi^2[2p_0^3-iA^3(1+3p_0^2/A^2)]g^2(p_0)$$
$$\frac{d\sigma}{d\Omega}=72p_0^4\frac{\cos^2\vartheta(1+\cos\vartheta)}{[4p_0^6+A^6(1+3p_0^2/A^2)^2]} \quad (3.14)$$

where $\vartheta=\mathbf{p}_0\cdot\mathbf{x}/|\mathbf{p}_0|\,|\mathbf{x}|$. Integrating over all directions gives

$$\sigma=96\pi p_0^4\frac{1}{[4p_0^6+A^6(1+3p_0^2/A^2)^2]}. \quad (3.15)$$

It is evident that this strong coupling value of the scattering cross section is much larger than the observed values. As was mentioned earlier, the cut-off momentum A cannot be taken much larger than μ on account of the actual range of the nuclear forces. It is true that σ, with p_0 increasing above A, falls off as p_0^{-2}, but this decrease is not fast enough and sets in too late to make the numerical values compatible with the measurements of Amaldi and Fidecaro at 200 Mev and above. A sharper cutoff would improve the situation for high energies, but for $p\sim A\sim\mu$ Eq. (3.15) would still give an unbelievably large cross section. A computational check of this point was made for $g(k)=(1+k^2/A^2)^{-2}$ which bears out the correctness of this conclusion.

Everything mentioned above about (3.14, 15) applies also to a more general interaction involving the isotopic spin operators. The scattering of either charged or neutral mesons without charge exchange would again be given by (3.14, 15) in the strong coupling approximation.

Equations (3.14, 15) may also be compared with the weak coupling value, obtained by ordinary perturbation theory (first-order approximation)

$$\frac{d\sigma}{d\Omega}=\frac{f}{16\pi^2}[p'g(p')]^4\frac{(1-\cos\vartheta')^2}{[(p'^2+\mu^2)^{\frac{1}{2}}+(p'^2+M^2)^{\frac{1}{2}}]^2} \quad (3.16)$$

$$\sigma=\frac{f}{3\pi}[p'g(p')]^4\frac{1}{[(p'^2+\mu^2)^{\frac{1}{2}}+(p'^2+M^2)^{\frac{1}{2}}]^2}. \quad (3.17)$$

All primed quantities are meant to refer to the center-of-mass coordinate system. (ϑ' = scattering angle.) Equations (3.16, 17) were already obtained by Wentzel[7] (his value in Eq. (22) of reference 7 should be multiplied by 4; $\eta=f/2\pi$)[3]. As mentioned in the Introduction, this approximation is even valid for intermediate coupling strengths, and the numerical values are not incompatible with the observed cross sections.

Before concluding the discussion of the one-nucleon problem, a few remarks may be added regarding the H_0 problem, i.e., the "binding" of mesons by a single nucleon leading to excited nucleon states. The main term in H^0 Eq. (2.15) is the one arising from the original interaction term ($\sim f$); neglecting the other terms in a first approximation, one is confronted with the eigenvalue problem

$$H_0{}^0F^0=E^0F^0$$
$$H_0{}^0=i(N\mathfrak{N})^{\frac{1}{2}}(f/2M)\boldsymbol{\sigma}\cdot\{\mathfrak{Q}^*\beta\gamma_5 Q+Q^*\beta\gamma_5\mathfrak{Q}\};$$

$i\beta\gamma_5$ may of course be chosen diagonal. For the sixteen operators Q_ρ and $\mathfrak{Q}_\rho{}^{(i)}$ which obey the usual Jordan-Wigner anticommutation relations (2.12) it seems simplest to take $Q_\rho{}^*Q_\rho$ and $\mathfrak{Q}_\rho{}^{(i)*}\mathfrak{Q}_\rho{}^{(i)}$ diagonal. So the problem which must be solved is the diagonalization of a matrix of 2^{16+1} rank. The various constants of motion reduce this $H_0{}^0$ to submatrices which are more manageable. The great number of these, however, makes the computation an almost impossible task.

4. THE TWO-NUCLEON INTERACTION

We consider two nucleons at the positions $\mathbf{x}_1$ and $\mathbf{x}_2$, with nonoverlapping sources, i.e., $|\mathbf{x}_1-\mathbf{x}_2|\gg A^{-1}$. Then the H^0 part of the Hamiltonian (2.14, 15^0) can be disregarded in the interaction problem, since it has no dependence on $|\mathbf{x}_1-\mathbf{x}_2|$. H', however, gives rise to an interaction, because the vacuum ψ'-field is changed by the presence of nucleons and this modification depends on the distances of the nucleons. Referring back to (2.17–23), let $E_m(r)$ be the energy of a stationary state m, as a function of $r=|\mathbf{x}_1-\mathbf{x}_2|$; then the interaction energy $J(r)$ is given by

$$J(r)=\textstyle\sum_m(-)[E_m(r)-E_m(\infty)]. \quad (4.1)$$

The sum is extended over all occupied negative energy states.[4]

For calculating the eigenvalues, E_m, it is initially necessary to introduce a periodicity condition giving

rise to Fourier series. Therefore, let

$$u(\mathbf{x})=8\pi^3V^{-1}\sum g(\mathbf{k})e^{i(\mathbf{k}\cdot\mathbf{x})} \quad \text{with} \quad g(\mathbf{k})=g^*(\mathbf{k})=g(-\mathbf{k}) \tag{4.2}$$

$$\phi(\mathbf{x})=8\pi^3V^{-1}\sum \varphi(\mathbf{k})e^{i(\mathbf{k}\cdot\mathbf{x})}. \tag{4.3}$$

V is the usual periodicity volume. The variational problem (2.21) then leads in the Fourier series representation of (2.22) to

$$(\boldsymbol{\alpha}\cdot\mathbf{k}+\mu\beta-E)\varphi(\mathbf{k})=g(k)\sum_{n=1}^{n=2}(\lambda_n+\boldsymbol{\Lambda}_n\cdot\mathbf{k})e^{-i(\mathbf{k}\cdot\mathbf{x}_n)} \tag{4.4}$$

$$\varphi(\mathbf{k})=g(k)\frac{(\boldsymbol{\alpha}\cdot\mathbf{k}+\mu\beta+E)}{k^2+\mu^2-E^2}\sum_{n=1}^{n=2}(\lambda_n+\boldsymbol{\Lambda}_n\cdot\mathbf{k})e^{-i(\mathbf{k}\cdot\mathbf{x}_n)}.$$

Note that no solution of the homogeneous equation, like the plane wave in (3.2), need be added since we are interested in determining stationary states m having a vanishing current density at infinity. Now, as before in the scattering problem, we resubstitute (4.4) into the Fourier transform of the constraints (2.17) and (2.18). These are

$$\int d^3x\phi(\mathbf{x})u(\mathbf{x}-\mathbf{x}_n)\sim\sum g(\mathbf{k})\varphi(\mathbf{k})e^{i(\mathbf{k}\cdot\mathbf{x}_n)}=0$$

$$\int d^3x\partial\phi/\partial x_\rho u(\mathbf{x}-\mathbf{x}_n)\sim\sum g(\mathbf{k})\varphi(\mathbf{k})k_\rho e^{i(\mathbf{k}\cdot\mathbf{x}_n)}=0.$$

One thus gets from them, respectively,

$$\sum_n\sum_k|g(k)|^2\frac{(\boldsymbol{\alpha}\cdot\mathbf{k}+\mu\beta+E)}{k^2+\mu^2-E^2}\times(\lambda_n+\boldsymbol{\Lambda}_n\cdot\mathbf{k})e^{-i\mathbf{k}\cdot(\mathbf{x}_n-\mathbf{x}_{n'})}=0 \tag{4.5}$$

$$\sum_n\sum_k|g(k)|^2k_\rho\frac{(\boldsymbol{\alpha}\cdot\mathbf{k}+\mu\beta+E)}{k^2+\mu^2-E^2}\times(\lambda_n+\boldsymbol{\Lambda}_n\cdot\mathbf{k})e^{-i\mathbf{k}\cdot(\mathbf{x}_n-\mathbf{x}_{n'})}=0. \tag{4.6}$$

In the two-nucleon case (4.5) and (4.6) form a system of 32 linear equations for the 32 components of $\lambda_{n\rho}$ and $\Lambda_{n\rho}{}^{(i)}$ whose nontrivial solution is determined by the vanishing of the determinant of their coefficients. The negative values E for which this determinant, denoted by $\Delta(E, r)$, vanishes are the eigenvalues $E_m(r)$ in (4.1). The calculation of $\Delta(E, r)$ is lengthy but straightforward and leads to the following simple result:

$$\Delta(E, r)=\Delta(E, \infty)[\chi(E, r)]^4. \tag{4.7}$$

The function χ will be described below.

When χ is known, one is able to find $J(r)$ by making use of the method of Wentzel.[5] Pauli and Hu[1] used this procedure to obtain for $J(r)$ the expression

$$J(r)=-\frac{1}{2\pi i}\int_C dE\ln\frac{\Delta(E, r)}{\Delta(E, \infty)}=-\frac{2}{\pi i}\int_C dE\ln\chi(E, r). \tag{4.8}$$

The counterclockwise path of this integral in the complex E plane is a loop chosen so as to enclose all the zeros of $\Delta(E, r)$ and $\Delta(E, \infty)$ on the negative (real) axis. χ may now be evaluated in the limit $V\to\infty$. This process causes χ to become discontinuous along the real E axis due to the continuous spread of the zeros. Explicit computation of χ shows that the limiting values, as the real E axis is approached from either side, are complex conjugates to each other. So if ϵ and κ are defined by $E=-[(\kappa^2+\mu^2)^{\frac{1}{2}}+i\epsilon]$, and introducing the notation

$$\chi^{\pm}(\kappa^2, r)=\lim_{\epsilon\to\pm0}\chi(E, r),$$

it turns out that $(\chi^+)^*=\chi^-$. Therefore, we may define a function $\vartheta(\kappa^2, r)$ by

$$\chi^+=\chi^-\exp[2i\vartheta(\kappa^2, r)]$$

and (4.8) may then be written as

$$J(r)=-\frac{4}{\pi}\int_0^\infty d\kappa\frac{\kappa}{(\kappa^2+\mu^2)^{\frac{1}{2}}}\vartheta(\kappa^2, r). \tag{4.9}$$

The phase $\vartheta(\kappa^2, r)$ is uniquely determined by the requirement

$$\lim_{r\to\infty}\vartheta(\kappa^2, r)=0 \quad (J(\infty)=0).$$

In (4.9), strictly speaking, a contour integral over a small circle in the E plane around the point $E=-\mu$ should be added. But it can be shown, with the formulas given later, that no contribution to $J(r)$ arises as the radius of the circle tends to zero. The k-space integrals‡ contained in $\chi^\pm$ and ϑ are expressible in terms of the following two types of integrals after angular integration:

$$I_\alpha{}^\pm(\kappa^2, r)=\lim_{\eta\to0}\int_{-\infty}^{\infty}\frac{k^\alpha e^{ikr}g^2(k)}{k^2-(\kappa^2\pm i\eta)}dk \quad (\alpha=1, 2, 3, 4) \tag{4.10}$$

$$(2n+1)J_n{}^\pm(\kappa^2)=\lim_{\eta\to0}\int_0^\infty\frac{k^{2(1+n)}g^2(k)}{k^2-(\kappa^2\pm i\eta)}dk \quad (n=0, 1).$$

[Note that for $\kappa^2<0$, or $E>-\mu$ one obtains $I_\alpha{}^+=I_\alpha{}^-$, $J_n{}^+=J_n{}^-$; this is the reason why only the region $\kappa^2>0$, or $E<-\mu$ contributes to the integrals (4.8) or (4.9).]

For further evaluation we choose again the simple source function (3.12), which allows one to carry out the k integration in (4.10) as contour integrations. The poles $k=iA$ in $I^\pm(\kappa^2, r)$ give rise to terms proportional to e^{-Ar} which will be neglected under the assumption $r\gg A^{-1}$ [see (2.10)]. Then the integrals of (4.10)

‡ $\left(\lim_{V\to\infty}V^{-1}\Sigma\to\frac{1}{8\pi^3}\int\right)$

become

$$(I_\alpha^+ + I_\alpha^-) = i\pi\kappa^{\alpha-1} g^2(\kappa)[e^{i\kappa r} + (-1)^{\alpha-1} e^{-i\kappa r}]$$
$$(I_\alpha^+ - I_\alpha^-) = i\pi\kappa^{\alpha-1} g^2(\kappa)[e^{i\kappa r} - (-1)^{\alpha-1} e^{-i\kappa r}]$$
$$(2n+1)(J_n^+ + J_n^-) = \pi A^{2n+1}(-1)^{n+1} g^2(\kappa) \times[(n-\tfrac{1}{2}) + (n+\tfrac{1}{2})\kappa^2/A^2] \quad (4.11)$$
$$(2n+1)(J_n^+ - J_n^-) = i\pi\kappa^{2n+1} g_s^2(\kappa).$$

We can now summarize the results for the function χ^+ in (4.8) with the choice (3.12) for the source function.

$$\chi^+ = (\chi^-)^* = \chi_1^+ \chi_2^+ = (\chi_1^- \chi_2^-)^*$$
$$\chi_1^+ = 1 + \frac{36}{y^2} \frac{(-4iy^3 + 14y^2 + 18iy - 9)}{(2iy^3 + 3z^2 y + z^3)^2} e^{2iy}$$
$$\chi_2^+ = 1 + \frac{36}{y^2} \frac{(2iy^8 - 17y^4 - 68iy^3 + 142y^2 + 162iy - 81)}{(2iy^3 + 3z^2 y + z^3)^2} e^{2iy}$$

where $y = \kappa r$ and $z = Ar$. The complete expression for χ_2^+ also contains a term with an e^{4iy} factor, which gives, however, a completely negligible contribution to $J(r)$.

In (4.9), χ_1 and χ_2 contribute in an additive manner ($\vartheta = \vartheta_1 + \vartheta_2$). The qualitative behavior of χ_1^+ and χ_2^+ is similar, and it will be sufficient to discuss χ_1^+. Three separate intervals on the κ or y axis may be distinguished.

(a) The neighborhood of the point $y = y_1$ defined such that the real part of χ_1^+ vanishes: $\Re(\chi_1^+(y_1)) = 0$; $y_1 \cong 18/z^3 \ll 1$. In this region the imaginary part, $\Im(\chi_1^+(y))$, is positive so that $\vartheta_1(y_1) = \pi/z$. The region (a) occupies a y domain, Δy_1, which includes all points where $|\Re(\chi_1^+(y))| \gtrsim |\Im(\chi_1^+(y))|$.

(b) If y, starting from y_1, increases toward infinity, χ_1^+ very rapidly approaches 1, i.e., ϑ_1 approaches 0.

(c) To the other side of y_1, y approaching 0, ϑ_1 tends rapidly toward the value π.

The region (a) is very narrow ($\Delta y_1 \sim y_1^4 \ll y_1 \ll 1$) and therefore a good approximation for the integral (4.9) is obtained by setting $\vartheta_1 \cong (\chi_1^+ - \chi_1^-)/2i$ in the interval b_1: $y_1 \leqslant y < \infty$, and $\vartheta_1 \cong \pi$ for c_1: $0 \leqslant y \leqslant y_1$.

Similarly one finds the contribution of χ_2^+ to be $\vartheta_2 \cong (\chi_2^+ - \chi_2^-)/2i$ in the interval b_2: $y_2 \leqslant y < \infty$, and $\vartheta_2 \cong \pi$ for c_2: $0 \leqslant y \leqslant y_2$ (there $y_2 \cong 54/z^3$). Then, according to (4.9)

$$J(r) = J_b(r) + J_c(r)$$
$$J_c(r) = J_{c1}(r) + J_{c2}(r) = -4/r[-2\mu r + (\mu^2 r^2 + y_1^2)^{\frac{1}{2}} + (\mu^2 r^2 + y_2^2)^{\frac{1}{2}}] \quad (4.12)$$
$$J_b(r) = J_{b1}(r) + J_{b2}(r) = -(288/A^6 r^7) f(\xi)$$

where

$$\xi = 2\mu r,$$
$$f(x) = 90 I(x) + x K_1(x)[101/2 + (19/16)x^2] + x^3 K_0(x)[41/4 + x^2/16]$$

and

$$I(x) = \int_0^\infty \frac{d\eta}{(\eta^2+1)^{\frac{1}{2}}} \left(\cos\eta x - \frac{\sin\eta x}{\eta x}\right)$$

and K_0, K_1 are Hankel functions of second kind with imaginary argument.[14] These are the same types of integrals as appear in the earlier work on pair theories.[1,6,15]

For two distinct r-intervals simpler expressions for J may be derived by inserting the asymptotic expansions of the Hankel functions: If $y_2 \ll 1 \ll \xi$; $r \gg 1/2\mu \gg (54)^{\frac{1}{3}}/A$ (supposing, here, $A \gg \mu$),

$$J(r) = -\frac{144}{(\pi\mu r)^{\frac{1}{2}}} \left(\frac{\mu}{A}\right)^4 \frac{1}{A^2 r^3} e^{-2\mu r}.$$

If, however, $\xi \ll y_2 \ll 1$; $(54)^{\frac{1}{3}}/A \ll r \ll 1/2\mu$ (again: $A \gg \mu$),

$$J(r) = -288/(A^2 r^4).$$

For all values of r covered by our calculations, i.e., $r \gg A^{-1}$, the potential is attractive.

At smaller values of r the source functions of the nucleons overlap and also H^0 contributes to the potential. This problem is even more complicated than the one-nucleon H^0 problem mentioned at the end of Sec. III.[16]

One inadequacy of a really strong coupling assumption appears rather certain, and this is the absence of long range spin-dependent forces of the proper magnitude. The Ω-interaction (2.15$^\Omega$) between the ψ'-field and the physical nucleons will certainly produce some spin-dependence of the forces, derivable by a second- (or perhaps fourth-) order perturbation treatment,[13] which, however, requires the knowledge of the H_0 eigenvalues and eigenfunctions. As long as the strong coupling condition (2.16) is fulfilled, the resulting spin-dependence will presumably be quite weak.

Since we would actually expect the coupling to be of intermediate strength, we want to present, in addition, the results of a weak coupling calculation, carried out with the usual perturbation methods. Here we adopt a charge-symmetric theory,[11] involving both charged and neutral mesons, because otherwise no resemblance with reality is obtained. The spin and isotopic spin dependence of the potential turns out to be the same as known from the pseudoscalar Yukawa theory, namely:

$$(8\pi^3)^2 J(\mathbf{r}) = (\boldsymbol{\tau}_1 \cdot \boldsymbol{\tau}_2)(\boldsymbol{\sigma}_1 \cdot \nabla)(\boldsymbol{\sigma}_2 \cdot \nabla) U(r)$$
$$= (\boldsymbol{\tau}_1 \cdot \boldsymbol{\tau}_2)\left[\left(\frac{(\boldsymbol{\sigma}_1 \cdot \mathbf{r})(\boldsymbol{\sigma}_2 \cdot \mathbf{r})}{r^2} - \frac{1}{3}(\boldsymbol{\sigma}_1 \cdot \boldsymbol{\sigma}_2)\right) r \frac{d}{dr}\left(\frac{1}{r}\frac{dU}{dr}\right) + \frac{1}{3}(\boldsymbol{\sigma}_1 \cdot \boldsymbol{\sigma}_2) \frac{1}{r^2}\frac{d}{dr}\left(r^2 \frac{dU}{dr}\right)\right]. \quad (4.13)$$

[14] See G. N. Watson, *A Treatise on the Theory of Bessel Functions* (The Macmillan Company, New York, 1944).
[15] J. Jauch (see reference 12).
[16] See Appendix II of reference 2.

The spatial dependence of $U(x)$, instead of being given by a simple momentum space integral as in Yukawa theory, is now expressible by the double integral

$$U(x)=\frac{f^2}{M^2}\int d^3p\int d^3q\frac{g^2(p)g^2(q)e^{i(\mathbf{p}-\mathbf{q})\cdot\mathbf{x}}}{[(p^2+\mu^2)^{\frac{1}{2}}+(q^2+\mu^2)^{\frac{1}{2}}]}\left[1+\frac{(\mathbf{p}\cdot\mathbf{q})+\mu^2}{(p^2+\mu^2)^{\frac{1}{2}}(q^2+\mu^2)^{\frac{1}{2}}}\right]. \tag{4.14}$$

After angular integrations this expression may be written as

$$U(x)=\frac{16\pi^2f^2}{M^2}\int pdp\int qdq\frac{g^2(p)g^2(q)}{(p^2+\mu^2)^{\frac{1}{2}}+(q^2+\mu^2)^{\frac{1}{2}}}\left[\sin px\sin qx\left(1+\frac{\mu^2}{(p^2+\mu^2)^{\frac{1}{2}}(q^2+\mu^2)^{\frac{1}{2}}}\right)\frac{1}{x^2}\right.$$
$$\left.+\frac{(px\cos px-\sin px)(qx\cos qx-\sin qx)}{(p^2+\mu^2)^{\frac{1}{2}}(q^2+\mu^2)^{\frac{1}{2}}}\frac{1}{x^4}\right]. \tag{4.15}$$

Again, the cutoff due to $g^2(p)$, $g^2(q)$ is essential for insuring the convergence of the integrals. In previous calculations[8] this was overlooked, and the results are therefore doubtful. Even for simple functions g, as (3.12), the integrals (4.15) are not expressible in terms of known functions, for arbitrary values of the parameters x, μ^{-1}, and A^{-1}. A first approximation for $x<\mu^{-1}$ is obtained by taking $\mu/A=0$. This appears sensible since, for $A>\mu$, the contribution that the integrand makes to $U(x)$ for p, $q<\mu$ is small. A convenient choice for g then is $g^2(p)=e^{-p/A'}$ (with $A'\sim A$). After the introduction of the coordinates $p=\rho\cos^2\vartheta$ and $q=\rho\sin^2\vartheta$ (4.15) may be evaluated in a straightforward computation with the result

$$U(x)=\frac{16\pi^2f^2}{M^2}A'^6\left[\frac{3}{2}\left\{\arctan A'x-\frac{A'x}{1+(A'x)^2}\right\}\frac{1}{(A'x)^5}\right.$$
$$\left.-\frac{1}{\{A'x[1+(A'x)^2]\}^2}\right]. \tag{4.16}$$

The substitution of this expression into $J(\mathbf{r})$ yields for the central-force term a strong short-range repulsion and attraction at larger distances. The tensor-force term, on the other hand, has always the same sign for all r values and it vanishes at $r=0$. Some characteristics of a charge-independent, "hard-core" type[17] of theory are therefore found in a weak coupling approximation of pseudoscalar μ-pair theory, especially the possibility of explaining nuclear saturation in terms of a short-range repulsion. It is easily checked that, for larger r values ($r\sim\mu^{-1}$), $J(\mathbf{r})$ exhibits qualitatively the same spin dependence as the pseudoscalar Yukawa theory. Therefore, as far as the weak coupling approximation goes, the spin and charge dependence of the forces agree, at least qualitatively, with the deuteron data, as, e.g., with the sign of the electric quadrupole moment. The range of the forces, for $A>\mu$, is, of course, given by A^{-1}, and so for $r>\mu^{-1}$ the potential is already negligibly small. For $(16\pi^2)(8\pi^3)^{-2}f^2A^5M^{-1}\sim 1$, $J(\mathbf{r})$ has roughly the right order of magnitude. It is, however, doubtful and hard to ascertain whether a perturbation treatment is legitimate for such f values.

Since for intermediate coupling strengths no computational method is known, the best one can do is to resort to a plain interpolation between the two extreme cases. Within this broad margin, and as far as our results go, there appears to be no serious discrepancy with experience.

In conclusion, I would like to express my gratitude to Professor G. Wentzel, who suggested this problem and gave me invaluable guidance and encouragement during the course of this work.

[17] R. Jastrow, Phys. Rev. **81**, 165 (1951).

The Second-Quantized Theory of Spin-½ Particles in the Nonrelativistic Limit*†

RICHARD K. OSBORN‡
Case Institute of Technology, Cleveland, Ohio
(Received September 17, 1951)

The second-quantized Dirac Hamiltonian for free electrons is transformed by a canonical transformation to a representation in which the positive and negative energy wave operators are separately represented by two-component operators. The transformation employed is the second-quantized analog of the one derived by Foldy and Wouthuysen in their discussion of the one-particle Dirac theory and its nonrelativistic limit. This transformation is then applied to the wave operators and the Hamiltonian in the second-quantized, charge-conjugate formalism for Dirac particles. The wave operators for positrons and electrons become linearly-independent two-component operators, and the Hamiltonian separates into an electron and a positron part, each of which contains only the corresponding two-component wave operators.

It is also shown that by means of an appropriate, readily determinable sequence of canonical transformations, Hamiltonians for fields of spin-½ particles interacting via intermediary fields can also be reduced to nonrelativistic form. This is accomplished by transforming the Hamiltonian to a representation in which it is exhibited effectively as a series expansion in powers of the Compton wavelength of the spin-½ particle. Illustration of the method is provided by detailed examination of the case of nucleons interacting via the pseudoscalar meson field.

I. INTRODUCTION

THEORIES of elementary particles and their interactions must at the present time be formulated in very general terms, since the mathematical difficulties of solution and the experimental difficulties of verification of detailed theories have as yet not been surmounted. The general requirements imposed upon theories of elementary particles and their interactions in a first-quantized formalism are usually that the equations describing the system shall be invariant under the group of Lorentz and gauge transformations, and that the function containing the physical description of the particle shall have certain special transformation properties corresponding to the known, or presumably known, spin of the particle.

However, because of the fact that the number of interacting particles is generally not constant throughout the course of the interaction, the mathematical description of such interacting systems is most easily obtained in the second-quantized formalism of field theory in which the state function becomes a vector in quantum number space instead of coordinate space, and the old one-particle functions whose transformation properties were prescribed by the ascribed spin of the particles go over into suitably transforming creation and destruction operators. The Lorentz and gauge invariance requirements are retained in the field formalism and are usually accomplished by first assuming that the proper conjugate variables, equations of motion, and Hamiltonians are derivable from some suitable Lagrangian regarded as a functional of the appropriate creation and destruction dynamical variables, and then prescribing that the Lagrangian shall be Lorentz and gauge invariant. Starting from this point of view, the commutation rules obeyed by the canonical variables of which the Hamiltonian is a function must be postulated, and the above invariance properties are required of them also.

But, though the most satisfactory mathematical approach to the problem of elementary particles and their interactions is accomplished in the second-quantized field theoretical formalism, there are many practical problems in which a nonrelativistic description of the interacting systems is adequate. The question arises immediately, therefore, relative to consideration of such problems, as to how, in a simple and rigorously satisfying way, the initial relativistically covariant formulation shall be reduced to a nonrelativistic form, which for purposes of calculation is generally simpler to deal with.

This question was answered in the one-particle, or first-quantized, formalism by a method derived by Foldy and Wouthuysen.[1] They pointed out that this question is especially obscure when particles with ½-integral spin are involved, for in that event many of the dynamical variables occuring in the relativistic formulation have no obvious analog in the corresponding nonrelativistic (Pauli) formalism. The nonrelativistic system of spin-½ particles is described in terms of two-component wave functions, whereas the relativistic system is usually described in terms of four-component wave functions, and the Hamiltonian generally contains odd operators which couple the upper and lower components of these functions.

If, however, it were possible to transform the Hamiltonian from the usual representation in which it contains odd operators to one in which it contains no odd operators, by means of one or more canonical trans-

* This research was supported in part by the AEC.
† From a thesis submitted to Case Institute of Technology in partial fulfillment of the requirements for the degree of Doctor of Philosophy.
‡ Now at Oak Ridge National Laboratory, Oak Ridge, Tennessee.

[1] L. L. Foldy and S. A. Wouthuysen, Phys. Rev. **78**, 29 (1950). Some of the results obtained in the paper relative to noninteracting particles have been previously obtained by Foldy and Wouthuysen in unpublished calculations.

formations, then it would be possible to describe the system by means of two unconnected sets of two-component wave functions. In this representation, if the transformation can be accomplished exactly, the nonrelativistic approximation can be obtained directly simply by stipulating that $p/mc \ll 1$. Transformations accomplishing the desired change of representation in the first-quantized formalism were deduced by Foldy and Wouthuysen for the free Dirac particle and the Dirac particle interacting with the electromagnetic field.

The purpose of this paper is to generalize this method so that it may be applied in the second-quantized formalism. In this formalism the spinor wave functions go over into four-component creation and destruction operators. Thus, when the Hamiltonian has been freed of odd Dirac operators by appropriate canonical transformations, it will be possible to decompose the four-component spinor operators into two sets of two-component operators, one set creating and destroying only positive energy states of spin-$\frac{1}{2}$ particles, the other set creating and destroying only negative energy states.

II. THE TRANSFORMATION IN THE CASE OF NO INTERACTION

The generalizations required for the case of free Dirac fields are fairly obvious, and the results obtained are, in the main, simply a second-quantized transcription of the results in the one-particle formalism. Consequently only a summary of the main points of procedure and results will be presented here.

The Hamiltonian in the usual representation,

$$H=\int \psi^*(\boldsymbol{\alpha}\cdot\mathbf{p}+\beta m)\psi d^3x,$$

is transformed by a unitary transformation

$$\exp(iS)=\exp\left[-\frac{\mathrm{i}}{2}\int\psi^*\beta\frac{\boldsymbol{\alpha}\cdot\mathbf{p}}{p}\tan^{-1}\left(\frac{\mathbf{p}}{m}\right)\psi d^3x\right],$$

to a representation in which it contains no odd operators, i.e.,

$$H'=e^{iS}He^{-iS}=\int\psi^*\beta(p^2+m^2)^{\frac{1}{2}}\psi d^3x. \qquad (1)$$

The proof of the correctness of Eq. (1) consists primarily in determining how the wave operators ψ transform since

$$H'=\int e^{iS}\psi^*e^{-iS}(\boldsymbol{\alpha}\cdot\mathbf{p}+\beta m)e^{iS}\psi e^{-iS}d^3x.$$

Thus, if one expands the transformed operator into the usual series of commutators

$$\psi'=e^{iS}\psi e^{-iS}=\sum_{n=0}^{\infty}\frac{i^n}{n!}[S,\psi]^n,$$

one finds that by inductive arguments the nth order commutator may be explicitly evaluated and the series summed. The result may be most conveniently expressed by the equation

$$\psi'=U\psi,$$

where

$$U=(E+m-\beta\boldsymbol{\alpha}\cdot\mathbf{p})/[2E(E+m)]^{\frac{1}{2}}.$$

Then

$$U^{-1}=(E+m+\beta\boldsymbol{\alpha}\cdot\mathbf{p})/[2E(E+m)]^{\frac{1}{2}},$$

and it is easily verified that

$$UU^{-1}=1,$$

and

$$U^{-1}(\boldsymbol{\alpha}\cdot\mathbf{p}+\beta m)U=\beta(p^2+m^2)^{\frac{1}{2}}.$$

In the representation in which H is free of odd operators, the four-component wave operators ψ decompose into two sets of two-component operators containing creation and destruction operators for either positive or negative energy states separately. One can also show that the momentum-space eigenfunctions $u(p,s)$ defined by[2]

$$\psi=\frac{1}{(2\pi)^{\frac{3}{2}}}\sum_s\int_p a(p,s)e^{i\mathbf{p}\cdot\mathbf{x}}u(p,s)d^3p$$

take on a particularly simple form in the new representation. Specifically, the functions u transform according to

$$u^{\pm\prime}=\left(\frac{2E}{E+m}\right)^{\frac{1}{2}}\left(\frac{1\pm\beta}{2}\right)\Lambda^{\pm}(p)u(p,s),$$

where

$$E=(m^2+p^2)^{\frac{1}{2}},\quad \Lambda^{\pm}(p)=[E\pm(\boldsymbol{\alpha}\cdot\mathbf{p}+\beta m)]/2E,$$

and, as a consequence,[3]

$$u^{+\prime}(p,1)=\{1,0,0,0\},$$
$$u^{+\prime}(p,2)=\{0,1,0,0\},$$
$$u^{-\prime}(p,3)=\{0,0,1,0\},$$
$$u^{-\prime}(p,4)=\{0,0,0,1\}.$$

A transformation to remove the odd operators from the Hamiltonian for noninteracting spin-$\frac{1}{2}$ particles in the charge-conjugate formalism was deduced, and the Hamiltonian in the new representation assumed a form that one would intuitively expect. The new Hamiltonian is reducible to a sum of three terms, two of which are functions of either two-component positron creation and destruction operators only, or two-component electron operators only. The third term is an infinite constant which arises as a consequence of the fact that the system has been transformed from a charge conjugate hole theory representation, in which the vacuum corresponds to a state of infinite negative energy, to a representation in which the vacuum cor-

[1] L. I. Schiff, *Quantum Mechanics* (McGraw-Hill Book Company, Inc., New York, 1949). p. 351.

[2] W. Heitler, *The Quantum Theory of Radiation* (Oxford University Press, London, 1949), second edition, p. 86.

responds to a state of zero energy. Thus, by the transformation, the eigenvalues of the energy operator have been shifted by an infinite amount corresponding to the "defining away" of the negative energy states. This infinite constant is in no sense a self-energy term.

III. THE TRANSFORMATION FOR THE CASES IN WHICH INTERACTIONS ARE CONSIDERED

When fields representing spin-$\frac{1}{2}$ particles interact with other fields, it no longer appears possible to go over to a representation in which the Hamiltonian is free of odd operators and in which the spinor operators have a two-component description, by means of a single canonical transformation. Foldy and Wouthuysen[1] showed, however, that in the one-particle formalism, the Hamiltonian for the interaction of a spin-$\frac{1}{2}$ particle and a given external field could be freed of odd operators to any desired order in the parameters, $(\hbar/mc^2)\partial/\partial t$ and $(\hbar/mc)\nabla$. The essence of their method consisted in obtaining the Hamiltonian in the form of a power series in these expansion parameters by a succession of readily determinable, unique canonical transformations. An investigation of the conditions under which this expansion is presumably physically significant (that is, that the field variables do not vary appreciably over spatial dimensions of the order of magnitude of the Compton wavelengths of the particles, or over time intervals of the order of the time required for light to travel a Compton wavelength for the particles) emphasizes the fact that the end results of the transformation procedures under consideration are indeed a reduction of the Hamiltonian to nonrelativistic form.

A. Interactions of Two Spin-$\frac{1}{2}$ Particles

1. *Different Particles*

The problem of removing the odd operators from the Hamiltonian in the cases in which the Dirac particles are presumed to interact with given external fields proceeds in strict analogy to the same problem in the one-particle formalism.

If, however, one considers cases in which two or more Dirac particles interact through the intermediation of another field, whether the Dirac particles be representable by different fields as in the case of neutrons and protons interacting via the meson field, or representable by a single field as in the case of two electrons interacting via the electromagnetic field, one encounters types of odd terms which at first sight present apparent difficulties in the application of the above method. The difficulty arises as a consequence of the generation of terms which are essentially products of two or more factors, each separately odd. In general these terms are neither even nor removable in the form in which they arise by further canonical transformations. The difficulty is merely apparent, however, and resolves itself after an examination of these terms in the light of their physical significance.

Though there is no difficulty in principle, it is too laborious to carry through the reduction of the Hamiltonian for arbitrarily interacting systems to a form free of odd operators to a given order in inverse powers of the masses. Consequently, the case of nucleonic interactions via the pseudoscalar meson field with both pseudoscalar and pseudovector coupling will be selected for detailed consideration. This example is chosen because of its current practical importance; because it satisfactorily illustrates the nature, source, and resolution of the difficulties commented upon above; and because it provides a statement of the equivalence theorem for pseudoscalar and pseudovector coupling in the nonrelativistic limit. To further reduce the length of the calculations involved, another restriction is made to the case of charged mesons only, and electromagnetic interactions will be omitted.

The Schrödinger equation for the system under consideration is

$$H\Phi = i\partial\Phi/\partial t,$$

where Φ is the time-dependent state function and $H=\int \mathcal{H} d^3x$ is the time-independent Hamiltonian. The Hamiltonian density $\mathcal{H}$ is obtainable most directly by derivation from a Lagrangian density $\mathcal{L}$ by the prescription

$$\mathcal{H} = -\mathcal{L} - \frac{\partial \mathcal{L}}{\partial(\partial\varphi_A/\partial x_\mu)} n_\mu n_\nu \frac{\partial \varphi_A}{\partial x_\nu}.$$

The φ_A are the various fields comprising the system and $\mathbf{n}$ is a unit four-vector normal to the space-time surface at the point x. Derivatives normal to the space-time surface may be eliminated from $\mathcal{H}$ by making use of the definitions of the momenta

$$P_A = -\frac{\partial \mathcal{L}}{\partial(\partial\varphi_A/\partial x_\mu)} n_\mu,$$

and then the noncovariant canonical formalism convenient for the discussion that follows is obtainable immediately by specializing to a flat space-like surface for which $n=(0,0,0,i)$. For the case to be discussed presently

$$\mathcal{L} = -\bar{\Psi}\left(\gamma^\mu \frac{\partial \Psi}{\partial x_\mu} + m\Psi\right) - \left(\frac{\partial \phi^*}{\partial x_\mu}\frac{\partial \phi}{\partial x_\mu} + \mu^2\phi^*\phi\right) - (R\phi^* + R^*\phi) - \left(\Gamma_\mu^* \frac{\partial \phi}{\partial x_\mu} + \Gamma_\mu \frac{\partial \phi^*}{\partial x_\mu}\right),$$

and the final form of $\mathcal{H}$ with which we have here to deal is

$$\begin{aligned}\mathcal{H} = \mathcal{H}_{m0} &+ \Psi^*\boldsymbol{\alpha}\cdot\mathbf{p}\Psi + \Psi^*\beta m\Psi + if\Psi^*\beta\gamma^5(\tau_-\phi + \tau_+\phi^*)\Psi \\ &- (g/\mu)\Psi^*\boldsymbol{\sigma}\cdot(\tau_-\nabla\phi + \tau_+\nabla\phi^*)\Psi \\ &+ (g/\mu)\Psi^*\gamma^5(\tau_-\pi^* + \tau_+\pi)\Psi \\ &+ \tfrac{1}{2}(g/\mu)^2[\Psi^*\gamma^5\tau_-\Psi\Psi^*\gamma^5\tau_+\Psi \\ &+ \Psi^*\gamma^5\tau_+\Psi\Psi^*\gamma^5\tau_-\Psi], \quad (2)\end{aligned}$$

where

$$R=if\bar{\Psi}\gamma^5\tau_+\Psi,$$
$$\Gamma_\mu=(ig/\mu)\bar{\Psi}\gamma^\mu\gamma^5\tau_+\Psi,$$
$$\mathcal{H}_{m0}=\pi^*\pi+\nabla\phi^*\cdot\nabla\phi+\mu^2\phi^*\phi.$$

The constants μ, f, and g are the meson mass and the pseudoscalar and pseudovector coupling constants, respectively. The nucleon wave operators Ψ and $\bar{\Psi}=\Psi^*\beta$ are eight-component column and row matrix operators $\{\psi_a, \psi_b\}$ where $\{\psi_a, 0\}$ represents the neutron and $\{0, \psi_b\}$ the proton;

$$\tau_+=\tfrac{1}{2}(\tau_x+i\tau_y) \quad \text{and} \quad \tau_-=\tfrac{1}{2}(\tau_x-i\tau_y)$$

are the operators that accomplish the change in charge state of the nucleons as a consequence of the interaction with the meson field; and the Dirac matrices $\gamma^\mu=(-i\beta\boldsymbol{\alpha}, \beta)$ have in this representation the form

$$\alpha=\begin{pmatrix}\alpha & 0\\ 0 & \alpha\end{pmatrix}.$$

The quantities ϕ and ϕ^* are the meson field operators, and π and π^* are their conjugate momenta. The commutation rules obeyed by the field operators are

$$\begin{aligned}[\phi^*, \pi^{*\prime}]_-=[\phi, \pi']_-=i\delta(\mathbf{x}-\mathbf{x}'),\\ [\Psi_i^*, \Psi_j']_+=\delta_{ij}\delta(\mathbf{x}-\mathbf{x}').\end{aligned} \tag{3}$$

The procedure that follows is prescribed by the requirement that odd operators be removed from the Hamiltonian to the order $(1/m^2)$. Further, explicit cognizance will be taken of the fact that $g/\mu\sim(f/m)$. Write

$$H=\sum_{i=1}^{7}H_i,$$

where

$$H_i=\int\mathcal{H}_i d^3x$$

and where

$$\begin{aligned}&\mathcal{H}_1=\Psi^*\beta m\Psi,\\ &\mathcal{H}_2=\mathcal{H}_{m0},\\ &\mathcal{H}_3=\Psi^*\boldsymbol{\alpha}\cdot\mathbf{p}\Psi,\\ &\mathcal{H}_4=if\Psi^*\beta\gamma^5(\tau_-\phi+\tau_+\phi^*)\Psi,\\ &\mathcal{H}_5=(g/\mu)\Psi^*\gamma^5(\tau_-\pi^*+\tau_+\pi)\Psi,\\ &\mathcal{H}_6=-(g/\mu)\Psi^*\boldsymbol{\sigma}\cdot(\tau_-\nabla\phi+\tau_+\nabla\phi^*)\Psi,\\ &\mathcal{H}_7=\tfrac{1}{2}(g/\mu)^2[\Psi^*\gamma^\circ\tau_-\Psi\Psi^*\gamma^5\tau_+\Psi+\Psi^*\gamma^5\tau_+\Psi\Psi^*\gamma^5\tau_-\Psi]\\ &\quad=\tfrac{1}{2}(g/\mu)^2(\mathrm{DI}),\end{aligned}$$

where (DI) stands for the direct interaction.

The lowest order odd operators, to be removed first, are the terms $\Psi^*\boldsymbol{\alpha}\cdot\mathbf{p}\Psi$, $if\Psi^*\beta\gamma^5(\tau_-\phi+\tau_+\phi^*)\Psi$, and $(g/\mu)\Psi^*\gamma^5(\tau_-\pi^*+\tau_+\pi)\Psi$. The transformation required is e^{iT}, where

$$T=-(i/2m)\int\Psi^*[\beta\boldsymbol{\alpha}\cdot\mathbf{p}+if\gamma^5(\tau_-\phi+\tau_+\phi^*)+(g/u)\beta\gamma^5(\tau_-\pi^*+\tau_+\pi)]\Psi d^3x. \tag{4}$$

Then

$$\mathcal{H}'=e^{iT}\mathcal{H}e^{-iT}=\mathcal{H}+i[T,\mathcal{H}]+\tfrac{1}{2}i^2[T,\mathcal{H}]^2+\tfrac{1}{6}i^3[T,\mathcal{H}_1]^3 \text{ to } \sim 1/m^2.$$

The commutators may be evaluated by straightforward calculation, the labor being considerably reduced by employment of the relation

$$\left[\int\Psi^*A\Psi a d^3x, \Psi^*B\Psi b\right]$$
$$=\int[a(x), b(x')]\Psi^*(x)A\Psi(x)\Psi^*(x')B\Psi(x')d^3x+b(x)a(x)\Psi^*(x)[A,B]\Psi(x),$$

where $a(x)$ and $b(x)$ are operators commuting with Ψ and Ψ^*, but such that $[a, b']$ is proportional to $\delta(\mathbf{x}-\mathbf{x}')$, and A and B are arbitrary functions of ∇, β, α, γ^5, τ_+, and τ_-. It is to be noted that, since the transformation removed odd terms of a given order because of the properties of the commutators of odd terms with the $(m\beta)$ term, each transformation will be of one higher order in reciprocal masses than the order of the term to be removed; hence, odd terms of the order $(1/m^2)$ or greater can always be removed without making further contribution and will consequently be ignored as they arise.

Evaluating the commutators indicated in (7) and collecting terms, one finds

$$\begin{aligned}\mathcal{H}'=\mathcal{H}_1+\mathcal{H}_2+\left(\frac{f}{2m}-\frac{g}{\mu}\right)\Psi^*\boldsymbol{\sigma}\cdot\boldsymbol{\nabla}(\tau_-\phi+\tau_+\phi^*)\Psi\\ +\frac{1}{2m}\Psi^*\beta p^2\Psi+\frac{f^2}{2m}\Psi^*\beta\phi^*\phi\Psi\\ -\left(\frac{if^2}{8m^2}-\frac{igf}{2\mu m}\right)\Psi^*\tau_*(\pi^*\phi^*-\pi\phi)\Psi\\ +\left[\frac{1}{2}\left(\frac{g}{\mu}\right)^2-\frac{gf}{4\mu m}+\frac{f^2}{8m^2}\right](\mathrm{DI})\\ +\frac{gf}{4\mu m}[\Psi^*\beta\gamma^5\tau_+\Psi\Psi^*\beta\gamma^5\tau_-\Psi\\ +\Psi^*\beta\gamma^5\tau_-\Psi\Psi^*\beta\gamma^5\tau_+\Psi]+\left(\frac{f}{8m^2}-\frac{g}{2\mu m}\right)\\ \times\Psi^*\beta\boldsymbol{\sigma}\cdot[\mathbf{p}(\tau_-\pi^*+\tau_+\pi)+(\tau_-\pi^*+\tau_+\pi)\mathbf{p}]\Psi\\ -\frac{f}{2m}\Psi^*\gamma^5(\tau_-\pi^*+\tau_+\pi)\Psi.\end{aligned} \tag{5}$$

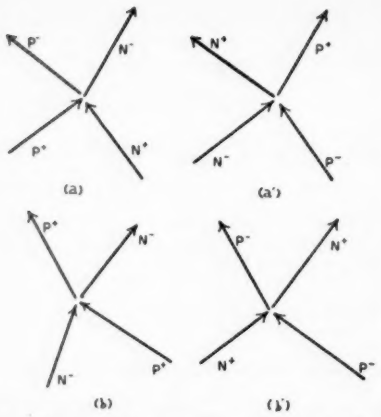

FIG. 1. Diagrams of the processes represented by the direct interaction terms.

The last term is odd and of the order $(1/M)$. However the transformation required to remove it will be of the order $(1/M^2)$, and the only commutator that it will have with $3\mathcal{C}'$ that will be proportional to $(1/M^2)$ will be the one with $3\mathcal{C}_2$. But this commutator will be odd; hence, the last term may now simply be dropped. The term involving the gradient of the meson momenta is also ignorable to this order. This is explicitly justified by noting that the term in question is, to the order $(1/m^2)$, simply the commutator of

$$G=-\left(\frac{f}{8m^2}-\frac{g}{2\mu m}\right)\int\Psi^*\beta\boldsymbol{\sigma}\cdot[\mathbf{p}(\tau_-\phi+\tau_+\phi^*)+(\tau_-\phi+\tau_+\phi^*)\mathbf{p}]\Psi d^3x \quad (6)$$

with $3\mathcal{C}'$, and hence is to this order simply $\partial G/\partial t=i[3\mathcal{C}', G]$. As a time derivative, it should have no diagonal matrix elements and therefore should be removable from this order by a canonical transformation. That this is true is obvious, and the transformation required is simply $\exp(-iG)$.

Consideration must now be given to the direct interaction terms in the Hamiltonian which, in the form in which they are exhibited, are neither even nor removable by canonical transformations. The terms to which attention shall be given are of the form

$$\Psi^*\gamma^5\tau_-\Psi\Psi^*\gamma^5\tau_+\Psi$$

and

$$\Psi^*\beta\gamma^5\tau_-\Psi\Psi^*\beta\gamma^5\tau_+\Psi.$$

If one rewrites the first of these in the form

$$\Psi^*\Gamma_1\tau_-\Psi\Psi^*\Gamma_2\tau_+\Psi+\Psi^*\Gamma_2\tau_-\Psi\Psi^*\Gamma_1\tau_+\Psi+\Psi^*\Gamma_1\tau_-\Psi\Psi^*\Gamma_1\tau_+\Psi+\Psi^*\Gamma_2\tau_-\Psi\Psi^*\Gamma_2\tau_+\Psi,$$

where

$$\Gamma_1=\left(\frac{1+\beta}{2}\right)\gamma^5\left(\frac{1-\beta}{2}\right),\quad \Gamma_2=\left(\frac{1-\beta}{2}\right)\gamma^5\left(\frac{1+\beta}{2}\right),$$

(the second term reducing to exactly the same form except that the unsymmetric terms are negative), one observes that there is a fundamental difference between the first two components which are unsymmetric in the Γ's and the second two symmetric components. The unsymmetric terms accomplish transitions during which there is no apparent change in the number of either positive or negative energy particles in the field, whereas the transitions resulting from the symmetric type terms do correspond to changes in the number of such particles. The nature of the difference implied here becomes clear immediately upon inspection of schematic diagrams representing the processes involved (Fig. 1).

Diagrams a and a' represent the processes accomplished by the symmetric terms in which the number of positive energy particles (P^+, N^+) and the number of negative energy particles (P^-, N^-) changes in the course of the interaction. However, the processes schematized in b and b' do not involve any apparent changes in the number of positive and/or negative energy particles.

Now, transitions involving such changes in the number of particles in the field require interaction energies at least of the order of the rest energies of the particles, and hence, correspond to fundamentally relativistic processes. Consequently, the symmetric components of the direct interaction terms should be removable from the Hamiltonian by means of a canonical transformation without generating any further contributions to the Hamiltonian of the same order as the terms themselves. This is indeed the case for

$$\left[\int\Psi^*\Gamma_1\tau_-\Psi\Psi^*\Gamma_1\tau_+\Psi d^3x,\ \Psi^*\beta m\Psi\right]=-2m\Psi^*\Gamma_1\tau_-\Psi\Psi^*\Gamma_1\tau_+\Psi.$$

Thus, if one chooses a canonical transformation whose generating function is

$$-(i/2m)\int\Psi^*\Gamma_1\tau_-\Psi\Psi^*\Gamma_1\tau_+\Psi d^3x,$$

the corresponding symmetric term will be canceled from $3\mathcal{C}$. It must be pointed out here that the removal of the relativistic components of the direct interactions does not in any way depend upon the assumption of equal masses for the interacting particles.

Conversely, the unsymmetric terms represent scattering in which the energy exchange may very well be small. Thus these terms should be even according to the criterion of commutativity with the βm term, as they are from the physical criterion that there is no observable coupling of positive and negative energy states. This one easily verifies by direct calculation.

The even character of the terms, as well as their physical significance, becomes still more obvious in the light of the following argument. Making use of the

relation

$$\int \Psi_r^* B_{rs} \Psi_s \Psi_i^* A_{ij} \Psi_j d^3x$$
$$= -\int \Psi_r^* \Psi_i^* B_{rs} A_{ij} \Psi_s \Psi_j d^3x + \int\int \Psi_r^*(x') \times B_{rs} A_{sj} \Psi_j(x) \delta(\mathbf{x}-\mathbf{x}') \delta(\mathbf{x}-\mathbf{x}') d^3x d^3x',$$

one easily deduces that

$$[\Psi^* \Gamma_1 \tau_- \Psi \Psi^* \Gamma_2 \tau_+ \Psi + \Psi^* \Gamma_2 \tau_+ \Psi \Psi^* \Gamma_1 \tau_- \Psi + \Psi^* \Gamma_2 \tau_- \Psi \Psi^* \Gamma_1 \tau_+ \Psi + \Psi^* \Gamma_1 \tau_+ \Psi \Psi^* \Gamma_2 \tau_- \Psi] d^3x$$
$$= \int\int \Psi^*(x') \Psi(x) \delta(\mathbf{x}-\mathbf{x}') \delta(\mathbf{x}-\mathbf{x}') d^3x d^3x'$$
$$-2\int \Psi_r^* \Psi_i^* (\Gamma_1 \tau_-)_{rs} (\Gamma_2 \tau_+)_{ij} \Psi_s \Psi_j d^3x$$
$$-2\int \Psi_r^* \Psi_i^* (\Gamma_2 \tau_-)_{rs} (\Gamma_1 \tau_+)_{ij} \Psi_s \Psi_j d^3x. \quad (7)$$

The first (infinite) term represents a self-energy contribution from the interaction, which presumably is removable by an appropriate renormalization of the original Hamiltonian. The second two terms may be still further clarified by transforming to momentum-space and noting that in the eight-dimensional matrix representation,

$$\Gamma_1 \tau_- = \begin{pmatrix} 0&0&0&0 \\ 0&0&0&0 \\ 0&I&0&0 \\ 0&0&0&0 \end{pmatrix}, \quad \Gamma_2 \tau_+ = \begin{pmatrix} 0&0&0&0 \\ 0&0&I&0 \\ 0&0&0&0 \\ 0&0&0&0 \end{pmatrix},$$

$$\Gamma_1 \tau_+ = \begin{pmatrix} 0&0&0&I \\ 0&0&0&0 \\ 0&0&0&0 \\ 0&0&0&0 \end{pmatrix}, \quad \Gamma_2 \tau_- = \begin{pmatrix} 0&0&0&0 \\ 0&0&0&0 \\ 0&0&0&0 \\ I&0&0&0 \end{pmatrix},$$

where I is the two-by-two unit matrix. One obtains (ignoring the infinite term)

$$-\frac{2}{(2\pi)^6} \sum_{s'''s''s's} \int d^3x d^3p''' d^3p'' d^3p' d^3p$$
$$\times \exp[-i\mathbf{x}\cdot(\mathbf{p}'''+\mathbf{p}''-\mathbf{p}'-\mathbf{p})]$$
$$\times a_{p'''s'''}^* a_{p''s''}^* a_{p's'} a_{ps}$$
$$\times u^*(p''', s_{3,6}''') I u(p', s_{3,4}')$$
$$\times u^*(p'', s_{3,4}'') I u(p, s_{3,6}), \quad (8)$$

$$-\frac{2}{(2\pi)^6} \sum_{s'''s''s's} \int d^3x d^3p''' d^3p'' d^3p' d^3p$$
$$\times \exp[-(i\mathbf{x}\cdot(\mathbf{p}'''+\mathbf{p}''-\mathbf{p}'-\mathbf{p})]$$
$$\times a_{p'''s'''}^* a_{p''s''}^* a_{p's'} a_{ps} u^*(p''', s_{7,8}''')$$
$$\times I u(p', s_{1,2}') u^*(p'', s_{1,2}'') I u(p, s_{7,8}),$$

where

$u(p, s_{1,2}) \rightarrow$ positive energy neutron, spin $\begin{Bmatrix} \text{up} \\ \text{down} \end{Bmatrix}$,

$u(p, s_{3,4}) \rightarrow$ negative energy neutron, spin $\begin{Bmatrix} \text{up} \\ \text{down} \end{Bmatrix}$,

$u(p, s_{5,6}) \rightarrow$ positive energy proton, spin $\begin{Bmatrix} \text{up} \\ \text{down} \end{Bmatrix}$,

$u(p, s_{7,8}) \rightarrow$ negative energy proton, spin $\begin{Bmatrix} \text{up} \\ \text{down} \end{Bmatrix}$.

It is to be noted that γ^5 behaves like a unit matrix in the two-dimensional spin sub-space, and therefore the interaction, in this case, does not involve spin transitions.

If the even, nonremovable part of the direct interaction be designated as (E of DI), the odd parts removed by canonical transformations, and the terms combined, keeping in mind that the even parts of the terms of the form

$$\Psi^* \beta \gamma^5 \tau_- \Psi \Psi^* \beta \gamma^5 \tau_+ \Psi$$

are of exactly the same form as those of the term types just discussed but opposite in sign, then the Hamiltonian density becomes

$$\mathcal{H} = \pi^* \pi + \nabla\phi^* \cdot \nabla\phi + \mu^2 \phi^* \phi + \Psi^* \beta m \Psi$$
$$+\frac{1}{2m} \Psi^* \beta p^2 \Psi + \left(\frac{f}{2m} - \frac{g}{\mu}\right) \Psi^* \boldsymbol{\sigma} \cdot \nabla (\tau_- \phi + \tau_+ \phi^*) \Psi$$
$$+\frac{f^2}{2m} \Psi^* \beta \phi^* \phi \Psi$$
$$-\left(\frac{if^2}{8m^2} - \frac{igf}{2\mu m}\right) \Psi^* \tau_3 (\pi^* \phi^* - \pi\phi) \Psi$$
$$+\left[\frac{1}{2}\left(\frac{g}{\mu}\right)^2 - \frac{gf}{2\mu m} + \frac{f^2}{8m^2}\right] (E \text{ of DI}). \quad (9)$$

Note that the Hamiltonian is now in a form such that, if the eight-component wave operators Ψ are replaced by two sets of four-component operators $\frac{1}{2}(1+\beta)\Psi$ and $\frac{1}{2}(1-\beta)\Psi$, it breaks up into a sum of essentially three different sets of terms. Two of these sets, resulting from the decomposition of those terms which are independent of the odd isotopic spin operators τ_- and τ_+ contain creation and destruction operators for either positive energy states of both protons and neutrons or negative energy states. The third set of terms is comprised of those which are odd in isotopic spin space; namely the terms resulting from the reduction to four-component description of the term $\Psi^* \boldsymbol{\sigma} \cdot \nabla (\tau_- \phi + \tau_+ \phi^*) \Psi$ and the even parts of the direct

interaction terms. Note that in the former the coupling is strictly between different charge states of the same energy character only, thus these reduced terms separate in the four-component description; whereas the latter do not separate—both sets of four-component wave operators are essential to the formulation of these terms—in spite of the fact that the coupling between nucleonic states of different energy character is observationally unreal.

It should be pointed out here that this represents a nonrelativistic statement of an "equivalence theorem" for pseudoscalar and pseudovector couplings in the pseudoscalar meson theory.[4] Such equivalence theorems have already been derived[5] for the case of a given external meson field. To the first order in the coupling constant it is seen that the nonrelativistic Hamiltonians for either pseudoscalar coupling or pseudovector coupling or both are completely equivalent, assuming an appropriate choice of the coupling constant. To the second order these three different Hamiltonians are equivalent only to within certain additive terms.

2. *Similar Particles*

One other case of interest should be mentioned here; namely, that of the interaction of two similar particles through the intermediation of a second field. As an example, the interactions of similar charged particles via the electromagnetic field will be considered. The question that arises is again relative to the removability of contact, or direct interaction, terms. The reason that the issue here requires some special attention is that, in this instance, there is only one Dirac field involved and hence formally the situation appears to differ considerably from the case previously discussed. However, as will be seen, this case is strictly analogous to the previous one, physically, and the decomposition of the direct interaction terms into odd, relativistic components and even, nonrelativistic components, and the removal of the odd components proceeds exactly as before.

Since it is of interest here merely to demonstrate the generation of "odd-odd" terms and discuss their reduction to nonrelativistic form, it is convenient for the sake of simplicity, and quite sufficient, to restrict ourselves to the particular case of the interaction of charged particles via the transverse electromagnetic field, omitting Coulomb interactions. The Hamiltonian may then be written as

$$\mathcal{H}=\mathcal{H}_{em}+\psi^*\beta m\psi+\psi^*\boldsymbol{\alpha}\cdot(\mathbf{p}-e\mathbf{A})\psi, \tag{10}$$

where

$$\mathcal{H}_{em}=\tfrac{1}{2}[|\mathbf{P}|^2+|\boldsymbol{\nabla}\times\mathbf{A}|^2],$$
$$[A_i(x),\, P_j(x')]_-=i\delta_{ij}\delta(\mathbf{x}-\mathbf{x}')$$

and $\mathbf{A}$ and $\mathbf{P}$ satisfy the operator equations

$$(\boldsymbol{\nabla}\cdot\mathbf{A})\Phi=0,\quad (\boldsymbol{\nabla}\cdot\mathbf{P})\Phi=0,$$

Φ being a state vector for the system.

If now one chooses a canonical transformation e^{iT}, where

$$T=-(i/2m)\int\psi^*\beta\boldsymbol{\alpha}\cdot(\mathbf{p}-e\mathbf{A})\psi d^3x, \tag{11}$$

then

$$\mathcal{H}'=e^{iT}\mathcal{H}e^{-iT}$$

will be free of odd operators to the order zero in $(1/m)$ and will contain as a consequence of $[T,\mathcal{H}_{em}]^2$ terms of the form $\psi^*\beta\boldsymbol{\alpha}\psi\cdot\psi^*\beta\boldsymbol{\alpha}\psi$ which are of the second order in $(1/m)$. This is of the type with which we are here concerned.

This term may be written as

$$\psi^*\boldsymbol{\Gamma}_1\psi\cdot\psi^*\boldsymbol{\Gamma}_1\psi+\psi^*\boldsymbol{\Gamma}_2\psi\cdot\psi^*\boldsymbol{\Gamma}_2\psi$$
$$-\psi^*\boldsymbol{\Gamma}_1\psi\cdot\psi^*\boldsymbol{\Gamma}_2\psi-\psi^*\boldsymbol{\Gamma}_2\psi\cdot\psi^*\boldsymbol{\Gamma}_1\psi,$$

where

$$\boldsymbol{\Gamma}_1=\left(\frac{1+\beta}{2}\right)\boldsymbol{\alpha}\left(\frac{1-\beta}{2}\right)$$

and

$$\boldsymbol{\Gamma}_2=\left(\frac{1-\beta}{2}\right)\boldsymbol{\alpha}\left(\frac{1+\beta}{2}\right).$$

The first two symmetric components are again odd and essentially relativistic; i.e., they represent the scattering of two positive energy particles (or two negative energy particles) into negative (or positive) energy states. Therefore, these terms should be and are removable for

$$\left[\lambda\int\psi^*\boldsymbol{\Gamma}_1\psi\cdot\psi^*\boldsymbol{\Gamma}_1\psi d^3x,\,\psi^*\beta m\psi\right]=-4m\lambda\psi^*\boldsymbol{\Gamma}_1\psi\cdot\psi^*\boldsymbol{\Gamma}_1\psi,$$

and similarly for the other odd term. Thus, by an appropriate choice of λ, the canonical transformation whose generating function is $\lambda\int\psi^*\boldsymbol{\Gamma}_1\psi\cdot\psi^*\boldsymbol{\Gamma}_1\psi d^3x$ will remove the odd components of the "odd-odd" terms.

The second two unsymmetric terms are even and essentially nonrelativistic in character, for they represent the scattering of one positive and one negative energy particle into negative and positive energy states, respectively. Thus, so far as an observer is concerned, these terms simply accomplish the scattering of electrons by positrons. The even character of these can readily be verified by straightforward calculation of their commutators with the βm term. If these terms are combined and then separated explicitly into their infinite and finite components, and the finite com-

[4] K. M. Case, Phys. Rev. **76**, 14 (1949). Note that the statement of the equivalence theorem obtained herein is not in agreement with the one derived by Case. The disagreement disappears if one chooses Case's relativistic statement of the theorem after altering the term $(2g/\hbar ck)(f-2k_0g/k)\phi^*\phi\bar{\psi}\psi$ to read $(2g/\hbar ck)(f-k_0g/k)\times\phi^*\phi\bar{\psi}\psi$ and then reduces the altered interaction Hamiltonian to nonrelativistic form.

[5] M. Sugarawara and Y. Ono, Prog. Theoret. Phys. **5**, 901 (1950).

ponents transformed into momentum-space and reduced to a description in spin sub-space as was done in the previous example, it will be seen that these even parts of the direct interaction terms accomplish spin transitions.[6]

[6] A related paper by S. Tani, Prog. Theoret. Phys. **6**, 267 (1951), has recently been published. In this paper, Tani employs the transformation for a detailed elucidation of the physical significance of the operators commonly occurring in theories of fermions interacting with fields in the single particle formalism.

The writer gratefully acknowledges his indebtedness to Dr. Leslie L. Foldy for suggesting this problem, and for his invaluable advice and criticism throughout the course of the work.

PHYSICAL REVIEW VOLUME 86, NUMBER 3 MAY 1, 1952

Radioisotopes of Bromine

S. C. FULTZ* AND M. L. POOL
Ohio State University, Columbus, Ohio
(Received December 31, 1951)

Selenium metal enriched with Se^{76} was bombarded with 7.3-Mev protons. A new 17.2-hour activity in bromine was observed and is assigned to Br^{76}. The radiations of Br^{82}, Br^{80}, Br^{77}, Br^{76}, and Br^{75} have been examined by use of a 180° focusing spectrometer and coincidence methods. Br^{82} emits a simple negatron spectrum with a maximum energy of 0.94±0.02 Mev. The ground state of Br^{80} emits a complex negatron spectrum with components: 1.97±0.03 Mev (80 percent), 1.1 Mev (11 percent), 0.7 Mev (9 percent). The gamma-rays of Br^{77} are associated with the K-capture process. The ground state of Br^{76} emits positrons having a complex spectrum with components 3.57±0.07 Mev (46 percent), 1.7 Mev (10 percent), 1.1 Mev (11 percent), 0.8 Mev (14 percent), 0.6 Mev (19 percent). Gamma-rays identified with Br^{76} have energies of 0.25, 0.32, 0.37, 0.42, 0.68, 0.75, 0.96, and 1.2 Mev. The ground state of Br^{75} decays by emission of positrons having a complex spectrum with components 1.70±0.02 Mev (46 percent), 0.8 Mev (20 percent), 0.6 Mev (15 percent), 0.3 Mev (19 percent).

INTRODUCTION

RADIATIONS from several radioisotopes of bromine have been studied by use of the beta-ray spectrometer and by absorption and coincidence measurements. The radioisotopes were obtained by proton and deuteron bombardments on selenium metal. Decay of their activities was followed with the aid of a Wulf electrometer filled with freon to a pressure of about 2 atmospheres. A magnetic field was used to separate positrons and negatrons, thus enabling decays of the activities giving rise to these particles to be determined separately by use of a G-M counter.

The spectrometer employed was of the 180° focusing type with a trajectory radius of 16 cm. The slits were made long in the direction of the magnetic field in order to obtain maximum possible intensity[1] for a predetermined resolution of about two percent. The spectrometer source consisted of fine particles of activated selenium metal evenly spread on a thin ribbon of Zapon and held in place by a thin layer of collodion. The density of the source and backing was about 10 mg/cm². The thickness of the G-M counter window was 2.5 mg/cm².

THE 17.2-HOUR Br^{76}

Two types of samples of selenium metal were bombarded with protons of 7.3-Mev energy. One type contained the natural isotopic mixture of stable selenium isotopes, while the other type contained Se^{76} enriched from 9.0 to 41.5 percent. In addition to the well-known bromine activities of 4.4-hour Br^{80}, 36-hour Br^{82}, and 2.4-day Br^{77}, a new activity of 17.2 hours was observed. Some evidence for the existence of a 15.7-hour activity had been observed previously[2] and early results for the work discussed below have already been reported.[3] Recently J. Hollander of the University of California privately communicated that a 16-hour bromine activity has been obtained by bombardment of arsenic with alpha-particles.

In Fig. 1 are shown decay curves obtained for the total activity and for the electromagnetically separated particles emitted from a Se^{76} enriched sample of selenium metal which was bombarded with protons of 7.3-Mev energy. Five components are present in the decay curve for the total activity. Their relative contributions to the total activity at the beginning of the measurements can be read from the intercepts of the straight lines. Similar sets of curves were obtained for samples of natural selenium bombarded in the same manner.

In Table I is given activity data obtained from three bombardments. The bottom row contains activities obtained when the bromine was chemically separated from the selenium metal. The activity values listed have been adjusted to take into account differences in

* Fellow, National Cancer Institute of the National Institutes of Health, Public Health Service, Federal Security Agency, Bethesda, Maryland.

[1] G. E. Owen, Rev. Sci. Instr. **20**, 916 (1949).

[2] G. T. Seaborg and I. Perlman, Revs. Modern Phys. **20**, 585 (1948).

[3] S. C. Fultz and M. L. Pool, Phys. Rev. **83**, 875 (1951).

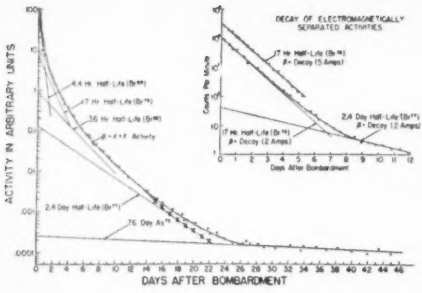
ACTIVITY IN ARBITRARY UNITS
DAYS AFTER BOMBARDMENT
DECAY OF ELECTROMAGNETICALLY SEPARATED ACTIVITIES
Counts Per Minute
Days After Bombardment
4.4 Hr. Half-Life (Br80)
17 Hr. Half-Life (Br77)
36 Hr. Half-Life (Br82)
β + γ + γ Activity
2.4 Day Half-Life (Br77)
76 Day As76
17 Hr. Half-Life (Br77) β+ Decay (5 Amps)
2.4 Day Half-Life (Br77) β+ Decay (2 Amps)
17 Hr. Half-Life (Br77) β+ Decay (2 Amps)

FIG. 1. Decay curves for bromine activities obtained by bombardment of Se^{76} with protons. The 17.2-hour activity is most distinct in the curves on the right for the magnetically separated components.

the cyclotron beam during the separate bombardments. In making these adjustments the 36-hour Br^{82} activity was chosen as a reference standard because it was produced by only a (p,n) reaction. The adjustment was achieved by equating the 36-hour activity to the isotopic abundance of Se^{82} for each type of sample. The 17.2-hour bromine activity may now be traced to the particular selenium isotope from which it was formed through proton bombardment by comparing the relative change in 17.2-hour bromine activity with the relative change in the isotopic abundance of each particular selenium isotope. As is seen in Table I such a comparison strongly favors the isotope Se^{76}. Hence it is concluded that the 17.2-hour bromine activity arises from the isotope Se^{76} under bombardment with 7.3-Mev protons.

Taking the 36-hour Br^{82} activity as a reference, as before, the ratio between the adjusted Br^{77} activities obtained from the enriched and natural samples of selenium is 0.79, which compares favorably with the isotopic abundance ratio of 0.90, for Se^{77}. However, if appreciable $Se^{76}(p,\gamma)Br^{77}$ reaction occurred, this ratio of adjusted activities would be greater than 0.90 because of the increase of Se^{76} relative to Se^{77}, in the enriched sample. Thus it is seen that within the limits of experimental error, no evidence for a (p,γ) reaction exists. Hence it is concluded that the 17.2-hour activity arises from Se^{76} by (p,n) reaction only, and is therefore assigned to Br^{76}.

RADIATIONS OF Br^{76}

Br^{76} disintegrates by emission of positrons, x-rays, and gamma-rays. A magnetic field was used to remove the positrons, and a decay curve was obtained for the x-rays. Using the activity value at the intercept of this curve, the ratio of the number of x-rays to number of positrons was estimated to be 0.7.

The Kurie plot for Br^{76} positrons, shown in Fig. 2, was obtained by use of the Coulomb correction given by Bethe and Bacher,[4] and checked with tables issued by the National Bureau of Standards.[5] It is evident that the spectrum is complex and that the highest energy component has the shape of an allowed spectrum. Results of analysis indicate that the spectrum may be composed of five groups having end-point energies and relative contributions of: 3.57 ± 0.07 Mev, 46 percent; 1.7 Mev, 10 percent; 1.1 Mev, 11 percent; 0.8 Mev, 14 percent; 0.6 Mev, 19 percent. The $\log(ft)$ values for the partial spectra therefore are 7.85, 7.1, 6.5, 6.1, and 5.8, respectively. The spectrum is also shown in Fig. 2.

Spectrometer measurements were also made on the internal conversion electrons and photoelectrons obtained from lead and uranium radiators. The activities available, however, were weak, so a statistical method was used to establish the small peaks. Bombardment conditions and isotopic ratios were changed in order to enhance some peaks at the expense of others. For each sample bombarded the negatron spectrum was scanned in detail several times to examine reproducibility and decay of the peaks. From the results of eight bombardments, a large number of gamma-rays were identified, some of which belonged to Br^{77} [6] and Br^{82}.[7] The following gamma-rays were attributed to Br^{76}: 0.25, 0.33, 0.37, 0.42, 0.68, 0.75, 0.96, and 1.21 Mev. Errors in energies are about 5 percent. From lead-absorption curves averaged gamma-ray energies of 0.6 and 1.4 Mev were obtained.

Coincidence measurements were made on Br^{76} positrons, which were selected by use of a magnetic field. Absorbers were used to eliminate all positrons except those from the high energy partial spectrum, and decay curves verified that the positrons selected belonged only to the 17.2-hour activity. The source and the beta- and gamma-counters were placed in a triangular arrangement such that the counters were on opposite sides of the source. About four inches of lead was then placed

TABLE I. Percent abundances and intensities.

Mass number	82	80	78	77	76	74	
				Percent abundance			
Enriched Se	5.0	30.2	16.1	6.8	41.5	0.5	
Natural Se	9.2	49.8	23.5	7.58	9.02	0.87	
Activities	Br^{82} 1.46 days	Br^{80} 4.4 hr		Br^{77} 2.4 days			17.2 hr
				Intensity of activity in arbitrary units			
Enriched Se	5.0	482	···	7.94	···	···	37.4
Natural Se (no chem.)	9.2	710	···	10.1	···	···	9.9
Natural Se (chem.)	9.2	872	···	···	···	···	8.3

[4] H. A. Bethe and R. F. Bacher, Revs. Modern Phys. **8**, 194 (1936).
[5] Fermi Function Table, preliminary copy, issued by the Computation Laboratory of the National Bureau of Standards. I. Feister, Phys. Rev. **78**, 375 (1950).
[6] R. Canada and A. C. G. Mitchell, Phys. Rev. **83**, 955 (1951).
[7] Siegbahn, Hedgran, and Deutsch, Phys. Rev. **76**, 1263 (1949).

between the counters. Radiations from the source could thus reach either counter, but annihilation radiation created in the beta-counter could not reach the gamma-counter. Thus a cause of false coincidences was eliminated. No true beta-gamma coincidences were recorded in a series of runs extending over a period of 96 hours or about six half-lives. It was therefore concluded that the high energy positrons of Br^{76} are transitions to the ground state of Se^{76}.

Br^{80}

Br^{80} was obtained by proton and deuteron bombardments of natural selenium. The negatron spectrum of the 18-minute isomer was examined while in equilibrium with the 4.4-hour parent isomer. The spectrum and its Kurie plot are shown in Fig. 3. The spectrum was analyzed into three groups having end-point energies and abundances of 1.97±0.03 Mev, 80 percent; 1.1 Mev, 11 percent; 0.7 Mev, 9 percent. The log(ft) values are: 5.48, 5.3, and 4.7, respectively. Coincidence measurements showed that the 1.97-Mev particles are emitted in a transition to the ground state of Kr^{80}.

Br^{77}

The radiations of Br^{77} have been examined previously by use of absorption methods[8] and more recently, with the aid of spectrometers.[6] The negatron spectrum was examined, and four internal conversion peaks were observed which decayed with a half-life of 2.4 days. The corresponding gamma-energies were 160±3, 234±3, 299±3, and 521±4 kev.

Coincidence experiments were conducted in two ways. First, coincidences were sought between positrons and gamma-rays. No true coincidences were found when

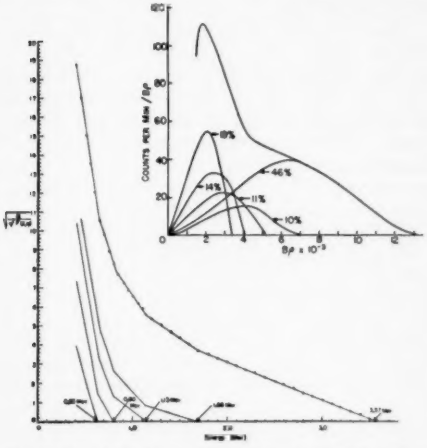

FIG. 2. (Above) Spectrum and partial spectra for Br^{78} positrons. (Below) Kurie plot for Br^{76} positrons showing end-point energies of partial spectra.

[8] Woodward, McCown, and Pool, Phys. Rev. 74, 870 (1948).

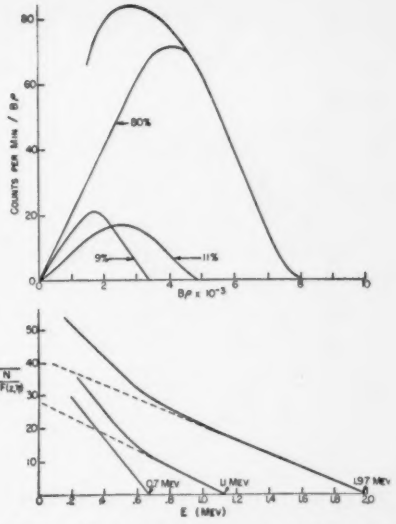

FIG. 3. (Above) Spectrum and partial spectra for Br^{80} negatrons. (Below) Kurie plot for Br^{80} negatrons showing end-point energies of partial spectra.

a wide range of positron energies were examined, so it was concluded that the positrons are emitted in a transition to the ground state of Se^{77}.

Second, coincidences between x-rays and gamma-rays were measured for various thicknesses of lead placed in front of the gamma-counter. The results of these measurements indicate that gamma-rays are emitted in the process of K-capture, and the energy of the unresolved gamma-rays, as given by the coincidence-absorption curve is 0.7 Mev, which is in agreement with the results of lead-absorption measurements previously made.[8] It is therefore evident that the gamma-rays emitted by Br^{77} occur during the K-capture process. The above information on the radiations of Br^{77} confirms two of the assumptions made in the proposed decay scheme of Canada and Mitchell.[6]

Br^{83}

Br^{83} was obtained by bombardment of selenium with deuterons. The negatrons were examined in the spectrometer and corrections were made for presence of other activities as well as its own decay. A Kurie plot indicated that the spectrum is simple and allowed, having an end-point energy of 0.94±0.02 Mev. This is in agreement with the value 0.94±0.01 Mev obtained by Duffield and Langer.[9]

Br^{75}

Br^{75} was obtained by proton bombardment of selenium metal enriched with Se^{74}. The positron spec-

[9] R. B. Duffield and L. M. Langer, Phys. Rev. 81, 203 (1951).

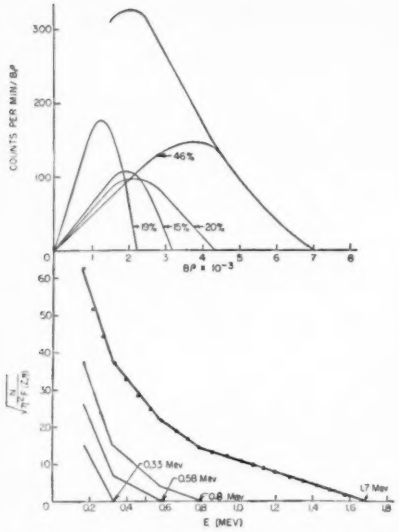

FIG. 4. (Above) Spectrum and partial spectra for Br^{76} positrons. (Below) Kurie plot for Br^{76} positrons showing end-point energies of partial spectra.

trum was examined in the spectrometer and was found to be highly complex. The spectrum and its Kurie plot are shown in Fig. 4. The spectrum has been analyzed into four partial spectra having end-point energies and abundances of 1.70±0.02 Mev, 46 percent; 0.8 Mev, 20 percent; 0.6 Mev, 15 percent; 0.3 Mev, 19 percent. The high energy component has the shape of an allowed spectrum. Assuming that the observed 1.7-hour half-life[8] is that of the ground state of Br^{76}, the log(ft) values are 5.6, 4.9, 4.7, and 4.7, respectively. The lead-absorption method gives an averaged gamma-ray energy of 0.61 Mev.

DISCUSSION

The negatron spectrum of Br^{80} had previously been classified as first forbidden[10,11] according to its log(ft) value. However, the Kurie plot for Br^{80}, as shown in Fig. 3 above, indicates that the negatrons are emitted by allowed transitions. The log(ft) values fall into the allowed group specified by more recent classification.[12,13] As deduced from the shell model[14] and the rules outlined by Nordheim[13] for odd-odd nuclei, the ground state of Br^{80} would be included in the following combinations of spin and parity:

(1)	$p_{3/2}+g_{9/2}$	6 (max)	odd
(2)	$f_{5/2}+p_{1/2}$	3 (max)	even
(3)	$f_{5/2}+g_{9/2}$	2	odd
(4)	$p_{3/2}+p_{1/2}$	1	even

Since Kr^{80} is even-even, its ground state is expected to have zero spin and even parity. Hence the selection rules for an allowed transition are obeyed only if the combination $p_{3/2}+p_{1/2}$ describes the ground state for Br^{80}. The 4.4-hour isomeric level[15] would be expected to be associated with the higher spin states.[11]

Br^{76} is an odd-odd nucleus which disintegrates by positron emission to the ground state of the even-even nucleus Se^{76}. The ground state of Br^{76} is included among the above combinations of spin and parity. The selection rules for the observed allowed beta-transition are again obeyed only for the combination $p_{3/2}+p_{1/2}$. However, the high log(ft) values obtained for Br^{76} are not consistent with the allowed positron spectra. This discrepancy might be explained by attributing the 17.2-hour half-life to an isomeric level which arises from the higher spin states.

The authors wish to acknowledge help received from the Development Fund of the Ohio State University, and financial assistance received by one of them (S.C.F.) from the National Institutes of Health. They also wish to thank Major C. Scoville, U.S.A.F., and Major D. Jones, U.S.A.F., for help in making some of the measurements.

[10] E. J. Konopinski, Revs. Modern Phys. **15**, 222 (1943).
[11] E. Segrè and A. C. Helmholz, Revs. Modern Phys. **21**, 271 (1949).
[12] C. S. Wu, Revs. Modern Phys. **22**, 386 (1950).
[13] L. W. Nordheim, Phys. Rev. **78**, 294 (1950).
[14] M. G. Mayer, Phys. Rev. **78**, 22 (1950).
[15] A. H. Snell, Phys. Rev. **52**, 1007 (1937).

The Dynamic Characteristics of a Low Pressure Discharge*

B. T. BARNES
Lamp Division, General Electric Company, Nela Park, Cleveland, Ohio
(Received December 17, 1951)

Square-wave modulation of current at a frequency of 167–400 cps was imposed on a dc discharge in a tube containing mercury vapor at a pressure of 6μ and argon at 3.5 mm (Hg). The intensity of λ2537 and other data were recorded on oscillograms. Each sudden change of the arc current i was accompanied by an instantaneous change in the same direction, of the longitudinal voltage gradient E, the electron temperature T_e, the 2537 output, and the ion current to the wall. These instantaneous changes were followed by much slower adjustments toward the steady-state values corresponding to the arc current. The time required for a rough adjustment was 0.2–0.5 msec when the current was increased, and 1–3 msec when it was decreased, for ratios of maximum to minimum current ranging from 1.6 to 3.9. When the current was decreased, there was an excess of ions that had to diffuse to the tube wall.

When the maximum arc current was 2.75 times the minimum value, the ratio of the electron concentration n_0 measured at the tube axis to that at the inner edge of the wall sheath (n_w) varied by a factor of 3 during each cycle. Some of this variation can be attributed to greater ion production per electron near the axis; some of it may be an artifact, since the wall probe may alter the radial distribution of electrons.

The number of electrons N_e per cm of arc was computed from the measured values of electron concentration by assuming that the radial variation follows the Bessel function $J_0(\mu r/a)$, where $J_0(\mu)=n_w/n_0$. The results for the major part of the cycle do not agree with those computed from the mobility equation. Part of the discrepancy can be ascribed to changes of the radial distribution of electrons during a short period when ion production is very high. Two-stage ionization predominates throughout the cycle.

Granovsky's approximate solutions of the basic equations for transient states of a low pressure discharge are not applicable to a Hg discharge with a rare-gas pressure of the order of 1 mm (Hg) or more. Since the concentrations of excited atoms are not single-valued functions of T_e, these equations are insoluble. However, step-by-step graphical or tabular solutions might be made for particular cases by use of experimental values of mean free paths and of the probabilities of exciting, ionizing, and radiative transitions. Useful relationships between i, E, T_e, and N_e can be obtained by combining the mobility and the energy-balance equations for the electrons. The variation in T_e during a transient depends mainly on the range of i/N_e. Instantaneous values of E are roughly proportional to the square root of the power expenditure w_e per electron. Since T_e is the principal factor fixing w_e, E and T_e are closely interdependent.

The modulation of radiant energy must decrease continuously with increasing frequency if a dc discharge is operated with a fixed amplitude of current modulation.

INTRODUCTION

IN the summer of 1943, the author was using an oscillograph to study the effects of a sudden change in the current through a fluorescent lamp operated on direct current. The purpose was merely to make measurements within a period over which the pressure of the mercury vapor was practically constant. However, the oscillograms showed an unexpected effect: an instantaneous change in lamp voltage that was much larger than the net long-term change, and in the opposite direction. This initial change was reversed in less than one millisecond when the change of current was an increase, and in one to five milliseconds when it was a decrease. It seemed certain that the transient was an indication of the time required for the ion concentrations in the discharge to increase or decrease to the equilibrium values corresponding to the new value of arc current.

Galkena and Granovsky[1] made similar observations on a low pressure discharge in mercury vapor without any rare gas present. In this case the mobility of the ions is many times greater than it is in a fluorescent lamp, hence the duration of the transient is only a few microseconds. Recently McClure and Holt[2] have reported results obtained by the use of current pulses with a duration of only 30 microseconds.

If the initial change of current is made by adding to the resistance in a lamp circuit or by shorting out part of it, the lamp current changes during the transient because the lamp impedance is changing. The results are more striking and more easily interpreted if the current is controlled by use of pentodes in series with the discharge, so that square-wave changes of current can be made, practically independent of subsequent changes in the impedance of the discharge.

EXPERIMENTAL TECHNIQUE

Circuits for square-wave control of current and for measuring the characteristics of the discharge during a transient have been described elsewhere.[3] The data in the present article have been taken on discharge tubes with an internal diameter of about 36 millimeters. The tubes had a well-distributed supply of liquid mercury and also contained argon (filling pressure 3.5 mm (Hg) at 27°C). They were operated fully immersed in a water bath which was held at 40°C. To prevent electrical leakage, the leads to the electrodes and to the probes were brought above the water level in glass tubing which was sealed to the discharge tube. The wall probe used to measure positive ion current was a disk 4.8 mm in diameter, surrounded by a guard ring with internal and external diameters of 6.2 and 9.5 mm. A mica disk behind the disk probe and its

* A preliminary report on this subject was made at the M.I.T. Conference on Physical Electronics, on April 2, 1948. Further results were given at the Conference on Gaseous Electronics at Pittsburgh, on November 5, 1949.

[1] Z. P. Galkena and V. L. Granovsky, J. Tech. Phys. (U.S.S.R.) **18**, 585 (1948).

[2] B. T. McClure and R. B. Holt, Phys. Rev. **83**, 878 (1951).

[3] B. T. Barnes and S. Eros, J. Appl. Phys. **21**, 1275 (1950).

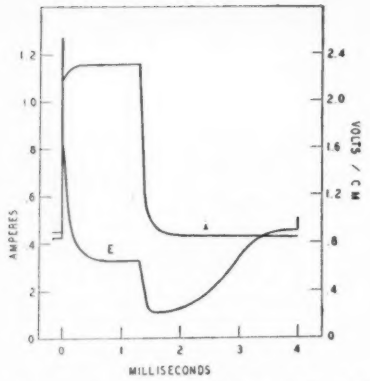

FIG. 1. Arc current i and longitudinal voltage gradient E during a cycle of modulation.

guard ring shielded their rear surfaces and the leads. The other probes were 3-mil wires with an exposed length of 5 mm, and with a short section adjacent to the collecting area surrounded by a thin-walled glass tube not quite in contact with the probe. This arrangement was intended to prevent extension of the collecting area by sputtered material from the probe, yet to provide the minimum interference with diffusion of electrons to the probe. There was a 5-mm gap between the wire probes used to measure electron temperature and a 12.3-cm spacing between the pair used to measure the longitudinal voltage gradient. The exposed areas of the probes were made small in order to reduce their effect on the discharge. The current drawn at space potential by a wire probe or by the wall probe, with the guard ring floating,[4] was 3–4 percent of the arc current.

At the middle of the discharge tube for which the intensity of λ2537 was determined, there was a side tube long enough to rise above water level, with a re-entrant section of the same length ending in a fused-quartz window. A heating coil prevented condensation of mercury between the inner and outer walls of this side tube.

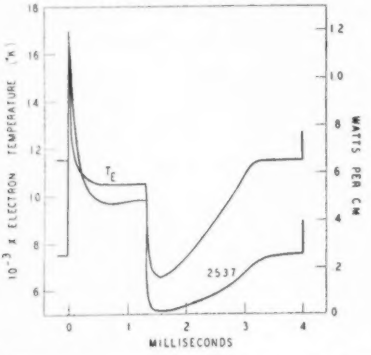

FIG. 2. Electron temperature T_e and output, per cm of arc, in 2537 line. Current modulation same as in Fig. 1.

[4] The guard ring was connected only for measurements of ion current.

RESULTS

The arc current i and the longitudinal voltage gradient E during a cycle of modulation are shown in Fig. 1. Each sudden change in arc current causes the voltage gradient to change by a slightly larger factor. When the current has been increased, the initial rise in voltage gradient is followed immediately by a very rapid decrease; when the current is reduced, a correspondingly rapid decrease in voltage gradient is followed by a relatively slow increase. In the latter case, the excess ions must flow to the wall of the discharge tube. The cycle is made long enough to permit the discharge to nearly reach its steady-state condition in each constant-current period.

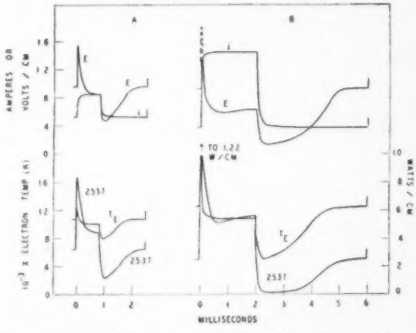

FIG. 3. Upper half of graph corresponds to Fig. 1, lower to Fig. 2, but amplitude of current modulation is less in case A, greater in case B.

The curves in Fig. 2 show the electron temperature T_e and the power output in the 2537 line. The curves for E, T_e, and λ2537 are quite similar, but T_e changes less and the 2537 output changes more than the voltage gradient does.

Figure 3 shows the effect of changing the amount of modulation while keeping the average arc current roughly constant. The adjustment toward equilibrium after a decrease in current becomes slower when one increases the factor by which the current is changed. This decrease in the speed of adjustment is caused by the greater reduction in T_e in the early part of the low current period, since the reduction in T_e produces a corresponding decrease in the rate of ambipolar diffusion. To offset this effect, one must reduce the frequency of modulation when the amplitude is increased, if each period at constant current is to be roughly of the same duration as the transient.

The voltage between the arc axis and the inner edge of the wall sheath is shown in Fig. 4. (The results given in Figs. 4–11 inclusive correspond to the amount of current modulation shown in Fig. 1.) The percentage variation in the radial voltage drop within the plasma is somewhat less than that of T_e (Fig. 2). If the radial distribution of electron concentration remained constant, one would expect the voltage drop to be proportional to T_e.

The rate at which ions arrive at the wall of the tube is plotted in Fig. 5. The sudden rise in ion current when the arc current increases abruptly is due to the increase in voltage gradient at every point along a radius of the tube, since ion velocities change proportionately. The subsequent gradual rise in ion current, in spite of falling T_e, reflects the increase in ion density during the period of high arc current. At the beginning of the low current period, the sudden fall in T_e causes a corresponding drop in ion current. The latter continues to fall throughout the period of low arc current because

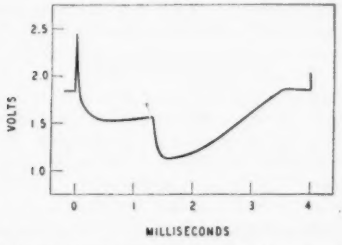

FIG. 4. Voltage between arc axis and inner edge of wall sheath. Current modulation same as in Fig. 1, for Figs. 4–11.

the ion concentrations decrease faster than the radial voltage gradients increase.

Figure 6(a) is an oscillogram of the current to a wire probe centered about the tube axis; 6(b) is the corresponding one for a wall probe. In each case the series of traces above the zero line was obtained by making successive changes of 1.5 volts in the bias voltage between an auxiliary probe and a special cathode-follower circuit[5] attached to the probe whose current was being recorded. By correcting for changes in the grid-cathode bias and for the varying voltage drop in the measuring resistor, one obtains data for a current-voltage characteristic for any instant during a cycle of modulation. Plotting these data, one finds the probe current at space potential and can then calculate the ion concentration in the region surrounding the probe.

Comparison of Figs. 6(a) and (b) shows that at the beginning of the high current period the current to a probe near the axis of the tube rises more rapidly than that to a wall probe. This indicates that the rate of ionization per electron is greater near the axis than

[5] See reference 3, Fig. 4.

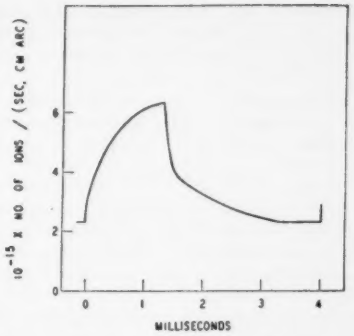

FIG. 5. Positive ion current to wall during a cycle.

near the wall—doubtless because the concentration of atoms in the 6^3P states is maximum at the axis.

The electron concentrations n_0 and n_w at the axis and at the inner edge of the wall sheath are shown in Fig. 7. The measured values of n_w for the latter part of the high current period are too low because only one 6L6 tube was used in the cathode-follower[6] when two were needed to prevent saturation. The dashed part of the curve in Fig. 7 probably represents the approximate course of n_w in this part of the cycle.

The values of n_w shown in Fig. 7 are based on the assumption that the concentration of electrons at the inner edge of the space charge sheath is not affected appreciably by the potential of a wall probe. With a mercury vapor pressure of a few microns and with no rare gas present, Langmuir and Mott-Smith obtained a ratio of electron current at space potential to positive ion current that was in reasonable agreement with this assumption.[6] With argon present at a pressure of 3.5 mm this might no longer be true. This point needs more detailed theoretical treatment. The wide variation of

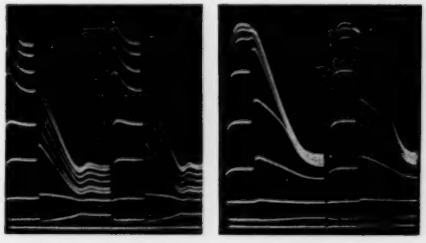

FIG. 6. Probe currents at voltages near space potential for probe centered about axis (a) and for wall probe (b). Bias voltage (between auxiliary probe and cathode follower connected to measurement probe) changed in 1.5-volt steps. Zero line at bottom.

[6] See L. Tonks and I. Langmuir, Phys. Rev. **34**, 917 (1929).

n_w/n_0 shown by Fig. 7 also deserves further investigation.

To compute the total number of electrons N_e per centimeter of arc from the data in Fig. 7, one must make an assumption as to the radial distribution of electron concentration. I have assumed that this distribution corresponded to the equation

$$n = n_0 J_0(\mu r/a), \tag{1}$$

where r = distance from the tube axis, a = tube radius, and J_0 is the zero-order Bessel function of the first kind. Values of μ for use in Eq. (1) were obtained from the curves shown in Fig. 7, using the relationship $J_0(\mu) = n_w/n_0$.

Equation (1) corresponds to the case where ionization is either single-stage or two-stage with no radial variation of the concentrations of atoms in the 6^3P states. Actually, the radial variation of n must be closer to a linear one than is indicated by Eq. (1), and the corresponding integration factors would be a few percent less than those with which N_e was computed. Since the radial variation of the concentration of metastable atoms is not known, the true integration factor cannot be computed.

A second method of computing N_e is available. The mobility equation for the electrons in a low pressure discharge may be written in the form[7]

$$i = 3.84 \times 10^{-10} N_e L_e E / T_e^{\frac{1}{2}}, \tag{2}$$

where i, E, and T_e are in amperes, volts/cm, and °K, respectively, and L_e is the electron mean free path (cm). Values of L_e for 3.5 mm (Hg) of argon plus 6μ of mercury vapor (both pressures reduced to terms of 0°C), have been published elsewhere.[8] These values were computed for Maxwellian distributions of electron velocity, taking into account the variation of the probability of collision with electron velocity.

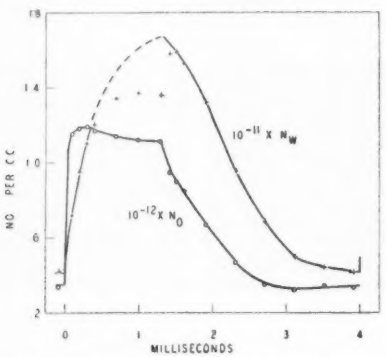

FIG. 7. Electron concentration at axis (n_0) and at inner edge of wall sheath (n_w) during a cycle.

The results obtained with these two methods of computing N_e are given in Fig. 8. The circles show the values calculated from n_0 and n_w using Eq. (1); the squares, those obtained from Eq. (2). In the early part of the high current period the discrepancy between the two curves is quite large. Here one would expect the values shown by the circles to be too high because most of the ions present have just been formed and are relatively near their points of origin. Under these conditions, the deviation of the radial distribution of electrons from that indicated by Eq. (1) is at its maximum, and the values of N_e obtained by use of this equation must be too high. However, it seems doubtful that this factor alone accounts for the disagreement between the curves in Fig. 8.

During the first part of the low current period, T_e is sufficiently low that ion production probably is almost negligible. If this is true, then Fig. 5 shows that N_e should be decreasing at the rate indicated by the curve drawn through the circled points. Later in the low current period, the rate of production of ions is not known and one cannot predict accurately the course of the curve for N_e. However, since the curve with the circled points seems to have the correct shape, it has been used in all subsequent calculations.

The rate of production of ions obviously is equal to the rate at which they flow to the wall plus the rate at which the number present in the discharge increases (Figs. 5 and 8). Figure 9 shows the ionization per electron, plotted against the reciprocal of T_e. Because of possible errors in dN_e/dt and in the data on ion flow to the walls, the computed values of ion production are not reliable when dN_e/dt is negative and nearly equal to the ion flow to the walls, per centimeter of arc. The curves through the circled points in Fig. 8 and the squares on Fig. 9 were drawn in such a way that these curves and the wall-current data (Fig. 5) are mutually consistent. This consistency, then, does not prove that the upper curve on Fig. 9 has the right slope, since the square that is farthest to the left on this graph could have been shifted up or down a relatively large distance by a comparatively small change in the course of the curve though the circled points on Fig. 8.

The dashed curve on Fig. 9 shows the computed rate of ionization for a single-stage process,[9] assuming a Maxwellian distribution of electron velocities and using the cross sections given by Nottingham.[10] In the discharge under investigation, one would expect a predominance of two-stage ionization. This is just what Fig. 9 shows.

The slope of the experimental curve on this graph has no special significance. At any value of T_e, the probability of two-stage ionization depends on the concentration of excited atoms. During a transient at roughly constant current, these concentrations may

[7] K. T. Compton and I. Langmuir, Revs. Modern Phys. **2**, 218 (1930), Eq. (107).

[8] Kenty, Easley, and Barnes, J. Appl. Phys. **22**, 1010 (1951).

[9] I am indebted to Miss M. A. Easley, who gave me these results.

[10] W. B. Nottingham, Phys. Rev. **55**, 214 (1939).

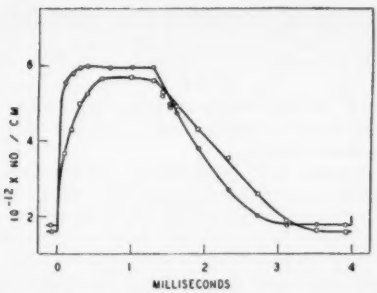

FIG. 8. Electrons per cm of arc computed from probe measurements of electron concentration (○) and from mobility equation for electrons (□).

differ considerably from those that would exist if the same values of T_e were obtained in the steady state by changing the arc current, the mercury vapor pressure, or both. Thus the variation with T_e of the ion production per electron may be quite different from that found in steady-state operation of a similar discharge.

BASIC EQUATIONS

Granovsky has made an extensive theoretical analysis[11] of nonstationary states of a low pressure discharge. Since the fundamental equations form such a complex system that they defy any attempt to find a general solution for them, Granovsky has made simplifying assumptions in order to derive solutions for special cases. Unfortunately several of his assumptions are not applicable to a discharge in mercury vapor plus a rare gas. The principal reasons why his analysis is not applicable are the following:

(1) In his derivation of the equation for the rate of change of the concentration of excited atoms, Granovsky ignores the effect of radiative transitions. In a typical low pressure discharge in mercury vapor, the loss of excitation by radiation of the 2537 line is much more important[12] than transitions from 6^3P levels to the ground level during collisions of the second kind.

(2) Granovsky assumes that the elastic loss per electron per second is proportional to $T_e - T_g$. (T_g = gas temperature in °K). In argon, because of the Ramsauer effect, the elastic loss per electron increases almost exponentially with T_e. In a discharge of the sort considered here (6μ Hg, 3.5 mm A), the elastic loss is almost entirely due to collisions of electrons with argon atoms.

(3) For determining the variation of inelastic losses with T_e, Granovsky suggests that measurements be made on steady-state discharges. This is not practical if either multiple excitation or collisions of the second kind play an important role, since the concentrations in the excited levels during a transient ordinarily will not have the equilibrium values, at a particular T_e, attained in steady-state operation.

(4) For the case where the concentrations in excited states approach a Boltzmann equilibrium with those in the normal level, Granovsky concludes that there is practically no variation in the concentrations in excited levels during a transient. However, T_e varies during every transient, and Boltzmann populations are exponential functions of T_e. Thus, if the transient is of sufficient duration, changes in the concentrations of excited atoms are an important factor. In the discharge described in the present article, the populations of the 6^3P levels are far from a Boltzmann equilibrium,[12] but even if this were not the case, the duration of transients is sufficient to allow large variations in the concentrations of excited atoms to take place when the amplitude of modulation is large.

A complete solution of the fundamental equations for transient states of a discharge seems unattainable, but there are several very useful relationships between the variables. The mobility equation for the electrons is applicable at every instant during a transient. It may be written in the following form:

$$E/i = 2.60 \times 10^9 T_e^{\frac{1}{2}}/(L_e N_e). \qquad (3)$$

The instantaneous power balance in the positive column is expressed by the equation

$$Ei = N_e(w_e + dW_e/dt), \qquad (4)$$

where W_e is the average energy of an electron and w_e is its average expenditure of power. This equation ignores the power spent by the longitudinal field in the acceleration of ions, but for a mercury discharge, this power is less than 0.1 percent of the input.

Rough calculations show that dW_e/dt is negligible compared to w_e except for a period of a few microseconds after a sudden large change in i. Since this short period of initial adjustment of T_e was not observable on the oscillograms on which Figs. 1–9 are based, one may use the following equation for the analysis of the

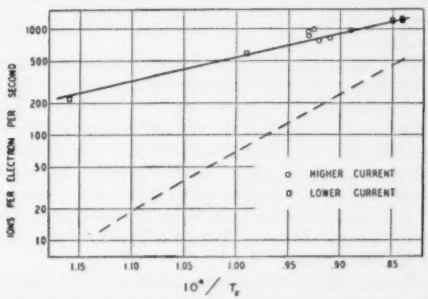

FIG. 9. Ion production per electron *vs* $10^4/T_e$ during a cycle of modulation. Dashed line shows values computed for a single-stage process, using Nottingham's data.

[11] B. Granovsky, J. Phys. U.S.S.R. **3**, 195 (1940).
[12] C. Kenty, J. Appl. Phys. **21**, 1309 (1950).

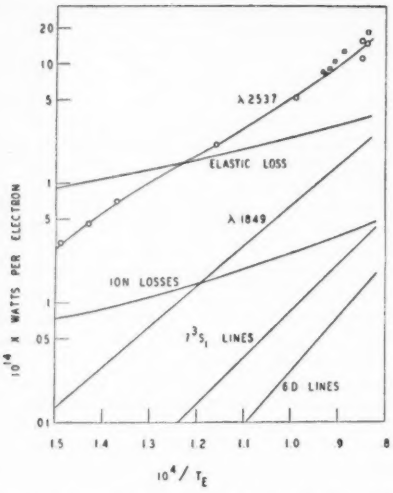

FIG. 10. Power per electron spent in elastic collisions, in flow of electrons and ions to wall, and in radiation of principal lines transmitted by or absorbed in tube wall.

data plotted on these graphs:

$$Ei = N_e w_e, \tag{5}$$

(3)÷(5) gives

$$w_e = 2.60\times10^9 \frac{T_e^{\frac{1}{2}}}{L_e}\left(\frac{i}{N_e}\right)^2 \tag{6}$$

and (3)×(5),

$$E = 5.1\times10^4 (T_e)^{\frac{1}{2}} (w_e/L_e)^{\frac{1}{2}}. \tag{7}$$

Since recombination of ions and electrons in the plasma of a low pressure discharge ordinarily is negligible, the variation of N_e during a transient obeys the following equation:

$$dN_e/dt = \lambda N_e - i_w/e, \tag{8}$$

where λ = number of ions formed per electron per sec, i_w = positive ion current to the wall per cm of arc, and e = electronic charge.

To what extent do the equations listed above define the behavior of a discharge during a transient? Since Eqs. (6) and (7) are derived from (3) and (5), these four equations fix the values of only two unknowns. If one assumes that i is determined solely by the external circuit, that N_e is known from the previous history of the discharge, and that the relationships of w_e and of L_e to T_e are known, then Eq. (5) can be used to compute instantaneous values of T_e and Eq. (3) shows the value of E at any instant.

To test some of the equations derived above, w_e will be determined by summing its component parts, each of which is known or can be computed as a function of T_e. This set of values will then be compared with those computed by substituting the values shown in Figs. 1, 2, and 8 into Eqs. (5) and (6).

One of the principle components in w_e is the λ2537 output per electron, which can be computed from Figs. 2 and 8. The other major component is the elastic loss per electron; its variation with T_e for Hg and A is shown in another article.[8]

The output in the 1849 line was not measured, but its order of magnitude is known from experiments in which the contribution of this line to the excitation of the phosphor in a fluorescent lamp was determined. The variation with T_e of the 1849 output is not known either, and cannot be calculated accurately because there is a possibility of appreciable two-stage excitation. As a rough approximation, the intensity has been assumed proportional to $E^{-6.7e/kT_e}$, where k is the Boltzmann constant. Similar exponentials have been used for the lines originating in the 7^3S_1 and in the $6D$ levels. Absolute values were computed from data obtained on ac and dc tubes similar to those operated on modulated direct current.

The power spent, per electron present, in accelerating ions toward the wall and in providing both ionization energy (10.4 ev) and the kinetic energy of the electrons ($3kT/2$) has been computed and labeled as ion losses. The result is plotted in Fig. 10, together with the other types of power expenditure discussed above. The values of w_e obtained from Fig. 10 are shown by the dashed line in Fig. 11; those computed from Eq. (6) are indicated by squares, and those from Eq. (5) by circles. The two sets of plotted points are in reasonable agreement, but the dashed line lies far below them at low values of T_e. Since elastic losses account for two-thirds of the computed expenditure of power at the lowest value of T_e, it seems likely that the curve given by Brode[13] for the probability of collisions of electrons with argon atoms is too low in the region where $\sqrt{V}<2$.

Equation (3) has been tested already, since it was used to compute one of the sets of N_e values plotted in Fig. 8. The agreement between the two curves on this figure is relatively poor, but the differences may be chiefly due to sources of error already mentioned: uncertainty as to L_e at low values of T_e, and difficulty in determining the correct integration factor for computing N_e from n_0.

In testing Eq. (7) one might use the values of w_e obtained from Eq. (6), but this would merely duplicate the results discussed in the preceding paragraph, since one obtains Eq. (3) when Eqs. (6) and (7) are combined. It seems more logical to test Eq. (7) by using the values of w_e obtained from Fig. 10. The dashed curve in Fig. 12 shows the result of this substitution, and the plotted points are the experimental values for two amplitudes of modulation. The curve through these points is in reasonable agreement with the computed curve except

[13] R. B. Brode, Revs. Modern Phys. **5**, 263 (1933).

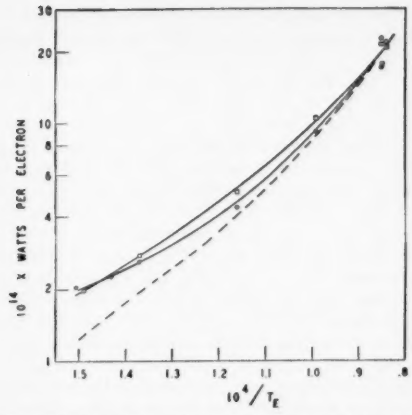

FIG. 11. Total power spent per electron, computed from input per cm arc and N_e values ○, from Eq. (6) □, and from sum of losses shown in Fig. 10 – – –.

at low values of T_e where the values of w_e obtained from Fig. 10 seem to be too low.

For a typical discharge in mercury vapor, computation of N_e by use of Eq. (8) is not possible because there are no detailed data on the probability of two-stage ionization. Klarfeld has estimated[14] that, for an equal excess of energy over the minimum required, the probability of ionization of an atom in a 6^3P level is an order of magnitude greater than that of an unexcited atom. Data accumulated here, but not analyzed in detail, indicate that for electron energies within 1–2 ev of the minimum for ionization, and for the same excess of energy above the minimum required value, the cross sections for ionization from the 6^3P_2 state are several times Nottingham's values[10] for the single-stage process. This tentative conclusion is based on measurements of ion production under steady-state conditions, which can be made fairly accurate, but it also involves computations of metastable atom concentrations and measurements of electron velocity distributions, both of which are much less reliable. Nevertheless, it should be possible to deduce curves for the cross sections for ionization from the 6^3P levels of mercury which would be useful over a considerable range of experimental conditions, even though one has insufficient data for confirmation of the details of the curves chosen to represent the ionization from the individual levels. If these cross sections were known, one could determine values of λ for use in Eq. (8), since fairly reliable computations of the concentrations in the 6^3P_1 and 6^3P_2 levels can be made,[12] and a rough estimate suffices for the 6^3P_0 one. With λ known, Eq. (8) would be usable and one could predict the behavior of a low pressure Hg discharge during any sort of transient.

[14] B. Klarfeld, J. Tech. Phys. (U.S.S.R.) **5**, 921 (1938).

DISCUSSION

Actually to use the equations in the preceding section, one would make a step-by-step computation of the changes in the variables over successive small intervals of time. This laborious procedure is necessary whenever two-stage processes are of importance because w_e and λ are not single-valued functions of T_e and of the pressure of mercury vapor. These two variables also depend on the concentrations of atoms in the 6^3P levels, and changes in these concentrations lag far behind changes in T_e. Thus, there are no simple expressions for w_e and λ that one can substitute in the equations describing the dynamic behavior of a discharge, in order to obtain a general solution for these equations.

The variation in T_e during a transient can be explained qualitatively by analyzing Eq. (6). This equation shows that $w_eL_eT_e^{-\frac{1}{2}}$ is proportional to $(i/N_e)^2$. Since L_e changes relatively slowly with changes in T_e, while w_e increases with T_e much faster than the first power, $w_eL_eT_e^{-\frac{1}{2}}$ always changes in the same direction as T_e. Thus an increase in i/N_e is accompanied by a rise in T_e; and a decrease, by a fall in T_e. Therefore, if a sudden change in i is made, T_e must change in the same direction initially, before N_e has adjusted to its equilibrium value for the new current.

During transients caused by sudden changes in current, the value of T_e at any particular instant will depend mainly on the value of i/N_e. This is illustrated by Fig. 13, which gives data for two of the three amplitudes of modulation shown in Figs. 1 and 3. The fact that, with the maximum modulation, the points for the high current period lie above the smooth curve through the other points may not be due to errors in the data. When the arc current is high, the concentration of atoms excited to the 6^3P levels is correspondingly high,

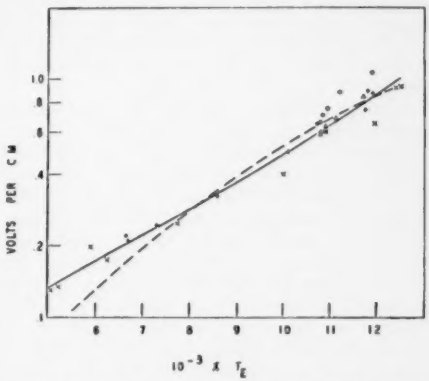

FIG. 12. Longitudinal voltage gradient *vs* $10^4/T_e$. Plotted points and full-line curve show experimental values; dashed curve was computed using Eq. (7). Values obtained at higher and lower currents with maximum modulation (Fig. 3) shown by △ and ×, respectively; those for medium modulation (Fig. 1) by ○ and +.

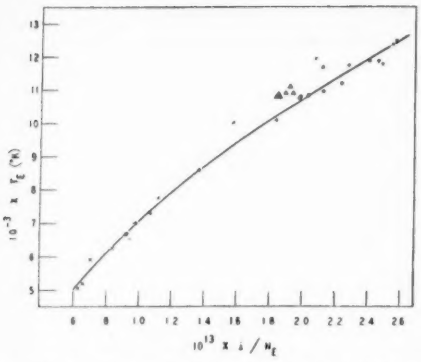

FIG. 13. Electron temperature *vs* i/N_e. Values at higher and lower currents at maximum modulation shown by △ and ×, respectively; those for medium modulation by ○ and +.

and a considerable proportion of the excitations to these levels are offset by collisions of the second kind which return the excitation energy to the electrons. As a result, the value of w_e is less for a particular T_e, and conversely [from Eq. (6)] the value of T_e corresponding to a particular value of i/N_e is greater than at lower currents.

Inspection of Eq. (7) shows that for a particular discharge E is nearly proportional to $w_e^{\frac{1}{2}}$, since $T_e^{\frac{1}{2}}$ and $L_e^{\frac{1}{2}}$ change relatively little during a transient. Since T_e is the principal factor determining the value of w_e, for a particular discharge tube, Eq. (7) shows that there is a close correlation between E and T_e. This was evident from the experimental data discussed earlier (Figs. 1 and 2).

Since the computation of λ [Eq. (8)] is the most difficult step in the use of Eqs. (3) to (8), these equations are particularly useful when $\lambda \doteqdot 0$. This is true in the early stages of a transient following a major reduction in current, since T_e is too low for appreciable ionization (see Fig. 2).

When the frequency of modulation or of ac operation is sufficiently high, instantaneous values of λ are of no importance because the number of ions formed during a cycle is small compared to the number present. Thus N_e varies relatively little during a cycle, and one needs to know only its average value in order to compute the dynamic properties of the discharge. Such a cumputation should shed some light on the factors which decrease the modulation of the radiant energy from a discharge as the frequency is increased, with the modulation of arc current held constant.[15] From Eq. (6), one sees that the modulation of T_e would decrease with increasing frequency because i/N_e would have a smaller range of values as N_e approached constancy. At still higher frequencies, one would have to use $w_e + dW_e/dt$ on the left side of Eq. (6). Since the ratio of the maximum to the minimum value of i/N_e would have become practically constant, w_e and therefore T_e would vary less when the frequency became high enough that dW_e/dt was of the same order of magnitude as w_e during a major part of the cycle.

Another factor which must be considered in the use of Eq. (6) for calculating the modulation of T_e is the storage of energy in metastable and resonance levels and its subsequent expenditure. These processes make w_e higher than one would otherwise expect when T_e is increasing, and lower when it is decreasing. With the modulation of w_e fixed by Eq. (6), any process which increases w_e at high values of T_e and decreases it when T_e is low reduces the variation of T_e during a cycle. Rough calculations indicate that the maximum rates of storage and expenditure of excitation energy will increase with frequency, even though the ratio of the maximum to the minimum stored energy decreases. If this is the case, this storage process will decrease the modulation of T_e with increasing frequency.

When the gas temperature is of the same order of magnitude as the electron temperature, storage of energy in the thermal motion of the gas atoms is another factor that reduces the modulation of T_e with increasing frequency. This effect was mentioned in the second article listed under reference 15.

All of the processes discussed in the preceding paragraphs make the radiant energy per electron vary less as the frequency of modulation is increased, with constant amplitude of current modulation. To find how the modulation of radiant energy changes, one must take account of the reduction in the fluctuation of N_e as the frequency is increased. Since N_e is higher at the maximum T_e and lower at the minimum, as the frequency is increased, the percentage modulation of the radiant intensity decreases less rapidly with increasing frequency than does the percentage variation of the radiated power per electron.

The detailed discussion of modulation given above illustrates the many factors to be considered when one uses Eqs. (3) to (8) to predict or interpret the dynamic behavior of a discharge. These equations obviously can also be used to analyze the wave shape of the voltage across an ac discharge, or the corresponding curve for the spectral intensity of some line from the discharge. Although the graphs refer to a particular discharge in mercury vapor with argon present, the equations and the method of analysis are applicable to any low pressure discharge.

ACKNOWLEDGMENT

I am indebted to Miss M. A. Easley, to Carl Kenty, and to C. G. Found, who furnished data on various dc and ac discharges in mercury vapor and discussed many phases of their behavior, thus contributing much of the background for this investigation.

[15] N. C. Beese, J. Opt. Soc. Am. **36**, 555 (1946). Frank, Huxford, and Wilson, J. Opt. Soc. Am. **37**, 718 (1947).

The Photodisintegration of the Deuteron at Intermediate Energies. I.

C. A. BARNES,* J. H. CARVER, G. H. STAFFORD,† AND D. H. WILKINSON
Cavendish Laboratory, University of Cambridge, Cambridge, England

(Received December 14, 1951)

Measurements have been made of the absolute cross section for photodisintegration of the deuteron at six gamma-ray energies in a range where the photomagnetic effect is small compared with the photoelectric. The methods of determining the gamma-ray flux are described as are the high pressure deuterium-filled ionization chamber and proportional counter used to determine the disintegration rate. The results are given in the following table, together with the reactions used to provide the gamma-rays.

Reaction	Gamma-ray energy (Mev)	Cross section ($\times 10^{28}$ cm^2)
$N^{15}(p, \alpha)C^{12*}$	4.45±0.04	24.3±1.7
$F^{19}(p, \alpha)O^{16*}$	6.14±0.01	21.9±1.0
$Be^9(p, \gamma)B^{10}$	7.39±0.15	18.4±1.5
$C^{13}(p, \gamma)N^{14}$	8.14±0.08	18.0±1.3
$B^{11}(p, \gamma)C^{12*}$	12.50±0.21	10.4±1.0
$Li^7(p, \gamma)Be^8$	17.6 ±0.2	7.7±0.9

INTRODUCTION

THE photodisintegration of the deuteron gives direct information about the neutron-proton system in the triplet state, for this state constitutes the bulk of the deuteron ground state. The total cross section for photodisintegration by gamma-rays of energy remote from the threshold, say above 4 Mev, is governed largely by the binding energy of the deuteron and by the effective range of the neutron-proton triplet interaction.[1–4] Although the absolute cross section depends on the details of the neutron-proton interaction, the form of the cross section's dependence on gamma-ray energy does not, provided this energy remains below about 20 Mev.[5,6]

Measurements of the cross section for photodisintegration of the deuteron have been made in the range of gamma-ray energy from 4.5 to 17.6 Mev. The first objective of these measurements was to determine the form of the dependence of the cross section on gamma-ray energy. Agreement between this form and that predicted by theory for forces of zero range[7] furnishes a check on the applicability of quantum mechanics to the calculation of transitions between states of the two-nucleon system. The second objective was the determination of the ratio between the cross sections and those predicted by theory for forces of zero range. This ratio then determines the effective range very directly.[3,4] A third objective was the provision of an anchor for high energy photodisintegration experiments where details of the neutron-proton interaction potential shape, for example, become important.[5,6] This demands the successful attainment of the first objective and the agreement between the effective range as deduced from these measurements and that derived by other means.

This paper describes the experiments; the following paper presents a discussion of the results.

GENERAL METHOD

Measurements have been made at 4.45, 6.14, 7.39, 8.14, 12.5, and 17.6 Mev. The method for all energies except the first was to irradiate a known mass of deuterium gas contained in an ionization chamber with a known flux of the gamma-rays in question and to determine the disintegration rate by counting the photoprotons. The cross section at 4.45 Mev was found by irradiating a proportional counter containing deuterium with known fluxes of 4.45- and 6.14-Mev gamma-rays. The ratio of the cross sections at the two energies was determined.

THE IONIZATION CHAMBER

Electrons must remain free in the gas of the ionization chamber. The gas pressure must be high because the cross section to be measured is small, and sufficient stopping power must be provided for the photoprotons to dissipate all their energy in the gas. The purity of the gas must then be very great.[8] The ionization chamber proper was spherical so that the geometrical effects of photoprotons striking the walls could be accurately calculated. The collecting electrode was a thin rod to minimize the inductive effects of positive ions. A steel envelope of thickness 0.67 cm closely surrounded the chamber proper, which was a spherical glass vessel of diameter 9.6 cm. The anode was an aluminum rod of diameter 0.3 cm and was held axially

* Now at the University of British Columbia, Vancouver, Canada.
† Now at the University of Pretoria, Pretoria, South Africa.
[1] J. M. Blatt and J. D. Jackson, Phys. Rev. **76**, 18 (1949).
[2] H. A. Bethe, Phys. Rev. **76**, 38 (1949).
[3] H. A. Bethe and C. Longmire, Phys. Rev. **77**, 647 (1950).
[4] E. E. Salpeter, Phys. Rev. **82**, 60 (1951).
[5] L. I. Schiff, Phys. Rev. **78**, 733 (1950).
[6] J. F. Marshall and E. Guth, Phys. Rev. **78**, 738 (1950).
[7] H. A. Bethe and R. Peierls, Proc. Roy. Soc. (London) **A148**, 146 (1935).
[8] D. H. Wilkinson, *Ionization Chambers and Counters* (Cambridge University Press, London, 1950).

within the sphere. There was no cathode within the glass chamber, but the outside of the vessel was painted with Aquadag to within 3 cm of the axis; this Aquadag coating was the cathode as in the Geiger counter of Maze.[9] The anode passed into small side-arms on which were painted Aquadag guard-rings. In this way a chamber of well-defined volume was achieved. The chamber was filled with distilled water and weighed; from the volume measured in this way was subtracted the calculated volumes of the side arms. The effective volume was 475 cc. The chamber was baked in an atmosphere of hydrogen for 8 hours at 400°C; it was then baked for a further 8 hours at a pressure of 10^{-6} mm Hg, flushed with pure hydrogen at a pressure of 10^{-3} mm Hg for 1 hour and sealed off. It was then mounted in the steel shell and was filled with pure deuterium by filtering this gas through palladium tubes which were attached to the glass chamber.[10] The pressure in the outer shell was increased at the rate of 1 atmosphere per hour. The pressure finally reached was 38.15 atmospheres (at 0°C). The measurement was made on the gas within the steel shell with a pressure gauge which had been calibrated by the National Physical Laboratory; it was made several weeks after filling to ensure that equilibrium had been reached. The chamber was operated under a potential difference of 10,000 volts: this was furnished by batteries. Under these conditions electron collection appeared to be complete.

THE RESOLUTION OF THE IONIZATION CHAMBER

There are three chief reasons why, on irradiation with monochromatic gamma-rays, this chamber does not yield a perfectly sharp group of photoproton pulses. One is that, due to the ballistics of the reaction, there exists a spread of about 20 percent in the photoproton energy. Another reason is the inductive effects of the positive ions; this means that the pulse produced by the liberation of a given amount of ionization depends on the location of that ionization within the chamber. This effect is calculable.[8] Calculations have been made for the present chamber under two approximations. The first approximation replaces the chamber by infinite coaxial cylinders of radii b and a, the second by confocal ellipsoids. The results of these two approximations differ only slightly, and the correct result lies between them: we assume that our chamber may be represented by infinite coaxial cylinders with $b^2/a^2=6000$. The result of the calculation of the inductive effects between confocal ellipsoids is stated in Appendix I. The ballistic spread and the inductive effect are combined analytically in Appendix II. The resolution of the chamber calculated in this way agreed very well with that experimentally observed and gave confidence that the apparatus was working properly. This calculation may also be used to demonstrate that, despite the fact that the ballistic spread is a function of gamma-ray energy while the inductive spread is not, the peak in the photoproton pulse distribution may be taken as a direct measure of the mean photoproton energy and so be directly related to the gamma-ray energy.[11,12]

The wall effect also distorts the pulse distribution. Some photoprotons strike the wall before reaching the end of their range and so give a reduced pulse. This effect may be simply calculated for a spherical chamber. The result is stated in Appendix III.

These considerations enable the expected pulse distribution to be computed with some accuracy, and, by comparing this with the experimental pulse distribution, the total disintegration rate may be accurately determined even though the photoproton range may become comparable with the dimensions of the chamber.

We have also considered the effects of collisions between deuterons of the chamber gas and the photoneutrons produced both within the chamber proper and between the glass chamber and the steel outer shell. Both effects are small.

The smearing effect on the calculated distributions of the noise due to the amplifier and to the building up of pulses due to fast electrons must be allowed for.

THE FINITE SIZE OF THE IONIZATION CHAMBER

Owing to the finite size of the ionization chamber we may not assume, for the purposes of relating the gamma-ray flux with the observed disintegration rate, that all the gas is concentrated at the center of the sphere. If the gamma-ray source is a disk of diameter small compared with that of the sphere, as it is under our experimental conditions, the departure from the inverse square law may be allowed for by dividing all the disintegration rates by

$$f(x)=\frac{3x^2}{2}\left\{1-\frac{x^2-1}{x}\log\left[\frac{x+1}{(x^2-1)^{\frac{1}{2}}}\right]\right\},$$

where x is the distance of the center of the sphere from the gamma-ray source divided by the radius of the sphere.

THE PROPORTIONAL COUNTER

The ionization chamber could not be applied directly to the measurements at 4.45 Mev because the pulses resulting from fast electrons became comparable in size with those resulting from photoprotons. A proportional counter was built for work at this energy. The body was a stainless steel cylinder of length 30 cm and diameter 10 cm; the wall thickness was 2 mm. A tungsten wire of diameter 40μ hung along the axis of the counter and was held taut by a nickel weight. The exposed length

[9] R. Maze, J. phys. et radium **7**, 164 (1946).
[10] G. H. Stafford, Nature **162**, 771 (1948).
[11] Provided that W, the energy required to create one ion pair, is a good constant for protons in deuterium. This is very probably so, and extra confidence is given by the fact that W for protons of 340 Mev in hydrogen is only 3 percent lower than for slow protons (see reference 12).
[12] C. J. Bakker and E. Segrè, Phys. Rev. **81**, 489 (1951).

of wire was 20 cm; it was led through the Kovar-glass seal by a nickel tube of outer diameter 1.5 mm. A purifier of the circulation type was attached to the counter. The gases were introduced into the counter via two needle valves, the moving parts of which were enclosed in bronze sylphon bellows so that no grease was in contact with the gas. The counter was always filled with mixtures of argon and deuterium and has operated satisfactorily at pressures up to ten atmospheres of argon plus one-half of an atmosphere of deuterium. The counter was well pumped and flamed; it was then filled to 1 atmosphere with argon, the purifier opened and about 1 cc of sodium dropped inside. The counter was thoroughly pumped and the sodium evaporated by heating. After further pumping at about 10^{-4} mm Hg for a day, the counter was filled; deuterium was put in first. The argon was of the commercial grade known as "oxygen free" and was passed in through a carbon dioxide trap. The deuterium was passed in through palladium. Before the counter was used the gases were circulated; the fresh sodium surface is an excellent purifier,[13] and we have had no trouble from electron attachment.

The work here reported was carried out with a filling of 2 atmospheres each of deuterium and argon; a gas amplification of 5.2 was achieved for an applied voltage of 3960.

THE RESOLUTION OF THE PROPORTIONAL COUNTER

The resolution is limited only by the inevitable ballistic spread and by the wall effect; positive ion induction does not occur in the same sense as in the ionization chamber.

The calculation of the wall effect is presented in Appendix IV.

THE MEASUREMENT OF THE GAMMA-RAY FLUX

The monitoring of the gamma-ray flux was carried out with a thick-walled brass Geiger counter whose sensitivity, which was checked from day to day with a standard gamma-ray source, did not change by 1 percent over a period of 650 days.

The calculation *ab initio* of the efficiency of a Geiger counter is uncertain and was not attempted; the counter was directly calibrated at 6.14 and 17.6 Mev.

When fluorine is bombarded with protons, many reactions occur. The one of chief concern here consists in the emission of an alpha-particle, leaving the residual nucleus O^{16} in an excited state at 6.14 ± 0.01 Mev.[14–16] If the resonance at a proton energy of 340 kev is used, 97½ percent of the alpha-particle transitions take place to this state at 6.14 Mev and 2½ percent to states at 6.9 and 7.1 Mev.[17] No other known gamma-ray emitting states in O^{16} are accessible. If these alpha-particles are observed at 90° to the proton beam, the relative contribution from alpha-particles making transitions to the ground state of O^{16} and the pair emitting state at 6.0 Mev is less than 1 percent.[18] Both alpha-particles and gamma-rays are emitted isotropically;[19,20] indeed, strong evidence[21–23] suggests that the level is formed by capture of *S*-wave protons. The radiative transition from the compound nucleus Ne^{20} is known[24–26] at a proton bombarding energy of 669 kev, but its intensity is low: it is negligible at the 340-kev resonance. At a bombarding energy of 900 kev the thick target yield of this energetic gamma-ray is roughly 0.2 percent of the 6- and 7-Mev gamma-rays combined.

Some gamma-rays will be internally converted or give rise to internal pair-creation. The 6.14-Mev gamma-ray from the 340-kev level is known to be (probably electric) octupole radiation.[21–23] The conversion coefficients to be expected are very small, being less than 10^{-6} and 2×10^{-3} for internal conversion and pair creation, respectively.[27,28]

It appears that the counting of alpha-particles at 90° to the proton beam constitutes an accurate method of measuring the flux of 6.14-Mev gamma-rays;[29] the alpha-particles preceding the emission of the 6.9- and 7.1-Mev gamma-rays are not counted, but their relative abundance is well known.[17,30] This method was first used by Van Allen and Smith.[31]

The sensitivity of the Geiger counter was determined at 6.14 Mev by counting the alpha-particles with a conventional fast ionization chamber in well-defined geometrical conditions. The natural effect in the Geiger counter and that associated with bombardment of a blank copper disk were respectively ½ percent and 1 percent of the effect resulting from the CaF_2 target at 33 cm. An inverse square law plot for the Geiger counter is shown in Fig. 1 to a distance from the target of 75 cm. The usual working distance was 33 cm. Loss of alpha-

[13] It is a common fallacy that sodium has a strong affinity for hydrogen; it is difficult to prepare NaH from the two elements by direct combination. We have looked for loss of deuterium over several days, but have found none (the sodium was at room temperature). We are indebted to Dr. A. G. Maddock for telling us of this useful property of sodium.

[14] Strait, Van Patter, Buechner, and Sperduto, Phys. Rev. **81**, 747 (1951).

[15] Hornyak, Lauritsen, Morrison, and Fowler, Revs. Modern Phys. **22**, 291 (1950).

[16] Millar, Bartholomew, and Kinsey, Phys. Rev. **81**, 150 (1951).

[17] J. M. Freeman, Phil. Mag. **41**, 1225 (1950).

[18] Streib, Fowler, and Lauritsen, Phys. Rev. **59**, 253 (1941).

[19] J. Van Allen and N. Smith, Phys. Rev. **59**, 501 (1941).

[20] S. Devons and M. G. N. Hine, Proc. Roy. Soc. (London) **A199**, 56 (1949).

[21] W. R. Arnold, Phys. Rev. **79**, 170 (1950).

[22] W. R. Arnold, Phys. Rev. **80**, 34 (1950).

[23] Barnes, French, and Devons, Nature **166**, 145 (1950).

[24] S. Devons and H. G. Hereward, Nature **162**, 331 (1948).

[25] Rae, Rutherglen, and Smith, Proc. Phys. Soc. (London) **A63**, 775 (1950).

[26] J. H. Carver and D. H. Wilkinson, Proc. Phys. Soc. (London) **A64**, 199 (1951).

[27] S. M. Dancoff and P. Morrison, Phys. Rev. **55**, 122 (1939).

[28] M. E. Rose and G. E. Uhlenbeck, Phys. Rev. **48**, 211 (1935).

[29] The distortion of the isotropic distribution by center-of-gravity motion should be considered, but is negligible (~0.3 percent) for observation near 90°.

[30] Chao, Tollestrup, Fowler, and Lauritsen, Phys. Rev. **79**, 108 (1950).

[31] J. Van Allen and N. Smith, Phys. Rev. **59**, 618 (1941).

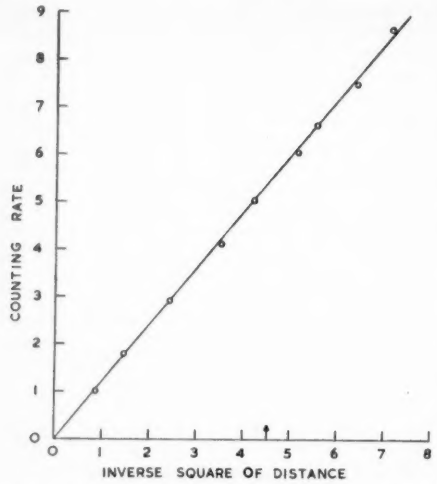

FIG. 1. Inverse square law for the Geiger counter during the alpha-particle calibration. Working point is indicated by the arrow.

particles by single and multiple scattering and their penetration of the edges of the aperture which defined their passage into the counter were computed. These effects were negligible.

The bias curve was analyzed with the help of considerations set out in Appendix V.

Several calibration runs were made over a period of days and a probable error in the calibration of the Geiger counter, based on internal consistency alone, of $\pm\frac{3}{4}$ percent[32] was determined.

A second calibration was made using a thick-walled current ionization chamber made of graphite, which contained a cylindrical cavity of radius 4.0 cm and depth 2.0 cm filled with pure nitrogen at a pressure of 76 cm Hg. Saturation was fully realized. This method is of common use.[33,34]

The ionization current was translated into gamma-ray flux by the theory of Lax.[35] A correction was computed on account of ionization produced by Compton-scattered photons. This correction amounted to 10 percent for gamma-rays of energy 6.14 Mev[36] and 3 percent for gamma-rays of energy 17.6 Mev. Absorption of gamma-rays in the graphite and surrounding aluminum can was also allowed for as were radiation losses, annihilation of positrons in flight, and the condensation effect in graphite.[37–40] The finite size of the cavity was taken into account in the same way as was the finite size of the deuterium chamber. Inverse square plots using various gamma-rays of energy up to 17.6 Mev showed that one may define an effective center of the chamber 0.45 ± 0.15 cm nearer the source than the geometrical center of the cavity.

The energy loss, W ev, of electrons in forming an ion pair in nitrogen must be known. For fast electrons in air Gray[41] recommends a value of 32.0 ev; the accuracy is about ±1 percent. A value for nitrogen may be found in two ways. Firstly, the measurements by Stetter[42] on the ionization produced by the alpha-particles of polonium in various gases suggest a ratio of 1.042 between W values in nitrogen and air. Secondly, we irradiated the graphite ionization chamber with the same gamma-ray flux both when filled with air and with nitrogen, and thereby derived the value 1.03 ± 0.01 for the preceding ratio. We adopted the value 1.03, obtaining $W=32.9$ ev for fast electrons in nitrogen.

Other sources of current are the various photodisintegration processes occurring in the graphite and in the nitrogen. These sources are negligible.

The current chamber was used with the 6.14-Mev gamma-rays from fluorine: it gave a value for their flux lower by $1\frac{1}{2}$ percent than that given by the counting of alpha-particles. This agreement gave some confidence in the elaborate computations which underlie the results obtained with the current chamber. The result of the alpha-particle calibration was that one count in the brass Geiger counter of wall thickness 0.95 cm, whose sensitive volume was of length 8 cm and diameter 2.6 cm, corresponded to the normal passage per cm^2 across a plane containing the counter's axis of 1.36 quanta of energy 6.14 Mev.

The current chamber was then used to calibrate the Geiger counter for the gamma-rays given by the bombardment of lithium with protons. Radiative capture takes place at a proton energy of about 440 kev, and gamma-rays of 14.8[43] and 17.6 Mev result.[44,45] We take an intensity ratio of 0.55:1 for these two components.[44,46]

[32] Throughout this paper $\pm$ means probable error.
[33] L. H. Gray, Proc. Roy. Soc. (London) **A156**, 578 (1936).
[34] G. C. Laurence, Can. J. Research **A15**, 16 (1937).
[35] M. Lax, Phys. Rev. **A72**, 61 (1947).
[36] This correction comprises 9 percent for the effect of photons which suffer a single Compton scattering and 1 percent for the effect of doubly-scattered photons.
[37] E. Fermi, Phys. Rev. **56**, 1242 (1939).
[38] E. Fermi, Phys. Rev. **57**, 485 (1940).
[39] O. Halpern and H. Hall, Phys. Rev. **73**, 477 (1948).
[40] F. L. Hereford, Phys. Rev. **74**, 574 (1948).
[41] L. H. Gray, Proc. Cambridge Phil. Soc. **40**, 72 (1944).
[42] G. Stetter, Z. Physik **120**, 639 (1943).
[43] This lower energy component is known as the 14.8-Mev component after the results of Walker and McDaniel (see reference 44). It is probable that the energy is a little less than this. Walker and McDaniel found the energy to be 14.8 ± 0.3 Mev: Carver and Wilkinson (see reference 26) have measured it as 14.4 ± 0.4 Mev. The best value for the mean position of the level in Be^8 to which the radiative transition occurs is 3.01 Mev (Burcham: private communication), and this corresponds to an energy of 14.60 Mev for the gamma-ray. This value we have used in reducing the results.
[44] R. L. Walker and B. D. McDaniel, Phys. Rev. **74**, 315 (1948).
[46] According to Nabholz, Stoll, and Wäffler, Phys. Rev. **82**, 963 (1951), a gamma-ray of 12.5 Mev is emitted in about 10 percent of the strength of the 17.6 Mev line. This introduces no significant uncertainty in our work.
[45] M. B. Stearns and B. D. McDaniel, Phys. Rev. **82**, 450 (1951).

We used a thick target of lithium hydroxide and protons of 510 kev. There is then no inelastic proton scattering in the level in Li^7 at 453 kev. We found a sensitivity of 0.376 quanta per cm^3 of 17.6 Mev for one count in the Geiger counter.[47] The intensity ratio may be as high as 0.8:1,[48] the sensitivity would then become 0.372 quanta per cm^3 of 17.6 Mev per count. We have used 0.55:1.

Our final measurements with the gamma-rays from fluorine were made at a proton bombarding energy of 900 kev. The constitution of the gamma-rays is then 73 parts of 6.14 Mev to 27 parts of 6.9 and 7.1 Mev combined.[17,30] Allowance for this inhomogeneity may accurately be made.

We have made the following estimates of the probable error in our knowledge of the Geiger counter calibration. For the 6.14-Mev gamma-rays, $\pm\frac{3}{4}$ percent for internal consistency as remarked above; $\pm 2\frac{1}{2}$ percent in interpretation of the alpha-particle bias curve; $\pm\frac{3}{4}$ percent for uncertainty in the composition of the gamma-rays at the 340-kev and higher resonances; geometrical errors $\pm 1\frac{1}{2}$ percent. These errors combine quadratically to ± 3.0 percent. For the 17.6-Mev gamma-rays, the good agreement of the two methods of flux measurement at 6.14 Mev suggest that ± 5 percent may be adequate.

These measurements reveal a Geiger counter efficiency increasing a little more rapidly than linearly with gamma-ray energy. For energies below 3 Mev the efficiency of such a counter varies almost linearly with energy.[49] The origin may therefore be used as a third point in the calibration. Little error is involved in estimating efficiencies between the two measured points and an error increasing uniformly from ± 3 percent at 6 Mev to ± 5 percent at 18 Mev has been assumed.

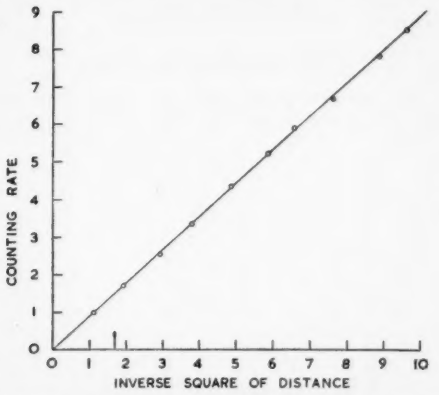

FIG. 2. Inverse square law for the Geiger counter during the disintegration experiment. Normal working point is indicated by the arrow.

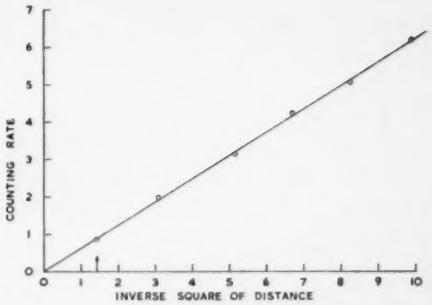

FIG. 3. Inverse square law for the photodisintegration chamber. Normal working point is indicated by the arrow.

For the work at 4.45 Mev we are only interested in the ratio of the Geiger counter efficiency at 4.45 and 6.14 Mev. We have taken an error of $\pm 2\frac{1}{2}$ percent in this ratio.

MEASUREMENTS AT 6.14 MEV

The cross-section measurements with the gamma-rays of 6.14 Mev was preceded by inverse square law investigations both for the Geiger counter and for the deuterium chamber to make sure that scattered radiation was of no importance. A proton energy of 900 kev was used. Figure 2 shows the results for the Geiger counter at distances from the target of 70 to 210 cm. The usual working distance was 172 cm. No background could be detected. Large masses placed near the target had no effect. The pulse distribution from the deuterium chamber was biased off close to the level of electron noise; the inverse square plot is shown in Fig. 3. Again no background could be found. The greatest distance from the target was 59 cm.

A molybdenum shutter could be inserted in the proton beam immediately in front of the target, and by this means we were assured that no significant gamma-ray flux had its origin other than in the fluoride.

Devons and Hine[50] suggest that the gamma-ray flux at 0° to the bombarding proton beam (the direction in which lay the ionization chamber) should be 1.09 in terms of that at 100° (the direction of the Geiger counter) for protons of 900 kev incident upon a thick target; Day, Chao, Fowler, and Perry[50] suggest 1.12 for this quantity. We found a value of 1.11 and adopted it.

The pulse distribution from the deuterium chamber was measured with a ninety-nine channel kick-sorter.[51] Typical distributions are shown in Figs. 4 and 5. Figure 4 is taken at a proton bombarding energy of 500 kev, where the radiation is largely of 6.14-Mev

[47] Strictly speaking, we derive a sensitivity for the mixed radiation, but the efficiency at the well-defined energy may very rapidly be arrived at by successive approximation.

[48] S. Devons and G. R. Lindsey, Proc. Phys. Soc. (London) **A63**, 1202 (1950).

[49] J. V. Dunworth, Rev. Sci. Instr. **11**, 167 (1940).

[50] Day, Chao, Fowler, and Perry, Phys. Rev. **80**, 131 (1950).

[51] D. H. Wilkinson, Proc. Cambridge Phil. Soc. **46**, 508 (1950).

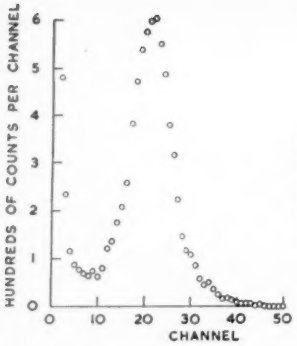

FIG. 4. Photoproton pulse distribution with gamma-rays of 6.14 Mev. Zero of the distribution lies at channel minus 15.

gamma-rays. Figure 5 is taken at 900 kev, where there is a 27 percent admixture of 6.9- and 7.1-Mev components. (The amplifier conditions are not the same for the two figures.) The distribution is noticeably broader in Fig. 5, but no resolution is to be expected in our conditions—the two higher energy peaks would lie at channels 34 and 36.

The possibility that some of these pulses may have been the result of deuterons recoiling from fast neutrons arising in secondary reactions was investigated by means of an ionization chamber identical with that described previously, but filled with ordinary hydrogen instead of deuterium. No significant effect was found.

The pulse distributions were interpreted with the aid of the calculations on resolution and wall effect previously discussed. All the results were corrected for the finite but accurately known dead time (0.0880 second) of the kick-sorter. Five successive runs yielded relative disintegration rates of 1, 1.005, 1.005, 0.979, 1.016; these ratios possess a statistical probable error of ± 0.017.

The absorption of gamma-rays between the source and the gas of the ionization chamber is important. It may be calculated,[52] but is of such a magnitude ($\sim$20 percent) that we investigated it experimentally. The bulk of the absorption took place in the steel outer wall of thickness 0.67 cm. Other absorbing bodies were the brass target backing (thickness 0.17 cm) and the glass inner envelope of the ionization chamber (thickness 0.2 cm). The absorption in the walls of the ionization chamber is not quite straightforward because some of the quanta which suffer Compton scattering, and which would then be regarded as absorbed on the simple view, in fact still lie above the photodisintegration threshold. The apparent absorption coefficient determined using the ionization chamber as the detector should be a function of the bias setting of the discriminator used to limit the pulse distribution. At zero bias the apparent absorption coefficient should be determined by the pair and photoelectric cross sections plus the Compton cross section for scattering of the gamma-rays below the photodisintegration threshold.

The absorption coefficient was determined by stacking steel plates immediately in front of the ionization chamber. Five plates were used, each of thickness 0.635 cm. A typical absorption curve is shown in Fig. 6. The dotted line indicates the thickness of the steel wall of the ionization chamber. We may not properly expect to be able to define an absorption coefficient at all, but the exponential plot of Fig. 6 shows that this may be done. The factor, derived from such plots, relating the counting rate to be expected without a wall to the chamber with that observed in practice was then determined as a function of discriminator bias; it is displayed in Fig. 7. The bias setting corresponding to the peak of the pulse distribution was 50 volts. The calculated value for "complete" absorption as shown at high bias settings was 1.17, and that for zero bias was 1.12. These figures accord well with the experimental results. The attenuation factor for the pulse size above which the distributions such as those of Figs. 4 and 5 were analyzed in detail was determined from Fig. 7 to be 1.15; the calculated value was 1.15. (In these calculations the form of the dependence of the photodisintegration cross section on gamma-ray energy given by the theory of Bethe and Peierls[7] was used.) The agreement of the experimental and calculated values of the absorption correction means that this correction may be applied with confidence. For all other gamma-rays the absorption correction was calculated. The corrections for absorption in the other bodies mentioned previously were much smaller and were calculated.

Results and Errors at 6.14 Mev

The principal errors are[53]—± 3.0 percent in the gamma-ray flux as previously detailed; ± 2.2 percent

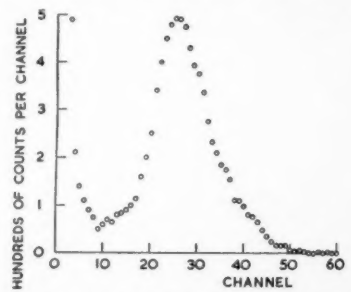

FIG. 5. Photoproton pulse distribution with gamma-rays of 6.14 and 7 Mev. Zero of the distribution lies at channel minus 15.

[52] W. Heitler, *The Quantum Theory of Radiation* (Oxford University Press, London, 1949).

[53] Where no direct estimate of a probable error was possible but only a maximum tolerance we have adopted one-half of this value as the associated probable error.

for the combined uncertainties in the interpretation of the kick-sorter distribution, wall effect estimate, statistical error in the 12,000 photoprotons counted and error due to the kick-sorter dead time; ±1.5 percent for the absorption correction; ±0.5 percent for possible Geiger counter fluctuations (the statistical error is negligible); ±0.35 percent for geometrical uncertainties; ±1.5 percent for uncertainty in the angular distributions; ±0.3 percent for possible background radiation in the Geiger counter; ±0.5 percent for deuterium pressure; ±0.5 percent for deuterium purity.[54] Assembling these errors quadratically we find ±4.5 percent as the total probable error in the cross section.

$$\sigma_{6.14}=(21.9\pm1.0)\times10^{-28}\ \text{cm}^2.$$

(A correction of 2.5 percent has been made for the mixed character of the gamma-rays. The form of variation of cross section with energy given by Bethe and Peierls[7] was used.)

MEASUREMENTS AT 7.39 MEV

When beryllium is bombarded with protons radiative capture takes place in a broad level centered at 998 kev. So far as is known decay takes place directly to the ground state of B^{10}.[18]

A sharp level formed with protons of 1.087 Mev decays via a state in B^{10} at 0.713 Mev; the main gamma-ray energy is then about 6.8 Mev. Our proton bombarding energy was 1000 kev and so we remained clear of this double transition. Several more known states in B^{10} could be involved in double transitions. We have assumed that they are not appreciably excited. It is known from the work of Walker[55] and others, that the low-lying states are not involved in more than a few percent of the strength of the main transition. We are not very sensitive to such transitions, because we should count both the photoprotons and the gamma-rays,[56] and so achieve a large measure of compensation for a small effect. A double transition of considerable danger, however, would be that involving the known state at 3.58 Mev, for we should see almost none of the photoprotons from either gamma-ray. A limit of about 10 percent on the relative probability of this transition is set by the work of Walker[55] (and private communication[57]). We are at the mercy of triple cascades in which the energy is more or less equally shared.

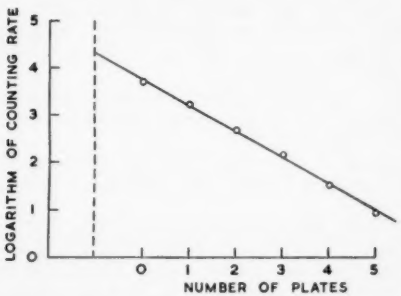

FIG. 6. Absorption curve of 6-Mev radiation in steel plates using the photodisintegration chamber as detector. The thickness of the steel wall of the chamber is indicated by the dotted line.

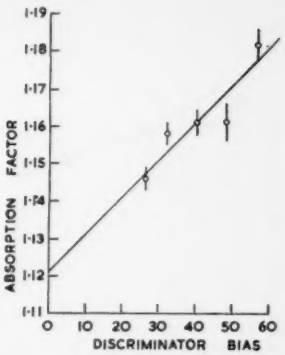

FIG. 7. Absorption factor for the steel wall of the chamber as a function of discriminator bias.

We have considered the production of gamma-rays from several competing reactions and decided that no significant contamination can occur. Be^9 possesses no known excited states below 1 Mev, so inelastic scattering of protons need not be feared.

It was with great annoyance that we discovered, in place of a well-defined photoproton spectrum, the pulse distribution shown in Fig. 8. The photopeak was expected at channel 35.

The explanation of this distressing phenomenon was that a substantial fast neutron flux was being generated. We are dealing with the second-order reactions $Be^9(p, d)Be^8$ followed by $Be^9(d, n)B^{10}$ and $Be^9(p, \alpha)Li^6$ followed by $Be^9(\alpha, n)C^{12}$.[58] The former pair is more probable under our conditions.

The run of Fig. 8 had been taken with a thick beryllium target, and the use of a thin target from which the deuterons could escape before losing much energy was demanded. A target of stopping power about 2 kev was used and yielded the pulse distribution shown in Fig. 9. A continuous pulse distribution was still observed, but superposed on it was a clear peak of photoprotons. The neutron spectrum from the two stage process should be closely the same for thick or thin targets; a small correction must be applied to

[54] This purity was measured by the mass spectrograph group at the laboratory of the National Research Council of Canada at Chalk River, Ontario, and found to be 96.98 percent and 96.62 percent on two separate samples of the gas.

[55] R. L. Walker, Phys. Rev. **79**, 172 (1950).

[56] The Geiger counter has an efficiency roughly proportional to gamma-ray energy and so detects single quantum transitions and cascades with approximately equal efficiency.

[57] We are indebted to Dr. Walker for making this estimate.

[58] The first pair of reactions has been commented on by Jennings, Sun, and Leiter, Phys. Rev. **80**, 109 (1950).

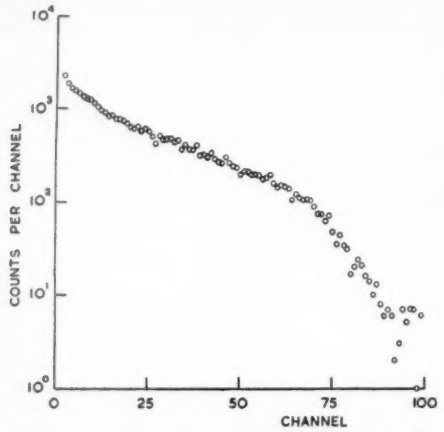

FIG. 8. Pulse distribution from protons of 1000 kev on a thick beryllium target. Zero of pulse distribution at channel minus 16.

the thick target pulse distribution to obtain that for the thin target. This correction was computed with the aid of the known excitation functions of the $Be^9(p, d)Be^8$ and $Be^9(d, n)B^{10}$ reactions and information on the change of neutron spectrum with deuteron energy. This corrected spectrum is shown as the full line in Fig. 9. In the peak the true photoproton counting rate is about five times the background, so the subtraction is not a serious one; when it is made a distribution of the expected shape results. (A small correction is made for the photoproton contribution to the distribution of Fig. 8.) Because of the suspicion always attaching to the subtraction of backgrounds, we have added an extra ± 5 percent to the error.

Two separate sets of final runs were made, 8 runs in the first set and 9 in the second. Internal consistency within each set was satisfactory, and the two sets agreed to within 3 percent; each contained about 10,000 photoprotons.

During these final runs the chamber was at a distance of 16.9 cm from the target and at 0° to the proton beam. The Geiger counter monitoring was carried out at 44.9 cm and 45°, and the usual corrections for absorption were made. There was a decrease in gamma-ray flux of 5 percent in going from 45° to 0°: this agrees with the results of Devons and Hine,[20] which lead one to expect a decrease of $4\frac{1}{2}$ percent.

The gamma-ray yield from excited states of B^{10} formed by $Be^9(d, n)B^{10}$ was not big enough to necessitate a correction to the Geiger counter counting rate.

The photoproton peak from the beryllium gamma-rays we locate with an error of ± 1.5 channels, that from the fluorine calibration gamma-ray to $\pm\frac{3}{4}$ percent. The gamma-ray energy is 7.39 ± 0.15 Mev.[59] The mass values predict a gamma-ray energy of 7.39 Mev from the 998-kev resonance.[60] Walker[55] has found an energy of 7.38 ± 0.07 Mev from a thick target and protons of 1.15 Mev, the chief contribution coming from the 998-kev resonance. We have taken 7.39 Mev.

Results and Errors at 7.39 Mev

Allowances of error above those discussed for the gamma-rays of 6.14 Mev are—± 5 percent for the subtraction of the neutron background; ± 4 percent for possible low energy gamma-rays (taking into account the partial compensation for their effects which obtains).

$$\sigma_{7.39} = (18.4 \pm 1.5) \times 10^{-28} \text{ cm}^2.$$

MEASUREMENTS AT 8.14 MEV

The radiative capture of protons by C^{13} in the resonance level at a proton energy of 554 kev gives a single quantum of about 8.1 Mev by a transition to the ground state of N^{14}. There is also a possible competing transition to the state in N^{14} at about 2.3 Mev. Lauritsen and Fowler[61] using a thick target report that these alternative transitions take place with equal intensity and find no other gamma-rays. Day[62] and Woodbury[63] find no evidence for the double cascade but an indication of a triple cascade of intensity about 13 percent of that of the direct transition. We are again sensitive to multiple transitions and the general remarks made previously in connection with the beryllium gamma-rays apply. However, we would have seen evidence of any other double transition of strength more than a percent or two of the 8.1-Mev line. Such transitions were not detected and, if present, would also be quite well compensated for; this is so even if they involved the state at 3.9 Mev almost midway between the initial and ground states, because the "electron-noise" cut-off does not occur until an equivalent gamma-ray energy of 4.2 Mev. We have assumed a 13 percent contribution of triple cascades in reducing the gamma-ray flux.

There are here no competing reactions and inelastic proton scattering need not be considered as no suitable levels are known in C^{13}.[15]

A target of C^{13} deposited on copper was bombarded with protons of 570 kev;[64] its thickness was estimated

[59] A notice of the gamma-ray energies derived in this work has been published by Carver and Wilkinson (see reference 26).

[60] No allowance for Doppler shift has been made in any of the calculated gamma-ray energies; the shift is never as much as $\frac{1}{2}$ percent.

[61] T. Lauritsen and W. A. Fowler, Phys. Rev. **58**, 193 (1940).

[62] Private communication.

[63] Ph.D. thesis. California Institute of Technology (1951).

[64] The resonance is centered at 554 kev and has a width at half-maximum of about 40 kev. We have sacrificed yield in working at 570 kev in order to keep away from the radiative capture resonance in C^{12} at 453 kev (width 35 kev). Our target was electromagnetically separated and so should be very free of C^{12}, but another source is deposition onto the target from oil of the diffusion pumps. All our other work, with the exception of

from the yield and reaction constants[65] as 20 kev, and so the effective proton energy was about 560 kev.

The ionization chamber was irradiated at 0° to the proton beam and at a distance from the target of 18.9 cm. The Geiger counter monitoring was done at 40° and 42.6 cm. The pulse distribution on which the estimate of the cross section was based is shown in Fig. 10. It is at once obvious that there is only one strong component in the gamma-ray spectrum. The ratio of width at half-maximum to peak position should be almost constant for our photoproton groups. This ratio for fluorine gamma-rays is about 0.28; for the main peak of Fig. 10 it is 0.29, demonstrating that this peak is not a superposition of two due to gamma-rays of significantly different energy. Some lower energy line is present; the photoprotons below the main group are only partly explained as wall effect. We determined the shape of the electron noise spectrum several channels below the zero of Fig. 10; this enabled us to extrapolate the noise into the region of the spectrum displayed in Fig. 10. The best account of the observed pulse distribution was given by a second line at about 5.8 Mev, whose intensity was 0.07 in terms of that of the 8.1-Mev line. The combined effects of these two lines plus their wall effects, and the extrapolated electron noise are shown by the dotted line. It is seen that this gives a decent account of the experimental points

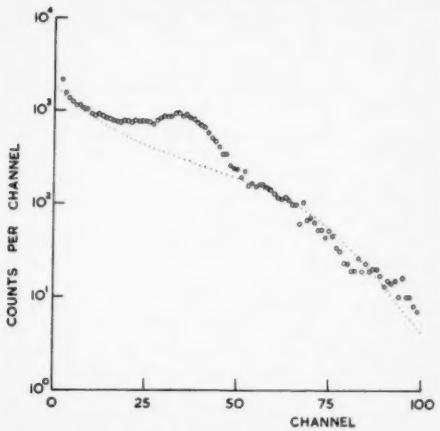

FIG. 9. Pulse distribution from protons of 1000 kev on a thin beryllium target. Zero of pulse distribution at channel minus 16.

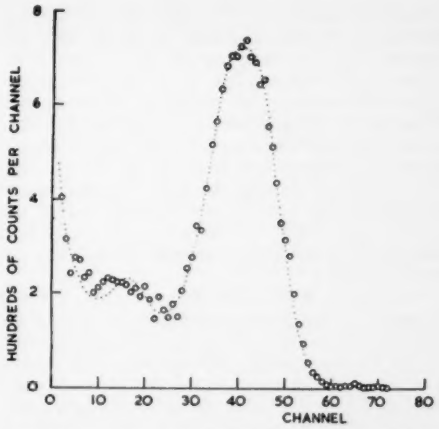

FIG. 10. Photoproton pulse distribution from protons of 570 kev on a "medium thin" target of C^{13}. Zero of pulse distribution at channel minus 20. Dotted curve "theoretical"—see text.

except, perhaps, for a few around channel 10. If a third line were present, its energy would be about 5.2 Mev, and its intensity about 0.015 of that of the 8.1-Mev line. This possibility is of little consequence for the absolute cross section.

There were four final runs; each contained about 3500 pulses and the relative yields of disintegrations per Geiger counter count were 1:0.98:0.98:1.01.

No correction was found necessary for angular distribution, and the absorption was calculated in the usual way.

The main peak we locate with an accuracy of ± 0.7 channels, the subsidiary peak to ± 2.5 channels and the calibrating fluorine peak to $\pm \frac{3}{4}$ percent. The gamma-ray energies are 8.14 ± 0.08 and 5.81 ± 0.25 Mev. From the mass values we expect, for the main line, 8.08 Mev. Lauritsen and Fowler[61] report 8.1 ± 0.2 Mev for this line. We have adopted 8.14 Mev.

It is possible that the lower energy line is the result of fluorine contamination; if this is so, the difference made to the final cross section is less than 1 percent.

Results and Errors at 8.14 Mev

We must again allow for the uncertainty in our knowledge of low energy components in the gamma-rays. The 13 percent strength of the triple cascade is not very accurate, and we have added ± 4 percent to our error on this account.

$$\sigma_{8.14} = (18.0 \pm 1.3) \times 10^{-28} \text{ cm}^2.$$

MEASUREMENTS AT 12.5 MEV

The radiative capture of protons by B^{11} provides gamma-rays of about 17 Mev by a transition to the ground state of C^{12}. More usually, a double transition

some using lithium, where the deposition of even a thick target of carbon would have been unimportant, has been carried out either at proton energies well below 450 kev or well above, where the deposit of a thin target of carbon would have no effect. Here we are constrained to work relatively close to the C^{13} resonance. The constancy in apparent position of the C^{13} resonance, and the internal consistency of the results show that if any carbon built up during the work, it did not have any effect.

[65] Fowler, Lauritsen, and Lauritsen, Revs. Modern Phys. **20**, 236 (1948).

is made via the state in C^{12} at 4.45 Mev, and it is the gamma-ray of about 12.5 Mev associated with this cascade which we have used in the present work. Unfortunately the reaction is not resonant around 1-Mev proton energy, so conditions are not so well defined as in the earlier work. With protons of 900 kev and a thick target, Fowler, Gaerttner, and Lauritsen[66] report single transitions and cascades in the ratio 0.15:1. Walker[55] gives for this ratio at proton energies of 510 kev and 1.2 Mev (thick target), 0.25:1 and 0.48:1, respectively. Rutherglen[67] suggests 0.19:1 at 700 kev. It is evident[55] that other cascades are not very frequent.

The reaction $B^{11}(p, \alpha)Be^8$ does not result, so far as is known, in any gamma-radiation as the bulk of the transitions go to the state at about 3 Mev in Be^8 which decays by alpha-particle emission. That only a small number of transitions go to the gamma-ray emitting state at 4.9 Mev in Be^8 is shown by the approximate equality which all workers find in the intensities of the 4.45-Mev and 12.5-Mev components. The first excited state in B^{11} is at 2.14 Mev, so inelastic proton scattering need not be considered. Another source of gamma-rays is the B^{10} contained in our natural boron target. There is little radiative capture; it has been observed by Walker[55] with a resonance at a proton energy of 1.16 Mev. The reaction $B^{10}(p, \alpha)Be^7$ is a source of gamma-rays of 0.43 Mev on account of the strong transition to the first excited state of Be^7. The correction was estimated for our experimental conditions by measuring the Geiger counter counting rate on bombarding a target of separated B^{10}; it was a little less than 10 percent.

A target of thickness about 200 kev was prepared by sedimentation of natural boron powder, and bombarded with protons of 950 kev. As with the thick beryllium target, there was no sign of a photoproton peak. The explanation is of the same type as before: the alpha-particles from $B^{11}(p, \alpha)Be^8$ act upon further boron nuclei, giving neutrons. The same remedy of using a very thin target could not be applied, for $B^{11}(p, \gamma)C^{12}$ is not resonant and the gamma-ray yield was low. Instead 15 cm of paraffin wax was placed between the target and the ionization chamber to scatter the neutrons. A pulse distribution, which revealed a high energy peak, was obtained; it is shown in Fig. 11. Some pulses below the peak are still caused by neutrons, but we know from the distribution without wax that if there is an appreciable number at channel 45 then there will be very few in the peak itself. We have no reliable subtraction recipe, and knowledge of the disintegration rate comes from the peak alone, which is due to the line at 12.5 Mev. The intensity of the line at about 17 Mev is low, and the pulses due to it would be almost all "wall-effect;" we should not then expect to see this line. An allowance for the contribution of the higher energy line to the peak must be made. Although the estimate of the disintegration rate due to 12.5-Mev gamma-rays varies with the assumed strength of the direct transition, the final answer for the cross section at 12.5 Mev does not vary much because, as we increase the percentage of the 17-Mev line and reduce the number of pulses in the peak to be ascribed to the 12.5-Mev line, so do we also reduce the gamma-ray flux associated with the 12.5-Mev line.

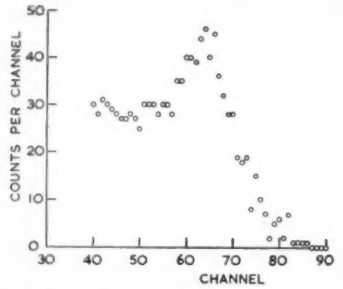

FIG. 11. Pulse distribution from the bombardment of boron with protons of 950 kev and 15 cm of paraffin wax interposed between source and ionization chamber. Zero of pulse distribution at channel minus 15.

[66] Fowler, Gaerttner, and Lauritsen, Phys. Rev. 53, 628 (1938).
[67] Private communication.

During the runs with wax the chamber was at a distance of 33 cm from the target and at 0° to the proton beam. The Geiger counter monitoring was carried out at 73 cm and 45°.

Six final runs were made, but the counts were so few in each that individual analysis was not profitable.

Combined allowance for angular distribution and gamma-ray absorption in the wax was made by comparing the counting rate of the Geiger counter in the monitoring position and at 0° (but at a distance of 2 meters, so that "good geometry" was achieved and the Compton scattered gamma-rays ignored).

The peak of Fig. 11 we locate to ± 1.5 channels, the fluorine calibration peak to $\pm\frac{3}{4}$ percent; the resulting gamma-ray energy is 12.50 ± 0.21 Mev. The energy expected for the direct transition from the mass tables at a proton energy of 900 kev is 16.75 Mev. The first excited state in C^{12} is at 4.46 Mev, and so the expected value of the energy for the first element of the cascade is 12.29 Mev. Other measurements are by Fowler, Gaerttner, and Lauritsen,[66] who obtained 11.8 ± 0.5 Mev from a thick target and protons of peak energy 0.9 Mev, and by Walker[55] who quotes 11.76 ± 0.18 Mev for protons of 0.51 Mev and 12.12 ± 0.12 Mev for protons of 1.15 Mev, both with thick targets. We have adopted 12.50 Mev.

Results and Errors at 12.5 Mev

This is a bad experiment. The errors introduced by our uncertainty of the constitution of the gamma-rays are small compared with the others. We have taken a probable error of ± 7 percent in the disintegration rate,

an additional ±3 percent on account of the absorption of the gamma-rays in the wax, and ±2 percent for the B^{10} correction. This gives a total error of ±10 percent

$$\sigma_{12.5}=(10.4\pm1.0)\times10^{-28}\ \text{cm}^2.$$

MEASUREMENTS AT 17.6 MEV

We have already discussed the gamma-rays emitted in the radiative capture of protons of 510 kev by Li^7. When they were used to irradiate the deuterium chamber, strong effects caused by fast neutrons were again in evidence. These neutrons arise from two sources. In the first the alpha-particles produced in the reaction $Li^7(p, \alpha)He^4$ act upon the lithium of the target; in the second the gamma-rays give (γ, n) reactions in the material of the laboratory and ionization chamber.

The second source was the stronger under our experimental conditions. (γ, p) reactions which could occur in the glass walls of the ionization chamber were considered, but may be neglected in our conditions. The high pressure hydrogen chamber was used to estimate the fast neutron background. The cross section for neutron collision, the energy transfer, and the angular distribution of recoil particles are all different for protons and deuterons. The use of the hydrogen chamber would therefore be unjustified but for a happy circumstance. We irradiated the two chambers identically with neutrons from a radium-beryllium source. These neutrons possess an extended neutron spectrum somewhat similar in range to that which must arise in (γ, n) reactions. The pulse distributions were measured and compared; when a suitable adjustment in scale had been made, they were indistinguishable over a considerable range at high energy.

The hydrogen chamber was then used to investigate the lithium "gamma-rays." The resulting distribution was treated according to the recipe derived from the neutron irradiations and subtracted from the distribution given by the deuterium chamber. Over the narrow range of subtraction recipes permitted by the data obtained with the radium-beryllium neutrons, the final subtracted photodisintegration distribution was almost unchanged. This fact lends confidence in the subtraction procedure, as does a comparison of the subtracted distribution with that calculated. The calculated distribution was smoothed and then "smeared" using the appropriate Gaussian distribution representing the amplifier and gamma-ray noise. As the wall effect was large a complete numerical integration was performed, taking into account the measured width of 2 Mev of the 14.8-Mev line as reported by Walker and McDaniel.[44] The result was, however, quite close to that given by the analytical formulas suitably modified to take account of inductive effects in the partial tracks. This modification is necessary at high gamma-ray energy where the tracks are very long and no longer confined to the region of the chamber near the wall where the inductive effects are small as they are for the lower energy gamma-rays. The calculated distribution is shown by the full line of Fig. 12. The experimental points have been grouped at intervals of three channels; the probable errors are purely statistical.

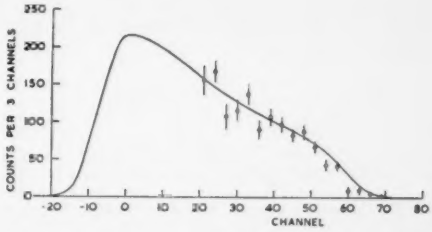

FIG. 12. Observed and calculated photoproton distributions for the gamma-rays from lithium. Zero of the distribution lies at channel minus 9.

The number of photodisintegrations was determined with a probable error which was estimated at ±10 percent by the extreme fittings of calculated and experimental distributions. There was no angular distribution correction.

Results and Errors at 17.6 Mev

The greatest error is the ±10 percent for the fitting of observed and calculated distributions. The other errors increase this to ±12 percent. The uncertainty in the composition of the gamma-rays is not very important; if the ratio of 14.8 to 17.6 Mev lines were as great as 0.8:1, the cross section would be lowered by only 4½ percent.

$$\sigma_{17.6}=(7.7\pm0.9)\times10^{-28}\ \text{cm}^2.$$

(Again we have corrected for the lower energy line using the form of dependence of cross section on energy given by Bethe and Peierls.[7])

MEASUREMENTS AT 4.45 MEV

When N^{15} is bombarded with protons of about 1 Mev, the reaction $N^{15}(p, \alpha)C^{12}$ takes place; it is similar to the reaction $F^{19}(p, \alpha)O^{16}$ in that at some resonances nearly all transitions leave the residual nucleus in an excited state.[68] We have used the resonance at a proton energy of 898 kev. The excited state in C^{12} is at about 4.5 Mev. It is believed that no excited states in C^{12} lie below 4.5 Mev;[15] neither are there accessible states above the one we use.

Radiative capture must be considered, it is reported[68] in a broad state around 1.0 Mev, giving gamma-rays of about 13 Mev. This transition is insignificant relative to the desired one at a proton energy of 900 kev which we used. We failed to find it with the high pressure chamber. There are no other competing reactions, and not even the ground-state alpha-particles can give the reaction $N^{15}(\alpha, n)F^{18}$. It was decided to measure

[68] Schardt, Fowler, and Lauritsen, Phys. Rev. **80**, 136 (1950).

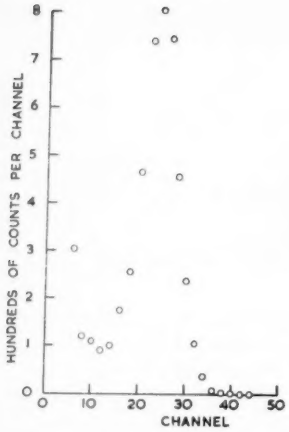

FIG. 13. Pulse distribution given by the proportional counter from protons of 890 kev on N^{15}. Zero of the distribution lies at channel minus 12.

the cross section at 4.45 Mev relative to that at 6.14 Mev.

The target was of N^{15} electromagnetically separated into molybdenum; it was effectively thin and on bombardment with protons of 890 kev it gave a just-adequate supply of the desired gamma-rays. The proportional counter was set up at 0° to the proton beam and 6.8 cm away from the target. The Geiger counter was at 19.6 cm and 115°. A typical pulse distribution is shown in Fig. 13. The ratio of width[69] at half-maximum to peak position is now 0.18 as against 0.28 for the pressure chamber; the value of this ratio expected from the ballistics of the reaction alone is 0.14. Similar results were obtained with fluorine irradiations at the 340-kev resonance which were interwoven with the N^{15} runs, and for which the proportional counter was set up in exactly the same position relative to the target. Four N^{15} runs were made, each containing about 1200 pulses. They bore relative yields per Geiger counter count of 1:1.05:1.02:1.05. The fluorine runs contained many more pulses. We believe that the relative yields of photoprotons have been determined to ± 2 percent in the statistics and ± 2 percent on account of the wall effects.

Another source of error was the large anisotropy which was found in the angular distribution of the gamma-rays; it could be roughly represented by $1+0.3\cos^2\theta$ though it rose more rapidly than this towards 0°. This necessitated a numerical integration over the volume of the proportional counter. We have increased the error by ± 2 percent on this account.

Two separate sets of N^{15} and F^{19} runs were compared to find the gamma-ray energy. In the first set the N^{15} peak was located to ± 0.1 channels (in 14), and the F^{19} peak to ± 0.15 channels (in 24), in the second set the errors were ± 0.2 channels (in 26) and ± 0.3 channels (in 45). The two sets agreed well and the resulting gamma-ray energy is 4.45 ± 0.04 Mev. This gamma-ray energy has been measured in the same reaction by Thomas and Lauritsen,[70] who find 4.465 ± 0.02 Mev. Estimates of the location of the level in C^{12} come from other sources. Schardt, Fowler, and Lauritsen[68] have measured the Q value of the short-range alpha-particle reaction as 0.529 ± 0.008 Mev; Strait *et al.*[14] have measured the Q-value of the ground-state transition as 4.960 ± 0.007; these measurements locate the state at 4.431 ± 0.011 Mev. Bradford and Bennett[71] locate the state at 4.45 Mev by a study of neutron groups from $Be^9(\alpha, n)C^{12}$; Pringle, Roulston, and Standil[72] report a gamma-ray of 4.40 ± 0.05 Mev, and Terrell[73] one of 4.45 ± 0.09 Mev from the same reaction. We have adopted 4.45 Mev.

Results and Errors at 4.45 Mev

All sources of error have been mentioned and we find

$$\sigma_{4.45}/\sigma_{6.14} = 1.11 \pm 0.06.$$

This result, combined with that quoted above for $\sigma_{6.14}$, gives

$$\sigma_{4.45} = (24.3 \pm 1.7) \times 10^{-28} \text{ cm}^2.$$

COLLECTED RESULTS

We gather together the gamma-ray sources, the value of the gamma-ray energy, and the total cross section. (See Table I.) The gamma-ray energy from fluorine is derived as explained previously, that from lithium is due to Walker and McDaniel,[44] and the rest are our own values based on the fluorine gamma-ray as standard. These results have already been published in preliminary form by Barnes, Stafford, and Wilkinson,[74] and by Carver and Wilkinson.[75] Few other measurements exist in this range of gamma-ray energy. They are summarized in Table II.[76–78]

ACKNOWLEDGMENTS

We would like to thank Dr. W. B. Lewis and the staff of the mass spectrometer group at the laboratory of the National Research Council of Canada, Chalk River, Ontario, for their analysis of the deuterium; Dr. C. Sykes, of Messrs. Firth-Brown, Sheffield, who supplied and heat-treated the steel from which the outer shells of the ionization chambers were made; Sir John Cockcroft and Dr. J. V. Dunworth, of the Atomic Energy Research Establishment, Harwell, for the graphite from which the graphite ionization chamber was made; Sir

[69] This width includes gas amplification and amplifier drifts over two hours.

[70] R. G. Thomas and T. Lauritsen, quoted in reference 15.
[71] C. E. Bradford and W. E. Bennett, Phys. Rev. **78**, 302 (1950).
[72] Pringle, Roulston, and Standil, Phys. Rev. **78**, 627 (1950).
[73] J. Terrell, Phys. Rev. **80**, 1076 (1950).
[74] Barnes, Stafford, and Wilkinson, Nature **165**, 69 (1950).
[75] J. H. Carver and D. H. Wilkinson, Nature **167**, 154 (1951).
[76] Phillips, Lawson, and Kruger, Phys. Rev. **80**, 326 (1950).
[77] P. V. C. Hough, Phys. Rev. **80**, 1069 (1950).
[78] H. Wäffler, Report to Chicago Conference (1951).

John Cockcroft and Dr. W. D. Allen for supplying us with the separated isotopes of many elements.

C. A. Barnes, J. H. Carver, and G. H. Stafford wish to thank respectively the Commissioners of the Exhibition of 1851 and the National Research Council of Canada; the Australian National University; the University of Cape Town and the South African C.S.I.R. for grants received in connection with this work.

APPENDIX I

Inductive Effects between Confocal Ellipsoids

Point ionizing events occur uniformly throughout the volume between two confocal ellipsoids; the outer ellipsoid, the cathode, has the form

$$\frac{x^2}{\lambda_0^2}+\frac{y^2+z^2}{\lambda_0^2-1}=1;$$

the inner ellipsoid, the anode, has the form

$$\frac{x^2}{\lambda_i^2}+\frac{y^2+z^2}{\lambda_i^2-1}=1 \quad 1<\lambda_i<\lambda_0.$$

The x axis is defined by the major axis of the anode. The result for the pulse distribution is most easily expressed in terms of $B(P)$, the probability that a pulse will exceed the relative size P. Neglecting the volume of the anode relative to that of the cathode,

$$B(P)=1-\frac{4XY^P(1+XY^P)}{(1-XY^P)^3}\cdot\frac{1}{(\lambda_0^2-1)\lambda_0},$$

where

$$X=\frac{\lambda_i^2-1}{(\lambda_i+1)^2} \quad Y=\frac{\lambda_0^2-1}{\lambda_i^2-1}\left\{\frac{\lambda_i+1}{\lambda_0+1}\right\}^2.$$

APPENDIX II

Ballistic Spread with Induction

Photodisintegration takes place uniformly between coaxial cylinders, the larger, the cathode, of radius b, the anode of radius a. Electric dipole transitions take place which, in the absence of induction, would yield a differential energy distribution

$$P(E)=1-(E-M)^2/K, \quad P\geqslant 0$$

(the normalizing factor is omitted). The proton energy is E; $M=\frac{1}{2}(h\nu-\epsilon)$; $h\nu$ is the energy of the gamma-ray and ϵ is the binding energy of the deuteron.

$$K=\frac{h^2\nu^2}{4mc^2}\left(h\nu-\epsilon-\frac{h^2\nu^2}{4mc^2}\right),$$

where m is the proton or neutron mass.

When induction is taken into account we obtain the distorted distribution

$$D(E)=\left[\overline{\mathrm{Ei}}(x)(A+B+C)-\frac{e^x}{x}\times\left(B+C\left(1+\frac{1}{x}\right)\right)\right]_{(E/E_{\max})\log(b^2/a^2)}^{(E/L)\log(b^2/a^2)}$$

(again the normalizing factor is omitted), where

$$\overline{\mathrm{Ei}}(x)=\int_{-\infty}^{x}e^z/z\,dz \quad \text{(tabulated by Jahnke and Emde[79])}$$

$$A=K-M^2, \quad B=2ME\log(b^2/a^2),$$
$$C=-\tfrac{1}{2}(E\log(b^2/a^2))^2, \quad E_{\max}=M+\sqrt{K}.$$

The limit L is $E_{\min}$, that is $M-\sqrt{K}$, for $E<E_{\min}$, and E for $E_{\min}\leqslant E\leqslant E_{\max}$.

TABLE I. Gamma-ray energies and deuteron photodisintegration cross sections.

Reaction	Gamma-ray energy (Mev)	Cross section ($\times 10^{28}$ cm^2)
$N^{15}(p,\alpha)C^{12}$[a]	4.45±0.04	24.3±1.7
$F^{19}(p,\alpha)O^{16}$[a]	6.14±0.01	21.9±1.0
$Be^9(p,\gamma)B^{10}$	7.39±0.15	18.4±1.5
$C^{13}(p,\gamma)N^{14}$	8.14±0.08	18.0±1.3
$B^{11}(p,\gamma)C^{12}$[a]	12.50±0.21	10.4±1.0
$Li^7(p,\gamma)Be^8$	17.6 ±0.2	7.7±0.9

TABLE II.

Workers	Gamma-ray energy (Mev)	Cross section ($\times 10^{28}$ cm^2)
Van Allen and Smith[a]	6.2	11.6±1.5
Phillips, Lawson, and Kruger[b]	6.14	26.9±3.8
Hough[c]	17.6	7.2±1.5
Wäffler[d]	17.6	7.1±2.0

[a] See reference 31. [b] See reference 76. [c] See reference 77. [d] See reference 78.

APPENDIX III

The Wall Effect in a Spherical Chamber

If infinitely long tracks originate at random throughout a sphere of radius r then, independent of their angular distribution relative to any specified direction, the probability $p(l)dl$ that any track should have a length l to $l+dl$ before striking the wall is given by

$$p(l)=(3/4r)[1-(l/2r)^2].$$

If the tracks have a maximum length of l_0, a fraction

$$\Phi_0=1-(3l_0/4r)(1-l_0^2/12r^2)$$

does not hit the wall. If we make the approximation that all the proton tracks have the same range, appropriate to the mean energy M, we distribute a fraction Φ_0 within the group whose form we have stated in Appendix II. The remainder is distributed according to the amount of their track which lies in the gas. No correction for positive ion induction effects need in general be made since these partial tracks lie near the wall where the induction is small. When Φ_0 becomes small, however, the induction effects play an appreci-

[79] E. Jahnke and F. Emde, *Tables of Functions* (Dover Publications, New York, 1945).

able rôle in modifying the shape of the distribution curve, and must be allowed for, as also must the real initial energy distribution of the protons. An approximation to the range-energy relation may be made in the form $R=cE^S$, R is the range of the particle. For hydrogen $S=1.77$ gives a good approximation in the energy range covered in this work.[80] If the probability is $\Phi(f)df$ that a proton spends a fraction f to $f+df$ of its energy in the chamber gas,

$$\Phi(f)=\tfrac{3}{4}S(M/E_r)^S(1-f)^{S-1}\times\{1-\tfrac{1}{4}(M/E_r)^{2S}[1-(1-f)^S]^2\},$$

where E_r is the energy of a proton whose range is equal to the radius of the chamber; this was 5.14 Mev.

APPENDIX IV

The Wall Effect in a Cylindrical Chamber

Gamma-rays are incident at right angles to the axis of an infinitely long cylinder of radius r and produce photodisintegrations by electric dipole transitions (the angular distribution is here of importance). The corrections because of the finite length of the counter are easily made and will not be discussed.

Let $f=l/2r$, where l is the residual track length in the chamber. We then seek $p(f)$, where $p(f)df$ is the probability that an infinitely long track should have a length f to $f+df$ contained within the cylinder.

$$p(f)=\frac{3}{\pi}\int_0^{\alpha_0}\sin^2\alpha(1+\cos^2\alpha)(1-f^2\sin^2\alpha)^{\frac{1}{2}}d\alpha$$

where

$$\alpha_0=\pi/2,\quad 0\leqslant f\leqslant 1$$
$$=\sin^{-1}(1/f),\quad 1<f.$$

This integral gives a solution in terms of closed elliptic integrals of the first and second kind (tabulated by Jahnke and Emde[79]). For $0\leqslant f\leqslant 1$

$$p(f)=\frac{3}{\pi f^2}\left\{K(f)\left[2(1-f^2)-\frac{3}{5f^2}(1+2f^2)(1-f^2)\right]-E(f)\left[2(1-2f^2)-\frac{1}{5f^2}(2+3f^2-8f^4)\right]\right\}.$$

For $1<f$, setting $g=1/f$,

$$p(f)=\frac{1}{5\pi g}\left\{K(g)(-12+13g^2-g^4)-E(g)(-12+7g^2-2g^4)\right\},$$

where

$$K(h)=\int_0^{\pi/2}\frac{d\theta}{(1-h^2\sin^2\theta)^{\frac{1}{2}}}$$

$$E(h)=\int_0^{\pi/2}(1-h^2\sin^2\theta)^{\frac{1}{2}}d\theta.$$

[80] H. A. Bethe, *Range-Energy Curves*, Brookhaven National Laboratory Report No. T-7 (1949).

For $f\ll 1$ asymptotic expressions for the elliptic integrals give expressions which are quite accurate throughout the range of f. The fraction of disintegrations which result in a track of length less than P is $P(f)$.

For $0\leqslant f\leqslant 1$

$$p(f)=\frac{1}{16}\left(15-\frac{21}{4}f^2-\frac{135}{128}f^4\right)$$

$$P(f)=\frac{f}{16}\left(15-\frac{7}{4}f^2-\frac{27}{128}f^4\right).$$

For $1<f$

$$p(f)=\frac{1}{40f^3}\left(15+\frac{75}{128}\cdot\frac{1}{f^4}\right)$$

$$P(f)=1-\frac{1}{80f^2}\left(15+\frac{75}{384}\cdot\frac{1}{f^4}\right).$$

At $f=1$ the expression valid for $f\ll 1$ and that valid for $f\gg 1$ differ by less than $\frac{1}{2}$ percent. To compute the energy distribution we have used the data of Bethe[80] for deuterium and of Hirschfelder and Magee[81] for argon.

APPENDIX V

The Alpha-Particle Bias-Curve Plus Noise

Owing to the finite size of the fast ionization chamber used to count the alpha-particles, there exist inductive effects which cannot be computed with accuracy, but which imply a pulse group more densely populated on the high energy side; this situation frequently obtains. We take the normalized group

$$\frac{k}{1-e^{-k}}e^{k(1-z)}\quad 0\leqslant z\leqslant 1,$$

where z is the pulse height in terms of the maximum. If the noise spectrum is Gaussian with variance σ^2, the probability of finding a pulse of height greater than z, is

$$B(z)=\frac{\exp(\frac{1}{2}k^2\sigma^2-k)}{2(1-e^{-k})}\left\{e^{kz}\left(\operatorname{erf}\left(\frac{1}{\sqrt{2}\sigma}z+\frac{k\sigma}{\sqrt{2}}\right)-\operatorname{erf}\left(\frac{1}{\sqrt{2}\sigma}(z-1)+\frac{k\sigma}{\sqrt{2}}\right)\right)+\exp(-\tfrac{1}{2}k^2\sigma^2+k)\operatorname{erf}\left(\frac{1}{\sqrt{2}\sigma}(z-1)\right)-\exp(-\tfrac{1}{2}k^2\sigma^2)\operatorname{erf}\left(\frac{z}{\sqrt{2}\sigma}\right)\right\},$$

where

$$\operatorname{erf}x=\frac{2}{(\pi)^{\frac{1}{2}}}\int_x^\infty\exp(-t^2)dt.$$

(It is tabulated by Jahnke and Emde.[79])

Appropriate values for our own work were $k\sim 10$, $\sigma\sim 0.1$.

[81] J. O. Hirschfelder and J. L. Magee, Phys. Rev. **73**, 207 (1948).

The Photodisintegration of the Deuteron at Intermediate Energies. II.

D. H. WILKINSON
Cavendish Laboratory, University of Cambridge, Cambridge, England
(Received December 14, 1951)

The measurements of Barnes, Carver, Stafford, and Wilkinson on the absolute cross section for photodisintegration of the deuteron in the range of gamma-ray energy from 4.45 to 17.6 Mev are analyzed. The cross sections for the electric dipole disintegration from the ^3S-state are obtained by subtracting small computed magnetic dipole and ^3D-state contributions. The electric dipole cross sections are analyzed from the point of view of both square well and Yukawa-type interactions and yield the following effective ranges (in units of 10^{-13} cm):

Effective range	Square well	Yukawa well
$\rho_t(-\epsilon, -\epsilon)$	1.73	1.79
$\rho_t(0, -\epsilon)$	1.75	1.70
$\rho_t(0, 0)$	1.77	1.62

The probable error in $\rho_t(-\epsilon, -\epsilon)$ is $\pm 0.09\times 10^{-13}$ cm. ^3P-state forces have been neglected. The meson mass associated with the Yukawa well is 291 ± 24 electron masses.

INTRODUCTION

THE preceding paper[1] described measurements of the absolute cross section for photodisintegration of the deuteron at six gamma-ray energies from 4.45 to 17.6 Mev. This paper discusses these measurements and analyzes them to yield the effective range of triplet neutron-proton interaction appropriate to the deuteron ground state.

THE ISOLATION OF THE ELECTRIC DIPOLE CROSS SECTION

The deuteron may be disintegrated by absorption of any order of multipole. We need here consider only dipole disintegration as, even at 17.6 Mev, the combined electric and magnetic quadrupole cross sections are less than ½ percent of the dipole cross section.[2,3] The electric dipole cross section σ_e and the magnetic dipole cross section σ_m combine to give the total cross section $\sigma_t=\sigma_e+\sigma_m$. We wish to find σ_e and so have chosen a range of gamma-ray energy where σ_m is never more than 4.3 percent of σ_m; although the theory of σ_m[4–7] is not yet free from objection, it is good enough to make this correction with adequate accuracy. We have tied σ_m to the neutron-proton capture cross section, and have assumed that the percentage contribution to the matrix element from meson interaction effects is independent of gamma-ray energy. We have used the neutron-proton capture cross section derived from the results of Whitehouse and Graham[8] and the cross section of boron for slow neutrons.[9]

Table I shows the calculated σ_m together with σ_t taken from I and the resulting σ_e. σ_m/σ_e shows the importance of the correction. As σ_m/σ_e is small and probably correct to 20 percent as a pessimistic estimate, we have applied the experimental error in σ_t to σ_e. The percentage probable error in σ_e is given in the last column. The gamma-ray energy is in Mev and the cross sections are in units of 10^{-28} cm^2.

Confidence that this calculation of σ_m is good enough derives from the experimental work of Hough[10] who finds, at 6.14 Mev, $\sigma_m/\sigma_e=0.03(+0.06, -0.03)$.

DISCUSSION

The calculation of the electric dipole cross section for forces of zero range, σ_{e0}, was made by Bethe and Peierls[11] who find

$$\sigma_{e0}=\frac{8\pi}{3}\frac{e^2}{\hbar c}\frac{\hbar^2}{m}\frac{\epsilon^{\frac{1}{2}}(h\nu-\epsilon)^{\frac{3}{2}}}{(h\nu)^3}, \quad (1)$$

where m is the nucleon mass, ϵ the binding energy of the deuteron, and $h\nu$ the photon energy.[12] We use $\epsilon=(2.227\pm 0.003)$ Mev,[13–16] then

$$\sigma_{e0}=11.39\times w^{3/2}(w+1)^{-3}\times 10^{-27}\text{ cm}^2.$$

$w=(h\nu/\epsilon)-1$. The error (± 0.1 percent)[17] in the constant is determined almost entirely by that in ϵ. This calculation assumes that the outgoing particles are free.

When forces of finite range are introduced Eq. (1)

[1] Barnes, Carver, Stafford, and Wilkinson, preceding paper [Phys. Rev. **85**, 359 (1952)], referred to as I.
[2] L. I. Schiff, Phys. Rev. **78**, 733 (1950).
[3] J. F. Marshall and E. Guth, Phys. Rev. **78**, 738 (1950).
[4] H. A. Bethe and C. Longmire, Phys. Rev. **77**, 647 (1950).
[5] E. E. Salpeter, Phys. Rev. **82**, 60 (1951).
[6] N. Austern and R. G. Sachs, Phys. Rev. **81**, 710 (1951).
[7] N. Austern, unpublished paper.
[8] W. J. Whitehouse and G. A. R. Graham, Can. J. Research **A25**, 261 (1947).
[9] Summarized by R. K. Adair, Revs. Modern Phys. **22**, 249 (1950).
[10] P. V. C. Hough, Phys. Rev. **80**, 1069 (1950).
[11] H. A. Bethe and R. E. Peierls, Proc. Roy. Soc. (London) **A148**, 146 (1935).
[12] We should use the energy of the gamma-ray in center-of-gravity space; this correction is about 10 kev at $E_\gamma=6$ Mev.
[13] R. E. Bell and L. G. Elliott, Phys. Rev. **79**, 282 (1950).
[14] R. C. Mobley and R. A. Laubenstein, Phys. Rev. **80**, 309 (1950).
[15] Taschek, Argo, Hemmendinger, and Jarvis, Phys. Rev. **76**, 325 (1949).
[16] T. R. Roberts and A. O. Nier, Phys. Rev. **77**, 746 (1950).
[17] Throughout this paper $\pm$ means probable error.

must be modified in several ways. For the moment we assume that the ground state of the deuteron is entirely a ^3S-state. The radial wave function multiplied by r has the asymptotic form (unnormalized)

$$\psi_g = e^{-\gamma r},$$

where

$$\gamma = \frac{1}{\hbar}(\epsilon m)^{\frac{1}{2}} = 0.2318 \times 10^{13}\ \text{cm}^{-1}.$$

The corresponding wave function for the outgoing ^3P-wave behaves as r^2 for small r; this leads to the well-known result that the matrix element for the transition is not strongly dependent on the behavior of the true ground-state wave function near the origin and that the asymptotic form may be used with fair accuracy. The matrix element computed using the asymptotic wave function must be multiplied by a factor F, close to unity, to take this approximation into account.

We must arrange that u_g, the true, unnormalized ground-state wave function, and ψ_g are asymptotic, but we must normalize the ground-state wave function on u_g. This leads immediately[4,5] to the result that σ_{e0} should be increased by a factor

$$\left(1 - 2\gamma \int_0^\infty (\psi_g^2 - u_g^2)dr\right)^{-1}$$

$$2\int_0^\infty (\psi_g^2 - u_g^2)dr = \rho_t'$$

is the effective range of neutron-proton triplet interaction appropriate to the deuteron ground state,[18,19] $\rho_t(-\epsilon, -\epsilon)$ in the notation of Bethe.[19] So

$$\sigma_e = \sigma_{e0}(1 - \gamma\rho_t')^{-1}F^2. \tag{2}$$

Equation (2) is accurate under three assumptions: (1) the ground state of the deuteron is a pure S-state; (2) the outgoing particles are free; (3) there are no specifically mesonic effects.

These assumptions must be considered separately.

(1) The deuteron ground state contains about 4 percent ^3D-state to account for the quadrupole moment of the deuteron. This diminishes the population of the ^3S-state and lowers the cross section; on the other hand, disintegrations can take place from the ^3D-state in compensation. It may be shown, as has been remarked by Austern[7] and others, that, if we neglect the disintegrations from the ^3D-state, then Eq. (2) remains correct. ρ_t must be re-interpreted, but is the same as that determined from neutron-proton scattering, which is modified in exactly the same way by the presence of the noncentral forces that generate the ^3D-wave. If, then, we are able to calculate the effect of transitions from the ^3D-state and subtract them out, we may still compare the effective range as determined from deuteron photodisintegration with that determined by neutron-proton scattering despite the existence of noncentral forces.[20] The importance of ^3D–^3P-transitions has been estimated by Austern[7] and amounts to a few tenths of a percent. The numerical correction is given later.

(2) The phenomena of high energy neutron-proton scattering imply that the strength of the P-state forces is not more than about 10 percent of that of the S-state forces, so the assumption of free outgoing particles is a good one. Detailed calculations at 6.14 Mev[21] suggest that the 10 percent limit corresponds to an uncertainty of 0.6 percent in the cross section. At 17.6 Mev[7] the uncertainty is about $1\frac{1}{2}$ percent, unless the noncentral forces have a very strong exchange character.[22] We have taken P-state forces to be zero.

(3) It has long been known[23] that there are no specifically mesonic effects in the electric dipole disintegration provided the Hamiltonian of the interaction between the gamma-ray and the deuteron is assumed to contain nucleon co-ordinates only.[24] The validity of this assumption has never been directly investigated, but it is expected to be good for the energies used in this investigation where the chief contribution to the matrix element comes from large nucleon separations.

TABLE I. Total, magnetic dipole, and electric dipole cross sections for photodisintegration of the deuteron, as functions of γ-ray energy.

E_γ	σ_t	σ_m	σ_e	σ_m/σ_e	±%
4.45	24.3	1.01	23.3	0.043	7.3
6.14	21.9	0.59	21.3	0.028	4.7
7.39	18.4	0.44	18.0	0.024	8.3
8.14	18.0	0.39	17.6	0.022	7.5
12.5	10.4	0.22	10.2	0.022	9.8
17.6	7.7	0.14	7.6	0.018	12

THE EFFECTIVE RANGE

Before evaluating the effective range from Eq. (2) we must know F. F depends on the shape of the interaction potential, and we have chosen to analyze the results in terms of extreme short- and long-tailed wells, namely, the square well and Yukawa well. For the square well F remains within 1 percent of unity throughout the range of gamma-ray energy used; we have set it equal to unity. For the Yukawa well F has been estimated through the approximation of Hulthén to the

[18] J. M. Blatt and J. D. Jackson, Phys. Rev. **76**, 18 (1949).
[19] H. A. Bethe, Phys. Rev. **76**, 38 (1949).

[20] There remains the question of the effect of noncentral forces on the energy dependence of the effective range; in the absence of detailed information we must assume that this dependence is unchanged.
[21] I. F. E. Hansson and L. Hulthén, Phys. Rev. **76**, 1163 (1949).
[22] Both these corrections refer to an interaction potential of Yukawa form.
[23] A. J. F. Siegert, Phys. Rev. **52**, 787 (1937).
[24] R. G. Sachs and N. Austern, Phys. Rev. **81**, 705 (1951).

Yukawa potential.[2,3,25] Then

$$F=1-\left(\frac{\gamma^2+k^2}{\beta^2+k^2}\right)^2, \qquad (3)$$

$$k^2=\frac{1}{\hbar^2}m(h\nu-\epsilon),$$

and β is the second constant of the Hulthén potential, chosen to give the correct effective range; we find $\beta=1.35\times10^{13}$ cm^{-1}. Although the Hulthén potential is a good stand-in for the Yukawa potential at high energies, we must expect some disagreement at the energies of these experiments. The only directly-computed value of F^2 for the Yukawa potential is at 6.14 Mev where its value is 0.984.[26] Equation (3) suggests 0.988. We have used F as given by Eq. (3) in the first instance. Table II shows the various quantities of interest. σ_D is the computed cross section for disintegration from the D-state; $\sigma_S=\sigma_\epsilon-\sigma_D$ is the deduced cross section from the S-state only. ρ_{tS}' and ρ_{tY}' are the effective ranges appropriate to square and Yukawa (Hulthén) wells, respectively. $\pm$ is the probable error in ρ_t'.[27]

The units of ρ are 10^{-13} cm, the rest as in Table I. ρ_t' is a good constant[28] over the range of E_γ; this establishes the first objective of this investigation (see I) namely that the form of dependence of σ_ϵ on E_γ is correctly given by quantum mechanics.[29] We cannot distinguish between well shapes on the basis of the constancy of ρ. The probable error in ρ we take to be ±0.09; it is largely governed by uncertainties common to all the cross sections. The weighted means are

$$\rho_{tS}'=1.73\times10^{-13}\text{ cm}.$$
$$\rho_{tY}'=1.78\times10^{-13}\text{ cm}.$$

The direct computation of F^2 at 6.14 Mev suggests that, in the lower energy region of our range where the most accurate experiments lie, the approximation for F^2 based on the Hulthén potential is too high by about 0.4 percent and that ρ should be accordingly increased by about 0.6 percent. We prefer the result deriving from the more physically-plausible Yukawa potential[30] and quote:

$$\rho_t(-\epsilon,-\epsilon)=(1.79\pm0.09)\times10^{-13}\text{ cm}.$$

The determination of this quantity was the second objective of this investigation.

TABLE II. Photodisintegration cross sections and effective ranges (for square well and Yukawa well), as functions of γ-ray energy.

E_γ	σ_ϵ	σ_D	σ_S	$\sigma_{\epsilon 0}$	F^2	ρ_{tS}'	ρ_{tY}'	$\pm$
4.45	23.3	0.10	23.2	14.23	0.994	1.67	1.69	0.18
6.14	21.3	0.13	21.2	12.65	0.988	1.74	1.77	0.12
7.39	18.0	0.14	17.9	11.00	0.982	1.67	1.72	0.21
8.14	17.6	0.14	17.5	10.09	0.980	1.83	1.88	0.18
12.5	10.2	0.14	10.1	6.37	0.958	1.59	1.69	0.24
17.6	7.6	0.14	7.5	4.18	0.925	1.89	2.06	0.35

COMPARISON WITH OTHER RESULTS ON THE EFFECTIVE RANGE

Photodisintegration is the most direct method for the determination of the triplet neutron-proton effective range. The only other measurements available are of $\rho_t(0,-\epsilon)$ and of these the most accurate is due to Hughes[31] who measures the hydrogen coherent scattering amplitude and combines it with the free proton cross section for slow neutrons[32] to find $\rho_t(0,-\epsilon)=(1.70\pm0.03)\times10^{-13}$ cm. Earlier measurements[33,34] gave a rather lower value of ρ_t with a considerably larger probable error.

In order to compare our results for $\rho_t(-\epsilon,-\epsilon)$ with this value of $\rho_t(0,-\epsilon)$ we must correct them for the energy dependence of ρ. This may be done using the data of Blatt and Jackson;[18] the shape-dependent parameter P of these authors is -0.04 and $+0.14$ for square and Yukawa wells, respectively; this leads to $\rho_t(0,-\epsilon)=1.75$ and $1.72_5\times10^{-13}$ cm for the two wells, respectively. It appears, however, that the linear dependence of ρ on energy as prescribed by effective range theory is not an accurate approximation, at least for the Yukawa potential. Hulthén and Nagel[26] have computed the energy dependence of ρ for the Yukawa potential and a better estimate of $\rho_t(0,-\epsilon)$ and $\rho_t(0,0)$ comes from their work. Table III shows the three effective ranges of chief interest. The two $\rho_t(-\epsilon,-\epsilon)$ are our own experimental values for the two wells; the others are derived from them for the square well by effective range theory[18] and for the Yukawa from the computations of Hulthén and Nagel.

The agreement between $\rho_t(0,-\epsilon)$ deduced from photodisintegration and that measured by Hughes and previously quoted is satisfactory. We can make no

[25] J. S. Levinger, Phys. Rev. **76**, 699 (1949).
[26] Bengt Nagel, private communication.
[27] The quantity which is determined experimentally is the range factor $R=(1-\gamma\rho)^{-1}$; $d\rho/\rho=(R-1)^{-1}dR/R$. $R\sim1.7$, so the percentage error in ρ is about 1.5 times that displayed in Table I for σ_ϵ.
[28] It might appear that ρ is too good a constant in view of the stated probable errors. These errors are in the absolute values of ρ; constancy of ρ is a matter for the relative cross sections which are considerably better known than the absolute ones, as some principal errors in σ_ϵ are common to all gamma-ray energies.
[29] E. G. Fuller [Phys. Rev. **79**, 303 (1950)] has investigated the relative variation of σ with E_γ over a range closely corresponding to ours. He finds a rather slower fall of σ with E_γ than given by quantum mechanics; this may be due to his use of a calculated betatron spectrum.
[30] The results of other long-tailed potentials such as the exponential are very close to this.
[31] Ringo, Burgy, and Hughes, Phys. Rev. **82**, 344 (1951).
[32] E. Melkonian, Phys. Rev. **76**, 1744 (1949).
[33] Sutton, Hall, Anderson, Bridge, de Wire, Lavatelli, Long, Snyder, and Williams, Phys. Rev. **72**, 1147 (1947).
[34] Shull, Wollan, Morton, and Davidson, Phys. Rev. **73**, 842 (1948).

TABLE III. The three effective ranges of chief interest.

Effective range	Square well	Yukawa well
$\rho_t(-\epsilon, -\epsilon)$	1.73	1.79
$\rho_t(0, -\epsilon)$	1.75	1.70
$\rho_t(0, 0)$	1.77	1.62

distinction between well shapes on the basis of this comparison. The achieving of this agreement constitutes the third objective of this investigation.

MESON MASS

It is tempting to inquire what meson mass m_π is implied if we accept the Yukawa potential. We may use our value of $\rho_t(0, 0)$ to compute an intrinsic range from which the meson mass is obtained immediately. This gives $m_\pi = (291 \pm 24) m_e$ where m_e is the electron mass. It is improper to regard the accord between these figures and the experimental π-meson mass[35] of (276.1 ± 2.3) as other than fortuitous.

CONCLUSION

The electric dipole component of the photodisintegration of the deuteron seems to be adequately represented by current quantum-mechanical theory up to gamma-ray energies of 10–20 Mev. No information about the shape of the interaction potential is forthcoming from this investigation.

ACKNOWLEDGMENTS

I am very much indebted to Professor L. Hulthén and Mr. Bengt Nagel for acquainting me with the results of their calculations and for much helpful comment.

I would like to thank Dr. Norman Austern, Dr. E. E. Salpeter, and Professor E. Guth for allowing me to see their papers prior to publication.

[35] Birnbaum, Smith, and Barkas, Phys. Rev. **83**, 895 (1951).

The Scattering of Neutrons by Systems of Heavy Nuclei*†

G. PLACZEK
Institute for Advanced Study, Princeton, New Jersey
(Received December 20, 1951)

It is shown that the scattering of neutrons by a system of heavy nuclei may, for neutron energies that are large compared with the level separation of the system, be described in terms of averages of simple two-particle operators over the initial state. Expressions are derived for the total and differential cross sections and for the first few moments of the energy transfer. The expression for the cross section can be explicitly evaluated even for complicated scattering systems and leads to an accurate representation of the energy dependence of the nuclear scattering. The results are applied to the problem of the detection of small electronic contributions to the cross section.

1. INTRODUCTION

WE consider the collision of a neutron of mass m, energy E_0, wave vector $\mathbf{k}_0$, and wave number k_0 with a system of N nuclei—such as a molecule, a gas, a liquid, or a crystal—in the state "a" of energy E_a. The standard Born approximation[1] leads to the scattering cross section,

$$\sigma^{(a)}=\frac{2}{k_0}\sum_b\int|(F(\boldsymbol{\kappa}))_a{}^b|^2\delta\left\{\kappa^2-2\mathbf{k}_0\cdot\boldsymbol{\kappa}+\frac{2m}{\hbar^2}(E_b-E_a)\right\}d\boldsymbol{\kappa}. \quad (1.1)$$

The summation extends over all states of the nuclear system, and the integration variable $\boldsymbol{\kappa}$ is the momentum transferred to the system, divided by $\hbar$. The delta-function expresses conservation of energy and the scattering amplitude $F(\boldsymbol{\kappa})$ is given by

$$F(\boldsymbol{\kappa})=\sum_{s=1}^{N}a_s\exp(i\boldsymbol{\kappa}\cdot\mathbf{r}_s). \quad (1.2)$$

Here $\mathbf{r}_s$ is the position vector of nucleus s and a_s its scattering length.

The scattering lengths will be taken to be independent of E_0 and $\boldsymbol{\kappa}$ in the energy region considered, they may, however, depend on the nuclear spin variables. For nuclei without spin the scattering length a_s is simply related to the scattering cross section σ_s of the bound nucleus by

$$\sigma_s=4\pi a_s^2, \quad (1.3)$$

and the matrix element of the scattering amplitude may here be written

$$F_a{}^b=\int\psi_b^*(\mathbf{r}_1,\cdots\mathbf{r}_N)F\psi_a(\mathbf{r}_1,\cdots\mathbf{r}_N)d\mathbf{r}_1\cdots d\mathbf{r}_N, \quad (1.4)$$

where the ψ's are the eigenfunctions of the Hamiltonian H of the motion of the nuclei in the field of the interatomic forces.

For nuclei with spin, (1.3) and (1.4) have to be modified which will be taken care of in Sec. 7.

The straightforward evaluation of (1.1) requires detailed knowledge of the eigenfunctions of all accessible states. It is therefore possible for the very simplest cases only, and even there it becomes progressively more laborious with increasing neutron energy. In the following it will be shown, however, that for systems of heavy nuclei the cross section may be expressed in terms of averages of simple operators over the initial state as soon as the neutron energy is large compared to the level separation of the system.

2. GENERAL CONSIDERATIONS

In the limit of infinite neutron energy, (1.1) goes over into[2]

$$\sigma_\infty{}^{(a)}=\sum_s\left(1+\frac{m}{M_s}\right)^{-2}\sigma_s, \quad (2.1)$$

where M_s is the mass of nucleus s. We shall have to determine, in particular, the behavior of the cross section on the approach to this limit. While certain general statements in regard to this problem may be made on the basis of the classical particle picture,[3] their application to the case of heavy nuclei would appear to be of limited practical use without a closer investigation. This may be seen as follows. In classical mechanics the collision—in our case of contact interaction—takes place instantaneously and the energy dependence of the cross section is determined by the momentum distribution of the scattering particles. The cross section of a system under the influence of forces will thus be equal to that of a free system with the same momentum distribution. A necessary condition for the description of the collision in classical particle terms requires that the collision time h/E_t, where E_t is the classical energy transfer, be short compared to the periods of the

* The results of this paper were presented at the International Conference on Nuclear Physics, Basel, September, 1949.

† Work partially supported by the AEC and ONR.

[1] For the justification of the use of the Born approximation in the treatment of this problem see E. Fermi, Ricerca sci. **7**, 13 (1936); G. Breit, Phys. Rev. **71**, 215 (1947).

[2] E. Fermi, Ricerca sci. **7**, 13 (1936).

[3] G. Placzek, Phys. Rev. **75**, 1295 (1949); and as quoted in reference 7.

system. Accordingly, the energy transfer $(m/M)E_0$ has to be large compared to the level separation of the system, and thus

$$E_0 \gg (M/m)\Delta, \tag{2.2}$$

where Δ is the level separation. Indeed, one can see immediately that unless condition (2.2) is satisfied the energy distribution of the scattered neutrons must differ appreciably from the classical energy distribution.

For heavy nuclei (2.2) becomes extremely restrictive and we shall therefore attempt to study the collision under the much less restrictive condition,

$$E_0 \gg \Delta. \tag{2.3}$$

For this purpose we start from the static approximation which results from neglecting the energy changes associated with the transition of the system. It is obtained by omitting the last term in the delta-function in (1.1). The summation over b can then be carried out immediately by closure so that (1.1) goes over into

$$\sigma^{(a)} = \frac{2}{k_0}\int (F^*(\boldsymbol{\kappa})F(\boldsymbol{\kappa}))_a{}^a \delta(\kappa^2 - 2\mathbf{k}_0\cdot\boldsymbol{\kappa})d\boldsymbol{\kappa}$$

$$= \int (|F(\mathbf{k}_0 - k_0\boldsymbol{\Omega})|^2)_a{}^a d\Omega, \tag{2.4}$$

where $\boldsymbol{\Omega}$ is a unit vector. Equation (2.4) represents the average of the cross section of a system, consisting of nuclei fixed in definite positions, over the configurations of the initial state of the real system. It may thus be referred to as the static approximation. This approximation forms the basis of the theory of x-ray scattering by molecules, crystals, and liquids.[4]

The cross section (2.4) has to be well distinguished from the elastic cross section (or more precisely, the cross section for scattering without change of quantum state) which from (1.1) is given by

$$\sigma_{el}{}^{(a)} = (2/k_0)\int |(F(\boldsymbol{\kappa}))_a{}^a|^2 \delta(\kappa^2 - 2\mathbf{k}_0\cdot\boldsymbol{\kappa})d\boldsymbol{\kappa}$$

$$= \int |(F(\mathbf{k}_0 - k_0\boldsymbol{\Omega}))_a{}^a|^2 d\Omega. \tag{2.5}$$

In the literature the cross section is frequently divided into an elastic and inelastic part and the energy dependence of each part is discussed separately. It is clear from (2.4) that in the static approximation this separation is an unnecessary complication which has to be avoided as far as possible. This situation will be shown later to hold also in higher approximations.

For systems consisting of one nucleus only, the static approximation leads to a constant cross section. Since here $|F|^2 = a_s^2$, we have from (2.4)

$$\sigma^{(a)} = \sigma_s. \tag{2.4a}$$

For systems consisting of several nuclei the evaluation of (2.4) involves the probability distribution of internuclear distances in the initial state (pair density). In the limit of infinite neutron energy the cross section (2.4) reduces here to

$$\sigma_\infty{}^{(a)} = \sum_s \sigma_s, \tag{2.6}$$

which differs from the correct result (2.1) by the absence of the reduced mass factors.

It will now be our problem to establish the exact conditions of validity of the static approximation which neglects the energy changes and to improve it by taking account of the energy changes. We shall limit ourselves to systems of random orientation. This will contribute to brevity and the generalization of the results to oriented systems such as single crystals will become quite obvious in the course of the treatment.

For systems of random orientation we may average the delta-function in (1.1) over all directions of $\mathbf{k}_0$, whereby (1.1) goes over into

$$\sigma^{(a)} = \frac{1}{2k_0^2}\sum_b{}^{E_b < E_0 + E_a} \int_{a,b} |F_a{}^b(\boldsymbol{\kappa})|^2 \frac{d\boldsymbol{\kappa}}{\kappa}, \tag{2.7}$$

where the subscript a, b under the integral sign indicates that the integration extends over a region in $\boldsymbol{\kappa}$-space bounded by the spheres of radius $k_0 + k_{ab}$ and $|k_0 - k_{ab}|$ with

$$k_{ab}{}^2 = 2mh^{-2}(E_0 + E_a - E_b). \tag{2.8}$$

Introducing the average $\phi_{ab}(\kappa^2)$ of the square of the matrix element over all directions of $\boldsymbol{\kappa}$

$$\phi_{ab}(\kappa^2) = (1/4\pi)\int |F_a{}^b(\boldsymbol{\kappa})|^2 d\Omega_\kappa \tag{2.9}$$

and putting

$$(E_b - E_a)/E_0 = x_{ab}, \tag{2.10}$$

we may write (2.7)

$$\sigma^{(a)} = \frac{\pi}{k_0{}^2}\sum_b{}^{x_{ab}<1} \int_{k_0{}^2[1-(1-x_{ab})^{\frac{1}{2}}]^2}^{k_0{}^2[1+(1-x_{ab})^{\frac{1}{2}}]^2} \phi_{ab}(\kappa^2)d\kappa^2. \tag{2.11}$$

If in this expression the quantities x_{ab} are neglected throughout, which implies also the replacement of the restricted sum over b by an unrestricted one, it goes over into

$$\sigma^{(a)} = \frac{\pi}{k_0{}^2}\int_0^{4k_0{}^2} (\sum_b \phi_{ab}(\kappa^2))d\kappa^2$$

$$= \frac{1}{4k_0{}^2}\int_0^{4k_0{}^2} d\kappa^2 \int_0 (|F(\boldsymbol{\kappa})|^2)_a{}^a d\Omega_\kappa, \tag{2.12}$$

[4] See the review article by M. Born in Reports of Progress of Physics **9**, 294 (1943).

which is the result of the static approximation (2.7), averaged over all directions of $\mathbf{k}_0$.

The expression (2.11) has a form suitable for taking the energy exchanges into account. For heavy nuclei, owing to the difficulty of large energy transfers between light and heavy particles, the quantities x_{ab} will be small for all transitions with appreciable matrix element, provided the neutron energy is large compared to the level spacing and the neutron velocity large compared to the average nuclear velocities. If these conditions—the latter of which only implies a very weak limitation on the admissible degree of initial excitation of the system—are satisfied, we may therefore expand the integrals in (2.11) in powers of x_{ab} and replace the restricted sum by an unrestricted one. This method will be carried out in the following sections. With appropriate changes it is also applicable to the treatment of other problems. For the scattering of x-rays by atoms, in particular, it leads to certain modifications of hitherto accepted results.[5]

3. AN EXPRESSION FOR THE CROSS SECTION IN TERMS OF AVERAGES OVER THE INITIAL STATE

With the notations $u=4k^2$, $t=\kappa^2$, (2.11) may be written

$$\sigma^{(a)}=\sum_b \sigma_{ab} \tag{3.1}$$

$$\sigma_{ab}=(\sigma_{ab})_+-(\sigma_{ab})_- \tag{3.2}$$

$$(\sigma_{ab})_\pm=\frac{4\pi}{u}\int_0^{t_\pm}\phi_{ab}(t)dt \tag{3.3}$$

$$t_\pm=(u/4)\{1\pm(1-x_{ab})^{\frac{1}{2}}\}^2.$$

The expansion of $(\sigma_{ab})_+$ in powers of x_{ab} is obtained by expanding the integral in powers of $u-t_+$ and expressing this quantity by its expansion in powers of x_{ab}

$$u-t_+=\frac{ux_{ab}}{2}\left\{1+\frac{x_{ab}}{8}+\frac{x_{ab}^2}{16}+\frac{5}{128}x_{ab}^3+\cdots\right\}. \tag{3.4}$$

This yields[6]

$$\frac{(\sigma_{ab})_+}{4\pi}=\frac{1}{u}\int_0^u\phi(t)dt-\frac{x}{2}\phi(u)+\frac{x^2}{16}\{-\phi(u)+2u\phi'(u)\}$$
$$+\frac{x^3}{32}\{-\phi(u)+u\phi'(u)-\tfrac{2}{3}u^2\phi''(u)\}$$
$$+\frac{x^4}{512}\{-10\phi(u)+9u\phi'(u)$$
$$-4u^2\phi''(u)+(4/3)u^3\phi'''(u)\}. \tag{3.5}$$

To expand $(\sigma_{ab})_-$, we expand ϕ in powers of t, integrate and expand t_- in powers of x

$$t_-=\tfrac{1}{16}ux^2(1+\tfrac{1}{2}x+\cdots). \tag{3.6}$$

Noting that $\phi_{ab}(0)=0$ for $a\neq b$ and $x_{ab}=0$ for $a=b$, we obtain

$$\frac{(\sigma_{ab})_-}{4\pi}=\frac{x^4}{512}u\phi'(u)+O(x^5). \tag{3.7}$$

The lower limit of the integrals in (2.11) thus gives rise to a fourth-order correction only.

The quantities σ_{ab} have now to be summed over b. At the same time we may average the cross section over the initial states of the system. Putting

$$\sigma=\textstyle\sum_a \gamma_a\sigma^{(a)}, \tag{3.8}$$

where γ_a is the probability of finding the system in state "a" before the collision and introducing sums S_n by

$$S_n(t)=\textstyle\sum_a \gamma_a S_n^{(a)}(t) \tag{3.9}$$

$$S_n^{(a)}(t)=\sum_b^{E_b<E_a+E_a}(E_b-E_a)^n\phi_{ab}(t), \tag{3.10}$$

we obtain for the cross section from (3.1), (3.2), (3.5), (3.7)–(3.10)

$$\frac{\sigma}{4\pi}=\frac{1}{u}\int_0^u S_0(t)dt-\frac{1}{2E_0}S_1(u)+\frac{1}{16E_0^2}\{-S_2(u)+2uS_2'(u)\}$$
$$+\frac{1}{32E_0^3}\{-S_3(u)+uS_3'(u)-\tfrac{2}{3}u^2S_3''(u)\}$$
$$+\frac{1}{512E_0^4}\{-10S_4(u)+u(9S_4'(u)-S_4'(0))$$
$$-4u^2S_4''(u)+(4/3)u^3S_4'''(u)\}. \tag{3.11}$$

We now have to discuss the quantities S_n. With (2.9) we may write (3.10)

$$S_n^{(a)}(\kappa^2)$$
$$=\frac{1}{4\pi}\int d\Omega_\kappa\sum_b^{E_b<E_a+E_a}(E_b-E_a)^n|(F(\kappa))_{ab}|^2. \tag{3.12}$$

For freely orientable systems such as molecules, the averaging over the directions of κ is superfluous since the sum over b will here depend on the magnitude of κ only. For systems showing the type of random orientation present in polycrystals, however, this averaging process is necessary.

Expressing E_b-E_a as the diagonal element of the operator $H-E_a$

$$E_b-E_a=(H-E_a)_{bb}$$

[5] G. Placzek, Bull. Am. Phys. Soc. **27**, No. 1, 13 (1952).

[6] In order to save indices, we write in the following x for x_{ab} and ϕ for ϕ_{ab}.

and neglecting the limitation of the sum in (3.12), we obtain by closure

$$\sum_b (E_b-E_a)^n|F_a{}^b|^2=\sum_b (F^*)_b{}^a(\{H-E_a\}^n)_b{}^b F_a{}^b$$

$$=(F^*\{H-E_a\}^n F)_a{}^a. \tag{3.13}$$

From the argument given at the end of the preceding section it may be concluded that under the conditions stated there the error committed by closure will be quite negligible for heavy nuclei and small n. In Sec. VI this will also be shown in somewhat greater detail for a specific example. Combining (3.9), (3.12), and (3.13) we obtain finally

$$S_n(\kappa^2)=\langle F^*(\boldsymbol{\kappa})(H-E_a)^n F(\boldsymbol{\kappa})\rangle_{\Delta\nu}, \tag{3.14}$$

where the average is to be taken (1) over the configuration of state "a," (2) over the distribution of states "a" initially present in the system, and (3) if necessary, over the directions of $\boldsymbol{\kappa}$. The first two averaging processes can sometimes be combined in the customary way by the use of transformation theory.

With the help of the relation,

$$\langle (H-E_a)O\rangle_{\Delta\nu}=\langle O(H-E_a)\rangle_{\Delta\nu}=0,$$

where O is a time-independent operator, (3.14) may be expressed in various ways. A convenient form is

$$\begin{aligned} S_0&=(F^*F)_{\Delta\nu}\\ S_1&=(F^*[HF])_{\Delta\nu}\\ S_2&=([F^*H][HF])_{\Delta\nu}\\ S_3&=([F^*H][H[HF]])_{\Delta\nu}\\ S_4&=([H[HF^*]][H[HF]])_{\Delta\nu}, \end{aligned} \tag{3.15}$$

where $[AB]$ is the commutator of the operators A and B. The evaluation of (3.15) will be carried out in Secs. V and VII.

The quantities S_n admit a simple physical interpretation. If a momentum $\hbar\kappa$ is imparted to the system, the average energy transfer accompanying this momentum transfer is given by $S_1(\kappa^2)/S_0(\kappa^2)$ and the n-th moment of the energy transfer by $S_n(\kappa^2)/S_0(\kappa^2)$. This will be used later in connection with the comparison of classical and quantum-mechanical results. The moments so defined are of course different from the moments of the energy transfer occurring in an actual collision. The latter are given by

$$\langle E^l\rangle_{\Delta\nu}=\textstyle\sum_a \gamma_a \sum_b (E_b-E_a)^l\sigma_{ab}/\sigma \tag{3.16}$$

and may be expressed in terms of the quantities S_n and their derivatives by noting that the denominator of (3.16) is given by (3.11) while the numerator results from (3.11) by simply replacing S_n by S_{n+l}. The moments (3.16) which are thus, for small n, obtainable by our method, are also simply related to the moments of the energy distribution of the scattered neutrons, given by $\langle (E_0-E)^l\rangle_{\Delta\nu}$.

4. THE DIFFERENTIAL CROSS SECTION

The treatment of the preceding section can be extended to the differential cross section. The differential cross section associated with the transition $a\to b$ is given by

$$d\sigma_{ab}/d\Omega=(1-x_{ab})^{\frac{1}{2}}\phi_{ab}(\kappa_{ab}{}^2). \tag{4.1}$$

The factor $(1-x_{ab})^{\frac{1}{2}}$ represents the ratio of the velocities of scattered and incoming neutron and $\kappa_{ab}{}^2$ is determined by the relation,

$$\boldsymbol{\kappa}_{ab}=\mathbf{k}_0-k_0(1-x_{ab})^{\frac{1}{2}}\boldsymbol{\Omega}, \tag{4.2}$$

where $\boldsymbol{\Omega}$ is a unit vector in the direction of scattering.

For scattering without energy change (4.2) goes over into

$$\boldsymbol{\kappa}_0=\mathbf{k}_0-k_0\boldsymbol{\Omega}. \tag{4.3}$$

$\kappa_0{}^2$ is related to the cosine μ_0 of the scattering angle by

$$\mu_0=1-\kappa_0{}^2/2k_0{}^2.$$

From (4.2) and (4.3) we have

$$\kappa_{ab}{}^2=k_0{}^2(1-x)^{\frac{1}{2}}+k^2(1-(1-x)^{\frac{1}{2}})^2. \tag{4.4}$$

One now expands $\phi_{ab}(\kappa_{ab}{}^2)$ in powers of $\kappa_{ab}{}^2-\kappa_0{}^2$ and substitutes

$$\kappa_0{}^2-\kappa_{ab}{}^2=\tfrac{1}{2}\kappa_0{}^2x_{ab}$$
$$+\tfrac{1}{4}(\tfrac{1}{2}\kappa_0{}^2-k^2)x_{ab}{}^2(1+\tfrac{1}{2}x_{ab}+\tfrac{5}{16}x_{ab}{}^2+\cdots).$$

Inserting the resulting expansion for ϕ as well as the expansion of $(1-x_{ab})^{\frac{1}{2}}$ into (4.1), one obtains, after summation over b and averaging over a, the following result, where again $u=4k_0{}^2$, the scattering angle is measured by

$$l=\kappa_0{}^2=\tfrac{1}{2}u(1-\mu_0)=u\sin^2(\theta/2) \tag{4.5}$$

and S_n stands for $S_n(l)$

$$\begin{aligned} \frac{d\sigma}{d\Omega}=S_0&-\frac{1}{2E_0}\{S_1+lS_1'\}\\ &-\frac{1}{16E_0{}^2}\{2S_2-(2l+u)S_2'-2l^2S_2''\}\\ &-\frac{1}{32E_0{}^3}\{2S_3-2lS_3'+luS_3''+\tfrac{2}{3}l^2S_3'''\}\\ &-\frac{1}{512E_0{}^4}\{20S_4-2(10l-u)S_4'+(4l^2+4lu-u^2)S_4''\\ &+4l^2(\tfrac{2}{3}l-u)S_4'''-(4/3)l^2S_4''''\}. \end{aligned} \tag{4.6}$$

As a check we integrate this expression over $d\Omega$. For this and other purposes it is convenient to write it in

the form,

$$\frac{d\sigma}{d\Omega}=S_0-\frac{1}{2E_0}\frac{\partial}{\partial t}tS_1+\frac{1}{16E^2}\frac{\partial}{\partial t}\{(u-2t)S_2+2t^2S_2'\}$$
$$+\frac{1}{32E_0^3}\frac{\partial}{\partial t}\{(u-2t)(S_3-tS_3')-\tfrac{2}{3}t^2S_3''\}$$
$$+\frac{1}{512E_0^4}\frac{\partial}{\partial t}\{(u-2t)(10S_4+(u-10t)S_4'$$
$$+4t^2S_4'')+(4/3)t^3S_4'''\}. \quad (4.7)$$

Introducing (4.7) into

$$\frac{\sigma}{4\pi}=\frac{1}{2}\int_{-1}^{1}\frac{d\sigma}{d\Omega}d\mu_0=\frac{1}{u}\int_0^u\frac{d\sigma}{d\Omega}dt \quad (4.8)$$

one immediately obtains (3.11).

Under actual experimental conditions, the measured differential cross section will depend on the variation of the detector sensitivity with energy. We shall concern ourselves with a $1/v$ detector. In this case the partial differential cross sections have to be multiplied by the ratio of the velocities of incident and scattered neutron before the summation over b. This will just compensate the factor $(1-x_{ab})^{\frac{1}{2}}$ in (4.1). It can be shown that the omission of this factor exempts the factors of S_n, S_n', S_n'', etc. in (4.7) from the operation $\partial/\partial t$. We find thus for the effective differential cross section measured by a $1/v$-detector

$$\left(\frac{d\sigma}{\partial\Omega}\right)_{eff}=S_0-\frac{tS_1'}{2E_0}+\frac{1}{16E_0^2}\{(u-2t)S_2'+2t^2S_2''\}$$
$$+\frac{1}{32E_0^3}\{(u-2t)(S_3'-tS_3'')-\tfrac{2}{3}t^2S_3'''\}$$
$$+\frac{1}{512E_0^4}\{(u-2t)(10S_4'+(u-10t)S_4''$$
$$+4t^2S_4''')+(4/3)t^3S_4''''\}. \quad (4.9)$$

5. SINGLE NUCLEUS

We take as the scattering system a single nucleus in the potential $V(\mathbf{r})$. The scattering amplitude is here given by a single term,

$$F=a_s\exp(iPz/\hbar), \quad (5.1)$$

where $P=\hbar\kappa$ is the momentum transferred to the nucleus and z the component of $\mathbf{r}$ in the direction of $\mathbf{P}$. From (5.1) and (3.15) we have

$$S_0=a_s^2. \quad (5.2)$$

With the Hamiltonian

$$H=p^2/2M+V(\mathbf{r}), \quad (5.3)$$

one obtains for the commutation relations:

$$[HF]=\frac{P}{M}F(\tfrac{1}{2}P+p_s) \quad (5.4)$$

$$[H[HF]]=\frac{P}{M}F\left\{-\frac{\hbar}{i}\frac{\partial V}{\partial z}+\frac{P}{M}(\tfrac{1}{2}P+p_s)^2\right\}, \quad (5.5)$$

where p_s is the component of the momentum of the nucleus in the direction of $\mathbf{P}$.

The expressions (5.4) and (5.5) are now introduced into (3.15). Integration by parts with real eigenfunctions and subsequent averaging over the directions of $\boldsymbol{\kappa}$ (i.e. $\mathbf{P}$) yields

$$\begin{aligned}S_1/S_0&=y\\ S_2/S_0&=y^2+(4/3)K_{\kappa}y\\ S_3/S_0&=y^3+4K_{\kappa}y^2+B_{\kappa}y\\ S_4/S_0&=y^4+8K_{\kappa}y^3+4(\tfrac{4}{5}\langle K^2\rangle_{\kappa}+B_{\kappa})y^2+2C_{\kappa}y,\end{aligned} \quad (5.6)$$

where

$$y=\hbar^2\kappa^2/2M=P^2/2M. \quad (5.7)$$

K is the kinetic energy of the nucleus and

$$B=\tfrac{1}{3}(\hbar^2/M)\nabla^2V \quad (5.8)$$

$$C=\tfrac{1}{3}(\hbar^2/M)(\mathrm{grad}V)^2. \quad (5.9)$$

It is instructive to compare the expressions (5.6) with their classical value. In classical mechanics the energy transfer accompanying the instantaneous transfer of momentum $\mathbf{P}$ to a particle of momentum $\mathbf{p}$ moving in the potential $V(\mathbf{r})$ is independent of the potential and given by

$$E=(1/2M)\{P^2+2\mathbf{P}\cdot\mathbf{p}\}. \quad (5.10)$$

Averaging the nth power of (5.10) over the momentum distribution and over the directions of $\mathbf{P}$ one obtains

$$S_n/S_0=\frac{1}{n+1}\sum_{l=0}^{[n/2]}4^l\binom{n+1}{2l+1}\langle K^l\rangle_{\kappa}y^{n-l}, \quad (5.11)$$

where $[n/2]$ stands for the largest integer smaller than or equal to $n/2$. Comparison with (5.6) shows that (5.6) is represented by (5.11) plus additional terms which depend on the potential and which appear for $n>2$ only.

We are now ready for the evaluation of the cross section. Observing that the value y_0 of y corresponding to $\kappa^2=u=4k_0^2$ is

$$y_0=4E_0/\mu \quad (5.12)$$

where $\mu=m/M$, we obtain from (3.11), (5.2), (1.3), and (5.6)

$$\frac{\sigma}{\sigma_s}=1-\frac{2}{\mu}+\frac{1}{\mu^2}\left(3+\frac{1}{3}\frac{\mu K_{\kappa}}{E_0}\right)-\frac{1}{\mu^3}\left(4+\frac{2}{3}\frac{\mu K_{\kappa}}{E_0}\right)$$
$$+\frac{1}{\mu^4}\left\{5+\frac{\mu K_{\kappa}}{E_0}-\frac{1}{32}\frac{\mu^3C_{\kappa}}{E_0^3}\right\}+\cdots. \quad (5.13)$$

The terms containing $\langle K^2\rangle_{Av}$ and B_{Av} have canceled; one-half of the term containing C_{Av} is contributed by the term $uS_4'(0)$ which arises from the lower limit of the integral in (2.11) and the other half by the terms $S_4(u)$ and $uS_4'(u)$. The terms starting with $1/\mu^n$ represent the terms containing S_n and its derivatives in (3.11). The expansion of the partial cross section σ_{ab} in powers of x_{ab} is thus found to lead to an expansion of the cross section σ in powers of $1/\mu$, where the characteristic energies of the system are measured in terms of E_0/μ. It is, however, important to observe that the quantities $K_{Av}/\mu^{-1}E_0$ and $C_{Av}/(\mu^{-1}E_0)^3$—the former of which represents the square of the ratio of the momenta of nucleus and neutron—may be large. The terms of (5.13) have therefore to be rearranged, by writing

$$\frac{\sigma}{\sigma_s}=\left(1-\frac{2}{\mu}+\frac{3}{\mu^2}-\frac{4}{\mu^3}+\frac{5}{\mu^4}\right)+\frac{1}{3}\frac{K_{Av}}{E_0}\left(1-\frac{2}{\mu}+\frac{3}{\mu^2}\right)-\frac{1}{32}\frac{C_{Av}}{\mu E_0^3}. \quad (5.14)$$

Here the first term represents the reduced mass effect, mentioned in Secs. I and II, the second term, of the order of the square of the velocity ratio, the Doppler effect and the third term the effect of the potential.

Introducing the cross section of the free nucleus at rest by

$$\sigma_{\text{free}}=\sigma_s(1+1/\mu)^{-2}, \quad (5.15)$$

we have thus

$$\sigma/\sigma_{\text{free}}=1+\tfrac{1}{3}K_{Av}/\mu E_0-\tfrac{1}{32}C_{Av}/\mu E_0^3. \quad (5.16)$$

The cross section is thus approximately equal to the cross section of the free nucleus with the same momentum distribution and the direct effect of the binding manifests itself only in the last term, which decreases as E_0^{-3}.

For the average energy transfer one obtains from (3.16) by replacing, in (3.11), S_n by S_{n+1}

$$(E_1)_{Av}=-\frac{2}{\mu}\left\{E_0\left(\frac{\mu}{\mu+1}\right)^2-\frac{4}{3}K_{Av}\left(1-\frac{17}{4\mu}+\cdots\right)+\frac{B_{Av}}{8E_0}\left(1-\frac{8}{3\mu}+\cdots\right)-\frac{4}{15}\frac{\langle K^2\rangle_{Av}}{\mu E_0}(1+O(1/\mu))\right\}. \quad (5.17)$$

In the higher moments of the energy transfer the direct influence of the binding becomes rapidly more important at low neutron energy. Here a potential term is appreciable in the second moment and leading in the third moment. The energy dependence of these higher moments shows how these quantum effects disappear as the neutron energy increases to a value large compared to μ times the level separation, as can be studied in detail on the basis of the data for an oscillator given in Sec. VI.

For the differential cross section one finds from (5.6) and (4.7)

$$\frac{4\pi}{\sigma_s}\frac{d\sigma}{d\Omega}=1-\frac{4}{\mu}+\frac{1}{\mu^2}\left(2\beta+6\beta^2+\frac{\mu}{3}\frac{K_{Av}}{E_0}\right)-\frac{4}{\mu^3}\beta\left\{3\beta+\frac{\mu K_{Av}}{E_0}(1-\beta)\right\}+\frac{2}{\mu^4}\left\{\beta^2(3+10\beta-5\beta^2)+\frac{3\mu K_{Av}}{E_0}\beta(1-\beta)+\frac{\mu^2 D}{8E_0^2}(1-6\beta+6\beta^2)+\frac{\mu^3 C_{Av}}{64E_0^3}\right\} \quad (5.18)$$

where

$$\beta=\sin^2(\theta/2)$$

and

$$D=\tfrac{4}{3}\langle K^2\rangle_{Av}+B_{Av}.$$

Rearranging terms and introducing (5.15), one has from (5.18)

$$\frac{d\sigma}{d\Omega}=\frac{\sigma_{\text{free}}}{4\pi}\left(1+\frac{1}{\mu}\left\{2\cos\theta+\frac{K_{Av}}{3E_0}-\frac{C_{Av}}{32E_0^3}+\cdots\right\}+\frac{1}{\mu^2}P_2(\cos\theta)\left\{1+\frac{2}{3}\frac{K_{Av}}{E_0}+\frac{\langle K^2\rangle_{Av}+(5/4)B_{Av}}{5E_0^2}+\cdots\right\}+\frac{1}{\mu^3}P_2(\cos\theta)\left\{\frac{K_{Av}}{3E_0}+\cdots\right\}+\frac{1}{\mu^4}\left\{\frac{(5\cos^2\theta-1)(1-\cos^2\theta)}{8}+\cdots\right\}\right). \quad (5.19)$$

Equation (5.19) contains two terms depending on the potential which are again small and the remainder is identical with the differential scattering cross section of a free nucleus with the same momentum distribution. Solving the latter problem in the usual way by transforming from center-of-mass to laboratory system and expanding the result in powers of the velocity ratio and the coefficients of this expansion in powers of $1/\mu$, one indeed finds again (5.19) except for the two potential terms.

The relative order of the various terms in (5.19) depends on the neutron energy and the degree of excitation of the system. For high excitation and low neutron energy, for example, it will not be consistent to carry the last two terms of (5.19) since under these conditions they will be smaller than terms which would arise if the original expansion (5.18) were carried to higher order than the fourth. Nevertheless, however, the terms contained in (5.19) are more than amply sufficient for an accurate representation of the differential cross section of heavy nuclei at all neutron energies satisfying the conditions stated at the end of Sec. II.

The effective differential cross section, obtained in the same way as (5.19), turns out to be

$$\left(\frac{d\sigma}{d\Omega}\right)_{\text{eff}} = 1+\frac{1}{\mu}\left\{1+\cos\theta\left(1+\frac{K_{\hbar\omega}}{3E_0}+\frac{B_{\hbar\omega}}{8E_0^2}+\frac{5C_{\hbar\omega}}{32E_0^3}+\cdots\right)\right\}+\frac{\cos\theta}{\mu^2}\left\{1+\frac{2K_{\hbar\omega}}{3E_0}+\frac{B_{\hbar\omega}+(2/5)\langle K^2\rangle_{\hbar\omega}}{2E_0^2}+\cdots\right\}+\frac{\cos\theta}{2\mu^3}\left\{\sin^2\theta+(11-9\cos^2\theta)\frac{K_{\hbar\omega}}{3E_0}+\cdots\right\}+\frac{\cos\theta}{2\mu^4}\{\sin^2\theta+\cdots\}. \quad (5.20)$$

From the results of this section it appears that, while the collision is describable in terms of the classical particle picture only if the neutron energy E_0 is large compared to μ times the level separation Δ, the quantum characteristics of the collision will, in the energy region $\Delta \ll E_0 \ll \mu\Delta$, manifest themselves primarily in the energy distribution of the scattered neutrons. The higher moments of the energy transfer show a strong explicit dependence on the binding potential. In the cross section and the differential cross sections, on the other hand, this dependence is much less pronounced and the binding affects these quantities mainly through its influence on the nuclear momentum distribution.

6. ISOTROPIC OSCILLATOR

As an example we consider a three-dimensional isotropic harmonic oscillator of frequency ω at a temperature T. For this system one finds easily

$$K_{\hbar\omega}=\tfrac{3}{2}T_{\text{eff}} \qquad B=(\hbar\omega)^2$$
$$\langle K^2\rangle_{\hbar\omega}=(15/4)T_{\text{eff}}^2 \qquad C_{\hbar\omega}=\tfrac{2}{3}BK_{\hbar\omega}=(\hbar\omega)^2T_{\text{eff}}, \quad (6.1)$$

where the effective temperature T_{eff} is related to the temperature T by

$$T_{\text{eff}}/T=(\hbar\omega/2T)\coth(\hbar\omega/2T). \quad (6.2)$$

For (5.16) we have thus for the cross section

$$\frac{\sigma}{\sigma_{\text{free}}}=1+\frac{T_{\text{eff}}}{2\mu E_0}\left\{1-\frac{1}{16}\left(\frac{\hbar\omega}{E_0}\right)^2\right\}. \quad (6.3)$$

The corresponding expressions for the differential cross sections and the moments of the energy transfer follow directly by insertion of (6.1) into the general formulas of the preceding section and will thus not be written down here.

For $T=0$, (6.3) goes over into

$$\frac{\sigma}{\sigma_{\text{free}}}=1+\frac{1}{4\mu n_0}\left(1-\frac{1}{16n_0^2}\right), \quad (6.4)$$

where $n_0=E_0/\hbar\omega$.

The asymptotic expression (6.4), valid for large n_0, may now be compared with the exact one. The transition probabilities are given by[7]

$$\phi_{0n}(\kappa^2)=a_s^2\xi^n\exp(-\xi)/n! \quad (6.5)$$

$$\xi=\hbar\kappa^2/2M\omega=P^2/2M\hbar\omega=y/\hbar\omega. \quad (6.5a)$$

Introduction of (6.5) into (3.1)-(3.3) yields

$$\frac{\sigma}{\sigma_{\text{free}}}=\frac{(\mu+1)^2}{4\mu n_0}\sum_{n=0}^{[n_0]}\{\Pi_n(\xi_n^{(-)})-\Pi_n(\xi_n^{(+)})\}, \quad (6.6)$$

where

$$\xi_n^{(\pm)}=(2/\mu)\{n_0-\tfrac{1}{2}n\pm[n_0(n_0-n)]^{\frac{1}{2}}\}$$

$$\Pi_n(x)=\frac{1}{n!}\int_x^\infty \xi^n e^{-\xi}d\xi=e^{-x}\sum_{l=0}^{n}\frac{x^l}{l!}$$

$$=1-\frac{x^{n+1}e^{-x}}{(n+1)!}\sum_{m=0}^{\infty}\frac{(n+1)!}{(n+m+1)!}xm. \quad (6.7)$$

Since for large μ the variation of the cross section with energy is a small effect, it is convenient to write the cross section in the form,

$$\frac{\sigma}{\sigma_{\text{free}}}=1+\frac{c(n_0)}{\mu n_0} \quad (6.8)$$

and discuss $c(n_0)$ rather than σ.

From (6.4) we have then

$$c(n_0)=\tfrac{1}{4}\{1-1/(4n_0)^2\} \quad (6.9)$$

while from (6.6)

$$c(n_0)=-\mu n_0+\frac{(\mu+1)^2}{2}\sum_{n=0}^{[n_0]}\{\Pi_n(\xi_n^-)-\Pi_n(\xi_n^+)\}. \quad (6.10)$$

Numerical comparison of these two expressions (see Fig. 1) shows, that for $\mu=12$ their difference becomes negligible at $n_0\approx 4.2$ and in the limit of large μ already at $n_0\approx 2$. Analytically, this may be seen as follows: Expanding (6.10) in powers of $1/\mu$,

$$c=c_0+c_1/\mu+c_2/\mu^2+\cdots, \quad (6.11)$$

one finds

$$c_0=\begin{cases}(2n_0-1)(n_0(n_0-1))^{\frac{1}{2}}-2n_0(n_0-1) & \text{for } n_0>1\\ 2n_0(1-n_0) & \text{for } n_0<1.\end{cases} \quad (6.12)$$

By expansion in powers of $1/n_0$, (6.12) goes over into (6.9). The quantities c_n/μ^n contribute asymptotically only to terms of higher order than (6.9) but reach their asymptotic form for $n_0 \gg n$ only. Consequently, the deviations of (6.10) from (6.9) will extend to higher and higher n_0 as μ decreases. For $\mu=1$, $c(n_0)$ becomes, for large n_0, a periodic function of n_0, with period 1 and average $\frac{1}{4}$.[3,7]

[7] A. Messiah, J. phys. et radium 12, 670 (1951).

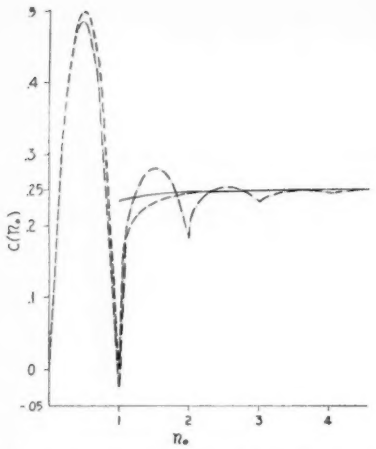

FIG. 1. The coefficient $c(n_0)$ in Eq. (6.8) for the cross section of isotropic oscillator at zero temperature; ———— asymptotic, Eq. (6.9); ·-·-·-·-·-· $\mu=12$, Eq. (6.10); — — — — $\mu=\infty$, Eq. (6.12).

It may also be noted that for the ground state of the oscillator the sums S_l can be evaluated explicitly. From (6.5) and (3.10) we have for the restricted sums

$$S_l(\xi, n_0)=a_s^2 e^{-\xi}\sum_n^{[n_0]}(n^l/n!)\xi^n, \tag{6.13}$$

where ξ is related to κ^2 and y by (6.5a).

For $l=0$ (6.13) becomes with (6.7)

$$S_0(\xi, n_0)=a_s^2\Pi_{[n_0]}(\xi). \tag{6.14}$$

S_l may be expressed in terms of S_0 by decomposing n^l into binomial coefficients. In this way one finds

$$\begin{aligned}
S_1(\xi, n_0)&=\xi S_0(\xi, n_0-1)\\
S_2(\xi, n_0)&=\xi^2 S_0(\xi, n_0-2)+\xi S_0(\xi, n_0-1)\\
S_3(\xi, n_0)&=\xi^3 S_0(\xi, n_0-3)+3\xi^2 S_0(\xi, n_0-2)+\xi S_0(\xi, n_0-1)\\
S_4(\xi, n_0)&=\xi^4 S_0(\xi, n_0-4)+6\xi^3 S_0(\xi, n_0-3)\\
&\quad+7\xi^2 S_0(\xi, n_0-2)+\xi S_0(\xi, n_0-1).
\end{aligned} \tag{6.15}$$

If $S_0(\xi, n_0-j)$ is replaced by $S_0(\xi, \infty)=a_s^2$, (6.15) goes over into (5.6) which can also be checked by introducing (6.1) into (5.6). The derivatives of S_l with respect to ξ may also be expressed in terms of S_0 with the aid of the relation,

$$\xi S_l'=S_{l+1}-\xi S_0. \tag{6.16}$$

From (6.14) we have for the relative error in S_0 caused by the closure approximation

$$\delta_0=\frac{S_0(\xi, \infty)-S_0(\xi, n_0)}{S_0(\xi, \infty)}=1-\Pi_{[n_0]}(4\beta n_0/\mu), \tag{6.17}$$

where

$$\beta=\kappa^2/4k_0^2=\mu\xi/4n_0<1.$$

If $4\beta/\mu$ is small compared to one, which for large μ will be true for all values of β, (6.17) goes over into

$$\delta_0=\frac{1}{[\frac{1}{2}([n_0]+1)]!}\left(\frac{4\beta n_0}{\mu}\right)^{[n_0]+1}\exp(-4\beta n_0/\mu). \tag{6.18}$$

For large n_0 we have, expressing $[n_0]$ by

$$[n_0]=n_0-1+\epsilon,$$

where ϵ varies between 0 and 1 and using Stirlings' formula,

$$\delta_0=(2\pi n_0)^{-\frac{1}{2}}(4\beta/\mu)^{\epsilon}\{(4\beta/\mu)\exp(1-4\beta/\mu)\}^{n_0}. \tag{6.19}$$

If μ is large, δ_0 will thus decrease exponentially with increasing energy for all values of β.

If $4\beta/\mu$ is no longer small, we have to revert to the original expression (6.17). From the integral representation of Π it is then seen that for $4\beta/\mu\geq 1$, δ_0 does not vanish for large n_0, but tends to the limit $\frac{1}{2}$. A more detailed analysis, taking compensation effects into account, shows, however, that the closure correction to $c(n_0)$ decreases for all $\mu>1$ as $\exp(-\alpha n_0)$ where

$$\begin{aligned}
&\alpha=-q-\log(1-q), \quad q=[(\mu-1)/(\mu+1)]^2. \qquad (6.20)\\
&\text{For} \quad 1-q\ll 1, \quad \alpha=\log(4/\mu)-1,\\
&\text{for} \quad\quad q\ll 1, \quad \alpha=\tfrac{1}{4}[(\mu-1)/(\mu+1)]^4.
\end{aligned}$$

7. SEVERAL NUCLEI

We now have to generalize the results of Sec. V to a system of N nuclei with the Hamiltonian

$$H=V(\mathbf{r}_1, \mathbf{r}_2, \cdots \mathbf{r}_N)+\textstyle\sum_s \mathbf{p}_s^2/2M_s. \tag{7.1}$$

At this stage it becomes necessary to consider the spin dependence of the scattering lengths. For a nucleus of spin j_s, the scattering length is given by[8]

$$\begin{aligned}
a_s=\frac{1}{2j_s+1}\{&(j_s+1)a_s^{(+)}+j_s a_s^{(-)}\\
&+2(\boldsymbol{\alpha}_n\cdot\boldsymbol{\alpha}_s)(a_s^{(+)}-a_s^{(-)})\}.
\end{aligned} \tag{7.2}$$

$a_s^{(+)}$ and $a_s^{(-)}$ are the scattering length associated with scattering processes leading to final states of the system nucleus plus neutron with spin $j_s+\frac{1}{2}$ and $j_s-\frac{1}{2}$, respectively, and $\boldsymbol{\alpha}_s$ and $\boldsymbol{\alpha}_n$ are the Pauli spin operators for nucleus and neutron.

Averaging over the orientations of the neutron spin, we have, with

$$\langle\boldsymbol{\alpha}_n\cdot\boldsymbol{\alpha}_s\rangle_{Av}=0; \quad \langle(\boldsymbol{\alpha}_n\cdot\boldsymbol{\alpha}_s)^2\rangle_{Av}=\tfrac{1}{4}j_s(j_s+1), \tag{7.3}$$

for the scattering cross section of the bound nucleus

$$\frac{\sigma_s}{4\pi}=\langle a_s^2\rangle_{Av}=\frac{1}{2j_s+1}\{(j_s+1)(a_s^{(+)})^2+j_s(a_s^{(-)})^2\}. \tag{7.4}$$

The definition of the matrix element (1.4) has now to be modified by inclusion of the spin coordinates. If the spins of different nuclei are not correlated—and this excludes homoeonuclear molecules at low temperatures, the averaging of (3.12) over position and spin coordinates may be carried out independently. As a consequence, the product $a_s a_{s'}$ has to be replaced by

$$\langle a_s a_{s'}\rangle_{Av}=\begin{cases}\langle a_s\rangle_{Av}\langle a_{s'}\rangle_{Av}=a_s^{(c)}a_{s'}^{(c)} & \text{for} \quad s'\neq s\\ \langle a_s^2\rangle_{Av}=\sigma_s/4\pi & \text{for} \quad s'=s,\end{cases} \tag{7.5}$$

where the coherent scattering length $a_s^{(c)}$ is defined by

$$a_s^{(c)}=\langle a_s\rangle_{Av}=\frac{1}{2j_s+1}\{(j_s+1)a_s^{(+)}+j_s a_s^{(-)}\} \tag{7.6}$$

and $\langle a_s^2\rangle_{Av}$ is given by (7.4).

[8] M. Hamermesh and J. Schwinger, Phys. Rev. **69**, 145 (1945).

The cross section (1.1) and the differential cross sections may then be written as a sum of two parts which are usually denoted as the coherent and the incoherent cross section. The coherent cross section is obtained by replacing a_s with $a_s^{(0)}$ throughout, while in the incoherent cross section the product terms with $s' \neq s$ are omitted and a_s^2 is replaced by

$$\langle a_s^2\rangle_{Av} - (\langle a_s\rangle_{Av})^2 = \frac{j_s(j_s+1)}{2j_s+1}(a_s^{(+)} - a_s^{(-)})^2.$$

The expressions of Sec. V for the total and the differential cross sections of a system containing a single nucleus will thus directly represent the incoherent cross section of a system of several nuclei with uncorrelated spins, if σ_{free} is replaced by the incoherent cross section $\sigma_{fs}^{(i)}$ of a free nucleus at rest

$$\sigma_{fs}^{(i)} = 4\pi\left(\frac{\mu_s}{\mu_s+1}\right)^2 \frac{j_s(j_s+1)}{2j_s+1}(a_s^{(+)} - a_s^{(-)})^2. \quad (7.7)$$

The averages entering these expressions are then to be taken for nucleus s and, in particular, the differentiations in the definitions (5.8) and (5.9) of B and C with respect to the coordinates of nucleus s. For the total incoherent scattering cross section we have thus

$$\sigma^{(i)} = \sum_s \sigma_{fs}^{(i)}\left\{1 + \frac{1}{3}\frac{\langle K_s\rangle_{Av}}{\mu_s E_0} - \frac{1}{32}\frac{\langle C_s\rangle_{Av}}{\mu_s E_0^3}\right\}. \quad (7.8)$$

As an example let us consider a Debye crystal containing a single type of nuclei. One has then

$$\begin{aligned} K_{Av} &= \frac{36T^4}{\Theta^3}\int_0^{\Theta/2T} x^3 \coth x\, dx \\ B_{Av} &= \tfrac{3}{5}\Theta^2 \\ C_{Av} &= \frac{96T^6}{\Theta^3}\int_0^{\Theta/2T} x^5 \coth x\, dx \\ \langle K^2\rangle_{Av} &= (5/3)(K_{Av})^2, \end{aligned} \quad (7.9)$$

where Θ is the Debye temperature.

For $T \ll \Theta$

$$\begin{aligned} K_{Av} &= \frac{9}{16}\Theta\left\{1 + \frac{8}{15}\left(\frac{\pi T}{\Theta}\right)^4\right\} \\ C_{Av} &= \frac{1}{4}\Theta^3\left\{1 + \frac{32}{21}\left(\frac{\pi T}{\Theta}\right)^6\right\} \end{aligned} \quad (7.10)$$

for $T \gg \Theta$

$$\begin{aligned} K_{Av} &= \frac{3}{2}T\left\{1 + \frac{1}{20}\left(\frac{\Theta}{T}\right)^2\right\} \\ C_{Av} &= \frac{3}{5}T\Theta^2\left\{1 + \frac{5}{84}\left(\frac{\Theta}{T}\right)^2\right\}. \end{aligned} \quad (7.11)$$

The incoherent cross section per nucleus becomes then

$$\frac{\sigma^{(i)}}{\sigma_{free}^{(i)}} = 1 + \frac{K_{Av}}{3\mu E_0}\left\{1 - \frac{\nu}{24}\left(\frac{\Theta}{E_0}\right)^2\right\}. \quad (7.12)$$

The coefficient ν depends but little on the temperature; it decreases from $\nu = 1$ for $T \ll \Theta$ to $\nu = 9/10$ for $T \gg \Theta$. For heavy nuclei (7.12) will hold as soon as the neutron energy is slightly larger than the Debye temperature. In the effective differential cross section the direct binding effect is somewhat larger as a result of the presence, in the first line at (5.20), of the term containing B_{Av} which at low temperatures and $E_0 = 2\Theta$ amounts to twenty percent of the Doppler term.[9]

Returning now to the general[6] problem it will be convenient to abandon the customary division of the cross section into a coherent and an incoherent part. Instead, we shall distinguish between diagonal terms ($s = s'$) and interference terms ($s \neq s'$). The diagonal terms are represented by the results of Sec. V,[10] so that we only have to calculate the interference terms. For this purpose we express the quantities S_n by

$$S_n = \sum_s \langle a_s^2\rangle_{Av} G_n^{(ss)} + \sum'_{ss'} a_s^{(0)} a_{s'}^{(0)} G_n^{(ss')}. \quad (7.13)$$

$G_n^{(ss)}$ is given by (5.6). For $G_n^{(ss')}$ we have from (3.12) with the notation

$$\begin{aligned} f_s &= \exp(i\boldsymbol{\kappa}\cdot\mathbf{r}_s) = \exp(iPz_s/\hbar), \\ G_0^{(ss')} &= \langle f_{s'}^* f_s\rangle_{Av} = \left\langle \frac{\sin\kappa r_{ss'}}{\kappa r_{ss'}}\right\rangle_{Av} \\ G_1^{(ss')} &= \langle f_{s'}^*[Hf_s]\rangle_{Av} \\ G_2^{(ss')} &= \langle [f_{s'}^* H][Hf_s]\rangle_{Av} \\ G_3^{(ss')} &= \langle [f_{s'}^* H][H[Hf_s]]\rangle_{Av}. \end{aligned} \quad (7.14)$$

[9] The statements made so far on the basis of the usual theory of neutron scattering by crystals [J. M. Cassels, *Progress in Nuclear Physics*, Vol. I (edited by O. R. Frisch, London-New York, 1950)] about the behavior of the cross section at high energies are either entirely erroneous because of inconsistent approximations [R. Weinstock, Phys. Rev. **65**, 1 (1944); R. J. Finkelstein, Phys. Rev. **72**, 907 (1947)], or very incomplete. [A. Akhiezer and I. Pomeranchuk, J. Phys. (U.S.S.R.) **11**, 167 (1947); D. A. Kleinman, thesis, Brown University (1951).] Akhiezer and Pomeranchuk have given an integral representation of the cross section. From its discussion they conclude that the neutron energy, at which the direct binding effects in the cross section become negligible, is determined by a condition which is essentially identical with Eq. (2.2) rather than (2.3) and which is therefore much too restrictive. Furthermore, their treatment leads to the same energy dependence for coherent and incoherent cross section at high energy. Actually, however, the derivatives of these two quantities with respect to the energy have opposite sign at high energy. The evaluation of the asymptotic interference term (7.21) for crystals [Placzek, Nijboer, and Van Hove, Phys. Rev. **82**, 392 (1951)] shows that this term, which has negative sign, is for heavy nuclei of considerably larger size than the Doppler term. At high energy therefore the coherent cross section increases with increasing energy, in contrast to the incoherent cross section which decreases with increasing energy.

[10] Adding the diagonal terms of the coherent cross section to the expressions (7.8) for the incoherent cross section is equivalent to replacing $\sigma_{fs}^{(i)}$ by the total free cross section σ_{fs}.

The commutation relations of f_s with the Hamiltonian (7.1) are identical with (5.4)–(5.5),

$$[Hf_s]=\frac{P}{M_s}f_s(\tfrac{1}{2}P+p_{ss}) \tag{7.15}$$

$$[H[Hf_s]]=\frac{P}{M_s}f_s\left\{-\frac{\hbar}{i}\frac{\partial V}{\partial z_s}+\frac{P}{M_s}(\tfrac{1}{2}P+p_{ss})^2\right\}. \tag{7.16}$$

With the aid of the relation

$$\langle f_s f_{s'}{}^*(\tfrac{1}{2}P+p_{ss})\rangle_{\mathrm{kr}}=\langle f_s f_{s'}{}^*(\tfrac{1}{2}P-p_{s's})\rangle_{\mathrm{kr}}=0 \quad \text{for} \quad s\neq s'$$

obtained through integration by parts, one finds from (7.14) and (7.15):

$$G_1^{(ss')}=0 \tag{7.17}$$

$$G_2^{(ss')}=\frac{P^2}{4M_sM_{s'}}G_0^{(ss')}+\frac{\hbar^2}{M_sM_{s'}}\langle\exp(i\boldsymbol{\kappa}\cdot\mathbf{r}_{ss'})(\mathbf{p}_s\cdot\boldsymbol{\kappa})(\mathbf{p}_{s'}\cdot\boldsymbol{\kappa})\rangle_{\mathrm{kr}}. \tag{7.18}$$

From (7.17) it follows that the first-order reduced mass correction does not apply to the interference terms. The second term in (7.18) is the analog of the Doppler term encountered previously and represents an effect caused by the correlation of the momenta of different nuclei. In classical statistics there is no such correlation and the term will thus vanish at high temperatures.

In a diatomic molecule, for example, the translational momenta of the two nuclei are fully correlated and the momenta of relative motion fully anticorrelated. At high temperatures, when the relative motion is fully excited, these two effects cancel out while at low temperatures the negative correlation prevails. The result of the evaluation of the term for a particular case will be given in the discussion of the cross sections; now let us just consider the average of the product of the momenta alone.

Expressing the momenta $\mathbf{p}_1$ and $\mathbf{p}_2$ of the nuclei in a diatomic molecule by the momentum $\mathbf{p}_c$ of the center of gravity and the momentum $\mathbf{p}$ of relative motion, we have

$$\mathbf{p}_1=\frac{M_1}{M_1+M_2}\mathbf{p}_c+\mathbf{p}, \quad \mathbf{p}_2=\frac{M_2}{M_1+M_2}\mathbf{p}_c-\mathbf{p},$$

$$(\mathbf{p}_1\cdot\mathbf{p}_2)_{\mathrm{kr}}=\frac{M_1M_2}{(M_1+M_2)^2}\langle p_c{}^2\rangle_{\mathrm{kr}}-\langle p^2\rangle_{\mathrm{kr}}=2M_r(E_t-E_i),$$

where E_t and E_i are the average kinetic energies of translation and internal motion. At high temperatures $E_t=E_i=\frac{3}{2}T$; at low temperatures, $T\ll\hbar\omega$, $E_t-E_i=-\hbar\omega/4+T/2$ or $-\hbar\omega/4+3T/2$ according to whether the temperature is large or small compared to the rotational quanta.

For G_3 one finds

$$G_3^{(ss')}=\frac{P^2}{M_s}G_2^{(ss')}+\frac{P^2}{M_sM_{s'}}\left\langle f_sf_{s'}{}^*\left\{\frac{\hbar^2}{2}\frac{\partial^2V}{\partial z_s\partial z_{s'}}+\frac{P}{M_s}p_{ss}{}^2(p_{s's}-\tfrac{1}{2}P)\right\}\right\rangle_{\mathrm{kr}}. \tag{7.19}$$

The expression for G_4 is longer and will not be given here. The discussion of the higher approximations in the preceding sections was necessary mainly to gain clear insight into the structure of the theory. This having been achieved we can limit ourselves, in the discussion of the interference effects, to the terms represented by S_0, S_1, and S_2. In this approximation one finds from (3.11) for the contribution of the interference terms to the cross section

$$\sigma_{\mathrm{int}}=8\pi\sum_{s,\,s'}^{s'<s}a_s{}^{(c)}a_{s'}{}^{(c)}\left\{\frac{1}{2k_0{}^2}\left\langle\frac{1}{r_{ss'}{}^2}\right\rangle_{\mathrm{kr}}-\frac{1}{2k_0{}^2}\left\langle\frac{\cos2k_0r_{ss'}}{r_{ss'}{}^2}\right\rangle_{\mathrm{kr}}+\frac{\langle 2k_0z_{ss'}\sin2k_0z_{ss'}v_{ss}v_{s's}\rangle_{\mathrm{kr}}}{v_0{}^2}+\frac{1}{\mu_s\mu_{s'}}\left\langle\frac{\sin2k_0r_{ss'}}{2k_0r_{ss'}}+\cos2k_0r_{ss'}\right\rangle_{\mathrm{kr}}\right\}. \tag{7.20}$$

Here v_0 denotes the neutron velocity, and v_{ss} and $v_{s's}$ components of the nuclear velocities; $z_{ss'}$ stands for $\mathbf{r}_{ss'}\cdot\mathbf{k}_0/k_0$ and v_{ss} for $\mathbf{v}_s\cdot\mathbf{k}_0/k_0$. It will of course be kept in mind that the quantities v_{ss} and $v_{s's}$ do not commute with $z_{ss'}$. The first two terms in (7.20) represent the static approximation and the rest the corrections resulting from G_2. At high temperatures the third term vanishes. For short neutron wavelength all the terms except the first one are not only rapidly fluctuating but also their magnitude goes to zero with decreasing wavelength.[11] The cross section is then represented by

$$\sigma_{\mathrm{int}}=\frac{4\pi}{k_0{}^2}\sum_{s,\,s'}^{s'<s}a_s{}^{(c)}a_{s'}{}^{(c)}\langle r_{ss'}{}^{-2}\rangle_{\mathrm{kr}}. \tag{7.21}$$

The wavelength at which (7.20) goes over into (7.21) depends upon the nature of the scattering system and its determination requires rather careful considerations.[12]

Introducing (7.13) and (7.18) into (4.7) or (4.9), one obtains simple but somewhat lengthy expressions for the contribution of the interference terms to the differential cross section. In an abbreviated form they may be written as follows:

$$\left(\frac{d\sigma_{\mathrm{int}}}{d\Omega}\right)_{\mathrm{eff}}=\varphi_0+\left\{(1-2\beta)\frac{\partial}{\partial\beta}+2\beta^2\frac{\partial^2}{\partial\beta^2}\right\}(\beta\varphi_1+\beta^2\varphi_2) \tag{7.22}$$

$$\frac{d\sigma_{\mathrm{int}}}{d\Omega}=\left(\frac{d\sigma_{\mathrm{int}}}{d\Omega}\right)_{\mathrm{eff}}+2\left(-1+2\beta\frac{\partial}{\partial\beta}\right)(\beta\varphi_1+\beta^2\varphi_2), \tag{7.23}$$

[11] This also holds for systems with long-range order; see reference 12.

[12] Placzek, Nijboer, and Van Hove, Phys. Rev. **82**, 392 (1951).

where $\beta=\sin^2\frac{1}{2}\theta$. The quantities φ_n are functions of $\kappa_0^2=4k_0^2\beta$

$$\varphi_0=2\sum_{s,s'}^{s'<s} a_s^{(c)}a_{s'}^{(c)}\left\langle\frac{\sin\kappa_0 r_{ss'}}{\kappa_0 r_{ss'}}\right\rangle_{Av}$$

$$\varphi_1=2\sum_{s,s'}^{s'<s} a_s^{(c)}a_{s'}^{(c)}\langle\cos\kappa_0 z_{ss'}v_{sz}v_{s'z}\rangle_{Av}/v_0^2$$

$$\varphi_2=2\sum_{s,s'}^{s'<s}\frac{a_s^{(c)}}{\mu_s}\frac{a_{s'}^{(c)}}{\mu_{s'}}\left\langle\frac{\sin\kappa_0 r_{ss'}}{\kappa_0 r_{ss'}}\right\rangle_{Av}.$$

For a diatomic molecule the differential cross sections may be expressed in terms of functions simply related to the error function of complex argument; if, in particular, the effective wavelength $1/\kappa_0$ is large compared to the vibrational amplitude the evaluation of φ_0 and φ_2 is trivial and for φ_1 one then finds for temperatures large compared to the rotational quanta

$$\varphi_1=2a_1^{(c)}a_2^{(c)}\langle(\cos\kappa_0 z_{12})v_{1z}v_{2z}\rangle_{Av}/v_0^2=$$
$$-a_1^{(c)}a_2^{(c)}\frac{(E_{vib}-T)}{3(\mu_1+\mu_2)E_0}\left(\frac{\pi}{2\kappa_0 r_0}\right)^{\frac{1}{2}}$$
$$\times\{J_{1/2}(\kappa_0 r_0)-2J_{3/2}(\kappa_0 r_0)\}. \quad (7.24)$$

Here r_0 is the equilibrium distance of the nuclei and E_{vib} the average total vibrational energy. (7.24) provides a simple example for the structure of momentum correlation term. For $T\gg\hbar\omega$, $E_{vib}-T=0$ and φ_1 vanishes.

8. APPLICATIONS

The isolation of small electronic contributions to the scattering cross section, which may be caused by ordinary magnetic effects,[13,14] scattering by spin waves[15] and the spin-independent interaction between neutron and electron[16,14] requires a very precise theoretical determination of the dependence of the nuclear scattering on neutron energy or scattering angle. Off hand this may seem too pretentious a task if the scattering system is as complex as in the transmission experiments of Rainwater, Rabi, and Havens on liquid bismuth.[17] On the basis of the results derived above, however, it can be approached with reasonable assurance. The characteristic temperature of liquid Bi, corresponding to the Debye temperature of a solid, is of the order of 100 degrees abs. The expressions (5.16) and (7.20) for the cross section will thus be valid for neutron energies large compared to 10^{-2} ev. Since $\mu=209$, the last term in (7.20), which is quadratic in the mass ratio, may be neglected. Since the melting temperature is 544 degrees abs and thus large compared to the characteristic temperature, the effect of the correlation of the momenta, given by the third term in (7.20) disappears, while in the second term of (5.16) $K_{kin}=3T/2$. With a slight modification[18,12] of the first two terms of (7.20) which is equivalent to neglecting deflections by an angle $k_0^2d^2$, where d is of the order of the total linear dimensions of the scattering system, the scattering cross section per nucleus is thus given by

$$\sigma=\sigma_{free}\left\{1+\frac{T}{2\mu E_0}\left(1-\frac{C_{kin}}{16TE_0^2}\right)\right\}$$
$$-\sigma_{coh}\frac{2\pi}{k_0^2}\int_0^\infty(1-\cos 2k_0 r)\{\rho-g(r)\}dr. \quad (8.1)$$

Here σ_{free} is, as before, the total scattering cross section of the free nucleus at rest and $\sigma_{coh}=4\pi(a_s^{(c)})^2$ the coherent cross section of the bound nucleus; $g(r)$ is the density at distance r from a given nucleus and ρ the ordinary density. The evaluation of the interference term in (8.1) has been carried out by Placzek, Nijboer, and Van Hove.[12] The third term in (8.1) depends on the average square of the force acting on the nucleus which cannot be calculated precisely for a liquid. Even the crudest estimates, however, are sufficient to show that at the relevant neutron energies this term cannot amount to more than a fraction of the Doppler term.

The discussion of the electronic contributions to the cross section has, in part, been given previously.[14,16] For an isolated rare gas atom paramagnetic scattering is absent and diamagnetic scattering negligible.[14] For liquid bismuth, on the other hand, the ordinary magnetic effects are hardly accessible to a satisfactory theoretical analysis. Although they do not interfere with the nuclear scattering the possibility that they might be of relevant size can by no means be excluded *a priori*. Since they are entirely caused by the outer electrons, however, their energy dependence will differ from that of the contribution of the spin-independent neutron-electron interaction which comes from all the electrons. The energy dependence of the latter has been calculated on the basis of the ordinary form factor.[16] Its isolation would thus seem to require a study of the variation with energy of the difference between the observed cross section and (8.1).

Among other applications of results derived here, the problem of the energy dependence and angular distribution of neutron scattering by heavy molecules might in particular be mentioned. The theory in the form developed here is valid for neutron energies large compared to the vibrational quanta, while many of the

[13] O. Halpern and M. H. Johnson, Phys. Rev. **55**, 898 (1939); O. Halpern, Phys. Rev. **72**, 746 (1947).
[14] E. Fermi and L. Marshall, Phys. Rev. **72**, 1139 (1947).
[15] R. G. Moorhouse, Proc. Phys. Soc. (London), **A64**, 207, 1097 (1951).
[16] Havens, Rainwater, and Rabi, Phys. Rev. **72**, 634 (1947).
[17] Rainwater, Rabi, and Havens, Phys. Rev. **75**, 1295 (1949); **82**, 345 (1951).
[18] F. Zernike and J. A. Prins, Z. Physik **41**, 184 (1927).

experiments[19,20] carried out so far concern neutron energies large compared to the rotational but small compared to the vibrational quanta. In order to extend the theory to this region the Hamiltonian (7.1) is replaced by the Hamiltonian of a rigid molecule. The results for the diagonal terms obtained in this way agree for high temperatures with the semiclassical mass tensor approximation[21] and differ from it for low temperatures to which it is not directly applicable. In addition one obtains the interference terms which are not given by the mass tensor approximation and which are particularly important for the angular distribution. The discussion of these results and their comparison with the experiments and with the approximation of Alcock and Hurst[20] will be given in a separate paper.

This paper is based on work begun at the General Electric Research Laboratory and carried out at The Institute for Advanced Study. I am indebted to H. A. Bethe for helpful discussions and to G. F. Chew and R. Jost for a critical reading of the manuscript.

[19] E. Melkonian, Phys. Rev. **76**, 1744 (1949).
[20] N. Z. Alcock and D. G. Hurst, Phys. Rev. **75**, 1609 (1949); **83**, 1100 (1951).
[21] R. G. Sachs and E. Teller, Phys. Rev. **60**, 18 (1941).

PHYSICAL REVIEW VOLUME 86, NUMBER 3 MAY 1, 1952

Triton Binding Energy by a Randomized Net-Point Method*

S. I. Rubinow†
University of Pennsylvania, Philadelphia, Pennsylvania
(Received November 27, 1951)

A numerical procedure is investigated for solving Schrödinger's equation for a system of particles. A net-point analysis is applied directly to the integral equation equivalent to Schrödinger's equation. A unique feature is the introduction of the concept of a "randomized" net of points. This is designed to cope with the problem of obtaining adequate covering of the space when many dimensions are involved.

The method is applied to the problem of finding the binding energy of the triton with the assumption of central forces. The result obtained for an exponential potential as determined by the most recent low energy scattering data is approximately 10 percent too deep. It may be concluded that more effective repulsion must be introduced into the "equivalent central potential" to bring about agreement with experiment.

I. THE RANDOMIZED NET-POINT PROCEDURE

A NUMERICAL net-point procedure for solving Schrödinger's equation has been investigated with special regard towards finding the lowest (ground state) eigenvalue for a system of three (or more) particles. The spin-free time independent Schrödinger equation for a system of particles may generally be written as

$$(\Delta - k^2)\psi = V\psi \tag{1}$$

and can be transformed into an equivalent integral equation by means of the appropriate Green's function $G(P, Q)$. Thus,

$$\lambda\psi(P) = -\int dQ G(P, Q) V(Q)\psi(Q), \tag{2}$$

where P is a point in an arbitrary n-dimensional space. If V is an attractive well, than the largest eigenvalue λ_0 corresponds to the binding energy of the system. The integral may be replaced by a sum over a discrete set of N points P_i yielding

$$\lambda\psi(P_i) = \sum_{j=1}^{N} \Delta Q_j G(P_i, Q_j) V(Q_j)\psi(Q_j), \tag{3}$$

where ΔQ_j is the volume element associated with the point Q_j.

Because the number of dimensions n may in general become large, the following unique manner of selecting the points P_i was introduced: Consider the set of N equally spaced points in each dimension. From each such set, choose a point at random; the aggregate of n of these taken together constitutes a single point P_i in n-dimensional space. This process is repeated with the remaining points until they are all exhausted. The final result is a set of N points in n-dimensional space.

The purpose of this mode of selection is to afford some compromise between the desires of having the points P_i equally spaced throughout the volume and of having the points randomly distributed throughout the volume. The latter desideratum is suggested by a random sampling procedure (Monte Carlo) for evaluating a multidimensional integral. It should be noted that the prescribed procedure selects points which are equally probable from the random sampling point of view. An advantage of randomly spacing the points is that it maximizes the number of coordinates chosen in each dimension.

* This work was carried out in partial fulfillment of the requirements of the degree of Doctor of Philosophy at the University of Pennsylvania.
† Now at the Massachusetts Institute of Technology, Cambridge, Massachusetts.

It should be mentioned that in Eq. (3) the case $j=i$ requires special consideration because the Green's function is generally singular when its argument is zero. This case may be conveniently treated by setting

$$G(P_i, Q_i)=(1/\Delta Q_i)\int dQ G(P_i, Q), \tag{4}$$

where the integration extends over a sphere whose center is at the point P_i and whose volume equals ΔQ_i. The largest eigenvalue λ_0 in Eq. (3) is just the dominant eigenvalue of the matrix $G_{ij}V_j\Delta Q_j$ and can be obtained by simple iteration.

In order to illustrate the procedure Schrödinger's equation for the three-dimensional square well was solved as a three-dimensional integral equation. In order to compare with a more usual net-point procedure, a "regular" choice of net points was chosen in addition to the randomized set of points. The results are given in Table I.

It can be seen from the table that the value of the dominant eigenvalue obtained for all cases is larger than the true value. This is a result of the fact that Eq. (4) systematically overestimates the value of G_{ii} because G is a monotonic decreasing function of R (as R increases). It can also be seen that the accuracy obtained with the use of the randomized net points is apparently significantly greater than that obtained for the regular choice of points. This can probably be attributed to the fact that a much greater sampling of the radial variable is obtained by use of the randomized net. Of course, a three-dimensional problem with a solution which is a function of only one variable was deliberately chosen in order to test in a favorable way the heuristic ideas of the randomized net-point method. It is believed that the randomized selection of net points is in general not inferior to a regular choice of net points and in addition may be superior in some cases.

II. APPLICATION TO THE BINDING ENERGY OF THE TRITON

On the basis of the encouraging results obtained for the square well it was decided to apply the method to the problem of finding the binding energy of the triton with the assumption of central forces. Schrödinger's equation for a system of three particles of equal mass m may be written with center-of-mass coordinates removed as

$$(\Delta_r+\Delta_s-k^2)\psi(\mathbf{r}, \mathbf{s})=(k^2/|E|)V(\mathbf{r}, \mathbf{s})\psi(\mathbf{r}, \mathbf{s}), \tag{5}$$

where $k^2=(4m/3\hbar^2)|E|$ and $\mathbf{r}=\frac{1}{2}\sqrt{3}(\mathbf{r}_3-\mathbf{r}_2)$, $\mathbf{s}=-\mathbf{r}_1+\frac{1}{2}(\mathbf{r}_2+\mathbf{r}_3)$. Transforming to the equivalent integral equation by means of the appropriate Green's function, there is obtained

$$\lambda\psi(\mathbf{r}, \mathbf{s})=-\int\int d\rho d\sigma[K_2(R)/R^2]V(\rho, \sigma)\psi(\rho, \sigma), \tag{6}$$

TABLE I. Values of the dominant eigenvalue obtained from a net-point analysis of the three-dimensional square well problem. The true value of the dominant eigenvalue is $\lambda_0=2.456$.

Choice of points	N	Dominant eigenvalue	Percentage error
Regular	8	3.55	44
Regular	13	3.20	31
Randomized	8	2.670	9
Randomized	24	2.541	3.5

where all lengths have been made nondimensional by multiplication by k, $\lambda=8\pi^2|E|$, and $K_2(R)$ is the Bessel function of pure imaginary argument. If now it is assumed that the potential $V(\rho, \sigma)$ is a central potential and a system of coordinates consisting of the particle interdistances and the Eulerian angles of the system is introduced, Eq. (6) may be reduced to the following three-dimensional integral equation:

$$\lambda\psi(r, s, \alpha)=-\int_0^\infty \rho^2 d\rho\int_0^\infty \sigma^2 d\sigma\int_0^\pi \sin\beta d\beta \times G(r, s, \alpha; \rho, \sigma, \beta)V(\rho, \sigma, \beta)\psi(\rho, \sigma, \beta), \tag{7}$$

where α is the angle between $\mathbf{r}$ and $\mathbf{s}$ and

$$G(r, s, \alpha; \rho, \sigma, \beta)=8\pi\int_0^\pi d\tau\frac{1}{v}\left[\frac{K_1(\sqrt{v_0-v})}{(v_0-v)^{\frac{1}{2}}}-\frac{K_1(\sqrt{v_0+v})}{(v_0+v)^{\frac{1}{2}}}\right],$$

$$v^2=v_1^2+v_2^2\cos\tau, \tag{8}$$

$$v_1^2=(2r\rho)^2+(2s\sigma)^2+2(2r\rho)(2s\sigma)\cos\alpha\cos\beta,$$

$$v_2^2=2(2r\rho)(2s\sigma)\sin\alpha\sin\beta,$$

$$v_0=r^2+s^2+\rho^2+\sigma^2.$$

In deriving Eq. (8), use has been made of the fact that the angular momentum operator is a function only of the Eulerian angles of the system. It was assumed that the ground state was a state of zero angular momentum so that Eq. (8) applies only to S-states.

In order to provide a measure of the accuracy obtainable by means of the randomized net-point analysis that was applied, application was first made to the central force potential consisting of effective singlet and triplet exponential well (n,p) and (p,p) interactions as determined by Rarita and Present[1] by use of an extensive variational procedure. In doing this, the wave function was assumed spacially symmetric with respect to the interchange of the two neutron coordinates. Then,

$$V(r, s, \alpha)=\tfrac{1}{4}[3T_{12}(r_{12})+3T_{13}(r_{13})+S_{12}(r_{12})+S_{13}(r_{13})+4S_{23}(r_{23})], \tag{9}$$

where S, T designate singlet and triplet wells, respectively.

[1] W. Rarita and R. D. Present, Phys. Rev. **51**, 788 (1937).

TABLE II. Errors in the values of the eigenvalues as compared to Rarita and Present's result, $|E| = 8.02$ Mev.

Alternative	1	2	3
Percentage error in value of lowest eigenvalue	0.5>	2<	8<

In applying Eq. (3), the approximations which follow were made. The infinite volume of integration was somewhat arbitrarily restricted to a finite volume, e.g.,

$$\int dQ \rightarrow \int_0^1 d\rho\rho^2 \int_0^1 d\sigma\sigma^2 \int_0^\pi d\beta \sin\beta. \qquad (10)$$

The values of $G_{ij}(i \neq j)$ were taken for simplicity of calculation from the equation

$$G(r, s, \alpha; \rho, \sigma, \beta) \approx \frac{8\pi^2}{v_1}\left[\frac{K_1(\sqrt{v_0 - v_1})}{(v_0 - v_1)^{\frac{1}{2}}} - \frac{K_1(\sqrt{v_0 + v_1})}{(v_0 + v_1)^{\frac{1}{2}}}\right], \qquad (11)$$

where the quantity on the right equals π times the midpoint of the integrand in Eq. (8). The value of G_{ii} was determined by Eq. (4) with the integration extended over the appropriate 6-dimensional hypersphere.

The accuracy obtained is indicated in Table II. The three alternatives represent different choices of sets of random net points and provide an indication of the variation in results to be expected as a result of different choices of net points. The number of net points chosen was $N = 24$.

The high accuracy obtained for such a relatively small amount of labor is somewhat fortuitous as a result of an explainable cancellation of errors involved; the errors inherent in the use of Eqs. (10) and (11) tend to underestimate the values of G_{ij} (and hence the value of λ_0), while the error involved in the use of Eq. (4) tends to overestimate the value of G_{ii} (and hence λ_0). Nevertheless, it was felt that the same circumstances would apply if only the values of the potential were changed in Eq. (3). This permitted some degree of confidence in the application of the Alternative 1 set of points to an exponential central potential as determined by the most recent low energy scattering data.[2] The result obtained for the binding energy of the trition was 9.3 Mev, approximately 10 percent greater than the experimental value.[3]

If the same potential was used to calculate the binding energy of the alpha-particle, it can be expected that the discrepancy with the experimentally determined value would be even more pronounced because the result reported is calibrated with Rarita-Present's work and their potential when applied to the calculation of the binding energy of the alpha-particle yielded an excessively large answer. From the point of view of an "effective central potential," it appears then that more repulsion must be introduced into the nuclear potential in order to fit the observed binding energy data of the light nuclei. It is, of course, impossible to tell whether the repulsion should be simply a repulsive inner region for the ordinary two-body forces or whether the repulsion is of the many-body type which will only come into play when three or more particles interact simultaneously.

The author wishes to thank Dr. T. A. Welton for suggesting this thesis and for many fruitful suggestions and discussions.

[2] E. E. Salpeter, Phys. Rev. **82**, 60 (1951).

[3] This value is corroborated by a recent variational calculation reported by J. Irving [Phil. Mag. **42**, 338 (1951)], who obtained a value of 9.5 Mev for a very similar assumed potential.

Photodisintegration of the Deuteron*

V. E. KROHN, JR. AND E. F. SHRADER
Case Institute of Technology, Cleveland, Ohio
(Received November 19, 1951)

The angular distribution of the protons from the $d(\gamma,n)p$ reaction has been investigated for 5–13-Mev gamma-rays by means of the D_2O loaded emulsion technique with the Case betatron serving as gamma-ray source. The results have been compared to a differential cross section of the form $d\sigma=\{a+(b+c\cos\theta)\sin^2\theta\}d\Omega$ in the center-of-mass system and the isotropy coefficient found consistent with the mean values: $a/b=0.04\pm0.03$ from 5 to 11 Mev and 0.24 ± 0.07 from 11 to 13 Mev. The forward asymmetry coefficient was determined for energies above 8 Mev and found to be $c/b=0.24\pm0.09$. These results are in agreement with the theoretical calculations of Marshall and Guth except for the isotropy coefficient observed above 11 Mev where the theory predicts $a/b\sim0.01$.

I. INTRODUCTION

THE determination of the angular distribution of protons arising from the photodisintegration of the deuteron is of interest in that it provides a test of the theory of nuclear forces as applied to this two-body problem. Considerable work has been done on the determination of the angular distribution at energies near the threshold for the process[1] and a number of recent experiments have been performed in the 4- to 20-Mev range.[2–8] The sources used in these latter works were the 6.1- and 7.0-Mev quanta from the $F^{19}+H^1$ reaction;[2,5–8] the 14.8- and 17.6-Mev quanta from the Li^7+H^1 reaction;[3,6] and 20-Mev bremsstrahlung.[4] The detecting systems employed were nuclear track plates loaded with calcium nitrate containing heavy water of crystallization;[2] track plates loaded by soaking in heavy water;[3,6–8] a scattering chamber containing D_2 gas with track plates as detectors;[4] a cloud chamber containing CD_4 gas;[5] and deuterated paraffin adjacent to a track plate.[6] The work to be described in this paper employs D_2O-loaded nuclear track plates and 14-, 17-, and 20-Mev bremsstrahlung.

An angular distribution function in the c.m. system of the form

$$d\sigma=\{a+(b+c\cos\theta)\sin^2\theta\}d\Omega$$

has been suggested by Marshall and Guth.[9] The coefficients a/b and c/b represent a measure of isotropy and forward asymmetry in the center-of-mass system, respectively. These quantities can be treated as parameters in a quantitative comparison of theory and experiment. The values of these parameters obtained by the various investigators have been collected in Table I.

II. EXPERIMENTAL

In this investigation the D_2O-loaded emulsion technique was used along with 14-, 17-, and 20-Mev bremsstrahlung from the Case betatron. A background plate loaded with H_2O was exposed with each D_2O plate and corresponding areas on the two plates were searched. About 85 percent of the data came from 200μ Kodak NTB plates while the remainder was from 150μ and 100μ NTB plates. The 200μ plates were exposed 3 m from the betatron target in a plastic microscope slide box. The beam was collimated to a diameter of about 2 cm and passed through the box along the length of the plates without touching the top, bottom, or sides of the box. This arrangement gave relatively less fog than earlier exposures with less collimation and smaller plate containers. All plates were exposed with the gamma-ray beam almost parallel to the surface of the emulsions. An incidence angle of 2° was used to reduce absorption of gamma-rays in the wet emulsions.

The plates were soaked for about two hours at room temperature in order to obtain loadings near saturation and were processed in the usual way immediately after the brief exposures. Track densities of order ten tracks per square millimeter were obtained. Work with the

TABLE I. Results of others as indicated by references.

Energy (Mev)	Isotropy coefficient a/b	Forward asymmetry coefficient c/b
5.	-0.07^a	0.2 ± 0.2^a
6.	0.09 ± 0.07^b	
6.5	$0.02^{+0.04}_{-0.02}{}^c$	$0.4^{+0.2}_{-0.3}{}^b$
	$\sim0^{d-f}$	
7.	0.17 ± 0.07^b	0.2 ± 0.2^a
	0.17^a	
9.	-0.12^a	0.21 ± 0.14^a
11.	-0.06^a	0.25 ± 0.14^a
13.	0.05^a	0.35 ± 0.14^a
17.	0.05 ± 0.15^g	0.33 ± 0.22^a
	$0.02^{+0.14}_{-0.02}{}^c$	
	0.22^a	

[a] E. G. Fuller, reference 4.
[b] G. Goldhaber, reference 7.
[c] P. V. C. Hough, reference 6.
[d] Gibson *et al.*, reference 2.
[e] Phillips *et al.*, reference 5.
[f] Gibson *et al.*, reference 8.
[g] H. Wäffler and S. Younis, reference 3.

* Work supported by the AEC.
[1] Bishop, Beghian, and Halban, Phys. Rev. **83**, 1052 (1951), and references.
[2] Gibson, Green, and Livesy, Nature **160**, 534 (1947).
[3] H. Wäffler and S. Younis, Helv. Phys. Acta **22**, 414 (1949).
[4] E. G. Fuller, Phys. Rev. **79**, 303 (1950).
[5] Phillips, Lawson, and Kruger, Phys. Rev. **80**, 326 (1950).
[6] P. V. C. Hough, Phys. Rev. **80**, 1069 (1950).
[7] G. Goldhaber, Phys. Rev. **81**, 930 (1951).
[8] Gibson, Grotdal, Orlin, and Trumpy, Phil. Mag. **42**, 555 (1951).
[9] J. F. Marshall and E. Guth, Phys. Rev. **78**, 738 (1950).

microscope included the standard determination of the orientation and sense of the tracks in space by measurement of the track depth normal to the plane of the emulsion and of the projections in the plane of the emulsion of the track length and angle from the gamma-ray beam. In addition, the distances between the track ends and the emulsion surfaces were measured and used to eliminate tracks which escaped or nearly escaped from the emulsion. Tracks were accepted for analysis if they had less than an arbitrary 45° dip in the wet emulsion and both ends cleared the surfaces of the processed plate by at least 7μ.

The total shrinkage factor varied from 5.7 to 7.0 depending on the water content of the plates. This factor was obtained by measuring the ordinary processing shrinkage factor and the way in which volumes of emulsion and water added. These measurements gave $S=2.4\pm0.1$ for the processing shrinkage factor and $P=1.00\pm0.06$ for the ratio of the swelling of the emulsion to the volume of water absorbed. The values of S and P obtained for each batch of plates were used in the calculations for all plates of the batch, the volume of water in each plate being determined by weighings. In addition, determination of the total shrinkage requires a knowledge of the amount of water absorbed by the gelatin base of the NTB plates (see reference 7). The thicknesses of the gelatin bases were determined by subtracting the processed emulsion thicknesses measured with a microscope from the total gelatin thicknesses measured with a micrometer. The total shrinkage factors used depend upon the assumption that the gelatin in the emulsion and the gelatin in the base absorb water in the ratio of their volumes. The error in the parameter a/b resulting from a possible 8 percent systematic error in the shrinkage factors has been calculated and a consequent uncertainty of ±0.02 has been included in our results for a/b listed in Table II.

III. CALCULATION

(A) Range *vs* Energy

Proton range-energy curves were obtained from calculations based on the experimental range-energy curves of Lattes *et al.*[10] for dry plates and the curves calculated by Aron *et al.*[11] for hydrogen and oxygen. Our results are given in Table III from which intermediate curves can be obtained by interpolation. The table gives ranges for various energies and several values of R_w, the volume of water in the emulsion divided by the sum of the water and emulsion volumes. In these calculations it was assumed that $P=1$ and that the stopping power and hence the density of the plates used would be the same as for those used by Lattes *et al.*

If the factor P is found to be different from unity or our measurement of the emulsion density differs from the 3.9 g/cm³ of the Ilford plates used by Lattes *et al.*, we correct the volume of emulsion used to calculate R_w and the ranges of the table assuming that the range-energy curves for the dry emulsions differ only by a constant factor multiplying the ranges. The measured densities of the plates used were in the range 3.5 ± 0.15 g/cm³.

Our reason for dealing with the relative volume R_w is that the results are sufficiently accurate for use with either heavy or ordinary water.

TABLE II. Results of this paper. In combining the results over energy intervals the isotropy coefficient obtained from 11 to 13 Mev has been combined separately, as it differs from the results at lower energies by more than the experimental error.

Energy (Mev)	Isotropy coefficient a/b	Forward asymmetry coefficient c/b
5–6	0.10 ± 0.06	···
6–7	0.04 ± 0.05	···
7–8	0.06 ± 0.05	···
8–9	-0.03 ± 0.06	0.26 ± 0.15
9–10	0.08 ± 0.07	0.24 ± 0.18
10–11	0.03 ± 0.07	0.31 ± 0.19
11–12	0.20 ± 0.08	0.09 ± 0.22
12–13	0.30 ± 0.11	-0.08 ± 0.29
5–11	0.04 ± 0.03	···
11–13	0.24 ± 0.07	···
8–13	···	0.24 ± 0.09

(B) Corrections

The fraction of the tracks that are retained (i.e., satisfy the criteria for acceptance given in Part II) is a function of θ and the ratio of the track length to the wet emulsion thickness considered, L/t (the layers near the surface of the emulsion not being considered). The values of θ and L/t were determined for each track studied and weights equal to the reciprocal of the probability of the track being retained were assigned to each track. This weighting factor, w, is given below for the three possible cases.

Case I. $t/L\geq\sin\theta\leq\sin45°$

$$\frac{1}{w}=1-\frac{2L}{\pi t}\sin\theta.$$

Case II. $\sin\theta\geq\sin45°\leq t/L$

$$\frac{1}{w}=\frac{2}{\pi}\left\{\sin^{-1}\left(\frac{\sin45°}{\sin\theta}\right)-\frac{L}{t}\left[\sin\theta-(\sin^2\theta-\sin^245°)^{\frac{1}{2}}\right]\right\}.$$

Case III. $\sin\theta\geq t/L\leq\sin45°$

$$\frac{1}{w}=\frac{2}{\pi}\left\{\sin^{-1}\left(\frac{t}{L\sin\theta}\right)-\frac{L}{t}\left[\sin\theta-\left(\sin^2\theta-\frac{t^2}{L^2}\right)^{\frac{1}{2}}\right]\right\}.$$

These weightings take account of our rejection of tracks with dip greater than 45° as well as loses from the emulsion.

[10] Lattes, Fowler, and Cuer, Proc. Phys. Soc. (London) **59**, 889 (1947).

[11] Aron, Hoffman, and Williams, University of California Radiation Laboratory—121 (1949).

(C) Determination of Parameters

Gamma-ray energies were obtained for each track from plots in terms of proton energy and space angle, θ, in the laboratory. The laboratory angles, θ, corresponding to 15° intervals of θ_{cm} in the center-of-mass system were calculated for each one-Mev interval in gamma-ray energy. The tracks were then grouped into one-Mev intervals of gamma-ray energy and 15° intervals of θ_{cm}. As values of θ were recorded to the nearest degree tracks with values of θ near one of the boundaries were divided between the intervals. For instance, if for a particular energy interval $\theta_{cm}=15°$ when $\theta=14°\ 15'$, one quarter of the tracks with $\theta=14°$ were assigned to the 15–30° interval in θ_{cm}.

The sum of the weights of the tracks in each interval minus the corresponding background was called the corrected number of tracks, Ni, in the interval. Assuming that the differential cross section is of the form indicated in the introduction the number of tracks to be expected in the ith θ_{cm} interval is $aA_i+bB_i+cC_i$ where

$$A_i=2\pi\int_{\theta_i}^{\theta_{i+1}}\sin\theta d\theta,\quad B_i=2\pi\int_{\theta_i}^{\theta_{i+1}}\sin^3\theta d\theta,$$

$$C_i=2\pi\int_{\theta_i}^{\theta_{i+1}}\sin^3\theta\cos\theta d\theta$$

with $\theta_i=0,\ 15,\ 30°$—etc.

The experimental values of a, b, and c were found for each energy interval by the method of least squares which requires that

$$\sum_{i=1}^{n}W_i(N_i-aA_i-bB_i-cC_i)^2$$

be a minimum. W_i is a weighting factor which varies inversely as the square of the probable error.

The foregoing method of correcting the data and obtaining the desired parameters avoids the use of average weighting factors and solid angle corrections for the relatively large intervals in θ. This is an advantage as the correct averages for such quantities depend upon the parameters one is measuring. For instance, in one alternative method of analysis the average solid angle for each interval of θ is divided into the data and an average weighting is used to correct for the loses from the emulsion in each interval. The corrected results are then plotted against an average value of $\sin^2\theta$. A straight line is obtained and the isotropy coefficient a/b appears as the negative intercept on the $\sin^2\theta$ axis. Each of the three quantities for which averages are required is a function of $\sin\theta$ so that the correct averages depend upon the parameters in the distribution function.

TABLE III. Calculated proton ranges for various values of R_w, assuming that $P=1$ and the range-energy curves for dry plates is identical with the determination of Lattes *et al.*

Proton energy (Mev)	R_w 0.5	0.6	0.65	0.7	0.75
1	17μ	18μ	18μ	19μ	19μ
2	50	53	54	56	58
3	97	102	105	109	113
4	157	167	173	180	187
5	231	247	255	265	276
6	316	338	350	364	379
7	412	441	457	476	495
8	520	555	575	600	625
9	635	685	710	740	770
10	765	820	855	890	930
11	905	970	1010	1050	1095
12	1050	1130	1175	1225	1280
13	1210	1300	1350	1410	1470
14	1380	1490	1550	1620	1690

(D) Errors and Correction for Uncertainty in Sense

The effect of various errors on the final results has been obtained by numerical calculations, except for the standard statistical error for which we obtain the formulas

$$\Delta(a/b)=\pm0.9n^{-\frac{1}{2}},\quad \Delta(c/b)=\pm2.2n^{-\frac{1}{2}}$$

for large values of the total uncorrected count, n. The effect of an error in the shrinkage factor on the result for (a/b) has been mentioned. Uncertainty in the sense of the tracks results in too low a result for c/b as a part of the forward asymmetry is not observed. This uncertainty was estimated from the opinions of observers who graded about a third of the tracks on an A, B, C, D basis and from the number of disagreements arising when two observers studied the same tracks. We estimate that for gamma-rays above 8 Mev the sense is correct in about 95 percent of the data. This corresponds to our missing 10 percent of the forward asymmetry including that between the laboratory and center-of-mass systems. Hence, 0.05 ± 0.03 has been added to our results for c/b. The uncertainty in sense rises rapidly as one proceeds to the shorter tracks and reliable values for c/b were not obtained below 8 Mev.

Several effects which might be expected to result in too large a value of a/b have been considered and found to contribute negligibly compared to the errors already mentioned. These were the 2° grazing incidence of the beam, variations in gamma-ray direction from the direction at the center of the plate, and random errors of $\pm1.5°$ in measuring θ.

Checks on the results from different observers and plates were found to agree within the statistical error.

(E) Azimuthal Distribution

The azimuthal distribution was calculated and tabulated from the data for 15° intervals of θ_{lab} and four energy intervals. The results were consistent within the statistical errors, and have been combined for presen-

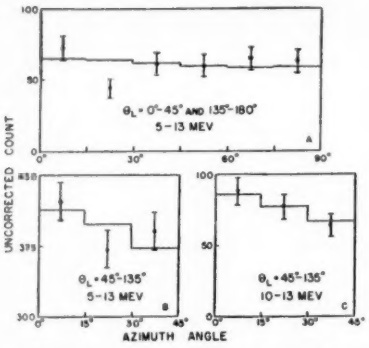

FIG. 1. Observed azimuthal distributions compared to distributions represented by solid histograms calculated for uniform azimuthal distributions altered by losses from the emulsions.

tation in Fig. 1 (A, B). Figure 1 (C) shows the energies and angles for which losses from the emulsion were largest. For $135°>\theta>45°$ and $\varphi>45°$ there are a few tracks, but the calculation was not carried out.

IV. RESULTS AND COMPARISON

The values obtained for a/b and c/b after correction of the latter for the uncertainty in track sense are presented in Table II. In Fig. 2 the folded histograms for 5–11 and 11–13 Mev are compared with the histograms calculated from the experimental values of a and b; while Fig. 3 shows the results from 8–13 Mev using the experimental values of a, b, and c (the correction of c/b does not affect this figure).

The results of other workers in the 4–20-Mev range are given in Table I. We have taken the results for the isotropy coefficient from Fuller's graphs rather than his conclusion in which he combined his results at 5 and 7 Mev to obtain $a/b\sim0.05$ and regarded the results at 9 and 11 Mev as an indication that a/b was near zero.

Theoretical calculations of Marshall and Guth, in which they neglect the possible effects of meson exchange currents and tensor forces, predict no appreciable contribution to the a/b term in the energy region 5 to 20 Mev other than the magnetic dipole contribution. The latter amounts to approximately two percent of the 90° cross section. The same calculations predict that the forward asymmetry coefficient, c/b, should rise from 0.12 at 6 Mev to 0.25 at 17 Mev. Details of the potentials used in the calculations result in differences of the parameters which are small compared to the errors arising in the angular distribution measurements which have been performed in this energy interval.

In the energy region around 7 Mev the experimental observations of the isotropy coefficient are in general agreement with values quoted above with the possible exception of Goldhaber's. Using the D_2O-loaded plate technique the determination of the forward asymmetry is inherently difficult in this energy range because of the large uncertainty in the direction sense of the low energy proton tracks. Fuller[4] has, however, observed a forward asymmetry which agrees with the theory within the experimental error.

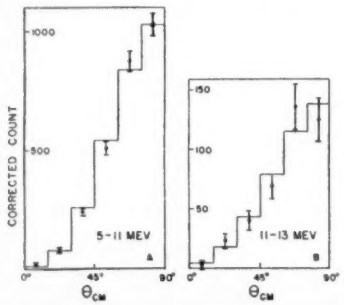

FIG. 2. Experimental angular distributions folded about 90° and compared with the solid histograms calculated from the distribution function using the empirical values of a and b.

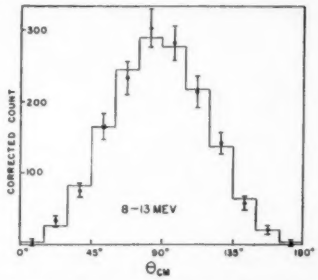

FIG. 3. Angular distribution found in the energy interval where a measure of the forward asymmetry was obtained. The solid histogram was calculated from the distribution function using the experimental values of a, b, and c prior to the correction of c/b for the uncertainty in track sense.

At higher energies the present work indicates a value for a/b of 0.24 ± 0.07 in the energy range 11 to 13 Mev as opposed to Fuller's value at zero in this range. His values, however, start at -0.12 at 9 Mev rising rapidly to 0.22 at 17 Mev. Other values of a/b given for 17.6 Mev are handicapped by large errors due to high background[3] or poor geometry.[6] The background tracks in the present work due to (γ,p) processes or knock-on protons constitute only eleven percent of the usable tracks in this energy region. The forward asymmetry parameter as given by this work is of the right order of magnitude but is subject to a large error. The large experimental error in this parameter, however, has no effect per se in the determination of the value of a/b.

Two papers on similar experiments[10,11] have appeared

[10] K. Phillips, Phil. Mag. **43**, 129 (1952).
[11] H. Wäffler and S. Younis, Helv. Phys. Acta **24**, 483 (1951).

in the literature since the present paper was submitted. The results quoted lead to values of c/b in agreement with the calculations of Marshall and Guth,[9] while the values reported for a/b suggest that this coefficient rises about 0.06 at 6 Mev to 0.14 at 15 Mev. These results are reasonably consistent with those reported here.

We are indebted to Mr. Herbert C. Field for his aid in searching and measuring plates and to Mr. William Voelker and Mr. J. W. Chastain of the Case betatron crew, and Professor E. C. Gregg, Jr., for their aid in obtaining the plate exposures. We are also indebted to Professor L. L. Foldy for suggestions on the treatment of the data and helpful discussions of the problem.

PHYSICAL REVIEW VOLUME 86, NUMBER 3 MAY 1, 1952

Covariant Theory of Radiation Damping

JEAN PIRENNE*
National Research Council, Ottawa, Canada
(Received November 19, 1951)

Schwinger's expression of the S matrix in the Cayley form, in terms of a Hermitian operator K, is shown to be identical with the previous noncovariant expression used in Heitler's theory of radiation damping. The comparison of the two formalisms leads, furthermore, to a clear understanding of mass renormalization which is necessary for internal consistency, quite independently of the eventual removal of divergences. For the computation of $\bar{K}$ in a covariant way, new formulas generalizing and connecting Gupta's and Fukuda and Miyazima's results are presented. The nth order approximations of $\bar{K}$ and S are closely related, and $\bar{K}_n$ may be expressed in terms of the S_p of order $p \leqq n$ or in terms of their anti-Hermitian parts only.

1. THE TWO FORMS OF THE S MATRIX

THE solution of the Schrödinger equation in the interaction representation

$$i\delta\Psi[\sigma]/\delta\sigma(x)=H(x)\Psi[\sigma] \tag{1}$$

by means of the usual perturbation method leads to the collision S matrix

$$S=1+\sum_{n=1}^{\infty} S_n, \tag{2}$$

with[1]

$$S_n=(-i)^n\int_{-\infty}^{+\infty}\cdots\int_{-\infty}^{+\infty} H(x_1)\theta^+(\sigma_1,\sigma_2)H(x_2)\times\theta^+(\sigma_2,\sigma_3)\cdots H(x_n)dx_1\cdots dx_n, \tag{3}$$

where

$$\theta^+(\sigma_1,\sigma_2)=\begin{cases}1 \text{ if } \sigma_1 \text{ is after } \sigma_2\\ 0 \text{ if } \sigma_1 \text{ is before } \sigma_2.\end{cases} \tag{4}$$

This expression of S has been extensively used because the presence of θ^+ functions alone, which are closely related to the principle of causality, leads very simply to the causal D^c functions of Stueckelberg and Feynman enabling a simple computation of (3) to be made by means of the Feynman rules.

However, even if all the S_n have been made convergent by a suitable regularization, it is not known whether the series (2) is always convergent, although it has a certain similarity with the development of an exponential, as was pointed out by Heisenberg.[2]

In any case, for large values of the coupling constant as in meson theories the convergence is presumably slow, and it is more indicative to write the unitary S matrix in the Cayley form

$$S=(1-\tfrac{1}{2}i\bar{K})/(1+\tfrac{1}{2}i\bar{K}), \tag{5}$$

which is closely connected with the effect of radiation damping. For the computation of transition probabilities one usually makes use of the alternative form

$$S=1-i\bar{R}, \tag{6}$$

which is equivalent to (5), provided $\bar{R}$ is deduced from the Heitler integral equation[3]

$$\bar{R}=\bar{K}-\tfrac{1}{2}i\bar{K}\cdot\bar{R}. \tag{7}$$

The scattering cross sections are then proportional to the square of the modulus of the corresponding matrix elements of $\bar{R}$.

The Hermitian operator $\bar{K}$ can be easily obtained as a series

$$\bar{K}=\sum_{n=1}^{\infty}\bar{K}_n \tag{8}$$

by a suitable perturbation method. According to Schwinger,[4]

$$\bar{K}_n=\left(-\frac{i}{2}\right)^{n-1}\int_{-\infty}^{+\infty}\cdots\int_{-\infty}^{+\infty} H(x_1)\epsilon(\sigma_1,\sigma_2)H(x_2)\times\epsilon(\sigma_2,\sigma_3)\cdots H(x_n)dx_1\cdots dx_n, \tag{9}$$

* National Research Laboratories Postdoctoral Fellow.

[1] F. J. Dyson, Phys. Rev. **75**, 486 (1949); D. Rivier, Helv Phys. Acta **22**, 965 (1949); A. Houriet and A. Kind, Helv. Phys. Acta **22**, 319 (1949).

[2] W. Heisenberg, Z. Naturforsch. **A5**, 251 (1950).

[3] W. Heitler, Proc. Cambridge Phil. Soc. **37**, 291 (1941).

[4] J. Schwinger, Phys. Rev. **74**, 439 (1948).

with

$$\epsilon(\sigma_1,\sigma_2)=\begin{cases}+1 \text{ if } \sigma_1 \text{ is after } \sigma_2\\ -1 \text{ if } \sigma_1 \text{ is before } \sigma_2.\end{cases} \tag{10}$$

Before the development of the present covariant formalism Pauli[8] gave the formula

$$(k|\bar{K}_n|0)=2\pi\delta(E_0-E_k)\times\sum_P\frac{(k|H|l)(l|H|m)\cdots(s|H|0)}{(E_0-E_l)\cdots(E_0-E_s)}, \tag{11}$$

where P indicates that the principal value must be used in integrating over the energy.

2. EQUIVALENCE OF THE OLD AND NEW FORMALISMS

The identity of Eqs. (9) and (11), which is not generally explicitly recognized, is immediately checked by means of the relation

$$\int_{-\infty}^{+\infty}\epsilon(t)e^{-i\omega t}dt=-\frac{2}{i}\frac{P}{\omega}, \tag{12}$$

where P means that the principal value must be taken in integrating over ω.

However, a more detailed comparison of the old and new formalism will be useful for the discussion of the mass renormalization. To derive the expression (11) of $\bar{K}_n$ in the old formalism Pauli wrote the wave function as the sum of an incident wave and an outgoing wave as follows:

$$(k|\Psi|0)=\delta_{k0}-2\pi i(k|R|0)\delta_+(E_0-E_k) \tag{13a}$$

with

$$\delta_+(\omega)=\frac{1}{2\pi}\int_0^\infty e^{i\omega t}dt=\frac{1}{2}\left\{\delta(\omega)-\frac{1}{i\pi\omega}\right\}. \tag{13b}$$

Inserting this wave function in the Schrödinger equation

$$(E-E_k)(k|\Psi|0)=\sum_l(k|H|l)(l|\Psi|0) \tag{14}$$

and assuming the energy E to be equal to the energy E_0 of the unperturbed incoming wave, one gets

$$(k|R|0)=(k|H|0)-i\pi\sum_l(k|H|l)(l|R|0)\delta(E_l-E_0)+\sum_l\frac{(k|H|l)(l|R|0)}{E_0-E_l}. \tag{15}$$

The solution of this equation by repeated substitution in the term containing the δ-function of the value of R given by the first member of (15) leads to the Heitler integral equation in the form

$$(k|R|0)=(k|K|0)-i\pi\sum_l(k|K|l)(l|R|0)\delta(E_0-E_l), \tag{16a}$$

where

$$(k|K|0)=(k|H|0)+\sum_{n=1}^{\infty}\sum_P\frac{(k|H|l)(l|H|m)\cdots(s|H|0)}{(E_0-E_l)\cdots(E_0-E_s)}. \tag{16b}$$

One finally obtains the Heitler integral equation in the form (7) by putting

$$\begin{aligned}(k|\bar{R}|0)&=2\pi\delta(E_0-E_k)(k|R|0),\\ (k|\bar{K}|0)&=2\pi\delta(E_0-E_k)(k|K|0).\end{aligned} \tag{17}$$

This straightforward derivation is easily put in covariant form by writing

$$\Psi[\sigma]=\left\{1-i\int_{-\infty}^{\sigma}R(x)dx\right\}\Psi[-\infty]. \tag{18}$$

Inserting this in the Schrödinger equation (1) we obtain

$$R(x)=H(x)-iH(x)\int_{-\infty}^{\sigma}R(x')dx', \tag{19a}$$

or by introducing the function ϵ given by (10)

$$R(x)=H(x)-\frac{i}{2}H(x)\int_{-\infty}^{+\infty}R(x')dx'-\frac{i}{2}H(x)\int_{-\infty}^{+\infty}\epsilon(\sigma,\sigma')R(x')dx'. \tag{19b}$$

Putting in the last term the value of $R(x')$ given by the first member of the same formula, we get

$$\begin{aligned}R(x)=H(x)&-\frac{i}{2}H(x)\cdot\int_{-\infty}^{+\infty}R(x')dx'\\ &-\frac{i}{2}\int_{-\infty}^{+\infty}H(x)\epsilon(\sigma,\sigma')H(x')dx'\\ &-\frac{i}{2}\int_{-\infty}^{+\infty}H(x)\epsilon(\sigma,\sigma')H(x')dx'\cdot\int_{-\infty}^{+\infty}R(x')dx'\\ &+\left(\frac{i}{2}\right)^2\int_{-\infty}^{\infty}H(x)\epsilon(\sigma,\sigma')H(x')\\ &\times\epsilon(\sigma',\sigma'')R(x'')dx'dx''.\end{aligned}$$

Inserting again in the last term the value of $R(x'')$ given by the first member of (19b) and repeating this operation indefinitely, we get the Heitler integral equation

$$R(x)=K(x)-\frac{i}{2}K(x)\int_{-\infty}^{+\infty}R(x')dx' \tag{20}$$

[8] W. Pauli, Phys. Soc. Cambridge Conference Report 5 (1947); W. Pauli, *Meson Theory* (Interscience Publishers, Inc., New York, 1948).

with

$$K(x)=H(x)+\sum\left(-\frac{i}{2}\right)^{n-1}\int_{-\infty}^{+\infty}\cdots\int_{-\infty}^{+\infty}H(x)$$
$$\times\epsilon(\sigma,\sigma')H(x')\epsilon(\sigma',\sigma'')\cdots H(x^{(n-1)})$$
$$\times dx'\cdots dx^{(n-1)}. \quad (20b)$$

This expression can be considered also as the solution, by iteration, of the integral equation

$$K(x)=H(x)-\frac{i}{2}\int_{-\infty}^{+\infty}H(x)\epsilon(\sigma,\sigma')K(x')dx'. \quad (20c)$$

Finally (20a) reduces to (7) by putting

$$\bar{R}=\int_{-\infty}^{+\infty}R(x)dx;\quad \bar{K}=\int_{-\infty}^{+\infty}K(x)dx. \quad (21)$$

The convergence condition of the series (8), representing $\bar{K}$, is no better known than that of the series (3), representing S. The two conditions might be different. If they are both fulfilled, the two developments will lead, of course, to the same unitary matrix S. However, for practical computations we have to break up one of them somewhere. In the case of series (8) this operation will not affect the hermiticity of $\bar{K}$ because each term $\bar{K}_n$ of the development is separately Hermitian, as is immediately verified by looking at formulas (9) or (11). Then the Cayley form might be more advantageous, because it is always unitary to any degree of approximation. This is no more true for the exponential-like development (3).

3. MASS RENORMALIZATION

The consistent subtraction of the self-energy in the construction of the S matrix in Cayley form, has already been treated[6,7] in the old noncovariant formulation. We remarked that the form (15) of the wave function is only consistent[8] with the picture of an incoming wave plus an outgoing wave if in $\delta_+(E_0-E_k)$ the energies of the system of "bare" particles are replaced by the actual total energies E_0' and E_k' with

$$E_k'=E_k+\Delta E_k, \quad (22)$$

ΔE_k being the contribution of the self-energies of the particles.

Moreover, in the Schrödinger equation the energy E of the system must be put equal to the perturbed energy E_0' of the incident wave. The Schrödinger equation can therefore be written in the form

$$(E_0'-E_k')(k|\Psi|0)=\sum_l(k|H'|l)(l|\Psi|0),$$

similar to the usual one, except that the perturbed energies have been substituted for the unperturbed energies and that $(k|H|l)$ has been replaced by

$$(k|H'|l)=(K|H|l)-\delta_{kl}\Delta E_k. \quad (23)$$

It was also shown that this substitution is necessary and sufficient to make $(k|R|0)$ free of singularities on the energy shell $E_k'=E_0'$, a condition which is indeed implied in the assumption that the second term of the wave function (13) describes an outgoing wave only, all the singularities being necessarily contained in the factor $\delta_+(E_0'-E_k')$. Finally, it was found that this condition of continuity is sufficient to determine completely the self-energies.

Now the substitution (23) is equivalent to the present covariant one

$$H'(x)=H(x)-\bar{\Psi}(x)\Psi(x)\delta mc^2. \quad (24)$$

If properly carried out, both should lead to the same results.

We see also now that the mass renormalization is not merely introduced, as is often believed, in order to subtract infinities and to obtain in this way finite physical results. In fact, it should still be performed, if the self-energies were made finite, but different from zero, as would be the case, for instance, in the nonrelativistic theory of extended particles. The actual mass renormalization is, therefore, only unsatisfactory because the self-energies are infinite and are nevertheless treated as small.

4. COVARIANT CALCULATION OF K

As S_n can be easily evaluated in a covariant way by means of the Feynman rules, it will be sufficient to show how to derive $\bar{K}_n$ from the $S_{n'}$.

To do this let us insert

$$\epsilon(x)=2\theta^+(x)-1 \quad (25)$$

in the expression (9) of $\bar{K}_n$. We get

$$-i\bar{K}_n=(-i)^n\int_{-\infty}^{+\infty}\cdots\int_{-\infty}^{+\infty}H(x_1)\{\theta^+(\sigma_1,\sigma_2)-\tfrac{1}{2}\}$$
$$\times H(x_2)\{\theta+(\sigma_2,\sigma_3)-\tfrac{1}{2}\}\cdots H(x_n)dx_1\cdots dx_n. \quad (26)$$

The term containing all the θ^+ is obviously identical with the expression (3) of S_n. Another term, containing r factors $\frac{1}{2}$, is easily identified by means of the same Eq. (3) with a product of r factors S_p or lower order, $S_{p_1}\cdots S_{p_r}$, with $p_1+p_2+\cdots+p_r=n$. We so obtain the general formula

$$-i\bar{K}_n=S_n-\tfrac{1}{2}\sum_{p=1}^{n-1}S_{n-p}S_p$$
$$+\tfrac{1}{4}\sum_{p=1}^{n-1}\sum_{q=1}^{p-1}S_{n-p}S_{p-q}S_q-\cdots, \quad (27)$$

which is for $n=1, 2, 3, 4$, identical with the particular expressions given by Gupta.[9]

[6] J. Pirenne, Helv. Phys. Acta **21**, 226 (1948).
[7] W. Heitler and S. T. Ma, Phil. Mag. **40**, 651 (1949).
[8] Heitler and Ma (see reference 7) start from analogous arguments of self-consistency but their treatment is somewhat different.
[9] S. N. Gupta, Proc. Cambridge Phil. Soc. **47**, 454 (1951).

Another useful general formula can be obtained by a suitable grouping of terms

$$-i\bar{K}_n=S_n-\tfrac{1}{2}\sum_{p=1}^{n-1}S_{n-p}\{S_p-\tfrac{1}{2}\sum_{q=1}^{p-1}S_{p-q}S_q+\cdots\}. \quad (28)$$

By (9) the bracket is equal to $-i\bar{K}_p$. Therefore,

$$-i\bar{K}_n=S_n+\frac{i}{2}\sum_{p=1}^{n-1}S_{n-p}\bar{K}_p. \quad (29)$$

But by a simple change of notation in the summations contained in (27) and a different grouping we can also obtain[9]

$$-i\bar{K}_n=S_n+\frac{i}{2}\sum_{p=1}^{n-1}\bar{K}_pS_{n-p}. \quad (30)$$

This is not surprising as $[S, K]=0$ and therefore

$$\sum_{p=1}^{n-1}[S_{n-p}, K_p]=0. \quad (31)$$

Taking the Hermitian conjugate of (30) and using the fact that $\bar{K}_p$ is Hermitian, we get

$$+i\bar{K}_n=S_n^{+}-\frac{i}{2}\sum_{p=1}^{n-1}S_{n-p}^{+}\bar{K}_p. \quad (30b)$$

Now let us introduce the Hermitian and anti-Hermitian parts of S_n:

$$S_n=H_n+iA_n. \quad (32)$$

By adding and subtracting (29) and (30) we find

$$-\bar{K}_n=A_n+\tfrac{1}{2}\sum_{p=1}^{n-1}H_{n-p}\bar{K}_p, \quad (33a)$$

$$0=H_n-\tfrac{1}{2}\sum_{p=1}^{n-1}A_{n-p}\bar{K}_p. \quad (33b)$$

Using now in (33a) the value of H_{n-p} given by (33b), we obtain the general formula

$$\bar{K}_n=-A_n-\tfrac{1}{2}\sum_{\substack{p>0,\ q>0\\ p+q<n-1}}A_{n-p-q}\bar{K}_p\bar{K}_q, \quad (34)$$

in which the order of the factors in the last term is, in fact, irrelevant because of (31).

This formula simplifies a great deal for low values of n. As

$$A_1=\int_{-\infty}^{+\infty}H(x)dx=0, \quad (35)$$

it follows that $\bar{K}_1=0$. Therefore, the second term of (34) will only bring a contribution if all the three indices are at least equal to 2. In other words

$$\bar{K}_n=-A_n \text{ for } n\leqq 5. \quad (36)$$

This simple rule was given without proof by Fukuda and Miyazima.[10] (34) is its generalization. For instance, for $n=6$ we have

$$\bar{K}_6=-A_6+\tfrac{1}{4}A_2^3. \quad (37)$$

In writing (35) we have implicity assumed that there is no external (static) field; if such a field exists, the Fukuda-Miyazima rule only applies for $n\leq 2$.

We have thus a rather simple way to compute $\bar{K}$ up to a certain degree of approximation p from the development of S limited to terms of the same order (which are themselves easily written down by means of the Feynman rules).

But, finally, for practical purposes we have to introduce that $\bar{K}$ into the Cayley formula (or into the Heitler integral equation) in order to obtain a certain S matrix, because it is S that we really need to compute transition probabilities.

It might therefore seem at first sight that we have not gained anything new. However, it must be realized that the S we have now obtained is unitary and constitutes, therefore, a quite different approximation from the initial nonunitary approximation of S from which $\bar{K}$ was derived. In addition to the limited number of terms considered in the initial development of S the new S will contain terms of higher order than p, arising from the successive powers of $\bar{K}$ in the development of S in terms of $\bar{K}$. These higher order terms result from the product of lower order process for each one of which the conservation laws of energy and momentum are both satisfied, as is the case for real processes. The appearance of these new terms corresponds to renormalization of the probability amplitudes of these low order real processes, which are really the only ones considered in the chosen approximation. This renormalization is an improvement which is the more necessary, the larger the transition probabilities.

The author wishes to thank Dr. T. Y. Wu, Dr. D. Rivier, and Dr. S. T. Ma for valuable discussions and the National Research Council of Canada for its support and hospitality.

[10] N. Fukuda and T. Miyazima, Prog. Theoret. Phys. **5**, 849 (1950).

Neutron-Proton Scattering with Spin-Orbit Coupling. I. General Expressions

JOHN M. BLATT, *University of Illinois, Urbana, Illinois*

AND

L. C. BIEDENHARN, *Oak Ridge National Laboratory, Oak Ridge, Tennessee*

(Received January 23, 1952)

Neutron-proton scattering in the triplet spin state is discussed under the following assumptions about the nuclear forces: (1) the forces are conservative, (2) they allow time-reversal, i.e., the reciprocity law is valid, (3) the spin vectors of the neutron and proton enter in a symmetrical way, so that the total spin of of the system is preserved during the collision, and (4) the forces have a finite range. We do not assume that the forces can be derived from a potential function (i.e., that they are velocity-independent).

General expressions are given for the scattering matrix and for the differential cross section. The matrix elements of the scattering matrix are expressed in terms of the minimum numbers of real, independent parameters. The energy dependence of these parameters near zero energy can be predicted uniquely on the basis of assumptions (1) to (4) above.

1. INTRODUCTION

THE analysis of neutron-proton scattering in the presence of spin-orbit coupling (e.g., the tensor force) is appreciably more involved than the analysis of the scattering in the absence of such coupling. There is considerable literature on this subject.[1] The purpose of the present paper is to give a general formula for the cross section in terms of the minimum number of independent real parameters and to discuss the behavior of these parameters near zero energy. We are preparing for publication a paper on low energy neutron-proton scattering with tensor forces, employing the effective range theory and giving numerical values of the relevant parameters for some representative choices of the nuclear force law. The general (but rather formal) results obtained in the present paper will be made use of in the subsequent paper.

We shall assume throughout that there are no transitions from the singlet to the triplet spin state of the neutron-proton system or vice versa. This is of course only an assumption. There is no absolute selection rule which would forbid a transition such as $^1P_1$ to $^3P_1$. However, if the spin vectors of neutron and proton enter symmetrically into the basic law of force, then such transitions would be excluded by the conservation of the spin symmetry character. In view of the unexpected difference between neutron-proton and proton-proton scattering at high energies, it is perhaps worth while to remark that transitions between the two spin states can occur in the neutron-proton scattering but are absolutely forbidden in proton-proton scattering due to the Pauli principle (e.g., in the transition cited above, the $^1P_1$ state is forbidden for two protons).

If we neglect the possibility of such transitions, we can treat scattering in the two spin states independently. The singlet state scattering presents no difficulties since spin-orbit coupling is impossible in that state. We shall restrict ourselves to scattering in the triplet state from here on, and all formulas will refer to pure triplet state scattering. Thus they must be multiplied by the statistical factor $\frac{3}{4}$, and the singlet contribution must be added before any comparison is made with experiment.

In this paper we shall use only those arguments which are independent of the details of the force law (e.g., whether or not the force is velocity-dependent). The results are correspondingly both general and formal. Specific numerical results can be obtained only by making more definite assumptions about the neutron-proton force. Such results are deferred to a second paper, now in preparation.

2. THE SCATTERING MATRIX AND ITS EIGENSTATES

Following Rarita and Schwinger, we classify the triplet states of the neutron-proton system according to their total angular momentum J and parity Π. Instead of the actual parity $\Pi=(-)^l$ it is useful to introduce the quantum number

$$\pi=(-1)^J\Pi. \tag{2.1}$$

$\pi=+1$ if $\Pi=(-)^J$, and $\pi=-1$ if $\Pi=-(-)^J$. For each value of J, except $J=0$, there are three possible values of the orbital angular momentum l, namely $l=J$, $l=J+1$, $l=J-1$. The first of these corresponds to $\pi=1$, the last two to $\pi=-1$. If we denote by N the number of different "channels" (choices of l) consistent with a given J and π, we get

$$N=1 \quad \text{for} \quad \pi=+1,$$
$$N=2 \quad \text{for} \quad \pi=-1, \quad (\text{except } J=0,\ \pi=-1). \tag{2.2}$$

The exceptional $^3P_0$ state is a single-channel state even though it has $\pi=-1$.

The spin and angle dependence of a wave function with total angular momentum J, z component thereof

[1] J. W. Rarita and J. Schwinger, Phys. Rev. **59**, 436, 556 (1941); C. Kittel and G. Breit, Phys. Rev. **56**, 744 (1939); J. M. Jauch, Phys. Rev. **67**, 125 (1945); F. Rohrlich and J. Eisenstein, Phys. Rev. **75**, 705 (1949); J. Ashkin and T. Y. Wu, Phys. Rev. **73**, 973 (1948); Massey, Burhop, and Hu, Phys. Rev. **73**, 1402 (1948); E. H. S. Burhop and H. N. Yadav, Proc. Roy. Soc. (London) **A197**, 505 (1949); W. Hepner and R. Peierls, Proc. Roy. Soc. (London) **A44**, 712 (1951); S. A. Kushneriuk and M. A. Preston, Proc. Phys. Soc. (London) **A44**, 712 (1951).

equal to M, orbital angular momentum l, and spin angular momentum s ($s=1$ for triplet states) is given by

$$\mathcal{Y}_{Jl}{}^{M}(\theta,\phi,\sigma)=\sum_{m_l+m_s=M}(lsm_l m_s|lsJM)\times Y_{lm_l}(\theta,\phi)\,\chi_{sm_s}(\sigma), \quad (2.3)$$

where $(lsm_l m_s|lsJM)$ is a Clebsch-Gordon coefficient in the notation of Condon and Shortley,[2] the Y's are spherical harmonics defined as in Condon and Shortley, and χ_{sm_s} is a spin function for spin s and z component of the spin equal to m_s.

Now consider a typical single-channel state with $\pi=+1$ and hence $l=J$. The wave function for this state can be written in the form

$$\psi=r^{-1}v_J(r)\mathcal{Y}_{JJ1}{}^{M}(\theta,\phi,\sigma). \quad (2.4)$$

No other state can be "mixed in" because of the selection rules. The radial function $v_J(r)$ has a complicated behavior as long as r is less than the range of the forces. For large values of r, however, $v_J(r)$ can be written as a linear superposition of an ingoing and an outgoing wave

$$v_J(r)=A\exp[-i(kr-\tfrac{1}{2}J\pi)]-B\exp[+i(kr-\tfrac{1}{2}J\pi)]. \quad (2.5)$$

If the incoming wave has a given amplitude A, the amplitude of the outgoing wave B is determined (mathematically the ratio of B to A is determined by the condition that v be that solution of the radial wave equation which vanishes at $r=0$). The scattering matrix, which in this case becomes just an ordinary number, is defined by

$$B=SA. \quad (2.6)$$

Since in pure elastic scattering the flux of the outgoing wave is equal to that of the ingoing wave, we get $|S|^2=1$ and hence S can be written in the form

$$S=\exp(2i\delta_{J,0}), \quad (2.7)$$

where the real quantity $\delta_{J,0}$ is called the phase shift. The asymptotic behavior of $v_J(r)$ is found by substituting (2.6) and (2.7) into (2.5), giving ($C=$constant)

$$v_J(r)=C\sin(kr-\tfrac{1}{2}J\pi+\delta_{J,0}). \quad (2.8)$$

We now apply the same method to the states with $\pi=-1$, where the orbital angular momentum can assume two values, $l=J-1$ and $l=J+1$. Corresponding to these two values of l there are two radial functions. The wave function as a whole for a state with total angular momentum J and $\pi=-1$ [parity$=(-1)^{J+1}$] can be written as

$$\psi=r^{-1}u_J(r)\mathcal{Y}_{J,J-1,1}{}^{M}(\theta,\phi,\sigma)+r^{-1}w_J(r)\mathcal{Y}_{J,J+1,1}{}^{M}(\theta,\phi,\sigma). \quad (2.9)$$

[2] E. U. Condon and G. H. Shortley, *Theory of Atomic Spectra* (Cambridge University Press, London, 1935).

For large values of r each radial wave function is a linear superposition of an ingoing and an outgoing wave, i.e.,

$$\begin{aligned}u_J(r)&=A_1\exp\{-i[kr-\tfrac{1}{2}(J-1)\pi]\}-B_1\exp\{+i[kr-\tfrac{1}{2}(J-1)\pi]\},\\ w_J(r)&=A_2\exp\{-i[kr-\tfrac{1}{2}(J+1)\pi]\}-B_2\exp\{+i[kr-\tfrac{1}{2}(J+1)\pi]\}.\end{aligned} \quad (2.10)$$

If the amplitudes of the incoming waves (A_1 and A_2) are given, the amplitudes of the outgoing waves (B_1 and B_2) are determined by the wave equation. The scattering matrix is now a 2-by-2 matrix, defined by

$$\begin{aligned}B_1&=S_{11}A_1+S_{12}A_2,\\ B_2&=S_{21}A_1+S_{22}A_2,\end{aligned} \quad (2.11)$$

or, in matrix notation[3]

$$b=Sa. \quad (2.11a)$$

According to general theorems the scattering matrix S must be unitary (conservation of probability) and symmetric (reciprocity). The most general unitary and symmetric 2-by-2 matrix contains 3 real independent parameters and can be written in the form

$$S=U^{-1}\exp(2i\Delta)\,U, \quad (2.12)$$

where U is an orthogonal matrix depending on only one real parameter which we shall call ϵ_J or just ϵ, when the value of J is understood.

$$U=\begin{pmatrix}\cos\epsilon & \sin\epsilon\\ -\sin\epsilon & \cos\epsilon\end{pmatrix}, \quad (2.13)$$

and Δ is a diagonal matrix whose diagonal elements are real and are the "eigen-phaseshifts" for the state J, $\pi=-1$:[4]

$$\Delta=\begin{pmatrix}\delta_{J\alpha} & 0\\ 0 & \delta_{J\beta}\end{pmatrix}=\begin{pmatrix}\delta_\alpha & 0\\ 0 & \delta_\beta\end{pmatrix}. \quad (2.14)$$

These parameters have the following interpretation: We can construct an incoming wave with a ratio $A_2:A_1$ such that the outgoing wave is a mixture of the two states $l=J-1$ and $l=J+1$ in the same proportion, i.e., such that $B_2:B_1=A_2:A_1$. Such a state is an eigenstate of the scattering matrix, in the sense that the scattering matrix produces merely a change of the phase of the outgoing wave with respect to that of the incoming wave, without admixing new states. There are two such eigenstates, which we shall call α and β, given by

$$A_{2\alpha}/A_{1\alpha}=\tan\epsilon, \quad A_{2\beta}/A_{1\beta}=-\cot\epsilon. \quad (2.15)$$

The equations connecting the amplitudes of the outgoing waves to those of the incoming waves then are

$$B_{1\alpha}=\exp(2i\delta_\alpha)\,A_{1\alpha}, \quad B_{1\beta}=\exp(2i\delta_\beta)\,A_{1\beta}. \quad (2.16)$$

[3] We use small letters, a, b for vectors (column matrices) and capital letters S, U, etc., for linear operators (square matrices).

[4] The use of the eigenstates of the scattering matrix is due to J. Schwinger (unpublished lectures, Harvard, 1947).

In each case B_2 is determined by (2.15) coupled with the condition that the ratio B_2/B_1 is identical with A_2/A_1.

It hardly needs to be emphasized that the eigenphaseshifts δ_α and δ_β are not to be thought of as phaseshifts for the states $l=J-1$ and $l=J+1$, respectively. There are no such phaseshifts, since neither of these two states is an eigenstate of the scattering matrix. The "mixture parameter" ϵ which determines the "correct" mixtures of these two states is an essential parameter in the scattering matrix and enters explicitly into the differential cross section.

It remains to identify the parameters δ_α, δ_β, and ϵ, which enter into the scattering matrix, in terms of the behavior of the radial wave functions $u_J(r)$ and $w_J(r)$ for large values of r. We substitute (2.15) and (2.16) into (2.10) and get, apart from constant factors,

$$\begin{aligned} u_{J\alpha}(r) &= \cos(\epsilon_J)\,\sin[kr-\tfrac{1}{2}(J-1)\pi+\delta_{J\alpha}], \\ w_{J\alpha}(r) &= \sin(\epsilon_J)\,\sin[kr-\tfrac{1}{2}(J+1)\pi+\delta_{J\alpha}], \end{aligned} \tag{2.17}$$

and

$$\begin{aligned} u_{J\beta}(r) &= -\sin(\epsilon_J)\,\sin[kr-\tfrac{1}{2}(J-1)\pi+\delta_{J\beta}], \\ w_{J\beta}(r) &= \cos(\epsilon_J)\,\sin[kr-\tfrac{1}{2}(J+1)\pi+\delta_{J\beta}]. \end{aligned} \tag{2.18}$$

Equations (2.17) and (2.18) show that the radial wave functions for the eigenstates of the scattering matrix are distinguished by having the same phaseshift δ appearing in the asymptotic formulas for both $u_J(r)$ and $w_J(r)$.

It is apparent from (2.17) and (2.18) that there is a relation between the ratio of the amplitudes of w to u in the "α" state and in the "β" state, namely

$$(w/u)_\alpha = -(u/w)_\beta \quad (\text{for } r\to\infty). \tag{2.19}$$

This relation is a consequence of (2.15) and is an expression of the fact that the eigenvectors of a unitary matrix (such as the scattering matrix S) are orthogonal to each other. The orthogonality relation reads

$$A_{1\alpha}{}^* A_{1\beta} + A_{2\alpha}{}^* A_{2\beta} = 0. \tag{2.20}$$

Equation (2.19) follows from (2.20) together with the additional observation that the eigenvectors are real; the latter observation follows from the reciprocity law (from the time reversal symmetry). We emphasize that these considerations do not depend on the particular force law (e.g., on the assumption that the force can be written as the gradient of a potential function), even though the usual proof depends on such assumptions.[5]

Finally, we observe that there is the following ambiguity inherent in the developments so far: There are two eigenstates of the scattering matrix, but so far no prescription has been given for calling one of them the "α" state and the other the "β" state. Indeed, all formulas so far are invariant under the interchange of δ_α and δ_β, provided that ϵ is simultaneously changed into $\epsilon'=\epsilon+\frac{1}{2}\pi$. We can make the assignments α and β unique in the following way: In the limit as the collision energy approaches zero, the difference between the centrifugal barrier effects for $l=J-1$ and $l=J+1$ is so pronounced that these two states become eigenstates. According to (2.17) and (2.18) this means that ϵ approaches either 0 or $\frac{1}{2}\pi$ in that limit. We now define the assignments α and β so that in that limit the α-wave corresponds to the state $l=J-1$ and the β-wave to the state $l=J+1$. That is, we require

$$\lim_{E\to 0} \epsilon_J = 0 \quad (\text{every } J). \tag{2.21}$$

Near zero energy the α-wave is then predominantly $l=J-1$, the β-wave is predominantly $l=J+1$. Of course, this is true only fairly close to zero energy, since ϵ_J is in general quite energy-dependent.

In addition to the above ambiguity which is now taken care of, there is the usual ambiguity inherent in all phaseshifts which is that we can add any integral multiple of π to δ_α or δ_β or both, as well as to ϵ, without changing the scattering matrix.

Finally, we have to include the exceptional ${}^3P_0$ state ($J=0$, $\pi=-1$) into the formalism. This can be done most simply by including it with the $\pi=+1$ states, since it is a one-channel state. However, for purely formal reasons involving convenience of writing the formulas later on, it is advantageous to use a somewhat different procedure. We define, for $J=0$ and $\pi=-1$,

$$\epsilon_J = \epsilon_0 \equiv 0, \quad \delta_{0\alpha} \equiv 0, \quad \delta_{0\beta} \equiv \delta({}^3P_0). \tag{2.22}$$

This is equivalent to the introduction of a formal state with $l=-1$ and associated phaseshift equal to 0. Of course, this formal state has no physical reality and drops out of the final formulas.

3. GENERAL FORMULA FOR THE CROSS SECTION

We are now in a position to write down the general formula for the differential scattering cross section for neutron-proton scattering in the triplet spin state. We use methods developed before.[6] The cross section can be written as a sum of Legendre polynomials of type

$$d\sigma = \frac{\lambda^2}{3} \sum_{L=0}^{\infty} B_L P_L(\cos\theta)\, d\Omega, \tag{3.1}$$

where B_L is given by formulas (4.25) and (4.26) of reference 6. We can simplify the appearance of the final formula somewhat by a notation which allows us to treat states of the same J but opposite parity together. We introduce an index ρ which can assume the three values $\rho=\alpha$, $\rho=\beta$, and $\rho=0$. The phaseshift δ_J is then equal to $\delta_{J\alpha}$, $\delta_{J\beta}$, and δ_{J0}, respectively. We also introduce the eigenvectors x_J corresponding to these three

[5] The usual proof employs the constancy of the Wronskian of the pair of coupled second-order differential equations for $u(r)$ and $w(r)$. We need not assume that u and w satisfy any differential equations.

[6] J. M. Blatt and L. C. Biedenharn (to be published).

values of ρ

$$x_{J\alpha}=(\cos\epsilon_J, 0, \sin\epsilon_J),$$
$$x_{J\beta}=(-\sin\epsilon_J, 0, \cos\epsilon_J), \tag{3.2}$$
$$x_{J0}=(0, 1, 0).$$

In each bracket the first symbol is the component of x_J belonging to $l=J-1$, the second is the component belonging to $l=J$, the third is the component for $l=J+1$.

We now introduce the quantity $X(J_1\rho_1J_2\rho_2, L)$ defined by

$$X(J_1\rho_1J_2\rho_2, L)=\sum_{l_1=J_1-1}^{J_1+1}\sum_{l_2=J_2-1}^{J_2+1}Z(l_1J_1l_2J_2, 1L)\times(x_{J_1\rho_1})_{l_1}(x_{J_2\rho_2})_{l_2}, \tag{3.3}$$

where the components $(x_{J\rho})_l$ are given explicitly in (3.2), and the Z coefficients for $s=1$ are tabulated in reference 6. The coefficient B_L in (3.1) is then given by

$$B_L=\sum_{J_1=0}^{\infty}\sum_{J_2=|J_1-L|}^{J_1+L}\sum_{\rho_1}\sum_{\rho_2}[X(J_1\rho_1J_2\rho_2, L)]^2\times\sin\delta_{J_1\rho_1}\sin\delta_{J_2\rho_2}\cos(\delta_{J_1\rho_1}-\delta_{J_2\rho_2}). \tag{3.4}$$

In order to illustrate the use of these formulas, we calculate explicitly the differential cross section for neutron-proton scattering in the triplet spin state at low energies. For low energies we can make the assumption that all phaseshifts vanish with the exception of the α-wave phaseshift $\delta_{1\alpha}$ associated with the ${}^3S_1+{}^3D_1$ state ($J=1$, $\pi=-1$). The β-wave phaseshift can be neglected at low energies, since the β-wave is a mixture of ${}^3S$ and ${}^3D$ with a predominant ${}^3D$ component, and we shall show in Sec. 4 that $\delta_{1\beta}$ behaves like a typical D wave phaseshift as far as its dependence on energy is concerned. Thus there are only two parameters necessary to describe the scattering, the phaseshift $\delta_{1\alpha}$ and the mixture parameter ϵ_1.[7] Equation (3.4) then becomes

$$B_L=[X(1\alpha1\alpha, L)]^2\sin^2(\delta_{1\alpha}). \tag{3.5}$$

We now use the tables in reference 6 to compute the relevant values of X

$$X(1\alpha1\alpha, 0)=\sqrt{3}(\cos^2\epsilon_1+\sin^2\epsilon_1)=\sqrt{3}, \tag{3.6}$$

$$X(1\alpha1\alpha, 2)=0\times\cos^2\epsilon_1+\sqrt{3}\cos\epsilon_1\sin\epsilon_1+\sqrt{3}\sin\epsilon_1\cos\epsilon_1+\sqrt{\tfrac{3}{2}}\sin^2\epsilon_1=\sqrt{3}\sin\epsilon_1(2\cos\epsilon_1+2^{-\frac{1}{2}}\sin\epsilon_1). \tag{3.7}$$

All other X vanish because of selection rules for the Z coefficients. Thus we get from (3.1)

$$d\sigma=\lambda^2\sin^2(\delta_{1\alpha})[1+\sin^2\epsilon_1(2\cos\epsilon_1+2^{-\frac{1}{2}}\sin\epsilon_1)^2P_2(\cos\theta)]d\Omega. \tag{3.8}$$

We see that the α-wave scattering is not equivalent to pure S wave scattering. It reduces to pure S wave scattering only if $\epsilon_1=0$.

The first few terms of the series (3.4) have been written by Rohrlich and Eisenstein (reference 1) and also by Biedenharn.[8] The quantity ζ_J used there is equal to $\tan\epsilon_J$ in the present notation.

4. THE BEHAVIOR OF THE SCATTERING MATRIX NEAR ZERO ENERGY

We now investigate the behavior of the parameters entering the scattering matrix (the phaseshifts $\delta_{J\alpha}$, $\delta_{J\beta}$, δ_{J0}, and the mixture parameter ϵ_J) at very low energies. One of the results of this section has been stated already in formula (2.21).

We shall make the assumption that the forces have a limited (even though perhaps a large) range, i.e., that there exists an inter-particle distance R such that, for $r\geqslant R$, the particles do not exert any forces on each other. We emphasize that this assumption does not mean that the forces must be derivable from a potential function. Velocity-dependent forces are permitted, provided that they have a finite range.

We use the derivative matrix of Wigner and Eisenbud.[9] Consider first the single-channel states, i.e., $\pi=+1$, $l=J$. The wave function is given by (2.4). But instead of the decomposition (2.5), we now decompose the radial wave function $v_J(r)$ in a different manner. Following Wigner and Eisenbud, we define two functions $\mathcal{S}_l(r)$ and $\mathcal{C}_l(r)$ by the requirements that both satisfy the radial equation for orbital angular momentum l in the absence of forces between the particles and furthermore that they satisfy the following boundary conditions at $r=R$:[10]

$$\mathcal{S}_l(R)=0, \qquad \mathcal{C}_l(R)=(M/2\hbar)^{\frac{1}{2}},$$
$$\mathcal{S}_l'(R)=(M/2\hbar)^{\frac{1}{2}}, \quad \mathcal{C}_l'(R)=-(l/R)(M/2\hbar)^{\frac{1}{2}}. \tag{4.1}$$

Since $\mathcal{S}_l(r)$ and $\mathcal{C}_l(r)$ both satisfy the force-free radial equation for orbital angular momentum l, both of them can be written as linear combinations of the standard

[7] Actually this argument is oversimplified. We shall derive the energy dependences of all the relevant parameters in Sec. 4 of this paper. When these energy dependences are substituted into the formula for the cross section at low energies, it can be seen that the approximations made here (neglecting all parameters other than $\delta_{1\alpha}$ and ϵ_1) are not really consistent, i.e., there are other terms in the cross section which are of the same order, or even lower order, in the energy than the terms we have kept in (3.8). Some of these other terms are connected with scattering in the P state ($l=1$); the present experimental data indicate that the P state scattering is very much smaller than expected and may even be altogether absent. However, the interference terms between the α-wave and the β-wave, as well as the interference terms between the α-wave and other waves involving D states, are of the same order in the energy as the angle-dependent term in (3.8), and they should be taken into account. Thus (3.8) should be considered an illustrative example rather than a consistent approximation formula.

[8] L. C. Biedenharn, M.I.T. thesis (1949).

[9] E. P. Wigner and L. Eisenbud, Phys. Rev. **72**, 29 (1947); E. P. Wigner, Phys. Rev. **73**, 1002 (1948). The developments of this section are a straightforward application of the methods of the second reference. We give the details of the derivation merely because the simple problem discussed here allows the use of an appreciably simpler notation.

[10] These are identical with the definitions of reference 8, if one observes that the "M" of that reference is the reduced mass in the channel, i.e., in our case equal to $\frac{1}{2}M$.

regular and irregular solutions of that equation, $F_l(r)$ and $G_l(r)$, where $F_l(r)$ and $G_l(r)$ are defined by their asymptotic behavior

$$F_l(r)\cong\sin(kr-\tfrac{1}{2}l\pi),\ G_l(r)\cong\cos(kr-\tfrac{1}{2}l\pi),\ (r\to\infty). \quad (4.2)$$

Indeed, simple substitution gives the relations[11]

$$\mathcal{S}_l(r)=k^{-1}(M/2\hbar)^{\frac{1}{2}}[G_l(R)F_l(r)-F_l(R)G_l(r)], \quad (4.3)$$

$$\mathcal{C}_l(r)=k^{-1}(M/2\hbar)^{\frac{1}{2}}\{[F_l'(R)+(l/R)F_l(R)]G_l(r) -[G_l'(R)+(l/R)G_l(R)]F_l(r)\}. \quad (4.4)$$

We now write the radial function $v_J(r)$ in (2.4) as a linear combination of $\mathcal{S}_J(r)$ and $\mathcal{C}_J(r)$

$$v_J(r)=A'\mathcal{S}_J(r)+B'\mathcal{C}_J(r) \quad (4.5)$$

and define the derivative matrix (which is a simple number here) by

$$B'=\mathcal{R}A'. \quad (4.6)$$

The coefficients A' and B' in (4.5) are of course related to the coefficients A and B in (2.5), and this relation can be determined by straightforward use of Eqs. (4.2), (4.3), and (4.4). We then get a relation between the derivative matrix and the scattering matrix $S=\exp(2i\delta_{J0})$ which can be stated as follows:

$$\tan\delta_{J0}=-\frac{F_J(R)-\mathcal{R}[F_J'(R)+(J/R)F_J(R)]}{G_J(R)-\mathcal{R}[G_J'(R)+(J/R)G_J(R)]}. \quad (4.7)$$

We now use the asymptotic forms of F and G for small values of kr

$$F_l(r)\cong(kr)^{l+1}/(2l+1)!!,\qquad G_l(r)\cong(2l-1)!!/(kr)^l, \quad (\text{for } kr\ll l) \quad (4.8)$$

where $(2l+1)!!\equiv1\times3\times5\times\cdots\times(2l+1)$. In addition we use the fact that *the derivative matrix $\mathcal{R}$ approaches a constant value as the energy approaches zero.* This can be seen from the fact that the derivative matrix can be defined in terms of "interior" quantities only, i.e., in terms of a boundary value problem for the domain $0\leqslant r\leqslant R$.[9] Substitution of (4.8) into (4.7) then gives the following relation which is valid near zero energy:

$$k\cot\delta_{J0}\cong\frac{[(2J-1)!!]^2}{(kR)^{2J}[\mathcal{R}-R/(2J+1)]} \quad (\text{for } kR\ll J). \quad (4.9)$$

Thus the phaseshift δ_{J0} is, in general, proportional to k^{2J+1}, which is the usual result for scattering with orbital angular momentum $l=J$. An exception occurs when the asymptotic value of the derivative matrix $\mathcal{R}$ at zero energy is equal to $R/(2J+1)$. This corresponds to a scattering resonance at exactly zero energy. We shall ignore this possibility in the remainder of the discussion.

We now proceed to the two-channel states, $\pi=-1$, $l=J\pm1$. The wave function is given by (2.9), and we introduce the derivative matrix as before by a decomposition of the radial functions $u_J(r)$ and $w_J(r)$ in terms of $\mathcal{S}(r)$ and $\mathcal{C}(r)$

$$u_J(r)=A_1'\mathcal{S}_{J-1}(r)+B_1'\mathcal{C}_{J-1}(r),\qquad w_J(r)=A_2'\mathcal{S}_{J+1}(r)+B_2'\mathcal{C}_{J+1}(r), \quad (4.10)$$

with the relations

$$B_1'=\mathcal{R}_{11}A_1'+\mathcal{R}_{12}A_2',\qquad B_2'=\mathcal{R}_{21}A_1'+\mathcal{R}_{22}A_2'. \quad (4.11)$$

Again the constants A', B' in (4.10) are related to the constants A, B in (2.10) through (4.2) and (4.3). The derivative matrix $\mathcal{R}_{ij}$ is real and symmetric and approaches a constant matrix as the energy approaches zero. Given the derivative matrix, the computation of the scattering matrix S is a straightforward procedure; the necessary relation is given in reference 8 but can be derived here directly without trouble. We then express the scattering matrix in the form (2.12), (2.13), (2.14), and approximate the radial functions by (4.8). We omit details. The results are[12]

$$\epsilon_J\cong\frac{(kR)^2}{2J+1}\frac{\mathcal{R}_{12}}{(2J-1)\mathcal{R}_{11}-R}, \quad (4.12)$$

$$k\cot\delta_{J\alpha}\cong\frac{[(2J-3)!!]^2}{(kR)^{2J-2}}\left[\mathcal{R}_{11}-\frac{R}{2J-1}\right]^{-1}, \quad (4.13)$$

$$k\cot\delta_{J\beta}\cong\frac{[(2J+1)!!]^2}{(kR)^{2J+2}}\times\left[\mathcal{R}_{22}-\frac{R}{2J+3}-\frac{(\mathcal{R}_{12})^2}{\mathcal{R}_{11}-R/(2J-1)}\right]^{-1}. \quad (4.14)$$

These expressions, valid near zero energy, show that the mixture parameter ϵ_J vanishes near zero energy; for low energies ϵ_J is proportional to k^2, i.e., to the energy. The mixture parameter is proportional also to the off-diagonal matrix element $\mathcal{R}_{12}$ of the derivative matrix, as should be expected. The α-wave phaseshift $\delta_{J\alpha}$ is proportional to k^{2J-1}, i.e., it behaves like a phaseshift for a pure $l=J-1$ state. Similarly the β-wave phaseshift $\delta_{J\beta}$ is proportional to k^{2J+2} just like a phaseshift for a pure $l=J+1$ state. This is to be expected, of course, because the fact that $\epsilon_J\to0$ as the energy approaches zero means that the eigenstates of the scattering matrix become pure $l=J-1$ and $l=J+1$ states, respectively.

Expressions (4.12), (4.13), and (4.14) suffer from the defect that the quantity R, the radius of the "interior" region, appears explicitly. Unlike resonance reactions, in neutron-proton scattering we can hardly expect to be able to give a good physical definition of R which is

[11] We use the Wronskian relation $F_l'(r)G_l(r)-F_l(r)G_l'(r)=k$.

[12] Equation (4.12) really contains $\frac{1}{2}\tan(2\epsilon_J)$ on the left-hand side. Hence ϵ_J approaches either 0 or $\frac{1}{4}\pi$ as the energy approaches zero. We then make the choice (2.21), i.e., $\epsilon_J\to0$ and replace $\frac{1}{2}\tan(2\epsilon_J)$ by ϵ_J.

free from ambiguities; the mathematical definition of R is quite indefinite. If $R=R_1$ satisfies the conditions of the derivative matrix theory, then any $R_2>R_1$ is also an acceptable value of R. Thus we need to define parameters which are invariant under the choice of R, i.e., parameters which are directly related to the scattering matrix. We define two scattering lengths, $a_{J\alpha}$ and $a_{J\beta}$, and a parameter q_J by the following relations, valid near zero energy:

$$\epsilon_J \cong q_J k^2, \tag{4.15}$$

$$\delta_{J\alpha} \cong -(ka_{J\alpha})^{2J-1}/[(2J-1)!!]^2, \tag{4.16}$$

$$\delta_{J\beta} = -(ka_{J\beta})^{2J+3}/[(2J+3)!!]^2. \tag{4.17}$$

In the special case of $J=1$, the ${}^1S_1+{}^3D_1$ state, $a_{J\alpha}=a_{1\alpha}$ is just the usual triplet scattering length, and we shall show in a subsequent paper that the quantity q_1 is to a first approximation proportional to the quadrupole moment of the deuteron.

We now wish to determine the asymptotic forms of the radial functions $u_J(r)$ and $w_J(r)$ for the α-wave and β-wave solutions in the limit of zero energy. The asymptotic forms in question are given by (2.17) and (2.18) for values of r such that $kr \gg J$. This condition cannot be fulfilled when k approaches zero. Hence we must first rewrite these asymptotic expressions in a form valid for all $r \geq R$. Using (4.2), we get

$$\begin{aligned} u_{J\alpha}(r) &= \cos(\epsilon_J)[\cos(\delta_{J\alpha})F_{J-1}(r)+\sin(\delta_{J\alpha})G_{J-1}(r)], \\ w_{J\alpha}(r) &= \sin(\epsilon_J)[\cos(\delta_{J\alpha})F_{J+1}(r)+\sin(\delta_{J\alpha})G_{J+1}(r)]. \end{aligned} \tag{4.18}$$

This equation reduces to (2.17) for $kr \gg J$ but is valid for all $r \geq R$. We now use the asymptotic forms (4.8) which are valid for very small k (more precisely, for $kr \ll J$) together with (4.15) and (4.16). We omit a common factor $k^J/(2J-1)!!$ in both $u_{J\alpha}$ and $w_{J\alpha}$ to get the result

$$\begin{aligned} u_{J\alpha}(r) &= r^J - (a_{J\alpha})^{2J-1}/[(2J-1)r^{J-1}], \\ w_{J\alpha}(r) &= -(2J+1)q_J(a_{J\alpha})^{2J-1}/r^{J+1}. \end{aligned} \qquad (k=0, r \geq R) \tag{4.19}$$

Thus *the α-wave solution at zero energy is recognizable by the fact that $w_{J\alpha}(r)$ does not contain a component proportional to r^{J+2}*. This condition leads to an eigenvalue problem for $a_{J\alpha}$ and q_J. Fortunately, this eigenvalue problem is of a very simple type and can be solved immediately if any two linearly independent pairs of solutions (u, w) are known at zero energy. Call them (u_1, w_1) and (u_2, w_2). For $r \geq R$, they assume the form (g_1, g_2, h_1, h_2, etc., are constants)

$$\begin{aligned} u_i(r) &= g_i r^J + h_i r^{-J+1}, \\ w_i(r) &= g_i' r^{J+2} + h_i' r^{-J-1}. \end{aligned} \qquad (i=1, 2) \tag{4.20}$$

The solution (u_α, w_α) is that particular linear superposition of (u_1, w_1) and (u_2, w_2) for which the coefficient of r^J in $u(r)$ is unity and the coefficient of r^{J+2} in $w(r)$ is zero. That is

$$\begin{aligned} u_\alpha(r) &= [g_2' u_1(r) - g_1' u_2(r)]/[g_1 g_2' - g_2 g_1'], \\ w_\alpha(r) &= [g_2' w_1(r) - g_1' w_2(r)]/[g_1 g_2' - g_2 g_1']. \end{aligned} \tag{4.21}$$

By comparing (4.20) and (4.21) with (4.19), we can express the quantities $a_{J\alpha}$ and q_J in terms of the g's and h's. This illustrates the advantage of starting the numerical solution of problems of this type at some energy $E \geq 0$ ($E=0$ is most convenient practically but any non-negative E could be treated by a similar method) rather than trying to start with numerical solutions for the energy of the bound state of the deuteron.

An entirely similar development for the β-wave leads to the following expressions valid at zero energy [we have omitted a common factor $k^{J+2}/(2J+3)!!$ in both $u_{J\beta}(r)$ and $w_{J\beta}(r)$]:

$$\begin{aligned} u_{J\beta}(r) &= -(2J+1)(2J+3)q_J r^J, \\ w_{J\beta}(r) &= r^{J+2} - (a_{J\beta})^{2J+1}/[(2J+3)r^{J+1}]. \end{aligned} \qquad (k=0, r \geq R) \tag{4.22}$$

Thus *the β-wave solution at zero energy is recognizable by the fact that $u_{J\beta}(r)$ does not contain a component proportional to r^{-J+1}*. Notice that the *decreasing* (with r) component is absent in $u_{J\beta}(r)$, whereas the *increasing* component was absent in $w_{J\alpha}(r)$. Given the numerical solutions (u_1, w_1) and (u_2, w_2), we can construct the solution (u_β, w_β) by a linear superposition analogous to (4.21), namely,

$$\begin{aligned} u_\beta(r) &= [h_2 u_1(r) - h_1 u_2(r)]/[h_2 g_1' - h_1 g_2'], \\ w_\beta(r) &= [h_2 w_1(r) - h_1 w_2(r)]/[h_2 g_1' - h_1 g_2']. \end{aligned} \tag{4.23}$$

By evaluating the quantity q_J first by the use of (4.21) and (4.19), then again by the use of (4.23) and (4.22), we obtain the following identity between the coefficients in the numerical solution (4.20):

$$(g_1 h_2 - g_2 h_1)/(g_1' h_2' - g_2' h_1') = -(2J+3)/(2J-1). \tag{4.24}$$

This (Wronskian) identity serves as a useful check on the accuracy of the numerical solutions (4.20).

The Yield of F^{18} from Medium and Heavy Elements with 420-Mev Protons

LUIS MARQUEZ
Institute for Nuclear Studies, University of Chicago, Chicago 37, Illinois
(Received January 28, 1952)

The yield of F^{18} from medium and heavy elements, when bombarded with 420-Mev protons, was determined. Chemical procedures and techniques are described and the cross sections varying from 2.2×10^{-4} barn for F to 4.4×10^{-6} for Au are given. Comparisons are made of these results with those of other heavy fragments obtained under similar conditions.

INTRODUCTION

PREVIOUS work[1,2] has definitely established that Li and Be are produced with 340-Mev protons, and some cosmic-ray evidence indicates that some heavier fragments are produced likewise.[3] The purpose of this work was to study the yield of one of these heavy fragments under controlled laboratory conditions as are available in the synchrocyclotron at the University of Chicago.

F^{18} was chosen because it has a fairly energetic positron of 0.64 Mev which makes its counting simple, and it has a half-life of 112 min which is also adequate for radiochemical measurements.

The experiments were carried out at 420 Mev instead of 450 Mev which is the maximum energy available to get higher cyclotron currents, since it drops fast in this region. It corresponds to a radius of 74 inches.

TARGETS AND CHEMICAL PROCEDURES

The elements bombarded were O, F, Al, Cl, Cu, Ag, Au. Oxygen was bombarded as Li_2CO_3 and as H_3BO_3, fluorine was bombarded as a teflon foil $(C_2F_4)_n$, chlorine was bombarded as NH_4Cl, and all the other elements were bombarded as metal foils. All the targets were of high chemical purity (99.9 percent or better). The metal foils were wrapped in foils of the same metal, and the powder targets were wrapped in foils of neighboring elements, for instance, Li_2CO_3 and H_3BO_3 were wrapped in cellulose acetate. The stack of foils was sandwiched between two aluminum foils of nearly the same size as the target, and they served as monitors to measure the cross sections through the reaction $Al^{27}(p,3pn)Na^{24}$.

Great care was taken that the aluminum and the inner target foil would not face each other to prevent recoiling F^{18} nuclei from reaching the target. The stack of foils was irradiated with the beam perpendicular or parallel to the direction of its thickness according to the desired yield; the size of the stack was always about 2 cm×1 cm×0.2 cm. The length of irradiation varied also from 15 sec to one hour. The check for the homogeneity of the bombardment was the closeness of the specific activities in the Al foils; they never differed by more than a factor of two in irradiations with the beam perpendicular to the direction of the thickness and a few percent with the bean parallel to the direction of the thickness.

The irradiations of H_3BO_3, teflon, and Al were counted without doing chemistry since all the activities could be accurately resolved.

To the other targets were added 20 to 40 mg of F^- carrier and dissolved in an appropriate solvent which was H_2O for NH_4Cl, HNO_3 for Cu and Ag, and aqua regia for Au; immediately diluted with water (gold was extracted with ethyl acetate) and 10 ml of 1.5M $BaCl_2$ added followed by ammonia. The BaF_2 precipitate was treated differently, according to the amount of contaminating activity remaining. But the basic steps were as follows: the BaF_2 was dissolved in 3N HCl and Ba^{++} removed with an excess of $SO_4^=$; 1 mg of carriers of suspected activities was added and the solution made basic with ammonia, several precipitations of $Fe(OH)_3$ made as scavenger and precipitation of sulfides with H_2S. The solution was made acid with HCl, the $SO_4^=$ removed with a large excess of Ba^{++}, and then when made basic with ammonia, the BaF_2 precipitated. It was dissolved and treated as previously but bubbling H_2S in acid solution this time and then scavenging with $Fe(OH)_3$ and the BaF_2 reprecipitated as described. Finally, the BaF_2 was again dissolved and the Ba removed with $SO_4^=$, diluted to 20 ml, made basic with NH_4OH, and 50 mg of Ca^{++} added to precipitate CaF_2. In this last step all reagents were kept to a minimum. The CaF_2 was centrifuged and thoroughly washed with H_2O and centrifuged twice, suspended in H_2O and placed in a tared Al dish, dried at 115°C and weighed as CaF_2.

From the basic procedure changes were made. For instance, for Cl only one iron scavenging was done before precipitating CaF_2, and for Au the whole purification scheme was done twice before precipitating CaF_2. Accordingly the chemical yield varied from 75 percent to 20 percent.

CROSS SECTIONS

The samples containing F^{18} were counted in an end-window Geiger counter at a distance of 3.4 cm from the window. The identity of F^{18} was not only established by the chemical procedure but also by an accurate determination of its half-life which never differs more

[1] S. Courtenay Wright, Phys. Rev. **79**, 838 (1950).
[2] L. Marquez and I. Perlman, Phys. Rev. **81**, 953 (1951).
[3] D. H. Perkins, Proc. Roy. Soc. (London) **203**, 399 (1950).

TABLE I. Yields of F^{18}, N^{13}, and C^{11} from various nuclei with 420-Mev protons.

Target nucleus	Product nucleus	Yield in barns	Estimated error (%)
O	F^{18}	8.3×10^{-5}	25
O^{18}	F^{18}	4.1×10^{-2}	25
F	F^{18}	2.2×10^{-2}	25
Al	F^{18}	8.4×10^{-3}	15
Cl	F^{18}	2.2×10^{-3}	25
Cu	F^{18}	8.0×10^{-5}	50
Ag	F^{18}	1.6×10^{-5}	50
Au	F^{18}	4.4×10^{-6}	50
O	C^{11}	3.1×10^{-2}	25
O	N^{13}	1.4×10^{-2}	25

than 2 min from the half-life of 112 min. This activity measurement, extrapolated back to the time of bombardment and properly corrected for the length of irradiation and for self-absorption and absorption in the air and in the window, was used to calculate the cross sections.

The Al monitors were counted about 24 hours after the irradiation; then it was only pure 15.1-hr Na^{24}. If it was counted later, however, it was followed through in order to deduct for the Na^{22} activity. The monitors were mounted in Al dishes equal to those where the CaF_2 were mounted; since back-scattering is independent of energy,[4] this eliminated automatically the back-scattering correction. To correct for self-absorption and absorption in the air and window the absorption coefficient of F^{18} and Na^{24} were measured with Al absorbers and found to be very close to those given by the formula $\mu=0.017E^{-1.43}$; as given by Gleason[5] this is of course under the assumption that absorption is exponential at the beginning. All cross sections are corrected for self-absorption and absorption in the air and window. The thickness of the Al foil was about 9 mg/cm^2, that of the CaF_2 precipitate about 10 mg/cm^2, and that of the air and window added up to 7 mg/cm^2. The cross section for the reaction Al(p,3pn)Na^{24} was found to be 10.8 ± 1.1 mb, as it will be described in the next section.

The cross section for the production of N^{13} from O and the cross section for the production of C^{11} in O were found as an incidental part of this work. These, together with the F^{18} cross sections are given in Table I. The value for O is given as the actual cross section, and the cross section was calculated as if all the F^{18} came from O^{18}, which is the most likely case.

The values quoted in estimated error are based upon reproducibility, estimates of the uncertainty of the CaF_2 yield in the heavy elements where the chemistry was more cumbersome, and uncertainty in the absorption correction, etc.

SPALLATION OF Al

It is a known experimental result that many cross sections for production of radio isotopes at high energies are very slowly varying functions of energy. In order to see if there is much change going from 340 Mev to 420 Mev, the spallation of Al at 420 Mev was studied. The results are compared in Table II. The values at 420 Mev are reported in two columns, first uncorrected, to compare with the uncorrected values taken at Berkeley[2] under very similar conditions and then the values corrected for self-absorption and absorption, which we consider better.

It can be seen that the results at 340 Mev and 420 Mev are identical within the experimental error. The values in Table II are estimated to be good within 15 percent, except the value of Na^{24} whose error is 10 percent.

The absolute cross section for the formation of Na^{24} from Al was measured at 450 Mev by irradiating an Al target in the circulating beam, the current was determined by measuring the heat evolved in the target and using the value of dE/dx from the formula from Bethe,[6] and the value of I was taken from the experimentally determined value of Segrè.[7] Besides this we added an estimate of the heat from nuclear events. For this estimate we took for the cross section for 420-Mev protons on Al the value 0.29 barn, which is one-half of the total neutron cross section at 240 Mev on Al,[8] and we guessed from other experiments that in each collision the ejected charged particles and the recoiling nucleus dissipate 30 Mev in the target which goes into heat.

The Al target was 4 Mev thick and was screwed tightly to an Al block, the whole weighing about 70 g. The block was insulated with a piece of plastic from the probe, and the temperature of the block was measured with a thermocouple; a plot of the rise in temperature against time indicated that this arrangement was a good calorimeter from which the heat deposited in the target was measured. The length of irradiation was 20 min. The rise in temperature was corrected for the small leakage of heat, and from the known heat capacity of the calorimeter, whose weight was accurately determined, the heat deposited in the target was measured. We estimate the error of this measurement to be 5 percent. The target was dissolved in HCl, several small aliquots ($\sim$1/20,000) taken, dried, and counted.

TABLE II. Yields of spallation products of Al with 335-Mev protons and 420-Mev protons.

Nucleus	Yields (barns) 335-Mev protons (uncorrected)	Yields (barns) 420-Mev protons (uncorrected)	Yields (barns) 420-Mev protons (corrected)
Na^{24}	1.02×10^{-2}	1.0×10^{-2}	1.08×10^{-2}
Na^{22}	1.2×10^{-2}	1.2×10^{-2}	1.7×10^{-2}
F^{18}	5.5×10^{-3}	6.3×10^{-3}	8.4×10^{-3}
N^{13}	not measured	8.9×10^{-4}	9.7×10^{-4}
C^{11}	1.9×10^{-3}	2.4×10^{-3}	2.8×10^{-3}
Be^7	1.4×10^{-3}	not measured	...

[4] L. E. Glendenin and A. K. Solomon, Science **112**, 623 (1950).
[5] Gleason, Taylor, and Tabern, Nucleonics **8**, No. 5, 12 (1951).
[6] M. S. Livingston and H. A. Bethe, Revs. Modern Phys. **9**, 263 (1937).
[7] R. Mather and E. Segrè, Phys. Rev. **84**, 191 (1951).
[8] J. DeJuren and B. J. Moyer, Phys. Rev. **81**, 919 (1951).

The backing was rubber hydrochloride of 1 mg/cm² thickness; the dried sample weighed about 1 mg/cm².

Two techniques were used to determine the absolute beta-disintegration rate of the sample. One was to count the sample and a RaD, E, F standard mounted on the same rubber hydrochloride in a technique as described by Novey.[9] The other was to count the sample in an arrangement of well-defined geometry as described by Gleason *et al.*[5] The average of these two methods had a probable error of 7 percent.

The heat evolved in nuclear events is about 8 percent of the heat evolved by ionization, and we estimate that our guess for this heat is right within a factor of two; however, if later experiments would show that this quantity is much different, the value of the cross section could be properly corrected.

The value for the cross section for the formation of Na^{24} from Al with 450-Mev protons thus found is 10.8 ± 1.1 mb. In the error quoted all sources of error that we know were included. It is very close to the value of 10 mb at 350 Mev found by Stevenson.[10]

RESULTS

All the results of this work at 420 Mev, together with previous results at 340 Mev and some recent results on yields obtained by Batzel and Seaborg[11] and by Greenberg and Miller,[12] are shown in Fig. 1. It also includes the value for $C^{12}(p,pn)C^{11}$ from Aamodt *et al.*[13] It will be noticed that the curves look alike in all the cases. At the beginning, from a peak there is a fast decrease of yield with increasing mass number which has the same shape for all of them, and then they turn and decrease more slowly. This is related to whether the nucleus is the product nucleus or the ejected nucleus.

It will be noticed also that the yield of the light fragments always turns sooner and crosses over the heavier ones. In the heavier elements the lightest fragments have larger yields. This seems to be somewhat related to the Coulombic barrier. But these yields, as pointed out previously,[2] are hard to reconcile with an evaporation process and are more likely knock-on products. That is, the high energy proton produces through some mechanism the ejection of the heavy fragment before the excitation energy is evenly distributed throughout the nucleus.

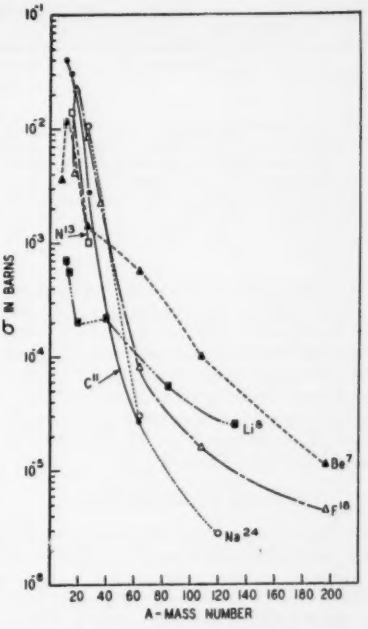

FIG. 1. Yield of heavy fragments in barns as a function of mass number with protons from 335 Mev to 420 Mev.

We are indebted to Dr. W. F. Libby for his suggestions and advice on the absorption corrections, to Dr. H. L. Anderson and the crew of the synchrocyclotron for their cooperation in the irradiations, and to G. W. Reed for the loan of two RaD, E, F standards.

[9] T. B. Novey, Rev. Sci. Instr. **21**, 280 (1950).
[10] P. C. Stevenson and R. L. Folger, private communication.
[11] R. E. Batzel and G. T. Seaborg, Phys. Rev. **82**, 607 (1951).
[12] D. H. Greenberg and J. M. Miller, Phys. Rev. **84**, 845 (1951).
[13] Aamodt, Peterson, and Phillips (University of California Radiation Laboratory Unclassified Report No. 526, November, 1949).

Atomic Masses from Titanium through Zinc*

THOMAS L. COLLINS, ALFRED O. NIER, AND WALTER H. JOHNSON, JR.
Department of Physics, University of Minnesota, Minneapolis 14, Minnesota
(Received January 21, 1951)

The double focusing mass spectrometer previously described has been used to measure 27 atomic masses in the region from titanium to zinc. When supplemented by our earlier values and nuclear reaction energies the data give the masses of 81 nuclides between mass numbers 31 and 70. A fit of the semi-empirical mass formula of Wigner indicates the existence of magic numbers at 20 and 28 protons and neutrons associated with discontinuities in the binding energy surface. The discontinuities are primarily changes in slope of the surface.

IN an earlier communication[1] we reported on the determination of atomic masses in the region about mass 40. The study has now been extended through zinc with the result that values are now available for almost every stable nuclide from S^{32} through Zn^{70}. The measurements were made with a double focusing mass spectrometer. A brief description of the apparatus and procedure of measurement has already been given[1,2] and hence will not be repeated here.

DOUBLET MEASUREMENTS

Table I gives the mass doublets investigated together with the mass differences found. As in previous work a "run" consisted of 10 or more consecutive tracings of the mass spectrum with alternate forward and backward sweep. Since readings are taken from half-height to half-height of the peaks compared—and on each side of the peak—the number given for the mass difference in a single run is the average of at least 20 readings. Runs were taken on different days over a period of several months. The errors given are probable errors computed statistically. As in previous work a given hydrocarbon peak may have an unresolved satellite produced by ions containing one less hydrogen atom but a C^{13} atom in place of one of the C^{12} atoms. From a measurement of intensity of the lighter hydrocarbon fragment a suitable correction may be made to the peak in question. The last column gives values for the corresponding doublets as found by other investigators.

ATOMIC MASSES

Table II gives the atomic masses computed from the present data. In order to follow a consistent procedure we have employed the masses for H^1 and C^{12} found in this laboratory. In our earlier paper[1] we discuss the discrepancies in the mass values for these atoms as given by different investigators. Should our values turn out to be slightly in error, the computed masses for the atoms now investigated would not change enough to affect the validity of the conclusions reached later in the present paper.

Table III compares some of our mass differences with values computed from nuclear reaction data. In general, the agreement is excellent. However, a discrepancy in the value for $Cr^{52}-V^{51}$ appears to be present.

COMPARISON WITH THE WIGNER FORMULA

By combining our mass spectroscopic data with nuclear reaction energies we have constructed an extensive table of masses from $A=31$ to $A=66$ in order to search for irregularities which could be associated with nuclear shell structure. This region includes proposed "magic numbers" 20 and 28 for both neutrons and protons. The odd-even fluctuations characteristic of the lighter nuclei make it difficult to see discontinuities in the binding energy surface or packing fraction curve. Others[3,4] have attempted to remove these effects by comparing masses with those predicted by the Bohr-Wheeler formula. We believe a better approach is to fit the Wigner formula to the data.

The binding energy of a nucleus may be expressed as the sum of a Coulomb energy, a kinetic energy, and a potential energy from nuclear forces. Wigner[5] proposed approximations for each of these terms. He computes the Coulomb energy for a uniformly charged sphere with a radius proportional to $A^{\frac{1}{3}}$. The radius constant may be evaluated from mirror nuclei giving

$$\mathrm{CE}=0.635Z(Z-1)/A^{\frac{1}{3}} \text{ milli-mass units.} \quad (1)$$

He computes the kinetic energy for a degenerate Fermi gas occupying the same volume. Using the radius constant from the Coulomb energy we find

$$\mathrm{KE}=14.640A+32.53(T^2+\tfrac{1}{2}\delta)/A \text{ mMU} \quad (2)$$

where $T=(N-Z)/2=$ isotopic spin.

$$\delta=\begin{cases}0 \text{ for even } Z, \text{ even } N.\\ 1 \text{ for even } Z, \text{ odd } N.\\ 1 \text{ for odd } Z, \text{ even } N.\\ 2 \text{ for odd } Z, \text{ odd } N.\end{cases}$$

* Research supported by the joint program of the ONR and AEC.

[1] Collins, Nier, and Johnson, Phys. Rev. **84**, 717 (1951).
[2] A. O. Nier and T. R. Roberts, Phys. Rev. **81**, 507 (1951).
[3] C. H. Townes and W. Low, Phys. Rev. **79**, 198 (1950).
[4] A. H. Wapstra, Phys. Rev. **84**, 837, 838 (1951).
[5] E. Wigner, University of Pennsylvania Bicentennial Conference (1941), University of Pennsylvania Press, Philadelphia. See also G. Gamow and C. L. Critchfield, *Atomic Nucleus and Nuclear Energy Sources* (Oxford Press, London, 1949).

Wigner expresses the potential energy in terms of two functions L' and L, where L' is the average magnitude of potential energy between pairs of nucleons from forces independent of symmetry. L is the average magnitude of the potential energy from forces which change sign with symmetry. Thus

$$\mathrm{PE} = -\tfrac{1}{2}A(A-1)L' - \Xi L \text{ mMU}, \qquad (3)$$

where Ξ is the number of symmetric minus the number of antisymmetric couplings. In our region of A, Ξ is a negative number and may be expressed for our purpose as

$$\Xi = 2A - \tfrac{1}{8}A^2 - \tfrac{1}{2}T(T+4) - \tfrac{3}{4}\delta. \qquad (4)$$

In the absence of spin orbit coupling AL and AL' should be approximately constant and should be smooth functions of A. The sum of terms (1) (2) (3) is the binding energy

$$\mathrm{BE} = \mathrm{CE} + \mathrm{KE} + \mathrm{PE}. \qquad (5)$$

The binding energy and potential energy are negative quantities.

The binding energy of the nucleus may be computed from the atomic mass M, neglecting the electronic binding energies,

$$\mathrm{BE} = M - (ZM_{\mathrm{H}} + NM_n), \qquad (6)$$

where M_{H} is the mass of the hydrogen atom and M_n is the mass of the neutron. In the absence of an adequate theory of nuclear forces we cannot compare the binding energies computed from expressions (5) and (6). Instead we combine the expressions and calculate the potential functions L and L'.

Table IV gives the data used to compute L and L'. The second column lists reaction energies giving the mass defects $(A-M)$ of unstable nuclei. If no reaction is listed the mass defect is from our mass spectroscopic data. The potential energy in the fourth column is computed by subtracting from the binding energy the Coulomb and kinetic energies. With 1.008146 for the mass of hydrogen and 1.008987 for the mass of the

TABLE I. Mass doublets.

Doublet	No. of runs	Δm in 10^{-4} amu	Previous work
CH_2S-Ti^{46}	3	354.0 ±0.4	349.0± 9.5[a]
CH_2S-Ti^{47}	4	438.3 ±0.9	444.2± 9.4[a]
C_4-Ti^{48}	6	522.0 ±0.6	521.6± 4.6[a]
C_4H-Ti^{49}	4	599.3 ±0.5	588.3± 5.1[a]
$C_4H_2-Ti^{50}$	6	708.92±0.29	694.6± 3.6[a]
$C_4H_3-V^{51}$	6	792.8 ±0.5	
$C_4H_2-Cr^{50}$	5	695.6 ±0.6	673.2± 3.7[b] 714.5± 2[c]
$C_4H_4-Cr^{52}$	4	908.8 ±0.9	920.3± 4.2[b] 908.4± 2[c]
$C_4H_5-Cr^{53}$	5	983.8 ±0.8	1008.7± 4.1[b]
$C_4H_6-Cr^{54}$	1	1079 ±2	1100.0± 4.6[b]
$C_4H_7-Mn^{55}$	5	1165.8 ±1.1	
$C_4H_6-Fe^{54}$	8	1072.0 ±0.5	1065.3± 4.7[b] 1075.1± 2.2[d]
$C_4H_8-Fe^{56}$	6	1278.2 ±1.0	1235 ±17[e] 1284.1± 3.9[f] 1271.3± 2.3[b]
$C_4H_9-Fe^{57}$	6	1350.9 ±0.9	1338.1± 5.0[b]
$C_4H_{10}-Fe^{58}$	1	1448 ±4	1458.8± 4.7[b]
$C_4H_{10}-Ni^{58}$	4	1433.8 ±0.9	1371.2± 3.9[g] 1434.3± 2.3[f] 1447.68[h]
C_5-Ni^{60}	5	702.0 ±2.9	695.9± 3.1[g] 714[h]
C_5H-Ni^{61}	4	782.9 ±2.3	735 ±15[g] 807.64[h]
$C_5H_2-Ni^{62}$	4	886.9 ±0.8	860.7±3.7[g] 913.88[h]
SO_2-Ni^{64}	3	346.9 ±0.7	
$C_5H_3-Cu^{63}$	6	943.9 ±0.5	
$C_5H_5-Cu^{65}$	7	1115.9 ±0.5	
SO_2-Zn^{64}	4	326.82±0.20	
$O_2-Zn^{64}/2$	4	252.46±0.22	
$C_5H_6-Zn^{66}$	4	1208.7 ±0.5	1213.8± 3.9[b]
$C_5H_7-Zn^{67}$	4	1280.8 ±0.5	1280.1± 6.3[b]
$C_5H_8-Zn^{68}$	4	1375.1 ±0.6	1355.5± 6.3[b]
$C_5H_{10}-Zn^{70}$	4	1528.8 ±0.5	1346 ±16[b]

[a] T. Okuda and K. Ogata, Phys. Rev. **60**, 690 (1941).
[b] K. Ogata, Phys. Rev. **75**, 200 (1949).
[c] H. E. Duckworth (private communication, December, 1951).
[d] H. E. Duckworth and H. A. Johnson, Phys. Rev. **78**, 179 (1950).
[e] Okuda, Ogata, Aoki, and Sugawara, Phys. Rev. **58**, 578 (1940).
[f] H. E. Duckworth and R. S. Preston, Phys. Rev. **79**, 402 (1950).
[g] Okuda, Ogata, Kuroda, Shima, and Shinda, Phys. Rev. **59**, 104 (1941).
[h] A. E. Shaw, Phys. Rev. **75**, 1011 (1949).

TABLE II. Atomic masses computed from data in Table I assuming $H^1 = 1.008146 \pm 3$ and $C^{12} = 12.003842 \pm 4$.

Ti^{46}	45.96697± 5	Ni^{58}	57.95345±10
Ti^{47}	46.96668±10	Ni^{60}	59.94901±29
Ti^{48}	47.96317± 6	Ni^{61}	60.94907±23
Ti^{49}	48.96358± 5	Ni^{62}	61.94681± 9
Ti^{50}	49.96077± 4	Ni^{64}	63.94755± 7
V^{51}	50.96052± 5	Cu^{63}	62.94926± 6
Cr^{50}	49.96210± 7	Cu^{65}	64.94835± 6
Cr^{52}	51.95707± 9	Zn^{64}	63.94955± 2
Cr^{53}	52.95772± 8	Zn^{66}	65.94722± 6
Cr^{54}	53.9563 ± 2	Zn^{67}	66.94815± 6
Mn^{55}	54.95581±10	Zn^{68}	67.94686± 7
Fe^{54}	53.95704± 5	Zn^{70}	69.94779± 6
Fe^{56}	55.95272±10		
Fe^{57}	56.95359±10		
Fe^{58}	57.9520 ± 4		

TABLE III. Comparison with some nuclear reactions.

	From Table I	From nuclear reactions	Reactions used
$Ti^{47}-Ti^{46}$	1−0.00029±11	1−0.00028±11	$Ti^{46}(d,p)Ti^{47a}$
$Ti^{48}-Ti^{47}$	1−0.00351±12	1−0.00355±14	$Ti^{47}(d,p)Ti^{48a}$
$Ti^{49}-Ti^{48}$	1.00041± 8	1.00045± 8	$Ti^{48}(d,p)Ti^{49a}$
$Cr^{52}-V^{51}$	1−0.00345±10	1−0.00262	$V^{51}(n,\gamma)V^{52b}$ $V^{52}(\beta)Cr^{52c}$
$Mn^{55}-Fe^{54}$	1−0.00123±11	1−0.00138± 4	$Mn^{55}(p,n)Fe^{55d}$ $Fe^{54}(n,\gamma)Fe^{55b}$
$Fe^{57}-Fe^{56}$	1.00087±14	1.00098± 1	$Fe^{56}(n,\gamma)Fe^{57b}$
$Ni^{61}-Ni^{60}$	1.00006±37	1.00020± 3	$Ni^{60}(n,\gamma)Ni^{61b}$

[a] J. A. Harvey, Phys. Rev. **81**, 353 (1951).
[b] Kinsey, Bartholomew, and Walker, Phys. Rev. **78**, 481 (1950).
[c] A. C. G. Mitchell, Revs. Modern Phys. **22**, 36 (1950).
[d] H. T. Smith and R. V. Richards, Phys. Rev. **74**, 1275 (1948).

TABLE IV. Data used in comparing experimental results with Wigner formula.

Nuclide	Reaction	Mev	Mass defect mMU	−PE mMU	−Ξ
S^{31}	(γ,n)	−14.8 ±4[a]	10.9 ±4	779.15	60
P^{32}	β	1.712±8[a]	15.93±1	803.44	68
S^{32}			17.76±1	808.37	64
S^{33}			17.87±5	832.36	72
S^{34}			21.24±5	859.10	79
S^{35}	β	0.167[a]	19.78±5	882.42	88
Cl^{35}			19.96±5	886.11	85
Cl^{36}	(n,γ)	8.56 ±3[b]	20.15±6	910.55	94
A^{36}			21.00±3	915.28	90
Cl^{37}			22.34±5	936.49	102
A^{37}	(p,n)	−1.598±3[a]	21.46±5	939.49	99
Cl^{38}	(n,γ)	6.11 ±3[b]	19.91±6	959.09	112
A^{38}			25.09±4	966.43	107
K^{38}	(γ,n)	−13.2 ±2[a]	18.8 ±2	966.07	107
K^{39}			23.94±3	994.08	114
Ca^{39}	(γ,n)	−15.9 ±4[a]	16.5 ±4	992.89	114
A^{39}			24.87±3	1014.88	126
K^{40}	(n,γ)	7.76 ±5[b]	23.26±4	1017.49	124
Ca^{40}			24.55±9	1023.37	120
A^{41}	(d,p)	3.84 ±3[a]	22.39±4	1037.67	137
K^{41}			25.10±4	1042.99	133
Ca^{41}	(d,p)	6.09[a]	24.60±20	1047.07	130
Sc^{41}	β^+	4.94[a]	18.20±20	1047.19	130
K^{42}	(d,p)	5.12 ±10[a]	24.01±10	1066.72	144
Ca^{42}			27.84±4	1073.54	139
Ca^{43}			27.49±6	1097.59	150
Ca^{44}			30.76±6	1124.84	160
Ca^{45}	β	0.254[a]	29.63±6	1148.75	172
Sc^{45}			29.90±5	1152.42	168
Ti^{46}			33.03±5	1183.96	175
Ti^{47}			33.32±10	1208.48	187
Ca^{48}			32.22±10	1226.74	208
Sc^{48}	β	2.954[a]	33.71±6	1230.32	204
Ti^{48}			36.88±6	1235.90	198
V^{48}	β^+	3.03[a]	32.53±7	1237.05	196
Ti^{49}			36.42±5	1260.29	211
Cr^{49}	(γ,n)	−13.4 ±2[c]	32.5 ±2	1266.33	204
Ti^{50}			39.23±4	1287.57	223
V^{50}	(γ,n)	−11.15 ±20[d]	36.5 ±2	1288.98	220
Cr^{50}			37.90±7	1294.87	215
V^{51}			39.48±5	1316.06	232
Cr^{51}	(p,n)	−1.534±3[a]	38.67±5	1319.73	228
V^{52}	(n,γ)	7.30 ±3[b]	38.34±6	1339.94	246
Cr^{52}			42.93±9	1347.76	240
Mn^{52}	β^+	4.116[a]	37.41±9	1348.32	238
Cr^{53}			42.28±8	1371.79	254
Mn^{53}	(p,n)	−1.380±8[e]	41.64±8	1375.97	250
Fe^{53}	(γ,n)	−13.8 ±2[a]	37.1 ±2	1377.81	247
Cr^{54}			43.7 ±2	1397.53	267
Mn^{54}	(p,n)	−2.162±5[e]	42.2 ±2	1400.84	264
Fe^{54}			42.96±5	1406.75	259
Mn^{55}			44.19±11	1426.83	277
Fe^{55}	(n,γ)	9.28 ±3[b]	43.96±6	1431.71	273
Co^{55}	β^+	2.42[a]	40.24±6	1434.65	270
Mn^{56}	(n,γ)	7.25 ±3[b]	42.76±7	1450.25	292
Fe^{56}			47.28±10	1458.73	286
Co^{56}	β^+	3.59[a]	42.33±10	1460.38	284
Fe^{57}			46.41±9	1482.38	301
Ni^{57}	(γ,n)	−11.7 ±2[a]	43.0 ±2	1491.36	294
Fe^{58}			48.0 ±4	1508.21	315
Ni^{58}			46.55±10	1517.95	307
Fe^{59}	β	1.56[a]	47.0 ±3	1532.16	331
Co^{59}	(n,γ)	7.73 ±4[b]	48.7 ±3	1538.15	326
Ni^{59}	(n,γ)	9.01 ±3[b]	47.24±11	1542.52	322
Co^{60}	β	2.811[a]	47.97±29	1562.15	342
Ni^{60}			50.99±29	1569.85	336
Co^{61}	β	1.42[f]	49.51±23	1588.06	357
Ni^{61}			50.93±23	1594.18	352
Ni^{62}			53.19±9	1620.53	367
Ni^{63}	β	0.063[a]	50.67±6	1642.85	384
Cu^{63}			50.74±6	1647.92	379
Zn^{63}	β^+	2.36[a]	47.11±6	1650.64	375
Ni^{64}			52.45±7	1669.18	400
Zn^{64}			50.45±2	1677.49	390
Ni^{65}	β	2.10[a]	49.39±6	1691.35	418
Cu^{65}			51.65±6	1697.64	412
Zn^{65}	(p,n)	2.17 ±1[a]	50.16±6	1701.47	407
Zn^{66}			52.78±6	1728.07	423

[a] *Nuclear Data*, Natl. Bur. Standards Circular 499 (1950).
[b] Kinsey, Bartholomew, and Walker, Phys. Rev. **78**, 481 (1950).
[c] W. E. Ogle and R. E. England, Phys. Rev. **78**, 63 (1950).
[d] Sher, Halpern, and Mann, Phys. Rev. **84**, 387 (1951).
[e] Lovington, McCue, and Preston, Technical Report No. 54, Laboratory of Nuclear Science and Engineering, M.I.T. (September, 1951).
[f] Smith, Haslam, and Taylor, Phys. Rev. **84**, 843 (1951).

neutron the expression is

$$-\mathrm{PE}=\text{mass defect}+8.146Z+8.987N+\mathrm{CE}+\mathrm{KE}\ \text{mMU}. \quad (7)$$

The final column gives the value of the symmetry function Ξ which is an integer from its definition.

From Eq. (3) one sees that the potential energy difference of isobars does not depend upon L'. Thus, using the data of Table IV, we have calculated L for many mass numbers from

$$L=\Delta(-\mathrm{PE})/\Delta\Xi, \quad (8)$$

excluding pairs which jump over the possible magic numbers 20 and 28. In the cases of three or more isobars, we computed the best value of L by least squares. Figure 1 shows the values of L (and AL) plotted against A. Contrary to expectation, L is not a smooth function of A but shows large discontinuities which are definitely associated with magic numbers 20 and 28. Region I contains nuclei with 20 or less neutrons, region II nuclei with 20 or more neutrons and 20 or less protons, and so on. The jumps are associated with 20 neutrons, 20 protons, 28 neutrons, 28 protons in order with increasing A. L increases on crossing a neutron number and decreases on crossing a proton number. The energy involved is surprisingly large, for example $\Delta L\Xi$ for the 28 neutron jump is 75 mMU. Between the discontinuities we have simply approximated L (or AL) by straight lines as shown. We assume AL is constant in regions I and II, but L is constant in regions III and IV. Region V does not have sufficient data to permit any approximation.

By substituting the average values of L or AL in the potential energy formula (3) we have computed L'. Figure 2 shows AL' plotted against A. Because we do not observe jumps of 75 mMU in the masses we expect L' to show discontinuities which almost cancel the effect of the discontinuities in L. Figure 2 shows that AL' can be represented in each region by a straight line with a small slope. In this way we arrive at the empirical

equations

$$(-\text{PE})=(A-1)(a_1+a_2A)+(\Xi/A)a_3 \text{ regions I, II,} \quad (9)$$

$$(-\text{PE})=(A-1)(a_1+a_2A)+\Xi a_3 \text{ regions III, IV,} \quad (10)$$

where a_1, a_2, and a_3 are constants characteristic of each region.

By means of the empirical equations we can investigate the effect of magic numbers upon the binding energy with due allowance for symmetry. The first step is to determine by least square the constants which best fit all nuclei of each region excluding magic number nuclei. The constants in mMU are:

region I, $AL=40.31$, $\frac{1}{2}AL'=25.963+0.0848A$;
region II, $AL=55.52$, $\frac{1}{2}AL'=27.363+0.0785A$;
region III, $L=0.8989$, $\frac{1}{2}AL'=23.316+0.1407A$;
region IV, $L=1.2316$, $\frac{1}{2}AL'=23.106+0.1752A$.

Table V (a), (b), (c), and (d) give the differences between the observed and computed binding energies in 10^{-4} atomic mass units. A positive value indicates that the nucleus has greater stability (more negative binding energy) than given by the empirical fit. The entries in heavy type are the residuals for the fitted region. The fit is satisfactory except, perhaps, in region III.

The next step is to extrapolate the empirical equations to the magic number nuclei and beyond. Table V also gives the differences between these computed and observed binding energies. Let us consider nuclei with 20 neutrons. Table V (a) shows that they can be grouped

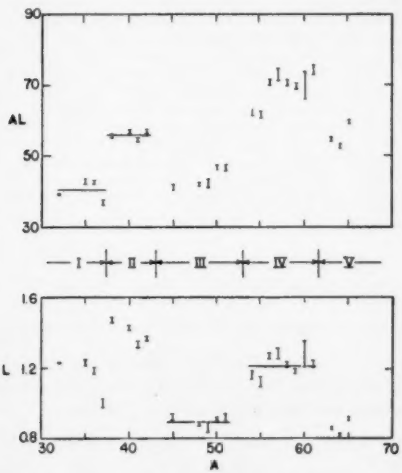

FIG. 1. Variation of the Wigner constant L (and AL) in mMU with mass number A for nuclides in region near magic numbers 20 and 28. Region *I* contains nuclides having 20 or less neutrons; region *II*, 20 or more neutrons and 20 or less protons; region *III*, 28 or less neutrons and 20 or more protons; region *IV*, 28 or more neutrons and 28 or less protons; and region *V*, 28 or more protons.

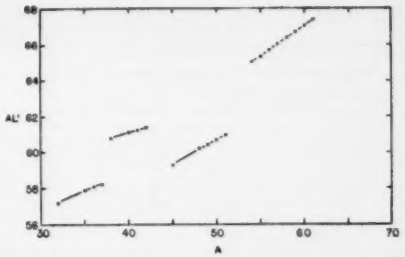

FIG. 2. Variation of the Wigner constant L' in mMU with mass number A computed from formula (3) with average values of L given in Fig. 1.

with nuclei having less than 20 neutrons, Table V (b) shows that they also can be grouped with nuclei having more than 20 neutrons but less than 20 protons. Each magic number shows similar properties. The errors become large when we extrapolate beyond the boundaries of the regions. From this we conclude that the effect of magic numbers is, primarily, changes of slope in the binding energy surface (however, with this form of empirical equation not more than two or possibly three nuclei could fit both ways exactly).

In our empirical equations we have attributed all of the effect of the magic numbers to the potential energy. The kinetic energy should require some modification and it is very possible that the assumptions of uniform charge and uniformly increasing radius used to compute the Coulomb energy should also be modified. These considerations do not invalidate the conclusions of the last paragraph but they do point out the doubtful theoretical significance of the empirical constants. Even as a method of predicting reaction energies, the empirical equations are limited. The residuals in the least square fits exceed the probable errors in the measurements and more accurate masses probably would not reduce them, so that we can expect predictions of individual masses to be in error by as much as 1 Mev.

From this attempt to fit a Wigner formula to our mass data we have reached the following conclusions. Both 20 and 28 are "magic" numbers associated with discontinuities in the binding energy surface. These discontinuities are primarily changes in the slope of the surface rather than discrete jumps in the binding energy. The regions between the magic numbers do not all have the same shape; the two regions below 20 protons require a different form of empirical equation from the two regions above 20 protons. Finally we believe the accuracy of mass measurements in this region now requires a considerable modification of the semi-empricial mass formulas before an adequate fit can be obtained.

The authors wish to acknowledge the very able assistance of Ruth C. Boe in making some of the measurements reported here. The construction of the

TABLE V. Difference in 10^{-4} amu between a fitted Wigner formula and experimental masses. The Wigner constants L and L' are obtained in each case by a least squares fit of the nuclides indicated by heavy type.

(a) Constants fitted to nuclides with less than 20 neutrons

Neutrons	P	S	Cl	A	K	Ca	Sc
24						−55	−75
23				−53	−57	−55	
22				−31	−39	−36	
21			−20		−25	−28	
20			−1	0	−4	−6	−27
19		1	2	**−3**	**−3**	−16	
18		**8**	**3**	**5**			
17	1	**−1**					
16		**0**					
15		**−6**					
	15	16	17	18	19	20	21
				Protons			

(b) Constants fitted to nuclides with more than 20 neutrons and less than 20 protons

Neutrons	S	Cl	A	K	Ca	Sc	Ti
24					16	3	14
23			**0**	**0**	3		
22			**2**	**−1**	3		
21		**0**		**0**	−1		
20		−1	0	3	3	0	
19	−17	−11	−16	−4	−9		
18	−29	−28	−25				
	16	17	18	19	20	21	22
			Protons				

(c) Constants fitted to nuclides with less than 28 neutrons and more than 20 protons

Neutrons	Cl	A	K	Ca	Sc	Ti	V	Cr	Mn	Fe	Co	Ni
33										−41		**−34**
32										−28	−27	**−19**
31									−30	−19		**−19**
30								−9	−12	0		**−3**
29							−12	−1	−3	1	−1	8
28				4		8	0	12	5	11	3	
27					4	**−2**	**−5**	**1**	**0**	**−4**		
26						**6**		**9**				
25				−12		**−2**	**−6**	**−4**				
24				−2	**−11**	**8**						
23		−26	−21	−10								
22		−7	−9	2								
21	−8		1	5								
20	14	21	20	24	6							
19	17	17	17	18								
18		23	28									
	17	18	19	20	21	22	23	24	25	26	27	28
						Protons						

(d) Constants fitted to nuclides with more than 28 neutrons and less than 28 protons

Neutrons	Ca	Sc	Ti	V	Cr	Mn	Fe	Co	Ni	Cu	Zn
36									−3	−26	−45
35									−11		−49
34								2	5	−22	−43
33							1	**−1**	1		−44
32							**−1**	**0**	2		
31						**−6**	**−1**		−6		
30					3	**−1**	**5**		−2		
29				**−1**	**3**	**−1**	**−1**	**−3**	2		
28	17		8	−3	3	−5	−3	−9			
27		3	−10	−15	−15	−16	−24				
26			−15		−18						
25	−30		−29	−28	−36						
	20	21	22	23	24	25	26	27	28	29	30
						Protons					

apparatus was aided materially by grants from the Graduate School and the Minnesota Technical Research Fund subscribed to by General Mills, Inc., Minneapolis Star and Tribune, Minnesota Mining and Manufacturing Company, Northern States Power Company, and Minneapolis Honeywell Regulator Company.

Letters to the Editor

PUBLICATION of brief reports of important discoveries in physics may be secured by addressing them to this department. The closing date for this department is five weeks prior to the date of issue. No proof will be sent to the authors. The Board of Editors does not hold itself responsible for the opinions expressed by the correspondents. Communications should not exceed 600 words in length, and should be submitted in duplicate.

Deuterium Total Cross Sections for Positive and Negative Pions*

H. L. ANDERSON, E. FERMI, D. E. NAGLE, AND G. B. YODH
Institute for Nuclear Studies, University of Chicago, Chicago, Illinois
(Received March 13, 1952)

RECENT communications from this laboratory report total cross sections of hydrogen for positive and negative pions.[1-3] In these experiments scintillation counters were used to measure the transmission of hydrogen in the several pion beams of the large Chicago cyclotron. In the present experiment similar techniques were used to compare the transmission of H_2O and D_2O cells for charged pions. The immediate result, which we call $(\sigma_D-\sigma_H)'$, is the difference between the cross sections of deuterium and hydrogen for those events which produce no ionizing particles within the angular acceptance of the last counter.

One type of cell for either H_2O or D_2O was 2 inches long, and a second type was 4 inches long. For each pair of cells the numbers of atoms/cm² were very nearly the same, so that the energy loss, Coulomb scattering, and nuclear events due to oxygen were very nearly the same. The difference between the $\frac{1}{2}(H_2O)$ and $\frac{1}{2}(D_2O)$ cross sections observed is then $(\sigma_D-\sigma_H)'$.

Table I presents the preliminary results. The solid angle is that of the last counter averaged over the absorber; hence it measures the "poorness" of the geometry. The energy band column lists the mean energy of the pions in the absorber, plus or minus half their energy spread. The energy spread is partly due to the spread in energy of the entering beam (±3 Mev), but mostly due to the energy loss in the absorber. This information comes partly from magnetic analysis of the beam, partly from range curves, and from calculations of the energy loss in the sample. The $(\sigma_D-\sigma_H)'$ entries have been corrected for the muon and electron contents of the beams, which in most channels is about 5 percent. The quoted error in $(\sigma_D-\sigma_H)'$ includes either the statistical or the consistency rms errors of the counts (whichever was greater), uncertainties in the corrections of the counting rates for chance coincidences (less the 1 percent), and uncertainties in the muon-electron correction (~2 percent).

TABLE I. Cross sections of deuterium and hydrogen for π^+ and π^- at several energies.

Solid angle steradians	Energy band Mev	Observed $(\sigma_D-\sigma_H)'$ 10^{-27} cm² π^-	Corrected $(\sigma_D-\sigma_H)$ 10^{-27} cm² π^-	σ_H 10^{-27} cm² π^+	σ_D 10^{-27} cm² π^-
0.63	79±10	31±10	34±10	48±10	54±13
0.63	109±15	66± 4	72± 5	80±10	103±10
0.088	115± 9	87± 7	88± 7	95±15	124±11
0.63	115± 9	77±18	84±18		
0.43	127±15	77± 7	84± 8	125±15	129±11
0.63	133± 9	66±13	76±15	135±15	128±16
0.088	164± 9	135±13	139±13		198±12
0.63	164± 9	119±11	128±14		
0.088	179± 9	170±10	172±10		234±12
0.63	179± 9	146± 9	163±12		
0.43	209±15	109±24	131±25		192±26
		π^+	π^+	π^-	π^+
0.43	72±17	24± 6	24± 6	15± 8	60± 9
0.63	79±10	30±13	31±13	20± 8	79±15
0.43	109±15	28±12	29±12	31± 9	109±16
0.43	127±15	25±15	26±15	45±10	151±21

It is desirable to correct the D−H difference for those specifically nuclear events which scatter particles into the last counter. For the purposes of this correction (which is of the order of 10 percent) we have taken $\sigma_D-\sigma_H$ for π^- equal to $\sigma_H(\pi^+)$. The correction was computed using the measured hydrogen cross sections[1,2] and assuming that the scattering is isotropic. Where $\sigma_H(\pi^+)$ was not available, we have taken $\sigma_H(\pi^+)=3\sigma_H(\pi^-)$ (see reference 3). For π^+ the corresponding corrections are much smaller because of the importance of the charge exchange process.[3] The fourth column of Table I gives the corrected $\sigma_D-\sigma_H$. Values from different geometries are seen to agree within the experimental error. Justification of the assumption of the equivalence of $\sigma_D-\sigma_H$ for $\pi^\pm$ and σ_H for $\pi^\mp$ is seen from a comparison of columns 4 and 5 in Table I. There is some indication of deviations at the higher energies.

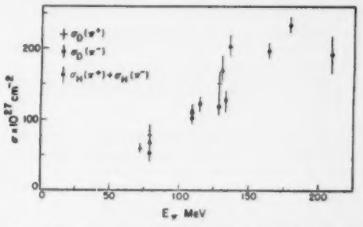

FIG. 1. Total cross sections of deuterium for positive and negative pions.

Adding σ_H to $\sigma_D-\sigma_H$, we obtain σ_D, as exhibited in column 6 of Table I and in Fig. 1. Within the experimental errors σ_D is the same for pions of either sign. This has also been observed at 60 Mev by the Columbia workers.[4] This equality is predicted by the principle of charge symmetry, which requires for the free neutron and proton

$$\sigma_N(\pi^+)=\sigma_H(\pi^-),\ \sigma_H(\pi^+)=\sigma_N(\pi^-).$$

For comparison, we have also plotted the sum $\sigma_H(\pi^+)+\sigma_H(\pi^-)$ in Fig. 1. It will be seen that σ_D does not differ greatly from this sum, in accordance with the idea that the neutron and the proton in the deuteron scatter pions fairly independently.

At energies above 115 Mev there is some indication that σ_D is less than $\sigma_H(\pi^+)+\sigma_H(\pi^-)$. From such an effect it may be possible to obtain information about the relative phase of the scattering from neutrons and protons. We hope to extend our study of this effect in the near future.

* This work was supported by the ONR and AEC.
[1] Anderson, Fermi, Long, Martin, and Nagle, Phys. Rev. **85**, 934 (1952).
[2] Anderson, Fermi, Long, and Nagle, Phys. Rev. **85**, 936 (1952).
[3] Fermi, Anderson, Lundby, Nagle, and Yodh, Phys. Rev. **85**, 935 (1952).
[4] Isaacs, Sachs, and Steinberger, Phys. Rev. **85**, 802 (1952).

Gamma-Gamma Angular Correlation in Pd^{106}

G. B. ARFKEN, E. D. KLEMA, AND F. K. MCGOWAN
Oak Ridge National Laboratory, Oak Ridge, Tennessee
(Received March 17, 1952)

SINCE the initial experiments of Brady and Deutsch,[1] the angular correlation of gamma-rays in Pd^{106} has constituted a puzzling discrepancy between experiment and theory. The shape of their correlation curve suggested spin assignments of 0-2-0 which yield a ratio of 2 for $W(\pi)/W(\frac{1}{2}\pi)$, while their measured ratio was about 1.5.

The angular correlation of the Pd^{106} gamma-rays from an aqueous ruthenium chloride source has been reinvestigated using NaI scintillation spectrometers with a resolution of 10 percent at 661 kev. The observed gamma-spectrum was in good agreement

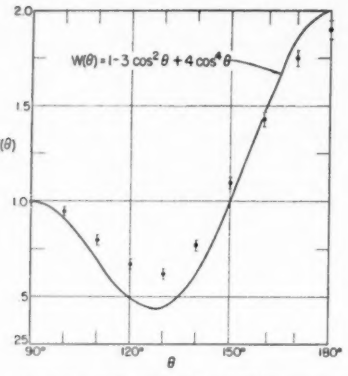

FIG. 1. Angular correlation of the 513- and 624-kev gamma-ray cascade in Pd^{108} (not corrected for finite solid angles).

with the decay scheme proposed by Alburger.[2] In preliminary runs the coincidence rate for the main cascade was observed as a function of angle in 10° increments from 90° to 180°, one spectrometer detecting the 513-kev photopeak, the other detecting the 624-kev photopeak. As shown in Fig. 1, the data follow closely the curve for Brady and Deutsch's conjectured spin assignments.

To check the agreement with this assignment some 40,000 counts were collected at 90°, 135°, and 180°. Various pulse-height spreads were tried, most of the data being taken with each spectrometer set to cover both photopeaks. The background was determined by introducing a 0.5-microsecond delay in one of the channels of the coincidence circuit. A typical set of runs corrected for the random background (0.160 counts/second) is shown in Table I. The average of the three entries at each angle represents some 12,000 counts. The correction for the 1024–513 kev cascade was determined by setting one spectrometer on the 513 photopeak and the other on the 1045 Compton distribution just above the 624 photopeak. A further 1 percent increase was attained by correcting for the counter solid angles. The ratio is rather insensitive to this geometric effect since $W(\theta)$ has a peak at both 90° and at 180°.

When the spectrometers were set to count all pulses above a certain height (integral), the ratio dropped, the decrease being greater the lower the integral setting. For example, counting all pulses above 300 kev, the observed ratio was 1.67. These decreases are explained partly though not completely by the calculated interference from the 1045–513 cascade. This suggests that the lack of energy resolution in earlier experiments is one of the main causes of the previous disagreement with the theoretical correlation function.

The corrected value of the 180°–90° ratio, 1.91 (with a possible 2 percent statistical error) is still some 4 or 5 percent less than the predicted ratio. This could be accounted for by a hyperfine coupling to the intermediate nuclear state. The necessary effect is within the limits of error Steffen[3] assigned to his experiment in the investigation of the effects of various sources. There is also the possibility of a small amount of interfering radiation.

TABLE I. Three determinations are given of the counting rates (corrected for background) of the 513-kev gamma-ray in coincidence with either the 624-kev or the 1045-kev gamma-ray. From their averages the separately determined 1045–513 counting rates are subtracted, yielding in the last line the coincidence rates for the 624–513 cascade alone.

Cascade	Counts/sec 180°	90°	$W(180°)/W(90°)$
624–513	1.272	0.688	1.85
+	1.245	0.673	1.85
1045–513	1.267	0.680	1.86
Average	1.261	0.680	1.85
1045–513	0.043	0.035	
624–513	1.218	0.645	1.89

Taking further advantage of the energy resolution of the scintillation spectrometers, the coincidence rate of the 1045-513 kev cascade was observed at 90°, 135°, and 180°. The data were reasonably consistent with the assignment of spin 2 to the 1.55-Mev level, the 1045-kev gamma being a mixture with β/α about 2 or 3, $\delta = 180°$ in the Ling-Falkoff[4] notation. The observed positive coefficient of the $\cos^4\theta$ term excludes the assignment of spin 1 or 3 for any possible dipole-quadrupole mixture. This confirms Alburger's suggestion[2] for the spin of the upper state.

[1] E. L. Brady and M. Deutsch, Phys. Rev. **74**, 1541 (1948); **78**, 558 (1950).
[2] D. E. Alburger, Phys. Rev. **85**, 700 (1952); Brookhaven Quarterly Progress Report No. BNL-132 (1951).
[3] R. M. Steffen, Bull. Am. Phys. Soc. **27**, No. 1, 57 (1952).
[4] D. S. Ling and D. L. Falkoff, Phys. Rev. **76**, 1639 (1949).

Helium II Transfer Rates on Lucite and Perspex Surfaces

B. S. CHANDRASEKHAR
Clarendon Laboratory, Oxford, England
(Received March 19, 1952)

DASH and Boorse[1] recently reported the curious dependence on temperature of the helium II transfer rate on Lucite, showing a sharp maximum at 1.5°K. It seemed of interest to look for a similar effect with Perspex, which, like Lucite, is a methyl methacrylate polymer. Experiments have now been done on the flow of beakers of both Perspex and Lucite (see Fig. 1).

The flow rate *versus* temperature curve for Perspex shows a striking dependence on the method used for polishing. Microscopic

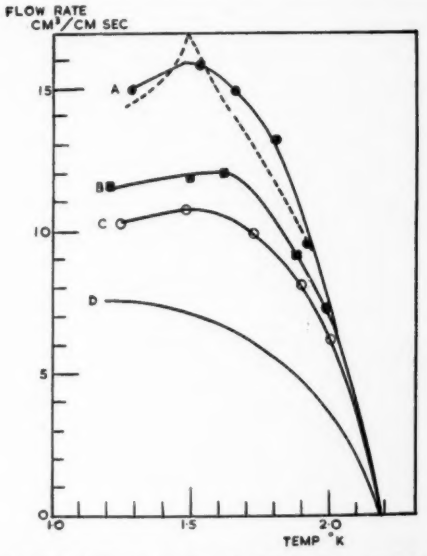

FIG. 1. The broken curve shows the results of Dash and Boorse for Lucite. Curve *A* is for Perspex polished with commercial liquid polish, *B* for rouge-polished Lucite, and *C* for rouge-polished Perspex. *D* is the curve for glass btainedo by Mendelssohn and White.

examination of the Perspex surface polished with a commercial liquid polish showed a rough streaky structure with "ridges" and "valleys" about 10^{-4} cm wide, while rouge polishing gave a comparatively smooth surface. The flow rates of curve *A* showed a considerably greater variation along the length of the beaker, than those of curve *C*, for a given temperature. Furthermore, the flow characteristics of rouge-polished Lucite and Perspex are very alike and have flatter maxima and are closer to the characteristic for glass.

These results, taken in conjunction with recent observations on the film flow out of specially polished stainless steel beakers,[2] seem to indicate that the observed flow on Lucite and Perspex can be regarded as being composed of two parts: (1) pure film flow giving a characteristic similar to the one observed on glass[3] (curve *D*); (2) a pressure dependent flow of bulk helium, which takes place when the surface irregularities are of a shape and size favorable to this type of siphon flow. The maxima in the flow characteristics would require this type of flow to decrease with decreasing temperature. It is interesting to note that a similar temperature dependence was observed in the case of flow of helium II through capillaries of about 10^{-2} cm diameter.[4] To verify this explanation, a flow experiment at 2.26°K, just above the λ-point, was done with a "rough" Perspex beaker carefully shielded from radiation, and a very small inflow was indeed observed. This flow was very strongly dependent on the difference of levels of helium outside and inside the beaker, increasing as the outer level was brought nearer the rim of the beaker with the inner level remaining constant. No such flow could be detected at 4.2°K. A detailed communication will appear shortly.

I wish to thank Dr. K. Mendelssohn for his guidance and many valuable discussions.

[1] J. G. Dash and H. A. Boorse, Phys. Rev. **82**, 851 (1951).
[2] B. S. Chandrasekhar and K. Mendelssohn, [to be published in Proc. Phys. Soc. (London)].
[3] K. Mendelssohn and G. K. White, Proc. Phys. Soc. (London) **A63**, 1328 (1950).
[4] J. F. Allen and A. D. Misener, Proc. Roy. Soc. (London) **A172**, 467 (1939).

Radioactivity in Neutron Activated Platinum

J. M. Cork, J. M. LeBlanc, F. B. Stumpf, and W. H. Nester
Department of Physics, University of Michigan, Ann Arbor, Michigan
(Received March 17, 1952)

In a previous report[1] some twenty-two electron conversion lines were noted from platinum irradiated in the pile. Since the spectrometric exposure was begun many hours after the end of the irradiation and only one spectrogram could be obtained from each specimen, it was naïvely concluded that all of the observed activity was associated with the 3.4-day decay of gold 199, formed from platinum 198. With stronger irradiated sources and shorter transit times, it becomes possible to make chemical separations and to obtain a sequence of exposures showing the different rates of decay for certain electron lines as shown in Fig. 1. It is apparent that lines characteristic of the 17.4-hour Pt^{197} activity are present. This electron group with work functions characteristic of gold, indicates the existence of two gamma-rays of energies 77.4 and 191.2 kev, as recently found in the *K*-capture decay of Hg^{197}. A chemical separation of gold from the platinum yields the electron lines shown in the bottom spectrogram of Fig. 1. The energies of the three gamma-rays, 49.8, 158.5, and 208.3 kev, agree well with values recently reported[2] by Hill.

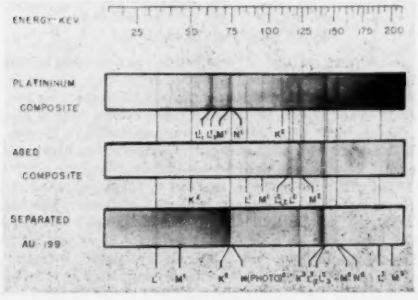

FIG. 1. Electron lines from freshly activated and aged platinum and separated gold.

TABLE I. Electron energies for composite platinum.

Electron energy	Interpretation	Energy sum	Electron energy	Interpretation	Energy sum
34.9 kev	*L* Hg	49.7 kev	110.5 kev	*K* Au	191.2 kev
46.3	*M* Hg	49.8	115.8	$L_{1,2}$ Pt	129.7
51.6	*K* Pt	130.0	118.2	L_3 Pt	129.8
53.2	Auger		125.3	*K* Hg	208.4
63.0	$L_{1,2}$ Au	77.4	126.9	*M* Pt	130.2
65.3	L_3 Au	77.2	129.1	*N* Pt	129.8
74.0	*M* Au	77.4	129.8	Photo *K* Pt	208.2
75.4	*K* Hg	158.5	144.3	$L_{1,2}$ Hg	158.5
76.8	*N* Au	77.6	146.4	L_3 Hg	158.7
77.8	Photo *K* Au	158.5	155.2	*M* Hg	158.7
80.2	Photo *K* Pt	158.6	157.7	*N* Hg	158.5
85.0	*L* Pt	98.9	193.4	*L* Hg	208.2
96.0	*M* Pt	99.3	204.6	*M* Hg	208.1

TABLE II. Gamma-energies.

Emitting isotope	Gamma energy, kev	*K*/*L* ratio
Au^{199}	49.8	
3.4-day	158.5	0.56; (*L*/*M*) 3.6
	208.3	4.5
Pt^{197}	77.4	
17.4-hour	191.2	6.0
Pt^{193m}	99.1	
4.4-day	129.8	0.1

Certain of the electron lines fall in neither of these groups and are associated with some other platinum activity. They decay with a half-life of the order of 4 days and appear to be satisfied by the work functions of platinum. It is, therefore, quite probable that no 4.4-day radioactivity exists in platinum 193 as had been assumed, but rather that an isomeric state exists, probably in platinum 195, since this mass could equally well satisfy every criterion used[2] in making the previous assignment. The gamma-energies of 99.1 and 129.8 kev are identical in value with those observed[4] after the beta-decay of a 180-day activity believed to be in Au^{195}. The relative intensity of the two gamma-rays, here found to be about equal, is quite different from that reported for the gold. This might be expected since in the latter case the beta-emission is complex so that about 90 percent of the beta-decays yield no 129.8-kev gamma-ray.

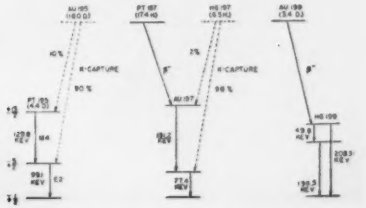

FIG. 2. Proposed nuclear levels in Pt^{193}, Au^{197}, and Hg^{199}.

The electron energies and their interpretations are shown in Table I, while the gamma-energies are tabulated in Table II. By the use of a recording microphotometer the densities of the photographic plates, and hence, the relative intensities have been found for certain of the lines as shown in Table II. By utilizing the data and tables as presented[5] by Goldhaber and Sunyar, the multipolarity of certain of the transitions appears to be as shown in Fig. 2. One unusual feature of the 129.8-kev isomeric transition seems to be that the intensity of the L_3 conversion is about equal to that for the L_1 line.

This project received the joint support of the AEC and ONR.

[1] Cork, Stoddard, Rutledge, Branyan, and LeBlanc, Phys. Rev. **77**, 843 (1950).
[2] R. D. Hill, Phys. Rev. **79**, 413 (1951).
[3] N. Hole, Arkiv Mat. Astr. Fys. **36A**, No. 9 (1948); G. Wilkinson, Phys. Rev. **75**, 1019 (1949).
[4] Steffen, Huber, and Humbel, Helv. Phys. Acta. **22**, 167 (1949).
[5] M. Goldhaber and A. Sunyar, Phys. Rev. **83**, 906 (1951).

Electrolysis of Thorium Oxide*

W. E. Danforth
Bartol Research Foundation, Franklin Institute, Swarthmore, Pennsylvania
(Received January 21, 1952)

THE electrolysis of homogeneous crystalline thorium oxide at elevated temperatures is being studied. Fused material obtained from the Norton Company is red when received and will bleach when heated in vacuum or hydrogen. The red color can be restored by heating in oxygen and, under certain circumstances, by radiation.

Optically clear specimens are cut with a diamond saw, ground and polished, and are mounted in a vacuum furnace in such a manner that visual observation is possible during passage of current. Preliminary studies have been made with tungsten electrodes and with molybdenum electrodes, the results being the same in both cases.

When a current of 100 ma/cm² is passed at a temperature of 1300°C, a darkening of the crystal is observed to form at the cathode end and to proceed toward the anode at a rate of approximately one mm per second. The crystal in the photograph is 10 mm long. After 7 seconds with 100 ma/cm² (and a field strength of about 50 v/cm) the dark region extends approximately 7 mm from the cathode end. Attention is drawn to the appearance of a metallic deposit on the crystal surface at the cathode end.

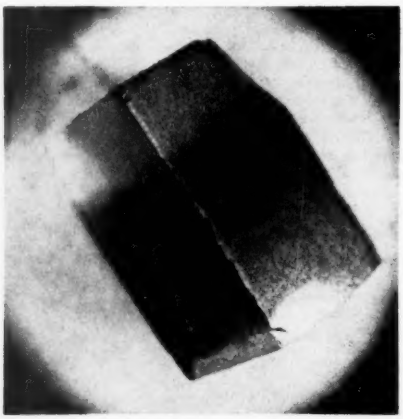

FIG. 1. A crystal of thorium oxide in an early stage of electrolysis.

When the drawing of current is continued the crystal becomes uniformly jet black and the metallic surface layer (presumably thorium) increases in area until it reaches the anode. This establishes an effective short circuit and electrolysis ceases.

If, starting with a specimen which has become completely covered with a metallic layer, one removes the layer by grinding, repolishes the crystal, and, subjects it to 1300°C for an hour or so, the black material diffuses to the surface and a metallic layer is again formed. It would appear, therefore, that the darkening is here associated with a stoichiometric excess of the metal, dispersed as ions, or possibly to some extent coagulated.

The particles responsible for the darkening are evidently charged since reversing the polarity of the applied field reverses the direction of motion of the dark region. However, wherever the dark region has reached the surface, a permanent discoloration remains. The charge responsible for the mobility appears to be neutralized (e.g., by stray electrons from outside) when the charge reaches the surface.

Certain evidence has led us to believe that the amount of thorium electrolyzed in the crystal in the photograph is not less than 10^{-3} mg. This is the result of the passage of 0.35 coulomb. If all the current were contributing to electrolysis, the quantity of thorium oxide electrolyzed by 0.35 coulomb would be 0.4 mg. This would indicate that, in single crystals, the fraction of current resulting in electrolysis is of the order of 10^{-2}.

It is of interest to compare the above result with that obtained from studies using finely divided thorium oxide. Measurements of the rate of disappearence of coated and sintered thoria cathodes show that the fraction of current producing electrolysis may be as low as 10^{-6}. The discrepancy may possibly be explained by a much higher electronic conduction in the activated cathodes than was present in the single crystals. It is also possible, however, that the large surface of the finely divided material plays an important part. The conductivity of the mass of particles may be of essentially different nature than that of a single crystal. Electrons in the surface region may possess higher mobility than in the interior. also it seems inescapable that metallic thorium will be liberated in the individual grains and migrate to their surfaces, giving rise to an even more involved electronic conductivity mechanism.

* This work is supported by the U. S. Navy, Bureau of Ships.

Alpha-Particles from the Li^7+T Reactions

J. T. Dewan,* T. P. Pepper, K. W. Allen,† and E. Almqvist
Atomic Energy Project, National Research Council of Canada, Chalk River, Ontario, Canada
(Received March 20, 1952)

THE interaction of tritons with Li^7 [1] may lead to the following exothermic reactions:

$$Li^7+T \rightarrow He^6+He^4+9.79 \text{ Mev}, \quad (1)$$
$$Li^7+T \rightarrow He^4+He^4+n+n+8.85 \text{ Mev}, \quad (2)$$
$$Li^7+T \rightarrow Be^9+n+10.43 \text{ Mev}. \quad (3)$$

In addition, reaction (2) may proceed as a two-step process via the formation of the unstable nuclei Be^8 or He^5. This letter discusses the energy distribution of the α-particles from the first two reactions and reports evidence for a new excited state of He^6.

Hydrogen, 15 percent tritium, was accelerated to 240 kev and the mass-three beam magnetically selected to bombard a $Li_2^7SO_4$ target.[2] The charged particles emitted at 90° to the beam were studied with a 90° magnetic analyzer by the technique previously reported[2] and also with a large proportional counter. This counter consisted of a dural cylinder 5 inches in diameter and 15 inches long provided with a side window of mica 1 mg per cm² thick. The inner conductor was a 0.010-inch diameter tungsten wire which passed through glass insulators supported by guard rings at each end. The counter was filled with A containing 1 percent CO_2 to a pressure of 70 cm of mercury and was usually operated at 2400 volts. The gas multiplication was about five. Under these

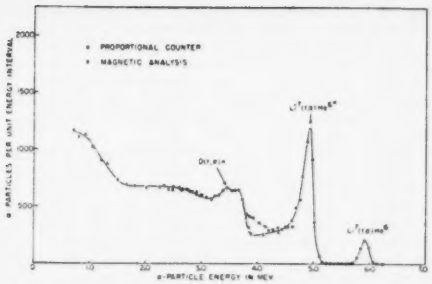

FIG. 1. The energy distribution of α-particles from the Li^7+T reactions observed at 90° to a 240-kev triton beam.

conditions and at the counting rates used, space charge did not noticeably affect the pulse heights obtained. The pulses from the counter were amplified and sorted according to size by a thirty-channel pulse-height analyzer. A correlation between pulse heights and α-particle energies was established by allowing α-particles of known energy to enter the counter immediately before and after each run. The following energy calibration points were obtained from the sources shown: U^{233}—4.82 Mev, Pu^{240}—5.16 Mev, Am^{241}—5.47 Mev, Cm^{242}—6.11 Mev, $T(d,\alpha)n$—3.43 Mev,[4] and $Li^7(p,\alpha)He^4$—8.75 Mev.[4]

In Fig. 1 is shown the energy distribution of the α-particles emitted at 90° to the beam. The data obtained by magnetic analysis have been corrected for charge exchange[5] in the target. At 5.95 Mev is a group attributed to α-particles associated with the formation of He^6 in its ground state. The energy of these α-particles was accurately determined by allowing them to enter the counter simultaneously with the α-particles from Cm^{242} which have nearly the same energy. An expanded portion of the pulse-height distribution (Fig. 2) shows the 6.11-Mev α-particles from the curium clearly resolved from the high energy group of α-particles from the reaction $Li^7(t,\alpha)He^6$. Using the measured separation of the two peaks of 0.165±0.017 Mev, the Q of reaction (1) is calculated to be 9.79±0.03 Mev. It can be shown that the energy equivalent of the mass difference He^6-Li^6 is $(Q_1+Q_3)-(Q_2+Q_4)$, where Q_1, Q_2, Q_3, and Q_4 are the Q values of the reactions $Li^7(p,\alpha)He^4$, $T(\beta^-)He^3$, $Li^6(p,\alpha)He^3$, and $Li^7(t,\alpha)He^6$, respectively. Taking 9.79±0.03 Mev for Q_4 and using the data of Li *et al.*,[6] the He^6-Li^6 mass difference is computed to be equivalent to 3.55±0.03 Mev. This value differs considerably from that of 3.215 ±0.015 Mev obtained by Perez-Mendez and Brown[7] for the end point of the He^6 β-spectrum. It is, however, in agreement with earlier determinations.[8] Knox[9] has found no evidence for a γ-ray associated with the He^6 β-particles.

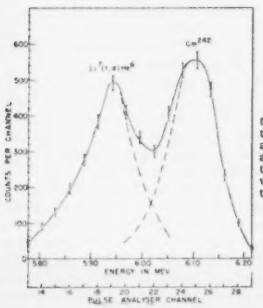

FIG. 2. The pulse-height distribution obtained when α-particles from the $Li^7(t,\alpha)He^6$ reaction and from Cm^{242} are admitted to the counter simultaneously through the same window. Observations at 90° to 240-kev triton beam.

The intense group of α-particles at 4.91±0.02 Mev is believed to be associated with an excited state of He^6 formed in the reaction $Li^7(t,\alpha)He^{6*}$. From the measured energy of the α-group, the Q of this reaction is computed to be 8.08±0.03 Mev. Thus the excited level in He^6 is 1.71±0.01 Mev above the ground state and is unstable by 0.78±0.03 Mev against break-up into an α-particle and two neutrons. The width of this level is probably less than 50 kev, as there is no observable broadening of the associated α-particle group.

In Fig. 1 the difference between the two sets of points in the neighorhood of 3.9 Mev represents the contribution of the ground state He^6 particles, whose ionization enables them to be detected in the proportional counter but whose magnetic rigidity is too great to permit their detection with the magnetic analyser. The small peak at about 3.4 Mev is due to α-particles from the $D(t,n)He^4$ reaction, which is usually present when low energy tritons are used as bombarding particles. Unless there are unresolved excited states of He^6, the broad continuum shown in Fig. 1 is composed of α-particles from reaction (2) proceeding via one or more steps and α-particles from the break-up of the observed excited state of He^6. If one subtracts the latter α-particles; the remaining continuum accounts for 80 percent of the disintegrations emitting particles at 90° to the beam.

* Now with Schlumberger Well Surveying Corporation, Houston, Texas.
† Now at the University of Liverpool, Liverpool, England.
[1] E. Almqvist, Can. J. Research **A28**, 433 (1950); Pepper, Allen, Almqvist, and Dewan, Phys. Rev. **81**, 315 (1951); R. W. Crews, Phys. Rev. **82**, 100 (1951).
[2] Lithium, 99.91 percent Li^7, 0.09 percent Li^6 kindly provided by the AEC.
[3] Pepper, Allen, Almqvist, and Dewan, Phys. Rev. **85**, 155 (1952).
[4] α-particle energy at 90° to the 240-kev beam.
[5] G. H. Briggs, Proc. Roy. Soc. (London) **A114**, 341 (1927).
[6] L. Whaling, Fowler, and Lauritsen, Phys. Rev. **83**, 512 (1951).
[7] V. Perez-Mendez and H. Brown, Phys. Rev. **77**, 404 (1950).
[8] T. Bjerge and K. J. Brostrøm, Kgl. Danske Videnskab. Selskab. Mat.-fys. Medd. **16**, No. 8 (1938); H. S. Sommers, Jr., and R. Sherr, Phys. Rev. **69**, 21 (1946); W. J. Knox, Phys. Rev. **74**, 1192 (1948).

$p-n$ Junction Method for Measuring Diffusion in Germanium*

W. C. DUNLAP, JR., AND D. E. BROWN
General Electric Research Laboratory, Schenectady, New York
(Received March 10, 1952)

THE diffusion of an n-type impurity into a p-type semiconductor creates a $p-n$ junction which can be detected electrically by the thermoelectric effect of a hot needle or by a rectification probe.[1] Study of the rate of penetration of the $p-n$ junction into the semiconductor can be used to measure the diffusion coefficients of various impurities in such semiconductors as germanium or silicon.

The object of the present study was to establish a foundation for the validity of this method by the direct measurement of diffusion, by the $p-n$ junction method, and by the radioactive tracer method. For this purpose, antimony 124 was chosen as the impurity to be used. This material served the double purpose of changing the conduction type from p to n as it diffused and, at the same time, creating a radioactive layer in which the concentration of the diffusing impurity could be evaluated by standard counting procedures.

Samples of single crystal p-type germanium were prepared in the form of wafers about 1 cm^2 in area and 50–60 mils thick. These samples were ground on a special grinder which made the surface flat and parallel to about 0.1 mil. After cleaning and etching with HF, a thin layer of the radioactive antimony (2–10 microgram/cm^2) was evaporated onto one face of the sample.

The sample was then sealed in small quartz tubes containing argon at a pressure of 70-cm Hg at room temperature. Following heating in a carefully controlled oven (±5°C) for the desired time, the tubes were broken open, and the surface activity removed by grinding from all parts of the sample except for one face. The sample was then ground off on the same grinder with which the faces were originally prepared. The surface layers were ground into

sheets of fine grade emery paper, in such a way that all the activity was retained on the paper. The $p-n$ character of each new face was checked by means of a thermoelectric probe. The activity of the paper was measured in a fixed geometry with a scintillation counter. The weight of the sample was measured after each grinding. The results for two samples are shown in Fig. 1. Here are

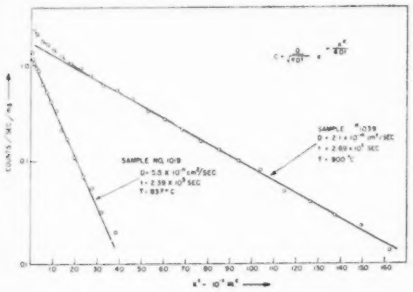

FIG. 1. Plot of log (counting rate) *vs* x^2 for the diffusion of radioactive antimony 124 into a germanium single crystal at two temperatures, 900°C and 837°C. The linearity of the plot on this chart is a test of the applicability of the "δ-function" solution of the diffusion equation.

plotted the counting rate per unit weight of material removed, *versus* the square of the distance from the original surface. This plot is chosen to check an important point. If the original surface layer could legitimately be considered to represent an infinitely sharp distribution (δ-function), the theoretical distribution of impurity should be given by the relation[3]

$$C=Q/(\pi Dt)^{\frac{1}{2}}\exp(-x^2/4Dt),$$

where C is the concentration of diffusing impurity (atoms/cm³), Q is the original surface density of impurity (atoms/cm²), x is the distance in centimeters, t the time in seconds, and D the diffusion coefficient (cm²/sec). Thus, the linearity of the curves on this plot is a check on the validity of the δ-function solution, and the slope of the lines obtained determines the diffusion coefficient. The good linearity obtained in all our tests shows that in spite of uncertainties that do exist regarding the actual initial conditions, including such effects as the formation of a liquid surface layer, 2-phase solid layers, effect of evaporation of the antimony, etc., all these effects either involve such a negligibly thin surface layer or are over within such a short time that they do not affect the diffusion in any important way.

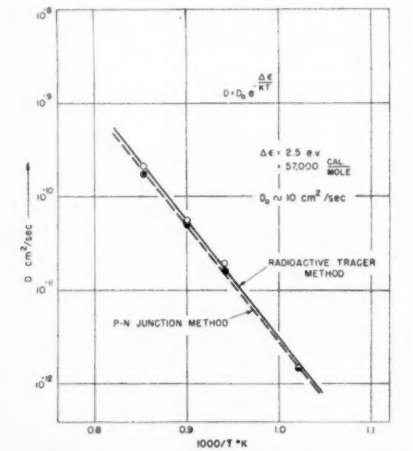

FIG. 2. Plot of the temperature variation of the diffusion coefficient for antimony in germanium determined by the $p-n$ junction method and by the radioactive tracer method. The good agreement observed justifies the use of the $p-n$ junction method for the measurement of diffusion in semiconductors.

Figure 2 shows the diffusion coefficients for antimony at various temperatures as measured by the $p-n$ junction method and by the radioactive tracer method. The results are seen to be in excellent agreement. The average difference between the values of D determined by the two methods is about 10 percent. The $p-n$ junction method gave uniformly lower values. The reason for this may be sought in the tendency of a thermoelectric probe to balance between p and n slightly on the n-type side, because of the tendency of surfaces to be p-type and because of the higher mobility of electrons than holes. However, a factor neglected in the radioactive tracer method was the absorption of the emitted β-rays in the germanium powder itself, and this may also affect the results slightly.

The activation energy determined from the slope was 2.5 ev, or 57,000 cal/mol. The value of D_0, the intercept of D on the $1/T=0$ axis, was about 10 cm²/sec. A calculation of D_0 based upon the Langmuir-Dushman[3] diffusion equation gave a value $D_0 \sim 0.3$. The two values are in satisfactory agreement considering the uncertainty involved in the Langmuir-Dushman equation, the error in extrapolating for D_0, and the possibility that the activation energy is slightly dependent on temperature. Thus the diffusion is a true volume diffusion and does not involve the "short circuits" found by Nowick[4] to play a part in many diffusion studies.

We should like to thank R. N. Hall for single crystal samples, and J. H. Hollomon, J. C. Fisher, D. Turnbull, J. A. Burton, and W. Shockley for helpful discussions.

* A partial report of these studies was presented at the meeting of the American Physical Society, January 31, 1952 [Bull. Am. Phys. Soc. **27**, No. 1, 41 (1952)].

[1] See W. C. Dunlap, Jr., Bull. Am. Phys. Soc. **27**, No. 1, 40 (1952).

[3] R. M. Barrer, *Diffusion in and through Solids* (University Press, Cambridge, England, 1941).

[3] I. Langmuir and S. Dushman, Phys. Rev. **20**, 113 (1922).

[4] A. S. Nowick, J. Appl. Phys. **22**, 1182 (1951).

Unusual $\pi-\mu$ Decays in Photographic Emulsions

W. F. FRY*
Department of Physics, University of Chicago, Chicago, Illinois†
and
Department of Physics, Iowa State College, Ames, Iowa‡
(Received March 17, 1952)

THE search for unusual $\pi-\mu$ decays in photographic emulsions has been continued.[1] Electron sensitive G-5 plates have been exposed in the positive meson beams[2] of the University of Chicago cyclotron. A total of 10,686 $\pi-\mu$ decays have been observed in C-2 and G-5 plates where both the π- and μ-meson tracks stopped in the emulsion. Thirteen unusual events were found among the 10,674 normal $\pi-\mu$ decays. The data concerning the unusual $\pi-\mu$ decays are given in Table I.

Event 12 is interpreted as a decay in flight of a negative π-meson and has been described elsewhere.[2] The μ-meson in event 13 did not stop in the emulsion. The length of the μ-meson track is 975 microns. The number of gaps along the μ-meson track has been measured and compared with the gap density along a μ-meson track from a π-decay which stops within 100 microns of the μ-meson track of event 13. Using this method it was found that the residual range of the μ-meson track in event 13 is about 60 microns. The long range of the meson track of event 13 is most probably due to the decay in flight of the positive π-meson. The observed short ranges of the μ-meson tracks in events 8 through 11 are possibly due to the decay in flight in the backward direction of the π-mesons. Assuming that the short ranges of the μ-meson tracks in

TABLE I. Characteristics of unusual $\pi-\mu$ decays.

Event	Type of emulsion	Range of μ-meson track in microns	Energy of μ-meson in Mev	Measured angle between directions of π- and μ-meson tracks	Energy in Mev of π-meson assuming decay in flight
1*	C-2	120	1.6	73	5.0
2*	C-2	185	2.1	20	10.6
3*	G-5	290	2.7	59	6.6
4*	G-5	416	3.3	51	8.3
5*	G-5	430	3.35	26	15.4
6*	G-5	441	3.4	56	5.1
7*	G-5	470	3.35	28	15.4
8	C-2	258	2.5	93	1.7
9	C-2	260	2.5	113	0.7
10	G-5	444	3.4	160	0.03
11	G-5	476	3.5	117	0.09
12	C-2	828	4.8	10	0.05
13	G-5	1035	5.5	55	0.5

* Events which do not appear to be decays in flight of the π-mesons.

events 1 through 7 are due to the decay in flight of the π-mesons, the energy of the π-mesons at the time they decayed can be calculated from the directions of the π- and μ-mesons and the ranges of the μ-meson tracks. In events 1 through 7 the grain density near the ends of the π-meson tracks is clearly inconsistent with the assumption of decay in flight of the π-mesons. However, it cannot be entirely ruled out that the π-mesons were scattered through a large angle in the last one or two grains and subsequently decayed in flight in the backward direction. From a study of the large angle scatterings near the end of the π-meson tracks of normal $\pi-\mu$ decays, it was found that the probability of large angle scatterings is quite small, hence the probability that a π-meson would be scattered and subsequently decay in flight is extremely small ($\sim 10^{-5}$). For this reason it seems quite certain that the short ranges of the μ-meson tracks in events 1 through 7 are not due to the decay in flight of the π-mesons. A decay electron track is observed from the end of each of the μ-meson tracks which stopped in G-5 plates. A study of the grain density and the total energy of the δ-rays along the μ-meson tracks indicate that the μ-mesons were ejected with a lower velocity than in normal $\pi-\mu$ decays. The range distribution of μ-mesons from π-meson decays in C-2 plates has been studied. From this study it is concluded that the events where the ranges of the μ-meson tracks are less than 480 microns cannot be due to straggling. Correcting for the increased probability that short μ-meson tracks will end in the emulsion, the ratio of unusual $\pi-\mu$ decays (range of the μ-meson track <480 microns) to normal $\pi-\mu$ decays is then $2.8\pm 1.2\times 10^{-4}$ if the events which can be explained by decay in flight are not included. A micro-projection drawing of event 4 is shown in Fig. 1.

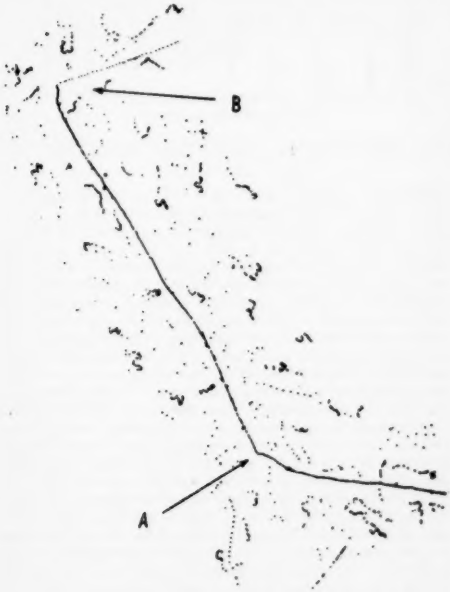

FIG. 1. An unusual $\pi-\mu-e$ decay which is listed as event 4. The $\pi-\mu$ junction is indicated by arrow A and the $\mu-e$ junction by arrow B. The range of the μ-meson track is 416 microns. The normal range of the μ-meson tracks from decays is about 600 microns.

Short μ-meson tracks from π-meson decays have also been found by Powell,[4] Smith,[5] and Seifert, Bramson, and Havens.[6] A theoretical explanation of the occurrence of unusual $\pi-\mu$ decays in terms of soft photon emission has been given independently by Primakoff,[7] Eguchi,[8] and Nakano, Nishimura, and Yamaguchi.[9] The percentage of unusual $\pi-\mu$ decays and the energy distribution of the μ-mesons appear to be in general agreement with the theoretical predictions based on a soft photon emission accompanying the charge acceleration of the μ-mesons from the π-meson decays.

The author is indebted to Dr. M. Schein for the use of the facilities of the cosmic-ray laboratory and for suggestions and encouragement. The author is also indebted to Dr. J. K. Knipp and Dr. J. J. Lord for many helpful and stimulating discussions. A portion of the plates was supplied by Dr. R. Sagane to whom the author is very grateful. The author is also indebted to Dr. H. L. Anderson and the cyclotron group for many exposures to the large cyclotron. Three of the unusual events were found by Miss M. McLean.

* AEC Postdoctoral Fellow.
† Supported in part by a joint program of the ONR and AEC.
‡ Supported in part by a grant from the Research Corporation.
[1] W. F. Fry, Nuovo cimento **8**, 590 (1951); W. F. Fry, Phys. Rev. **83**, 1268 (1951).
[2] H. L. Anderson, University of Chicago Cyclotron Status Report, November (1951), unpublished.
[3] W. F. Fry, Phys. Rev. **84**, 385 (1951).
[4] C. F. Powell, in *Cosmic Radiation, Colston Papers* (Butterworth Scientific Publications, London, England, 1949).
[5] F. M. Smith, report at the Washington Meeting, of the American Physical Society (1951).
[6] Seifert, Bramson, and Havens, Bull. Am. Phys. Soc. **27**, No. 1, 28 (1952).
[7] H. Primakoff, Phys. Rev. **84**, 1255 (1951).
[8] T. Eguchi, Phys. Rev. **85**, 943 (1952) and private communications.
[9] Nakano, Nishimura, and Yamaguchi, private communications.

Polarization of D-D Neutrons*

H. J. LONGLEY, R. N. LITTLE, JR., AND J. M. SLYE
University of Texas, Austin, Texas
(Received March 19, 1952)

AN attempt has been made to detect the polarization of the fast neutrons of the D-D reaction at very low bombarding energies. Various descriptions[1,2] of the interactions in the D-D reaction result in the possibility of a polarization of the D-D neutrons. A method proposed by Schwinger[3] to detect polarization of fast neutrons was used in this experiment. The experimental arrangement is shown in Fig. 1.

Following Schwinger's notation, $P_1(\theta_1)$ is the fraction polarized of neutrons emerging from source at angle θ_1 and $P_2(\theta_2)$ is the fraction of the neutrons polarized by the Pb scatterer emerging from the scatterer at angle θ_2. The ratio of the neutron intensities, I, at positions 1 and 2 is given by

$$R=\frac{I_2}{I_1}=\frac{1+P_1(\theta_1)P_2(\theta_2)}{1-P_1(\theta_1)P_2(\theta_2)}.$$

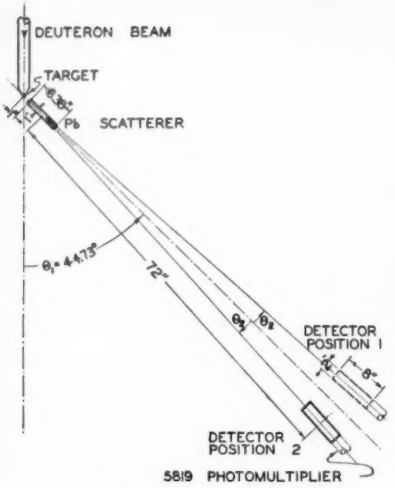

FIG. 1. Experimental arrangement.

For a given θ_1 this ratio may be solved for the polarization $P_1(\theta_1)$ if $P_2(\theta_2)$ is known.

θ_1 was 45° in center-of-mass coordinates, and the ratio R was measured for two angles $\theta_2=3.23°$ and 4.47°. At $\theta_2=4.47°$, $R=1.2\pm0.2$; and at $\theta_2=3.23°$, $R=1.5\pm0.2$. The value of $P_2(\theta_2)$ can be computed as in Schwinger's discussion, giving values of the polarization $P_1(45°)$ to be 30 percent from R at $\theta_2=4.47°$ and 40 percent ±20 percent from R at $\theta_2=3.23°$.

The chief uncertainty in the experimental data is due to the background count, and the experiment is being repeated to lower the uncertainties.

The neutrons were detected by a liquid xylene-terphenyl mixture coupled to a 5819 photomultiplier. The details of the experimental arrangement and the revised data will appear in a subsequent article.

* This work was supported in part by the Research Institute of the University of Texas, the Air Research and Development Command, and the AEC.

[1] E. J. Konopinski and E. Teller, Phys. Rev. **73**, 822 (1948).
[2] L. Wolfenstein, Phys. Rev. **75**, 342 (1949).
[3] J. Schwinger, Phys. Rev. **73**, 407 (1948).

The Decay of Rubidium 87

M. H. MACGREGOR* AND M. L. WIEDENBECK
Department of Physics, University of Michigan, Ann Arbor, Michigan
(Received March 17, 1952)

SINCE the discovery of natural radioactivity in rubidium by Thomson[1] in 1905, much work has been done in an attempt to evaluate its properties. Strassman and Walling,[2] evaluating the half-life from a determination of the ratio of Sr^{87} to Rb^{87} in a lepidolite sample of known geologic age, obtained the value $T_{\frac{1}{2}}=6.3\times10^{10}$ years. In addition many determinations of the half-life have been made by counting methods.[3-6] Recent results range from $5.8\pm1.0\times10^{10}$ years to $6.5\pm0.6\times10^{10}$ years. Most of the values obtained must be carefully evaluated, since in many of the cases thick sources or backings were used, and in some it was found necessary to make assumptions concerning the decay scheme.

Experiments giving information about the decay products have been in disagreement. By means of absorption measures, Hoffman[6] (1924) and Mühlhoff[7] (1930) found evidence of a weak beta-radiation accompanying a stronger one. Ollano[8] (1941) reported at least five electron lines lying over a continuous background. The absorption work of Eklund[9] (1945) indicated simple beta-decay. Haxel *et al.*[4] (1948) found up to 30 percent coincidences between the front and back sides of the source and attributed them to a beta-particle in coincidence with a 100-percent-converted gamma-ray. Curran *et al.*[5] (1951), using a proportional counter, obtained an energy spectrum of the beta-disintegration from which they concluded that the process is simple beta-decay.

The present work was undertaken to re-evaluate the half-life and to provide further information about the decay scheme. In measuring the half-life of Rb^{87}, the cell counter described by Sawyer and Wiedenbeck[9] was used. A thin aluminized zapon film of about 0.025 mg/cm², upon which RbCl was vaporized, served as the cathode. The two sections were operated in parallel. With this arrangement the results are essentially independent of the decay scheme. Data were obtained for various source and backing thicknesses (Fig. 1). The specific activity extrapolated to zero thickness is 478 counts/g RbCl/sec; this, combined with Nier's value[10] for the isotopic abundance, gives $T_{\frac{1}{2}}=6.23\pm0.3\times10^{10}$ years. (Using Paul's[11] more recent value for this abundance, one obtains $T_{\frac{1}{2}}=6.29\times0.3\times10^{10}$ years.)

An investigation was then carried out to determine whether or not there are coincidences between beta-particles and conversion electrons. The counter mentioned above was modified by insulating the source from the rest of the counter and placing wire screens on both sides of the source, between the source and the cell counters. The screens were placed about 2 cm from the source, thus enabling a negative screen potential to discriminate against low energy electrons coming from the source. The two cell counters were

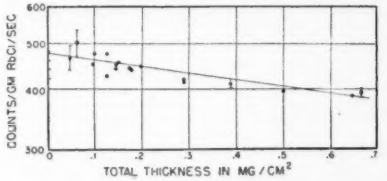

FIG. 1. Counting rate *versus* total source-plus-backing thickness. A zero-thickness activity of 478 counts per g RbCl per sec was obtained.

operated in coincidence, and a third cell counter was placed in anticoincidence to eliminate cosmic-ray effects. Coincidences which occur when the screen is at a negative potential arise either from a two-particle disintegration in which each particle has sufficient energy to traverse the 2 cm of counter gas between the source and the screen, or else from a single particle disintegration in which the particle is scattered from the sensitive region of one counter into the sensitive region of the other counter. When the screens are positive with respect to the source, there is superimposed on the above effect those real coincidences which arise from low energy particles which cannot traverse the 2 cm of counter gas, as well as coincidences due to a single particle which is scattered from one side of the source to the other in the region between the two screens.

Preliminary work was carried out with a group of single beta-emitters having different upper energies. These included Ni^{63}(50 kev), S^{35}(169 kev), Ca^{45}(260 kev), and P^{32}(1.7 Mev). The coincidence curves for these elements varied slightly with the energy of the emitted radiation. Changing the source activity by a factor of 100 and the resolving time of the coincidence circuit from 8 to 30 microseconds had no effect on the shape of the curves. Decreasing the gas pressure in the counter lowered the curves on the screen positive side (by reducing gas scattering), and it raised the curves on the screen-negative side (by increasing the mean free path).

Curves were taken for Rb^{87} sources of varying thicknesses. The Curve obtained for the thinnest source, 0.04 mg/cm², most closely resembled the curves for S^{35} and Ca^{45}. Figure 2 shows the curves

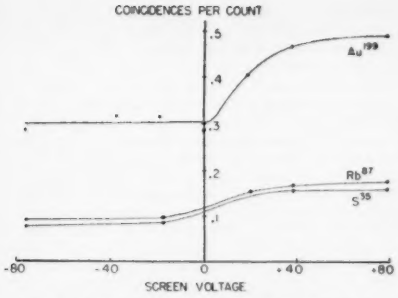

FIG. 2. Coincidence curves for Au^{199}, Rb^{87}, and S^{35}, plotted as a function of screen voltage.

for S^{35} and Rb^{87}, as well as the curve for Au^{199}, all obtained with a total source plus backing thickness of about 0.1 mg/cm^2. The close agreement of Rb^{87} with S^{35} is apparent. Au^{199}, which emits beta-radiation followed approximately 40 percent of the time by conversion electrons,[12] has a much higher coincidence rate.

On the basis of these results, it seems safe to conclude that the disintegration of Rb^{87} consists of a simple beta-decay.

This work was supported, in part, by funds from the Michigan Memorial Phoenix Project.

* AEC Predoctoral Fellow.

[1] J. J. Thomson, Phil. Mag. **10**, 584 (1905).
[2] F. Strassman and E. Walling, Ber. deut. chem. Ges. **71**, 1B, 1 (1938).
[3] S. Eklund, Arkiv Mat. Astr. Phys. **33A**, 60 (1946).
[4] Haxel, Houtermans, and Kemmerich, Phys. Rev. **74**, 1886 (1948).
[5] Curran, Dixon, and Wilson, Phys. Rev. **84**, 151 (1951).
[6] G. Hoffman, Z. Physik **25**, 177 (1924).
[7] W. Mühlhoff, Ann. Phys. **7**, 205 (1930).
[8] Z. Oilano, Nuovo cimento **18**, 11 (1941).
[9] G. A. Sawyer and M. L. Wiedenbeck, Phys. Rev. **79**, 490 (1950).
[10] A. O. Nier, Phys. Rev. **50**, 1041 (1936).
[11] W. Paul, Z. Physik **124**, 244 (1948).
[12] P. M. Sherk and R. D. Hill, Phys. Rev. **83**, 1097 (1951).

Transmission of X-Rays through Calcite near the Bragg Angle

GUENTER SCHWARZ AND GEORGE L. ROGOSA
Department of Physics, Florida State University, Tallahassee, Florida
(Received March 17, 1952)

RECENTLY Campbell[1] has reconsidered the problem of the transmission of x-ray radiation through a crystal when set at the Bragg angle. This same problem has also been investigated experimentally by Bragg, Bosanquet, and James[2] and Borrmann.[3,4] When a monochromatic beam of x-rays falls on a thin crystal, as this crystal is rotated through the Bragg angle, part of the incident beam is reflected and part of it is transmitted straight through. Bragg, using a rocksalt crystal, has observed that this transmitted intensity at a wavelength of about 0.5A will decrease at the Bragg angle, whereas Campbell at about 1.5A has measured an increase in this intensity for various crystals.

We have measured the transmitted intensity at the Bragg angle for single crystals of calcite using monochromatic radiation from 0.7A to 2.3A. A double crystal spectrometer served as a monochromator. When working at the wavelength of a strong emission line, sufficient intensity was available to use the $(1, +1)$ position at the peak of the line. When using the continuum from a W target, because of intensity limitation, the $(1, -1)$ position was used to obtain limited monochromatization. The crystal under investigation was mounted on the axis of an Allison-type spectrometer and could be rotated by a synchronous motor drive at an angular speed of 27 sec/min. Crystals with the reflecting planes parallel to the surface using both external and internal reflections were investigated. In some cases crystals were cut with planes perpendicular to the surface. An indication of the perfection of the crystal was obtained from the width of the $(1, -1)$ diffraction pattern which in all cases was a symmetrical curve.[5] The intensity was measured with an argon filled Geiger counter and a General Radio counting rate meter, the output of which was recorded with an Esterline-Angus recording milliameter.

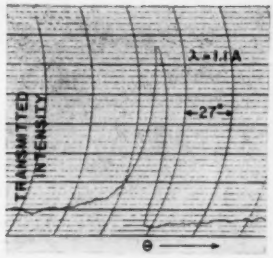

FIG. 1. Transmission curve for a calcite crystal.

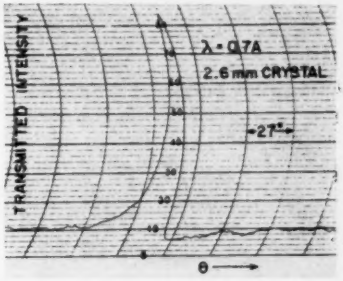

FIG. 2. Transmission curve for a 2.6-mm calcite crystal.

The results of both Bragg and Campbell were confirmed using the peaks of Mo $K\alpha 1$ and Cu $K\alpha 1$. The expected decrease in the transmitted intensity was observed at the short wavelength and the expected increase was observed at the longer wavelength. By using Cr $K\alpha$ radiation a large increase in transmitted intensity at the Bragg angle was also observed. With the spectrometer set to pass radiation of about 1.1A, the transmitted intensity was found to show a dip on the long wavelength side of the Bragg angle and a substantial increase at the Bragg angle as shown in Fig. 1. The absorption on the two sides of the Bragg angle was not the same.

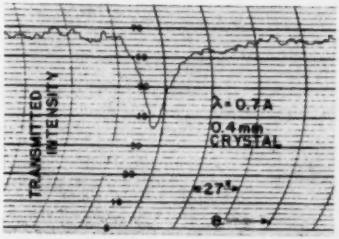

FIG. 3. Transmission curve for a 0.4-mm calcite crystal.

This effect was observed with two different crystals. In the $(1, -1)$ position, for the W continuum at 0.7A, the results depended on the crystal thickness. Figures 2, 3, and 4 show this effect for three

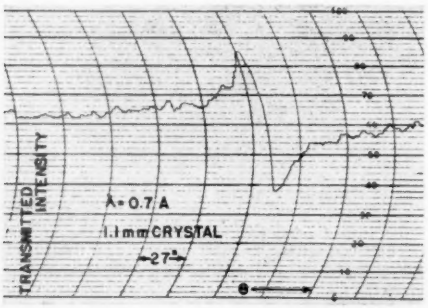

FIG. 4. Transmission curve for a 1.1-mm calcite crystal.

different crystals. Using the internal planes of a cleaved crystal of 2.6-mm thickness, the transmitted intensity showed an increase at the Bragg angle; a thin crystal of 0.4-mm thickness showed a decrease while a 1.1-mm thick crystal showed both a minimum and maximum. Further experiments on the transmitted intensity as a function of wavelength and crystal thickness are in progress.

We wish to express our appreciation to Professor S. K. Allison for the loan of a spectrometer. This work was supported by a grant from the Research Corporation.

[1] H. N. Campbell, J. Appl. Phys. **22**, 1139 (1951).
[2] Bragg, Bosanquet, and James, Phil. Mag. **42**, 1 (1921).
[3] G. Borrmann, Physik Z. **42**, 157 (1941).
[4] G. Borrmann, Z. Physik. **127**, 297 (1950).
[5] $(1, -1)$ with respect to the investigated crystal refers to a parallel alignment of its planes with that of the second crystal on the monochromator.

The Gamma-Radiations from V^{48} and Nb^{92}†

HAROLD K. TICHO, DAVID GREEN, AND J. REGINALD RICHARDSON
Department of Physics, University of California, Los Angeles, California
(Received March 10, 1952)

THE disintegration of the isotope V^{48} is followed by the emission of two gamma-rays[1,2] of energy 1.320 Mev and 0.990 Mev in cascade.

A gamma-ray of higher energy has also been reported by Fluharty and Deutsch[3] in 1 percent of the disintegrations. They reported that the energy was between 1.6 Mev and 2.2 Mev. Zobel[4] found a high energy gamma-ray in 3.5 percent of the disintegrations. By observing the absorption of the Compton electrons he concluded that the energy was consistent with the 2.31 Mev to be assigned to a cross-over gamma-ray.

We have observed the gamma-radiation emitted from a V^{48} sample prepared by the p, n reaction from titanium bombarded in the FM cyclotron at UCLA. The observations were made on a NaI spectrometer[5] of the Hofstadter type. The vanadium fraction was chemically separated.[6]

Figure 1 shows the comparison spectra of Na^{22}, V^{48}, and Na^{24}. Microdensitometer traces of these spectra were used to evaluate the high energy V^{48} line in terms of the 1.277-Mev photoline of Na^{22}, the 1.380-Mev photoline of Na^{24}, the 2.76-Mev photoline of Na^{24}, the 1.74-Mev pair line of Na^{24}, and the 1.320-Mev photoline of V^{48}. The result of these comparisons gave a spread of less than 1 percent and may be stated as 2.22 ± 0.02 Mev. This line is therefore clearly not a cross-over line which would involve the sum of the 0.990-Mev and 1.320-Mev energies. A small pair peak corresponding to the 2.22-Mev line was observed between the photoline of the 0.99-Mev and 1.32-Mev radiations.

An estimate of the relative number of the 2.22-Mev and 1.32-Mev quanta was made in the following manner. A series of five exposures were made of the V^{48} of varying length, 15 sec, 30 sec, 1 min, 15 min, 30 min, all on a single film. By comparing the times required for equal darkening of the 2.22- and 1.32-Mev photolines an estimate was made of the relative number of pulses per unit energy interval at the peaks of the lines. This was also done with Na^{24} for the 1.38-Mev and 2.76-Mev photolines. Assuming that the number of quanta in this latter case were equal we then drew a calibration curve for our particular spectrometer. This curve was drawn between the Na^{24} points with the help of the theoretical cross section involved and remembering the dependence of peak width on energy. In this manner we obtain that in the case of V^{48} the number of 2.22-Mev quanta is 3.6 percent of the 1.32-Mev quanta. We consider that the limit of error in this estimate is a factor of two. The chemically separated sample of V^{48} was followed in this way over several half-lives, and it was found that the

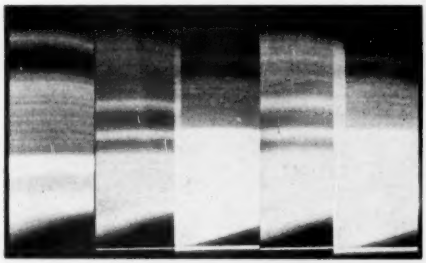

(a) (b) (c) (d) (e)

FIG. 1. Comparison gamma-ray spectra: (a) Na^{22}, (b) Na^{24}, (c) V^{48}, (d) Na^{24}, (e) V^{48}. The gain for (a) Na^{22} was increased by a factor of 1.96 relative to the others.

ratio of 2.22-Mev to 1.32-Mev quanta remained constant within the experimental uncertainty.

An unsuccessful search was made for a possible 90-kev gamma-ray which might be in cascade with the 2.22-Mev line. However, the fact that we did not find this radiation may not be significant in view of the possible masking by the large amount of annihilation radiation present. The upper limit to the number of cross-over gamma-rays of 2.31 Mev can be set from our measurements at 0.5 percent of the number of 1.32-Mev quanta.

Nb^{92} was bombarded by 20-Mev protons. Chemical separation was performed.[6] The spectrum indicated the presence of two lines, one very intense line with an energy of 0.933 ± 0.009 Mev and one weak line of energy 1.84 ± 0.02 Mev. Relative intensity measurements as a function of time indicated that although the decay of the 0.93-Mev line was consistent with the 10-day half-life of Nb^{92}, the 1.84-Mev line corresponded to a much longer half-life. Bombardments at varying proton energies indicated that the 1.84-Mev line should probably be assigned to the 42-day isomer of Nb^{92} produced by $Nb^{93}(p, p)Nb^{93*}$. The energy of the 0.93-Mev line agrees well with other measurements.[7,8]

† This work was supported in part by the joint program of the ONR and AEC.
[1] W. C. Peacock and M. Deutsch, Phys. Rev. **69**, 306 (1946).
[2] Robinson, Ter-Pogossian, and Cook, Phys. Rev. **75**, 1099 (1949).
[3] R. G. Fluharty and M. Deutsch, Phys. Rev. **76**, 182 (1949).
[4] W. Zobel, Tech. Ref. No. 4, Purdue University, October, 1950, unpublished.
[5] Harold K. Ticho, Phys. Rev. **84**, 847 (1951).
[6] We wish to thank Professor Ralph James for performing the chemical separations.
[7] D. N. Kundu and M. L. Pool, Phys. Rev. **71**, 140 (1947).
[8] P. Preiswerk and P. Stahelin, Helv. Phys. Acta. **24**, 300 (1951).

The Disintegration Scheme of K^{40}

M. PAGANELLI AND G. QUARENI
Istituto di Fisica dell' Universita di Padova, Italy
(Received March 18, 1952)

THE disintegration scheme of K^{40}, which is considered at present to be the more tenable, was proposed by Suess[1] in 1948 (Fig. 1). It is assumed in this scheme that the γ-radiation is associated with the K-capture. As no direct proof had yet been obtained for this association, we have attempted to establish its existence by an experiment based on the detection of coincidences between the γ-radiation and the products of K-capture, namely

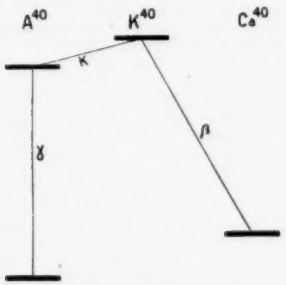

FIG. 1. Disintegration scheme of K^{40}.

Auger electrons[2] and x-rays.[3] The experimental arrangement is shown in Fig. 2. In position X may be placed Geiger counters (5×50 cm^3) of two types: ordinary counters and counters having the cathode coated internally with a layer of a salt of potassium. Five counters of the second type, indicated by (a), (b), (c), (d), and (e), were used. The chemical composition of the layers is given in the second column of Table I. In the third and fourth columns of the same table are listed the mean thicknesses in g/cm^2 and the total masses of potassium contained in each counter, respectively. The layers were deposited by spraying solutions of the salts. On examination under a microscope they showed small agglomerations of crystals whose dimensions were between 1 and 40 microns. Taking this fact into account we have evaluated the total surface area of the layers of counter (a) to be 400 cm^2 and of counters (b), (c), and (d) to be 1300 cm^2, with an error estimated not to exceed 30 percent.

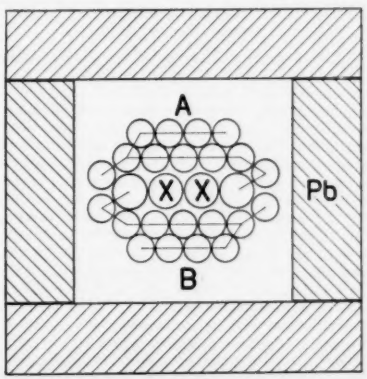

FIG. 2. Experimental arrangement.

TABLE I. Experimental data.

	Salts of K	g/cm^2	Grams of K	Pressure in mm of Hg	N coinc/hr
(a)	KCl	0.53×10^{-4}	0.022	95	0.45 ± 0.15
(b)	KI	11.7×10^{-4}	0.212	95	1.11 ± 0.17
(c)	KCl	5.3×10^{-4}	0.219	95	1.21 ± 0.18
(d)	KF	4.3×10^{-4}	0.225	95	1.90 ± 0.21
(e)	KF	$14-\times10^{-4}$	0.730	95	3.12 ± 0.72
(c')	KCl	5.3×10^{-4}	0.219	400	1.43 ± 0.18
(d')	KF	4.3×10^{-4}	0.225	400	2.38 ± 0.18

The counters located in position X are surrounded by 24 ordinary counters (4×70 cm^2) forming two groups of 12 each. All of the counters used in this experiment have a brass cathode 1 mm thick.

Triple coincidences A-X-B and double coincidences X-AB are recorded separately. The resolution time of the circuit is $(12.4\pm0.5)\times10^{-6}$ sec.

We may expect that the K^{40} would give double coincidences X-AB for the following events:

(1) An Auger electron or an x-ray resulting from K-capture initiates a discharge in the central counter; the associated γ-quantum (following the assumed hypothesis) may discharge one counter of group AB;

(2) the central counter detects a β-particle which, after having traversed the sensitive volume, comes to rest in the wall of the counter; the group AB may be discharged due to a photon produced by bremsstrahlung (internal or external) associated with the electron;

(3) a γ-ray may produce an electron by Compton effect in the brass wall of the central counter; the electron is detected by the central counter while AB detects the scattered photon.

Other double coincidences may be the result of:

(4) cosmic rays; practically all produce a triple coincidence as well;

(5) radioactivity of the surroundings;

(6) casual coincidences.

In order to separate the double coincidences actually due to K^{40}, the resultant coincidence counts from counters containing K and from ordinary counters are considered. The number of coincidences caused by K^{40} due to the effects listed in points (1), (2), (3) may be expressed as follows:

$$N=(D-T)-(D'-T')-(C-C'),$$

where D, T, C are, respectively, the double coinc/hr, the triple coinc/hr, and the casual double coinc/hr with counters containing potassium, and where D', T', C' are the corresponding coinc/hr for ordinary counters.

In order to reduce as far as possible the background count, represented by $D'-T'$, we have placed the equipment in a cave under 150 m of rock and have surrounded the counters with a shield of 10 cm of lead. The number N of coincidences per hour is listed in Table I, column six. The counters (c') and (d') are the same counters (c) and (d) with the increased filling pressure indicated in column five. It can be seen from the table that N does not vary proportionally to the mass of the potassium used. The results relative to counters (b), (c), and (d) show also that for a given mass of potassium, N varies appreciably with the chemical composition of the layer.

The events which we have considered in points 2 and 3 cannot account for these effects. They can be explained by assuming a coincidence between a penetrating radiation discharging the counters AB and a radiation of very short range discharging the central counter. If this range is much shorter than the linear dimensions of the crystals which compose the layer, the relative intensity of the radiation will be proportional to the surface area of the layer and not to the mass of the potassium it contains. The results are in agreement with the hypothesis that there is an association between γ-radiation and the Auger electrons. The latter have a 90 percent probability to follow the K-capture and have energy of $\sim$3 kev and range less than 0.3 micron in the salts

we have used. Comparing the results obtained with counters (c') and (d') with the corresponding results obtained from (c) and (d), a small increase in the coincidence rate is noted. Considering the fact that the counters (c') and (d') are more sensitive to photons of low energy, the increase in the number of coincidences observed can be explained by the hypothesis that a fraction of the coincidences are due to the association between γ-radiation and x-rays subsequent to K-capture. A sensible increase in N is obtained only for counters with KF ($N_{d'}-N_d=0.48\pm0.26$) and not for those with KCl. This agrees with the hypothesis that the increase is actually caused by x-rays of the K_α line of argon which are strongly absorbed in chlorine.

The hypothesis that there is an association between K-capture and γ-radiation justifies the magnitude of the observed effect.

Further details on this experiment will be found in a paper to appear shortly in *Nuovo cimento*.

We are indebted to Professor A. Rostagni for suggesting this investigation, to Dr. M. Ceccarelli for his assistance in the first phase of the experiment, to S. A. D. E. for the facilities afforded us, and to Soc. Montevecchio for lending the lead.

[1] H. E. Suess, Phys. Rev. **73**, 1209 (1948).
[2] G. A. Sawyer and M. L. Wiedenbeck, Phys. Rev. **79**, 490 (1950).
[3] Ceccarelli, Quareni, and Rostagni, Nuovo cimento **8**, 132 (1951).

Detection of Millimeter Wave Solar Radiation*

WILLIAM M. SINTON
Department of Physics, the Johns Hopkins University, Baltimore, Maryland
(Received March 10, 1952)

VAN VLECK has calculated the transmission of the atmosphere in the millimeter wave region.[1] His results show that the region from one to three millimeters, with the exception of the vicinity of the 2_2-3_{-2} rotation line of water vapor predicted at 1.6 mm (6.15 cm^{-1}), will be substantially transparent to solar radiation. Radiation in this region has now been detected from the sun. The detecting equipment consisted of a Golay infrared detector at the focus of a modified, 24-inch searchlight. The filters used to isolate these long wavelengths were three sheets of photographic wrapping paper, the quartz window of the detector, and the pure rotation spectrum of the water vapor in the atmosphere. The rotation spectrum of the water vapor removes the region 50 to 1000 microns, and black paper is opaque from the visible to 100 microns or more but is found to be transparent to these radiations.

Figure 1 shows two records which were obtained by allowing the sun to drift across the sensitive field of the millimeter wave telescope. The reduction in the signal which was obtained on February 2 was due more to the higher water vapor content of the air than to the clouds. Measurements indicate that clouds are quite transparent.

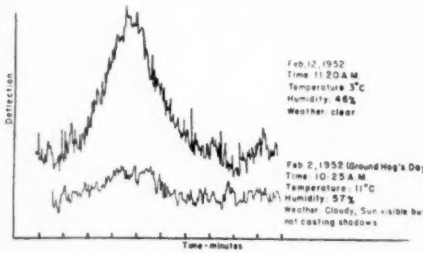

FIG. 1. Transits of the sun across the field of the millimeter wave telescope.

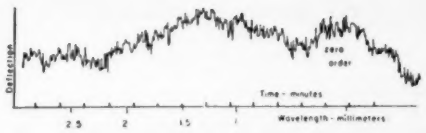

FIG. 2. Solar spectrum obtained with an echelette grating.

Assuming that the sun radiates as a blackbody at 6000°K, then the illumination just outside the earth's atmosphere is 9.5×10^{-11} watts per cm^2 in the wavelength region one to three millimeters. The maximum signal so far received was 6×10^{-12} watts per cm^2 which was obtained when the ground level atmosphere contained 2.7 grams of water per cubic meter. This signal was estimated by comparison to the signal received from a blackbody source of the same apparent diameter as the sun. The amount of water vapor absorption in the 45-foot path to the blackbody was estimated from ground level absorption measurements made in the laboratory.

One way in which the wavelength of this radiation has been checked involved measurements of the extinction coefficient of rocksalt. This has been measured in the far infrared by McCubbin and Sinton[2] and in the microwaves by von Hippel. A linear interpolation for the intervening wavelengths is sufficient since they are well removed from any eigenfrequency. The average wavelength found from the measured extinction coefficient is 1.4 mm.

A coarse transmission echelette grating was used to obtain the spectrum of the solar radiation. It was made of paraffin and had six lines per foot and an echelette angle of two degrees. Figure 2 shows the spectrum which was obtained when this grating was placed in front of the telescope and the sun allowed to move ahead without the telescope tracking. It is uncertain whether the dip in the spectrum near two mm is the 2_2-3_{-2} line of water vapor, or whether the peak after two mm is the second order of the shorter wavelength radiation. However, since the wavelength of the blaze is calculated to be one mm, the second order of this wavelength should be nearly absent.[3]

This work was carried out under the supervision of John Strong.

* This research was supported by a Navy contract.
[1] J. H. Van Vleck, Phys. Rev. **71**, 413 and 425 (1947).
[2] T. K. McCubbin and W. M. Sinton, J. Opt. Soc. Am. **40**, 537 (1950).

Hexagonal Iron-Oxide Compounds as Permanent-Magnet Materials

J. J. WENT,* G. W. RATHENAU, E. W. GORTER, AND G. W. VAN OOSTERHOUT
Philips Research Laboratories, N. V. Philips' Gloeilampenfabrieken, Eindhoven, Netherlands
(Received March 11, 1952)

A CLASS of oxides with hexagonal crystal structure has been the subject of a detailed magnetic investigation. These oxides are characterized by the formulas $MeO\cdot6Fe_2O_3$, and $MeO\cdot2Fe_2O_4\cdot6Fe_2O_3$, respectively, where Me stands for the divalent metals Ba, Sr, or Pb. Only the Ba-compounds will be dealt with in this communication. The saturation magnetic moment per gram as measured for small single crystals along the direction of preferred magnetization is plotted in Fig. 1 as a function of temperature. The value of the saturation magnetization at absolute zero temperature can be accounted for on the basis of the crystal structure[1,2] as being caused by noncompensated antiferromagnetism, along the lines of Néel's[3] and Anderson's[4] theories. The paramagnetic behavior above the Curie point (at about 450°C) is shown in Fig. 2 for the compound $BaO\cdot6Fe_2O_3$. It points equally to noncompensated antiferromagnetism.

The crystal anisotropy of the hexagonal compounds is large. Approximate values of the anisotropy constant K (in erg/cm^3) for $BaO\cdot6Fe_2O_3$ have been plotted against temperature in Fig. 3. K is defined by the relation: crystalline energy $=K\sin^2\varphi$, where φ is the angle between the magnetization and the hexagonal axis.

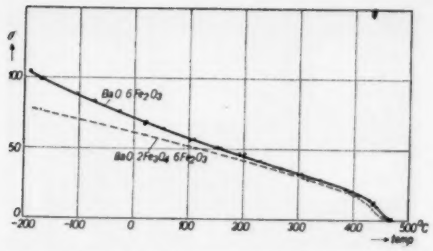

FIG. 1. Saturation magnetic moment per gram, measured for small single crystals along the direction of preferred magnetization, as a function of temperature.

The hexagonal axis is the direction of preferred magnetization while no anisotropy has been found within the basal plane.

The ratio K/I_s, which is related to the coercive force expected for pure rotation, does not decrease appreciably with temperature up to 300°C. I_s denotes the volume magnetization. The critical crystal size, which must be exceeded to allow the formation of a stable Bloch-wall within an isolated single crystal in its own demagnetizing field, contains as the temperature-dependent part the ratio $K^{\frac{1}{2}}/I_s$.[5,6] This ratio increases with rising temperature up to about 400°C.

Figure 4 shows the intrinsic coercive force ${}_IH_c$ for a fine-grained sintered sample of $BaO \cdot 6Fe_2O_3$ as a function of temperature. The curve shown cannot be explained by pure rotational processes since the observed values of ${}_IH_c$, though large, are appreciably lower than K/I_s, while also the shape of the curve differs from that of the curve K/I_s *versus* temperature. We believe that the maximum of ${}_IH_c$ at about 250°C is due to the interplay of two effects: the decrease of the number of stable Bloch-walls at higher temperatures, of which only the most stable will probably persist, and the increase of the mobility of a particular wall when K decreases. It may be added that, because of the high anisotropy coupled with a relatively low saturation magnetization single domain crystals can be expected at much larger crystal sizes than is the case with ordinary materials.

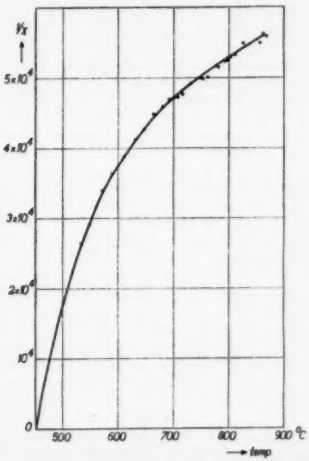

FIG. 2. Paramagnetic behavior of $BaO \cdot 6Fe_2O_3$ above the Curie point.

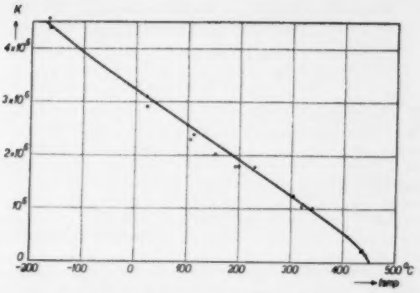

FIG. 3. Anisotropy constant K for $BaO \cdot 6Fe_2O_3$, as a function of temperature.

In connection with the increase of the coercive force ${}_IH_c$ with temperature the following experiment is interesting. A magnetized specimen of $BaO \cdot 6Fe_2O_3$ (demagnetization factor 0.1) is heated up to 400°C, whereby the remanence decreases to about 30 percent of the room-temperature value, and cooled to room temperature again without application of an external magnetic field. The room-temperature value of the remanence is again obtained.

The $(BH)_{max}$ value of fine-grained sintered material at 20°C amounts to about 0.85×10^6 gauss oersted at $B = 1100$ gauss. The

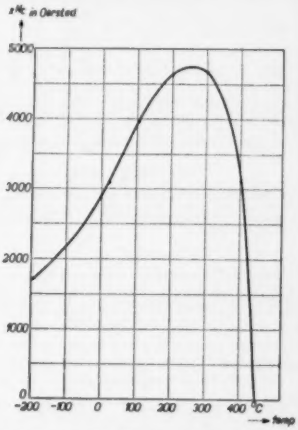

FIG. 4. Intrinsic coercive force ${}_IH_c$ for a fine-grained sintered sample of $BaO \cdot 6Fe_2O_3$, as a function of temperature.

material contains only trivalent iron ions and accordingly shows a high resistivity (well above 10^7 ohm cm at room temperature).[7]

A detailed publication will appear elsewhere.[8]

* Now with N.V. K.E.M.A., Arnhem (Netherlands).

[1] V. Adelsköld, Arkiv Kemi, Mineral Geol. **12A**, No. 29, 1 (1938). (For $MeO \cdot 6Fe_2O_3$).

[2] P. B. Braun (to be published) (for $MeO \cdot 2Fe_2O_3 \cdot 6Fe_2O_3$).

[3] L. Néel, Ann. phys. **3**, 137 (1948).

[4] P. H. Anderson, Phys. Rev. **79**, 350, 705 (1950).

[5] C. Kittel, Revs. Modern Phys. **21**, 541 (1949).

[6] The equations for the critical diameter in reference 5 have been corrected so as to take into account the fact that the exchange interaction decreases with temperature as I_s^2/I_0^2, I_0 being the volume magnetization at zero absolute temperature.

[7] J. H. de Boer and E. J. W. Verwey, Proc. Phys. Soc. (London) **49**, 59 (1937).

[8] Went, Rathenau, Gorter, and van Oosterhout, Philips Tech. Rev. (January 1952).

Magnetic Domains on Silicon Iron by the Longitudinal Kerr Effect*

C. A. FOWLER, JR., AND E. M. FRYER
Department of Physics, Pomona College, Claremont, California
(Received March 14, 1952)

USE of the normal Kerr magneto-optic effect to observe domain patterns in ferromagnetic substances having free surface poles has been described by Williams, Foster, and Wood.[1] Since plane polarized light reflected normally from a polished magnetic surface is not affected by magnetization in the plane of the surface, oblique reflection using the longitudinal Kerr magneto-optic effect[2] has been investigated as a means of observing domains in a single crystal of silicon iron where the magnetization is in the plane of the crystal surface. The plane of polarization of the reflected light suffers a positive or negative rotation depending upon the direction of magnetization. For magnetic saturation this rotation amounts to about 4 minutes at an angle of incidence of 60°. Ambiguity with the transverse Kerr effect is avoided by polarizing the light at right angles to the plane of incidence, for which direction the transverse Kerr effect is zero.[3]

Two methods have been used to observe domain structure on the (100) surface of the silicon iron crystal. Observations of Kerr effects over local portions of the surface have been made by illuminating the surface with a small optical probe, passing the reflected beam through a nicol analyzer set about 2° from extinction, and measuring the intensity of the transmitted light with a sensitive multiplier phototube circuit. A traverse of the crystal in an unmagnetized state with a 0.5-mm probe of light, when compared with a similar traverse after application of a small external field, indicates those regions in which there has been a change in surface magnetization. Figure 1 is the result of such analysis for traverses in the [001] direction across the central portion of the (100) surface.

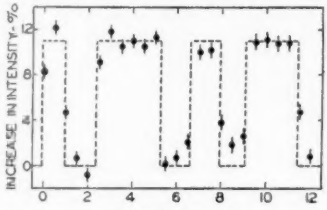

FIG. 1. Percentage increase in transmitted light with magnetization of silicon iron crystal along a line through the center of the crystal in the [001] direction. The broken line indicates the domain configuration suggested and substantiated in (b) of Fig. 2.

Since the contrast between regions magnetized in antiparallel directions is about 10 percent, photographic observations are possible with a suitable optical system. Figure 2 shows oblique photographs of the crystal with the same domain arrangement as that scanned photoelectrically. (a) and (b) differ 180° in the position of the crystal, resulting in the reversal of the relative intensities of adjacent domains. (c) is the result of magnetizing the crystal along the direction of the original domains, namely the [010] direction. This is the long dimension of the crystal although it appears otherwise because of the angle at which the picture was taken. While the crystal was electro-polished to a mirror surface, oblique photography and the need for increasing the contrast in development and printing have magnified surface imperfections and resulted in its rough appearance.

It is interesting to note that a particular domain pattern is generally quite stable and persists indefinitely under normal conditions of handling. Magnetization and subsequent demagnetization generally result in different domain bands, always parallel to the long side of the crystal surface. There is some evidence, however, that patterns may eventually reoccur.

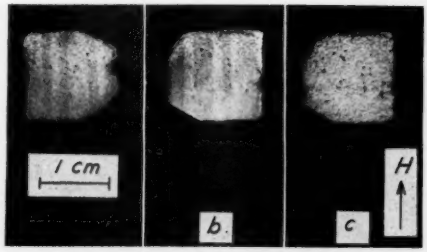

FIG. 2. Oblique photographs of the (100) surface of the crystal. In (a) and (b) the crystal is unmagnetized. An external field in the direction shown was applied in (c).

Results seem comparable with the magnetic powder patterns obtained by Williams, Bozorth, and Shockley[4] although we have not yet employed their method on this particular crystal.

We wish to thank R. M. Bozorth and H. J. Williams of the Bell Telephone Laboratories for loan of the single crystal of silicon iron[5] and for discussions concerning the investigation. We are also indebted to the Office of Naval Research for support of this research and to Burton Henke for assistance on the project.

* Supported by the ONR.

[1] Williams, Foster, and Wood, Phys. Rev. **82**, 119 (1951).
[2] *International Critical Tables* (McGraw-Hill Book Company, Inc., New York, 1929), first edition, Vol. VI, p. 438.
[3] L. R. Ingersoll, Phys. Rev. **35**, 312 (1912).
[4] Williams, Bozorth, and Shockley, Phys. Rev. **75**, 155 (1949).
[5] H. J. Williams, Phys. Rev. **52**, 747 (1937).

The Occurrence of Heavy Mesons in Penetrating Showers*

R. B. LEIGHTON AND S. D. WANLASS
California Institute of Technology, Pasadena, California
(Received March 17, 1952)

IN the course of a cloud chamber study of penetrating showers, two events have been observed which probably represent the decay in flight of τ-mesons,[1] and one event which probably represents the decay in flight of a κ-meson.[2]

One of the τ-meson decays is shown in Fig. 1. The particle enters the chamber at the top, traverses the 2.5-cm lead plate with no detectable deflection, and decays in the lower section of the chamber into three charged particles. All of the tracks except that of the left-hand secondary are at, or very near, minimum ionization; the ionization of the latter secondary is estimated to be 1.4–2.2 times minimum. The momentum of the τ-meson, based upon its curvature in the 5000-gauss magnetic field, is 600 ± 100 Mev/c, and the momenta of the three secondary particles are, from the left to right, 155 ± 30, 350 ± 75, and 210 ± 50 Mev/c. The masses of the secondaries are therefore 350 ± 75 m_e, less than 600 m_e, and less than 300 m_e, respectively, and are thus all consistent with π-mesons, but none can be a proton. Charge is conserved, and the measured momenta are consistent with conservation of momentum in the decay. The mass of the τ-meson, calculated from the above momenta, is about 975 m_e, which corresponds to an energy release of about 75 Mev.[1] It would be extremely difficult to interpret this event as a collision phenomenon.

The second τ-meson decay is similar in appearance to the above one, but the momenta are higher, making the mass limits on all of the particles less sharp. Both of these τ-mesons, which are the only ones we have so far observed to decay, travel much farther inside the chamber before decaying than do V-particles; this suggests that their mean life is considerably longer than that of V-particles—perhaps 10^{-9} sec or even longer.

The κ-meson decay is shown in Fig. 2. The particle (heavily ionizing) enters the upper chamber from the right, proceeds downward toward the left, and decays above the plate, producing a single charged particle (which travels upward toward the left) and presumably one or more neutral particles. The momentum of the κ is 185 ± 20 Mev/c, and its ionization, estimated visually, is 6–10 times minimum. Thus its mass is 1200 ± 300 m_e. The momentum of the secondary particle is 150 ± 15 Mev/c, and its ionization is about 1.2–1.6 times minimum, indicating a mass of 250 ± 50 m_e, a value consistent with either a π- or μ-meson. The kinetic energy of the meson (assumed to be a μ) in the center-of-mass system is 82 Mev.

This event might alternatively be interpreted as the decay of a V^0 or V^- particle. However, the absence of a nearby origin from which either of these particles could have come suggests, rather, a longer-lived particle which can decay at a great distance from its point of origin, even though it is moving slowly. Furthermore, if the event were to represent the decay of a V^0-particle, the latter would have to be traveling upward, and would thus be the only one to do this out of more than 150 observed V^0-particles.

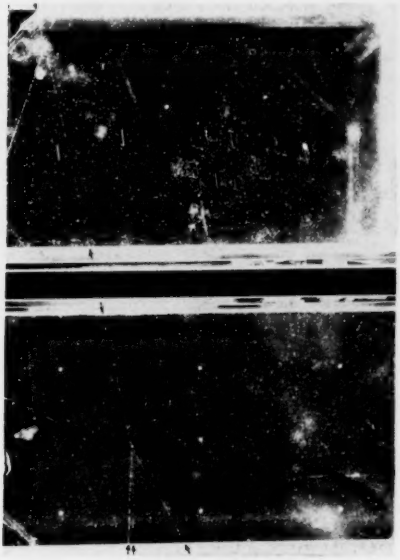

FIG. 1. The decay of a τ-meson.

The presence of both $\tau-\kappa$-mesons in penetrating showers is also indicated by direct estimates of the masses of heavily-ionizing particles in these showers. Preliminary results suggest that the flux of τ- and κ-mesons may be rather great—perhaps much greater than that of V-particles.

In addition to several τ- and κ-meson tracks, this preliminary survey has also yielded three tracks which may indicate the existence of a particle whose mass lies in the range 400–650 m_e. The momenta of these particles are 180 ± 20, 100 ± 15, and 135 ± 15 Mev/c, and their ionizations, estimated visually by comparing them with time-coincident protons, mesons, and electrons on the same photographs, are 2–3, 3–6, and 4–8 times minimum, respectively. These measurements indicate masses of 550 ± 150 m_e, 450 ± 150 m_e, and 750 ± 150 m_e, respectively. Only with great difficulty can the first two tracks be reconciled with those of either π- or τ-mesons; the third cannot be a π-meson, but might conceivably be a τ-meson.

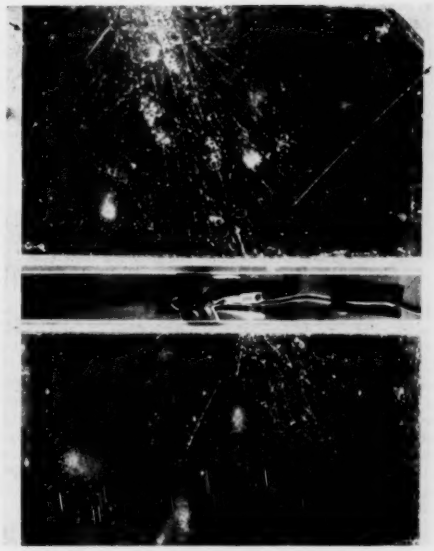

FIG. 2. The decay of a κ-meson.

It should perhaps be mentioned that there are indications, mainly from the division of momentum between V^0-particle secondaries, that particles of mass 500–700 m_e are sometimes produced in V^0 decay.

* Supported in part by the joint program of the ONR and AEC.

[1] Brown, Camerini, Fowler, Muirhead, Powell, and Ritson, Nature **163**, 82 (1949).

[2] C. O'Ceallaigh, Phil. Mag. **42**, 1032 (1951).

Motion of an Electron in a Perturbed Periodic Potential

EDWARD N. ADAMS, II
Institute for Nuclear Studies, University of Chicago, Chicago, Illinois
(Received March 10, 1952)

IN a previous publication[1] (referred to as I) a generalized multiband form of Wannier's theory[2] was derived and used to establish the region of validity of Luttinger's[3] generalization of the one-band theory. In the presentation of the theory a logical gap was overlooked, so it was necessary to note in proof that the diagonal part of the operator ξ^μ, which represents the μ-component of the electron coordinate, need not have the form used throughout the last half of the paper. Accordingly, it was stated that the equations of (I) were to be modified so that the part of ξ^μ in the nth band became $x^\mu+\xi(p)_{nn}{}^\mu$ instead of x^μ, $\xi(p)_{nn}{}^\mu$ being some periodic function of p. Now such a form for ξ^μ is not objectionable for the formal structure of the theory. However, it is a great inconvenience in a calculation because of the additional complexity which it introduces into the commutation rules as a result of the p dependence of $\xi_{nn}{}^\mu$. For this reason, one would want to simplify the form of $\xi_{nn}{}^\mu$ as much as possible. It will be shown that in every case $\xi_{nn}{}^\mu$ can be made independent of both p and x, and hence is a constant which will be called $X_n{}^\mu$. $X_n{}^\mu$ has a simple significance.

The mean value of the coordinate of the electron taken over the Wannier localized function $\varphi_{ln}(x)$ is

$$(\varphi_{ln}(x),\ x^\mu\varphi_{ln}(x))=x_l^\mu+X_n^\mu. \tag{1}$$

Thus X_n^μ is the mean displacement of the center of charge from the origin in unit cell.

It was shown in (I) that for any choice of phase of the Bloch functions ψ_{kn} so that they are periodic in p space, there exists a function $\eta_n(p)$ such that

$$\xi_{nn}{}^\mu=\frac{\partial}{\partial p^\mu}\eta_n(p). \tag{2}$$

The error made in (I) was to treat η_n as a periodic function of p, whereas it had been proven only that $\xi_{nn}{}^\mu$ was a periodic function. Since $\xi_{nn}{}^\mu$ is periodic, however, the most general form of η_n is

$$\eta_n(p)=\eta_n'(p)+X_n{}^\mu p^\mu. \tag{3}$$

In a band n for which some of the $X_n{}^\mu$ are different from zero, the treatment of (I) requires that across some plane in the Brillouin zone the phase of the wave function ψ_{kn} jumps by the increment of $X_n{}^\mu p^\mu$ across the zone. The difficulty noted in the footnotes to (I) is that derivatives of the ψ_{kn} by k do not converge on this plane.

There is, of course, an arbitrariness in the definition of the Bloch functions ψ_{kn} on which the theory is based, since it has been assumed of them only that they are eigenfunctions of H_0 and are continuous periodic functions of k. An equally suitable set of basic functions $\bar{\psi}_{kn}$ are obtained from the ψ_{kn} by multiplying them by a factor $U(hk, n)$ which is any continuous and periodic function of k with modulus unity. If $U(hk, n)$ is chosen to be

$$U(hk, n)=\exp[-i\eta_n'/\hbar], \tag{4}$$

and the $\bar{\psi}_{kn}$ used as the basic functions one gets

$$\xi_{nn}{}^\mu=X_n{}^\mu. \tag{5}$$

Further, by a suitable choice of $U(hk, n)$, $X_n{}^\mu$ can always be made so small that if plotted from the center of unit cell it does not extend past the surface of the cell. The change of phase of basic functions is accomplished by transforming all operators in the Wannier theory with the unitary operator

$$\mathbf{U}=\Sigma_n\mathfrak{r}_{nn}U(p, n). \tag{6}$$

As a consequence of the argument above, one can now show that the treatment of the problems discussed in (I) is essentially correct. In particular, the chief modification in the equation of motion in a magnetic field is that Luttinger's Hamiltonian should involve $E_n(p+(e/c)\mathfrak{A}(x+X_n))$ rather than $E_n(p+(e/c)\mathfrak{A}(x))$. By proper choice of the origin in unit cell one could always arrange that for any one band $X^\mu=0$. Therefore, the conclusions originally drawn as to the validity of Luttinger's form of Wannier's one-band theory remain unchanged.

[1] E. N. Adams, II, Phys. Rev. **85**, 41 (1952).
[2] G. H. Wannier, Phys. Rev. **52**, 191 (1937); William Slater, Phys. Rev. **76**, 1592 (1944).
[3] J. M. Luttinger, Phys. Rev. **84**, 814 (1951).

The Saturation Property of Nuclear Forces

HIDEO KANAZAWA
College of General Education, Tokyo University, Tokyo, Japan
(Received February 25, 1952)

IN the Fermi gas model of heavy nuclei all the lowest states of neutrons and protons are occupied up to those with a maximum momentum. On account of the Pauli principle the interaction potentials between nucleons in heavy nuclei are expected to be different from those between free nucleons.

The matrix element for the transition from an initial state in which two nucleons have momenta $\mathbf{p}_1$, $\mathbf{p}_2$ to a final state with the momenta $\mathbf{p}_1-\mathbf{k}$, $\mathbf{p}_2+\mathbf{k}$ *via* a neutral scalar meson field is given by

$$g^2f(p_1)f(p_2)[1-f(p_1-k)][1-f(p_2+k)]\left\{\frac{1}{E(p_1)-E(p_1-k)-\omega_k}+\frac{1}{E(p_2)-E(p_2+k)-\omega_k}\right\}\exp i(\mathbf{k}, \mathbf{x}_2-\mathbf{x}_1)(\psi_1'^*\beta\psi_1)(\psi_2'^*\beta\psi_2).$$

Here $f(\mathbf{p})$ is the probability that the state $\mathbf{p}$ is occupied and E, ω are the energies of the nucleon and the meson, respectively. The interaction potential between two nucleons having momenta $\mathbf{p}_1$, $\mathbf{p}_2$ within the Fermi sphere is given by

$$V(1, 2)=g^2\beta^{(1)}\beta^{(2)}\int[1-f(p_1-k)][1-f(p_2+k)]\times\left\{\frac{1}{E(p_1)-E(p_1-k)-\omega_k}+\frac{1}{E(p_2)-E(p_2+k)-\omega_k}\right\}\times\exp i(\mathbf{k}, \mathbf{x}_2-\mathbf{x}_1)\frac{d\mathbf{k}}{(2\pi)^3}.$$

If we apply the energy law, two nucleons within the Fermi sphere cannot go over to the states outside the fermi sphere. However, according to Araki and Huzinaga,[1] the energy law cannot be made use of in general when forces between fermions in bound states are to be derived. In nonrelativistic approximation we get the following potential

$$V(1, 2)=-g^2\int[1-f(p_1-k)][1-f(p_2+k)]\frac{\exp i(\mathbf{k}, \mathbf{x}_2-\mathbf{x}_1)}{\omega_k{}^2}\frac{d\mathbf{k}}{(2\pi)^3}.$$

We now calculate the mean energy of $V=\frac{1}{2}\Sigma_{i,k}V(i, k)$ using the Fermi gas model.

$$\bar{V}=\bar{V}_{\text{ord}}+\bar{V}_{\text{exc}}$$

$$\bar{V}_{\text{ord}}=\frac{1}{2}\Big\{\sum_{p_1,p_2}{}^{(+)}\int\psi_{p_1}{}^*(x_1)\psi_{p_2}{}^*(x_2)V(1, 2)\psi_{p_1}(x_1)\psi_{p_2}(x_2)dx_1dx_2+\sum_{p_1,p_2}{}^{(-)}\int\psi_{p_1}{}^*(x_1)\psi_{p_2}{}^*(x_2)V(1, 2)\psi_{p_1}(x_1)\psi_{p_2}(x_2)dx_1dx_2+2\sum_{p_1}{}^{(+)}\sum_{p_2}{}^{(-)}\int\psi_{p_1}{}^*(x_1)\psi_{p_2}{}^*(x_2)V(1, 2)\psi_{p_1}(x_1)\psi_{p_2}(x_2)dx_1dx_2\Big\}.$$

$$\bar{V}_{\text{exc}}=\frac{-1}{2}\Big\{\sum_{p_1,p_2}{}^{(+)}\int\psi_{p_1}{}^*(x_1)\psi_{p_2}{}^*(x_2)V(1, 2)\psi_{p_2}(x_1)\psi_{p_1}(x_2)dx_1dx_2+\sum_{p_1,p_2}{}^{(-)}\int\psi_{p_1}{}^*(x_1)\psi_{p_2}{}^*(x_2)V(1, 2)\psi_{p_2}(x_1)\psi_{p_1}(x_2)dx_1dx_2\Big\},$$

where $\psi_p(x)=\Omega^{-\frac{1}{2}}\exp i(\mathbf{p}, \mathbf{x})$ and $\Sigma^{(+)}$, $\Sigma^{(-)}$ represent summations extending over the occupied neutron states and proton states, respectively. If we first perform the integration over x, we find that only $k=0$ contributes to $\bar{V}_{\text{ord}}$, but $[1-f(p_1)][1-f(p_2)]$ vanishes because of $f(p_1)=f(p_2)=1$. So the nonsaturating $\bar{V}_{\text{ord}}$ vanishes, but $\bar{V}_{\text{exc}}$ does not.

The details will be published elsewhere.

[1] G. Araki and S. Huzinaga, Prog. Theoret. Phys. **6**, 673 (1951).

β-Decay of Mirror Nuclei and the Shell Model

O. KOFOED-HANSEN AND AAGE WINTHER
Institute for Theoretical Physics, University of Copenhagen, Copenhagen, Denmark
(Received March 14, 1952)

SPIN and parity predictions from the nuclear shell model are in good agreement with nearly all experimental β-decay data.[1] For mirror nuclei the ft-values agree within a factor two with the theoretical nuclear matrix elements for suitably chosen β-decay coupling constants.[2-3]

It is the intention in this note to base a determination of these coupling constants on those mirror nuclei which have closed shells (0, 2, 8, 20) in both neutrons and protons±one particle. For these

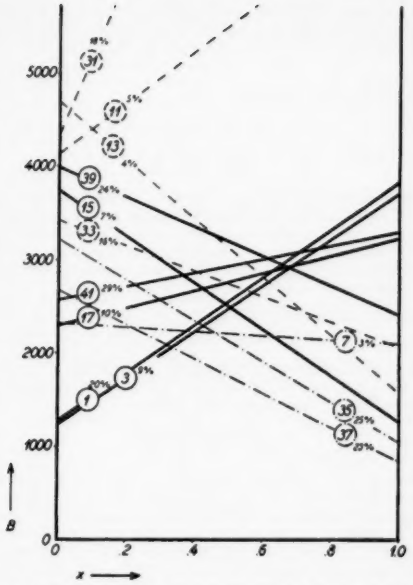

FIG. 1. B as a function of x for some mirror nuclei. The mass number is given in a circle at each curve and the experimental uncertainty in ft is indicated. ——— represents data in Table I. — — — — — represents data in Table II. — — — — — represents data in Table III.

nuclei one would expect the shell model to prescribe the wave functions with the least ambiguity. The view that these nuclei have a simple structure is also supported by the fact that their magnetic moments lie close to the Schmidt lines.

The nuclear wave functions are thus taken as single particle wave functions, and the normalization of the coupling is evident when it is noted that the square of the Fermi matrix element between $s_{1/2}$ states is given by $|F|^2=|\langle s_{1/2}|1|s_{1/2}\rangle|^2=1$ and that the corresponding Gamow-Teller (G−T) matrix element squared is $|G|^2=|\langle s_{1/2}|\sigma|s_{1/2}\rangle|^2=3$. The results are given in Table I.[4]

The decay constant is given by

$$\lambda=\frac{\ln 2}{t}=\frac{g^2m^5c^4}{2\pi^3\hbar^7}[(1-x)|F|^2+x|G|^2]f,$$

where x is the relative contribution from the G−T coupling; i.e., the partial coupling constant for G−T transitions equals $g[x]^{\frac{1}{2}}$, and correspondingly $g[1-x]^{\frac{1}{2}}$ is the partial Fermi coupling constant.

With

$$B=2\pi^3\hbar^7\ln 2/(g^2m^5c^4),$$

we get

$$B=ft[(1-x)|F|^2+x|G|^2].$$

In an x, B-diagram this represents a straight line connecting $B=ft|F|^2$ for $x=0$ and $B=ft|G|^2$ for $x=1$. For each of the transitions listed in Table I this straight line is given as a full drawn curve in Fig. 1. If the data are consistent with a single value of x and B all these lines ought to pass through a common point. This is actually the case within the limits of the experimental uncertainties. A least square fit of the data yields $B=2600\pm 85$ and $x=0.50\pm 0.05$, where the errors given are mean square deviations computed from internal consistency of the data. From this value of B we find $g=(2.19\pm 0.03)\times 10^{-49}$ erg cm^3.

These values differ somewhat from those given by Moszkowski[5] who based his determination on H^3, Be^7 (see below) and on He^6.

It should be emphasized that the above uncertainties of course do not contain the changes which might arise from refinements in the nuclear wave functions.

It is clear that more precise experimental investigations would be of great value in deciding whether the shell model is sufficiently accurate to provide a unique intersection point for the transitions listed in Table I. At the same time one would obtain an improved determination of B and x.

TABLE I. Mirror nuclei with closed shells 0, 2, 8, 20 ±one particle.

Transition	Spin	Configuration	Maximum kinetic energy, Mev	Half-life, t	ft[a]	$\|F\|^2$	$\|G\|^2$
$_0n^1-{}_1H^1$	1/2	$s_{1/2}$	0.782 ±0.001	12.8 ±2.5 min	1280±20%	1	3
$_1H^3-{}_2He^3$	1/2	$-s_{1/2}$[b]	0.0191±0.0005	12.45±0.20 yr	1240± 9%	1	3
$_8O^{15}-{}_7N^{15}$	1/2	$-p_{1/2}$	1.68 ±0.01	2.1 ±0.1 min	3750± 7%	1	1/3
$_8F^{17}-{}_8O^{17}$	5/2	$d_{5/2}$	1.72 ±0.03	70 ±3 sec	2300±10%	1	7/5
$_{19}Ca^{39}-{}_{18}K^{39}$	3/2	$-d_{3/2}$	5.13 ±0.15	1.1 ±0.2 sec	3990±24%	1	3/5
$_{21}Sc^{41}-{}_{20}Ca^{41}$		$f_{7/2}$	4.9 ±0.3	0.87±0.05 sec	2570±29%	1	9/7

[a] The Fermi integral f is determined from the formulas of Feenberg and Trigg (reference 4).
[b] The symbol $-s_{1/2}$ indicates that one $s_{1/2}$ particle will fill up the shell.

TABLE II. Mirror nuclei with closed shells 6, 16 ±one particle.

Transition	Spin	Configuration	Maximum kinetic energy, Mev	Half-life, t	ft	$\|F\|^2$	$\|G\|^2$
$_6C^{11}-{}_5B^{11}$	3/2	$-p_{3/2}$	0.975±0.010	20.5±0.2 min	4130± 5%	1	5/3
$_7N^{13}-{}_6C^{13}$	1/2	$p_{1/2}$	1.24 ±0.02	10.1±0.2 min	4700± 4%	1	1/3
$_{16}S^{31}-{}_{15}P^{31}$	1/2	$-s_{1/2}$	4.06 ±0.12	3.2±0.3 sec	4320±18%	1	3
$_{17}Cl^{33}-{}_{16}S^{33}$	3/2	$d_{3/2}$	4.43 ±0.13	1.8±0.1 sec	3440±16%	1	3/5

TABLE III. Unique $J-T$ multiplet mirror nuclei.

Transition	Spin	Configuration	Maximum kinetic energy, Mev	Half-life, t	ft	$\|F\|^2$	$\|G\|^2$
$_4Be^7-{}_3Li^7$	3/2	$(p^3_{3/2})_{3/2}{}^{1/2}$[a]	0.863±0.002[b]	54 ±1 day	2330± 3%	1	121/135
$_{18}A^{35}-{}_{17}Cl^{35}$	3/2	$(d^3_{3/2})_{3/2}{}^{1/2}$	4.4 ±0.2	1.90±0.05 sec	3220±25%	1	121/375
$_{19}K^{37}-{}_{18}A^{37}$		$(d^3_{3/2})_{3/2}{}^{1/2}$	4.57 ±0.13	1.2 ±0.2 sec	2700±23%	1	121/375

[a] The upper right index 1/2 means $T=1/2$.
[b] K-capture.

We have also calculated $|F|^2$ and $|G|^2$ for mirror nuclei having 6 protons and neutrons±one nucleon and 16 protons and neutrons±one nucleon, since the numbers 6 and 16 are assumed to represent closed configurations. The data are listed in Table II and shown in Fig. 1. Especially for the nuclei of mass numbers 11 and 31 the fit is bad. This can hardly be explained without the assumption of a rather strong distortion of the nuclear wave functions. Also the magnetic moments of these nuclei show that one does not have pure single particle states. Estimates indicate that perturbations of the order of magnitude required may arise from the coupling between the single particle motion and nuclear surface deformations.[6,7]

For the more complicated mirror nuclei the shell model wavefunctions are more ambiguous. However, in a few cases included in Table III the states are given uniquely by the $j-j$ coupling shell model together with the charge symmetry requirements. The results for these nuclei are plotted in Fig. 1, and it is seen that the matrix elements are slightly too small.

A more detailed account of β-matrix elements derived from nuclear shell models will appear in Dan. Mat. Fys. Medd.

We wish to thank Professor N. Bohr for his interest in our work, and we are indebted to Dr. Ben Mottelson and Mr. Aage Bohr for many valuable discussions and suggestions.

[1] Mayer, Moszkowski, and Nordheim, Argonne National Laboratory Report No. 4626 (1951); and Revs. Modern Phys. (to be published).
[2] E. P. Wigner, *Notes on Nuclear Structure and Beta Theory* (University of Wisconsin, Madison, Wisconsin, 1951).
[3] G. L. Trigg (private communication).
[4] E. Feenberg and G. L. Trigg, Revs. Modern Phys. **22**, 399 (1950).
[5] S. A. Moszkowski, Phys. Rev. **82**, 118 (1951).
[6] Aage Bohr, Dan. Mat. Fys. Medd. **26**, 14 (1952).
[7] Aage Bohr and B. Mottelson, Dan. Mat. Fys. Medd. (to be published).

Tests of Charge Independence from Pion Production in Nuclear Collisions*

A. M. L. MESSIAH
University of Rochester, Rochester, New York
(Received March 6, 1952)

NEW possibilities of testing the hypothesis of charge independence[1] arise in connection with studies of pion production in nuclear collisons. Formally, charge independence is most conveniently expressed with the help of the isotopic spin formalism which can be extended to include pions; it amounts to assuming that the total isotopic spin is a good quantum number in reactions involving nucleons and pions only.[2] If this assumption is true, it turns out that the cross sections for the production of charged and neutral pions in nuclear collisions must satisfy rather stringent relations.

Thus, consider a production process,

$$N_1+N_2\rightarrow N+\pi, \tag{1}$$

where N_1 and N_2 designate the colliding nuclei and N the outgoing nuclear fragments (bound or unbound). We designate by t_1, t_2, t, ϑ the isotopic spins of N_1, N_2, N, and π, respectively, ($\vartheta=1$) and by T the total isotopic spin ($|t_1-t_2|\leqslant T\leqslant t_1+t_2$).

The simplest case is $t_1=0$, $t_2=0$ (e.g., $d+\alpha$, $\alpha+\alpha$, $d+C^{12}$, $\cdots$); then $T=0$ and the cross sections σ_+, σ_0, σ_-, for the production of π^+, π^0, π^- at a given solid angle and with a given energy must be equal since there exists no preferred direction in charge space:

$$\sigma_+=\sigma_0=\sigma_-. \tag{2}$$

The equality of σ_+ and σ_- is merely a consequence of charge symmetry; therefore one must measure the π^0 yield if one wishes to use (2) as a test of charge independence.

When $t_1=0$, $t_2=\frac{1}{2}$ (e.g., $p+d$, $p+\alpha$, $p+C^{13}$, $\cdots$, $d+Be^9$, $\cdots$), $T=\frac{1}{2}$; therefore t may assume two values: $\frac{1}{2}$ or $\frac{3}{2}$. For convenience, we treat the particular case of p-d collisions; it will become apparent that the general case leads to identical results. The 3-nucleon system leads to one quartet and two doublets; the corresponding charge functions will be designated by the symbols ξ_q, ξ'_q, ξ''_q, respectively, where the subscript q stands for the total charge of the nuclear system (with the convention that the proton has isotopic spin $+\frac{1}{2}$, $q=t_z+\frac{1}{2}$) and ϑ_+, ϑ_0, ϑ_- will designate the charge functions of the 3 types of pions. Only 3 mutually orthogonal charge states can be formed with 3 nucleons and 1 pion, having the proper values $T=\frac{1}{2}$, $T_z=\frac{1}{2}$:

$$\begin{aligned}\chi&=\sqrt{\tfrac{1}{3}}\xi_1\vartheta_+-\sqrt{\tfrac{1}{3}}\xi_2\vartheta_0+\sqrt{\tfrac{1}{3}}\xi_3\vartheta_-\\ \chi'&=\sqrt{\tfrac{2}{3}}\xi_1'\vartheta_+-\sqrt{\tfrac{1}{3}}\xi_2'\vartheta_0\\ \chi''&=\sqrt{\tfrac{2}{3}}\xi_1''\vartheta_+-\sqrt{\tfrac{1}{3}}\xi_2''\vartheta_0.\end{aligned} \tag{3}$$

Therefore, the scattered wave function assumes the form $\Psi_\chi+\Psi'_{\chi'}+\Psi''_{\chi''}$ where Ψ, Ψ', and Ψ'' depend on the nucleon spins, the relative coordinates of the nucleons and the coordinate $\mathbf{r}$ of the pion relative to the center of mass of the nucleons. Using Eq. (3), this scattered wave can be rewritten in order to separate the terms corresponding to mesons of different charge, namely

$$\begin{aligned}&[\sqrt{\tfrac{1}{3}}\Psi\xi_1+\sqrt{\tfrac{2}{3}}(\Psi'\xi_1'+\Psi''\xi_1'')]\vartheta_+\\ &\quad-[\sqrt{\tfrac{1}{3}}\Psi\xi_2+\sqrt{\tfrac{1}{3}}(\Psi'\xi_2'+\Psi''\xi_2'')]\vartheta_0+[\sqrt{\tfrac{1}{3}}\Psi\xi_3]\vartheta_-.\end{aligned} \tag{4}$$

Let us consider first the cross sections for producing π^++H^3 and π^0+He^3, respectively. In this case, $t=\frac{1}{2}$ and the nuclear wave functions in the final state assume the form

$$\begin{aligned}\Phi_{H^3}&=\phi'\xi_1'+\phi''\xi_1''\\ \Phi_{He^3}&=\phi'\xi_2'+\phi''\xi_2'',\end{aligned} \tag{5}$$

where ϕ', ϕ'' are functions of the space and spin coordinates of the nucleons. That the same ϕ', ϕ'' appear in both wave functions in the way indicated is a consequence of the assumption of charge independence of nuclear forces. To find the desired cross sections, we take the scalar products of the scattered wave (4) with $\Phi_{H^3}\vartheta_+$ and with $\Phi_{He^3}\vartheta_0$ obtaining,

$$\begin{aligned}F_+(\mathbf{r})&=\sqrt{\tfrac{2}{3}}[\langle\phi'|\Psi'\rangle+\langle\phi''|\Psi''\rangle]\\ F_0(\mathbf{r})&=-\sqrt{\tfrac{1}{3}}[\langle\phi'|\Psi'\rangle+\langle\phi''|\Psi''\rangle].\end{aligned} \tag{6}$$

Since, according to (6), $F_+(\mathbf{r})=-2F_0(\mathbf{r})$, the same relationship holds between the scattering amplitudes; taking then the absolute squares,

$$\sigma(p+d\rightarrow H^3+\pi^+)=2\sigma(p+d\rightarrow He^3+\pi_0). \tag{7}$$

It is clear that relation (7) would hold if one replaced the two final states considered above, H^3 and He^3, by any other charge doublet.[3] In the same way, one finds that the cross sections for the production of π^+, π^0, π^- leading to nuclei in charge quartet states go as 1:2:3, to be compared with the ratios 2:1:0 found for doublet transitions. It follows that the cross sections σ_+, σ_0, σ_- defined above satisfy the relations,

$$\sigma_+/(1+2\rho)=\sigma_0/(2+\rho)=\sigma_-/3, \tag{8}$$

where ρ is the ratio of the doublet to quartet contribution. Equation (8) leads to the (rather weak) inequality: $\sigma_-<3\sigma_+$ and, by elimination of ρ, to

$$\sigma_0=\tfrac{1}{4}[\sigma_-+\sigma_+]. \tag{9}$$

The type of derivation given above applies to the more complicated cases and relations similar to (9) can be derived for any value of t_1 and t_2. In particular, in nucleon-nucleon collisions one finds

$$\sigma_0^{np}+\sigma_0^{pp}=\tfrac{1}{2}\sigma_+^{pp}+\sigma_+^{np}, \tag{10}$$

where the superscripts indicate the charge of the colliding nucleons, the subscript the charge of the meson produced. Equation (10) is valid provided the initial beams (n or p) have the same energy, and the mesons are observed with the same energy and at the same angle.[4] An interesting particular case of Eq. (10) is obtained by considering π^0 and π^+ production with deuteron formation;[5] then

$$\sigma(n+p\rightarrow d+\pi^0)=\tfrac{1}{2}\sigma(p+p\rightarrow d+\pi^+). \tag{11}$$

Relations (2), (9), (10) and their particular exemplifications like (7) and (11) provide many possible tests of the charge independence hypothesis. In order to eliminate small uncertainties in

the predictions associated with the mass difference between the charged and neutral pion and between the proton and neutron on one hand, and with Coulomb effects on the other, experiments should be conducted with light nuclei at the highest possible meson energies.

The role of the constancy of the isotopic spin in nucleon-pion problems was called to the author's attention by Professor Fermi's stimulating lectures on pion scattering at the University of Rochester last January. Thanks are due to Dr. Marshak for his interest in this research and for several helpful comments and criticisms.

Note added in proof:—Since this letter was sent in, Dr. J. M. Luttinger has informed me that he has independently derived Eqs. (9) and (10).

* This work was supported jointly by the AEC and the French Direction des Mines. Some of the calculations were presented at the Rochester Conference on Meson Physics (January 11–12, 1952).

[1] As usual, "charge independence" denotes the equality of $n-p$, $p-p$, and $n-n$ forces for states of the same spin and partity; "charge symmetry" refers to the equality of $n-n$ and $p-p$ forces alone.

[2] For a general discussion of the applications of charge independence to pion-nucleon problems and of the extension of the isotopic spin formalism to the pion field, the reader is referred to the treatment of K. M. Watson [Phys. Rev. **85**, 852 (1952)] and also to W. Heitler [Proc. Roy. Irish Acad. **51**, 33 (1946)] and K. M. Watson and K. K. Brueckner [Phys. Rev. **83**, 1 (1951)].

[3] In particular for final states containing the deuteron, as was pointed out by Dr. Chew.

[4] Equation (10) reduces to Eq. (21) of Watson and Brueckner (reference 2) when, in accordance with their assumptions, the production of π^0 in $p-p$ collisions is forbidden.

[5] Equation (11) arose out of a discussion between Dr. Marshak, Mr. Petschek, and the author.

Regularities in the Total Cross Sections for Fast Neutrons*

H. H. Barschall
University of Wisconsin, Madison, Wisconsin,
and
Los Alamos Scientific Laboratory, Los Alamos, New Mexico
(Received March 17, 1952)

RECENTLY Miller, Adair, and others[1] have measured the total cross sections for fast neutrons of many of the heavier elements in the energy range from about 0.1 to 3 Mev. It was found that, disregarding the effect of individual resonances, neighboring elements show very similar variations of cross section with energy while there are marked differences in the shape of the cross section curves between elements of appreciably different atomic number. This behavior is shown in Fig. 1. In this figure the measured cross sections divided by the geometrical area of the nucleus are plotted against neutron energy. The nuclear area was calculated for a nuclear radius of $1.45\times A^{\frac{1}{3}}\times 10^{-13}$ cm. The elements are arranged according to their atomic weight A, since in the case of Te and I it was found that a smoother surface resulted from such an arrangement than if the elements were ordered according to their atomic number. No attempt has been made to include details of the fluctuations in cross section; in particular, the behavior at thermal and epithermal energies has been ignored, since the cross sections at the lowest energies depend primarily on the presence of individual resonances.

An interesting feature of the surface shown in Fig. 1 is the large value of the cross section at low energies for elements around Sr. This peak appears to shift to higher energies with increasing atomic weight. Furthermore, the cross section of the elements heavier than Ir exhibit a minimum at neutron energies around 1 Mev.

The behavior shown in Fig. 1 is in disagreement with the continuum theory proposed by Weisskopf and his collaborators,[2] since this theory predicts a monotonic decrease of the total cross section with energy. Following a suggestion by Wigner, Weisskopf[3] has more recently calculated the energy dependence of the cross section on the basis of a single particle interaction and finds that variations of the total cross section with energy similar to those shown in Fig. 1 may be obtained.

* Work performed under the auspices of the AEC.
[1] Miller, Fields, and Bockelman, Phys. Rev. **85**, 704 (1952); more complete reports will be published later.
[2] Feshbach, Peaslee, and Weisskopf, Phys. Rev. **71**, 145 (1947); H. Feshbach and V. F. Weisskopf, Phys. Rev. **76**, 1550 (1949).
[3] V. F. Weisskopf, Bull. Am. Phys. Soc. **27**, No. 1, 7 (1952).

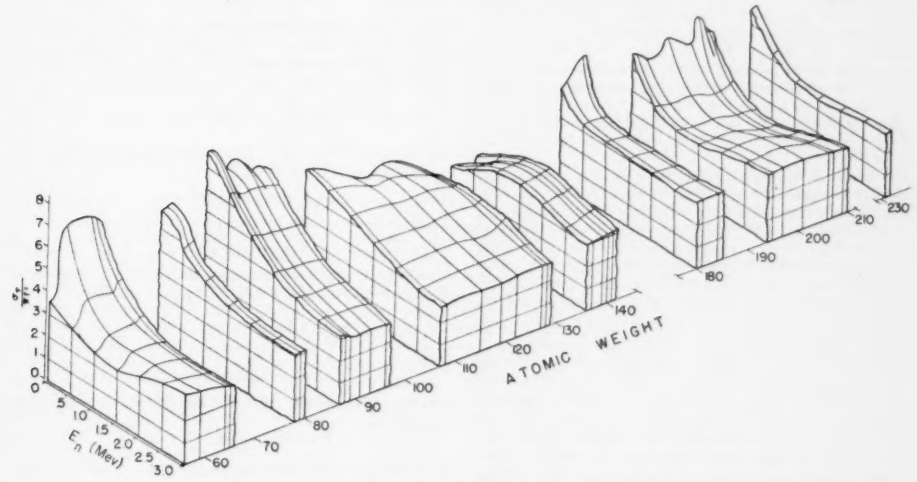

FIG. 1. Total neutron cross sections of elements heavier than Mn as a function of neutron energy. The surface is based on measurements for the atomic weights at which straight vertical lines appear in the figure.

An Investigation of the Magnetic Properties of Liquid He^3†

E. F. HAMMEL, H. L. LAQUER, S. G. SYDORIAK, AND W. E. MCGEE
Los Alamos Scientific Laboratory, Los Alamos, New Mexico
(Received March 5, 1952)

CONTINUED interest in the magnetic properties of liquid He^3 [1-3] has prompted the authors to place on record their results already briefly communicated.[4] Although Goldstein[1] showed that the possibility of nuclear ferromagnetism in liquid He^3 was very slight, experimental examination of its magnetic properties seemed desirable. Two methods were employed. The first was a heterodyne beat method. A coil of inductance L surrounding the sample formed part of an oscillating circuit, the frequency of which was essentially $\nu=[2\pi(LC)^{\frac{1}{2}}]^{-1}$. Since the inductance of the coil is proportional to the permeability of the medium surrounding it, condensation of any material within the coil results in a frequency shift $-d\nu/\nu=dL/L=fd\mu/2\mu=2\pi f\kappa$, where f is the filling factor for the coil equal to 0.098 for the coil used, μ is the permeability of the sample, and κ is its volume susceptibility. The oscillator was operated at 1.47 Mc. The system was calibrated with liquid oxygen ($d\nu=272\pm3$ cycles). He^4 condensed inside the coil gave no sudden shift larger than ±5 cycles although a gradual drift in the frequency occurred, probably due to change in bath level. With He^3 at 2.08°K and at 1.27°K there was no frequency shift larger than 5 cycles. Hence the volume susceptibility (κ) of liquid He^3 at these temperatures is less than 5×10^{-6}. If liquid He^3 were a nuclear ferromagnetic, long relaxation times for the domains would give a null result, as would magnetic saturation of the sample by the earth's field. The second method employed was, therefore, a low frequency (60 cycles) method which avoided these objections, unless the relaxation time was of the order of hours. Two matched 6000-turn coils were mounted above one another and connected in opposition. A Pyrex sample bulb several cubic millimeters in volume was situated in the upper search coil, and the whole assembly was located in a cryostat around which was wound a Helmholtz coil. The earth's field in the vicinity of the search coils plus that from the permanent magnetization of the associated equipment yielded a resultant field almost horizontal equal to 0.65 oersted. By operating the Helmholtz coil to give a 60-cycle oscillating field of 0.65-oersted maximum, the resultant field oscillating over a 90° arc, beginning 45° from the vertical. The signal from the search coils was taken through a phase adjusting and amplitude balancing network, and then through amplifiers to the Y-plates of an oscilloscope. The X-plates were connected across the Helmholtz coil input. With the sample bulb evacuated, the phase and amplitude of any remaining signal from the search coils was balanced to give only a horizontal line on the oscilloscope. Introduction of a substance of high permeability in the upper coil would then have transformed the oscilloscope trace into an ellipse.

Calibration of the system indicated that a 7-μv peak-to-peak signal from the search coils could be observed. The effective linkage of the number of turns of the search coil with the sample was determined to lie between 5 and 22 percent as follows: The initial and constant (for very low fields) permeability of a bundle of pure iron wire was measured. A sample of this iron was placed in a glass capillary (similar to the one used with the He^3), inserted in the search coil and the signal measured. From this the ratio of the effective number of turns to the total number was calculated to be 22 percent. Measurement of the paramagnetic susceptibility of oxygen using the same coil system but a higher gain amplifier and improved phase shifting network gave a filling factor of 5 percent.

If liquid He^3 were ferromagnetic, the induced emf for the above mentioned apparatus would be $\epsilon_{ind}=dF/dt=-\omega(4\pi\eta\mu)NAf\sin\omega t=2.75f$ millivolts peak-to-peak, where $F=\Delta BANf\cos\omega t$, $\Delta B=$ difference in flux through sample area with and without sample, $A=$area of sample, $N=$number of turns in search coil, $f=$filling factor, $\eta=$the number of He^3 atoms/cc$=1.6\times10^{22}$,[5] and $\mu=$magnetic moment of $He^3=1.07\times10^{-23}$ cgs units.[6] Using the above values for filling factor, the observed signal should have been $140<\epsilon_{obs}<600$ μv (peak-to-peak).

Two experiments were carried out with this apparatus. In the first, the sample bulb was flushed with O_2 gas before cooling the assembly and condensing the He^3 in an attempt to decrease the relaxation time.[7] The temperature, measured by the vapor pressure of the He^3, was 0.904°K. No change in the oscilloscope signal was observed upon condensation of the He^3. The sample was held at this temperature for about 40 minutes. In the second experiment, the He^3 was condensed at 2.51°K. The temperature was then gradually reduced to 1.35°K over a 45 minute period. Again, no change in the oscilloscope signal was observed.

The authors are indebted to Dr. L. Goldstein of this Laboratory, who suggested this problem, together with Dr. F. G. Brickwedde and Professor E. Teller, consultants to the Los Alamos Scientific Laboratory, for stimulating discussions, and also to Mr. R. W. Freyman, Dr. W. L. Briscoe, and Mr. C. W. Johnstone of the Laboratory for assistance with some of the electronic components.

† This paper is based on work performed under University of California contract with the AEC.

[1] L. Goldstein, J. Chem. Phys. **18**, 538 (1950).
[2] R. A. Buckingham and H. N. V. Temperley, Phys. Rev. **78**, 482 (1950).
[3] I. Pomeranchuk, J. Exptl. Theoret. Phys. (U.S.S.R.) **20**, 919 (1950).
[4] S. G. Sydoriak and E. F. Hammel, Proc. Int. Conf. Physics Very Low Temp., M.I.T., Cambridge, Mass., Sept. 6-10 (1949), p. 42.
[5] Grilly, Hammel, and Sydoriak, Phys. Rev. **75**, 1103 (1949).
[6] H. Anderson and A. Novick, Phys. Rev. **73**, 919 (1948).
[7] Bloch, Hansen, and Packard, Phys. Rev. **70**, 474 (1946).

The Virial Theorem for a Dirac Particle*

M. E. ROSE AND T. A. WELTON
Oak Ridge National Laboratory, Oak Ridge, Tennessee
(Received January 28, 1952)

THE authors have recently had occasion to use a number of identities, satisfied by Dirac wave functions, which take the form of a virial theorem in the relativistic quantum case. In the hope that these results may prove useful to others they are communicated herewith.

The well-known relativistic virial theorem in the classical case is

$$-\overline{\mathbf{r}\cdot\mathbf{F}}=\bar{T}+\bar{L}_0, \tag{1}$$

where T and L_0 are the kinetic energy and Lagrangian for a free particle, the bar indicates a time average and $\mathbf{F}$ is the Lorentz force and in the quantum mechanical case we obtain the corresponding result by considering the expectation value

$$\left\langle\frac{d}{dt}\mathbf{r}\cdot\mathbf{p}\right\rangle=i\langle\mathbf{r}\cdot(H,\mathbf{p})+(H,\mathbf{r})\cdot\mathbf{p}\rangle=0, \tag{2}$$

where the round brackets in Eq. (2) designate commutators and the single particle Hamiltonian is

$$H=e\phi+\boldsymbol{\alpha}\cdot(\mathbf{p}-e\mathbf{A})+\beta. \tag{3}$$

We use $\hbar=m=c=1$. From (2) and (3) we obtain

$$\langle\boldsymbol{\alpha}\cdot\mathbf{p}\rangle=e\langle\mathbf{r}\cdot\nabla(\phi-\boldsymbol{\alpha}\cdot\mathbf{A})\rangle. \tag{4}$$

In addition, we may consider the expectation value of the operator with $\boldsymbol{\pi}=\mathbf{p}-e\mathbf{A}$ replacing $\mathbf{p}$ in (2). Then it follows that

$$\left\langle\frac{d}{dt}\mathbf{r}\cdot\mathbf{A}\right\rangle=\langle\boldsymbol{\alpha}\cdot\mathbf{A}\rangle+\langle\mathbf{r}\cdot(\boldsymbol{\alpha}\cdot\nabla)\mathbf{A}\rangle=0.$$

Using

$$\nabla\boldsymbol{\alpha}\cdot\mathbf{A}=\boldsymbol{\alpha}\times\mathrm{curl}\mathbf{A}+(\boldsymbol{\alpha}\cdot\nabla)\mathbf{A},$$

the relativistic quantum-mechanical virial theorem may be written in the form

$$-\langle\mathbf{r}\cdot\mathbf{F}\rangle=\langle\boldsymbol{\alpha}\cdot(\mathbf{p}-e\mathbf{A})\rangle=\langle E-e\phi-\beta\rangle, \tag{5}$$

where E is the energy including rest energy and the Lorentz force operator is interpreted as follows,

$$\mathbf{F}=e(-\nabla\phi+\boldsymbol{\alpha}\times\mathrm{curl}\mathbf{A}).$$

This corresponds to the classical virial theorem, since in the presence of a magnetic field the right-hand side of (1) is replaced by $\langle \boldsymbol{\alpha}\cdot\boldsymbol{\pi}\rangle$ in the quantum case.

Perhaps the most useful form of the virial theorem is the case corresponding to no magnetic field,

$$-\langle \mathbf{r}\cdot\mathbf{F}\rangle = \langle \boldsymbol{\alpha}\cdot\mathbf{p}\rangle = \langle E - e\phi - \beta\rangle. \tag{6}$$

It is clear that (5) and (6) do not apply for continuum states. For example, for a free particle $\langle \boldsymbol{\alpha}\cdot\mathbf{p}\rangle = \langle p^2/E\rangle$.

Alternatively, for a static potential ϕ, we consider the expectation value for any stationary state of the anticommutator of β and H to obtain

$$\langle \beta(E - e\phi)\rangle = 1, \tag{7}$$

(that is, $\langle \beta\boldsymbol{\alpha}\cdot\mathbf{p}\rangle = 0$) which gives the well-known result $\langle\beta\rangle = 1/E$ for a free particle. However, for a bound state in the Coulomb field, it follows from (6) that

$$\langle\beta\rangle = E, \tag{7a}$$

so that in this case,

$$e\langle\beta\phi\rangle = E^2 - 1. \tag{7b}$$

The nonrelativistic limit $e\langle\phi\rangle = -2\langle T\rangle$, T the nonrelativistic kinetic energy operator, follows from (7b); and more generally from (6) the usual limiting form $e\langle \mathbf{r}\cdot\nabla\phi\rangle = 2\langle T\rangle$ results.

* This paper is based on work performed for the AEC at the Oak Ridge National Laboratory.

Soft and Hard *F*-Centers

JORDAN J. MARKHAM
Applied Physics Laboratory, Johns Hopkins University, Silver Spring, Maryland
(Received March 19, 1952)

OBERLY[1] has suggested that two types of *F*-centers exist. The soft type can be bleached easily by light, while the hard type is relatively unaffected. The suggestion is based on his photoconductivity measurements and work by Petroff.[2] The author would like to explain the observations in an alternate manner which does not require two types of centers and agrees with the conventional model.[3]

Using x-rayed KBr, Oberly measured at room temperature the changes of $\eta\omega$ (η is the quantum yield and ω is the electron range) caused by irradiation with *F*-light. He measured $\eta\omega$ as a function of wavelength after a 7- and a 23-minute exposure to *F*-light. Between 550 mμ and 1000 mμ, $\eta\omega$ decreases between the 7- and the 23-minute measurements while the reverse is true in the violet beyond the *F*-band.

One interpretation is that η changes because the soft centers disappear. This requires, in the author's opinion, soft and hard *F*, *R*, *M*, and *N* centers.

The author would like to suggest that ω changes. During the exposure to *F*-light negative-ion vacancies are formed from those centers which release electrons. We shall assume that negative-ion vacancies remain as incipient vacancies during the course of the experiments. Thus when the crystal is exposed to *F*-light, the concentration of negative-ion vacancies and the corresponding macroscopic cross section for an electron to be captured by a vacancy increases; the latter in turn decreases ω. Oberly's data is explained as follows: (1) The photoconductivity between 550 mμ and 1200 mμ is due to electrons whose ω decreases during *F*-light exposure. (2) The photoconductivity between 470 mμ and 550 mμ is due to holes whose ω is not affected by the concentration of negative-ion vacancies. (3) Oberly observed that an exposure to *F*-light affects photoconductivity measurements more than absorption measurements. The reason seems to be that absorption depends only on the concentration of *F*-centers, while photoconductivity depends critically on the concentration of negative-ion vacancies as well as the concentration of *F*-centers.

Another reason which might cause one to believe that there are two types of *F*-centers is that the half-width of the band varies experimentally.[4] Some *F*-centers may be surrounded by a perfect lattice, while other *F*-centers may be near vacancy clusters or dislocations. The centers near a perturbation in the lattice probably have a different half-width than those in a nearly perfect lattice. The method of excitation and the past history of the crystal would seem to determine the location of the *F*-centers and their half-width. The variation in the *F*-centers seems to be a matter of degree rather than a matter of having two types with distinct η.

Petroff has suggested two types of *F*-centers to explain the rate of growth of the *M*-band. Seitz[3] has proposed that an *M*-center is an electron attached to two negative and one positive-ion vacancy. It seems probable that the *M*-band is formed by breaking up vacancy clusters and that the intermediate state may be a vacancy complex which gives no absorption rather than a center hidden under the *F*-band.

There seems to be the possibility of explaining Oberly's data without changing the present picture of color centers. The author will not attempt to explain some secondary effects observed by Oberly which need further experimental exploration. At present there seems to be no reason to believe that these secondary effects will require a more elaborate model.

The author would like to thank Professor F. Seitz and Mr. W. H. Deurig for helpful discussions of these ideas.

* Supported by the Bureau of Ordnance, U. S. Navy.
[1] J. J. Oberly, Phys. Rev. **84**, 1257 (1951).
[2] St. Petroff, Z. Physik **127**, 443 (1950).
[3] F. Seitz, Revs. Modern Phys. **18**, 384 (1946).
[4] See, for example, A. Smakula, Z. Physik **59**, 603 (1930).

Optical Focusing in Constant Radius Accelerators

DAVID C. DEPACKH
Nucleonics Division, Naval Research Laboratory, Washington, D. C.
(Received March 19, 1952)

THAT the focusing forces are weak at low energies and large radii in electron accelerators with magnetic fields characterized by the usual parameter n can be readily deduced from the definition of this quantity, namely,

$$n \equiv -(R/H_z)(\partial H_z/\partial r) \equiv -(R/H_r)(\partial H_r/\partial z),$$

where R is the equilibrium orbit radius, H_z is the vertical field at the orbit, and H_r is the radial field at the orbit. We find in fact that

$$\Delta z/\Delta H_r = n^{-1}R^2/(RH_z), \quad \Delta r/\Delta H_z = (1-n)^{-1}R^2/(RH_z).$$

The quantity on the left is a direct measure of the orbit shift due to a stray field ΔH_r or ΔH_z and thus of the amount the particle will go astray due to this field. RH_z depends only on the particle energy, which must be considered at its lowest value, namely, the injection energy. The value of n is of course restricted to lie between 0 and 1.

It is evident that for machines of large radius a stronger focusing force at injection is very desirable. Such a force can be supplied by a sequence of magnetic lenses regularly spaced around the acceleration tube. Because of the axial symmetry of this arrangement there is no theoretical limit, short of the fact that the lenses must be discrete, on the amount of focusing force available. It will be assumed that the field strength of the lenses is constant in the time, at least after a certain time. This condition must be fulfilled because of the size limitation of the lenses, which must fit into the available aperture. The calculations show that there is no adiabatic variation of oscillation amplitude with particle acceleration if the lens fields are constant. It may thus be desirable to supply a small increase in the lens field during the early part of the acceleration cycle to insure that the orbits will lie within the acceleration tube.

The separation of the lenses should be considerably less than four focal lengths, the theoretical maximum. The individual lens separations and focal lengths should be held constant with respect to the average to a tolerance of about 1 percent for an average machine to avoid catastrophic resonance effects as the high transverse oscillation frequency corresponding to the relatively strong low-energy focusing force is gradually reduced with increase in the particle energy. It is of course necessary to provide the usual transverse field focusing at high energies.

Preliminary tests of twelve lenses equally spaced on the Naval Research Laboratory small aperture accelerator (radius 2½ feet, aperture cross section 30-mm diameter) gave excellent focusing and evidence of many electron circuits through the tube on a fluorescent screen inserted into the path of the particles. This behavior was not possible at the injection energy of about 30 kv prior to the use of lens focusing.

A paper dealing with the theoretical aspects of the problem as well as with experimental results using more accurately spaced and wound lenses will be issued when the latter information has been obtained.

The Electron Neutron Interaction

BURTON D. FRIED
Department of Physics, University of Chicago, Chicago, Illinois
(Received March 14, 1952)

A WEAK, attractive interaction between neutrons and electrons has been observed experimentally.[1-4] From a qualitative point of view, such an effect is in accord with meson theory, for if a neutron can dissociate into charged particles,

$$N \leftrightarrow P + \pi^-,$$

it should have some interaction with an electric field. However, although several authors[5-8] have treated this problem in detail, there has been some confusion as to just what value meson theory gives for this interaction. For instance, using the same type of theory—pseudoscalar mesons, pseudoscalar coupling, with the usual weak coupling perturbation theory carried to second order in the meson-nucleon coupling—different methods of calculation have produced different answers. Thus, Slotnick and Heitler, and Dancoff and Drell obtain values about four times larger than do Case and Borowitz and Kohn. Moreover, Foldy's phenomenological treatment[9] gives a value lying between these two results.

Of course, meson theory weak coupling calculations of such effects cannot be taken too seriously—for instance, they do not even give the correct neutron to proton magnetic moment ratio. Nevertheless, in view of recent interest in the electron-neutron interaction[10,11] it seems desirable to state definitely just what value pseudoscalar meson theory does predict for this effect and to explain the relation of the various results referred to above. This note summarizes the results of an investigation aimed at settling these questions. A calculation of the electromagnetic properties of neutrons has been carried out with special attention to the matter of interpretation of the terms obtained from field theory. A more detailed account will be submitted for publication shortly.

As in previous calculations, the meson-nucleon coupling term in the Hamiltonian density is taken to be

$$\mathcal{H}' = g\sqrt{2}(\psi_N^\dagger \gamma^5 \psi_P \phi^* + \psi_P^\dagger \gamma^5 \psi_N \phi),$$

where ϕ is the charged meson field and ψ_P, ψ_N are the nucleon fields. (The electromagnetic properties of neutrons are the same for both charged and symmetric meson theories.) With the usual Feynman-Dyson techniques it can be shown that as a consequence of this coupling, the (first-quantized) Dirac equation for a single neutron becomes

$$(m\beta + \boldsymbol{\alpha}\cdot\mathbf{p} + H_1)\psi = i\dot{\psi}, \tag{1}$$

where, dropping terms which contain higher order derivatives of the external potential A_μ or higher powers of g,

$$H_1 = -\tfrac{1}{2}\mu\beta F_{\mu\nu}\sigma_{\mu\nu} - i\lambda\beta\Box^2 A_\mu\gamma^\mu,$$

with

$$\mu = -(eg^2/8\pi^2 M) f_0(\eta), \quad \lambda = (eg^2/8\pi^2 M^3) f_1(\eta),$$
$$f_0(\eta) = 1 - \eta\log\eta^{\frac{1}{2}} + (\eta-2)\eta^{\frac{1}{2}}(4-\eta)^{-\frac{1}{2}}\cos^{-1}(\eta^{\frac{1}{2}}/2),$$
$$f_1(\eta) = (13-4\eta)(12-3\eta)^{-1} + (\tfrac{1}{4} - \tfrac{2}{3}\eta)\log\eta$$
$$+ \eta^{\frac{1}{2}}(4-\eta)^{-\frac{1}{2}}(-35/3 + 17\eta/2 - 4\eta^2/3)\cos^{-1}(\eta^{\frac{1}{2}}/2). \tag{2}$$

M is the nucleon mass, and η is the square of the meson to nucleon mass ratio.

An unambiguous interpretation of the additional term H_1 can best be obtained by considering the two-component Pauli equation to which (1) reduces in the nonrelativistic limit. (The experiments always use slow neutrons.) This is

$$[M + p^2/2M - \mu\mathbf{H}\cdot\boldsymbol{\sigma} - (\mu/2M + \lambda)\,\mathrm{div}\mathbf{E}]\psi = i\dot{\psi}, \tag{3}$$

showing that while the first term of H_1 alone is responsible for the magnetic moment, both terms contribute to the interaction with an electric field—in fact, as shown below, the two contributions are of the same order of magnitude. (An additional Thomas type term has been omitted from (3) since it cannot contribute to the observed scattering effects.[1])

To express these results in conventional form, take the source of $\mathbf{E}$ to be an electron, so that $\mathrm{div}\mathbf{E} = -4\pi e\rho_0$, where ρ_0 is the electron particle density, $\int d\tau\rho_0 = 1$. Then the effective potential which the neutron sees is

$$V = (e^2 g^2/2\pi M^2)(-\tfrac{1}{2}f_0 + f_1).$$

The conventional "equivalent well depth," V_0, defined in terms of the classical electron radius $r_e = e^2/m$, is

$$V_0 = \int d\tau V \Big/ \frac{4\pi}{3} r_e^3 = \frac{3}{2\pi}\frac{g^2}{4\pi}\left(\frac{m}{M}\right)^2 \frac{m}{e^4}(-\tfrac{1}{2}f_0 + f_1). \tag{4}$$

Using $\sqrt{\eta} = 0.151$[12] for the meson-nucleon mass ratio gives $f_0 = 0.820$; $f_1 = -0.131$; $(-\frac{1}{2}f_0 + f_1) = -0.541$. Adjusting g so that the neutron magnetic moment μ is given correctly[13] by (2) leads to

$$g^2/4\pi\hbar c = 7.33, \tag{5}$$

so that

$$V_0 = -5.38 \text{ kev}, \tag{6}$$

in fair agreement with the recent experimental figures of (5300 $\pm$1000)[2] and (4100$\pm$1000)[4] electron volts.

The relation of these results to those of other authors can be expressed quite simply. Case and Borowitz and Kohn neglect the contribution of the first term of H_1 to the electron-neutron interaction. This is equivalent to replacing $(-\frac{1}{2}f_0 + f_1)$ in (4) by just f_1, which, with the choice (5) for the coupling constant, gives

$$V_{C;B,K} = -1.30 \text{ kev}. \tag{7}$$

On the other hand, a phenomenological treatment like Foldy's, in which the magnitude of the electron-neutron interaction is deduced from the value of the magnetic moment only, corresponds to using just $\frac{1}{2}f_0$ in (4), leading to

$$V_F = -4.08 \text{ kev}. \tag{8}$$

Finally, the calculations by Slotnick and Heitler, and Dancoff and Drell of the matrix element for neutron scattering in an electric field in nonrelativistic approximation give, with the present choice of coupling constant,

$$V_{S,H} = -4.99 \text{ kev}, \quad V_{D,D} = -6.10 \text{ kev}. \tag{9}$$

These nearly agree with the value (6), thus supporting Foldy's suggestion that neglect of the first term in H_1 is largely responsible for the discrepancy between (7) and (9).

The author is indebted to Professor G. Wentzel, who suggested this problem. Thanks are due to Professor Wentzel, Dr. M. Goldberger, and Dr. M. Gell-Mann for many helpful discussions and to

Dr. Hamermesh, Dr. Ringo, and Dr. Wattenberg for communicating the results of their measurement in advance of publication.

[1] E. Fermi and L. Marshall, Phys. Rev. **72**, 1139 (1947).
[2] Havens, Rabi, and Rainwater, Phys. Rev. **72**, 634 (1947); Phys. Rev. **75**, 1295 (1949).
[3] Havens, Rainwater, and Rabi, Phys. Rev. **82**, 345 (1951).
[4] Hamermesh, Ringo, and Wattenberg, Phys. Rev. **85**, 483 (1952).
[5] M. Slotnick and W. Heitler, Phys. Rev. **75**, 1645 (1949).
[6] K. M. Case, Phys. Rev. **76**, 1 (1949).
[7] S. M. Dancoff and S. D. Drell, Phys. Rev. **76**, 205 (1949).
[8] S. Borowitz and W. Kohn, Phys. Rev. **76**, 818 (1949).
[9] L. L. Foldy, Phys. Rev. **83**, 688 (1951).
[10] G. Breit, Proc. Natl. Acad. Sci. **37**, 837 (1951).
[11] D. J. Hughes, Bull. Am. Phys. Soc. **27**, 31 (1952).
[12] Barkas, Smith, and Gardner, Phys. Rev. **82**, 102 (1951).
[13] Bloch, Nicodemus, and Staub, Phys. Rev. **74**, 1025 (1949).

Spin and Parity of the First (603-kev) Excited State of Te^{124}†

FRANZ R. METZGER
Physics Department, University of Illinois, Urbana, Illinois
(Received March 17, 1952)

SIXTY-DAY Sb^{124} and 4-day I^{124} decay into Te^{124} by β^- emission, and by β^+ emission and K-capture, respectively. Both decays are rather complex, especially the disintegration of Sb^{124}. However, it seems well established that the 603-kev gamma-ray, which is the most intense gamma-ray in both decays, is the transition from the first excited level to the even-even ground state of Te^{124}.

In the Sb^{124} decay the number of conversion electrons due to the 603-kev gamma-ray is 0.2 percent of the total number of beta-rays.[1,2] Assuming practically all the disintegrations of Sb^{124} to go through the 603-kev state, Langer, Moffat, and Price[3] identified this ratio of conversion electrons to beta-rays with the conversion coefficient of the 603-kev transition. They concluded that the 603-kev gamma-ray was electric dipole and therefore assigned spin one, odd parity, to the first excited state of Te^{124}, thus providing one of the few exceptions to Goldhaber and Sunyar's rule.[5]

TABLE I. Comparison of the theoretical conversion coefficients for the 603-kev gamma-ray in Te^{124} with the experimental value.

	Electric dipole	Magnetic dipole	Electric quadrupole	Experimental value
$10^3 \times \alpha_K$	1.6	5.6	4.3	4.25 ± 0.3

New interest in the properties of the 603-kev level arose in connection with the observation of a large beta-gamma angular correlation in Sb^{124}.[4] The two most recent investigations[6] of this correlation are in good agreement with one another, both with respect to energy dependence and magnitude of the correlation. Both authors consider the assignments 1–1–0 and 3–2–0 the most probable ones.

We have determined the K-conversion coefficient of the 603-kev gamma-ray using the following method: A beta-ray source and a photoelectron source were prepared and their activities compared by counting the gamma-rays with a scintillation counter. The K-conversion and K-photoelectron lines due to the gamma-ray of interest were then measured in a beta-ray spectrometer. The efficiency of the standardized photoelectron arrangement was determined using gamma-rays with known conversion coefficients.

From the relative source strength, the converter efficiency, and the ratio of the areas under the conversion and photoelectron lines, one obtains the conversion coefficient N_e/N_γ without reference to the decay scheme.

Using this method we find for the K-conversion coefficient of the 603-kev gamma-ray in Te^{124} the value $\alpha_K = (4.25 \pm 0.3) \times 10^{-3}$. In Table I this experimental value is compared with the theoretical conversion coefficients given by Rose, *et al.*[6]

The 603-kev gamma-ray is thus unambiguously characterized as electric quadrupole and the first (603-kev) excited state of Te^{124} as 2, even.

A comparison of the measured conversion coefficient with the above mentioned ratio of conversion electrons to beta-rays indicates that the 603-kev gamma-ray is only connected with 40–50 percent of the Sb^{124} disintegrations. The presently accepted decay scheme therefore will have to be revised as soon as better data regarding the relative intensities of the gamma-rays are available.

Concerning the ground state of Sb^{124}, one is inclined to accept the spin value 3, as suggested by the correlation experiments. The large ft-value (10.3) of the 2.29-Mev transition, the deviation from the allowed shape,[7] and the presence of two isomeric states indicate that, here too, further studies will be necessary.

† Supported by the joint program of the ONR and AEC.
[1] Kern, Zaffarano, and Mitchell, Phys. Rev. **73**, 1142 (1948).
[2] Langer, Moffat, and Price, Phys. Rev. **79**, 808 (1950).
[3] M. Goldhaber and A. W. Sunyar, Phys. Rev. **83**, 906 (1951).
[4] S. L. Ridgway, Phys. Rev. **78**, 821 (1950).
[5] D. T. Stevenson and M. Deutsch, Phys. Rev. **83**, 1202 (1951); E. K. Darby, Can. J. Phys. **29**, 569 (1951).
[6] Rose, Goertzel, Spinrad, Harr, and Strong, Phys. Rev. **83**, 79 (1951).
[7] See reference 2 and also Nakamura, Umezawa, and Takebe, Phys. Rev. **83**, 1273 (1951); L. M. Langer, Phys. Rev. **84**, 1059 (1951).

The Emission of Deuterons from the Nucleus

A. G. W. CAMERON
Department of Physics, University of Saskatchewan, Saskatoon, Saskatchewan, Canada
(Received March 17, 1952)

THREE experiments have been carried out which indicate that deuterons are emitted in photonuclear reactions very much more easily than would be expected from considerations of the statistical theory of nuclear reactions.[1] The reaction $S^{32}(\gamma, d)P^{30}$ may be readily detected at energies down to the photodeuteron threshold;[2,3] at only one Mev above this threshold the (γ, d) to (γ, p) cross section ratio has already reached the value 0.001. Byerly and Stephens[4] have observed that the ratio of deuterons to protons produced in copper irradiated with 24-Mev x-rays is 0.31. For 65-Mev bremsstrahlung this ratio has risen to 0.5 ± 0.15.[5] These ratios are several orders of magnitude larger than the statistical theory would predict.[4]

These facts indicate that there might be some mechanism by means of which low energy deuterons may penetrate potential barriers more easily than can a single particle such as a proton. Schiff[6] has suggested that deuterons may be more easily emitted from the nucleus if they are radially polarized, with the neutron component of the deuteron forming a "bridge" to the nucleus which causes a lowering of the potential barrier in the neighborhood of the outgoing deuteron.

It is the purpose of this note to suggest an experiment which might test this hypothesis. The first excited level of the deuteron is a singlet state about 64 kev above the dissociation energy.[7] If a deuteron in this first excited level were emitted from the nucleus, the neutron and proton resulting from its subsequent disintegration would travel in nearly the same direction, since only a small transverse momentum would be imparted by the break-up. The angle between the directions of motion of the neutron and proton would range up to 40° for deuteron kinetic energies of 4 Mev and greater. One might expect that deuterons in the excited and ground states would have emission probabilities in somewhat less than the ratio of the multiplicities of the levels (1:3), since there would be less residual energy of nuclear excitation following the emission of the singlet deuteron. However, even if the emission probability of a singlet deuteron were less than that for the independent emission of a proton and a neutron by a little more than an order of magnitude, such emission could readily be detected in a

coincidence experiment through the strong angular correlation between the directions of emission.

If there were any significant amount of radial polarization of the emitted singlet deuterons, the disintegration of these particles would impart much less transverse momentum to the two nucleon products. A measurement of the angular correlation between the disintegration products of singlet deuterons emitted in nuclear reactions would therefore give valuable information concerning the mechanism of barrier penetration. From the experimental point of view, such a coincidence experiment would be easier to perform if the nuclear reaction initiating the deuteron emission were produced by a steady beam of bombarding particles, rather than by short pulses of radiation such as produced in betatrons and synchrotrons.

I am indebted to Dr. L. Katz for valuable discussions of this problem.

[1] V. F. Weisskopf and D. H. Ewing, Phys. Rev. **57**, 472 (1940).
[2] L. Katz and A. S. Penfold, Phys. Rev. **81**, 815 (1951).
[3] L. Katz and A. G. W. Cameron, Can. J. Phys. **29**, 518 (1951).
[4] P. R. Byerly, Jr. and W. E. Stephens, Phys. Rev. **83**, 54 (1951).
[5] W. H. Smith, Bull. Am. Phys. Soc. **27**, No. 1, 18 (1952).
[6] L. I. Schiff, private communication.
[7] W. M. Woodward and I. Halpern, Phys. Rev. **76**, 107 (1949).

CONTENTS

The Fermion Simple ... Page Number

Monte Carlo Study of ... Number ...

Comparative Models ... D. ...

Reflection Effects in ... of ...

Relativistic Hartree-Fock ... Johnson and ...

Signs of the Quadrupole ... L. Cook, ...

Radiochemistry ... Jr., ...

Energy Levels of C^{11} and ... Vincent ...

New "Double Resonance" ... Lamb, ...
Eq. 19 ...

Effect of the Atomic Core on ... R. ...

Integration of Equations ... Comparison ...

Nuclear Resonance Fluorescence ... Cook, ...

Second-Quantized Theory of ... Comparison ...

Radioisotopes of Francium ... S. Corliss and ...

Dynamic Characteristics of ... Resonance ...

Photodisintegration of the ... L. ... Cook, John D. ...

Photodisintegration of ... R. ... D. ...

Scattering of Electrons by ... of Heavy ...

Triton Binding Energy by ... Comparison ...

Photodisintegration of ... Comparison ...

Covariant Theory of ... Deuteron ...

Neutron-Proton Scattering ... Comparison ...

Yield of F^{18} from ... Reaction ... Lamb, ...

Atomic Masses from ... Spectra ... Wapstra, ...

Letters to the Editor:

Relativistic Hartree-Fock ... A. E. S. Green, ...

Spectra of Neutron-Rich ... A. E. S. Green, ...

Effect of Tensor Forces ... A. E. S. Green, ...

Reflectivity in ... A. ... ...

Energetics of Thermal ... ...

Alpha Emission from ... ...

... Potential ... ...

Resonance ... ...

Polarization of ... ...

Decay of ... ...

Determination of ... ...

... ...

... ...

Dependence of ... ...

Detection of ... ...

Magnetic ... ...

... ...

Measurement of ... ...

Modes of ... ...

... ...

... ...

... ...

... ...

... ...

... ...

Mass Number of a ... ...

Soft and Hard ... ...

Optical Reactivity ... ...

Neutron Fluxes, ...

Rate and Depth of ... ...

Reduction of ... ...